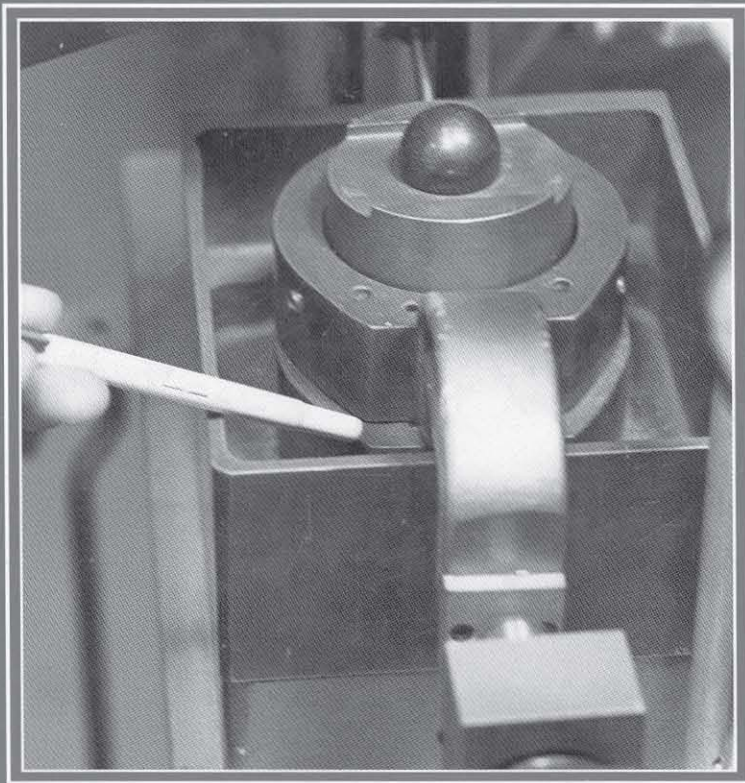


DISK INCLUDED



EXPERIMENTAL SOIL MECHANICS



JEAN-PIERRE BARDET

EXPERIMENTAL SOIL MECHANICS

Jean-Pierre Bardet

Civil Engineering Department
University of Southern California, Los Angeles



PRENTICE HALL
Upper Saddle River, New Jersey 07458

Library of Congress Cataloging-in-Publication Data

Bardet, J. P. (Jean Pierre)

Experimental soil mechanics / by J. P. Bardet.

p. cm.

Includes bibliographical references and index.

ISBN 0-13-374935-5

1. Soils--Testing--Data processing. I. Title.

TA710.5.B34 1997

624.1'5136'078--dc20

96-320

CIP

Acquisitions editor: **BILL STENQUIST**

Editor-in-chief: **MARCIA HORTON**

Production editor: **IRWIN ZUCKER**

Managing editor: **BAYANI MENDOZA DE LEON**

Cover designer: **JAYNE CONTE**

Director of production and manufacturing: **DAVID W. RICCARDI**

Manufacturing buyer: **JULIA MEEHAN**

Editorial assistant: **MARGARET WEIST**

Prentice
Hall

© 1997 by Prentice Hall, Inc.
Upper Saddle River, NJ 07458

All rights reserved. No part of this book may be reproduced, in any form or by any means, without permission in writing from the publisher.

The author and publisher of this book have used their best efforts in preparing this book. These efforts include the development, research, and testing of the theories and programs to determine their effectiveness. The author and publisher make no warranty of any kind, expressed or implied, with regard to these programs or the documentation contained in this book. The author and publisher shall not be liable in any event for incidental or consequential damages in connection with, or arising out of, the furnishing, performance, or use of these programs.

Printed in the United States of America

10 9 8 7 6 5 4

ISBN 0-13-374935-5

Prentice-Hall International (UK) Limited, *London*

Prentice-Hall of Australia Pty. Limited, *Sydney*

Prentice-Hall of Canada, Inc., *Toronto*

Prentice-Hall Hispanoamericana, S. A., *Mexico*

Prentice-Hall of India Private Limited, *New Delhi*

Prentice-Hall of Japan, Inc., *Tokyo*

Prentice-Hall Asia Pte. Ltd., *Singapore*

Editora Prentice-Hall do Brasil, Ltda., *Rio de Janeiro*



Contents

Preface	vi
Introduction	1
Laboratory soil testing	1
Standard procedures for soil testing	4
1 Grain Size Distribution	8
✓ 1-1 Principles of grain size analysis	9
1-2 Sieve analysis	22
✓ 1-3 Principles of sedimentation analysis	31
1-4 Hydrometer analysis	42
1-5 Pipette analysis	55
1-6 Buoyancy analysis	65
1-7 Combined grain size analysis	71
2 Plasticity, Shrinkage, and Soil Classification	74
✓ 2-1 Principles of liquid and plastic limits tests	75
2-2 Determination of water content	84
2-3 Liquid limit test	86

- 2-4 One-point liquid limit test 92
- 2-5 Plastic limit test 96
- 2-6 Principles of shrinkage limit analysis 101
- 2-7 Shrinkage limit analysis with mercury 106
- 2-8 Shrinkage limit analysis with wax 112
- ✓2-9 Engineering classification of soils 116

3 Density and Compaction 128

- ✓3-1 Weight-volume relationships 129
- 3-2 Unit weight of cohesive soils 136
- 3-3 Determination of specific gravity 142
- 3-4 Principles of compaction 147
- 3-5 Compaction tests 155
- 3-6 Sand cone method 166

4 Permeability and Seepage 176

- 4-1 Principles of permeability tests 177
- 4-2 Constant head permeability test 189
- 4-3 Falling head permeability test 202
- 4-4 Electrical analogy of seepage problems 207
- 4-5 Finite difference solutions of seepage problems 217

5 Stress - Strain - Strength Properties 234

- 5-1 Stress in soils 235
- 5-2 Strain in soils 251
- 5-3 Stress - strain relations 261
- 5-4 Laboratory tests for determination of stress - strain - strength of soils 265
- 5-5 Elastic properties of soils 277

6 Consolidation 296

- 6-1 Principles of consolidation 297
- 6-2 Consolidation test 343

7 Shear Strength 360

- 7-1 Shear strength of soils 361
- 7-2 Principles of the unconfined compression test 404

- 7-3 Unconfined compression test 411
- 7-4 Principles of direct shear tests 421
- 7-5 Direct shear test 430
- 7-6 Principles of triaxial tests 443
- 7-7 Triaxial tests on coarse-grained soils 449
- 7-8 Triaxial tests on fine-grained soils 465

8 Elements of Experimental Techniques 470

- 8-1 Review of data modeling 471
- 8-2 Review of statistics 482
- 8-3 Error analysis 489
- 8-4 Dimensions and units 495
- 8-5 Report writing 499

9 Data Processing with Spreadsheets 508

- 9-1 Basics of spreadsheets 509
- 9-2 User-defined functions 517
- 9-3 Worked examples 520

Appendix: Conversion factors 540

Data Sheets 544

Index 579



Preface

In 1983, when I started to teach experimental soil mechanics to the undergraduate students in civil engineering at the University of Southern California, I thought that laboratory soil testing was well covered by textbooks. However, I stumbled on three unexpected but major problems when I attempted to select a textbook for my course: the reliance on standardized testing procedures, outdated data processing, and the absence of typical test results.

In reference to the first problem, most recent textbooks describe soil testing as a set of standardized procedures with little reference to the theories prompting these tests. They are useful for training laboratory technicians in testing companies but are less informative to student engineers. Any standardized testing procedure is not engraved in stone—it only provides guidelines which, when followed carefully, guarantee the quality and repeatability of test results. As an educator I feel strongly that standardized tests should not eclipse the principles that motivated the tests.

In reference to the problem of outdated data processing, the textbooks on soil testing that I examined were filled with complicated and numerous data sheets. They required students to write down their measurements and calculate results with hand calculators and archaic nomographs, such as for the hydrometer test. In this age of personal computers, such tedious data reduction is as outdated as slide rules. To update the data processing I wrote two generations of BASIC programs for personal computers. The first generation produced poor graphics and barely improved the hand calculator results. The second generation had advanced graphic and input/output features but had to be sealed hermetically because it was too complicated. Both versions created many difficulties in entering data and unnecessarily confused soil testing. I found myself asking more fundamental questions. Does the computer improve or hinder students' understanding? Do students benefit from a program they do not understand?

These concerns motivated the use of spreadsheet programs that have an open calculation structure (e.g., Lotus 123, Quattro Pro, and Microsoft Excel). Initially, spreadsheets were intended for business purposes, but now they have mathematical functions and programmable custom functions that make them suit-

able for engineering. They can reduce experimental data, plot graphs, and print reports. The spreadsheet approach eased my apprehensions about using computers in teaching experimental techniques. In fact, spreadsheets enhanced the ways my students understood physical phenomena and processed their measurements. For instance, by using Stokes' and buoyancy laws directly, instead of applying esoteric nomographs, they better understood the principles and limitations of hydrometer analysis. With spreadsheets, I was therefore capable of addressing two of the problems found in textbooks on soil testing: the advanced data processing techniques actually helped to emphasize the principles of soil mechanics. My students also benefited in other ways, enhancing their communication and presentation skills, and producing well-organized laboratory reports.

The third problem with existing textbooks is that there has been no way for students to know if they have performed the test correctly. In the professional world, we look to published experimental results constantly. If our results deviate significantly from normal results, we must either correct our own errors or explain the discrepancy. To establish normal test results for comparison, I have compiled typical results on soil properties from various sources, and included a few useful empirical correlations between soil properties. Empirical correlations are often discredited from the scientific point of view due to their lack of physical and rational explanations; however, some correlations are useful in the laboratory to check approximate agreement between different soil properties. With typical results and empirical correlations, my students have a basic knowledge of values for soil properties and some points of reference for discussing the validity of their experimental results.

Since 1983, my students have been using the spreadsheets programs, comparing their test results, and gaining a thorough understanding of the theories behind the tests. In effect, they have learned much more than basic standardized testing procedures. I hope that *Experimental Soil Mechanics* will benefit other teachers and students in geotechnical engineering.

Organization of materials

The book has nine chapters. The first seven chapters introduce the laboratory experiments (soil classification, density and compaction, permeability and seepage, consolidation, and shear strength) in the order in which most instructors present the material in geotechnical engineering. A systematic and consistent approach to each laboratory experiment covers theory, equipment, experimental procedure, and data processing. This presentation stresses that experiment and theory are meaningful only when considered together. All theories are based on experiments, and all experiments need a theory to explain and apply their results. Each test procedure is illustrated with photographs and line illustrations. Last are review questions and exercises to check understanding.

The eighth chapter covers the basic elements of experimental techniques, such as dimensions and units, data modeling, error analysis, and report writing. The ninth chapter reviews the use of spreadsheet programs relevant to data processing and the tabular and graphical presentation of laboratory results. It is versatile enough to apply not only to soil testing but also to various engineering fields. The spreadsheet experts may skip this section, provided that their expertise takes them through the worked examples.

Suggestions

For students, the theoretical sections should be studied before the experimental procedure and data processing sections. I suggest developing a basic knowledge

of spreadsheet calculation and programming before moving on to the data processing of soil experiments. The book covers a sufficiently large number of experiments to fully occupy a one-semester course. Several unprocessed data sets included in the exercises can be used to substitute for unsuccessful experiments in the laboratory.

My publisher and I have made all possible efforts to correct typographical mistakes. However, there may still be some errors in this first edition. Report them by using the world wide web site for Prentice Hall (<http://www.prenhall.com>) so that I can correct them in the next editions. I also welcome suggestions and comments which may help me to improve the quality and usefulness of this book.

Acknowledgments

I would like to express my thanks to all my students, especially G. Bowyer, P. Chraghchian, G. Gunawan, Q. Huang, M. M. Kapuskar, S. Karimi, N. Mace, A. Mahdi, J. Ramadan, S. Richards, A. Shiv, and J. Young. I extend my thanks to E. Amirkhanian, who assisted in taking photographs. I am also indebted to my wife, Marilyn, for her support and encouragement, and for proofreading the manuscripts.

Jean-Pierre Bardet

*To Benoit, Fabienne, Jacques,
Marcel, Marie-Thérèse, and
Marilyn.*



Introduction

In geotechnical engineering, the design and analysis of soil structures, such as earthdams, retaining walls, excavations, slopes, and foundations, are based on the theory of soil mechanics and the experimental determination of soil properties. *Soil mechanics* applies the *principles* of mechanics including kinematics, dynamics, fluid mechanics, and mechanics of materials to soils. Soil mechanics identifies and relates the main engineering properties of soils such as their density, compressibility, and resistance to shear. However, all these theoretical developments largely depend on experiments on soil properties in the laboratory and in the field.

LABORATORY SOIL TESTING

This book is about *experimental soil mechanics*. It reviews the basic *theory* of soil mechanics and describes the experiments which determine soil properties in the laboratory. It covers the tests listed in Table 1. These tests fall into five major categories: Soil classification, density and compaction, seepage, consolidation, and shear strength. Following is a breakdown of the categories and objectives of the experiments in Table 1.

Soil classification categorizes soils according to their probable engineering behavior. By knowing the soil classification, the engineer already has a fairly good idea of the way the soil will behave during construction. However, a soil classification does not eliminate the need for detailed testing for engineering properties.

Density, water content, void ratio, specific gravity, etc. are elementary soil properties which characterize the state of soils in the laboratory and in the field. Some of these soil properties such as soil density can be altered by *compaction* to control and improve other types of engineering properties such as seepage, compressibility and shear strength.

Seepage refers to the flow of water through soils, which takes place in water-retaining structures such as earthdams and levees. Permeability is the primary soil property required to analyze seepage problems, which can be solved using methods such as electrical analogy and finite differences.

Consolidation is the deferred compressibility of soils following the application of construction loads. This phenomenon is primarily responsible for the long-term settlement of buildings with time, which may take years to be completed.

Shear strength includes the soil properties that characterize the ability of soils to withstand construction loads. Shear strength properties are used in the stability analysis of structures including slopes, retaining walls, and foundations.

Field sampling and field testing

Laboratory testing relies on *field sampling* for taking representative samples of soils from the field. In general, the removal of soil from its natural environment disturbs its natural state. Some sampling techniques minimize this disturbance and produce so-called *undisturbed* samples, which are hermetically sealed in sampling tubes to preserve their moisture content. Other sampling techniques yield *disturbed* samples which are broken into smaller fragments and have density and structures different from the soils in the field. The sampling technique to be used depends on the type of information required and the characteristics of the soil to be sampled. For classification purposes, disturbed samples are sufficient, but for the determination of engineering properties of soil in the laboratory, undisturbed samples are usually required. A description of the types of samplers available and their utilization can be found in Lowe and Zaccheo (1991).

Field testing, also referred to as *in-situ testing*, is an efficient means to determine soil properties in the field. It produces abundant and detailed information on soil profiles at a location, such as *stratigraphy* of soil layers and spatial variation of their properties. The determination of soil properties from field measurements is generally based on empirical correlations between quantities measured in the field and soil properties measured in the laboratory (e.g., Kulhawy and Mayne, 1990). Recent developments in field testing are surveyed by Jamiolkowski et al. (1985).

Report of Laboratory Tests

Suggestions and guidelines for the preparation of soil reports can be found in Chapter 8-5. It is useful to compare experimental results recently obtained with those from other sources to check the validity of the results, and to understand possible similarities and discrepancies. This book provides some data on soil properties taken from various sources including Biarez and Hicher, 1994; Bowles, 1992; Head, 1984, 1986, and 1988; Holtz and Kovacz, 1981; Lambe, 1951; Lambe and Whitman, 1979; and Mitchell, 1993.

In the practice of geotechnical engineering, soil testing addresses real problems. In the academic context, it is instructive to recreate such a goal-oriented approach by posing practical yet simple problems which require the measurement of several soil properties. A few examples of this goal-oriented approach are given in Projects.

TABLE 1

Categories and objectives of the laboratory experiments in this book

Category and main objectives	Laboratory tests	Specific objectives
Engineering soil classification Categorize soils according to their probable engineering behavior	<ul style="list-style-type: none"> • <u>Grain size analysis</u> <ul style="list-style-type: none"> • Sieve analysis • Sedimentation analysis <ul style="list-style-type: none"> • Hydrometer • Pipette • Buoyancy • Combined analysis • <u>Atterberg limit tests</u> <ul style="list-style-type: none"> • Plastic limit test • Liquid limit test • Shrinkage limit analysis <ul style="list-style-type: none"> • Mercury method • Wax method • Engineering soil classification 	<ul style="list-style-type: none"> • Determine grain size distribution curve <ul style="list-style-type: none"> • Test for coarse-grained soils • Test for fine-grained soils <ul style="list-style-type: none"> • ASTM • British Standards • Combine sieve and sedimentation analysis • Determine plasticity of fine-grained soils <ul style="list-style-type: none"> • Measure plastic limit PL • Measure liquid limit LL • Define the shrinkage and swelling potential of fine-grained soils • Identify soil group in USCS and AASHTO engineering soil classification based on results of grain size analysis and Atterberg limit tests
Density and compaction Determine basic states of soils in the laboratory and in the field	<ul style="list-style-type: none"> • Determination of unit weight • Determination of specific gravity • Standard and improved laboratory compaction tests • Sand cone test 	<ul style="list-style-type: none"> • Determine unit weight, void ratio, degree of saturation, and water content of fine-grained soils • Determine the unit weight of soil minerals • Define the optimum water content and maximum density for soils • Control the soil density in the field after field compaction
Seepage Calculate total head, water pressure, total flow, and hydraulic gradients in seepage problems	<ul style="list-style-type: none"> • Permeability tests <ul style="list-style-type: none"> • Constant head test • Falling head test • Electrical analogy of seepage problems • Finite difference solution of seepage problems 	<ul style="list-style-type: none"> • Measure the permeability coefficient of soils <ul style="list-style-type: none"> • Test for coarse-grained soils • Test for fine-grained soils • Solve seepage problems (e.g., flow of water under a sheetpile wall) with a physical means • Solve seepage problems with numerical methods and spreadsheets
Consolidation Calculate long term settlement of structures	<ul style="list-style-type: none"> • Consolidation test 	<ul style="list-style-type: none"> • Determine the properties of fine-grained soils for calculating the amplitude and rate of settlement of structures <ul style="list-style-type: none"> • Compressibility • Overconsolidation ratio and pressure • Consolidation coefficients (primary and secondary)
Shear strength Determine the soil properties (undrained shear strength S_u , friction angle ϕ' and cohesion c') for analyzing the stability of foundations, excavations, slopes, retaining walls, etc.	<ul style="list-style-type: none"> • Unconfined compression test (UC) • Direct shear test (DS) • Triaxial tests <ul style="list-style-type: none"> • CD and CU triaxial tests on coarse-grained soils • CD, CU, and UU triaxial tests on fine-grained soils 	<ul style="list-style-type: none"> • Measure rapidly but approximately S_u • Measure shear strength (S_u, ϕ' and c') on a predetermined surface of rupture (slopes, foundation, etc.) • Measure shear strength (S_u, ϕ' and c') under various stress conditions, including drained and undrained loadings. Better control of initial stresses and loading stress paths than UC and DS tests (except for UU tests)

STANDARD PROCEDURES FOR SOIL TESTING

In the United States of America, Great Britain, and many other countries, most of the experimental procedures in laboratory soil testing are described by standards. Standards provide guidelines and minimum requirements to obtain reliable and repeatable test results. Tables 2 and 3 give the correspondence between the laboratory experiments covered in each test, and the relevant test methods and guides of the American Society for Testing and Materials (ASTM) and the British Standard Institutions (BS). Further information can be found in these guidelines and in Head (1984, 1986, and 1988).

TABLE 2

Experiments covered in this book and related ASTM test methods (ASTM, 1995a and 1995b)

Experiment	Chapter	ASTM number	ASTM description
Sieve analysis	1-2	D 422-63	Test Method of Particle-Size Analysis of Soils
		D 1556-90	Test Method for Amount of Material in Soils Finer than the No. 200 (75 mm) Sieve
		D 421-85	Practice for Dry Preparation of Soil Samples for Particle-Size Analysis and Determination of Soil Constants
		D 2217-85	Practice for Wet Preparation of Soil Samples for Particle-Size Analysis and Determination of Soil Constants
		E 11-87	Specifications for Wire-Cloth Sieves for Testing Purposes
Hydrometer analysis	1-4	D 422-63	Test Method of Particle-Size Analysis of Soils
		D 421-85	Practice for Dry Preparation of Soil Samples for Particle-Size Analysis and Determination of Soil Constants
		E 100-94	Specifications for ASTM Hydrometers
Determination of water content	2-2	D 2216-90	Method of Laboratory Determination of Water (Moisture) Content of Soil, Rock, and Soil-Aggregate Mixtures
		D 4944-89	Test Method for Field Determination of Water (Moisture) Content of Soil by Calcium Carbide Gas Pressure Tester Method
		D 4643-93	Test Method for Determination of Water (Moisture) Content of Soil by the Microwave Oven Method
		D 4959-89	Test Method for Determination of Water (Moisture) Content of Soil by Direct Heating Method
Atterberg limit test	2-3 to 2-5	D 4318-93	Test Method for Liquid Limit, Plastic Limit, and Plasticity Index of Soils
Shrinkage limit	2-7 and 2-8	D 427-93	Test Method for Shrinkage Factor of Soils by the Mercury Method
		D 4943-89	Test Method for Shrinkage Factor of Soils by the Wax Method
Engineering classification of soils	2-9	D 2487-93	Test Method for Classification of Soils for Engineering Purposes (Unified Soil Classification System)
		D 3282-93	Test Method for Classification of Soils and Soil-Aggregates Mixtures for Highway Construction Purposes
		D 2488-93	Practice for Description and Identification of Soils (Visual/Manual Procedure)
		D 448-86	Classification for Sizes of Aggregate for Road and Bridge Construction
Determination of density	3-2	D 4253-93	Test Methods for Maximum Index Density and Unit Weight of Soils Using a Vibratory Table
		D 4254-91	Test Methods for Minimum Index Density and Unit Weight of Soils and Calculation of Relative Density
		D 4718-87	Practice for Correction of Unit Weight and Water Content for Soils Containing Oversize Particles

TABLE 2 (cont.)

Experiments covered in this book and related ASTM test methods (ASTM, 1995a and 1995b)

Experiment	Chapter	ASTM number	ASTM description
Determination of specific gravity	3-3	D 854-92	Standard Test Method for Specific Gravity of Soils
		C 127-88	Test Method for Specific Gravity and Absorption of Coarse Aggregate
		D 5550-94	Test Method for Soil Solids by Gas Pycnometer
Compaction tests	3-5	D 1140-54	Test Method for Laboratory Compaction Characteristics of Soil Using Standard Effort (12,400 ft-lbf/ft ³ (600 kN-m/m ³))
		D 1557-91	Test Method for Laboratory Compaction Characteristics of Soil Using Modified Effort (56,000 ft-lbf/ft ³ (2700 kN-m/m ³))
		D 2168-90	Test Method for Calibration of Laboratory Mechanical Rammer Soil Compactors
		D 5080-93	Test Method for Rapid Determination of Percent Compaction
In-situ density determination	3-6	D 1556-90	Test Method for Density of Soil In Place by the Sand-Cone Method
		D 2167-94	Test Method for Density and Unit Weight of Soil In Place by the Rubber Balloon Method
		D 2922-91	Test Method for Density of Soil and Soil-Aggregate In-Place by Nuclear Methods (Shallow Depth)
		D 5195-91	Test Method for Density of Soil and Rock In-Place at Depths Below the Surface by Nuclear Methods
		D 2937-94	Test Method for Density of Soil In Place by the Drive-Cylinder Method
		D 4564-93	Test Method for Density of Soil In Place by the Sleeve Method
		D 4914-89	Test Method for Density of Soil and Rock In Place by the Sand Replacement Method in a Test Pit
		D 5030-89	Test Method for Density of Soil and Rock In Place by the Water Replacement Method in a Test Pit
		D 3017-88	Test Method for Density of Soil and Rock In-Place by Nuclear Methods (Shallow Depth)
D 5220-92	Test Method for Density of Soil and Rock In-Place by the Neutron Depth Probe Method		
Permeability test	4-2	D 2434-68	Test Method for Permeability of Granular Soils (Constant Head)
		D 5084-90	Test Method for Measurement of Hydraulic Conductivity of Saturated Porous Materials Using a Flexible Wall Permeameter
Consolidation test	6-2	D 2435-90	Test Method for One-Dimensional Consolidation Properties of Soils
		D 4186-89	Test Method for One-Dimensional Consolidation Properties of Soils Using Controlled-Strain Loading
		D 5333-92	Test Method for Measurement of Collapse Potential of Soils
		D 4546-90	Test Method for One-Dimensional Swell or Settlement Potential of Cohesive Soils
Unconfined compression test	7-3	D 2166-91	Test Method for Unconfined Compressive Strength of Cohesive Soils
Direct shear test	7-5	D 3080-90	Test Method for Direct Shear Test of Soils Under Consolidated Drained Conditions
Triaxial tests	7-8	D 4767-88	Test Method for Consolidated-Undrained Triaxial Compression Test on Cohesive Soils
		D 2850-87	Test Method for Unconsolidated, Undrained Compressive Strength of Cohesive Soils in Triaxial Compression
Units	8-4	E 380	Excerpts from Standard Practice for Use of the International System of Units (SI) (the Modernized Metric System)

TABLE 3

Experiments covered in this book and related BS 1377 (1975) test methods

Experiment	Chapter	Test number	BS description
Sieve analysis	1-2	7B	Test Sieves (BS 410, 1969)
		7A	Dry Sieving
		7D	Wet Sieving
Hydrometer analysis	1-4	7D	Hydrometer Analysis
Pipette analysis	1-5	7C	Pipette Analysis
Determination of water content	2-2	1A	Oven Drying
		1B	Sand Bath Method
Atterberg limit test	2-3 to 2-5	2B	Casagrande Method
		2C	Liquid Limit-Casagrande One-point Method
		2A	Cone Penetrometer Method
		3	Plastic Limit
Determination of density	3-2	15F	Water Displacement
		15E	Weighing in Water
		6B	Density Bottle
Determination of specific gravity	3-3	6A	Gas Jar Method
		6B	Pycnometer
Compaction tests	3-5	12	Ordinary Compaction Test
		13	Heavy Compaction
		14	Compaction by Vibration; Vibrating Hammer Method
Consolidation test	6-2	17	Oedometer Consolidation
Unconfined compression test	7-3	20	Autographic Unconfined Compression
Triaxial tests	7-8	21	Triaxial Compression

REFERENCES

- ASTM, 1995a, *Annual book of ASTM Standards, Soil and Rock (I)*, Vol. 04.08, American Society for Testing and Materials, ASTM, Philadelphia, PA, p. 981.
- ASTM, 1995b, *Annual book of ASTM Standards, Soil and Rock (II)*, Vol. 04.09, American Society for Testing and Materials, ASTM, Philadelphia, PA, p. 625.
- BS 1370, 1975, *Methods of Tests for Soil for Civil Engineering Purposes*, British Standards Institution, London, UK.
- BIAREZ, J., and P.-Y. HICHER, 1994, *Elementary Mechanics of Soil Behaviour, Saturated Remoulded Soils*, A. A. Balkema, Rotterdam, Netherlands.
- BOWLES, J. E., 1992, *Engineering Properties of Soils and their Measurement*, Fourth edition, McGraw-Hill, New York.
- HEAD, K. H., 1984, *Manual of Soil Laboratory Testing. Volume 1, Soil Classification and Compaction Tests*, Pentech Press, London.
- HEAD, K. H., 1986, *Manual of Soil Laboratory Testing. Volume 3, Effective Stress Tests*, Pentech Press, London.
- HEAD, K. H., 1988, *Manual of Soil Laboratory Testing. Volume 2, Permeability, Shear Strength, and Compressibility*, Pentech Press, London.
- Holtz, R. D., and W. D. Kovacz, 1981, *An Introduction to Geotechnical Engineering*, Prentice-Hall, Englewoods Cliffs, N.J.
- JAMIOLKOWSKI, C. C. LADD, J. T. GERMAINE, and R. LANCELOTTA, 1985, "Recent development in field and laboratory testing of soils," *Proceedings of the 11th International Conference on Soil Mechanics and Foundation Engineering*, San Francisco, CA, Vol. 1, pp. 57-153.

- KULHAWY, F. H., and P. W. MAYNE, 1990, *Manual on Estimating Soil Properties for Foundation Design*, Report EL-9800 to Electric Power Research Institute, Cornell University, Ithaca, New York.
- LAMBE, T. W., 1951, *Soil Testing for Engineers*, John Wiley & Sons, New York.
- LAMBE, T. W., and R. V. WHITMAN, 1979, *Soil mechanics, SI version*, John Wiley & Sons, New York.
- LOWE III, J., and P. F. ZACCHEO, 1991, "Subsurface exploration and sampling," in *Foundation Engineering Handbook*, 2d ed., H.-Y. Fang, ed., Chapman & Hall, New York, pp. 1-71.
- MITCHELL, J. K., 1993, *Fundamentals of Soil Behavior*, 2nd ed., John Wiley & Sons, New York.

PROJECTS

The following projects include several types of experiments on the same soil, and require comprehensive reports with recommendations and conclusions. They may require several weeks to be completed.

1. Classify a soil based on the results of the sieve and sedimentation analysis, then determine if the soil is appropriate for the following applications:
 - 1.1 Core of earthdam
 - 1.2 Shell of earthdam
 - 1.3 Fill resistant to frost heave
 - 1.4 Workable construction materials.
2. Compare the results of hydrometer, pipette and buoyancy analyses on the same soil. Conclude on the pros and cons of each method. Write a recommendation for your company which is about to select one of these methods.
3. In a site which has previously been compacted, compare the optimum water and density from laboratory tests with the corresponding values in the field. Conclude on the degree of compaction in the field.
4. Solve one of the seepage problems of Chapters 4-4 and 4-5 for the permeability you measured in the laboratory.
5. Solve one of the seepage problems of Chapters 4-4 and 4-5 by using both electrical analogy and finite difference. Superimpose and compare the flow nets obtained from each method.
6. Compare the values of permeability coefficients measured in the fixed wall permeameter and triaxial cell.
7. Compare the values of permeability coefficients measured in the falling head permeameter and consolidation cell.
8. For a given embankment or tank, calculate the settlement for the soil properties you measured in the laboratory.
9. Compare the values of undrained shear strength on the same fine-grained material obtained from the unconfined compression test, direct shear test, and CU triaxial test. Compare your results and conclusions with those given in Chapter 7-2.
10. For a given slope stability problem, calculate the factor of safety of the slope based on the laboratory test which you believe is the most appropriate.



1

Grain Size Distribution

- 1-1** Principles of grain size analysis
- 1-2** Sieve analysis
- 1-3** Principles of sedimentation analysis
- 1-4** Hydrometer analysis
- 1-5** Pipette analysis
- 1-6** Buoyancy analysis
- 1-7** Combined grain size analysis

1-1

Principles of Grain Size Analysis

SCOPE

As shown in Figure 1, a soil consists of particles of various shapes, sizes, and quantity. The grain size analysis divides these particles into size groups and determines their relative proportions by weight. Grain size analysis is a basic laboratory test required to identify soils in engineering soil classification systems.



Figure 1 The particles of this soil were divided into six size groups in the laboratory. The largest particle shown is 15 mm in diameter. The largest sizes in each group from left to right are 0.07, 0.3, 1, 2, 5, and 15 mm, respectively.

GROUPS OF PARTICLE SIZES

As shown in Table 1, the engineering soil classification systems such as ASTM D 422, BS 1377, AASHTO, and USCS, divide soil particles on the basis of size into

categories—boulders, cobbles, gravel, sand, silt, and clay—with an optional subdivision indicating coarse, medium and fine. Soil particles have sizes ranging from greater than 200 mm down to less than 0.002 mm. The ratio between these extremes is $10^5 : 1$. As the particle size D decreases, the number of particles contained in a unit mass of soil increases proportionally to $1/D^3$ and their individual mass decreases in the same ratio. For illustration, the mass of several spheres with diameters ranging from 100 to 0.001 mm is calculated in Table 2 for a typical mineral unit mass $\rho_s = 2.65 \text{ g/cm}^3$ (unit mass is the mass per unit volume). The ratio of smallest and largest masses is enormous $\sim 10^{15} : 1$.

Specific surface, which is the total surface area of particles per unit mass, is an important characteristic of small soil particles. It largely influences the interaction between small soil particles which depends on electrostatic forces. The dimension of specific surface is squared length divided by mass, and its unit is mm^2/g or m^2/g . As shown in Table 2, the specific surface of spheres increases proportionally to $1/D$. However, natural soil particles have much more complicated shapes than those of spheres, and their specific surface is even higher than those shown in Table 2. For instance, the specific surface of fine sand particles is about $0.03 \text{ m}^2/\text{g}$, while those of flat and platelike clay particles such as kaolinite and montmorillonite are 10 and $1000 \text{ m}^2/\text{g}$.

TABLE 1

Classification of particle size in the BS 1377, USCS, AASHTO and ASTM engineering soil classification systems.

BS	Silt			Sand			Gravel			Cobbles	Boulders			
	Clay	Fine	Medium	Coarse	Fine	Medium	Coarse	Fine	Medium			Coarse		
	0.002	0.006	0.02	0.06	0.2	0.6	2	6	20	60	200			
USCS	Fines (silt, clay)				Sand			Gravel		Cobbles	Boulders			
					Fine	Medium	Coarse	Fine	Coarse					
					0.075	0.425	2	4.75	19	75	300			
AASHTO	Clay	Silt		Sand			Gravel		Boulders					
				Fine	Coarse									
		0.005	0.075	0.425	2					75				
ASTM	Clay	Silt		Sand			Gravel		Cobbles	Boulders				
				Fine	Medium	Coarse								
		0.001	0.005	0.01	0.075	0.1	0.425	1	4.75	10	75	100	300	1000

TABLE 2

Particle Size, Mass, and Surface Area of Spheres.

Equivalent soil category	Particle size D (mm)	Particle mass m (g)	Number of particles per gram	Specific surface area (m^2/g)
Cobble	100.0	1.4×10^3	7.2×10^{-4}	2.3×10^{-5}
Gravel	10.0	1.4	7.2×10^{-1}	2.3×10^{-4}
Coarse sand	1.0	1.4×10^{-3}	7.2×10^2	2.3×10^{-3}
Fine sand	0.1	1.4×10^{-6}	7.2×10^5	2.3×10^{-2}
Medium silt	0.01	1.4×10^{-9}	7.2×10^8	2.3×10^{-1}
Clay	0.001	1.4×10^{-12}	7.2×10^{11}	2.3

$$m = \rho_s \frac{\pi}{6} D^3 = \text{mass of sphere of diameter } D \text{ and unit mass } \rho_s$$

$$(\rho_s = 2.65 \text{ g/cm}^3)$$

$$\frac{6}{\rho_s \pi D^3} = \text{number of particles per gram}$$

$$\frac{6\pi D^2}{\pi \rho_s D^3} = \frac{6}{\rho_s D} = \text{specific surface of}$$

PARTICLE SIZE DISTRIBUTION CURVE

In Table 1, six categories of particle sizes were defined: boulder, cobble, gravel, sand, silt, and clay. However, natural soils are often made of a mixture of particles that do not fall entirely within only one of these size ranges covering two or more categories. It would be too tedious to count individually all the different sizes of particles because of the enormous number (see Table 2). Therefore, the grain distribution within the various size categories is generally represented by using the cumulative distribution of statistics. The grain size distribution curve is plotted as the percentage finer than a given size versus the particle sizes on a logarithmic scale. Figure 2 shows a typical particle size distribution curve. Grain-size distribution curves are always increasing because they are cumulative distribution. Plotting particle size data on a standard chart enables engineers to recognize instantly the grading characteristics of a soil. The position of a curve on the chart indicates the soil fineness or coarseness. The steepness, flatness, and general shape indicate the distribution of grain sizes. Other types of charts are also found in practice. For example, the horizontal axis may have an opposite orientation, with cobbles and gravel to the left. The vertical axis may also represent percent coarser by weight, instead of percent finer by weight.

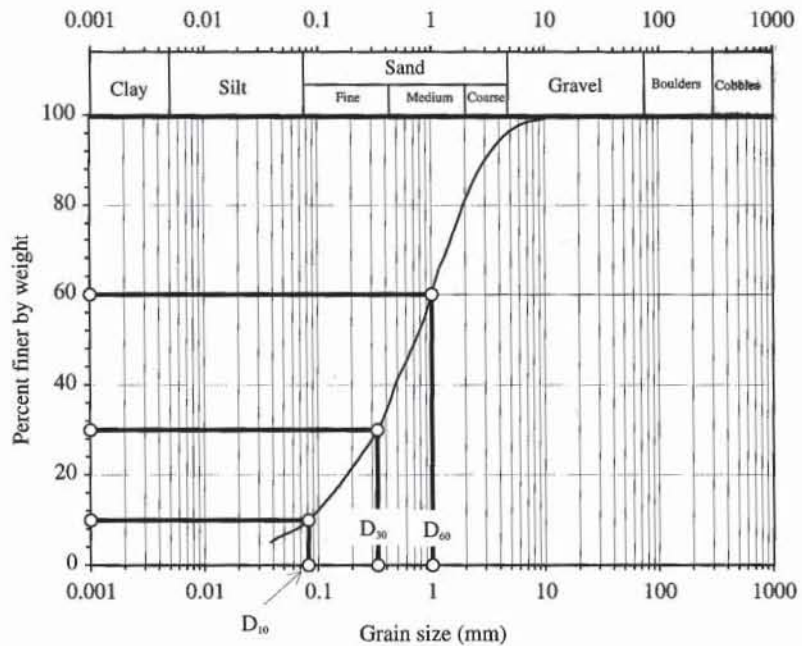


Figure 2 Grain size distribution chart.

In addition to the cumulative frequency distributions, there are other graphical representations for particle size distribution, such as frequency distributions. In this case, the percentage by mass between certain sizes is plotted versus the logarithm of the grain size. These representations are used in powder technology (e.g., Allen, 1974). The semilogarithmic cumulative grain size distribution curve remains the most commonly used representation for soils.

APPLICATION OF GRAIN SIZE DISTRIBUTION CURVES

Grain size distribution curves provide a means by which soils can be classified and their engineering properties assessed. This classification, which applies primarily to sands and gravels, will be completed in Chapter 2-9.

Classification of Sands and Gravels

Grain size distribution curves enable sands and gravels to be classified into three main types: uniform, well graded, and poorly graded.

Uniform soils. In uniform soils, the majority of grains are nearly the same size. The grading curve is very steep, as shown by curve A in Fig. 3, which represents a uniform sand. The uniformity in soils is characterized by the uniformity coefficient C_u :

$$C_u = \frac{D_{60}}{D_{10}} \quad (1)$$

where D_{10} is the grain size corresponding to 10% finer and D_{60} is the grain size corresponding to 60% finer. D_{10} and D_{60} are obtained by interpolation between the experimental points of the grain size distribution curve (see Fig. 2). C_u represents the average slope of the grain size distribution between 10 and 60%. For instance, in Fig. 2, $D_{10} = 0.082$ mm, $D_{60} = 1.008$ mm, and $C_u = 12.35$. The smallest possible value for C_u is equal to 1 and corresponds to a perfectly uniform assemblage of grains of identical size.

Well-graded soils. Well-graded soils contain a wide and even distribution of particle sizes. A well-graded silty sand and gravel is shown by curve B in Fig. 3. The smooth concave upward-grading curve is typical of well-graded material. Curve B' of Fig. 3 represents an idealized material in which the particles fit together in the densest possible state of packing (Fuller grading), as illustrated in Fig. 4. The interstices of the largest particles of size D_{\max} are filled in a regular pattern with smaller and smaller particles that occupy the void without holding the neighboring particles apart. The Fuller grading has the smooth shape shown in Fig. 3 and is determined using the equation

$$P = 100 \sqrt{\frac{D}{D_{\max}}} \quad (2)$$

where P is the percentage by weight of particles finer than diameter D and D_{\max} is the maximum particle size ($D_{\max} = 75$ mm in the example of Fig. 3).

Particle size distribution can be characterized by its curvature, and more specifically by the coefficient of curvature C_c :

$$C_c = \frac{D_{30}^2}{D_{10}D_{60}} \quad (3)$$

where D_{30} is the grain size corresponding to 30% finer (see Fig. 2). By definition, gravels are considered to be well graded when $C_u > 4$ and $1 < C_c < 3$. Sands are considered to be well graded when $C_u > 6$ and $1 < C_c < 3$. For example, in Fig. 2, $D_{10} = 0.082$ mm, $D_{30} = 0.334$ mm, $D_{60} = 1.008$ mm, and $C_c = 1.35$. As found previously, $C_u = 12.35$; therefore, the sand of Fig. 2 is well graded.

Poorly graded soils. The term *poorly graded* applies to any soil, including uniform soil, which does not comply with the description of well graded. Poorly graded soils are deficient in certain sizes. Gap-graded materials are examples of poorly graded materials with missing ranges of particle sizes. For example, curve C in Fig. 3 has a flat part indicating that there are only a few particles in the range 1 to 10 mm. In practice, gap-graded materials are generally found in the coarse

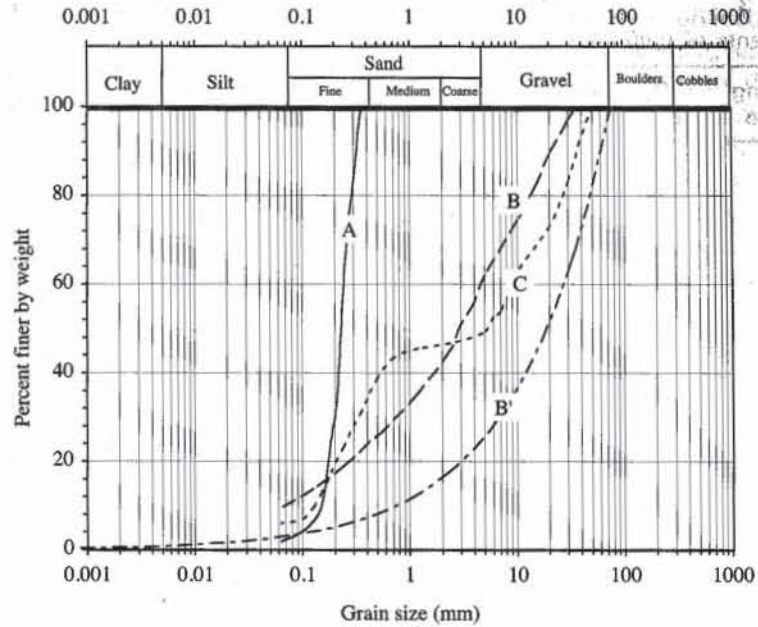


Figure 3 Examples of grain size distribution curves for sands and gravels (data after Head, 1984).

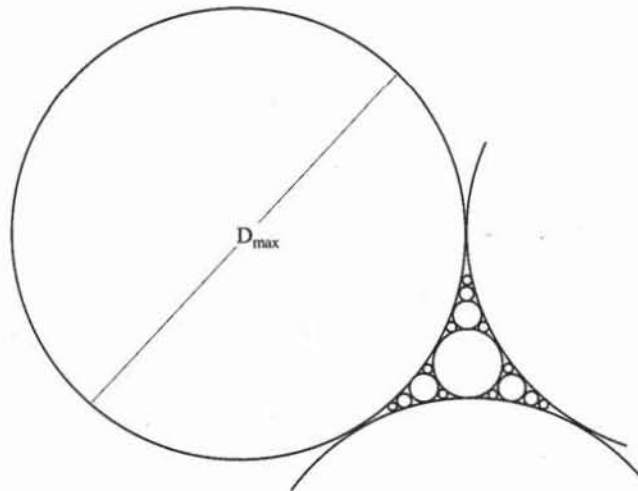


Figure 4 Idealized Fuller packing (two-dimensional representation).

sand–fine gravel range. The values of D_{10} , D_{30} , D_{60} , C_u , and C_c , for materials A, B, and C, and Fuller packing are summarized in Table 3.

Classification of Clays and Silts

Soils consisting entirely of clay- or silt-size particles are rarely found in nature. Most clays contain silt-size particles, and most material described as silt includes some clay or some sandy material, or both. Some typical grading curves of clays and silts are shown in Fig. 5.

Curve D is described as clay, although it consists of 56% clay-and 44% silt-size particles. Curve E shows a well-graded soil consisting primarily of silt, with a

TABLE 3

Coefficients of uniformity and curvature for soils in Figs. 3 and 5.

Grading curve	D_{10} (mm)	D_{30} (mm)	D_{50} (mm)	D_{60} (mm)	C_u	C_c	Description
A	0.148	0.196	0.229	0.242	1.64	1.07	Uniform fine sand
B	0.069	0.745	2.880	4.642	67.10	1.73	Well-graded silty sand and gravel
B'	0.730	6.551	18.750	26.203	35.89	2.24	Idealized Fuller grading
C	0.125	0.332	5.068	8.971	72.03	0.10	Gap graded silty sand and gravel
D	-	-	0.001	0.003	-	-	Clay
E	0.001	0.003	0.010	0.017	21.68	0.51	Sandy and silty clay
F	0.004	0.018	0.048	0.066	17.97	1.32	Sandy silt
G	0.001	0.013	0.401	1.642	2693.84	0.10	Gravelly sandy silty clay

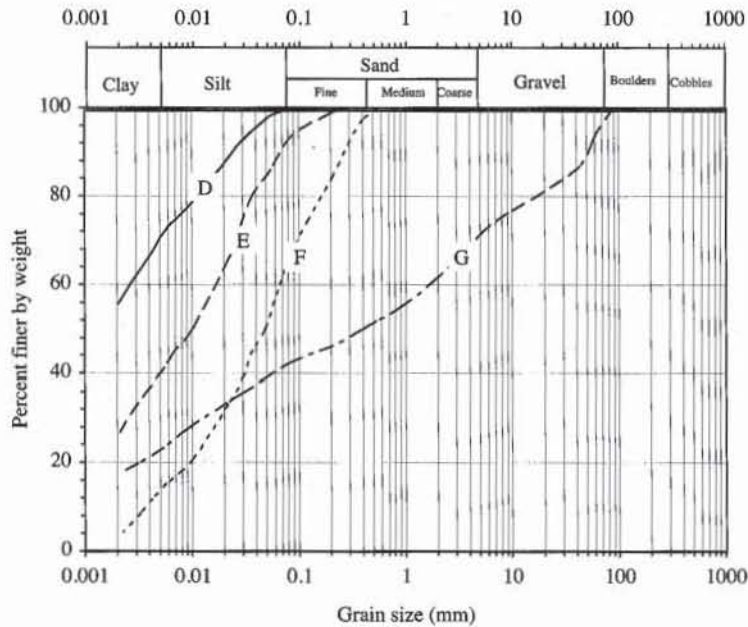


Figure 5 Examples of grain size distribution curves (data after Head, 1984).

clay fraction of less than 2% which is described as sandy silt with a trace of clay. Curve *F* has a mixture of clay, silt, and sand. The soil is described as silty clay with sand. Curve *G* represents a well-graded soil containing particles of all sizes from cobbles down to clay. It is described as gravelly sandy silty clay. This type of soil, which is found as glacial till, is often called boulder clay.

The values of D_{10} , D_{30} , D_{60} , C_u , and C_c for materials *D*, *E*, *F*, and *G* are given in Table 3. The particle size corresponding to 10% finer for material *D* is outside the range of the grain size distribution chart; D_{10} , C_u , and C_c cannot be determined for this material.

The clay fraction is defined as the percent by weight finer than 2 μm . Its values for soils *A* to *G* are listed in Table 4.

TRIANGULAR CLASSIFICATION CHART

A triangular classification chart is an alternative representation of the grain size distribution of soils. Less commonly used than the semilogarithmic representation, it is convenient for comparing clay-silt-sand mixtures on the proportions of

each constituent. As shown in Fig. 6, each side of the triangle is divided into 100 parts, representing the percentage of three soil constituents: clay, silt, and sand. A point within the triangle indicates the percentage of these constituents, the sum of which adds up to 100%. The triangular chart can also be used to show (clay + silt)–sand–gravel mixtures, or any other three main constituents of soil. The triangular coordinates of samples A through G in Figs. 3 and 5, are listed in Table 4 and are plotted as points on the triangular chart of Fig. 7. This triangular chart was introduced by the U.S. Bureau of Reclamation (1974).

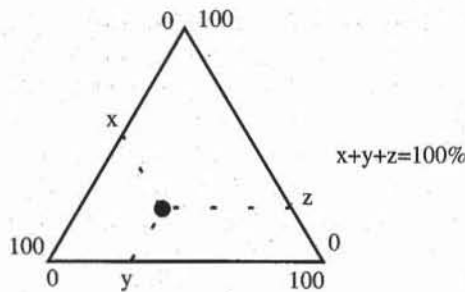


Figure 6 Definition of coordinates on a triangular classification chart.

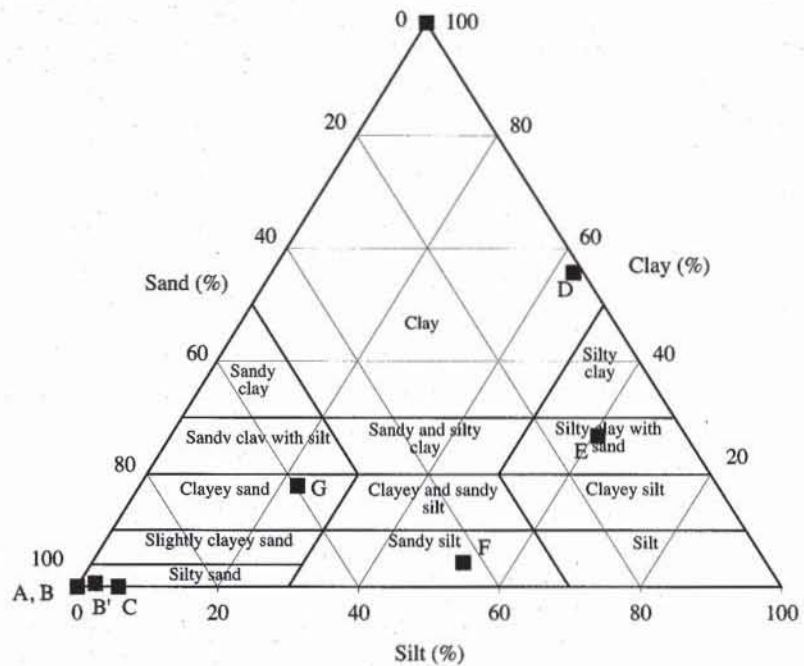


Figure 7 Representation of samples A to G of Table 3 on a triangular classification chart.

FREQUENCY DISTRIBUTIONS

As noted earlier, grain size distributions are usually represented as cumulative distributions in soil mechanics. Figures 8 and 9 show an alternative representation: the frequency distributions corresponding to the samples of Figs. 3 and 5. The frequency f_i associated with a particular size d_i is calculated from the cumulative values p_i (e.g., percent by weight finer) by using the relation

$$f_i = p_{i+1} - p_i \tag{4}$$

TABLE 4

Coordinates of samples A to G of Table 3 for triangular classification chart (after Head, 1984)

Material	Sand fraction (%)	Silt fraction (%)	Clay fraction (%)
A	100.0	0.0	0.0
B	100.0	0.0	0.0
B'	97.1	2.3	0.6
C	94.1	5.9	0.0
D	1.4	42.9	55.7
E	12.5	60.7	26.8
F	43.0	52.7	4.3
G	59.7	22.4	17.9

The sum of f_i should equal 100%. As shown in Fig. 8, sample A (uniform sand) displays a unique peak at 0.2 mm, while sample B' (Fuller material) has a continuous and decreasing distribution. As shown in Figs. 8 and 9, all other samples have a multimodal, rather than a unimodal distribution with several peaks. In all cases, their frequency distribution appears more complicated than their cumulative distribution.

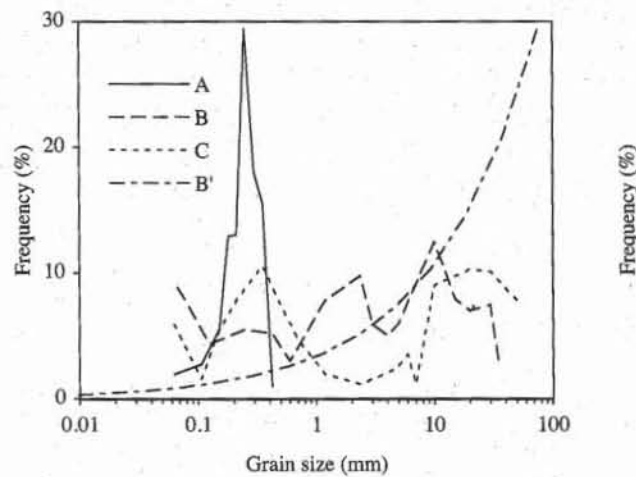


Figure 8 Frequency distributions corresponding to the cumulative distributions of Fig. 3.

APPLICATIONS OF GRAIN SIZE ANALYSIS IN ENGINEERING PRACTICE

In geotechnical engineering, particle size analyses are useful for various practical applications, ranging from the selection of fill and aggregate materials, to road construction, drainage, filters, and grouting.

Selection of Fill Materials

Soils used for the construction of embankments and earth dams are required to be within specified limits as defined by particle size distribution curves. The various zones of an earth dam, for instance, have different gradation characteristics.

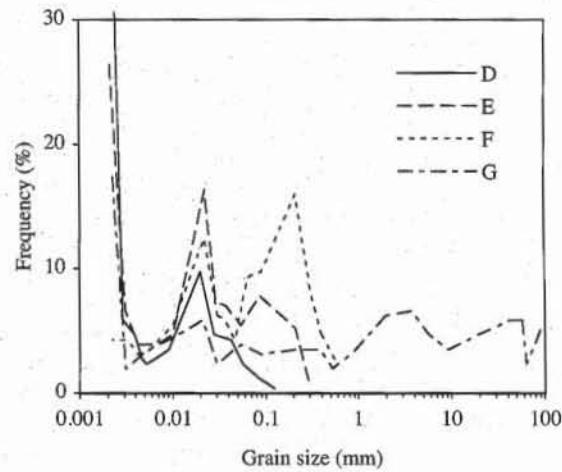


Figure 9 Frequency distributions corresponding to the cumulative distributions of Fig. 5.

Selection of Aggregate Materials

Sands and gravels for use as concrete aggregates are divided by particle size distribution curves into various types. In the exploration for sand and gravel resources, particle size analysis is the main criterion for selection of sites for potential development.

Road Subbase Materials

Each layer of a road or airfield runway subbase must comply to a particular grading specification to provide a mechanical stable foundation (see the description of the AASHTO classification system in Chapter 2-9).

Drainage Filters

The grading specification for a filter layer must be related in certain ways to the grading of the adjacent ground or of the next filter layer. This specification, referred to as the filter requirement, prevents small particles from being dragged by seepage forces and avoids the clogging of pores between large particles.

Groundwater Drainage

The drainage characteristics of the ground depend largely on the proportion of fines (silts and clay-size particles) present in the soil.

Grouting and Chemical Injection

Grouting and chemical injections consist of injecting liquids with predefined mechanical or chemical characteristics inside the soil interstices to decrease the ground permeability and/or to improve its mechanical properties. The most suitable grouting process and the extent to which the ground can be impregnated depend mainly on the grading characteristics of soils.

LIMITATIONS OF PARTICLE SIZE ANALYSIS

Particle size analysis helps to classify soils, especially coarse soils. It is possible to tell from grain size distribution analysis whether the soil consists of predominantly gravel, sand, silt, or clay, and to a limited extent, which of these size ranges is likely to control the soil engineering properties. Particle size analysis is of greater value if supplemented by descriptive details such as color and particle shape. But the engineering behavior of soils also depends on factors other than particle sizes, such as mineral, structural, and geological history. The physical behavior of clays, such as plastic consistency, controls more of its mechanical behavior than its particle size distribution, and for this the Atterberg limits test (see Chapters 2-3 to 2-5) provides more significant information than is provided by grain size analysis.

TYPES OF GRAIN SIZE ANALYSES

There are two separate procedures for obtaining the grain size distribution of soils: sieve analysis and sedimentation analysis. Sieve analysis is used for gravel- and sand-size particles (coarse-grained soils with grain size larger than 75 μm) but cannot be used for silt- and clay- size particles (fine-grained soils with grain size smaller than 75 μm). A sedimentation procedure (e.g., hydrometer, pipette, or buoyancy analysis) is used instead. Sieve and sedimentation analyses are combined to define the grain size distribution of soils having fine and coarse grains. The grain size distribution of soils by sieving, sedimentation, and combined analyses are described in subsequent chapters.

REFERENCES

- See Introduction for references to ASTM procedures (pages 4 to 6).
- AASHTO, 1974, *Specifications (M 145-73)*, American Association of State Highway and Transportation Officials, pt. 1.
- Allen, T., 1974, *Particle Size Measurement*, Chapman & Hall, London.
- BS 1370, 1975, *Methods of tests for soil for civil engineering purposes*, British Standards Institution, London, UK.
- Head, K. H., 1984, *Manual of Soil Laboratory Testing, Vol. 1: Soil Classification and Compaction Tests*, Pentech Press, London.
- U.S. Bureau of Reclamation, 1974, *Earth Manual*, 2nd ed., Test Designation E.7, Part C, US Government Printing Office, Washington, DC.
- U.S. Army Engineer Waterways Experiment Station, 1960, "The Unified Soil Classification System," *Technical Memorandum No. 3-357*. Appendix A, Characteristics of Soil Groups Pertaining to Embankment and Foundations, 1953; Appendix B, Characteristics of Soil Groups Pertaining to Roads and Airfields, 1957.

REVIEW QUESTIONS

1. Name the six categories of particle sizes that are identified in soil mechanics.
2. What is a specific surface? In what unit is it expressed? Can you give a typical value for the specific surface of montmorillonite?
3. What is a Fuller material?
4. What axes do we generally use in soil mechanics to represent a grain size

- distribution curve? Are there other types of representation?
- Define *coefficient of uniformity* C_u and the *coefficient of curvature* C_c . What are their physical meanings?
 - Is it always possible to determine the coefficient of uniformity C_u and the coefficient of curvature C_c for all types of soils?
 - What are the two main experimental techniques used in soil mechanics to determine a grain size distribution curve? Define their range of application.
 - Is it possible for a grain size distribution curve to have a bump (i.e., to increase, then to decrease)?
 - Define *poorly graded soil* and *well-graded soil*. What is a gap-graded material?
 - Material *A* has $C_u = 1$ and material *B* has $C_u = 4$. Which material is a better filter, and which is a better drain?
 - Explain why the percent by weight finer value always increases with the particle diameter.
 - Calculate analytically C_u and C_c for a Fuller material ($P = 100\sqrt{D/D_{\max}}$).
 - What is the coefficient C_u for a set of marbles having identical size?
 - Draw the grain size distribution curve of an assembly of marbles knowing that the marbles have only two sizes. There is 1 kg of 8-mm-diameter marbles and 1 kg of 10-mm-diameter marbles.

EXERCISES

- The result of a grain size analysis is given below. Plot the grain size distribution curve, and calculate D_{10} , D_{30} , D_{60} , C_u , and C_c . Compare your results to those in Fig. 1.

Particle size (mm)	Percent finer (%)
15.00	100.00
10.00	99.22
6.00	97.67
4.00	94.19
2.80	88.76
2.00	81.00
1.40	70.00
1.18	65.89
1.00	59.69
0.85	54.00
0.60	45.00
0.50	41.09
0.36	31.01
0.18	20.00
0.13	15.00
0.08	9.00
0.05	6.20
0.04	5.00

- The tabulated data of four grain distribution curves of sands and gravels are given below. Plot these grain size distribution curves by using semilogarithmic axes as shown in Fig. 3. Calculate D_{10} , D_{30} , D_{60} , C_u , and C_c .

Sample A		Sample B		Sample C		Fuller	
Particle size (mm)	Percent finer (%)	Particle size (mm)	Percent finer (%)	Particle size (mm)	Percent finer (%)	Particle size (mm)	Percent finer (%)
0.425	100.0	35.000	100.0	50.000	100.0	75.000	100.0
0.355	99.0	30.000	96.9	38.000	92.1	37.500	70.7
0.300	83.5	20.000	89.4	30.000	83.1	18.750	50.0
0.250	65.5	15.000	82.4	20.000	73.0	9.375	35.3
0.212	36.1	10.000	74.5	10.000	62.7	4.688	25.0
0.180	23.1	5.000	62.0	7.000	53.7	2.344	17.6
0.150	10.2	4.000	56.0	6.000	52.5	1.172	12.5
0.106	4.7	3.000	51.0	4.750	49.0	0.586	8.8
0.063	1.9	2.360	45.1	2.360	46.6	0.293	6.2
		1.180	35.3	1.180	45.4	0.146	4.4
		0.600	27.5	0.710	43.5	0.073	3.1
		0.425	24.5	0.500	38.8	0.037	2.2
		0.250	19.3	0.355	31.3	0.018	1.5
		0.125	13.8	0.212	20.7	0.009	1.1
		0.063	9.4	0.150	12.9	0.005	0.7
				0.106	7.4	0.002	0.5
				0.063	5.8	0.001	0.4

3. The tabulated data of four grain distribution curves of silts and clays are given below. Plot these grain size distribution curves by using semilogarithmic axes as shown in Fig. 5. Calculate D_{10} , D_{30} , D_{60} , C_u , and C_c , and compare your results to those of Table 3.

Sample D		Sample E		Sample F		Sample G	
Particle size (mm)	Percent finer (%)	Particle size (mm)	Percent finer (%)	Particle size (mm)	Percent finer (%)	Particle size (mm)	Percent finer (%)
0.124	100	0.289	100.0	0.552	100.0	90.252	100.0
0.085	100	0.209	99.0	0.399	97.2	63.719	94.9
0.057	98	0.088	93.7	0.304	92.6	57.686	92.6
0.043	96	0.055	85.9	0.209	84.4	42.804	86.7
0.028	92	0.038	80.5	0.090	68.4	19.316	80.9
0.020	87	0.029	73.5	0.063	58.7	9.161	76.2
0.009	77	0.022	66.1	0.047	49.4	5.712	72.7
0.006	74	0.010	49.8	0.037	45.1	3.743	68.0
0.005	71	0.007	45.1	0.030	39.3	1.961	61.4
0.005	69	0.006	41.2	0.022	33.0	0.930	55.2
0.004	66	0.004	37.3	0.010	20.6	0.525	51.7
0.003	61	0.003	33.4	0.006	15.1	0.389	49.8
0.002	56	0.002	26.8	0.004	11.6	0.209	46.3
				0.003	8.5	0.090	42.8
				0.002	4.2	0.055	39.6
						0.030	35.7
						0.021	33.4
						0.009	27.6
						0.005	23.3
						0.003	19.8
						0.002	17.8

4. By using the tabulated data of Exercises 2 and 3, compute the sand, silt, and clay fractions of samples A through G. Plot these fractions, each of which should add up to 100%, on a triangular chart. Compare your results with those of Table 4 and Fig. 7.

5. Write a spreadsheet function that calculates the x - y Cartesian (horizontal and vertical) coordinates of a point to be plotted in a triangular chart.
6. Plot the frequency distributions corresponding to the cumulative distributions of samples A , B , C , B' , D , E , F , and G that are given in the tables of Exercises 2 and 3. Compare your results to those of Figs. 8 and 9.
7. Derive the equation that relates the percentage by weight finer P to the grain size D for a Fuller material having for maximum grain size D_{\max} .
8. In the case of a Log normal distribution, calculate the analytical expression for the coefficients of uniformity and curvature in terms of the mean value μ and standard deviation σ .

1-2 Sieve Analysis

OBJECTIVE

The sieve analysis determines the grain size distribution curve of soil samples by passing them through a stack of sieves of decreasing mesh opening sizes and by measuring the weight retained on each sieve. The sieve analysis is generally applied to the soil fraction larger than $75\ \mu\text{m}$. Grains smaller than $75\ \mu\text{m}$ are sorted by using sedimentation (e.g., hydrometer or pipette analysis). Sieving can be performed in either wet or dry conditions. Dry sieving is used only for soils with a negligible amount of plastic fines, such as gravels and clean sands, whereas wet sieving is applied to soils with plastic fines.

EQUIPMENT

The equipment used in sieve analysis includes:

- Series of standard sieves with openings ranging from 7.5 cm to $75\ \mu\text{m}$, including a cover plate and bottom pan. Figure 1 shows an example of a stack of sieves. Sieves are generally constructed of wire screens with square openings of standard size. Table 1 lists the number and mesh opening sizes of the U.S. standard sieves. Only a few sieves in Table 1 are selected for the sieve analysis. The total number and mesh sizes of the sieves are selected to cover the range of grain sizes in an even distribution on a logarithmic scale.
- Sieve shake (Fig. 2).
- Balances sensitive to 0.1 g.
- Soft wire brush.
- Sample splitter or riffle for dividing large soil samples into smaller samples with identical grain size distribution.
- Mortar and rubber-covered pestle, for breaking up aggregations of soil particles.

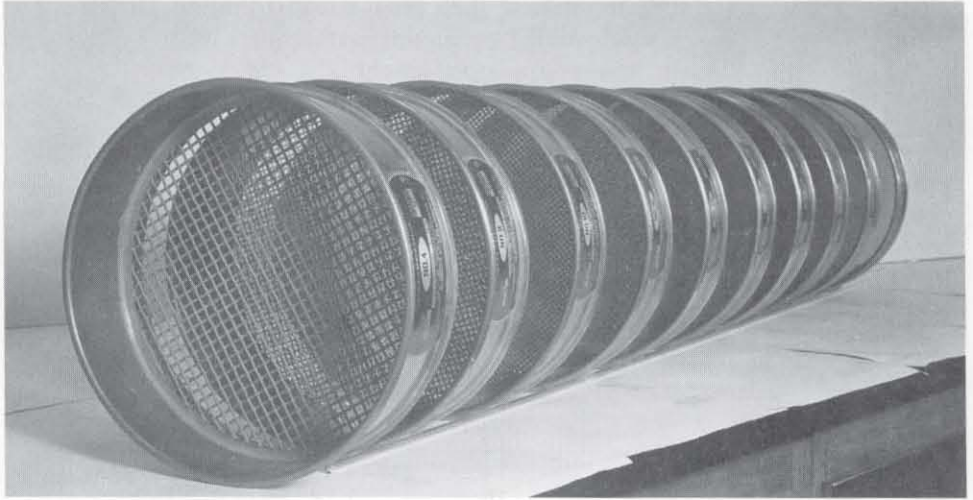


Figure 1 Typical stack of sieves for grain size analysis. The sieves are stacked by decreasing mesh opening size, with the largest mesh opening at the top of the stack.



Figure 2 The stack of sieves is mounted on a mechanical shaker.

PREPARATION OF SOIL SAMPLE

The material to be tested is first air dried. Aggregations or lumps are thoroughly broken up with the fingers or with the mortar and pestle. The specimen to be tested should be large enough to be representative of the soil in the field. It should also be small enough not to overload sieves. Large soil samples are divided by using a

riffle to preserve their grain-size distribution. The size of a representative specimen depends on the maximum particle size. Table 2 gives some guidelines for selecting the minimum sample weight.

TABLE 1
Numbers and openings of U.S. standard sieves

Sieve number	Sieve opening (mm)	Sieve number	Sieve opening (mm)
4	4.75	45	0.355
5	4	50	0.3
6	3.35	60	0.25
7	2.8	70	0.212
8	2.36	80	0.18
10	2	100	0.15
12	1.7	120	0.125
14	1.4	140	0.106
16	1.18	170	0.09
18	1	200	0.075
20	0.85	230	0.063
25	0.71	270	0.053
30	0.6	325	0.045
35	0.5	400	0.038
40	0.425		

TABLE 2
Approximate sample weight for sieve analysis

Maximum particle size	Minimum weight of sample (g)
7.5 cm	6,000
5 cm	4,000
2.5 cm	2,000
1 cm	1,000
Finer than No. 4 sieve	200
Finer than No. 10 sieve	100

PROCEDURE

There are two different procedures for dry and wet sievings. Wet sieving is used when the small particles aggregate and form hard lumps, or coat the coarser particles.

Dry Sieving

1. Oven dry the sample, allow it to cool, and measure its weight.
2. Select a stack of sieves suitable to the soil being tested. The choice of sieves usually depends on experience, judgment, and the intended applications of grain size analysis. A stack of six or seven sieves is generally sufficient for most soils and applications. The top sieve should have an opening slightly larger than the largest particles. Arrange the stack of sieves so that the largest mesh opening is at the top and the smallest is at the bottom (see Fig. 1).
3. Attach a pan at the bottom of the sieve stack. Pour the sample on the top sieve as shown in Fig. 3. Add a cover plate to avoid dust and loss of particles while shaking.



Figure 3 The soil sample is poured on the stack of sieves with a pan at the bottom.

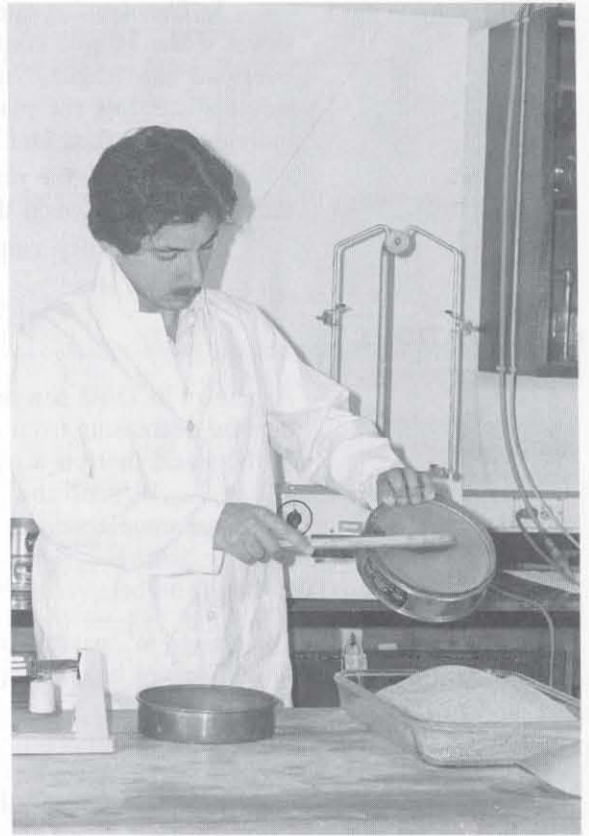


Figure 4 The soil particles stuck in the mesh opening of the sieves are removed with a brush.

4. Place the stack of sieves in the mechanical shaker as shown in Fig. 2, and shake for about 10 min or until additional shaking does not produce appreciable changes in the amounts of material retained in each sieve.

5. Remove the stack of sieves from the shaker. Beginning with the top sieve, transfer its contents to a piece of paper or a large recipient. Carefully empty the sieve without losing any material, and use a brush to remove grains stuck in its mesh opening, as shown in Fig. 4. Measure the weight of soil retained in each sieve and note the corresponding sieve mesh opening and number.

6. Repeat step 5 for each sieve. As a preliminary check, the weights retained on all the sieves and the bottom pan are added, and their sum is compared to the initial sample weight. Both weights should be within about 1%. If the difference is greater than 1%, too much material was lost, and weighing and/or sieving should be repeated.

Wet Sieving

1. Weigh the dry specimen as for dry sieving.

2. If the sample contains plastic fines, which tend to form hard lumps or to coat the coarser particles, place the oven-dried sample in a pan filled with enough water to cover all the material and allow it to soak until all the soil lumps or coatings have disintegrated. Soaking may take 2 to 24 hours, depending on the soil.

3. Transfer the sample to a No. 200 sieve, or to a set of No. 4 to No. 200 sieves if the sample contains an appreciable amount of coarse particles. Do not overload the fragile No. 200 sieve. Wash the sample thoroughly through the sieves, discarding the material passing the No. 200 sieve. Larger particles may be individually washed and removed from the sieves.

4. Oven dry the retained material, and weigh it after it has cooled. Record the difference between the dry weights before and after washing.

5. Use the dry sample for dry sieving starting at step 2.

COMPUTATIONS

As shown in Table 3, a generic stack of sieves is made of n sieves having an opening size decreasing from top to bottom, and numbered from 1 to n . At the bottom of the stack, there is a pan numbered $n + 1$. The weight retained on each sieve is W_1, W_2, \dots, W_n , and the weight retained on the pan is W_{n+1} , as shown in Table 3. The total sample weight W_{tot} is the sum of all retained weights:

$$W_{\text{tot}} = W_1 + W_2 + \dots + W_{n-1} + W_n + W_{n+1} \quad (1)$$

The weight W'_j passing the j th sieve is the sum of weights retained in the pan and sieves located below the j th sieve. The weight passing the top sieve ($j = 1$) is

$$W'_1 = W_{\text{tot}} - W_1 \quad (2)$$

and the weight passing the j th sieve ($n \geq j \geq 1$) is

$$W'_j = W'_{j-1} - W_j \quad (3)$$

$W'_{n+1} = 0$ because no material passes through the pan. The percentage in weight of material finer than the mesh opening of the j th sieve is p_j :

$$p_j = 100 \frac{W'_j}{W_{\text{tot}}} \quad (4)$$

As shown in Table 3, p_j always decreases with j because W'_j decreases continuously with j .

TABLE 3
Summary of calculations for sieve analysis

Sieve number	Weight retained	Weight passing	Percent finer
1 (top)	W_1	$W'_1 = W_2 + W_3 + \dots + W_{n+1} = W_{\text{tot}} - W_1$	$100 W'_1 / W_{\text{tot}}$
2	W_2	$W'_2 = W_3 + W_4 + \dots + W_{n+1} = W'_1 - W_2$	$100 W'_2 / W_{\text{tot}}$
j	W_j	$W'_j = W_{j+1} + \dots + W_{n+1} = W'_{j-1} - W_j$	$100 W'_j / W_{\text{tot}}$
n	W_n	$W'_n = W_{n+1}$	$100 W'_n / W_{\text{tot}}$
$n + 1$ (pan)	W_{n+1}	$W'_{n+1} = 0$	0

The coefficients of uniformity C_u and curvature C_c are defined from D_{10} , D_{30} , and D_{60} , the grain size corresponding to 10, 30, and 60% by weight finer. D_{10} , D_{30} , and D_{60} are obtained by using a semilogarithmic interpolation between



$$y = y_1 + (\log(x) - \log(x_1)) \left[\frac{y_2 - y_1}{\log x_2 - \log x_1} \right]$$

$$\log y = \log y_1 + (x - x_1) \left[\frac{\log y_2 - \log y_1}{x_2 - x_1} \right] \quad 27$$

the data points of the grain size distribution curve. For instance, when $p_i \leq 10 \leq p_{i+1}$,

$$\log(D_{10}) = \log(d_i) + \frac{\log(d_{i+1}) - \log(d_i)}{p_{i+1} - p_i} (10 - p_i) \quad (5)$$

where d_i and d_{i+1} are the sieve openings corresponding to p_i and p_{i+1} . Therefore, D_{10} is

$$D_{10} = d_i \left(\frac{d_{i+1}}{d_i} \right)^{(10 - p_i)/(p_{i+1} - p_i)} \quad (6)$$

D_{30} and D_{60} are calculated similarly to D_{10} .

Error Analysis

The results of sieve analyses are checked by comparing the accumulated weight W_{tot} and initial sample weight W_0 . If W_{tot} is smaller than W_0 , material was lost or data were recorded incorrectly. W_{tot} may also be slightly larger than W_0 , owing to added measurement errors. Equation 1 implies that the error ΔW_{tot} on W_{tot} is

$$\Delta W_{tot} \leq (n + 1)\Delta W \quad (7)$$

where ΔW is the scale accuracy and n is the number of sieves. Because all weights are measured on the same scale, the error ΔW_0 on W_0 is also equal to ΔW . Therefore, the error $\Delta(W_{tot} - W_0)$ on $W_{tot} - W_0$ is

$$\Delta(W_{tot} - W_0) \leq (n + 2)\Delta W \quad (8)$$

If the sieve analysis was correctly performed, $|W_{tot} - W_0|$ should be smaller than $(n + 2)\Delta W$. The analysis should be repeated if $|W_{tot} - W_0|$ is larger than $(n + 2)\Delta W$.

EXAMPLE

Figures 5 and 6 show the results of a sieve analysis for a fine-grained sand. As shown in Fig. 5, the results are presented in the form of a grain size distribution curve, which is obtained by plotting grain size (i.e., sieve opening)

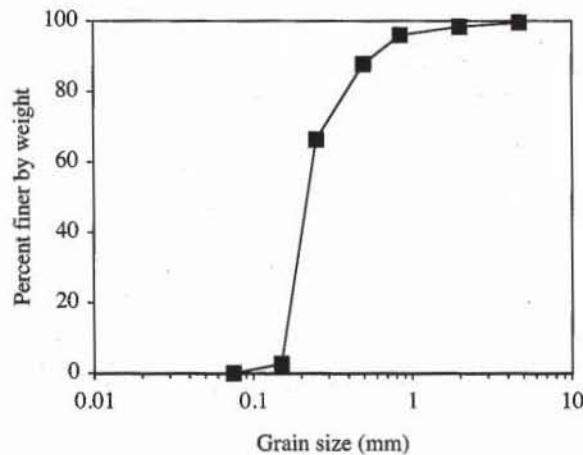


Figure 5 Example of grain size distribution curve obtained by sieve analysis.

on the abscissa and the percent finer by weight on the ordinate. A logarithmic scale is used for the grain size, and a linear scale is used for the percent finer values.

Figure 7 shows the formulas used in Fig. 6. The coefficients D_{10} , D_{30} , and D_{60} are calculated by using the semilogarithmic interpolation of Eq. 6, which is performed by the user-defined function INTER (See Chapter 8-1).

	A	B	C	D	E
1	Sieve analysis				
2					
3	Analyst name: Mike Kapuskar				
4	Test date: 13-11-1990				
5	Sample description: San FranciscoMarina sample #3/20 (beach sand)				
6	Sample mass $M_0 = 191.10$ g				
7					
8	US sieve number	Sieve opening (mm)	Mass retained (g)	Mass passing (g)	Percent finer by weight
9		d	M	M_p	p
10	4	4.750	0.00	190.20	99.53
11	10	2.000	2.10	188.10	98.43
12	20	0.850	4.60	183.50	96.02
13	35	0.500	15.80	167.70	87.76
14	60	0.250	40.90	126.80	66.35
15	100	0.150	122.00	4.80	2.51
16	200	0.075	4.70	0.10	0.05
17	pan		0.10	0.00	0.00
18	Total mass $M_{tot} = 190.20$ g				
19	$D_{10} = 0.159$ mm		$C_u = 1.492$		
20	$D_{30} = 0.187$ mm		$C_c = 0.923$		
21	$D_{60} = 0.238$ mm				

Figure 6 Example of data set for grain size analysis.

	A	B	C	D	E
8	US sieve number	Sieve opening (mm)	Mass retained (g)	Mass passing (g)	Percent finer by weight
9		d	M	M_p	p
10	4	4.75	0	=Mtot-M	=(Mp/M0)*100
11	10	2	2.1	=D10-M	=(Mp/M0)*100
12	20	0.85	4.6	=D11-M	=(Mp/M0)*100
13	35	0.5	15.8	=D12-M	=(Mp/M0)*100
14	60	0.25	40.9	=D13-M	=(Mp/M0)*100
15	100	0.15	122	=D14-M	=(Mp/M0)*100
16	200	0.075	4.7	=D15-M	=(Mp/M0)*100
17	pan		0.1	=D16-M	=(Mp/M0)*100
18	Total mass $M_{tot} = \text{SUM}(M)$				
19	$D_{10} = \text{inter}(10,p,d)$		$C_u = =D.60/D.10$		
20	$D_{30} = \text{inter}(30,p,d)$		$C_c = =D.30^2/D.10/D.60$		
21	$D_{60} = \text{inter}(60,p,d)$				

Figure 7 Formulas used in Fig. 6.

REFERENCES

- See Introduction for references to ASTM procedures (pages 4 to 6).
- AASHTO T87, Sample preparation. American Association of State Highway Transportation Officials, Washington, DC.
- AASHTO T88, Standard test method for particle size analysis of soil.
- BS 410, 1969, *Test Sieves*, British Standards Institution, London.

REVIEW QUESTIONS

1. What is the purpose of grain size analysis?
2. Under what conditions should you use wet sieving instead of dry sieving?
3. On which basis do you select the number and opening of sieves for the sieve analysis of a given soil?
4. How can you quickly verify the results of dry sieving?
5. What are the smallest and largest mesh openings used in practice for determining grain size distribution?
6. A mass of volcanic ashes with highly crushable grains is brought to the laboratory. What precaution do you take to determine its grain size distribution?
7. On what range of particle size does the sieve analysis apply?
8. Is it possible to carry out a sieve analysis on a sample of clay?

EXERCISES

1. The following masses of soil are retained on sieves.

US Sieve No.	4	10	20	40	100	200	pan
Mass retained (g)	100	150	200	250	200	100	5

- Draw the grain size distribution curve and determine C_c and C_u .
2. Determine the formulas that define the error on the percent by weight finer in terms of the retained weights and the experimental errors. Include these formulas in the spreadsheet calculation.
 3. Modify the spreadsheet to obtain a grain size distribution curve that has percent coarser by weight, as the vertical axis rather than percent finer by weight.
 4. In your laboratory report, calculate coefficients D_{10} , D_{30} , and D_{60} by using a linear interpolation instead of the nonlinear interpolation of Eq. 6. Compare the values obtained by both interpolations.
 5. Plot the following grain size distribution as a frequency distribution and a cumulative distribution. Calculate the range, average, and standard deviation of this distribution. Attempt to fit the experimental distribution with a lognormal distribution.

Sieve number	Mass retained (g)
8	76
10	38
20	374
40	538
50	226
60	74
80	142
100	44
200	104
pan	60

Sample mass, 1684 g.

6. Plot the following grain size distributions as cumulative distributions. Calculate the coefficients of uniformity and curvature.

Sieve number	Mass retained (g)
4	0
8	98
10	46
20	394
40	594
50	240
60	88
80	144
100	50
200	104
pan	56

Sample mass, 1814 g.

Sieve number	Mass retained (g)
4	0
9	118
16	160
20	184
30	214
40	270
60	264
80	118
100	56
200	102
pan	62

Sample mass, 1560 g.

7. Write a report on the results of the following sieve analyses. Include a discussion of the experimental errors assuming that the scale accuracy is 0.5 g. Plot the grain size distribution curves, and classify the soils by using their coefficients of uniformity and curvature.

Sieve number	Mass retained (g)
4	0
8	76
10	38
20	374
40	538
50	226
60	74
80	142
100	44
200	104
pan	60

Sample mass, 1684 g.

Sieve number	Mass retained (g)
4	0
10	124
16	168
20	200
30	240
40	274
60	328
80	136
100	52
200	114
pan	58

Sample mass, 1698 g.

1-3

Principles of Sedimentation Analysis

OBJECTIVE

Sedimentation analysis (hydrometer, pipette, and buoyancy analysis) defines the grain size distribution curve of soils that are too fine to be tested with sieves. Sedimentation analysis sorts soil particles by size using the physical process of sedimentation, a process that is described by Stokes' law (Stokes, 1891). The grain size is calculated from the distance of sedimentation of soil particles. The percent by weight finer is determined by measuring the unit weight of the soil-fluid suspension.

STOKES' LAW

The rigid sphere of Fig. 1 with diameter D is immersed in a viscous fluid of viscosity η and having velocity U far away from the sphere. According to Stokes' law, slowly moving viscous fluids exert drag force F on the sphere:

$$F = 3\pi\eta UD \quad (1)$$

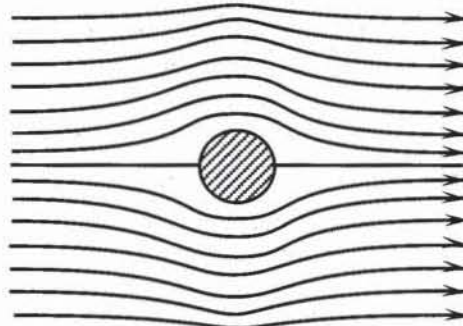


Figure 1 Flow past a fixed sphere for low Reynolds numbers.

The fluid viscosity η has the dimension of mass divided by length and time, and its unit is generally g/cm·s.

Stokes' law is applicable to slowly moving fluids that display the laminar flow patterns of Fig. 1 when the Reynolds number is smaller than 1. By definition, the Reynolds number R_e is the dimensionless ratio of inertial and viscous forces. In the particular case of the flow around a sphere, R_e is

$$R_e = \frac{\rho UD}{\eta} \quad (2)$$

where ρ is the fluid unit mass (i.e., the fluid mass in a unit volume). Stokes' law is no longer applicable when $R_e \gg 1$ because of the changes taking place in the flow pattern.

These changes in flow patterns around a sphere are illustrated in Fig. 2 by considering the flow around a cylinder. After the laminar flow of Fig. 2a, a circulation appears in Fig. 2b behind the cylinder with two vortices rotating in opposite directions. When $R_e \approx 40$, there is a sudden change in the character of the motion. One of the vortices behind the object gets so long that it breaks off and travels downstream with the fluid. Then the fluid curls around behind the sphere and makes another vortex. The vortices peel off alternately on each side, so an instantaneous view of the flow looks roughly like that sketched in Fig. 2c. As the velocity gets higher and higher, there is less and less time for the vorticity to diffuse in a larger region of fluid. When $R_e \approx 10^4$, the flow is chaotic and irregular. As R_e is increased further, the turbulent region moves toward the cylinder and forms a turbulent boundary layer.

The drag force F defined for spheres in Eq. 1 may be generalized to other shapes by expressing it in terms of a drag coefficient C_d times the stagnation pressure $\frac{1}{2}\rho U^2$ and the projected area A_p of the body normal to the flow:

$$F = \frac{1}{2} C_d A_p \rho U^2 \quad (3)$$

In the case of a sphere, A_p and C_d are

$$A_p = \frac{\pi}{4} D^2 \quad \text{and} \quad C_d = 24 \frac{\eta}{\rho UD} = \frac{24}{R_e} \quad (4)$$

Figure 3 shows the theoretical and measured drag coefficients C_d for spheres, disks, and long circular cylinders. Equation 4 predicts that C_d is inversely proportional to R_e , which translates into a straight line of slope equal to -1 in the log-log scale of Fig. 3. As shown in Fig. 3, Eq. 4 reproduces reasonably well the measured values of C_d for spheres provided that $R_e < 1$. But it breaks down when $R_e > 1$ for spheres and other shapes, as indicated by departure of experimental points from the theoretical straight line in Fig. 3.

APPLICATION OF STOKES' LAW TO FALLING SPHERES

When a sphere of radius a falls at a constant velocity U in a fluid of viscosity η , it is subjected to three forces: its weight, $+\frac{4}{3}\pi a^3\gamma_s$; the drag force, $-6\pi\eta Ua$; and the buoyancy force, $-\frac{4}{3}\pi a^3\gamma_w$ where γ_s is the sphere unit weight and γ_w is the fluid unit weight. By definition, the unit weight is the weight of a unit volume. The buoyancy and drag forces are acting in the direction opposite to the weight that is arbitrarily taken positive. When the particle velocity reaches a constant velocity, the forces are in equilibrium:

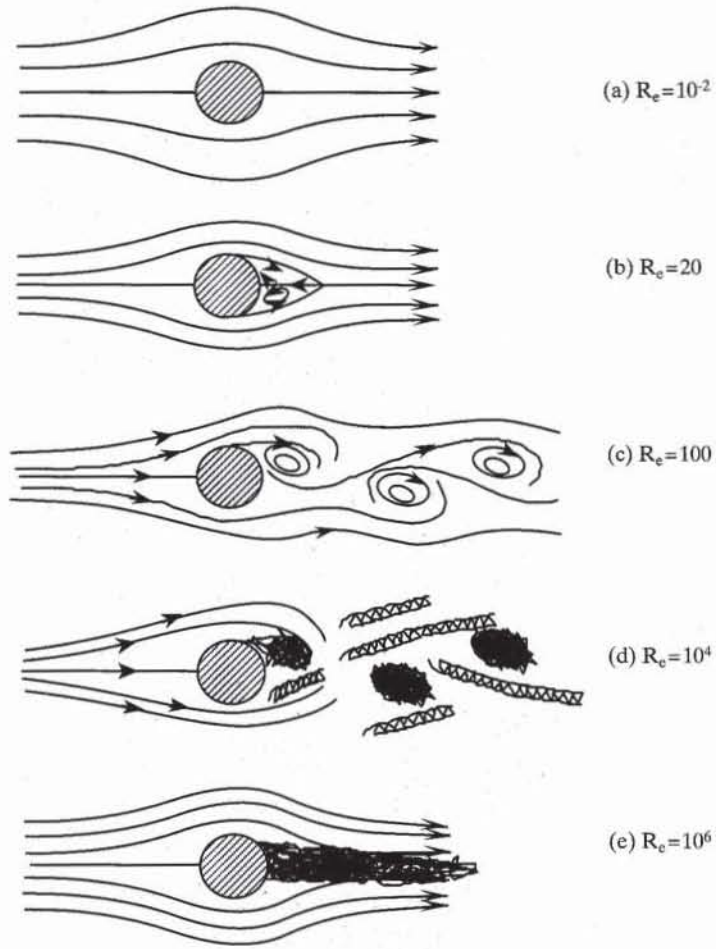


Figure 2 Flow past a fixed cylinder for various Reynolds numbers.

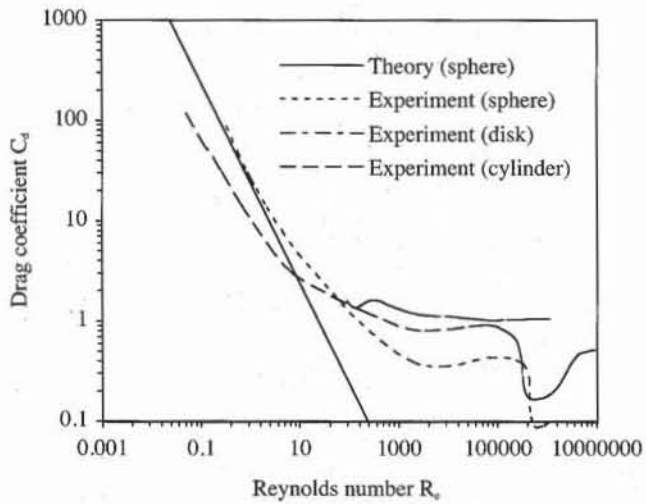


Figure 3 Measured and theoretical drag coefficient for spheres, disks, and cylinders (data after Roberson and Crowe, 1993).

$$\frac{4}{3}\pi a^3\gamma_s - \frac{4}{3}\pi a^3\gamma_w - 6\pi\eta Ua = 0 \quad (5)$$

The sphere velocity U is proportional to a^2 :

$$U = \frac{2}{9} \frac{\gamma_s - \gamma_w}{\eta} a^2 \quad (6)$$

while R_e is proportional to a^3 :

$$R_e = \frac{4}{9} \frac{\gamma_s - \gamma_w}{\eta^2} \rho_w a^3 \quad (7)$$

where ρ_w is the fluid unit mass.

The terminal velocity U and R_e values of spheres made of a typical soil mineral and falling in water are given in Table 1. Stokes' law does not apply to spheres with a radius larger than 0.1 mm, because $R_e > 1$. The diameter of 0.1 mm gives an approximate upper limit of particle size for which Eq. 6 applies. Equation 6 does not hold also for colloids that are particles smaller than 1 μ m. Colloids are influenced predominantly by the electrostatic forces acting on their surfaces. In this case the gravitational forces of Eq. 5, which are proportional to particle volume, become negligible with respect to electrostatic forces. The motion of colloids is random and is referred to as *Brownian*.

As a consequence of Eq. 6, the sphere of radius a initially at the liquid surface at time $t = 0$ will reach the depth H at time t :

$$H = \frac{2}{9} \frac{\gamma_s - \gamma_w}{\eta} a^2 t \quad (8)$$

TABLE 1

Velocity and Reynolds number
of a sphere falling in water ($\rho_s = 2.7 \text{ g/cm}^3$,
 $\rho_w = 1.0 \text{ g/cm}^3$, $\eta = 0.01 \text{ g/cm}\cdot\text{s}$)

a (mm)	U (cm/s)	R_e
1.0	3.7×10^2	7.4×10^3
0.1	3.7	7.4
0.01	3.7×10^{-2}	7.4×10^{-3}
0.001	3.7×10^{-4}	7.4×10^{-6}

THE SEDIMENTATION PROCESS

The model of Fig. 4 illustrates the suspension process with four particle sizes. The particles are settling in a 50-cm-high container filled with water. The particle diameters and terminal velocities calculated by using Eq. 6 are given in Table 2. Although it oversimplifies soils that contain many more particle sizes, this model is still useful to understand what happens in suspensions at various time intervals.

Initially the particles are distributed uniformly by shaking the suspension. The sedimentation process starts at time $t = 0$ immediately after the suspension stops being shaken. All the particles are assumed to reach their terminal velocity within a very short time. At $t = 10$ s, the coarse silt particles A have traveled about 1 cm, whereas the clay particles have only fallen 40 μ m. At $t = 15$ min, all

the coarse silt particles have reached the bottom. At $t = 3$ h, all medium silt particles have settled at the bottom. At $t = 8$ h, only the clay particles remain in suspension. The sedimentation process sorts small particles by size in the same way that sieves separates coarse particles.

Instead of four sizes, soil may have n different particle sizes a_1, a_2, \dots, a_n , where $a_1 > a_2 > \dots > a_n$. These particles when mixed with water make a soil-water mixture which is hereafter referred to as a *suspension*. The concentrations W_1, W_2, \dots, W_n denote the total weights of particles of size a_1, a_2, \dots, a_n in 1 L. $W_{\text{tot}} = W_1 + W_2 + \dots + W_n$ is the total weight of particles. The percent p_j by weight finer than size a_j is

$$p_j = \frac{100}{W_{\text{tot}}} \sum_{i=j+1}^n W_i \quad (\%) \quad (9)$$

In a random suspension, particles are evenly scattered. The weight of particles and percent finer for a given particle size is identical at all depths. The sedimentation process sorts the particles as illustrated in Fig. 4. At time $t > 0$, all the particles above depth H have a radius smaller than a :

$$a = \sqrt{\frac{9}{2} \frac{\eta}{\gamma_s - \gamma_w} \frac{H}{t}} \quad (10)$$

At depth H , the concentration of particles of radius a is constant from $t = 0$ until $t = H/U$, where U is the velocity of the particles of radius a . At time $t > H/U$,

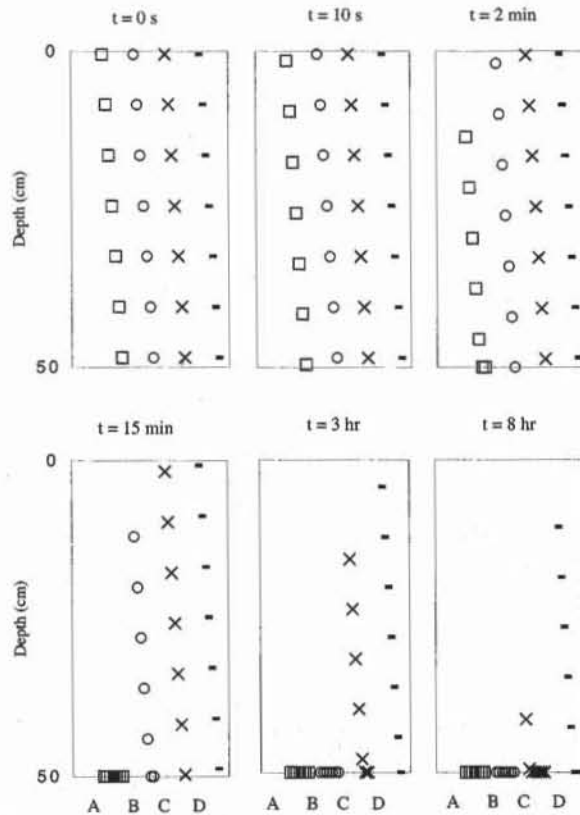


Figure 4 Schematic representation of the sedimentation process of particle sizes A, B, C, and D in Table 2 (after Head, 1984).

there is no longer a particle of radius a at depth H . The percent by weight finer than a can therefore be determined from the concentration of particles of size a at depth H at time t .

TABLE 2

Terminal velocities of particles in suspension in Fig. 4.

Type of particle	Diameter (μm)	Terminal velocity (cm/s)
A: Coarse silt	35	0.1090
B: Medium silt	12	0.0128
C: Fine silt	4	0.0014
D: Clay	2	0.0004

UNIT WEIGHT OF A MIXTURE OF FLUID AND PARTICLES

The weight of a mixture of water and soil particles is

$$V\gamma_{av} = x + \left(V - \frac{x}{\gamma_s}\right)\gamma_w \quad (11)$$

where γ_{av} is the average unit weight, V is the total volume of the suspension, x the weight of particles in the volume V , γ_s the unit weight of the solid particles, and γ_w the unit weight of the water. Therefore, the weight x of particles in volume V is

$$x = \frac{G_s}{G_s - 1} (\gamma_{av} - \gamma_w)V \quad (12)$$

where G_s is the specific gravity of soil grains:

$$G_s = \frac{\gamma_s}{\gamma_w} \quad (13)$$

The average unit weight γ_{av} of the suspension is

$$\gamma_{av} = \frac{x}{V} \left(1 - \frac{\gamma_w}{\gamma_s}\right) + \gamma_w \quad (14)$$

Equation 14 implies that $\gamma_{av} > \gamma_w$ when $\gamma_s > \gamma_w$. When particles settle down, x gradually decreases toward zero and γ_{av} slowly decreases toward γ_w . The unit weight γ_{av} of a sedimenting mixture, which varies with depth and time, can be measured with a hydrometer.

HYDROMETER

As shown in Fig. 5, the hydrometer has a graduated stem and a weighted bulb. When it floats, its weight W_h compensates the buoyancy force:

$$W_h = \int_0^{h_t} S(z)\gamma(z) dz \quad (15)$$

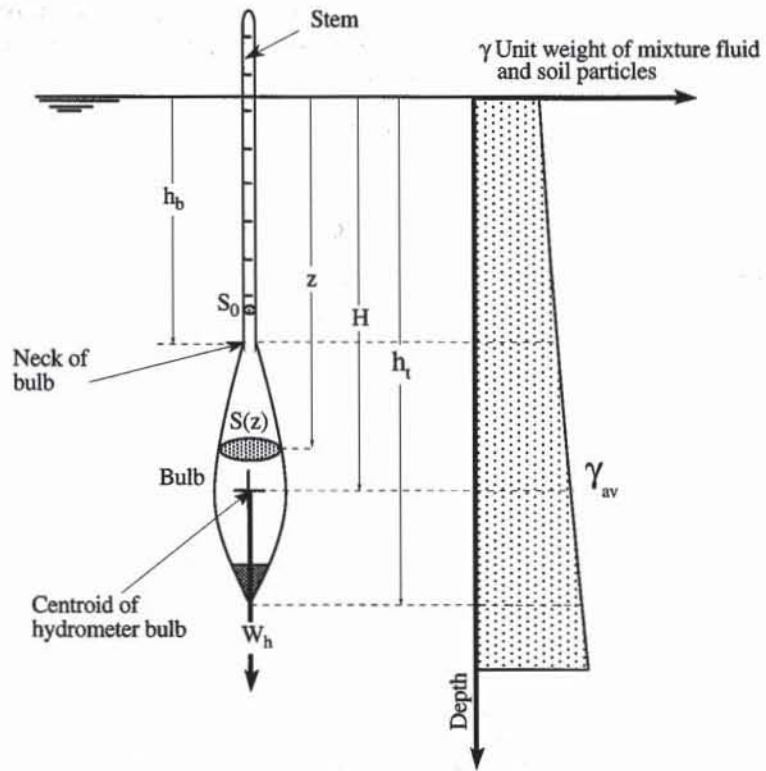


Figure 5 Schematic view of the hydrometer in a sedimenting mixture.

where z is the depth measured from the free surface, $S(z)$ the cross-sectional area of the hydrometer at depth z , $\gamma(z)$ the fluid unit weight at depth z , and h_t the wetted length of the hydrometer at time t . The buoyancy force is the sum of the buoyancy forces applied to bulb and stem:

$$W_h = \int_{h_b}^{h_t} S(z)\gamma(z)dz + S_0 \int_0^{h_b} \gamma(z)dz \quad (16)$$

where h_b is the depth of the bulb neck and S_0 is the constant cross-sectional area of the stem. Because the stem volume is much smaller than the bulb volume V_b , the second integral of Eq. 16 is small compared to the first one. Therefore, the hydrometer measures the average unit weight γ_{av} of the fluid between depths h_b and h_t :

$$\gamma_{av} = \frac{1}{\int_{h_b}^{h_t} S(z)dz} \int_{h_b}^{h_t} S(z)\gamma(z)dz = \frac{1}{V_b} \int_{h_b}^{h_t} S(z)\gamma(z)dz \quad (17)$$

As shown in Fig. 5, when the suspension density gradually varies with depth, γ_{av} is approximately equal to the suspension unit weight at depth H where the bulb is centered. Since the hydrometer weight W_h is constant, Eq. 16 implies that a decrease in mixture density between depths h_b and h_t is balanced by an increase in the wetted length h_t . Therefore, the hydrometer stem can be graduated to measure the suspension unit weight.

The 152H hydrometers (ASTM E 100-94) are graduated to measure the weight x of soil in 1 L assuming that $G_s = 2.65$. When the soil has another specific density G_s , the corrected weight x' of soil per liter of suspension is

$$x' = \frac{2.65 - 1}{2.65} \frac{G_s}{G_s - 1} x = 0.6226 \frac{G_s}{G_s - 1} x \quad (18)$$

DETERMINATION OF PERCENT BY WEIGHT FINER

The hydrometer gives the weight x of particles located around the bulb centroid but not of those located above or below. If W_{tot} is the initial concentration of particles, the percent by weight finer than size a is

$$p = \frac{x}{W_{\text{tot}}} \times 100 \quad (\%) \quad (19)$$

As shown in Fig. 6, when the hydrometer is immersed in a burette of finite size, the water level rises, which changes the distance particles fall relative to the free surface. The water surface rises the distance V_b/A , where V_b is the volume of the hydrometer bulb and A is the cross-sectional area of the sedimentation burette, whereas the water at the elevation of the bulb centroid only rises the amount $V_b/2A$. Therefore, the particles at depth H where the bulb centroid is located have indeed fallen the distance H_R :

$$H_R = H - \frac{V_b}{2A} \quad (20)$$

The substitution of H_R into Eq. 10 gives the grain size a corresponding to p in Eq. 19.

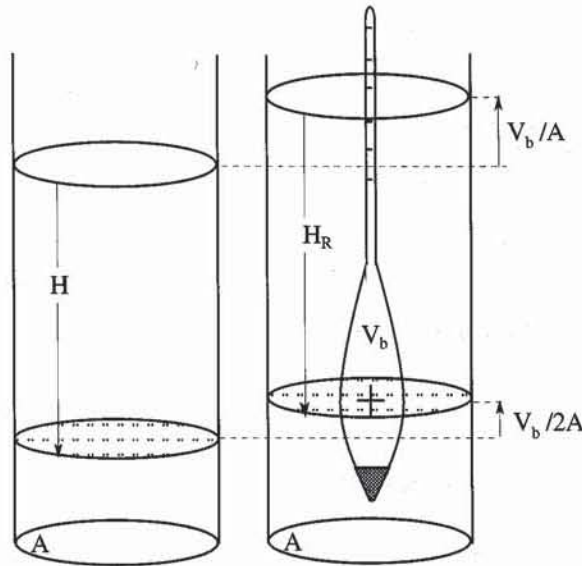


Figure 6 Effect of finite size of burette on distance of sedimentation.

UNIT MASS AND VISCOSITY OF WATER

As indicated in Table 3, the unit mass ρ_w and the viscosity η of the water are functions of temperature T . As shown in Figs. 7 and 8, the values of ρ_w and η that are listed in Table 3 may be fitted by using a cubic polynomial:

$$\eta = 0.0178 - 5.684 \times 10^{-4}T + 1.115 \times 10^{-5}T^2 - 1.017 \times 10^{-7}T^3 \quad (21)$$

$$\rho_w = 0.99991 + 5.202 \times 10^{-5}T - 7.512 \times 10^{-6}T^2 + 3.605 \times 10^{-8}T^3 \quad (22)$$

The values of ρ_w and η at temperature T may also be calculated by linear interpolation of values in Table 3. For instance, if T is between temperatures T_i and T_{i+1} , then η is

$$\eta = \eta_i + (\eta_{i+1} - \eta_i) \frac{T - T_i}{T_{i+1} - T_i} \quad (23)$$

where η_{i+1} is the viscosity at temperature T_{i+1} and η_i is the viscosity at temperature T_i . In a similar way, ρ_w at temperature T is

$$\rho_w = \rho_i + (\rho_{i+1} - \rho_i) \frac{T - T_i}{T_{i+1} - T_i} \quad (24)$$

where ρ_{i+1} is the water unit mass at temperature T_{i+1} , and ρ_i is the water unit mass at temperature T_i .

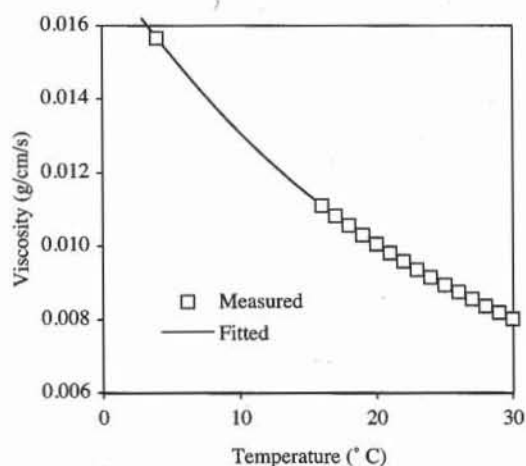


Figure 7 Variation of viscosity of water with temperature.

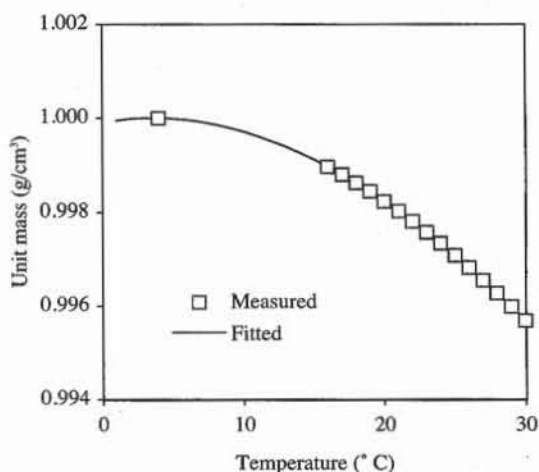


Figure 8 Variation of unit mass of water with temperature.

LIMITATIONS OF SEDIMENTATION ANALYSIS

The sedimentation analysis assumes that soil particles (1) are spherical, (2) have similar specific gravity G_s , (3) are separated from one another, and (4) do not interact during sedimentation. These assumptions are not always verified, which limits the application of sedimentation principles to grain size analysis.

TABLE 3

Viscosity and density of distilled water
at various temperatures (International Critical Tables, 1928)

Temperature (°C)	Dynamic viscosity (g/s·cm)	Unit mass (g/cm ³)
4.0	0.01567	1.00000
16.0	0.01111	0.99897
17.0	0.01083	0.99880
18.0	0.01056	0.99862
19.0	0.01030	0.99844
20.0	0.01005	0.99823
21.0	0.00981	0.99802
22.0	0.00958	0.99780
23.0	0.00936	0.99757
24.0	0.00914	0.99733
25.0	0.00894	0.99708
26.0	0.00874	0.99682
27.0	0.00855	0.99655
28.0	0.00836	0.99627
29.0	0.00818	0.99598
30.0	0.00801	0.99568

1. As described later in Chapter 2-1, small particles such as clay and silt particles are usually not spherical but similar to "corn flakes." Therefore, the drag coefficients C_d of these non-spherical objects can be different from that of Stokes' law.
2. Natural soils may consist of particles having several minerals, different values of G_s , and various tendencies to break down into small fragments. In this case, the particle velocity and size may not be described by using an average value of G_s .
3. Particles in suspension are usually separated by using a chemical agent which creates repulsive forces between particles. However it is difficult to prevent some particles from clustering together and falling faster than individual particles.
4. Finally, the flow patterns around falling particles, which are assumed to be laminar, may become complicated when they interact with one another. It is assumed that this effect is limited when the concentration of soil particles is smaller than 50 g/L.

In spite of these limitations, the principle of sedimentation is still used to determine the grain size distribution of fine-grained soils in geotechnical engineering. It may lead to results which do not fully agree with those of more advanced techniques used in the powder industry (e.g., Allen, 1974). However, the sedimentation analysis is not expensive to perform, and produces consistent results which are sufficient to classify soils for engineering purposes.

REFERENCES

- ALLEN, T., 1974, *Particle Size Measurement*, Chapman & Hall, London.
- HEAD, K. H., 1984, *Manual of Soil Laboratory Testing, Vol. 1: Soil Classification and Compaction Tests*, Pentech Press, London.
- INTERNATIONAL CRITICAL TABLES, 1928, Vols. III and V, McGraw-Hill Book Co., New York.

- ROBERSON, J. A., and C. T. CROWE, 1993, *Engineering Fluid Mechanics*, Fifth Ed., Houghton Mifflin Company, Boston, pp. 502–508.
- STOKES, G., 1891, *Mathematical and Physical Paper III*, Cambridge University Press, Cambridge, U.K.

REVIEW QUESTIONS

1. What is Stokes' law? Which physical quantities does it relate?
2. What is the physical dimension of the viscosity used in Stokes' law? In which unit is it usually expressed? What is the approximate value of the water viscosity at 20°C?
3. State the Reynolds number of a sphere of radius R in a fluid of viscosity η and unit mass ρ flowing with velocity U .
4. What is the approximate range of Reynolds numbers to which Stokes' law applies?
5. What is the drag coefficient of a sphere calculated by using Stokes' law?
6. What is the terminal velocity of a sphere of radius 0.2 mm and specific gravity $G_s = 2.65$ that falls into pure water at 20°C?
7. Does Stokes' law apply to the particles of medium sand falling in the sedimentation burette?
8. Do the water viscosity and water density increase or decrease with temperature?
9. What physical law prevents the particles smaller than 1 μm from falling when they are in suspension?
10. What shape is assumed for the soil particles when interpreting the results of a sedimentation analysis? Does this assumption apply to clay particles?
11. Does the addition of salt to distilled water increase or decrease the unit mass of water?

1-4

Hydrometer Analysis

OBJECTIVE

Hydrometer analysis is used to determine the grain size distribution of fine-grained soils having particle sizes smaller than $75 \mu\text{m}$. If soil samples have particle sizes ranging from sand to silt or clay, sieving and sedimentation analysis are combined as explained in Chapter 1-7. The principle of hydrometer analysis is based on Stokes' law. It assumes that dispersed soil particles of various shapes and sizes fall in water under their own weight as non-interacting spheres.

EQUIPMENT

The equipment used in hydrometer analysis includes:

- Soil hydrometer. There are two different types of hydrometers. One is graduated in the specific gravity of fluids and is calibrated to read 1.000 g/cm^3 in pure water at 20°C . The other is graduated in grams of soil and is calibrated at 0 g/L in pure water at 20°C . The capacity and accuracy of both types of hydrometer are indicated in Table 1. Hereafter, we will use the 152H hydrometer graduated in grams of soil per liter (ASTM D422).

TABLE 1
Capacity and Accuracy of Hydrometers

Hydrometer type	Capacity	Accuracy	Unit
Fluid specific gravity	0.995–1.04	0.001	g/cm^3
Grams of soil per liter	0.0–50.0	1.0	g/L

- Dispersion apparatus, a high-speed mechanical stirrer equipped with an electric motor, which rotates a stirring paddle at high speed (Fig. 1). The dispersion apparatus disperses the mixture of soil, chemicals, and water. If no conventional stirrer is available, a malt mixer or blender can be used.



Figure 1 Equipment for hydrometer analysis. From left to right, two graduated cylinders, also called sedimentation cylinders, a thermometer, a hydrometer, dispersion apparatus, two porcelain evaporating dishes, a stock solution of sodium hexametaphosphate, and a scale.

- Two sedimentation cylinders of glass, essentially 45 cm high and 6.6 cm in diameter, marked for a volume of 1000 mL.
- Thermometer, ranging from 0 to 50°C, accurate to 0.5°C.
- Stopwatch.
- Balance accurate to 0.01 g.
- Measuring cylinder, 100 mL.
- Two porcelain evaporating dishes about 100 mm in diameter.
- Drying oven, 105°-110°C.
- Glass rod about 12 mm in diameter and about 400 mm long.
- 500 mL of hydrogen peroxide.
- 500 mL of stock solution of sodium hexametaphosphate with a concentration of 40 g per liter of distilled or demineralized water. This solution should be prepared frequently, and should be less than a month old.
- 3 L of distilled or demineralized water. The water should be at the temperature that is expected to prevail during the hydrometer test.

PREPARATION AND PRETREATMENT OF SAMPLE

1. The test specimen is obtained from the fraction of soil sample that is smaller than 75 μm . The approximate weight of the dry specimen may be selected as shown in Table 3.

TABLE 2

Stock Solution for Dispersing Agent

Chemical	Quantity	Unit
Sodium hexametaphosphate Buffered with Na ₂ CO ₃ (commercial name "Calgon")	40.0	g
Water	1.0	L

TABLE 3

Approximate Quantity of Material for Sedimentation Analysis.

Soil type	Dry weight (g)
Fat clays	30.0
Lean clays and silty soils	50.0

2. Organic soils must be treated with chemicals to remove organic matter. The organic matter is removed from soils by oxidation and is accomplished by mixing the soil sample with a solution of 30% hydrogen peroxide. The air-dried test specimen is placed in a 1000-mL conical beaker, 150 mL of the hydrogen peroxide solution is added, and the mixture is stirred gently for a few minutes with a glass rod. The oxidation process may be accelerated by heating the mixture gently. Very organic soils may require several additions of hydrogen peroxide, and the oxidation process may take 2 to 3 days. The oxidation process is completed when there are no more gas bubbles. After the pretreatment, the volume of liquid may be reduced to about 50 mL by boiling.

3. Very fine soil grains will normally tend to flocculate in a suspension (i.e., will adhere to each other and settle together). A dispersing agent is added to all samples to prevent grains from flocculating. A 125-cm³ quantity of stock solution of sodium hexametaphosphate (40 g/L) is usually sufficient to disperse most soils. After placing the dry sample in a dish, distilled or demineralized water is added until the sample is submerged; then the 125 cm³ of dispersing agent is added. The sample should be allowed to soak overnight or until all soil lumps have disintegrated.

HYDROMETER AND CYLINDER CALIBRATION

Prior to the hydrometer test, the hydrometer and sedimentation cylinder are calibrated as follows.

1. The cross-sectional area A of the sedimentation cylinder is determined by measuring its internal diameter.

2. The volume of the hydrometer bulb V_b is obtained by immersing it in a graduated cylinder and measuring the rise of water level.

3. The distances between the bulb center and graduation marks 0, 10, 20, 30, 40, 50, and 60 g/L are noted $h_0, h_{10}, h_{20}, h_{30}, h_{40}, h_{50},$ and h_{60} , respectively. As shown in Fig. 2, they are determined by adding h and N to $l_0, l_{10}, l_{20}, l_{30}, l_{40}, l_{50},$ and l_{60} , where N is the distance between bulb neck and lowest stem mark and h is the distance between the bulb centroid and bulb neck. For instance, the distance between the bulb center and the 30-g/L graduation is h_{30} :

$$h_{30} = l_{30} + N + h \quad (1)$$

For a symmetrical bulb, h is half the bulb height. Typical results of a hydrometer and cylinder calibration are reported in Table 3. As shown in Fig. 3, the distance between the graduations marks and bulb centroid are linearly related and can be fitted by linear regression.

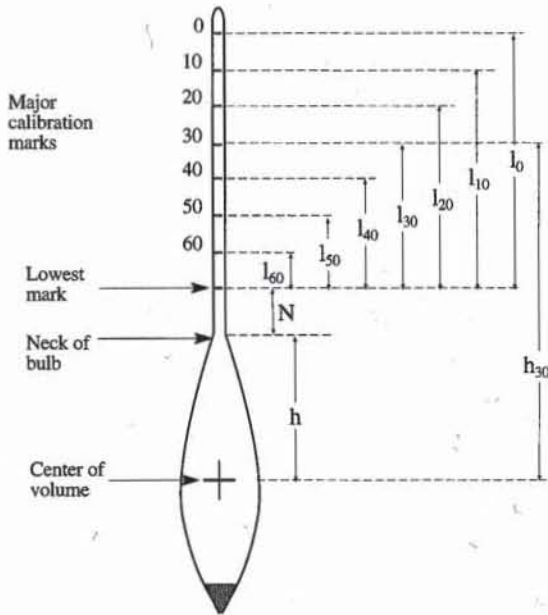


Figure 2 Measurements for calibration of hydrometer.

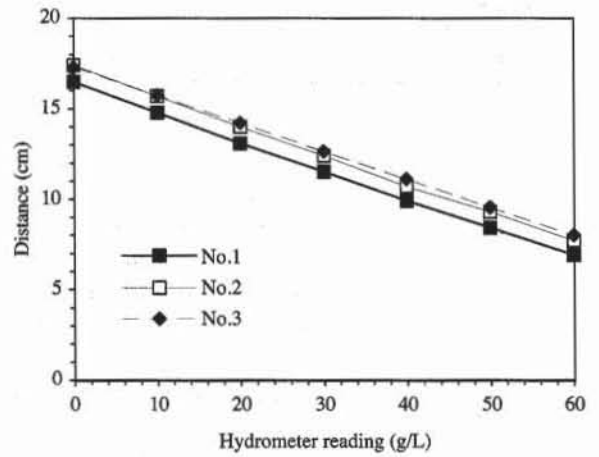


Figure 3 Relation between hydrometer readings and distance to bulb center for the hydrometers of Table 3.

TABLE 4
Example of Calibration Results for Three Soil Hydrometers.

Graduation mark on stem (g/L)	Distance to bulb center (cm)		
	Hydrometer 1	Hydrometer 2	Hydrometer 3
0	16.5	17.4	17.3
10	14.8	15.7	15.75
20	13.1	14	14.2
30	11.5	12.4	12.65
40	9.9	10.7	11.1
50	8.4	9.3	9.55
60	6.9	7.7	8
Bulb volume (mL)	60	60	60
Slope (cm L/g)	-0.16	-0.16	-0.16
Intercept (cm)	16.39	17.30	17.30

CORRECTION OF HYDROMETER READING

Three corrections are applied to the hydrometer reading R : C_m , the meniscus correction; m , the temperature correction; and C_d , the dispersing agent correction. C_m applies to the calculations of grain size and percent by weight finer, whereas m and C_d apply only to the calculation of percent by weight finer.

Meniscus Correction

Hydrometers are calibrated to read correctly at the surface of a transparent liquid, which is represented by level A in Fig. 4. But soil suspensions are not transparent, making such a reading impossible. Therefore, the hydrometer is read

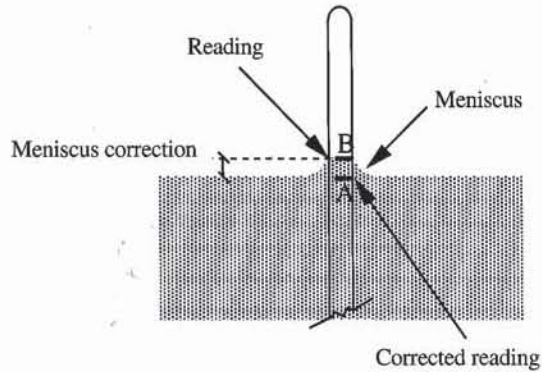


Figure 4 Reading a hydrometer, and determination of meniscus correction.

systematically at the upper rim of the meniscus, which corresponds to point *B* in Fig. 4. C_m is determined by immersing the hydrometer in clear water and measuring the difference between the hydrometer reading made at points *A* and *B*. C_m is always positive and is a constant for a given hydrometer. C_m is equal to approximately 0.5 g/L for most 152H hydrometers. The corrected hydrometer reading R' is

$$R' = R + C_m \quad (2)$$

where R is the reading above the meniscus.

Temperature Correction

Temperature influences the solution density and hydrometer volume (caused by thermal contraction or expansion) and consequently the density reading. Since the hydrometer is calibrated at 20°C, a temperature correction factor m must be added algebraically to each hydrometer reading. The following temperature correction m (g/L) was determined experimentally for a particular type of hydrometer

$$m = 1000 [0.99823 - \rho_w - 0.000025 (T - 20)] \quad (3)$$

where T is the temperature of water (°C) and ρ_w is the water unit mass (g/cm³) at temperature T . As shown in Fig. 5, the correction m is equal to zero for $T = 20^\circ\text{C}$, and is positive or negative, depending on T .

Dispersing Agent Correction

The addition of a dispersing agent to water increases the liquid density. C_d is the hydrometer reading in water and dispersing agent. C_d is always positive and should be subtracted from the corrected hydrometer reading R' when calculating percent by weight finer. The maximum value of C_d is estimated from the concentration of dispersing agent as follows:

$$C_d = 0.001 X_d V_d \quad \text{g/L} \quad (4)$$

where X_d is the concentration of dispersing agent in stock solution (g/L), and V_d is the volume of stock solution in 1 L. When $X_d = 40$ g/L and $V_d = 125$ mL, Eq. 4 gives $C_d = 5$ g/L, a value which is slightly different from the measured value of C_d because the dispersing agent has a smaller specific density than soils.

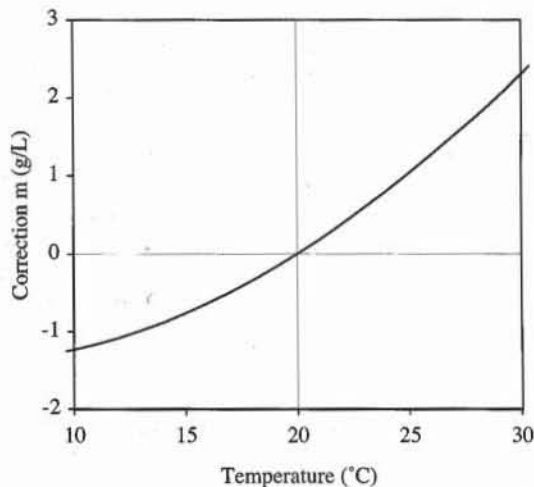


Figure 5 Variation of temperature correction factor m for a particular type of hydrometer.

TEST PROCEDURE

Following the removal of organic matter, addition of dispersing agent, and hydrometer and cylinder calibration, the test procedure consists of the following steps:

1. Determine the dispersing agent correction C_d and the meniscus correction C_m .
2. Measure the specific gravity of solids G_s .
3. Transfer the soil-water slurry from the dish to a dispersion cup, washing any residue from the dish with distilled or demineralized water. As shown in Fig. 6, add distilled water to the dispersion cup until the water surface is 5 to 8 cm below the top of the cup. If the cup contains too much water, it will splash out while mixing. Place the cup in the dispersing machine and disperse the suspension for 1 to 10 min.
4. Transfer the suspension into a 1000-mL sedimentation cylinder and add distilled or demineralized water to fill the 1000 mL cylinder (Fig. 7).
5. About 1 min before starting the test, take the graduate in one hand and, using the palm of the other hand or a suitable rubber cap as a stopper, shake the suspension vigorously for a few seconds to mix the sediment at the bottom of the graduate into a uniform suspension. Repeat this agitation several times by turning the cylinder upside down. Sometimes it is necessary to loosen the sediment at the bottom of the cylinder by means of a hand agitator (Fig. 8). Sustain a uniform suspension until the test begins.
6. Slowly immerse the hydrometer in the liquid 20 to 25 s before each reading. Immerse and remove it very slowly, as shown in Fig. 9, to prevent disturbance of the suspension.
7. Record the hydrometer reading after 1 and 2 min has elapsed from the time agitation has stopped (Fig. 10). As soon as the 2-min reading has been taken, carefully remove the hydrometer from the suspension and place it in clean water as shown in Fig. 11. If a hydrometer is left in a soil suspension too long, material will settle on or adhere to the hydrometer bulb, and this will cause a sig-



Figure 6 The soil sample is placed in a dispersion cup and the dispersing agent is added.



Figure 7 After dispersion, the soil suspension is poured into the sedimentation cylinder.

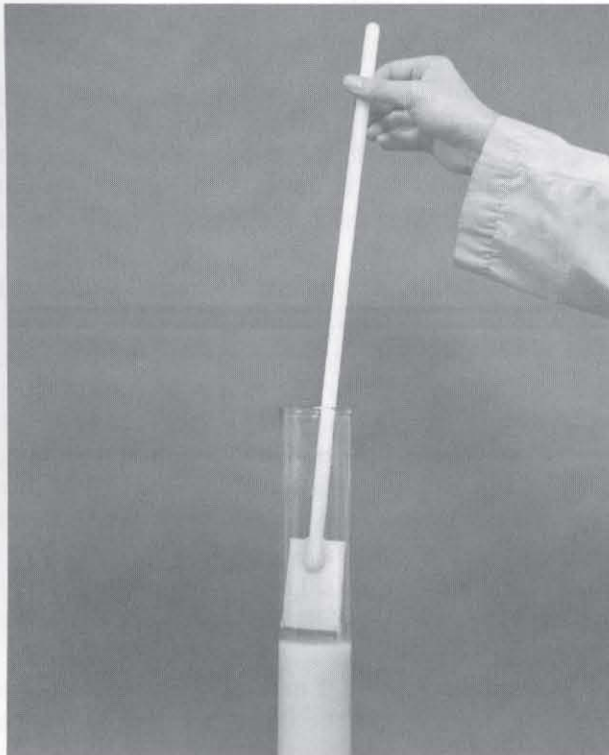


Figure 8 A uniform suspension may be obtained by using a hand agitator.



Figure 9 At selected time intervals, the hydrometer is slowly and carefully immersed.

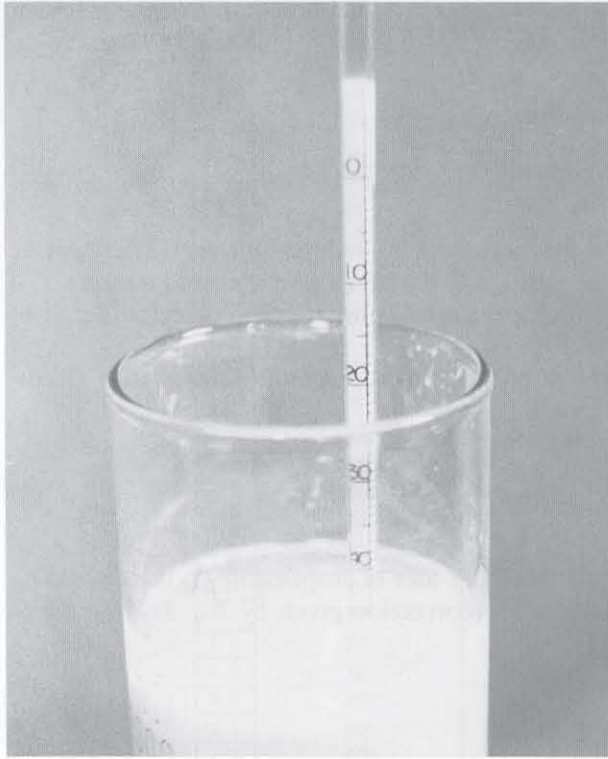


Figure 10 When the hydrometer stops moving, the reading is made at the top of the meniscus.

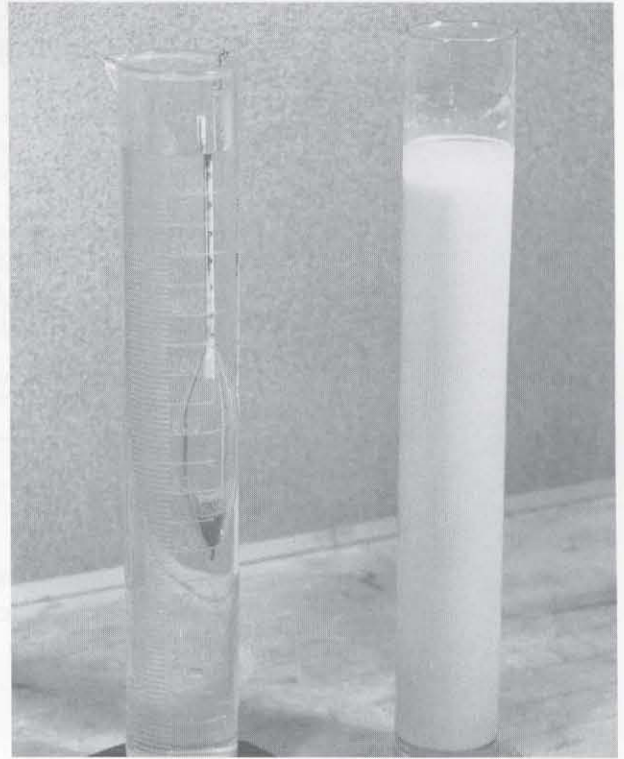


Figure 11 Once the measurement is completed, the hydrometer is removed slowly and carefully, and immersed in a second cylinder filled with clean water.

nificant error in the reading. Insert the hydrometer in the suspension again and record readings after 4, 15, 30, 60, 120, 240, and 1240 min.

8. At the end of 2 min and after each hydrometer reading, record the water temperature. Temperature changes of the soil suspension during the test affect test results. Variations in temperature can be minimized by keeping the suspension away from heat sources, such as radiators, sunlight, or open windows.

COMPUTATION

The corrected hydrometer reading $R' = R_t + C_m$, where R_t is the hydrometer reading at time t and C_m is the meniscus correction. The depth of fall H is calculated by linear interpolation of R' . For instance, when $20 \leq R' \leq 30$ g/L, H corresponding to R' is

$$H = h_{20} + (h_{30} - h_{20}) \frac{R' - 20}{30 - 20} \quad (5)$$

where h_{20} and h_{30} correspond to the marks 20 and 30 g/L, respectively, as defined in the hydrometer calibration. The corrected depth of fall H_R is defined to account for the rise of water level when the hydrometer is immersed:

$$H_R = H - \frac{V_b}{2A} \quad (6)$$

where V_b is the bulb volume, $A = (\pi/4) d_c^2$ the cross-sectional area of the cylinder, and d_c the diameter of the cylinder. According to Stokes' equation, the particle diameter D (mm) is

$$D = \sqrt{\frac{30\eta H_R}{981(G_s - 1)\rho_w t}} \quad (7)$$

where t is the time (min) after the beginning of sedimentation, G_s the specific gravity of the soil particles, ρ_w the unit mass of water (g/cm^3) at temperature T , η the viscosity of water ($\text{g/cm}\cdot\text{s}$) at temperature T , and H_R the corrected depth of fall (cm).

The percentage p by weight of particles with diameter smaller than D corresponding to R' is

$$p = \frac{0.6226}{W_0} (R' - C_d + m) \frac{G_s}{G_s - 1} \times 100 \quad (\%) \quad (8)$$

where W_0 is the oven-dried weight of soil per liter of suspension, C_d the dispersing agent correction, and m the temperature correction given by Eq. 3. The unit of W_0 , R' , C_d , and m is g/L.

EXAMPLE

Figures 12 and 13 show the results of a hydrometer analysis of a silt. As shown in Fig. 12, the results are presented on the same type of grain size distribution curve as the sieve analysis. Figure 13 shows the input/output data corresponding to Fig. 12, and Fig. 14 shows the formulas used in Fig. 13. Figure 15 lists the user-defined functions DENS1, VISCO, and M. DENS1 and VISCO return the water unit mass in (g/cm^3) and water viscosity in ($\text{g/cm}\cdot\text{s}$) at temperature T ($^\circ\text{C}$). M calculates changes in the hydrometer reading as a function of temperature T ($^\circ\text{C}$) (see Eq. 3). The user-defined function INTERL is also used to calculate the distance of fall by linear interpolation. The clay fraction, which the percent by weight finer than $2 \mu\text{m}$, is calculated by using the user-defined INTER (see Chapter 8-1).

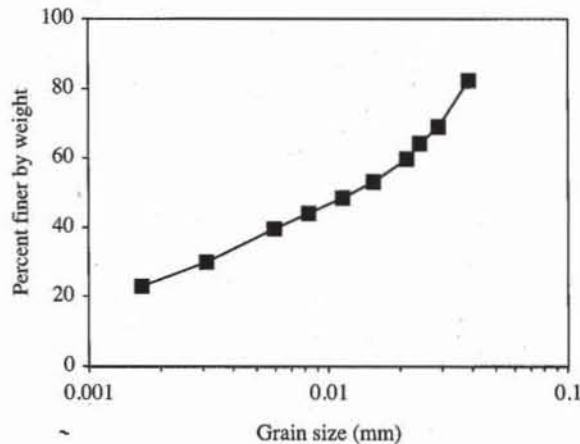


Figure 12 Example of grain size distribution obtained by hydrometer analysis.

	A	B	C	D	E	F
1	Hydrometer analysis					
2						
3	Analyst name: <i>Mike Kapuskar</i>					
4	Test date: <i>11/13/90</i>					
5	Sample description:					
6						
7	Mass in suspension $W_0 =$ <i>45.00</i> g					
8	Specific unit weight $G_s =$ <i>2.65</i>					
9	Dispersing agent correction $C_d =$ <i>4.00</i> g/L					
10	Meniscus correction $C_m =$ <i>0.50</i> g/L					
11	Cylinder diameter $d_c =$ <i>5.95</i> cm					
12	Hydrometer bulb volume $V_b =$ <i>60</i> cm ³					
13						
	Graduation mark on hydrometer stem (g/L)		Distance to bulb center (cm)			
14	R_s		H_s			
15						
16	<i>0</i>		<i>16.5</i>			
17	<i>10</i>		<i>14.8</i>			
18	<i>20</i>		<i>13.1</i>			
19	<i>30</i>		<i>11.5</i>			
20	<i>40</i>		<i>9.9</i>			
21	<i>50</i>		<i>8.4</i>			
22	<i>60</i>		<i>6.9</i>			
23						
	Time (min)	Hydrometer reading (g/L)	Temperature (°C)	Corrected distance of fall (cm)	Grain size (mm)	Percent finer by weight
24						
25	t	R_t	T_e	HR	D	p
26	<i>1</i>	<i>40.0</i>	<i>22.5</i>	<i>8.54</i>	<i>0.0388</i>	<i>82.2</i>
27	<i>2</i>	<i>34.0</i>	<i>22.5</i>	<i>9.56</i>	<i>0.0290</i>	<i>68.8</i>
28	<i>3</i>	<i>32.0</i>	<i>22.0</i>	<i>9.90</i>	<i>0.0243</i>	<i>64.2</i>
29	<i>4</i>	<i>30.0</i>	<i>22.0</i>	<i>10.24</i>	<i>0.0214</i>	<i>59.7</i>
30	<i>8</i>	<i>27.0</i>	<i>22.0</i>	<i>10.75</i>	<i>0.0155</i>	<i>53.1</i>
31	<i>15</i>	<i>25.0</i>	<i>21.5</i>	<i>11.09</i>	<i>0.0116</i>	<i>48.4</i>
32	<i>30</i>	<i>23.0</i>	<i>21.5</i>	<i>11.43</i>	<i>0.0083</i>	<i>43.9</i>
33	<i>60</i>	<i>21.0</i>	<i>21.5</i>	<i>11.77</i>	<i>0.0060</i>	<i>39.5</i>
34	<i>240</i>	<i>17.0</i>	<i>20.0</i>	<i>12.45</i>	<i>0.0031</i>	<i>30.0</i>
35	<i>900</i>	<i>14.0</i>	<i>19.0</i>	<i>12.96</i>	<i>0.0017</i>	<i>22.9</i>
36	Clay fraction (%) = <i>24.4</i>					

Figure 13 Example of data set.

REFERENCE

See Introduction for references on ASTM procedures (pages 4 to 6).

REVIEW QUESTIONS

1. What is the purpose of hydrometer analysis? On which physical principles is hydrometer analysis founded?
2. Does hydrometer analysis determine the size of soil particles exactly?

D		E	
2 4	Corrected distance of fall (cm)	Grain size (mm)	
2 5	HR	D	
2 6	=INTERL(Rt+ABS(Cm),Rs,Hs)-Vb/(2*PI()*dc^2/4)	=SQRT(30*VISCO(Te)*Hr/(Gs-1)/981/DENSI(Te)/t)	

F	
2 4	Percent finer by weight
2 5	p
2 6	=100/W0*(Rt-ABS(Cd)+ABS(Cm)+M(Te))*0.6226*Gs/(Gs-1)

B	C
3 6	Clay fraction (%) = =INTER(0.002,D,p)

Figure 14 Formulas used in Fig. 13.

A		B
1	VISCO	viscosity of water
2	=RESULT(1)	in g/cm/s as a function of
3	=ARGUMENT("T",1)	temperature T in degree Celsius
4	=RETURN(0.0178-5.684/10^4*T+1.115/10^5*T^2-1.017/10^7*T^3)	
5		
6	DENSI	density of water
7	=RESULT(1)	in gr/cm3 as a function pf
8	=ARGUMENT("T",1)	temperature T in degree Celsius
9	=RETURN(0.99991+5.202/10^5*T-7.512/10^6*T^2+3.605/10^8*T^3)	
10		
11	M	temperature correction
12	=RESULT(1)	factor for hydrometer
13	=ARGUMENT("T",1)	as a function of temperature T
14	=RETURN(1000*(0.99823-DENSI(T)-0.000025*(T-20)))	in degree Celsius

Figure 15 User-defined functions VISCO, DENSI, and M used in Fig. 14.

- Why do you correct the distance of fall of particles during hydrometer analysis?
- What physical quantity is read on the stem of a 152H hydrometer? In what unit is this quantity expressed?
- What corrections are made on the hydrometer reading?
- What modifications would be required if one wanted to carry out a hydrometer analysis in a 2000-mL cylinder instead of a 1000-mL cylinder?
- Does the hydrometer go up or down during the sedimentation of soil particles?
- What is the purpose of the dispersing agent? Does its use require a correction?
- Why should you remove the hydrometer from the sedimentation burette after each reading?
- Is there a correction for the specific gravity of soil particles when one uses a 152H hydrometer?
- What physical quantity does the hydrometer measure? At what location does it measure it?
- Why must you slowly insert and remove the hydrometer in the sedimentation burette?

13. Why do you measure the water temperature during the hydrometer analysis?
14. What is the purpose of the hydrometer calibration? What quantities does it relate?
15. Why does the meniscus correction always have the same sign? What is this sign?
16. For what reason do you agitate the suspension at the beginning of the hydrometer test?
17. What is the usual duration of a hydrometer analysis? Why does the sedimentation part take so much time?
18. Suppose that one wants to calibrate the hydrometer analysis with an assembly of spherical particles having only one radius: say $a = 0.05$ mm. Describe qualitatively what will happen to the hydrometer as a function of time. Will it sink gradually from the beginning of the sedimentation? Sketch the variation of hydrometer penetration versus time.

EXERCISES

1. Equation 3 was assumed to account for the effect m of temperature on the hydrometer reading. Verify experimentally this relation.
2. The calibration of the hydrometer requires measurement of the distances h for the readings $R = 0, 10, 20, 30, 40, 50,$ and 60 g/L. By using a linear regression, give an approximate expression that relates R and h for the following hydrometer:

R (g/L)	0	10	20	30	40	50	60
h (cm)	17.4	15.7	14.0	12.4	10.7	9.3	7.7

3. Modify the example of Fig. 13 in order to use the fitting between the hydrometer reading R and the distance h between readings and the bulb center when processing the experimental results of the hydrometer test.
4. Draw the grain size distribution curve for the following hydrometer analysis results.

Soil data	Hydrometer calibration			Hydrometer test		
	Graduation mark on stem (g/L)	Distance to bulb center (cm)	Time (min)	Hydrometer reading (g/L)	Temperature (°C)	
Mass retained on No. 200 sieve	0 g	0	16.5	1	20.0	24
Mass in suspension	30.02 g	10	14.8	2	19.5	24
Specific unit weight	2.65	20	13.1	4	18.7	24
Dispersing agent correction	3 g/L	30	11.5	15	16.0	24
Meniscus correction	0.5 g/L	40	9.9	30	14.5	24
Burette diameter	5.44 cm	50	8.4	60	13.0	24
Bulb volume	65 cm ³	60	6.9	120	12.0	23
				240	10.0	29
				1240	9.5	23.5

5. Draw the grain size distribution curve for the following hydrometer analysis results.

Soil data	Hydrometer calibration			Hydrometer test		
	Graduation mark on stem (g/L)	Distance to bulb center (cm)	Time (min)	Hydrometer reading (g/L)	Temperature (°C)	
Mass retained on No. 200 sieve	0 g	0	18.15	1	40.0	25
Mass in suspension	45 g	10	16.7	2	38.5	25
Specific unit weight	2.65	20	15.25	4	38.0	25
Dispersing agent correction	3.5 g/L	30	13.8	15	37.5	25
Meniscus correction	0.5 g/L	40	12.35	30	36.5	25
Burette diameter	5.44 cm	50	10.9	60	35.5	25
Bulb volume	65 cm ³	60	120	33.0	24.5	
			240	31.2	24	
			1240	26.0	23	

6. Draw the grain size distribution curve for the following hydrometer analysis results.

Soil data	Hydrometer calibration			Hydrometer test		
	Graduation mark on stem (g/L)	Distance to bulb center (cm)	Time (min)	Hydrometer reading (g/L)	Temperature (°C)	
Mass retained on No. 200 sieve	0 g	0	24.5	1	20.0	24
Mass in suspension	30.02 g	10	22.9	2	19.0	24
Specific unit weight	2.65	20	21.3	4	18.0	24
Dispersing agent correction	3 g/L	30	19.7	15	16.0	24
Meniscus correction	0.5 g/L	40	18.1	30	14.5	24
Burette diameter	5.44 cm	50	16.5	60	13.5	23
Bulb volume	65 cm ³	60	120	12.5	24	
			240	12.0	23	
			1240	9.5	23	

7. Draw the grain size distribution curve for the following hydrometer analysis results.

Soil data	Hydrometer calibration			Hydrometer test		
	Graduation mark on stem (g/L)	Distance to bulb center (cm)	Time (min)	Hydrometer reading (g/L)	Temperature (°C)	
Mass retained on No. 200 sieve	0 g	0	17.8	1	30.0	28
Mass in suspension	30.04 g	10	16.1	2	28.0	28
Specific unit weight	2.65	20	14.4	4	27.0	28
Dispersing agent correction	2.25 g/L	30	12.7	15	25.0	28
Meniscus correction	0.5 g/L	40	11	30	23.0	28.5
Burette diameter	5.95	50	9.3	60	20.0	25
Bulb volume	65 cm ³	60	120	17.0	25	
			244	15.0	24	
			1059	11.0	23	

8. Derive Eq. 4 which determines the approximate C_d dispersing agent correction when a volume V_d of stock solution with a concentration X_d is used in a liter of soil suspension.

1-5 Pipette Analysis

OBJECTIVE

Like hydrometer analysis, pipette analysis is used to determine the grain size distribution of fine-grained soils having particle size smaller than 75 μm . If soil samples have fine and coarse particles, including sand, silt, and clay particles, sieving and pipette analysis are combined as explained in Chapter 1-7. Pipette analysis is based on Stokes' law and assumes that dispersed soil particles of various shapes and sizes fall in a liquid under the action of gravitational forces as noninteracting spheres.

In the United States, pipette analysis is less commonly used than hydrometer analysis and is not described by ASTM. However, in the United Kingdom, the British Standard (BS 1377, 1975) refers to pipette analysis as the primary method for determining the grain size distribution of fine-grained soils. Pipette analysis gives faster results than hydrometer analysis but requires accurate measurements of small weights.

EQUIPMENT

The equipment used in pipette analysis includes:

- Sampling pipette, either an Andreasen pipette or a regular pipette, capable of measuring 10 ± 0.2 mL of liquid, with a lowering and raising support (Fig. 1). The Andreasen pipette shown in Figs. 1, 2 and 3 has its own sedimentation cylinder and its own support for adjustment of sampling depth. As shown in Figs. 4 and 5, a regular pipette can also be used.
- Dispersion apparatus (same as that used for hydrometer analysis).
- Two sedimentation cylinders (same as those used for hydrometer analysis).
- Thermometer, ranging from 0 to 50°C, accurate to 0.5°C.
- Stopwatch.
- Balance accurate to 0.001 g.

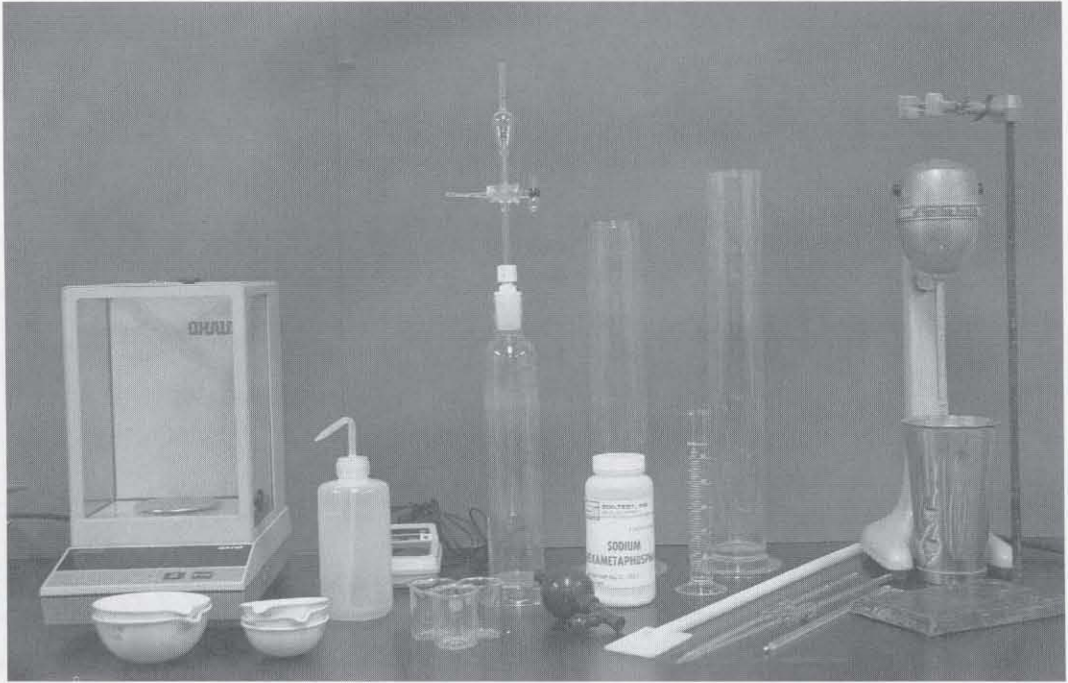


Figure 1 Equipment for pipette analysis. Two sedimentation cylinders, a thermometer, an Andreassen pipette, a 10-mL pipette, a dispersion apparatus, porcelain evaporating dishes, and a stock solution of sodium hexametaphosphate, and a 1-mg sensitive scale.

- Measuring cylinder, 100 mL.
- Porcelain evaporating dishes about 10 cm and 5 cm in diameter.
- Drying oven, 105°–110°C.
- Hand agitator about 400 mm long.
- 500 mL of hydrogen peroxide.
- 500 mL of stock solution of sodium hexametaphosphate prepared as in the hydrometer test.
- 2 L of distilled or demineralized water.

SAMPLE PREPARATION AND PRETREATMENT

The test specimen is selected, pretreated for removal of organic matter, and mixed with a dispersing agent as described for hydrometer analysis. For the pipette analysis, it is recommended to use 500 mL of soil-water suspension and 65 mL of stock solution of sodium hexametaphosphate (i.e., half the quantities used for hydrometer analysis).

PIPETTE CALIBRATION

The pipette volume V must be calibrated. This calibration does not need to be repeated before each experiment. The pipette, which has first been cleaned and dried, is filled with distilled water until the bottom of the water meniscus reaches the graduation mark on the pipette stem. Then the pipette contents are emptied



Figure 2 The Andreasen pipette, its sedimentation cylinder, and a rubber pumping and sucking device.

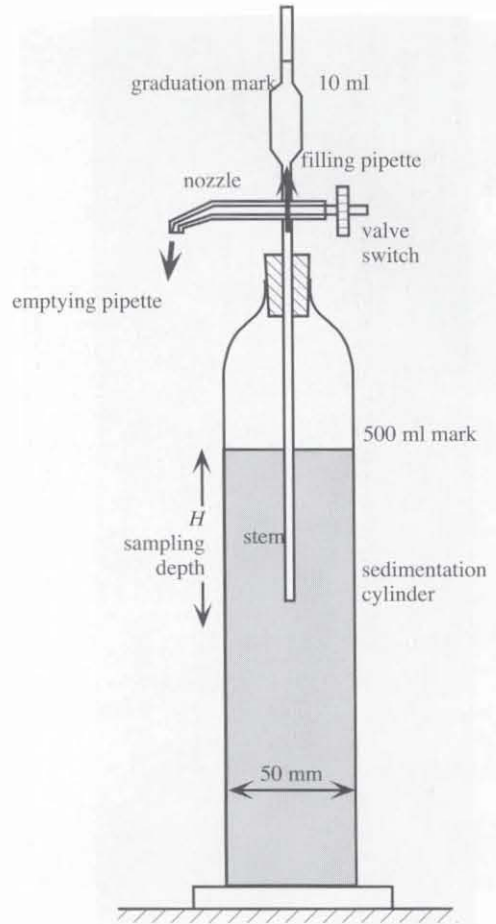


Figure 3 In the Andreasen pipette, the sample can be taken without removing the pipette. The sampling depth may be adjusted by varying the pipette position.

into a dish and the mass of water is measured. The volume V in milliliters is equal to the mass of water in grams. Make three determinations of V , and take the average for volume V .

TEST PROCEDURE

There are two pipette methods: wet and dry. In the *wet method*, samples are weighed without being dried, whereas in the *dry method*, samples are dried prior to being weighed. After the removal of organic matter, addition of dispersing agent, and pipette calibration, the test procedures consist of the following steps:

1. Follow steps 2 to 5 of the hydrometer analysis, except for the total volume of the suspension, which is now 500 mL, and the stock solution volume, which is now 65 mL.
2. Pipette samples are to be taken at several specified time intervals corresponding to the particle size equal to 20, 10, 6, and 2 μm , as shown in Table 1. No sampling is made for 75 and 60 μm because there is simply not enough time. The last sampling operation takes place about 7 h after the be-

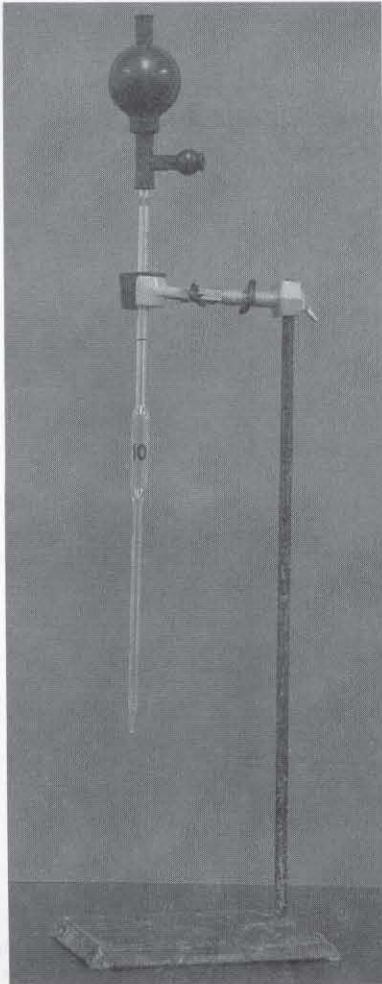


Figure 4 Regular pipette capable of measuring 10 mL of liquid. It is mounted on a stand with a lowering and raising device.

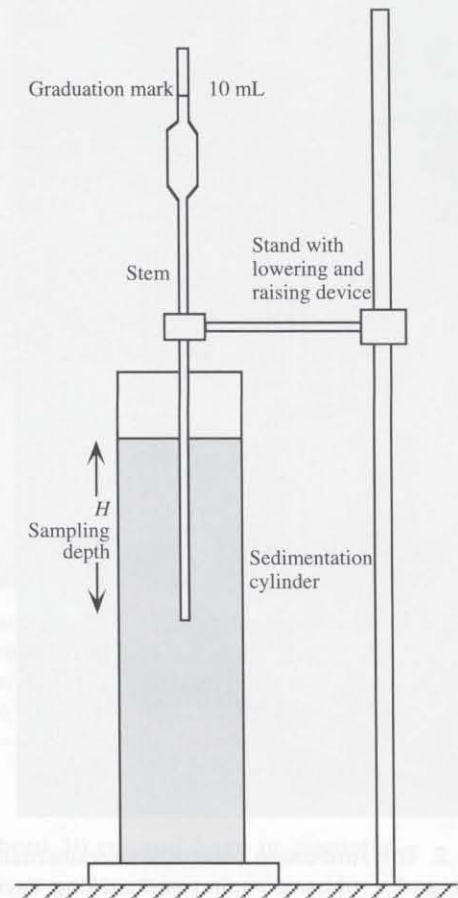


Figure 5 Regular pipette mounted on a stand and lowered into suspension just before sampling.

ginning of the test. Therefore, the pipette analysis can be completed three times faster than hydrometer analysis. The sampling times t of Table 1 are calculated by using the following equation for a temperature of 25°C:

$$t = \frac{18 \times 10^8 \eta H}{(G_s - 1)981 \rho_w D^2} \quad (\text{s}) \quad (1)$$

where G_s is the specific gravity of the soil particles, ρ_w the unit mass of the water (g/cm^3), η the viscosity of the water ($\text{g}/\text{cm}\cdot\text{s}$), H the sampling depth (cm), and D the particle size (μm).

- 3. Regular pipette.** Move the pipette over the sedimentation cylinder, and lower it until its tip touches the water surface (Fig. 6). About 15 s before a sample is due, steadily lower the pipette 100 mm into the suspension, slowly enough not to disturb the suspension. Draw a sample into the pipette until the bottom of the liquid meniscus reaches the graduation mark. A convenient way of drawing the sample is to use a rubber pump attachment (see Fig. 7). The drawing operation should take about 10 s. Then gently withdraw the pipette from the suspension.

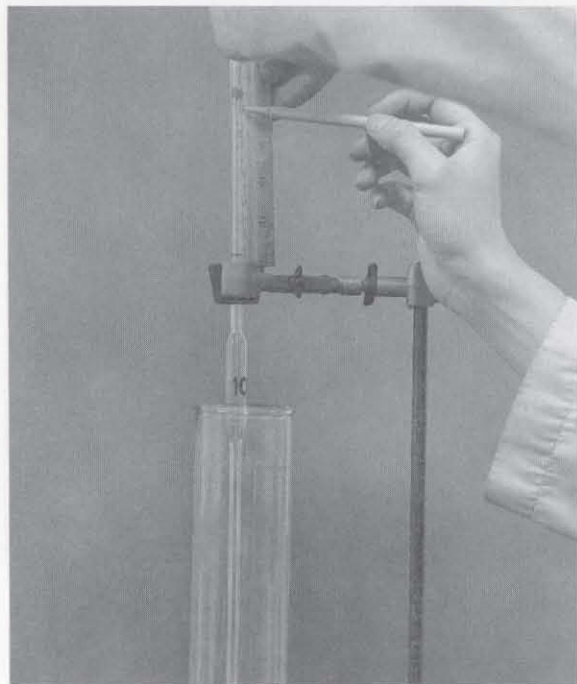


Figure 6 The pipette is first positioned to touch the liquid surface, then steadily and slowly lowered into the suspension to the sampling depth.

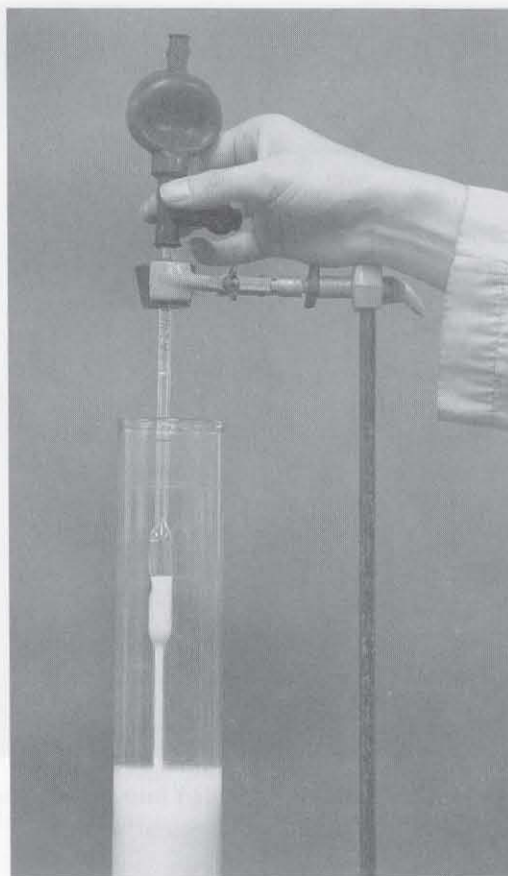


Figure 7 Open the pipette tap and draw a sample into the pipette until the bottom of the liquid meniscus reaches the graduation mark.

Andreasen pipette. Slowly draw a sample into the pipette until the bottom of the liquid meniscus reaches the graduation mark. Switch the two-way valve to empty the pipette.

4. Carefully empty the pipette contents, without losing a drop, into a weighing dish previously weighed (Figs. 8 and 9). Squeeze the rubber pump attachment several times to remove all sample traces from the pipette.

5. *Wet method.* Measure the sample weight with an accuracy smaller than or equal to 1 mg.

Dry method. Place the weighing dish and sample in an oven at 105°C, and weigh it when the sample is dry. Accurate weighing is important because the sample weights are very small.

6. After each sampling, record the water temperature. The temperature should not vary excessively during the experiment.

7. At a convenient time between samplings, the mass of dispersing agent in solution is measured. Take a sample of water and dispersing agent from another sedimentation cylinder, which contains the same amount of dispersing agent and water as the test cylinder but no soil. The sampling time is not critical because the dispersing agent does not settle. Empty the pipette sample into a weighing dish.

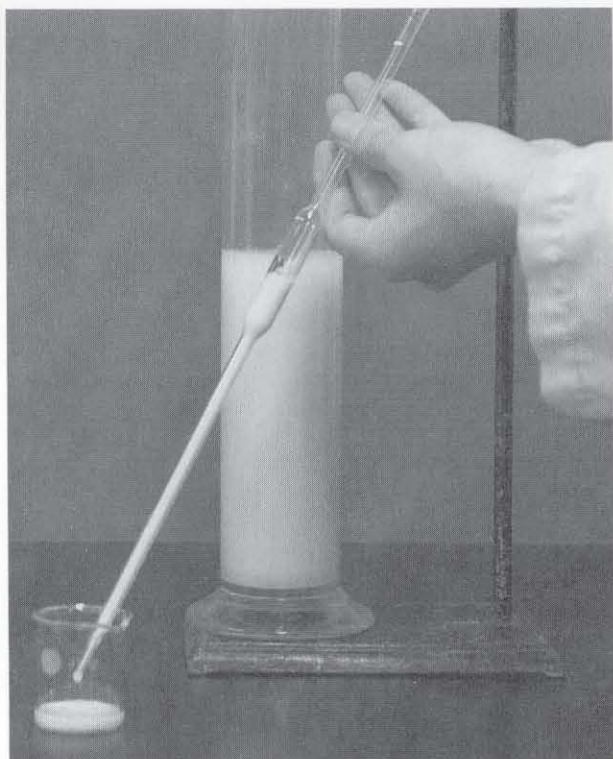


Figure 8 The pipette is emptied into a weighing dish.

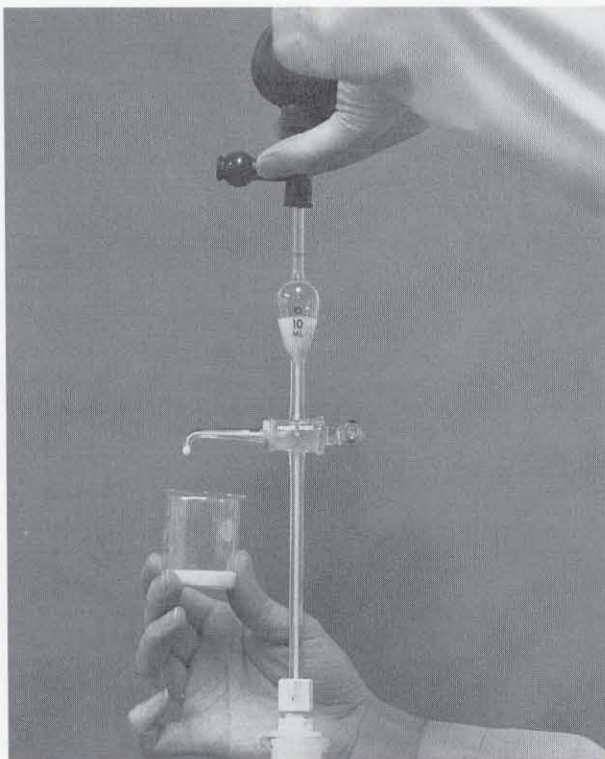


Figure 9 In contrast to a regular pipette, the Andreasen pipette is emptied without being removed from the sedimentation cylinder.

8. *Wet method.* Weigh the sample of dispersing agent.

Dry method. Dry the sample of dispersing agent in an oven at 105°C, and weigh it when it is dry.

TABLE 1

Approximate Sampling Times

G_s	Diameter of particle (μm)					
	75	60	20	10	6	2
2.5	20 s	31 s	04 min 35 s	18 min 20 s	50 min 57 s	07 h 38 min
2.55	19 s	30 s	04 min 26 s	17 min 45 s	49 min 18 s	07 h 23 min
2.6	18 s	29 s	04 min 18 s	17 min 12 s	47 min 46 s	07 h 09 min
2.65	18 s	28 s	04 min 10 s	16 min 40 s	46 min 19 s	06 h 56 min
2.7	17 s	27 s	04 min 03 s	16 min 11 s	44 min 57 s	06 h 44 min
2.75	17 s	26 s	03 min 56 s	15 min 43 s	43 min 40 s	06 h 33 min
2.8	16 s	25 s	03 min 49 s	15 min 17 s	42 min 27 s	06 h 22 min
2.85	16 s	25 s	03 min 43 s	14 min 52 s	41 min 18 s	06 h 11 min
2.9	15 s	24 s	03 min 37 s	14 min 29 s	40 min 13 s	06 h 01 min
2.95	15 s	24 s	03 min 32 s	14 min 06 s	39 min 11 s	05 h 52 min
3	15 s	23 s	03 min 26 s	13 min 45 s	38 min 13 s	05 h 43 min
3.05	14 s	22 s	03 min 21 s	13 min 25 s	37 min 17 s	05 h 35 min
3.1	14 s	22 s	03 min 17 s	13 min 06 s	36 min 23 s	05 h 27 min
3.15	14 s	21 s	03 min 12 s	12 min 48 s	35 min 33 s	05 h 19 min
3.2	13 s	21 s	03 min 08 s	12 min 30 s	34 min 44 s	05 h 12 min

Depth of sampling, 10 cm; temperature, 25°C; G_s , specific gravity.

COMPUTATION

For both dry and wet pipette methods, the grain size D is

$$D = \sqrt{\frac{30 \eta H}{(G_s - 1)981 \rho_w t}} \quad (\text{mm}) \quad (2)$$

where t is the time (min) after the beginning of sedimentation, G_s the specific gravity of the soil particles, ρ_w the unit mass of the water (g/cm^3) at temperature T , η the viscosity of the water in ($\text{g/cm}\cdot\text{s}$) at temperature T , and H the sampling depth (cm).

In the dry pipette method, the percentage p by weight of particles with diameter smaller than D is

$$p = \frac{V_t M_s - M_b - M_d}{V M_0} \times 100 \quad (\%) \quad (3)$$

where M_0 is the total mass of the oven-dried soil in suspension (g), M_b the mass of the empty weighing dish (g), M_s the mass of the weighing dish and sample of oven-dried soil (g), V_t the total volume of the suspension (mL), V the volume of the pipette (mL), and M_d the mass of the dispersing agent in volume V (g). The mass M_d of the dispersing agent in volume V is measured directly. It can also be estimated as follows:

$$M_d = 0.001 \frac{V}{V_t} C_d V_d \quad (\text{g}) \quad (4)$$

where C_d is the concentration of the dispersing agent in stock solution (g/L), V_d the volume of the stock solution in total volume (mL), and V_t the volume of the suspension (mL). In general, Eq. 4 slightly overestimates the measured value of M_d when the dispersing agent is not completely dissolved.

In the wet pipette method, the percentage p by weight of particles with diameter smaller than D is

$$p = \frac{\rho_s V_t}{\rho_s V - M_{dw}} \frac{M_{sw} - M_b - M_{dw}}{M_0} \times 100 \quad (\%) \quad (5)$$

where M_0 is the total mass of the oven-dry soil in suspension (g), M_b the mass of the empty weighing dish (g), M_{sw} the mass of the weighing dish and sample of soil suspension (g), V_t the total volume of suspension (mL), V the volume of the pipette (mL), ρ_s the unit mass of the solid (i.e., $\rho_s = G_s \rho_w$) (g/mL), and M_{dw} the mass of water and dispersing agent in volume V (g). M_{dw} is measured directly. It can also be estimated as follows:

$$M_{dw} = V \rho_w + 0.001 \frac{V}{V_t} C_d V_d \left(1 - \frac{1}{G_c}\right) \quad (\text{g}) \quad (6)$$

where G_c is the specific gravity of the dispersing agent. Equation 6 slightly overestimates the measured value of M_{dw} for the same reason as Eq. 4.

EXAMPLE

Figures 10 and 12 show the results of a dry pipette analysis obtained for a silt from Lucerne Valley, California. As shown in Fig. 10, the results are presented in a grain size distribution curve similar to that of sieve and hydrometer analyses. Figure 13 shows the formulas used in Fig. 12. Figures 11, 14, and 15 give the results, data set, and formulas of a wet pipette analysis on a silt from Barnard, Vermont. Both dry and wet methods use the user-defined functions DENSI and VISCO, which are defined in Chapter 1-4. DENSI and VISCO return the water unit mass (g/cm^3) and water viscosity ($\text{g}/\text{cm}\cdot\text{s}$), respectively, at temperature T ($^{\circ}\text{C}$).

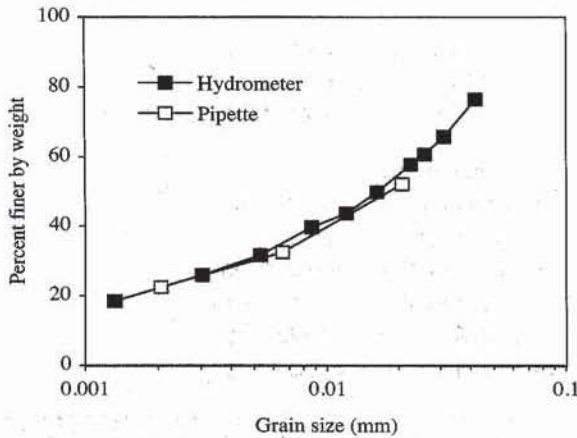


Figure 10 Comparison of results for hydrometer and dry pipette analysis on a silt from Lucerne Valley, California.

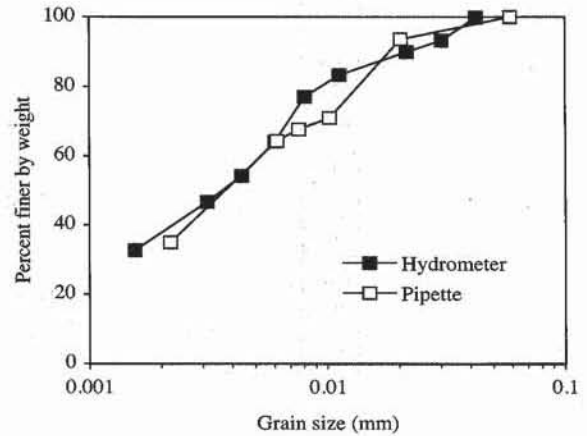


Figure 11 Comparison of results for hydrometer and wet pipette analysis on a silt from Barnard, Vermont.

	A	B	C	D	E	F	G
1	Pipette analysis						
2							
3	Analyst name: <i>Qiang Huang</i>						
4	Test date: <i>16-Feb-92</i>						
5	Sample description: <i>P.V. No.1 silt from Lucerne Valley, California</i>						
6							
7	Dry method						
8	Total mass in suspension $M_0 =$		25.017		g		
9	Soil specific density $G_s =$		2.65				
10	Volume of pipette $V =$		10		mL		
11	Total volume of suspension $V_t =$		500		mL		
12	Mass of dry agent and bottle $M_d =$		45.968		g		
13	Mass of bottle $M_{bd} =$		45.950		g		
14							
15	Time (min)	Depth of sampling (cm)	Temperature ($^{\circ}\text{C}$)	Mass of bottle (g)	Mass of dry sample and bottle (g)	Grain size (mm)	Percent finer by weight
16	t	H	T_s	M_b	M_s	D	p
17	4	10.0	23.0	44.5987	44.8772	0.0209	52.06
18	40	10.0	23.0	47.7586	47.9397	0.0066	32.60
19	410	10.0	23.8	43.2441	43.3748	0.0020	22.52

Figure 12 Example of data set for dry pipette analysis.

	F	G
15	Grain size (mm)	Percent finer by weight
16	D	p
17	$=20 \cdot \text{SQRT}(4.5 \cdot \text{VISCO}(\text{Te}) \cdot \text{H} / ((\text{Gs}-1) \cdot \text{DENSI}(\text{Te}) \cdot 981 \cdot 60 \cdot \text{t}))$	$=100 \cdot (\text{Ms}-\text{Mb}-\text{Md}+\text{Mbd}) / \text{M0} \cdot \text{Vt} / \text{V}$

Figure 13 Formulas used in Fig. 12.

	A	B	C	D	E	F	G
1	Pipette analysis						
2	Analyst: <i>Henry T. Guapo</i>						
3	Test date: <i>8-Feb-93</i>						
4	Sample: <i>Silt from Barnard, Vermont</i>						
5							
6	Wet method						
7	Total mass in suspension $M_0 = 25.020$ g						
8	Soil specific density $G_s = 2.65$						
9	Volume of pipette $V = 9.900$ mL						
10	Total volume of suspension $V_t = 500$ mL						
11	Mass of sampled water, agent and bottle $M_{dw} = 54.442$ g						
12	Mass of bottle $M_{bd} = 44.530$ g						
13							
14	Time (min)	Sampling depth (cm)	Temperature (°C)	Mass of bottle (g)	Mass of sample and bottle (g)	Grain size (mm)	Percent finer by weight
15	t	H	T_s	M_b	M_s	D	p
16	0.5	10.0	23	16.960	27.180	0.0591	100.07
17	4.2	10.0	23	16.000	26.200	0.0205	93.58
18	8.3	5.0	23	86.790	96.920	0.0102	70.83
19	15.0	5.0	23	45.160	55.280	0.0076	67.58
20	23.1	5.0	23	45.950	56.060	0.0061	64.33
21	180.5	5.0	23	47.080	57.100	0.0022	35.09

Figure 14 Example of data set for wet pipette analysis.

	F	G
14	Grain size (mm)	Percent finer by weight
15	D	p
16	$=20 \cdot \text{SQRT}(4.5 \cdot \text{VISCO}(\text{Te}) \cdot \text{H} / ((\text{Gs}-1) \cdot \text{DENSI}(\text{Te}) \cdot 981 \cdot 60 \cdot \text{t}))$	$=100 \cdot (\text{Msw}-\text{Mb}-\text{Mdw}+\text{Mbd}) / \text{M0} \cdot \text{Vt} / (\text{V} - (\text{Mdw}-\text{Mbd}) / \text{Gs} / \text{DENSI}(\text{Te}))$

Figure 15 Formulas used in Fig. 14.

COMPARISON OF HYDROMETER AND PIPETTE ANALYSES

Pipette analysis has several advantages over hydrometer analysis. It takes less time because the sampling depth is adjustable, whereas it is fixed in hydrometer analysis. The calculations are also simpler and there is no need to account for the correction of meniscus or hydrometer dilation. However, compared to hydrometer analysis, pipette analysis is less adapted to the conditions encountered in a field laboratory. It requires accurate weight measurement. As shown in Figs. 10

and 11, hydrometer and pipette analyses give similar grain size distribution curves. This similarity is not surprising because both analyses are based on sedimentation (Stokes' law) and sample preparation is identical.

REVIEW QUESTIONS

1. What is the purpose of pipette analysis? On which physical principle is pipette analysis founded?
2. Does pipette analysis determine the size of soil particles exactly?
3. Compare pipette analysis and hydrometer analysis based on their principles and experimental procedures.
4. What is the purpose of a dispersing agent? Does its use require a correction in pipette analysis?
5. Why is a constant temperature required during the sedimentation process?
6. What is the purpose of pipette calibration? Do you have to repeat it before each sampling?
7. For what reason do you agitate the suspension at the beginning of a pipette test?
8. When does the analysis time start in pipette analysis?
9. If one wanted to sample at a depth of 5 cm (instead of 10 cm) during pipette analysis, what would be the effect of this change?
10. What is the average duration of a pipette analysis? Why does pipette analysis require less time than hydrometer analysis?
11. Why is it difficult to measure the particles with a diameter larger than 75 μm by using pipette analysis?

EXERCISES

1. Using a spreadsheet program, construct a table of sampling times similar to Table 1, but for $H = 15$ cm and $T = 20^\circ\text{C}$ instead of $H = 10$ cm and $T = 25^\circ\text{C}$.
2. Derive Eqs. 4 and 6, which estimate the mass of dispersing agent in the pipette for the dry and wet methods.

1-6

Buoyancy Analysis

OBJECTIVE

The buoyancy analysis is based on the same physical principles as hydrometer and pipette analyses. The buoyancy analysis can be used to determine the grain size distribution of fine-grained soils having particle size smaller than $75\mu\text{m}$. If soil samples have fine and coarse particles including sand, silt and clay particles, sieving and buoyancy analyses are combined as explained in Chapter 1-7.

To our knowledge, the buoyancy analysis is a new type of experiment for grain size analysis. Compared to the hydrometer analysis, it gives faster results but requires accurate weight measurement. Compared to the pipette analysis, it has fewer and less complicated experimental steps.

EQUIPMENT

The equipment of the buoyancy analysis includes the following:

- Teflon sphere about 2.5 cm in diameter attached to a 0.1 mm thick nylon line by using a small point of rapid glue. As shown in Fig. 1 the line is attached to a light frame which can sit on the platen of a sensitive scale.
- Dispersion apparatus (same as for hydrometer analysis).
- Two 1000 mL sedimentation cylinders (same as for hydrometer analysis).
- Thermometer, ranging from 0 to 50°C , accurate to 0.5°C .
- Stop-watch.
- Balance accurate to 1 mg mounted on a cantilever support as shown in Fig. 1.
- Measuring cylinder, 100 mL.
- Drying oven.
- Hand agitator about 400 mm long.
- 500 mL of Hydrogen peroxide.
- 1000 mL of stock solution of sodium hexametaphosphate prepared as in hydrometer test.

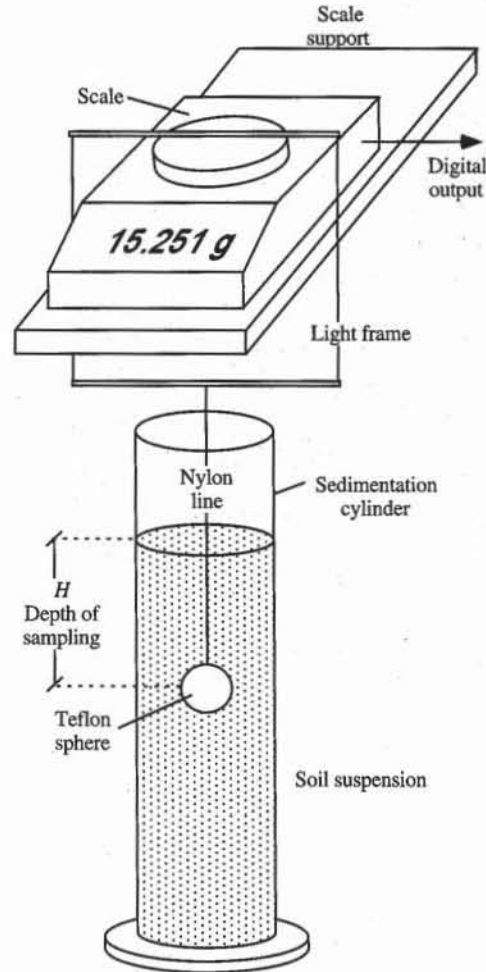


Figure 1 Equipment for buoyancy analysis. A sphere about 2.5 cm in diameter is attached to a nylon line and a light frame.

SAMPLE PREPARATION AND PRETREATMENT

The test specimen is selected, pretreated for removal of organic matter, and mixed with a dispersing agent as described in Chapter 1-4.

INSTRUMENT CALIBRATION

Before each experiment, the following calibration steps are performed:

1. Clean and dry the sphere and measure its mass M_a suspended in the air (Fig. 2a).
2. Immerse the sphere in water and measure its mass M_w and the water temperature (Fig. 2b).
3. Pour 125 mL of stock solution of sodium hexametaphosphate into a 1000 mL graduate, and add distilled or demineralized water to reach the 1000 mL

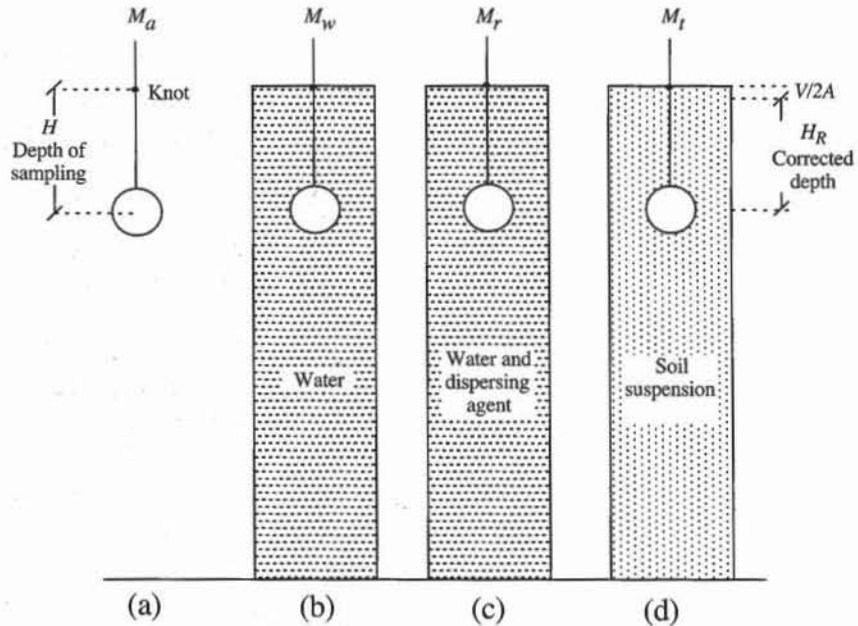


Figure 2 Measurements of mass M_a , M_w , M_r , and M_t , and definition of corrected sampling depth during the buoyancy analysis.

mark. Immerse the sphere in the graduate, and measure its mass M_r and the temperature of the dispersing agent solution (Fig. 2c). The temperature should be similar to the water temperature in step 2.

TEST PROCEDURE

After the removal of organic matter, addition of dispersing agent (see Chapter 1-4), and calibration, the test procedures consist of the following steps:

1. Follow steps 2 to 5 of the hydrometer analysis.
2. At the following times t after the beginning of sedimentation: $t = 0.5, 1, 2, 4, 15, 30, 60, 120, 240,$ and 480 minutes, slowly immerse the sphere in the soil suspension to a depth $H = 10$ cm, and measure mass M_t (Fig. 2d). The sampling depth and time series defined above should cover grain sizes ranging from 1 to $75 \mu\text{m}$. The time t and depth H of sampling are related to grain size D as follows:

$$t = \frac{30\eta H}{(G_s - 1)981\rho_w D^2} \text{ (min)} \quad (1)$$

where G_s is the specific gravity of soil particles, ρ_w the unit mass of water (g/cm^3), η the viscosity of water (g/cm/s), H the sampling depth (cm), and D the grain size (mm). There should be no air circulation around the scale to avoid fluctuation in readout.

3. After each sampling, measure the water temperature T_t , which should not vary excessively during the experiment. If T_t is largely different from the temperature at which M_a , M_w and M_r were measured then these quantities must be measured again at temperature T_t .

- After removing the sphere from the soil suspension, use a wash bottle to clean it of soil particles which may be attached to it. Then immerse the sphere in water at the same temperature as the soil suspension.

COMPUTATION

The grain size D (mm) is:

$$D = \sqrt{\frac{30\eta H_R}{(G_s - 1)981\rho_w t}} \quad (2)$$

where t is the time (min) after the beginning of sedimentation, G_s the specific gravity of soil particles, ρ_w the unit mass of water (g/cm^3) at temperature T_t , and η the viscosity of water (g/cm/s) at temperature T_t . The corrected sampling depth H_R (cm), which accounts for the rise in water level when the sphere is immersed in the suspension, is

$$H_R = H - \frac{V}{2A}, \quad V = \frac{M_a - M_w}{\rho_w}, \quad \text{and} \quad A = \frac{\pi}{4} d_c^2 \quad (3)$$

where H is the sampling depth (cm), d_c the internal diameter of the sedimentation cylinder (cm), M_w the mass of the sphere in water (g), and M_a the mass of the sphere in air (g). The volume of the sphere can also be calculated from its diameter.

The percentage p by weight of particles with diameter smaller than D is:

$$p = \frac{V_{tot}}{M_{tot}} \frac{\rho_w G_s (M_r - M_t)}{(G_s - 1)M_a - G_s M_w + M_r} \times 100 \quad (\%) \quad (4)$$

where M_{tot} is the total mass of oven-dry soil in suspension (g), V_{tot} the total volume of suspension (mL), ρ_w the unit mass of water (g/cm^3) at temperature T_t , G_s the specific gravity of soil particles, M_t the mass of sphere in suspension at time t (g), and M_w the mass of sphere in water and dispersing agent (g).

EXAMPLE

Figures 3 and 4 show the results of buoyancy analysis obtained for a silt from Los Angeles, California. The results are presented in a grain-size distribution

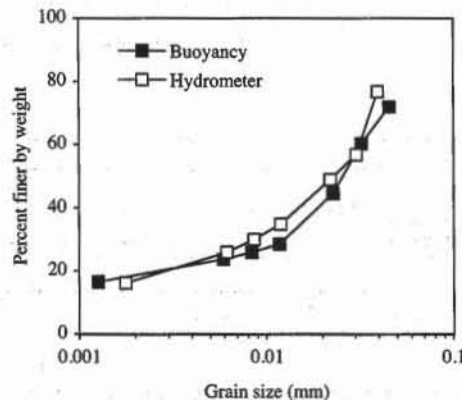


Figure 3 Comparison of results for buoyancy and hydrometer analyses on a silt from Los Angeles, California.

curve similar to that of hydrometer analyses. Figure 5 shows the formulas used in Fig. 3. Figures 3 and 6 give the results of a hydrometer analysis performed on the same material as the buoyancy analysis. Both analyses use the user-defined functions DENSI and VISCO (see Chapter 1-4). DENSI and VISCO return the water unit mass (g/cm^3) and water viscosity (g/cm/s), respectively, at temperature T ($^{\circ}\text{C}$).

	A	B	C	D	E	F
1	Buoyancy analysis					
2	Analyst name: <i>Julie Young</i>					
3	Test date: <i>10-Feb-96</i>					
4	Sample description: <i>Silt from Los Angeles, CA</i>					
5	Depth of sampling $H =$ <i>12.6</i> cm					
6	Specific gravity $G_s =$ <i>2.65</i>					
7	Total mass of soil in suspension $M_{tot} =$ <i>50</i> g					
8	Total volume of suspension $V_{tot} =$ <i>1000</i> cm^3					
9	Mass of sphere in air $M_a =$ <i>25.593</i> g					
10	Mass of sphere in water $M_w =$ <i>17.035</i> g					
11	Mass of sphere in water and dispersing agent $M_r =$ <i>17.019</i> g					
12	Diameter of sedimentation cylinder $d =$ <i>5.95</i> cm					
13	Unit mass of water and dispersing agent $r_r =$ <i>0.999</i> g/cm^3					
14	Volume of sphere $V =$ <i>8.58</i> cm^3					
15						
16						
17	Time (min)	Mass of sphere in suspension (g)	Temperature ($^{\circ}\text{C}$)	Grain size (mm)	Percent finer by weight	
18	t	M_r	T_a			
19	<i>1</i>	<i>16.827</i>	<i>24.5</i>	<i>0.046</i>	<i>71.94</i>	
20	<i>2</i>	<i>16.858</i>	<i>24.5</i>	<i>0.032</i>	<i>60.33</i>	
21	<i>4</i>	<i>16.9</i>	<i>24.5</i>	<i>0.023</i>	<i>44.59</i>	
22	<i>15</i>	<i>16.943</i>	<i>24.5</i>	<i>0.012</i>	<i>28.48</i>	
23	<i>30</i>	<i>16.95</i>	<i>24.5</i>	<i>0.008</i>	<i>25.86</i>	
24	<i>60</i>	<i>16.956</i>	<i>24.5</i>	<i>0.006</i>	<i>23.61</i>	
25	<i>1300</i>	<i>16.975</i>	<i>24.5</i>	<i>0.001</i>	<i>16.49</i>	

Figure 4 Example of data set for buoyancy analysis.

	D	E	F
13	Unit mass of water and dispersing agent $r_r = (M_a - M_r)/V$		g/cm^3
14	Volume of sphere $V = (M_a - M_w)/\text{DENSI}(24.5)$		cm^3

	D	E
17	Grain size (mm)	Percent finer by weight
18		
19	$=\text{SQRT}(30 \cdot \text{VISCO}(T_e) \cdot (H - V) / (2 \cdot \text{PI}() \cdot D^2 / 4)) / (G_s - 1) / 981 / T$	$=\text{DENSI}(T_e) \cdot G_s \cdot (M_r - M_t) / (M_a \cdot (G_s - 1) - M_w \cdot G_s + M_r) \cdot V_{tot} / M_{tot} \cdot 100$

Figure 5 Formulas used in Fig. 4.

COMPARISON OF BUOYANCY, HYDROMETER AND PIPETTE ANALYSES

The buoyancy analysis offers advantages over the hydrometer and pipette analyses. It takes less time to complete than the hydrometer analysis, and requires fewer and less complicated steps than the pipette analysis. However, like the pipette analysis and in contrast to the hydrometer analysis, the buoyancy analysis requires accurate weight measurement. As shown in Fig. 3, the buoyancy and hydrometer analyses give similar grain size distribution curves. This similarity is not surprising because both analyses are based on the same physical principle (i.e., Stokes' law), and sample preparation.

REFERENCES

See Introduction for references to ASTM procedures (pages 4 to 6).
BS 1370, 1975, *Methods of tests for soil for civil engineering purposes*, British Standards Institution, London, UK.

REVIEW QUESTIONS

1. What is the purpose of the buoyancy analysis? On which physical principle is this analysis based?
2. Does the buoyancy analysis determine exactly the size of soil particles?
3. Compare the principle and experimental procedure of the buoyancy, pipette and hydrometer analyses.
4. What is the purpose of the dispersing agent? Does its use require a correction in the buoyancy analysis?
5. Why is a constant temperature required during the sedimentation process?
6. For what reason do you agitate the suspension at the beginning of the buoyancy test?

1-7

Combined Grain Size Analysis

OBJECTIVE

A combined grain size analysis is required when neither the fraction of soil particles smaller than 75 μm nor that with particles larger than 75 μm can be neglected. A sieve analysis is performed on the fraction with particles larger than 75 μm , and a sedimentation (hydrometer, pipette, or buoyancy) analysis is performed on the fraction with particles smaller than 75 μm . The combined analysis gives a grain size distribution curve over a wide range of grain size.

EQUIPMENT

The equipment for the combined analysis is identical to that used for sedimentation and sieve analyses.

PREPARATION OF SAMPLE

The total amount of the sample should be sufficient to yield the required amounts of material for both sieve and sedimentation analyses. Samples of soils having fines with little or no plasticity are oven dried, weighed, and then separated on a No. 200 sieve. Samples of soils having plastic fines are soaked in water as explained for wet sieving (see Chapter 1-2), then washed over a No. 200 sieve.

PROCEDURE

1. Perform a sieve analysis on a representative portion of the sample, and measure the weight passing through a No. 200 sieve.
2. Perform a sedimentation (hydrometer, pipette, or buoyancy) analysis on a sample passing through a No. 200 sieve.

COMPUTATION

Combined analysis and sieve analysis have identical grain size distribution curves for particles retained in No. 200 sieves. However, for particles tested in the sedimentation analysis, the total percent by weight finer becomes:

$$p = \frac{W_{200}}{W_{\text{tot}}} p_h \quad (1)$$

where W_{200} is the weight of dry sample passing a No. 200 sieve, W_{tot} the weight of total dry sample in sieve analysis, and p_h the percent by weight finer calculated in sedimentation analysis alone. The clay fraction, which is the percent by weight finer than 2 μm , should be calculated by using the combined percent by weight finer calculation of Eq. 1.

EXAMPLE

The results of the combined analysis are presented on a grain size distribution curve similar to the one used for sieve and sedimentation analyses. As shown in Fig. 1, the curves obtained from sieve and sedimentation analyses may not connect smoothly. This offset is caused partly by the breakdown of Stokes' law for large particles in hydrometer analysis and the difficulty of wet-sieving fine particles in the presence of surficial tension in the sieve analysis. As shown in Fig. 1, both curves are joined by constructing a smooth curve between them. The data of Fig. 1 are listed in Fig. 2, and Fig. 3 shows the formulas used in Fig. 2.

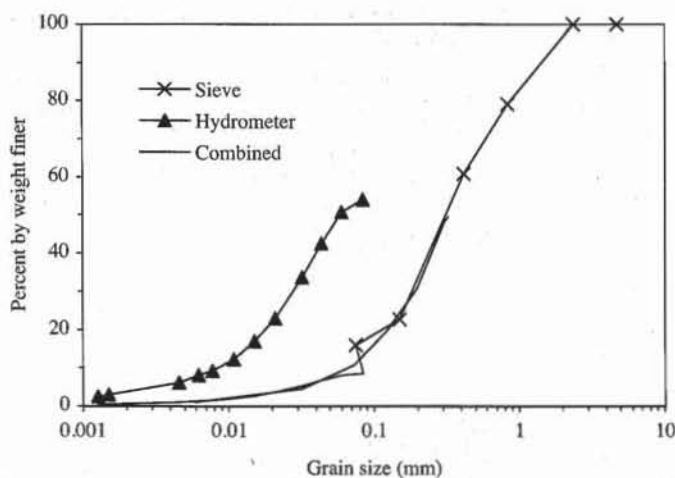


Figure 1 Grain size distribution curves from sieve and hydrometer analyses (after Lambe, 1951).

REFERENCE

See Introduction for references to ASTM procedures (pages 4 to 6).

LAMBE, T. W., 1951, *Soil Testing for Engineers*, John Wiley & Sons, New York.

	A	B	C	D	E
1	Combined analysis				
2	Analyst name: <i>T.W. Lambe</i>				
3	Test date: <i>14-Oct-49</i>				
4	Sample description: <i>Silty sand; grayish brown; well graded.</i>				
5					
6					
7		Grain size (mm)	Separate percent finer by weight	Combined percent finer by weight	
8		d	p	P _c	
9	Sieve analysis		4.760	100.00	100.00
10	Mass passing No. 200 sieve W _{N200} (g) = 67.6		2.380	100.00	100.00
11	Total sample mass W _{tot} (g) = 424.7		0.840	79.16	79.16
12			0.420	60.81	60.81
13			0.150	22.75	22.75
14			0.075	15.92	15.92
15	Hydrometer analysis		0.0845	53.97	8.59
16			0.0604	50.74	8.08
17			0.0440	42.45	6.76
18			0.0321	33.56	5.34
19			0.0210	22.84	3.64
20			0.0151	16.98	2.70
21			0.0108	12.13	1.93
22			0.0077	9.30	1.48
23			0.0062	8.09	1.29
24			0.0046	6.06	0.97
25			0.0015	2.99	0.48
26			0.0013	2.43	0.39
27	Clay fraction (%) = 0.5				

Figure 2 Example of data set for combined analysis (after Lambe, 1951).

	E
7	Combined percent finer by weight
8	P _c
9	=p
10	=p
11	=p
12	=p
13	=p
14	=p
15	=p*WN200/Wtot
16	=p*WN200/Wtot
17	=p*WN200/Wtot

	D	E
27	Clay fraction (%) = =INTER(0.002,d,pc)	

Figure 3 Formulas used in Fig. 2.

REVIEW QUESTIONS

1. What is the purpose of a combined grain size analysis? On what type of soils do you need to carry out a combined grain size analysis?
2. Is it possible for the grain size distribution curves of sieve and sedimentation analyses to overlap?

2

Plasticity, Shrinkage, and Soil Classification

- 2-1** Principles of liquid and plastic limits tests
- 2-2** Determination of water content
- 2-3** Liquid limit test
- 2-4** One-point liquid limit test
- 2-5** Plastic limit test
- 2-6** Principles of shrinkage limit analysis
- 2-7** Shrinkage limit analysis with mercury
- 2-8** Shrinkage limit analysis with wax
- 2-9** Engineering classification of soils

2-1

Principles of Liquid and Plastic Limits Tests

The engineering behavior of fine-grained soils depends on factors other than particle size distribution. It is influenced primarily by their mineral and structural composition and the amount of water they contain, which is referred to as *water content* (or *moisture content*). The liquid and plastic limits tests characterize the effects of water content on fine-grained soils and help to classify fine-grained soils and to assess their mineral composition and engineering properties.

WATER CONTENT

Soils are made of solid particles with voids between. These voids are generally filled with air and water. The water content w of a soil is

$$w = \frac{W_w}{W_s} \times 100 \quad (\%) \quad (1)$$

where W_w is the weight of water removed from the soil by oven drying at 105° to 110°C and W_s is the weight of the dried soil. A soil is considered to be dry when its mass does not change by oven drying, which may usually require about 12 to 24 h.

Oven drying removes the water completely from soils without clay particles, but partially from soils with clay particles. Clay particles are made of clay minerals and have plate-like shapes smaller than 2 μm . Table 1 lists four common clay minerals and typical values of their specific surfaces. Kaolinite, the largest clay mineral, has a thickness or edge dimension of about 1 μm , while montmorillonite, one of the smallest clay minerals, has a thickness of only a few nanometers.

The clay minerals relate to water in several complex ways, which give three main categories of water around a clay particle as shown in Fig. 1:

1. Adsorbed water, held on the particle surface by powerful electrical forces and virtually in a solid state. This layer is about two water molecules thick

TABLE 1

Average values of relative sizes, thicknesses, and specific surfaces of four common clay minerals (after Yong and Warkentin, 1975).

Clay mineral	Typical thickness (μm)	Typical diameter (μm)	Specific surface (m ² /g)
Montmorillonite	0.003	0.1–1	800
Illite and Chlorite	0.03	10	80
Kaolinite	0.05–2	0.3–4	15

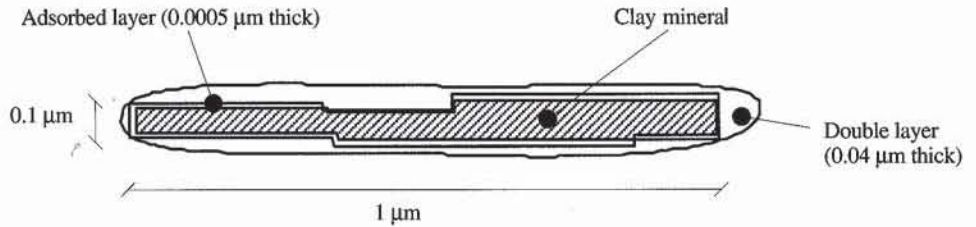


Figure 1 Schematic side-view representation of a typical particle of kaolinite, with its adsorbed layer and double layer.

(i.e., 0.0005 μm). The adsorbed water cannot be removed by oven drying at 110°C and is considered to be part of the soil particles.

2. Chemically combined water, in the form of water of hydration within the crystal structure. This layer is referred to as the *double layer*. Its thickness varies with clay minerals, type, and concentration of ions in the water, and other factors (Yeung, 1992). As shown in Fig. 1, the double layer is about 0.04 μm thick for a kaolinite clay particle. Except for gypsum and some tropical clays, this water is not generally removable by oven drying.
3. Interstitial water, not so tightly held as chemically combined and adsorbed waters. It can be removed by drainage, air drying, or oven drying.

LIQUID AND PLASTIC LIMITS

The mechanical properties of a clay are altered by changing the water content. A clay softens when water is added, and with sufficient water, forms a slurry that behaves as a viscous liquid; this is known as the *liquid state*. If the water content is gradually reduced by drying it slowly, the clay eventually begins to hold together and to offer some resistance to deformation; this is the *plastic state*. With further loss of water, the clay shrinks and its stiffness increases until it becomes brittle; this is the *semisolid state*. As drying continues, the clay continues to shrink until it reaches a constant minimum volume. Beyond that point, further drying causes no further decrease in volume; this is the *solid state*. These four states are shown in Fig. 2. The change from one state to the next is not abrupt, but gradual.

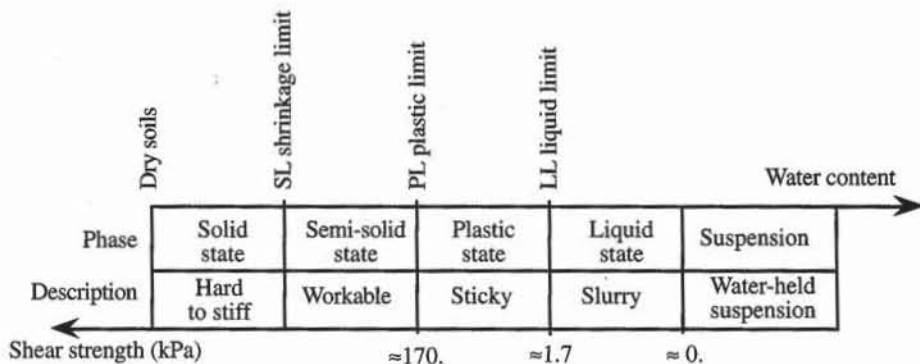


Figure 2 Variation of consistency of fine-grained soils with water content.

These smooth transitions are empirically defined by introducing the liquid limit LL , plastic limit PL , and shrinkage limit SL . The moisture content between PL and LL is the plasticity index PI :

$$PI = LL - PL \quad (2)$$

PI is a measure of the plasticity of a clay.

The liquid and plastic limit tests provide a means of measuring and describing the plasticity range of clay soils. Liquid and plastic limits are also referred to as *Atterberg limits*, after the Swedish scientist A. Atterberg, who first defined them for the classification of agricultural soils in 1911. Originally, the limits were determined by simple tests using an evaporating dish (Bauer, 1959). The procedures were defined more precisely for engineering purposes by Casagrande (1932). The mechanical device he designed for determining the liquid limit is still known as the Casagrande apparatus (Casagrande, 1958). A cone penetrometer apparatus can also be used instead of the *Casagrande apparatus*, but we will not describe this technique.

PLASTICITY CHART

Sedimentation tests (e.g., hydrometer tests) give the clay fraction but unfortunately, no information about the type of clay. Clay particles are too small to be examined visually except by using an electron microscope. The identification of clay minerals in soils with x-ray diffraction would also be too lengthy and expensive for engineering practices. The liquid and plastic limit tests are two basic engineering experiments that enable the classification of clay soils and assessment of their probable types of clay minerals.

Fine-grained soils are usually classified by using the plasticity chart. The plasticity chart is a graphical plot of the liquid limit LL against the plasticity index PI . The standard plasticity chart is shown in Fig. 3. When the values of LL and PI for inorganic clays are plotted on this chart, most of the points lie just above the line marked *A-line* and in a narrow band parallel to it. The *A-line* is defined by the relationship

$$PI = 0.73 (LL - 20) \quad (3)$$

where PI and LL are in percent. The *A-line* is a reference line derived from experimental observations. It does not represent a well-defined boundary between

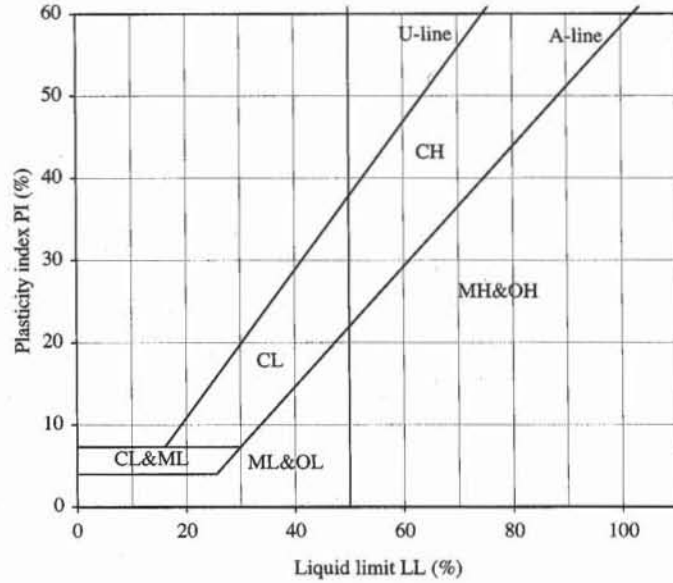


Figure 3 Plasticity chart.

soil types. The *U-line* of Fig. 3 is a tentative upper limit for all soils, which was also drawn from experimental data. The *U-line* has the equation

$$PI = 0.9 (LL - 8) \tag{4}$$

Table 2 provides us with a few examples of liquid limits, plastic limits and plastic indexes for various clay minerals and soils. The data points of Table 1 are plotted by using two different scales in Figs. 4 and 5. Most points are lined up along the *A-line*.

Based on a compilation of experimental results on the Atterberg limits of various clay minerals, Holtz and Kovacs (1981) observed that the clay minerals can be determined by using the Atterberg limits and the plasticity chart (see Fig. 6). As shown in Figs. 4 and 5, montmorillonites are very high on the chart, close to the *U-line*, whereas illites and kaolinites are close to the *A-line*.

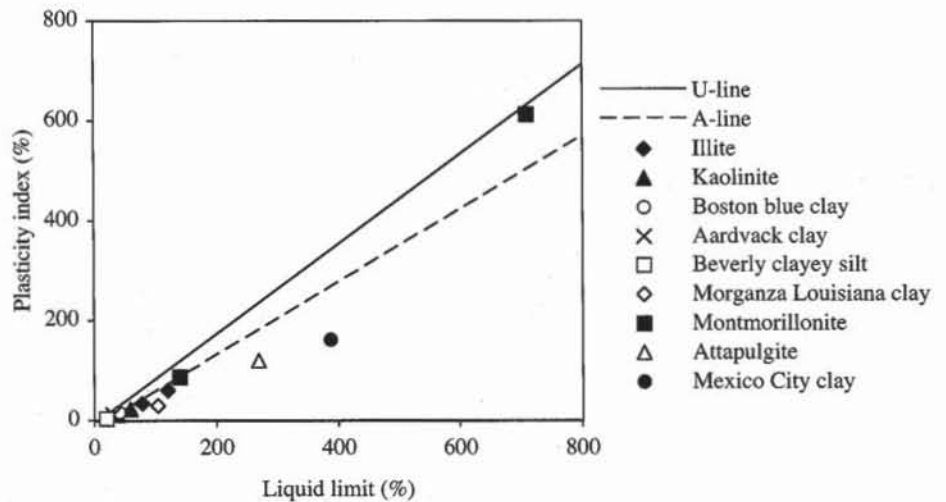


Figure 4 Representation of various clay minerals and natural soils on the plasticity chart (0 < LL < 800%).

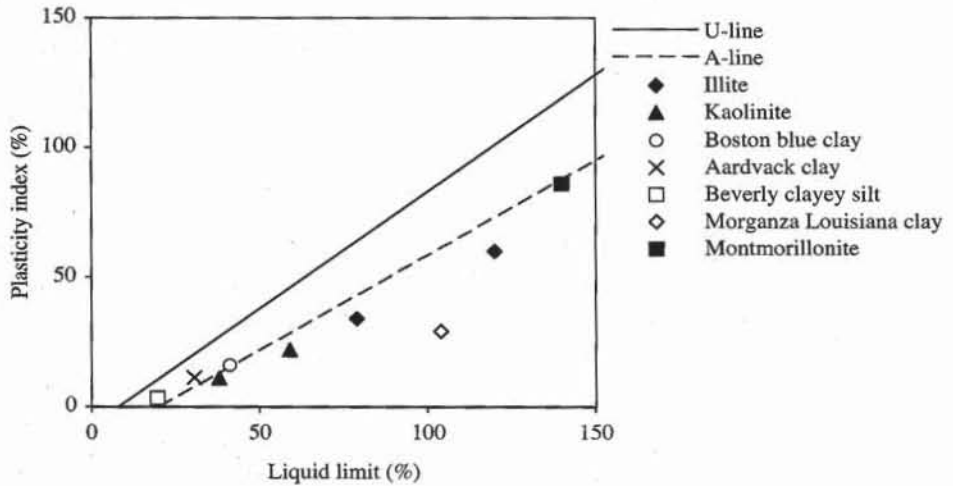


Figure 5 Representation of various clay minerals and natural soils on the plasticity chart ($0 < LL < 200\%$).

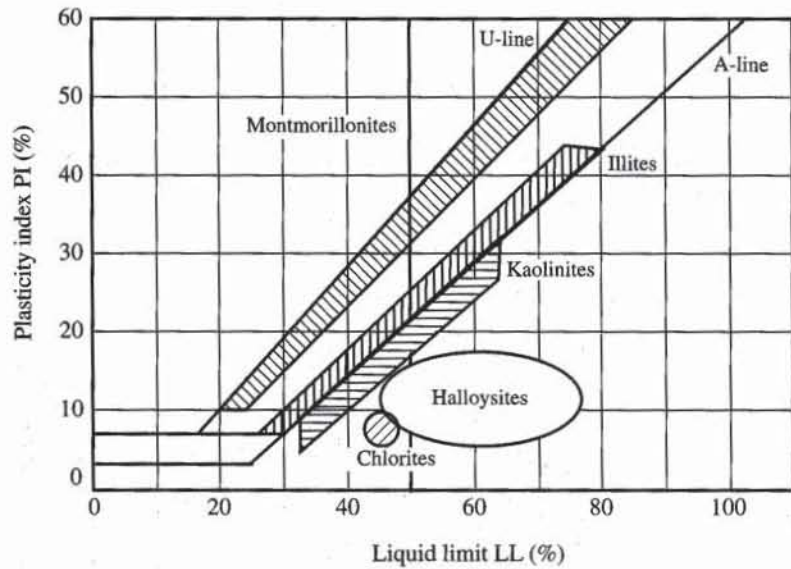


Figure 6 Location of common clay minerals on the plasticity chart (after Holtz and Kovacs, 1981).

CONSISTENCY OF CLAYS

The state of a clay cannot be defined solely by its water content. Two different clays with identical water content may exhibit quite different characteristics. It is therefore preferable to characterize the state of a clay by the liquidity index *LI*, which relates its water content to its liquid and plastic limits as follows:

$$LI = \frac{w - PL}{LL - PL} = \frac{w - PL}{PI} \tag{5}$$

LI provides us with a normalized representation of water content in relation to the plasticity range. Below the plastic range (i.e., $w \leq PL$), *LI* is negative. At the liquid limit (i.e., $LI = 1$), a slowly drying slurry first begins to show a small but

TABLE 2

Typical ranges of index properties of some common clay minerals and natural soils (after Lambe and Whitman, 1979; and Lambe, 1951).

Mineral	Exchangeable ion	Liquid limit (%)	Plastic limit (%)	Plastic index (%)
Montmorillonite	Na	710	54	656
	K	660	98	562
	Ca	510	81	429
	Mg	410	60	350
	Fe	290	75	215
Illite	Na	120	53	67
	K	120	60	60
	Ca	100	45	55
	Mg	95	46	49
	Fe	110	49	61
Kaolinite	Na	53	32	21
	K	49	29	20
	Ca	38	27	11
	Mg	54	31	23
	Fe	59	37	22
Attapulgite	H	270	150	120
Mexico City clay		388	226	162
Boston blue clay (illite)		41	25	16
Aardvack clay		30.6	19.6	11
Morganza Louisiana clay		104	74.8	29.2
Beverly clayey silt (illite)		19.5	16.3	3.2

definite shear strength. As the moisture content decreases and LI approaches zero, the shear strength increases considerably, and at the plastic limit ($LI = 0$) the shear strength may be 100 times greater than at the liquid limit LL .

ACTIVITY OF CLAYS

The Atterberg limits are related to the combined effects of particle size and mineral composition. In Fig. 7, Skempton (1953) showed that the plasticity index depends on the clay fraction—percent by weight of particles finer than $2 \mu\text{m}$ —and that the plasticity index/clay fraction ratio was constant for a given clay mineral.

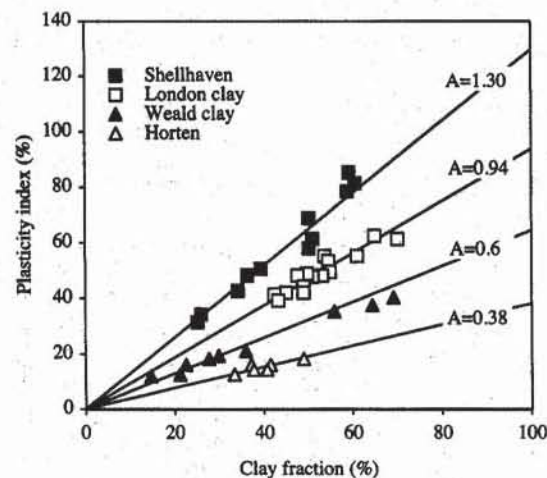


Figure 7 Relation between plasticity index and clay fraction (after Skempton, 1953).

The slope of the linear relationship between PI and the clay fraction of a particular clay is called the activity A :

$$A = \frac{PI(\%)}{\text{clay fraction}(\%)} \quad (6)$$

On the basis of their A values, clays can be classified into the four groups of Table 3. Approximate values of A for some clay minerals are listed in Table 4. Montmorillonites are highly active because they have very small particles and large plasticity indices.

TABLE 3
Activity of clays

Description	Activity
Inactive	< 0.75
Normal	0.75–1.25
Active	1.25–2.
Highly active	> 2
(e.g., bentonite)	6 or more

TABLE 4
Activity of various minerals
(after Skempton, 1953; and Mitchell, 1993)

Mineral	Activity
Na-montmorillonite	4–7
Ca-montmorillonite	1.5
Illite	0.5–1.3
Kaolinite	0.3–0.5
Halloysite (dehydrated)	0.5
Halloysite (hydrated)	0.1
Attapulgite	0.5–1.2
Allophane	0.5–1.2
Mica (muscovite)	0.2
Calcite	0.2
Quartz	0.

REFERENCES

- BAUER, E. E., 1959, History and development of the Atterberg limit tests, ASTM STP 254, American Society for Testing and Materials, pp. 160–167.
- CASAGRANDE, A., 1932, Research on the Atterberg limits of soils, *Public Roads*, Vol. 8, pp. 121–136.
- CASAGRANDE, A., 1958, Notes on the design of the liquid limit device, *Géotechnique*, Vol. 8, pp. 84–91.
- HOLTZ, R. D., and W. D., KOVACS, 1981, *An Introduction to Geotechnical Engineering*, Prentice Hall, Englewood Cliffs, NJ, 733 pp.
- LAMBE, T. W., 1951, *Soil Testing for Engineers*, John Wiley & Sons, New York, 165 pp.
- LAMBE, T. W. and R. V. WHITMAN, 1979, *Soil Mechanics, SI Version*, John Wiley & Sons, New York, 553 pp.
- MITCHELL, J. K., 1993, *Fundamentals of Soil Behavior*, Second Edition, John Wiley & Sons, New York.
- SKEMPTON, A. W., 1953, The colloidal activity of clays, *Proceedings of the Third*

International Conference on Soil Mechanics and Foundation Engineering, Vol. 1, pp. 57–61.

YEUNG, A. T., 1992, Diffuse double layer equations in SI units," *Journal of Geotechnical Engineering, ASCE*, Vol. 118, No 12, pp. 2000–2005.

YONG, R. N., and B. P. WARKENTIN, 1975, *Soil Properties, and Behavior*, Elsevier Scientific Publishing Co., New York, 449 p.

REVIEW QUESTIONS

1. Why do we use Atterberg limits to characterize fine-grained soils? Why is the result of the hydrometer analysis insufficient for this purpose?
2. Define water content? Give an example of a maximum value for the water content in soils.
3. How many categories of water can we distinguish around clay particles? Can you name these categories?
4. What are the definitions of liquid and plastic limits? Are these definitions based on theoretical or empirical concepts?
5. Does the shear strength increase or decrease with water content in fine-grained soils?
6. Is it possible for a soil to have a liquid limit and a plasticity index both equal to 30%? Why?
7. Define *activity of clays*. What is it used for?
8. Is it meaningful to define the activity of a sand?
9. Define *clay fraction*.
10. A sample of wet clay and its container weigh 102 g. After oven drying, the sample and the container weigh 60 g. What is the water content?
11. It is possible for a sample of clay to have a water content equal to 700%? Can you give an example?
12. Which clay mineral has the largest activity? Why is it so active?

EXERCISES

1. Calculate the activity of the clay from the following test results.

Soils	Clay fraction (%)	Plasticity index (%)
Shellhaven	59.3	85.2
	60.6	81.3
	58.9	78.4
	50.2	68.8
	51.1	61.4
	50.2	58.0
	39.4	50.6
	36.4	48.3
	34.2	42.6
	26.0	34.1
	25.1	31.3

Soils	Clay fraction (%)	Plasticity index (%)
London clay	70.1	61.4
	64.9	62.5
	61.0	55.1
	53.7	55.1
	54.5	53.4
	55.0	49.4
	53.2	48.3
	51.1	47.7
	49.8	48.9
	47.6	48.3
	48.9	44.3
	48.9	42.0
	45.0	42.0
	42.4	41.5
43.3	39.2	
41.1	37.5	

2. Calculate the activity of the clay from the following test results.

Soils	Clay fraction (%)	Plasticity index (%)
Weald clay	69.3	40.3
	64.5	37.5
	55.8	35.2
	35.9	21.0
	29.9	19.3
	27.7	18.2
	22.5	15.9
	21.2	12.5
	14.7	11.9

Soils	Clay fraction (%)	Plasticity index (%)
Horten	48.9	18.2
	41.6	15.9
	40.7	14.2
	37.2	15.9
	37.7	14.2
	33.3	12.5

2-2

Determination of Water Content

DEFINITION

By definition, water content, w , is the ratio of the weight of water in a given soil mass to the weight of solid particles. The standard and recommended method for determining the water content of soils is the oven-drying method with a drying temperature of 105° to 110°C. Alternative methods include the sand bath method, the carbide method, and the alcohol method. Detailed instructions on these alternative procedures are given by Head (1984).

EQUIPMENT

The equipment for determining water content includes:

- Thermostatically controlled drying oven, capable of maintaining a temperature of 105° to 110° C. A microwave oven may be used for fast and approximate determination of water content (see ASTM D6643).
- Balance accurate to 0.2% of the sample weight.
- Small metal containers with lids. Containers and lids should be as light as practicable in relation to the amount of material. They should be washed clean and dried thoroughly before use.

PROCEDURE

1. Clean, dry, and weigh the container and its lid. Make sure that both have the same labels.

2. Select the test sample to be representative of the soil from which it is taken. It is recommended to determine two or three separate moisture contents and to average them. However, if only a very small quantity of soil is available, it is better to use it all for one measurement. It is recommended to select the approximate mass of the specimen depending on soil types as follows:

Soil type	Mass
Homogeneous clay and silts	30 g
Medium-grained soils	300 g
Coarse-grained soils	3 kg

3. Place the specimen in the container and immediately determine the weight of the container, lid, and wet soil. Each sample should be weighed as soon as possible. If weighing is delayed, the lid must be fitted tightly to avoid loss of water by evaporation.

4. Before placing the specimen in the oven, remove the lid and place it under or next to the container in the oven. Leave the specimen in the oven until it has dried to reach a constant weight. The time required for drying will vary depending on the type of soil, size of specimen, and type of oven. It takes a few minutes in the microwave oven but can take several hours in a standard oven.

5. When the specimen is estimated to be dry, remove its container from the oven and close it with its lid. Allow the container to cool until it can be handled comfortably with bare hands, then determine its dry weight. If the specimen is not weighed immediately after cooling, it must be placed in the oven again to remove the moisture that it has absorbed from the atmosphere.

COMPUTATION

The water content w is calculated as follows:

$$w = \frac{W_w - W_d}{W_d - W_c} \times 100 \quad (\%) \quad (1)$$

where W_c is the weight of the container, W_w the weight of the container and wet soil, and W_d the weight of the container and dry soil. If two or three separate measurements have been made on the same soil specimen, the average value of w is then calculated.

REFERENCES

See Introduction for references to ASTM procedures (pages 4 to 6).

HEAD, K. H., *Manual of Soil Laboratory Testing*, Pentech Press, London, 1984.

REVIEW QUESTIONS

1. Why is it not recommended to leave an oven-dried sample in the open air for a long time before measuring its dry weight?
2. Excluding oven drying, are there other methods to determine the water content of soils?
3. Is it possible to measure the water content of sands?
4. Why do we use a fixed temperature range to dry soils? What is the effect on soils of microwave drying?
5. What is the function of the container lid when determining the water content of a soil?

2-3 Liquid Limit Test

OBJECTIVE

The liquid limit test determines the liquid limit of a soil. By convention, the liquid limit is defined as the water content at which the groove cut into the soil pat in the standard liquid limit device requires 25 blows to close along a distance of 13 mm.

EQUIPMENT

The equipment for the liquid limit test includes:

- Mechanical device shown in Fig. 1. The cup must fall freely from a height equal to 10 ± 0.2 mm above the base. The material and construction must conform to ASTM D4318-93.
- Grooving tool as illustrated in Fig. 2. The V-groove profile must not differ more than 0.25mm from those specified in Fig. 2. The gage for checking the height of drop of the cup is to be 10 ± 0.2 mm.

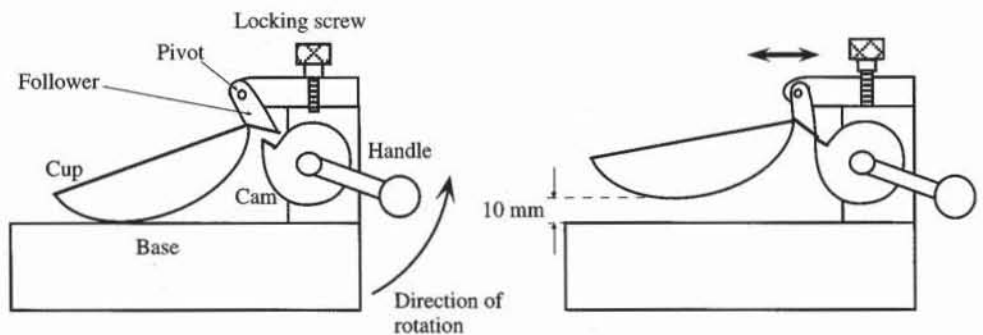


Figure 1 Side-view of Casagrande apparatus.

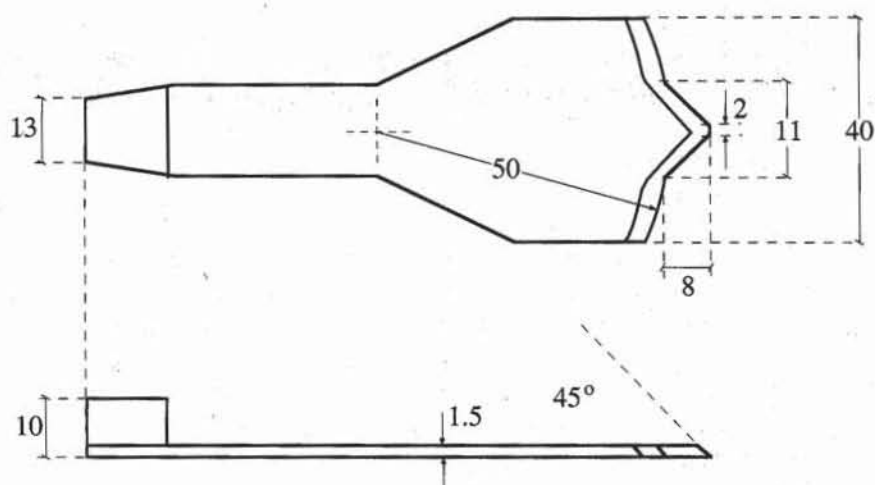


Figure 2 Grooving tool for Casagrande apparatus (dimensions in mm).

- Spatula, with a blade about 10 cm long and about 2 cm wide.
- Mixing dish or bowl.
- Specimen containers. Metal containers with lids are recommended. The containers should be resistant to corrosion. Containers approximately 2 cm high by 5 cm in diameter are adequate.
- Balance, sensitive to 0.01 g.
- Drying oven.
- Sieve, U.S. Standard No. 40 (0.42 mm).

PROCEDURE

1. The liquid limit device must first be calibrated. Its bowl must be clean, dry, and oil-free. The height of drop is checked by using the spacer gage on the grooving tool handle (see Fig. 2). This 10-mm-thick steel block should just pass between cup and base when the cup is at its maximum height (see Fig. 1). The locknut is tightened after adjustment and the maximum height rechecked with the gage.
2. Whenever possible, the soil used for Atterberg limits tests should not be dried prior to testing. Oven-drying alters the index properties of soils, especially of organic clays. The test material should be free from coarse particles (e.g., larger than 425 μm). If sieving is required, the soil may be air dried before testing. About 250 g of dry soil is needed for both the liquid and plastic limit tests. An essential step in the sample preparation is thorough mixing of the soil with water. Natural or distilled water is preferable to tap water, to avoid ion exchange between soil and water impurities, which may affect the soil plasticity. Water and soil are mixed on a glass plate by using a spatula until the mixture is uniform and behaves as a soft paste that can be shaped with a spatula.
3. Place 50 to 80 g of the specimen in the bowl and level it off to a depth of approximately 1 cm. The surface of the soil paste should be smoothed off level and parallel to the base, giving a depth at the greatest thickness of 10 mm (Fig. 3).

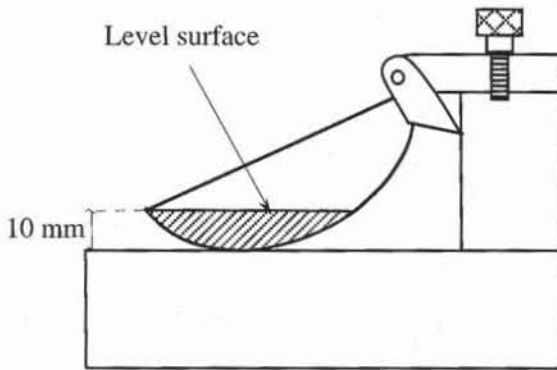


Figure 3 Soil placed in a Casagrande bowl.

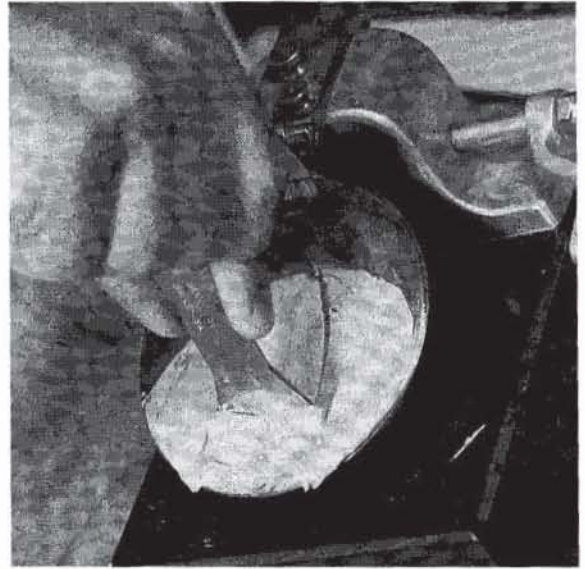


Figure 4 A groove is cut through the sample from back to front.

4. As shown in Fig. 4, a groove is cut through the sample from back to front, dividing it into two equal halves. Starting near the hinge, draw the grooving tool toward the front in a continuous movement with a circular motion, keeping the tool normal to the cup surface and its chamfered edge in the direction of movement. The tip of the tool should scrape the bowl lightly. The completed groove must be clean and sharp.
5. Turn the crank handle at a steady rate of two revolutions per second, so that the bowl is lifted and dropped. Continue turning until the two halves of the soil pat come in contact at the bottom of the groove along a distance of 13 mm, as shown in Fig. 5. During the test, the soil should slump and flow plastically in the bowl. It should not slide on the bowl surface. Record the number of blows required to close the groove.
6. Remove 5 to 10 g of soil from the sample and use it to determine the water content of the complete specimen.
7. Repeat the run. Transfer the soil remaining in the cup to the mixing dish, and repeat steps 3 to 6 for three additional specimens with various water contents. The water content can be lowered by drying the specimen through continued mixing with a spatula and a hair dryer. It is recommended that the water content be adjusted to obtain two specimens between 15 and 25 blows, and two others between 25 and 35 blows. Material left over in the mixing dish should be preserved for the plastic limit test.

COMPUTATION

The water content w_i corresponding to the blow counts N_i is calculated as in Chapter 2-2. The line passing through n data points $(\log N_i, w_i)$ is determined by linear regression,

$$w = A \log N + B \quad (1)$$

where the slope A and intercept B are

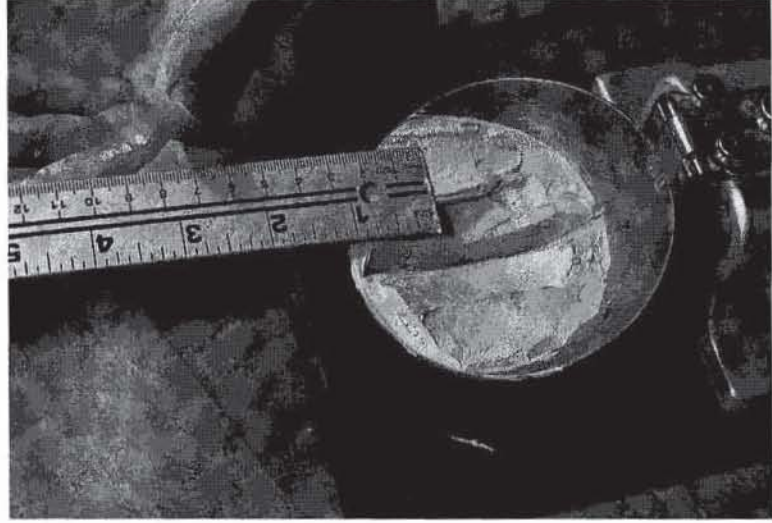


Figure 5 For the liquid limit, the groove is assumed to be closed when the two soil parts come in contact along a distance of 13 mm.

$$A = \frac{n \sum_{i=1}^n w_i \log N_i - \sum_{i=1}^n w_i \sum_{i=1}^n \log N_i}{n \sum_{i=1}^n (\log N_i)^2 - \left(\sum_{i=1}^n \log N_i \right)^2},$$

and

$$B = \frac{\sum_{i=1}^n w_i \sum_{i=1}^n (\log N_i)^2 - \sum_{i=1}^n \log N_i \sum_{i=1}^n w_i \log N_i}{n \sum_{i=1}^n (\log N_i)^2 - \left(\sum_{i=1}^n \log N_i \right)^2} \quad (2)$$

The liquid limit corresponds to $N = 25$ on the line $w = A \log N + B$

$$LL = A \log(25) + B \quad (3)$$

EXAMPLE

As shown in Figs. 6 to 8, four different specimens of a particular clay were used to find the liquid limit. In Fig. 6 the logarithmic horizontal axis represents the number of blows N_i , and the vertical axis represents the corresponding moisture content w_i . In Fig. 6, the straight line drawn through the experimental points was defined by using a linear regression on four data points $(\log N_i, w_i)$. All the formulas used in Fig. 7 are listed in Fig. 8. The liquid limit is calculated by using Eq. 3 calibrated with the coefficients A and B found by linear regression.

Figure 9 shows additional examples of results for the liquid limit tests on several clays (data after Casagrande, 1932). The points (N, w) are lined up along straight lines, even for a wide range of N values.

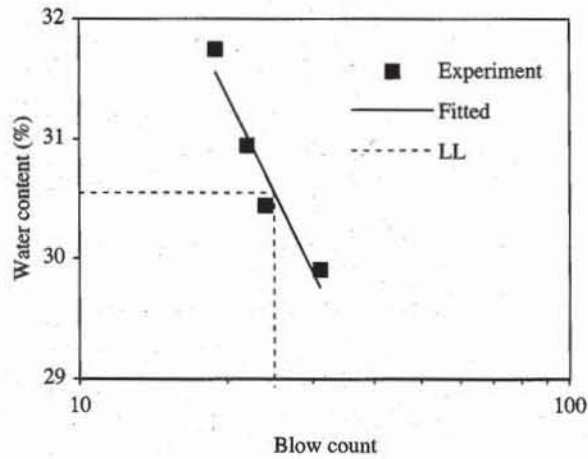


Figure 6 Example of linear regression for finding the flow line.

	A	B	C	D	E	F	G
1	Liquid limit						
2	Analyst name: <i>Henry T. Guapo</i>						
3	Test date: <i>20-Feb-94</i>						
4	Sample description: <i>Aardvark modeling clay</i>						
5							
6	Set number	Tare mass (g)	Tare with wet soil (g)	Tare with dry soil (g)	Blow count	Water content (%)	Water content fitted (%)
7		W_c	W_w	W_d	N	w	
8	1	47.72	59.89	57.05	24	30.44	30.70
9	2	43.21	59.76	55.95	31	29.91	29.76
10	3	45.17	61.25	57.45	22	30.94	31.02
11	4	45.81	58.26	55.26	19	31.75	31.56
12	Liquid limit (%) = 30.55						
13	Slope of flow line = 0.119						

Figure 7 Example of data set for liquid limit test.

	F	G
6	Water content (%)	Water content fitted (%)
7	w	
8	$=100*(Ww-Wd)/(Wd-Wc)$	$=TREND(w,LOG10(N),LOG10(E8))$
9	$=100*(Ww-Wd)/(Wd-Wc)$	$=TREND(w,LOG10(N),LOG10(E9))$

	B	C
12	Liquid limit (%) = $=TREND(w,LOG10(N),LOG10(\{25\}))$	
13	Slope of flow line = $=-SLOPE(LOG(w),LOG(N))$	

Figure 8 Formulas used in Fig. 7.

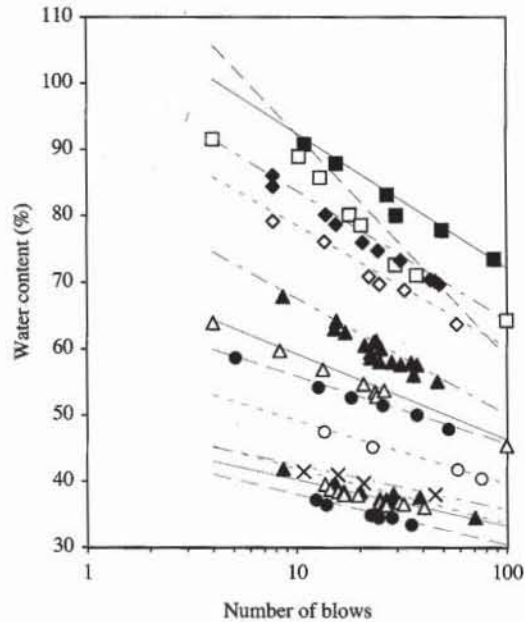


Figure 9 Additional examples of results for liquid limit tests on several clays (data after Casagrande, 1932).

REFERENCES

See Introduction for references to ASTM procedures (pages 4 to 6).

CASAGRANDE, A., 1932, Research on the Atterberg limits of soils," *Public Roads*, Vol. 8, pp. 121-136.

REVIEW QUESTIONS

1. What is the purpose of the liquid limit test?
2. How do you define *liquid limit*?
3. Why do you use a special cup and cranking device to determine the liquid limit? Why not use another shape for the cup?
4. Should you add or remove water to obtain a lower blow count?
5. What is the minimum number of data points required to determine the liquid limit?
6. What is the purpose of calibration of the Atterberg device?
7. Under what conditions would you use seawater to moisten a clay sample?
8. Is there a typical value for the liquid limit for clean fine sand? Justify your answer.

EXERCISE

1. Determine the liquid limit from the following experimental results.

Set number	Tare mass (g)	Tare with wet soil (g)	Tare with dry soil (g)	Blow count
1	47.11	73.87	67.86	34
2	47.11	82.44	73.86	29
3	47.07	75.70	69.09	20
4	47.07	76.99	69.41	14

2-4

One-point Liquid Limit Test

OBJECTIVE

The one-point liquid limit test is a quick means of determining the liquid limit of a soil. It requires one moisture content measurement instead of four measurements as in the standard liquid limit test in Chapter 2-3. However, the one-point liquid limit test is likely to be less reliable than the standard liquid limit test.

DEFINITION

In the test results of Fig. 1 obtained for various types of soil, the points ($\log N$, $\log w$) are lined up along parallel straight lines having a constant inclination. These straight lines are called flow lines. Therefore, $\log(w)$ and $\log(N)$ are related through

$$\log(w) = A' \log(N) + B'' \quad (1)$$

where A' is the constant slope of flow lines. Because Eq. 1 applies to point (25, LL);

$$\log(w) - A' \log(N) = \log(LL) - A' \log(25) \quad (2)$$

one obtains the following relation between liquid limit LL , water content w , and number of blows N :

$$LL = w \left(\frac{N}{25} \right)^{A'} \quad (3)$$

For most soils, A' was found approximately equal to 0.104. Therefore, LL can be determined by using Eq. 3 for only one point (N, w). This is the shortcut used by the one-point limit test. As shown in Table 1, the liquid limits calculated by using Eq. 3 and $A' = 0.104$ are generally close to those determined with the standard liquid limit test.

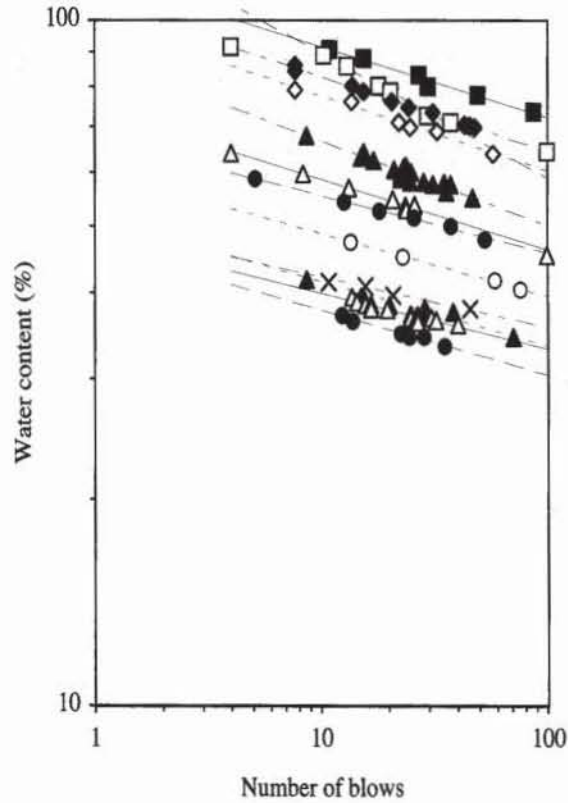


Figure 1 Examples of $\log(N) - \log(w)$ curves (data after Casagrande, 1932).

TABLE 1

Measured liquid limits, calculated one-point liquid limits, and slope of flow lines for several clays (data after Casagrande, 1932)

Set	Liquid limit (%)	One point liquid limit (%)	Slope of flow line	Error (%)
1	83.4	83.6	0.103	0.2
2	75.9	76.9	0.182	1.4
3	75.0	76.2	0.110	1.6
4	70.3	70.1	0.110	0.4
5	59.5	60.7	0.123	2.0
6	53.3	53.2	0.102	0.1
7	51.4	49.7	0.084	3.3
8	45.0	44.5	0.091	0.9
9	39.4	38.0	0.073	3.7
10	38.2	38.9	0.093	1.8
11	37.1	37.1	0.080	0.0
12	34.6	34.5	0.094	0.3

EQUIPMENT AND PREPARATION OF SAMPLE

The equipment and sample preparation are the same as for the standard liquid limit test, except for the soil sample, which is prepared slightly more plastic.

PROCEDURE

Same as for the standard liquid limit test in Chapter 2-3. The number of blows should be between 20 and 30.

COMPUTATION

The liquid limit is calculated using Eq. 3 and $A' = 0.104$. A liquid limit value should be computed for two trials of water content determination, and the average of the two is taken as the final liquid limit. The test is considered valid when the difference between the two liquid limit values is less than 2% of their average.

REFERENCE

CASAGRANDE, A., 1932, Research on the Atterberg limits of soils, *Public Roads*, Vol. 8, pp. 121-136.

REVIEW QUESTION

1. What is the purpose of the one-point liquid limit test? What is the main difference between the one-point liquid limit test and the usual liquid limit test?

EXERCISES

1. Verify Eq. 1 from the results of your standard liquid limit tests and calculate the slope of the flow line.
2. Verify Eq. 3 for the following results of standard liquid limit tests. Calculate the slope of the flow line. Compare the liquid limits calculated by the four-point and one-point methods.

Set number	Number of blows	Water content (%)	Set number	Number of blows	Water content (%)
1	11	90.8	6	8	59.7
	16	87.9		13	56.8
	27	83.2		21	54.7
	30	80.0		24	53.4
	49	77.8		24	52.8
	87	73.4		26	53.6
2	10	88.9	7	5	58.6
	13	85.7		13	54.2
	18	80.1		18	52.6
	20	78.6		26	51.4
	30	72.6		37	49.9
	37	71.0		53	47.8
3	8	86.1	8	14	47.5
	8	84.4		23	45.1
	14	80.1		59	41.7
	16	78.7		76	40.4
	21	76.0			
	25	74.7			
	31	73.2			
	43	70.4			
	46	70.2			
48	69.6				

3. For the following test results, compare the liquid limits calculated by the four-point and one point methods.

Set number	Number of blows	Water content (%)
4	8	79.2
	14	76.1
	22	70.9
	25	69.6
	33	68.8
	58	63.7
5	9	67.8
	16	64.1
	15	63.0
	17	62.4
	24	61.1
	23	60.9
	21	60.4
	25	60.0
	23	59.4
	23	58.6
	25	58.1
	29	57.9
	31	57.5
	35	57.8
	37	57.5
36	56.0	
47	55.0	

Set number	Number of blows	Water content (%)
9	11	41.4
	16	40.9
	21	39.7
	46	37.9
10	10	43.0
	9	41.8
	15	39.5
	16	39.2
	20	38.4
	29	38.1
	29	37.3
	38	37.5
71	34.5	

Set number	Number of blows	Water content (%)
11	14	39.5
	14	38.8
	16	38.5
	17	38.5
	17	37.9
	20	37.8
	25	37.2
	25	36.8
	27	37.1
	26	36.8
	27	36.4
	27	36.3
	31	36.8
	32	36.5
	40	36.0
12	12	37.1
	14	36.4
	23	34.9
	24	34.9
	25	34.5
	29	34.5
35	33.4	

2-5 Plastic Limit Test

OBJECTIVE

The plastic limit test is used to determine the lowest moisture content at which the soil behaves plastically. It is carried out only on the soil fraction passing No. 40 sieve (425 μm) and is usually performed in conjunction with the liquid limit test. By convention, the plastic limit of a soil is defined as the water content at which the soil begins to crumble when rolled into a thread 3 mm in diameter.

EQUIPMENT

The equipment for the plastic limit test includes:

- Surface for rolling the thread, such as a glass or plastic plate or smooth linoleum tabletop.
- Short metal rod of 3 mm diameter.
- Spatula with a blade about 10 cm long and about 2 cm wide.
- Specimen containers for determination of water content (see Chapter 2-3).
- Balance sensitive to 0.01 g.
- Hair dryer.
- Drying oven.

PROCEDURE

1. About 20 g of soil is prepared as for the liquid limit test. The sample may be obtained by air drying and sieving through a No. 40 sieve or by taking the natural soil and removing coarse particles by hand. If it is initially too wet, the sample should be allowed to dry partially in air on the glass plate until the right consistency is achieved. Drying may be accelerated by mixing with a spatula and by using a hair dryer.



Figure 1 The soil specimen is rolled under the fingers into a thread 3 mm in diameter.



Figure 2 The 3-mm-diameter soil thread crumbles when the water content is equal to the plastic limit.

2. When the soil is plastic enough, it is kneaded and shaped into a 1- to 2-cm-diameter ball. The material should be plastic enough not to stick to the fingers when squeezed.
3. The ball is formed into a thread by rolling it under the fingers against the test surface (Fig. 1). Use just enough pressure to roll the soil into a thread 3 mm in diameter as shown in Fig. 2. Gage this diameter by using metal rod 3 mm in diameter as reference. The pressure required for rolling the thread varies greatly depending on the soil toughness. Some tough clays may require firm pressure as they become harder near the plastic limit. Very silty and organic clays that have a soft and spongy consistency at the plastic limit must be rolled gently. If the thread diameter gets smaller than 3 mm without crumbling, fold and knead the thread into a ball again and repeat the rolling process. Knead and roll the soil thread until it has dried to the point of crumbling and breaking into numerous pieces about 3 to 9 mm in length when the thread diameter reaches approximately 3 mm. As shown in Fig. 2, the crumbling of the soil thread, which corresponds to longitudinal and transverse cracking, should be the result of the decrease in water content, not the result of excessive hand pressure.
4. As soon as the soil thread crumbles, collect part of it and determine its water content. Repeat steps 2 and 3 with another portion of the prepared material, and check that two successive runs give approximately the same plastic limit. If the two test values vary more than 5% from the average, additional tests should be performed.

COMPUTATION

The plastic limit *PL* is reported as the average of two similar values. If it is not possible to obtain a plastic limit in the plastic limit test, the soil is reported as nonplastic. This also applies if $PL \geq LL$. Errors in computing the liquid or plastic limits can be detected by plotting the point (*LL*, *PI*) on the plasticity chart. This point should fall under the U-line.

EXAMPLE

An example of plastic limit determination is given in Figs. 3 to 5. Figure 3 summarizes the measured plastic limits, and Fig. 5 lists the formulas used in Fig. 4. In this example, four measurements were made. The plastic limit is the average of these four measurements. As shown in Fig. 3, all these measurements vary by less than 5% from their mean value, and two tests would have been sufficient to determine the plastic limit.

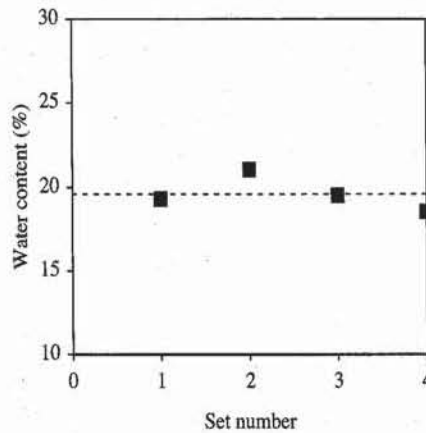


Figure 3 Variation of the plastic limits in four different tests.

	A	B	C	D	E
1	Plastic limit				
2	Analyst name: <i>Mike Kapuskar</i>				
3	Test date: <i>11/13/90</i>				
4	Sample description: <i>Aardvark modeling clay</i>				
5					
	Set number	Mass of container (g)	Mass of container with wet soil (g)	Mass of container with dry soil (g)	Water content (%)
6		M_c	M_w	M_d	w
7					
8	1	20.10	30.00	28.40	19.28
9	2	22.40	29.30	28.10	21.05
10	3	21.20	31.00	29.40	19.51
11	4	23	35.80	33.80	18.52
12	Plastic limit (%) = 19.59				

Figure 4 Data set for plastic limit test.

	E
	Water content (%)
6	
7	w
8	$= (M_w - M_d) / (M_d - M_c) * 100$

	A	B
12	Plastic limit (%) = =AVERAGE(w)	

Figure 5 Formulas used in Fig. 4.

REFERENCE

See Introduction for references to ASTM procedures (pages 4 to 6).

EXERCISES

- Determine the plastic limit from the experimental results of Table E1.

TABLE E1

Set number	Tare mass (g)	Tare with wet soil (g)	Tare with dry soil (g)
1	47.12	77.12	71.44
2	45.67	75.67	69.94
3	45.66	75.66	70.05
4	45.67	75.67	69.68

- Same as Exercise 1 but for the experimental results of Table E2.

TABLE E2

Set number	Tare mass (g)	Tare with wet soil (g)	Tare with dry soil (g)
1	47.11	48.63	48.47
2	43.21	44.96	44.75
3	47.12	48.71	48.47
4	104.19	106.49	106.19

- Same as Exercise 1 but for the experimental results of Table E3.

TABLE E3

Set number	Tare mass (g)	Tare with wet soil (g)	Tare with dry soil (g)
1	47.12	54.70	53.59
2	46.69	47.84	47.63
3	45.61	47.03	46.66
4	45.81	47.77	47.49

4. Same as Exercise 1 but for the experimental results of Table E4.

TABLE E4

Set number	Tare mass (g)	Tare with wet soil (g)	Tare with dry soil (g)
1	46.70	49.14	48.85
2	47.72	51.50	51.02
3	47.08	49.33	49.05
4	47.72	50.17	49.82

2-6 Principles of Shrinkage Limit Analysis

DEFINITIONS

Fine-grained soils shrink continuously when the water content decreases, until the water content reaches the shrinkage limit. At that point the soil particles are in close contact, and the soil volume can no longer decrease, even if the water content is reduced further. Clays are more susceptible to shrinkage than are silts and sands. In most cohesive soils, the shrinkage limit is appreciably smaller than the plastic limit, except for silts, which have similar shrinkage and plastic limits.

Shrinkage Limit

Figure 1 shows the typical variation of volume measured for clays when the water content decreases. The volume change decreases proportionally to the loss of water content w between points A and B , where $w > PL$. However, between points C and D , where $w < PL$, there is no further decrease in volume as the soil dries. The shrinkage limit SL is the water content at the intersection of lines AB and CD . The intercept of line AB (i.e., point F) corresponds to the total volume of dry soil particles.

Shrinkage Ratio

Related to Fig. 1, Fig. 2 shows the corresponding variation of volume ratio V/V_0 , where V is the total soil volume and V_0 is the dry soil volume. The shrinkage ratio SR is the slope of line AF in Fig. 2:

$$SR = \frac{(V_1 - V_2)/V_0}{w_1 - w_2} \quad (1)$$

where V_1 is the volume corresponding to water content w_1 and V_2 is the volume corresponding to water content w_2 . The columns of Fig. 2 illustrate the variation of the volumes of soil and its air, water, and solid constituents at various drying

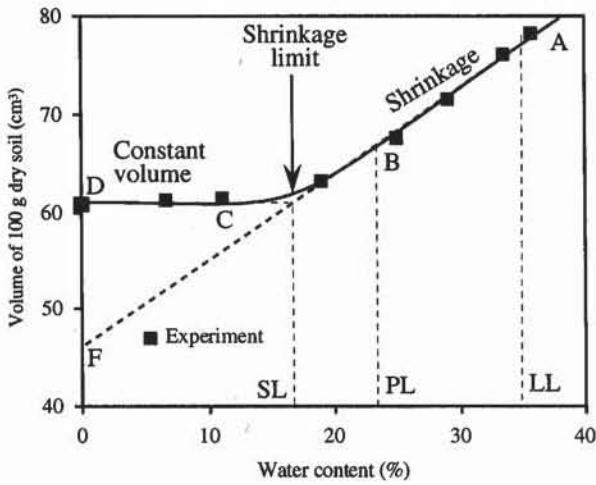


Figure 1 Typical shrinkage curve for clay soil (data after Head, 1984).

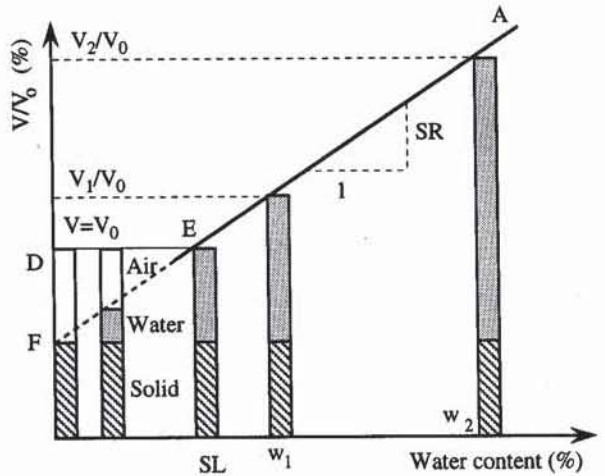


Figure 2 Definition of shrinkage ratio *SR*.

stages. For large water content, the soil is fully saturated, and its volume varies linearly with w . The volume of the solid fraction is always constant and equal to the volume at point F . At point E the soil particles cannot get closer together even though water is being removed, and air starts to fill voids as drying continues. When V_1 and V_2 are both larger than V_0 , the water content decreases linearly with the volume change:

$$w_1 - w_2 = \frac{\rho_w}{M_0} (V_1 - V_2) \tag{2}$$

where ρ_w is the water unit mass and M_0 is the mass of dry soil. Therefore, *SR* is

$$SR = \frac{M_0}{\rho_w V_0} \tag{3}$$

Linear Shrinkage

The linear shrinkage ratio *LS* characterizes the change in length induced by drying a cylindrical sample of soil initially about its liquid limit. *LS* is

$$LS = \frac{L - L_0}{L} \times 100 \quad (\%) \tag{4}$$

where L is the original length of the sample at about the liquid limit and L_0 is the length of the dry sample. *LS* gives an indication on the amount of axial strain that drying may cause to soil samples. *LS* can also be determined from volume changes provided that the soil shrinks uniformly in all directions:

$$LS = \left(1 - \sqrt[3]{\frac{V_0}{V}}\right) \times 100 \quad (\%) \tag{5}$$

where V is the initial soil volume close to the liquid limit and V_0 is the dry soil volume. In the case of most British soils (Head, 1984), *LS* was found to be approxi-

mately related to the plasticity index PI through

$$PI = 2.13LS \quad (\%) \quad (6)$$

TYPICAL VALUES FOR SHRINKAGE LIMIT

Table 1 lists some typical values of shrinkage limits for clay minerals and soils.

TABLE 1

Liquid, plastic, and shrinkage limits for several clay minerals and natural soils (after Lambe and Whitman, 1979; and Lambe, 1951)

Mineral	Exchangeable ion	Liquid limit (%)	Plastic limit (%)	Plasticity index (%)	Shrinkage limit (%)	Shrinkage limit calculated by method 1 (%)	Shrinkage limit calculated by method 2 (%)
Montmorillonite	Na	710	54	656	9.9	-132.3	6.2
	K	660	98	562	9.3	-74.8	10.1
	Ca	510	81	429	10.5	-51.3	10.5
	Mg	410	60	350	14.7	-45.3	9.5
	Fe	290	75	215	10.3	2.1	15.7
Illite	Na	120	53	67	15.4	26.0	23.4
	K	120	60	60	17.5	33.0	27.8
	Ca	100	45	55	16.8	23.4	22.1
	Mg	95	46	49	14.7	25.8	23.8
	Fe	110	49	61	15.3	24.7	22.8
Kaolinite	Na	53	32	21	26.8	23.1	22.9
	K	49	29	20	21.2	21.1	
	Ca	38	27	11	24.5	22.1	22.4
	Mg	54	31	23	28.7	21.8	21.7
	Fe	59	37	22	29.2	26.5	26.0
Attapulgite	H	270	150	120	7.6	82.5	43.9
Mexico City clay		388	226	162	43	126.6	52.5
Boston blue clay (illite)		41	25	16	18.7	19.3	19.3
Aardvack clay		30.6	19.6	11	12.17	16.7	16.4
Morganza Louisiana clay		104	74.8	29.2	13.7	52.1	47.0
Beverly clayey silt (illite)		19.5	16.3	3.2	13.3	16.4	15.4

APPROXIMATE DETERMINATION OF SHRINKAGE LIMIT

There are two empirical methods to estimate SL from the liquid and plastic limits.

Method 1

The shrinkage limit SL is estimated as follows (Holtz and Kovacs, 1981):

$$SL = 5.4 + 0.73LL - PI \quad (\%) \quad (7)$$

where LL is the liquid limit and PI is the plasticity index. Table 1 compares the measured shrinkage limits with those estimated using Eq. 7. Eq. 7 is a very crude approximation of the measured shrinkage limits. Equation 7 even predicts an unrealistic negative value of the shrinkage limit for montmorillonite.

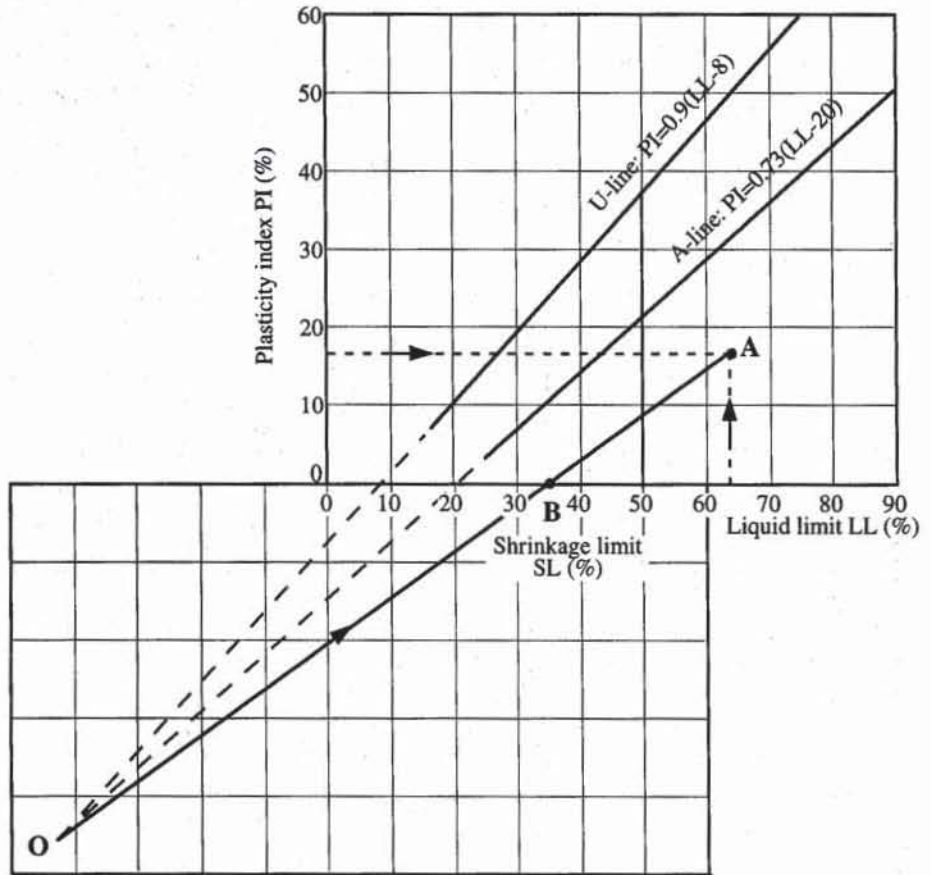


Figure 3 Method 2 for estimating the shrinkage limit from liquid and plastic limits.

Method 2

As shown in Fig. 3, the U- and A-lines of the plasticity chart intersect at point *O* with coordinates -43.53 and -46.38 . The shrinkage limit *SL* of a soil with liquid limit *LL* and plasticity index *PI* can be estimated as the liquid limit of the intersection point *B* between line *OA* and the liquid limit axis, where *A* has for coordinates *LL* and *PI* (Holtz and Kovacs, 1981). This graphical construction corresponds to

$$SL = 46.38 \frac{LL + 43.53}{PI + 46.38} - 43.53 \quad (\%) \quad (8)$$

where *LL* is the liquid limit (%) and *PI* is the plastic index (%). As shown in Table 1, Eq. 8 provides a more accurate approximation of measured shrinkage limits than does Eq. 7.

ENGINEERING SIGNIFICANCE OF SHRINKAGE

The effects of shrinkage of fine-grained soils are of considerable significance from a geotechnical engineering point of view. Shrinkage cracks are caused by the evaporation from the surface in dry climates and lowering the groundwater table.

When the climate changes and the soils again have access to water, they tend to increase in volume and swell. The volume changes resulting from both shrinkage and swelling of fine-grained soils are often large enough to cause serious damage to small buildings and highway pavements. In 1973, Jones and Holtz estimated that shrinking and swelling soils caused about \$2.3 billion in damage annually in the United States alone, which, to put things in perspective, was more than twice the annual cost of damage from floods, hurricanes, tornadoes, and earthquakes combined.

REFERENCES

- HEAD, K. H., 1984, *Manual of Soil Laboratory Testing*, Vol. 1: Soil Classification and Compaction Tests, Pentech Press, London.
- HOLTZ, R. D., and W. D. KOVACS, 1981, *An Introduction to Geotechnical Engineering*, Prentice Hall, Englewood Cliffs, NJ, 733 pp.
- JONES, D. E., and R. D. HOLTZ, 1973, Expansive soil—the hidden disaster, *Civil Eng., ASCE*, Vol. 43, No. 8, pp. 49–51.
- LAMBE, T. W., 1951, *Soil Testing for Engineers*, John Wiley & Sons, NY, 165 pp.
- LAMBE, T. W., and R. V. WHITMAN, 1979, *Soil Mechanics, SI Version*, John Wiley & Sons, New York, 553 pp.

REVIEW QUESTIONS

1. Define *shrinkage limit*. What is the position of the shrinkage limit with respect to the liquid and plastic limits?
2. Define *shrinkage ratio*.
3. Is it meaningful to define a shrinkage limit for sands?
4. Is the shrinkage limit larger or smaller than the plastic limit?
5. Which methods are used to estimate the shrinkage limits from liquid and plastic limits?

2-7

Shrinkage Limit Analysis with Mercury

OBJECTIVE

Shrinkage limit analysis determines the shrinkage limit and shrinkage ratio of fine-grained soils. The *shrinkage limit* is the water content below which a soil undergoes no further volume change. The shrinkage ratio provides an estimate of the amount of volume change during drying and wetting. There are two methods to determine the shrinkage limit: the mercury method and the wax method. The mercury method is described in this chapter, the wax method in Chapter 2-8.

EQUIPMENT

The equipment for shrinkage limit analysis with mercury includes:

- Shrinkage dish, porcelain or metal, about 42 mm in diameter and 12 mm deep (Fig. 1).
- Immersion glass cup about 57 mm in diameter and 38 mm deep, with the rim ground flat.
- Prong plate, transparent, fitted with three prongs and large enough to cover the immersion glass cup.
- Mercury, a little more than 1 kg, to fill the glass cup completely. Mercury is a harmful substance—avoid direct skin contact with mercury. After the experiment, pour the mercury back into its container without leaving any mercury trace on the laboratory equipment, bench, or floor. Handling of mercury can be hazardous unless the appropriate precautionary measures are taken. Mercury vapour is poisonous when its concentration exceeds $100 \mu\text{g}/\text{m}^3$. It is important to control the surface area of mercury exposed to the air (absolutely no spillage of mercury on the floor or laboratory bench) and have a normal ventilation in the room.
- Large evaporating dish and tray, to prevent mercury from spilling.

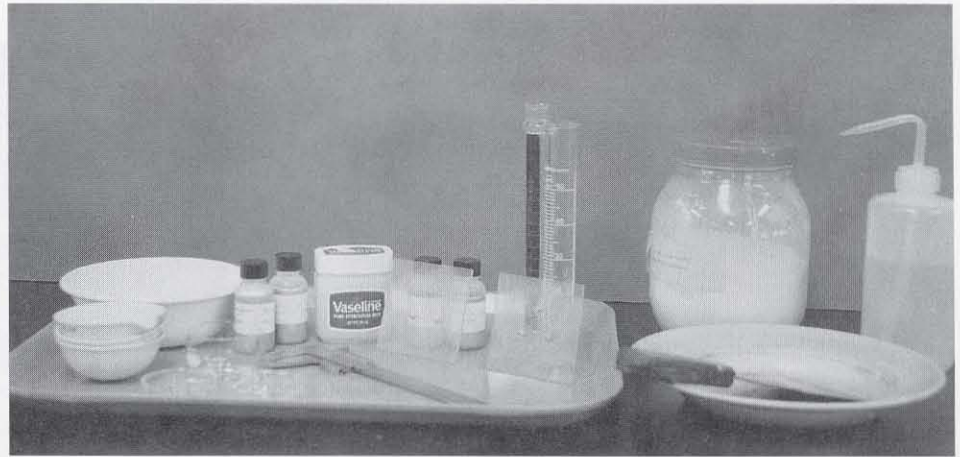


Figure 1 Equipment for shrinkage limit analysis. Shrinkage dish, prong plate, container of mercury, petroleum jelly, spatula, large evaporating dish, and large tray.

- Petroleum jelly, silicon grease, or Teflon powder spray to lubricate shrinkage dish.
- Balance accurate to 0.01 g.
- Measuring cylinder, 100 mL.
- Drying oven.
- Straight-edge spatula.

TEST PROCEDURE

1. Take about 40 g of the material used for the liquid and plastic limit tests. This material should pass a No. 40 sieve. Place the soil in an evaporating dish and, use a spatula to mix thoroughly with distilled water to obtain a soil paste with a water content higher than the liquid limit.
2. Measure the weights of the shrinkage limit dish, first dry, then filled with water, to determine its volume.
3. Lightly coat the inside of the dish with petroleum jelly or silicon grease (Fig. 2). This coating will prevent the soil from sticking to the dish or forming cracks upon drying. Measure the weight of the coated dish.
4. Fill about one-third of the dish with the soil paste (Fig. 3). Tap the dish with the spatula handle to cause the soil paste to flow to the edges of the dish and to release air bubbles. Add a second layer of soil, about the same size as the first, and again tap the sample to release entrapped air. Add more soil and overtop the dish slightly. Strike off the excess soil with a straight-edge and clean off adhering soil from the outside of the shrinkage dish. Measure the weight of the wet soil and dish.
5. Leave the soil in the shrinkage dish to dry in the laboratory until the soil surface changes to a light color (about 5 to 6 h). Place it in the oven at 105 to 110°C and dry it to constant weight (about 12 to 18 h). Measure the weight of the dry soil and container.
6. Remove the dried soil-pat carefully from the shrinkage dish. It should be intact if it was adequately air dried before oven drying. Place the immersion cup in a clean evaporating dish, itself located inside a large tray (Fig. 4). Fill



Figure 2 Lightly coat the inside of the shrinkage limit dish with petroleum jelly or silicon grease.

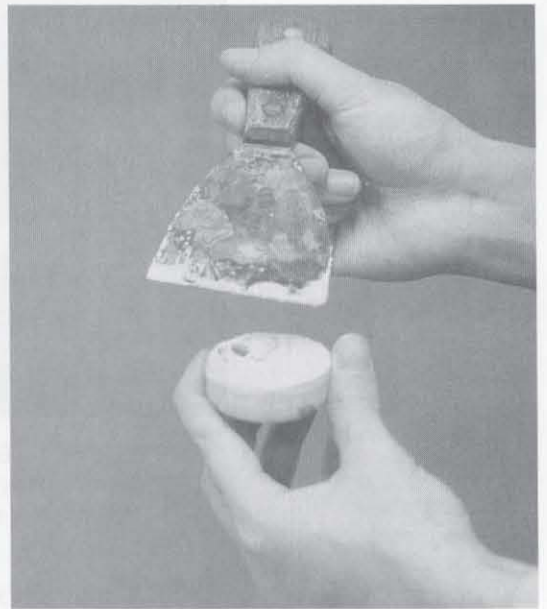


Figure 3 The shrinkage dish is filled with soil paste. The dish is tapped with a spatula handle to cause the soil to flow to the edges of the dish. When the dish is completely filled with an excess standing out, strike off the excess with a straightedge.



Figure 4 Place the immersion cup in a clean evaporating dish, itself located inside a large tray. Place the dry soil pat on the mercury surface.



Figure 5 Press the three prongs of the prong plate carefully onto the sample and force it under the mercury.

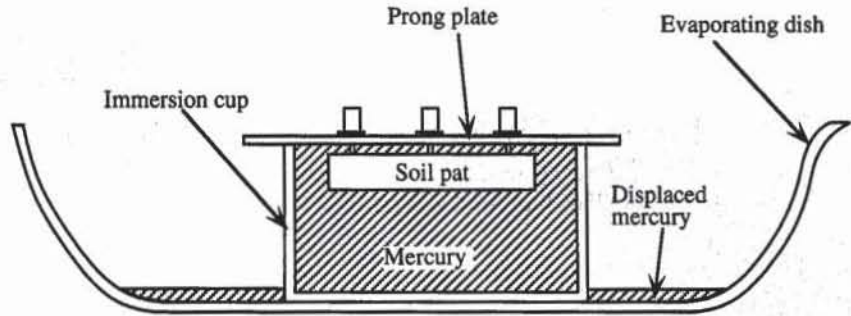


Figure 6 The three prongs push the dry soil pat into the mercury, and displace mercury from the immersion cup to the evaporating dish.

the cup to overflowing with mercury, and remove the mercury excess by pressing the glass prong plate firmly on the top of the cup. Press slowly to avoid trapping air under the glass plate. Carefully remove the prong plate. Transfer the excess mercury collected in the evaporating dish into its original container without spilling.

7. Place the soil pat on the mercury surface (Fig. 4). The soil pat will float because the mercury is much denser than any soil. Press the three prongs of the prong plate carefully on the sample and force it under the mercury (Fig. 5). Avoid trapping any air. Press the plate firmly onto the dish. Displaced mercury will be held in the evaporating dish. Brush off any droplets of mercury adhering to the cup into the evaporating dish (Fig. 6). Transfer all the displaced mercury to the measuring cylinder and measure the weight of displaced mercury. The volume of displaced mercury is equal to the volume of the dry soil pat.
8. Transfer the mercury back into its original container, by working above a large tray, without spilling.

COMPUTATION

The initial water content w of the wet soil pat is

$$w = \frac{M - M_0}{M_0} \tag{1}$$

where M is the mass of the wet soil and M_0 is the mass of the dry soil. The shrinkage limit SL is calculated from w by removing the change in water content from V to V_0 :

$$SL = w - \rho_w \frac{V - V_0}{M_0} \tag{2}$$

where V is the volume of the wet soil pat, V_0 the volume of the dry soil pat, and ρ_w the unit mass of water. V is equal to the volume of the mold where the pat is formed.

V_0 is equal to the volume of mercury that is displaced by immersion of the dry pat into the mercury bowl:

$$V_0 = \frac{M_{Hg}}{\rho_{Hg}} \tag{3}$$

where M_{Hg} is the mass of the displaced mercury and ρ_{Hg} is the unit mass of the mercury = 13.6 g/cm³. The shrinkage ratio is

$$SR = \frac{M_0}{\rho_w V_0} \tag{4}$$

The linear shrinkage ratio LS is

$$LS = 1 - \sqrt[3]{\frac{V_0}{V}} \tag{5}$$

EXAMPLE

Figure 7 shows an example of input/output data for the shrinkage limit test, and Fig. 8 shows the formulas used in Fig. 7.

	A	B	C	D
1	Shrinkage Test			
2				
3	Analyst name: <i>Henry Guapo</i>			
4	Test date: <i>2/22/93</i>			
5	Sample description: <i>Aardvark modeling clay</i>			
6				
7	MERCURY METHOD	Sample 1	Sample 2	
8	Mass of coated dish M_c (g)	17.51	15.64	
9	Mass of coated dish and wet soil M_w (g)	78.07	76.47	
10	Mass of coated dish and dry soil M_d (g)	64.41	62.56	
11	Volume of wet soil V (cm ³)	32.42	32.85	
12	Mass of dish M_t (g)	130.00	130.00	
13	Mass of dish and displaced mercury M_{Hg} (g)	462.00	466.00	
14	Unit mass of Mercury ρ_{Hg} (g/cm ³)	13.60		
15	Volume of dry soil V_0 (cm ³)	24.41	24.71	Average
16	Initial water content w	29.13%	29.64%	29.38%
17	Shrinkage limit SL	12.06%	12.28%	12.17%
18	Shrinkage ratio SR	1.92	1.90	1.91
19	Linear Shrinkage LS	9.02%	9.06%	9.04%

Figure 7 Example of data set.

	A	B	C	D
15	Volume of dry soil V_0 (cm ³)	$=(M_{Hg}-M_t)/r_{Hg}$	$=(M_{Hg}-M_t)/r_{Hg}$	Average
16	Initial water content w	$=(M_w-M_d)/(M_d-M_c)$	$=(M_w-M_d)/(M_d-M_c)$	=AVERAGE(w)
17	Shrinkage limit SL	$=w-(V-V_0)/(M_d-M_c)$	$=w-(V-V_0)/(M_d-M_c)$	=AVERAGE(SL)
18	Shrinkage ratio SR	$=(M_d-M_c)/V_0$	$=(M_d-M_c)/V_0$	=AVERAGE(SR)
19	Linear Shrinkage LS	$=(1-(V_0/V)^{1/3})$	$=(1-(V_0/V)^{1/3})$	=AVERAGE(LS)

Figure 8 List of formulas used in Fig. 7.

REVIEW QUESTIONS

1. What is the purpose of the shrinkage limit?
2. Why do we use mercury in the shrinkage limit test? Is there another technique to define the shrinkage limit? Which one?
3. Why do we coat the shrinkage dish with petroleum jelly or silicon grease?

EXERCISES

1. Calculate the ratio between the plasticity index PI and linear shrinkage ratio LS . Compare your value to that found for British soils ($PI/LS = 2.13$).
2. Calculate the shrinkage limit, shrinkage ratio, and linear shrinkage ratio from the following test results.

	Sample 1	Sample 2
Mass of coated dish (g)	17.04	13.61
Mass of coated dish + wet soil (g)	74.24	68.88
Mass of coated dish + dry soil (g)	56.61	51.62
Volume of wet soil (cm ³)	32.41	34.96
Mass of dish (g)	134.00	134.00
Mass of dish + displaced mercury (g)	400.00	438.00
Unit mass of mercury	13.60	13.60

	Sample 1	Sample 2
Mass of coated dish (g)	17.51	13.97
Mass of coated dish + wet soil (g)	78.07	72.97
Mass of coated dish + dry soil (g)	64.41	59.80
Volume of wet soil (cm ³)	32.42	34.95
Mass of dish (g)	0.00	0.00
Mass of dish + displaced mercury (g)	316.00	355.00
Unit mass of mercury	13.60	13.60

2-8

Shrinkage Limit Analysis with Wax

OBJECTIVE

The shrinkage limit analysis with wax has the same objective as the shrinkage limit analysis with mercury (Chapter 2-7). It determines the shrinkage limit and shrinkage ratio of fine-grained soils by using wax instead of mercury. Because wax is less toxic than mercury, this method is recommended in an academic environment. The wax method assumes that wax, similar to mercury, does not wet or expand dry soils.

EQUIPMENT

The equipment for shrinkage limit analysis with wax includes:

- Shrinkage dish, porcelain or metal, about 42 mm in diameter and 12 mm deep.
- Petroleum jelly, silicon grease, or Teflon powder spray to lubricate shrinkage dish.
- Straight-edge spatula.
- Balance accurate to 0.01 g.
- Support frame for suspending the sample below the balance (see Chapter 3-2).
- Paraffin wax and wax bath.
- Container filled with water.
- Drying oven.
- Evaporating dish.

TEST PROCEDURE

The procedure combines several steps of the shrinkage limit analysis with mercury and the determination of the unit weight of cohesive soils (refer to Chapters 2-7 and 3-2 for details).

1. Construct the soil pat and dry it as specified in steps 1 to and 4 of the test procedure in Chapter 2-7. Measure the weight of the coated dish, the weight of the coated dish and wet soil, the weight of the coated dish and dry soil, and the volume of wet soil.
2. Measure the volume of the dry soil pat as specified in steps 2 to and 6 of the determination of the unit weight of cohesive soils in Chapter 3-2. If the pat has a tendency to crumble, apply thin layers of hot wax on it with a brush before immersing it completely in the heated wax bath. Measure the total and buoyant weights of the dry pat and wax.
3. The wax unit mass should be determined as described in Chapter 3-2.

COMPUTATION

The moisture content w of the initial wet soil pat, the shrinkage limit SL , the shrinkage ratio SR , and the linear shrinkage ratio LS are given in Eqs. 1, 2, 4, and 5 of Chapter 2-7. However, in the wax method, V_0 is calculated from the weight of displaced water corrected for the additional volume of wax:

$$V_0 = \frac{M_{sp} - M_{bsp}}{\rho_w} - \frac{M_p}{\rho_p} \tag{1}$$

where M_{sp} is the mass of the dry soil covered with wax, M_{bsp} the buoyant mass of the dry soil covered with wax, M_p the mass of wax covering the dry pat, ρ_w the unit mass of water, and ρ_p the unit mass of wax.

EXAMPLE

Figure 1 shows an example of input/output data for the shrinkage limit analysis with wax, and Fig. 2 shows the formulas used in Fig. 1.

	A	B	C	D
1	Shrinkage Test			
2	Analyst name: <i>Henry Guapo</i>			
3	Test date: <i>2/22/93</i>			
4	Sample description: <i>Aardvark modeling clay</i>			
5				
6	WAX METHOD	Sample 1	Sample 2	
7	Mass of coated dish M_c (g)	15.64	13.90	
8	Mass of coated dish and wet soil M_w (g)	76.47	76.08	
9	Mass of coated dish and dry soil M_d (g)	62.56	61.43	
10	Volume of wet soil V (cm ³)	32.85	33.75	
11	Mass of soil and wax M_{sp} (g)	51.85	48.40	
12	Buoyant mass of soil and wax M_{bsp} (g)	22.05	22.70	
13	Unit mass of wax ρ_{wax} (g/cm ³)	0.95	0.95	
14	Volume of dry soil V_0 (cm ³)	24.61	24.78	Average
15	Initial water content w	29.64%	30.83%	30.23%
16	Shrinkage limit SL	12.08%	11.96%	12.02%
17	Shrinkage ratio SR	1.91	1.92	1.91
18	Linear Shrinkage LS	9.17%	9.78%	9.48%

Figure 1 Example of data set.

	A	B	C	D
14	Volume of dry soil V_0 (cm ³)	$= (M_{sp} - M_{bsp}) - (M_{sp} - (M_d - M_c)) / r_{wax}$	$= (M_{sp} - M_{bsp}) - (M_{sp} - (M_d - M_c)) / r_{wax}$	Average
15	Initial water content w	$= (M_w - M_d) / (M_d - M_c)$	$= (M_w - M_d) / (M_d - M_c)$	=AVERAGE(w)
16	Shrinkage limit SL	$= w - (V - V_0) / (M_d - M_c)$	$= w - (V - V_0) / (M_d - M_c)$	=AVERAGE(SL)
17	Shrinkage ratio SR	$= (M_d - M_c) / V_0$	$= (M_d - M_c) / V_0$	=AVERAGE(SR)
18	Linear Shrinkage LS	$= (1 - (V_0/V)^{1/3})$	$= (1 - (V_0/V)^{1/3})$	=AVERAGE(LS)

Figure 2 Formulas used in Fig. 1.

COMPARISON OF WAX AND MERCURY METHODS

The shrinkage limit analyses with wax and mercury were performed successively for some particular soils and were found to yield similar results. The volume of a dry soil pat can be measured by using first mercury, then wax. As shown in Fig. 3, $SL = 12.06$ and 12.28% for the mercury method, while $SL = 12.08$ and 11.96% for the wax method.

Shrinkage Test

Analyst name: *Henry Guapo*Test date: *2/22/93*Sample description: *Aardvark modeling clay*

	Sample 1	Sample 2	Sample 3
Mass of coated dish (g)	17.51	15.64	13.90
Mass of coated dish and wet soil (g)	78.07	76.47	76.08
Mass of coated dish and dry soil (g)	64.41	62.56	61.43
Volume of wet soil (cm ³)	32.42	32.85	33.75
MERCURY METHOD			
Mass of dish (g)	130.00	130.00	
Mass of dish and displaced mercury (g)	462.00	466.00	
Unit mass of Mercury (g/cm ³)	13.60	13.60	
Initial water content	29.13%	29.64%	30.83%
Volume of dry soil (cm ³)	24.41	24.71	
Shrinkage limit (%)	12.06%	12.28%	
Shrinkage ratio	1.92	1.90	
Linear Shrinkage (%)	9.02%	9.06%	
WAX METHOD			
Mass of soil and wax (g)		51.85	48.40
Bouyant mass of soil and wax (g)		22.05	22.70
Unit mass of wax (g/cm ³)		0.95	0.95
Volume of dry soil (cm ³)		24.61	24.78
Shrinkage limit (%)		12.08%	11.96%
Shrinkage ratio		1.91	1.92
Linear Shrinkage (%)		9.17%	9.78%

Figure 3 Comparison of shrinkage limits obtained by using the wax and mercury methods.

REVIEW QUESTIONS

1. What are the differences between the wax and mercury methods of determining the shrinkage limit?
2. How do you determine the unit weight of wax?
3. What is the main function of the wax in the wax method?

EXERCISE

1. Calculate the shrinkage limit, shrinkage ratio, and linear shrinkage ratio from the following test results obtained from the wax and mercury methods. Compare the results obtained by the wax method and mercury method.

	Sample 1	Sample 2	Sample 3	Sample 4
Mass of coated dish (g)	17.51	13.97	0.00	0.00
Mass of coated dish + wet soil (g)	78.07	72.97	60.56	59.00
Mass of coated dish + dry soil (g)	64.41	59.80	47.20	45.80
Volume of wet soil (cm ³)	32.42	34.95	33.75	33.75
Mercury method				
Mass of dish (g)	0.00	0.00		
Mass of dish + displaced mercury (g)	316.00	355.00		
Unit mass of Mercury (g/cm ³)	13.60	13.60		
Wax method				
Mass of soil and wax (g)			54.55	53.75
Buoyant weight of soil and wax (g)			22.10	20.40
Unit mass of wax (g/cm ³)			0.95	0.95

2-9

Engineering Classification of Soils

INTRODUCTION

Soil classification systems attribute to soils a label or designation that represents their most significant properties for specific engineering applications. They are based on measurable parameters, such as coefficient of uniformity, clay fraction, activity, and liquid limit. Several soil classification systems were developed to meet specific engineering needs. Some examples in the United States are the AASHTO classification system (ASTM D 3282) and the Unified Soil Classification System (ASTM D 2487). These engineering soil classifications are based on the results of Atterberg limits tests and grain size analyses.

UNIFIED SOIL CLASSIFICATION SYSTEM

The Unified Soil Classification System (USCS), originally developed by Casagrande, is one of the most commonly used systems. It classifies soils into groups defined by a primary and a secondary letter. The letters and their meanings are given in Table 1. Normally, two letters are used. For example, SW indicates well-graded sand. However, soils having the characteristics of two groups are classified using dual symbols (e.g., CL-CH). The flowchart of Fig. 1 specifies the steps for classifying soils. Coarse-grained soils (e.g., sands and gravels) are classified using their grain size distribution curve, whereas fine-grained soils (e.g., silts and clays) are classified using their liquid and plastic limits. Under the USCS, many soils fall within one of two general categories. Coarse-grained soils, which include sands and gravels, have either G or S for the first letter and W, P, M, or C for the second. Fine-grained soils have M, C, or O for the first letter and L or H for the second. A third group of soils—highly organic soils, or Pt—consists of peat, muck, and so on. They are typically spongy, crumbly, and compressible and are undesirable for use in supporting structures.

TABLE 1

Primary and secondary letters used in the Unified Soil Classification System.

Primary letter		Secondary letter	
G	Gravel	W	Well graded
S	Sand	P	Poorly graded
M	Silt	M	With nonplastic fines
C	Clay	C	With plastic fines
O	Organic	L	Of low plasticity ($LL < 50\%$)
Pt	Peat	H	Of high plasticity ($LL > 50\%$)

EXAMPLE

The results of grain size analysis and the Atterberg limit for a soil are as follows:

U.S. sieve size	Percent passing
No. 4	100
No. 10	85.6
No. 40	72.3
No. 200	58.8
Liquid limit	$LL = 46.2\%$
Plastic limit	$PL = 21.9\%$

The plasticity index is $PI = LL - PL = 46.2 - 21.9 = 24.3\%$.

The soil is fine-grained (right branch of Fig. 1) because more than 50% passes a No. 200 sieve. Its liquid limit $LL = 46.2\%$ is less than 50%. The point $(LL, PI) = (46.2, 24.3)$ falls above the A-line of the plasticity chart. The soil is classified as CL.

AASHTO CLASSIFICATION SYSTEM

"AASHTO" stands for the "American Association of State Highway and Transportation Officials." This classification system is widely used in highway work. The system intends to indicate a soil's acceptability as a highway and road subgrade and base course, partially by the use of a numerical measure of the soil quality, termed the *group index GI*.

AASHTO classifies soils by using the results of grain size analysis and liquid and plastic limit tests. The necessary parameters are listed in the first column of Table 2. With the values of these parameters known, one enters the column of Table 2 labeled A-1a and determines whether or not the parameters meet the limiting values of that column. If they do, the soil classification is A-1a. If they do not, one enters the next column to the right and determines whether or not the parameters meet the limiting values of that column. The procedure is repeated until the parameters meet all the limiting values of a column. The soil classification is given at the top of that particular column. In addition to its group name, a soil is further classified by its group index *GI*:

$$GI = (F-35)[0.2 + 0.005(LL-40)] + 0.01(F-15)(PI-10) \quad (1)$$

where F is the percentage of soil passing a No. 200 sieve, LL the liquid limit, and PI the plasticity index. GI is rounded off to the nearest whole number and, if

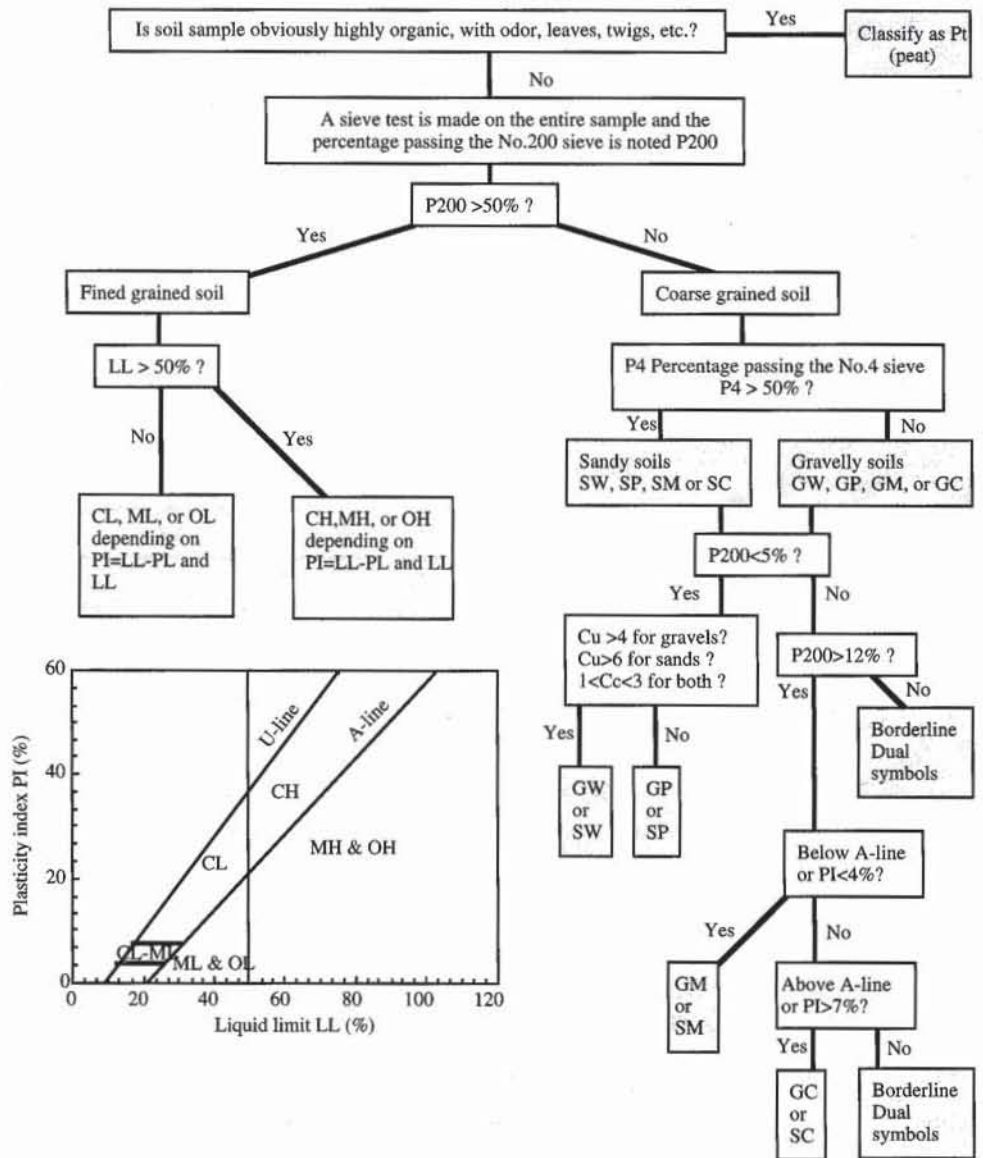


Figure 1 Flowchart of Unified Soil Classification System.

negative, set equal to zero. The result of the AASHTO classification is reported by appending *GI* in parentheses to the group designation.

EXAMPLE

With 85.6% passing a No. 10 sieve, 72.3% passing a No. 40 sieve, 58.8% passing a No. 200 sieve, a liquid limit of 42.6%, and a plasticity index of 24.3%, one proceeds across Table 2 from left to right until the first column is reached in which these parameters meet the limiting values in that column. The result is A-7. The group index is determined using Eq. 1.

$$GI = (58.8 - 35)[0.2 + 0.005(46.2 - 40)] + 0.01(58.8 - 15)(24.3 - 10) = 11.8 \approx 12$$

Therefore, this soil is classified as A-7 (12).

TABLE 2

AASHTO classification of soils and soil-aggregate mixtures

General classification	Granular materials (35% or less passing .075 mm)							Silt-clay materials (more than 35% passing .075 mm)			
Group classification	A-1		A-3	A-2				A-4	A-5	A-6	A-7 A-7-5 A-7-6
	A-1a	A-1b		A-2-4	A-2-5	A-2-6	A-2-7				
Percent passing 2.00 mm (No. 10) 0.425 mm (No. 40) 0.075 mm (No. 200)	50 max. 30 max. 15 max.	50 max. 25 max.	51 max. 10 max.	35 max.	35 max.	35 max.	35 max.	36 min.	36 min.	36 min.	36 min.
Fraction passing 0.425 mm (No. 40) Liquid limit Plasticity index	6 max.		N.P.	40 max. 10 max.	41 min. 10 max.	40 max. 11 min.	41 min. 11 min.	40 max. 10 max.	41 min. 10 max.	40 max. 11 min.	41 min. 11 min.
Usual types of significant constituent materials	Stone fragments Gravel and sand		Fine sand	Silty or clayey gravel sand				Silty soils		Clayey soils	
General rating as subgrade	Excellent to good							Fair to poor			

Classification procedure: Given the required test data, proceed from left to right in chart; the correct group will be found by the process of elimination. The first group from the left consistent with the test data is the correct classification. The A-7 group is subdivided into A-7-5 or A-7-6, depending on the plastic limit. For $PL < 30$, the classification is A-7-6; for $PL > 30$, A-7-5. N.P. denotes "nonplastic."

COMPARISON OF USCS AND AASHTO CLASSIFICATION SYSTEMS

There are significant differences between the USCS and AASHTO soil classification systems, which result from their different histories and purposes. Tables 3 and 4 compare the two systems in terms of the probable corresponding soil groups.

TABLE 3

Comparable soil groups in the AASHTO and USCS systems (after Liu, 1970)

Soil group in USCS	Comparable soil groups in AASHTO system		
	Most probable	Possible	Possible but improbable
GW	A-1a	—	A-2-4, A-2-5, A-2-6, A-2-7
GP	A-1a	A-1b	A-3, A-2-4, A-2-5, A-2-6, A-2-7
GM	A-1b, A-2-4, A-2-5, A-2-7	A-2-6	A-4, A-5, A-6, A-7-5, A-7-6, A-1a
GC	A-2-6, A-2-7	A-2-4, A-6	A-4, A-7-6, A-7-5
SW	A-1b	A-1a	A-3, A-2-4, A-2-5, A-2-6, A-2-7
SP	A-3, A-1b	A-1a	A-2-4, A-2-5, A-2-6, A-2-7
SM	A-1b, A-2-4, A-2-5, A-2-7	A-2-6, A-4,	A-6, A-7-5, A-5, A-7-6, A-1a
SC	A-2-6, A-2-7	A-2-4, A-6, A-4, A-7-6	A-7-5
ML	A-4, A-5	A-6, A-7-5	—
CL	A-6, A-7-6	A-4	—
OL	A-4, A-5	A-6, A-7-5, A-7-6	—
MH	A-7-5, A-5	—	A-7-6
CH	A-7-6	A-7-5	—
OH	A-7-5, A-5	—	A-7-6
Pt	—	—	—

TABLE 4

Comparable soil groups in the AASHTO and USCS systems (after Liu, 1970)

Soil group in AASHTO system	Comparable soil groups in USCS system		
	Most probable	Possible	Possible but improbable
A-1a	GW, GP	SW, SP	GM, SM
A-1b	SW, SP, GM, SM	GP	—
A-3	SP	—	SW, GP
A-2-4	GM, SM	GC, SC	GW, GP, SW, SP
A-2-5	GM, SM	—	GW, GP
A-2-6	GC, SC	GM, SM	GW, GP
A-2-7	GM, GC, SM, SC	—	GW, GP, SW, SP
A-4	ML, OL	CL, SM, SC	GM, GC
A-5	OH, MH, ML, OL	—	SM, GM
A-6	CL	ML, OL, SC	GC, GM, SM
A-7-5	OH, MH	ML, OL, CH	GM, SM, GC, SC
A-7-6	CH, CL	ML, OL, SC	OH, MH, GC, GM, SM

EXAMPLE OF UNIFIED SOIL CLASSIFICATION

An example of classification with the USCS is given in Figs. 2 to 5. The formulas used in Fig. 2 are listed in Fig. 3. Figure 4 shows the user-defined function for USCS. The input data in Fig. 2 are given in the arguments of the USC function.

In Fig. 2 the soil is classified as CL (i.e., a clay of low plasticity). The results of the USC function can be verified by plotting the point (*LL,PI*) on the plasticity chart of Fig. 5. In this case the point (*LL,PI*) is not a borderline case because it is far from the boundaries between two classifications.

	A	B
1	Example of Unified Soil Classification	
2	Clean Sand (Sieve analysis) SP	
3	Clay sample CL	
4	Liquid limit (%) = 34	
5	Plastic limit (%) = 20	

Figure 2. Example of Unified Soil Classification.

	B
2	=USC(0,99,0.05,1.48,0.96,0,0)
3	=USC(0,100,100, 0, 0,B4,B5)

Figure 3 Formulas used in Fig. 2.

	A	B
1	USC	Unified Soil Classification (USC)
2	=RESULT(2)	Returns a classification code
3	=ARGUMENT("Organic",1)	Amount of organic matter in%
4	=ARGUMENT("pf4",1)	Percent passing #4 sieve
5	=ARGUMENT("pf200",1)	Percent passing #200 sieve
6	=ARGUMENT("Cu",1)	Coefficient of uniformity
7	=ARGUMENT("Cc",1)	Coefficient of curvature
8	=ARGUMENT("LL",1)	Liquid limit in %
9	=ARGUMENT("PL",1)	Lastic limit in %
10	=LL-PL	Plasticity index
11	=IF(pf4<pf200,RETURN("ERR: % passing No.4 must be larger than % passing No.200"))	Error messages
12	=IF(LL<PL,RETURN("ERR: liquid limit must be larger or equal to plastic limit"))	
13	=IF(Organic>99.9,RETURN("Pt"))	Purely organic clay or silt
14	=IF(pf200>50)	Classify according to plasticity chart
15	= IF(AND(A10>0.9*(LL-8),A10>7.3),RETURN("ERR: above U line in plasticity chart"))	Above U line
16	= IF(OR(A10<=0.73*(LL-20),A10<=4))	
17	= IF(LL>50,IF(Organic<=1,RETURN("MH"),RETURN("OH")))	Under A line
18	= IF(Organic<=1,RETURN("ML"),RETURN("OL"))	
19	= ELSE.IF(A10>=7.3)	
20	= IF(LL>50,RETURN("CH"),RETURN("CL"))	
21	= ELSE.IF(AND(A10>4,A10<=7.3))	
22	= RETURN("CL-ML")	
23	= END.IF()	
24	=ELSE.IF(AND(pf200>=5,pf200<=12))	
25	= IF(pf4>50,RETURN("SC-SM"),RETURN("GC-GM"))	
26	=ELSE.IF(pf200>12)	
27	= IF(AND(A10>0.9*(LL-8),A10>7.3),RETURN("ERR: above U line in plasticity chart"))	
28	= IF(AND(A10>0.73*(LL-20),A10>7),IF(pf4<50,RETURN("GC"),RETURN("SC")))	
29	= IF(OR(A10<=0.73*(LL-20),A10<4),IF(pf4<50,RETURN("GM"),RETURN("SM")))	
30	= IF(pf4<50,RETURN("GM-GC"),RETURN("SM-SC"))	
31	=ELSE()	
32	= IF(Cu<1,RETURN("Cu must be greater than or equal to 1"))	
33	= IF(pf4>50)	
34	= IF(AND(Cu>6,Cc>1,Cc<3),RETURN("SW"),RETURN("SP"))	
35	= ELSE()	
36	= IF(AND(Cu>4,Cc>1,Cc<3),RETURN("GW"),RETURN("GP"))	
37	= END.IF()	
38	=END.IF()	
39	=RETURN("ERR")	

Figure 4 User-defined function for Unified Soil Classification.

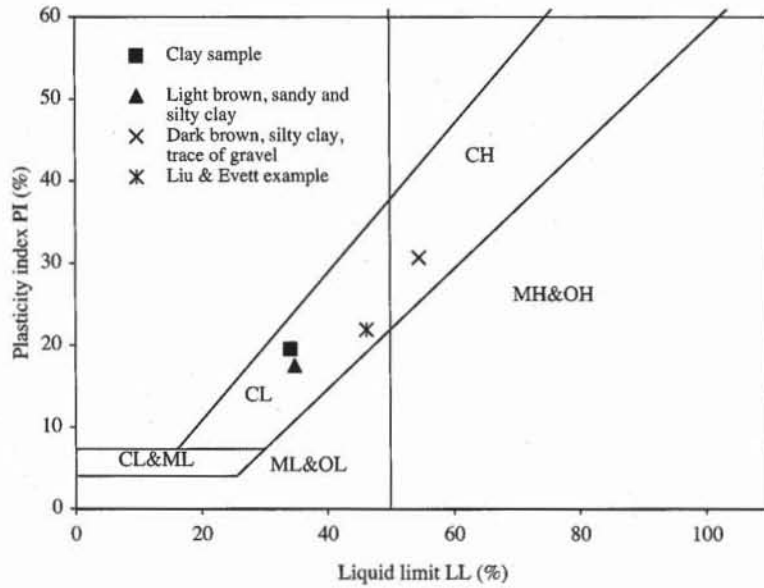


Figure 5 Position of USCS and AASHTO classification examples of Figs. 2 and 7 on plasticity chart.

EXAMPLE OF AASHTO SOIL CLASSIFICATION

Figure 6 lists the user-defined function for AASHTO classification, Fig. 7 is an example of AASHTO soil classification, and Fig. 8 lists the formulas used in Fig. 7. This function exactly follows the instructions of Table 2.

A		B
40	AASHTO	AASHTO Classification System
41	=RESULT(2)	Returns a Classification Code
42	=ARGUMENT("PP10",1)	Percent Passing No.10 Sieve
43	=ARGUMENT("PP40",1)	Percent Passing No.40 Sieve
44	=ARGUMENT("PP200",1)	Percent Passing No.200 Sieve
45	=ARGUMENT("LL",1)	Liquid Limit in %
46	=ARGUMENT("PL",1)	Plastic Limit in %
47	=LL-PL	Plasticity Index
48	="&TEXT(MAX(INT((PP200-35)*(0.2+0.005*(LL-40))+0.01*(PP200-15)*(A47-10))),0,"0")&")	Group Index
49	=IF(PP10<PP40,RETURN("ERROR: % passing No.10 must be larger than % passing No.40"))	
50	=IF(PP40<PP200,RETURN("ERROR: % passing No.40 must be larger than % passing No.200"))	
51	=IF(LL<PL,RETURN("ERROR: liquid limit must be larger or equal plastic limit"))	
52	=IF(AND(PP10<50,PP40<30,PP200<15,A47<6),RETURN("A-1a"))	
53	=IF(AND(PP40<50,PP200<25,A47<6),RETURN("A-1b"))	
54	=IF(AND(PP40<51,PP200<10,PL<=0),RETURN("A-3"))	
55	=IF(AND(PP200<35,LL<40,A47<10),RETURN("A-2-4"&A48))	
56	=IF(AND(PP200<35,LL>41,A47<10),RETURN("A-2-5"&A48))	
57	=IF(AND(PP200<35,LL<40,A47>11),RETURN("A-2-6"&A48))	
58	=IF(AND(PP200<35,LL>41,A47>11),RETURN("A-2-7"&A48))	
59	=IF(AND(PP200>=36,LL<40,A47<10),RETURN("A-4"&A48))	
60	=IF(AND(PP200>=36,LL>41,A47<10),RETURN("A-5"&A48))	
61	=IF(AND(PP200>=36,LL<40,A47>11),RETURN("A-6"&A48))	
62	=IF(AND(PP200>=36,LL>41,A47>11,PL>30),RETURN("A-7-5"&A48))	
63	=IF(AND(PP200>=36,LL>41,A47>11,PL<30),RETURN("A-7-6"&A48))	
64	=RETURN("N-C")	

Figure 6 User-defined function for AASHTO classification.

	A	B
6	Example of AASHTO Classification	
7	Light brown, sandy and silty clay	A-2-6(0)
8	Liquid limit (%) =	34.8
9	Plastic limit (%) =	17.5
10	Dark brown, silty clay, trace of gravel	A-7-5(10)
11	Liquid limit (%) =	54.5
12	Plastic limit (%) =	30.7
13	Medium brown, very gravelly, coarse sand	A-1b
14	Liu & Evett example	A-7-6(11)
15	Liquid limit (%) =	46.2
16	Plastic limit (%) =	21.9

Figure 7 Result of AASHTO classification.

	B
7	=AASHTO(68.5,36.1,18.1,B8,B9)
8	34.8
9	17.5
10	=AASHTO(79.5,69,54.3,B11,B12)
11	54.5
12	30.7
13	=AASHTO(59.1,38.5,5.1,0,0)
14	=AASHTO(85.6,72.3,58.8,B15,B16)

Figure 8 Formulas used in Fig. 7.

USE OF SOIL CLASSIFICATION

Table 5 gives a general indication of engineering properties such as permeability (Chapter 4-1), compressibility (Chapter 6-1), and strength (Chapter 7-1) of the various soil groups in USCS. Table 5 also gives an indication of the relative desirability of each group for use in earth dams, canal sections, foundations and runaways. Table 6 lists some typical values of engineering properties for compacted soils (Chapter 3-4) which may be used for preliminary analysis. However, for final analysis, the engineering soil properties must be determined from laboratory or field tests.

Soil classification is a valuable tool which provides the soil engineer with some empirical guidance through the results of field experience. However, as pointed out by Lambe and Whitman (1979), solving flow, compression, and stability problems merely on the basis of soil classification can lead to disastrous results. Empirical correlations between index properties and fundamental soil behavior have many large deviations.

TABLE 6

Typical properties of compacted soils based on results of USCS classification (after NAVFAC, 1982).

Typical names and soil groups	Group symbol	Range of maximum dry unit weight (kN/m ³)	Range of optimum moisture content (%)	Typical value of compressibility (1/MPa)		Typical strength characteristics			Typical coefficient of permeability (cm/s)
				m _v at 140 kPa	m _v at 350 kPa	Cohesion c' as compacted (kPa)	Cohesion c' as saturated (kPa)	Effective stress envelope ψ' (deg)	
Well graded gravels, gravel-sand mixtures, little or no fines	<i>GW</i>	19.6-21.2	8-11	0.02	0.02	0	0	> 38	0.03
Poorly graded gravels, gravel-sand mixtures, little or no fines	<i>GP</i>	18.1-19.6	11-14	0.03	0.03	0	0	> 37	0.05
Silty gravels, poorly graded gravel-sand-silt mixtures	<i>GM</i>	18.9-21.2	8-12	0.04	0.03	-	-	> 34	> 5 × 10 ⁻⁷
Clayey gravels, poorly graded gravel-sand-silt mixtures	<i>GC</i>	18.1-20.4	9-14	0.05	0.05	-	-	> 31	> 5 × 10 ⁻⁸
Well graded sands, gravelly sands, little or no fines	<i>SW</i>	17.3-20.4	9-16	0.04	0.03	0	0	38	> 5 × 10 ⁻⁴
Poorly graded sands, gravelly sands, little or no fines	<i>SP</i>	15.7-18.9	12-21	0.06	0.04	0	0	37	> 5 × 10 ⁻⁴
Silty sands, poorly graded sand-silt mixtures	<i>SM</i>	17.3-19.6	11-16	0.06	0.05	50	20	34	> 3 × 10 ⁻⁵
Sand-silt-clay mixture with slightly plastic fines	<i>SM-SC</i>	17.3-20.4	11-15	0.06	0.04	50	14	33	> 1 × 10 ⁻⁶
Clayey sands, poorly graded sand-clay mixtures	<i>SC</i>	16.5-19.6	11-19	0.08	0.06	74	11	31	> 3 × 10 ⁻⁷
Inorganic silts and very fine sands, rock flour, silty or clayey fine sands with slight plasticity	<i>ML</i>	14.9-18.9	12-24	0.06	0.05	67	11	32	> 5 × 10 ⁻⁶
Mixture of inorganic silt and clay	<i>ML-CL</i>	15.7-18.9	12-22	0.07	0.06	65	9	32	> 3 × 10 ⁻⁷
Inorganic clays of low to medium plasticity, gravelly clays, sandy clays, silty clays, lean clays	<i>CL</i>	14.9-18.9	12-24	0.09	0.07	65	22	28	> 5 × 10 ⁻⁸
Organic silts and organic silt-clays of low plasticity	<i>OL</i>	12.6-15.7	21-33	-	-	86	13	-	-
Inorganic silts, micaceous or diatomaceous fine sandy or silty soils, elastic silts	<i>MH</i>	11.0-14.9	24-40	0.14	0.11	72	20	25	> 3 × 10 ⁻⁷
Inorganic clays of high plasticity, fat clays	<i>CH</i>	11.8-16.5	19-36	0.19	0.11	103	11	19	> 5 × 10 ⁻⁸
Organic clays of medium to high plasticity, fat clays	<i>OH</i>	10.2-15.7	21-45	-	-	-	-	-	-

REFERENCES

- See Introduction for references to ASTM procedures (pages 4 to 6).
- LAMBE, T.W., and R.V. WHITMAN, 1979, *Soil Mechanics, SI Version*, John Wiley & Sons, Inc., New York, 553 p.
- LIU, T.K., 1970, "A review of Engineering Soil Classification Systems," *Special Procedures for Testing Soil and Rock for Engineering Purposes*, 5th Ed., American Society for Testing and Materials, ASTM Special Technical Publication No. 479, pp. 361-382.
- NAVFAC, 1982, *Soil Mechanics (Design Manual 7.1)*, Naval Facilities Engineering Command, Alexandria, 355 p.
- WAGNER, A.A., 1957, "The use of the Unified Soil Classification System by the Bureau of Reclamation," *Proceedings of the 4th International Conference on Soil Mechanics and Foundation Engineering*, London, Vol. 1, p. 125.

REVIEW QUESTIONS

1. What is the purpose of a soil classification? How many soil classification systems can you name?
2. In the USCS, what material properties are used to classify coarse-grained soils?
3. In the USCS, what material properties are used to classify fine-grained soils?

EXERCISES

1. The results of particle size analyses, and where appropriate, limit tests on samples of four soils are given below. Classify each soil according to the USCS.

Particle size	Percentage smaller			
	Soil A	Soil B	Soil C	Soil D
63 mm	100	—	100	—
20 mm	64	—	76	—
6.3 mm	39	100	65	—
2 mm	24	98	59	—
600 μm	12	90	54	—
212 μm	5	9	47	100
63 μm	0	3	34	95
20 μm	—	—	23	69
6 μm	—	—	14	46
2 μm	—	—	7	31
Liquid limit	—	—	26	42
Plastic index	—	—	9	18

2. Same as Exercise 2 but for the AASHTO classification system.
3. Determine the extreme values of soil parameters that give GW in the USCS. You may find the necessary parameters and their extreme values by working the flowchart of Fig. 1 backward or by using the custom function of the USCS. Having determined the necessary parameters and their extreme values, use those to determine the possible AASHTO classifications. Compare your results with those in Table 3.

4. Repeat Exercise 4 for one of the following USCS classifications: GP, GM, GC, SW, SP, SM, SC, ML, CL, O, MH, CH, and OH. Compare your results with those in Table 3.
5. Determine the extreme values of soil parameters that give A-1a in the AASHTO classification system. You may find the necessary parameters and their extreme values in Table 2. Having determined the necessary parameters and their extreme values, use those to determine the possible USCS classifications. Compare your results with those in Table 4.
6. Repeat Exercise 5 for one of the following AASHTO classifications: A-1b, A-3, A-2-4, A-2-5, A-2-6, A-2-7, A-4, A-5, A-6, A-7-5, and A-7-6. Compare your results with those in Table 4.

3

Density and Compaction

- 3-1** Weight-volume relationships
- 3-2** Unit weight of cohesive soils
- 3-3** Determination of specific gravity
- 3-4** Principles of compaction
- 3-5** Compaction tests
- 3-6** Sand cone method

3-1 Weight-Volume Relationships

DEFINITIONS

As illustrated in Fig. 1a, soils are made of solid particles with voids in between. For most soils the particles are made of soil minerals, and the voids are filled with air and water. Soils are three-phase materials with solid, liquid, and air constituents. Figure 1a shows a soil sample of total volume V and weight W . In Fig. 1b, the volumes and weight of its solid, water, and air constituents are related through

$$W = W_w + W_s \quad V = V_v + V_s = V_a + V_w + V_s \quad V_v = V_a + V_w \quad (1)$$

where W_s is the weight of solid grains, W_w the weight of water, V_s the volume of soil grains, V_w the volume of water, V_a the volume of air, and V_v the volume of voids occupied by water and air. It is assumed that the weight of air W_a is negligible (i.e., $W_a = 0$).

The unit weights of the water constituent and solid constituent are denoted γ_w and γ_s , respectively, where

$$\gamma_s = \frac{W_s}{V_s} \quad \text{and} \quad \gamma_w = \frac{W_w}{V_w} \quad (2)$$

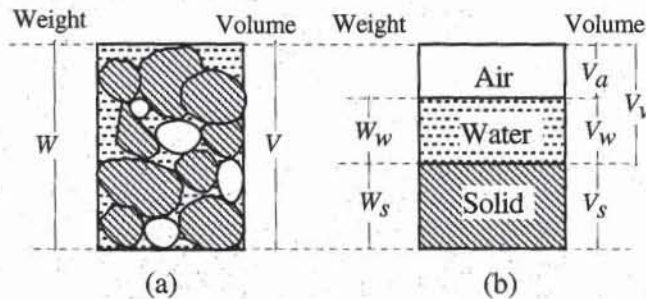


Figure 1 Definition of (a) the weight and volume of a soil sample, and (b) the weights and volumes of its solid, water, and air constituents.

The specific gravity G_s is the ratio of the solid and water unit weights:

$$G_s = \frac{\gamma_s}{\gamma_w} \quad (3)$$

The total or bulk unit weight γ of the sample of Fig. 1a is

$$\gamma = \frac{W}{V} \quad (4)$$

When the sample of Fig. 1b has no water but the same total volume V , its dry unit weight γ_d is

$$\gamma_d = \frac{W_s}{V} \quad (5)$$

When the sample has its voids filled completely with water, it is said to be fully saturated. When its total volume V is still equal to V after saturation, its saturated unit weight γ_{sat} is

$$\gamma_{\text{sat}} = \frac{W_s + V_v \gamma_w}{V} \quad (6)$$

In soil mechanics, it is also common to define the buoyant unit weight γ_b , which is the unit weight of the saturated soils immersed in water (i.e., uplifted by the buoyancy force $= \gamma_w V$):

$$\gamma_b = \frac{W_s + V_v \gamma_w - V \gamma_w}{V} = \gamma_{\text{sat}} - \gamma_w \quad (7)$$

The total unit mass ρ , dry unit mass ρ_d , saturated unit mass ρ_{sat} , buoyant unit mass ρ_b , water unit mass ρ_w , and solid unit mass ρ_s are related to their unit weight counterparts through

$$\gamma = \rho g, \quad \gamma_s = \rho_s g, \quad \gamma_w = \rho_w g, \quad \gamma_{\text{sat}} = \rho_{\text{sat}} g, \quad \gamma_d = \rho_d g, \quad \text{and} \quad \gamma_b = \rho_b g \quad (8)$$

where g is the earth gravity acceleration (i.e., $g = 9.81 \text{ m/s}^2$). The dimensions of unit weight is force divided by volume, whereas the dimension of unit mass is mass divided by volume:

$$[\gamma] = [\gamma_s] = [\gamma_w] = [\gamma_{\text{sat}}] = [\gamma_d] = [\gamma_b] = FL^{-3} = MLT^{-2}L^{-3} = MT^{-2}L^{-2}$$

$$[\rho] = [\rho_s] = [\rho_w] = [\rho_{\text{sat}}] = [\rho_d] = [\rho_b] = ML^{-3} \quad (9)$$

where F , M , L , and T represent the dimension of force, mass, length, and time, respectively. The metric unit generally used for all unit weights is kN/m^3 , whereas the units for unit mass can be g/cm^3 , kg/m^3 , or tons/m^3 .

In soil mechanics, the proportions of the solid, liquid, and air constituents are characterized by five additional dimensionless quantities: e , n , w , S_r , and D_r . The void ratio e is the ratio of the volume of voids to the solid volume:

$$e = \frac{V_v}{V_s} \quad (10)$$

The porosity n is the ratio of the volume of voids to the total volume:

$$n = \frac{V_v}{V} \quad (11)$$

The water content w is the ratio of the weight of water to the dry weight:

$$w = \frac{W_w}{W_s} \times 100 \quad (\%) \quad (12)$$

The degree of saturation S_r is the ratio of the volume of water to the volume of voids:

$$S_r = \frac{V_w}{V_v} \times 100 \quad (\%) \quad (13)$$

In the case of coarse-grained soils, the relative density D_r is defined to characterize the degree of compaction:

$$D_r = \frac{e_{\max} - e}{e_{\max} - e_{\min}} \times 100 \quad (\%) \quad (14)$$

where e_{\max} is the maximum void ratio, e_{\min} the minimum void ratio, and e the present void ratio. D_r varies from 0 when $e = e_{\max}$ to 100% when $e = e_{\min}$. In reality, e_{\min} and e_{\max} are not the absolute maximum and minimum void ratios of a soil, respectively. They are just index void ratios obtained by standard procedures. In general, the values of w , S_r , and D_r are expressed in percent, whereas those of e and n are expressed as decimal numbers.

RELATIONS

Various relations can be obtained directly between γ , γ_d , γ_{sat} , γ_b , G_s , e , n , w , and S_r by using Fig. 2, where all the volumes and weights of Fig. 1b are divided by the solid volume V_s (i.e., by selecting $V_s = 1$). The following relations were also used in obtaining Fig. 2:

$$\frac{W_w}{V_s} = \frac{W_w}{W_s} \frac{W_s}{V_s} = w\gamma_s = wG_s\gamma_w \quad \text{and} \quad \frac{V_w}{V_s} = \frac{V_w}{W_w} \frac{W_w}{V_s} = \frac{wG_s\gamma_w}{\gamma_w} = wG_s \quad (15)$$

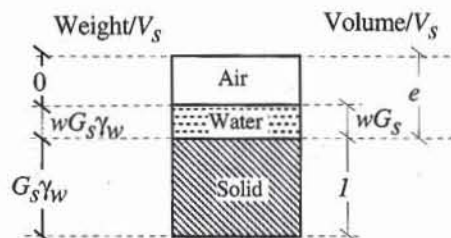


Figure 2 Schematic definition of the weight and volume for a soil sample having a unit solid volume ($V_s = 1$).

A few useful relations are

$$n = \frac{e}{1+e} \quad \text{and} \quad e = \frac{n}{1-n} \quad (16)$$

$$S_r = \frac{G_s w}{e} \quad (17)$$

$$\gamma = \gamma_w \frac{G_s(1+w)}{1+e} = \gamma_w \frac{G_s + S_r e}{1+e} = \gamma_w \frac{G_s(1+w)}{1 + G_s(w/S_r)} \quad (18)$$

$$\gamma_d = \gamma_w \frac{G_s}{1+e} = \frac{\gamma}{1+w} = \gamma_w \frac{G_s}{1 + G_s(w/S_r)} \quad (19)$$

$$\gamma_{\text{sat}} = \gamma_w \frac{G_s + e}{1+e} = \gamma_w \frac{G_s(1+w)}{1 + G_s w} \quad (20)$$

Table 1 lists some additional useful relations that were obtained after some algebraic manipulations. Note that the water content w in Table 1 is the saturated water content, which is required to get a full saturation (i.e., $S_r = 100\%$). When using Eqs. 16 to 20 and those of Table 1, make sure to use decimal values (e.g., 0.1) and not percents (e.g., 10%) for w , S_r , and D_r .

TYPICAL VALUES

By definition, S_r and D_r must be between 0 and 100%. They cannot be negative or larger than 100%. $S_r = 0\%$ corresponds to a dry soil, whereas $S_r = 100\%$ corresponds to a fully saturated soil. $D_r = 0\%$ corresponds to the loosest state of a coarse-grained soil, whereas $D_r = 100\%$ corresponds to its densest state. Tables 2 and 3 list some values of specific gravity of solids for minerals and typical soils. Table 4 and 5 list some values of dry unit weight, bulk (or natural) unit weight, saturated unit weight, porosity, and void ratio for typical soils.

REFERENCES

- DJOENAI, W.J., 1985, A compendium of soil properties and correlations, M. Eng. Sci. thesis, University of Sydney, Sydney, Australia.
- JUMIKIS, A.R., 1962, *Soil Mechanics*, Van Nostrand Co., Princeton, NJ, pp. 90-91.
- KEDZI, A., 1974, *Handbook of Soil Mechanics*, Vol. I: Soil Physics, Elsevier Publishing Co., Amsterdam, 294 pp.
- LAMBE, T.W., and R.V. WHITMAN, 1979, *Soil Mechanics, SI Version*, John Wiley & Sons, New York, 553 pp.

REVIEW QUESTIONS

1. Define *specific gravity of soil*.
2. Define *total weight, dry weight, and saturated unit weight*.
3. Define *void ratio, porosity, and relative density*.
4. What are typical values of specific gravity for soils?

Continues on page 134

TABLE 1

Relation between G_s , γ_d , γ_{sat} , saturated w , n , and e (After Jumikis, 1962)

	G_s	γ_d	γ_{sat}	Saturated w	n	e
G_s, γ_d			$(1 - \frac{1}{G_s})\gamma_d + \gamma_w$	$\frac{\gamma_w}{\gamma_d} - \frac{1}{G_s}$	$1 - \frac{\gamma_d}{G_s \gamma_w}$	$\frac{G_s \gamma_w}{\gamma_d} - 1$
G_s, γ_{sat}		$\frac{\gamma_{sat} - \gamma_w}{G_s - 1} G_s$		$\frac{\gamma_w - \gamma_{sat}/G_s}{\gamma_{sat} - \gamma_w}$	$\frac{G_s - \gamma_{sat}/\gamma_w}{G_s - 1}$	$\frac{G_s \gamma_w - \gamma_{sat}}{\gamma_{sat} - \gamma_w}$
G_s, w		$\frac{G_s}{1 + w G_s} \gamma_w$	$\frac{1 + w}{1 + w G_s} G_s \gamma_w$		$\frac{w G_s}{1 + w G_s}$	$w G_s$
G_s, n		$G_s(1 - n)\gamma_w$	$(G_s - n(G_s - 1))\gamma_w$	$\frac{n}{(1 - n)G_s}$		$\frac{n}{1 - n}$
G_s, e		$\frac{G_s}{1 + e} \gamma_w$	$\frac{G_s + e}{1 + e} \gamma_w$	$\frac{e}{G_s}$	$\frac{e}{1 + e}$	
γ_d, γ_{sat}	$\frac{\gamma_d}{\gamma_d + \gamma_w - \gamma_{sat}}$			$\frac{\gamma_{sat}}{\gamma_d} - 1$	$\frac{\gamma_{sat} - \gamma_d}{\gamma_w}$	$\frac{\gamma_{sat} - \gamma_d}{\gamma_d + \gamma_w - \gamma_{sat}}$
γ_d, w	$\frac{\gamma_d}{\gamma_w - w\gamma_d}$		$(1 + w)\gamma_d$		$w \frac{\gamma_d}{\gamma_w}$	$\frac{w\gamma_d}{\gamma_w - w\gamma_d}$
γ_d, n	$\frac{\gamma_d}{(1 - n)\gamma_w}$		$\gamma_d + n\gamma_w$	$\frac{n\gamma_w}{\gamma_d}$		$\frac{n}{1 - n}$
γ_d, e	$(1 + e)\frac{\gamma_d}{\gamma_w}$		$\frac{e\gamma_w}{1 + e} + \gamma_d$	$\frac{e}{1 + e} \frac{\gamma_w}{\gamma_d}$	$\frac{e}{1 + e}$	
γ_{sat}, w	$\frac{\gamma_{sat}}{\gamma_w + w(\gamma_{sat} - \gamma_w)}$	$\frac{\gamma_{sat}}{1 + w}$			$\frac{w\gamma_{sat}}{(1 + w)\gamma_w}$	$\frac{w\gamma_{sat}}{\gamma_w - w(\gamma_{sat} - \gamma_w)}$
γ_{sat}, n	$\frac{\gamma_{sat} - n\gamma_w}{(1 - n)\gamma_w}$	$\gamma_{sat} - n\gamma_w$		$\frac{n\gamma_w}{\gamma_{sat} - n\gamma_w}$		$\frac{n}{1 - n}$
γ_{sat}, e	$(1 + e)\frac{\gamma_{sat}}{\gamma_w} - e$	$\gamma_{sat} - \frac{e}{1 + e} \gamma_w$		$\frac{e\gamma_w}{\gamma_{sat} + e(\gamma_{sat} - \gamma_w)}$	$\frac{e}{1 + e}$	
w, n	$\frac{n}{(1 - n)w}$	$\frac{n}{w} \gamma_w$	$n \frac{1 + w}{w} \gamma_w$			$\frac{n}{1 - n}$
w, e	$\frac{e}{w}$	$\frac{e}{(1 - e)w} \gamma_w$	$\frac{(1 + w)e}{(1 + e)w} \gamma_w$		$\frac{e}{1 + e}$	

TABLE 2

Specific gravity of minerals
(after Lambe and Whitman, 1979)

Mineral	Specific gravity
Quartz	2.65
K-feldspars	2.54-2.57
Na-Ca-feldspars	2.62-2.76
Calcite	2.72
Dolomite	2.85
Muscovite	2.7-3.2
Biotite	2.8-3.2
Chlorite	2.6-2.9
Pyrophyllite	2.84
Serpentine	2.2-2.7
Kaolinite	2.62-2.66
Halloysite	2.55
Illite	2.60-2.86
Montmorillonite	2.75-2.78
Attapulgitite	2.30

TABLE 3

Typical values of specific gravity of various soils (after Djoenaidi, 1985)

Type of soil		Specific gravity
Inorganic	Gravel	2.65
	Coarse and medium sand	2.65
	Fine sand (silty)	2.65
	loess, rock flour, sandy silt	2.67
Inorganic	Slightly clayey sand	2.65
	Sandy silt	2.66
	Silt	2.67–2.70
	Clayey sand	2.67
	Clayey sandy silt	2.67
	Clayey silt	2.68
	Sand–clay	2.68
	Sand–silt–clay	2.69
	Silt–clay	2.71
	Sandy clay	2.70
	Silty clay	2.75
	Lean clay	2.75
	Clay	2.72–2.80
	Organic	Silts with traces of organic matter
Organic alluvial muds		2.13–2.60
Peat		1.50–2.15

TABLE 4

Maximum and minimum values of void ratio and dry unit weight for granular soils (after Lambe and Whitman, 1979)

Description	Void ratio		Dry unit weight (kN/m ³)	
	e_{\max}	e_{\min}	$\gamma_{d\min}$	$\gamma_{d\max}$
Uniform spheres	0.92	0.35	—	—
Standard Ottawa sand	0.80	0.50	14.5	17.3
Clean Uniform sand	1.0	0.4	13.0	18.5
Uniform inorganic silt	1.1	0.4	12.6	18.5
Silty sand	0.9	0.3	13.7	20.0
Fine to coarse sand	0.95	0.2	13.4	21.7
Micaceous sand	1.2	0.4	11.9	18.9
Silty sand and gravel	0.85	0.14	14.0	22.9

REVIEW QUESTIONS cont.

5. What are typical values of total, dry, and saturated unit weights?
6. What are typical values of void ratio for sands and clays?
7. Define *degree of saturation*. Is it possible for a soil to have a degree of saturation of 120%?

EXERCISES

1. For a moist soil, given $V = 1.2 \text{ m}^3$; $W = 23.04 \text{ kN}$; $w = 8.6\%$; and $G_s = 2.71$, determine the bulk unit weight, dry unit weight, void ratio, porosity, degree of saturation, and volume of water V_w .
2. The following laboratory measurement were made on a sample of soft clay taken under the water table: total volume $V = 31.3 \text{ cm}^3$; total weight $W = 0.47 \text{ N}$; weight after oven drying $W_{\text{dry}} = 0.258 \text{ N}$; and specific gravity

TABLE 5

Range of values of void ratio, porosity and unit weight of typical soils (after Kedzi, 1974)

Soil type	State of soil	Porosity (%)	Void ratio	Unit weight (kN/m ³)			
				Dry	Natural	Saturated	Buoyant
Sandy gravel	Loose	38-42	0.61-0.72	14-17	18-20	18-21	8-11
	Dense	18-25	0.22-0.33	19-21	20-23	21-23	12-14
Coarse sand, medium sand	Loose	40-45	0.67-0.82	13-15	16-19	17-19	8-10
	Dense	25-32	0.33-0.47	17-18	18-21	20-21	10-11
Uniform fine sand	Loose	45-48	0.82-0.92	14-15	15-19	19-20	9-10
	Dense	33-36	0.49-0.56	17-18	18-21	21-22	11-12
Coarse silt	Loose	45-55	0.82-1.22	13-15	15-19	18-20	8-10
	Dense	35-40	0.54-0.67	16-17	17-21	20-21	10-11
Silt	Soft	45-50	0.82-1.00	13-15	16-20	18-20	8-10
	Slightly plastic	35-40	0.54-0.67	16-17	17-21	20-21	10-11
	Hard	30-35	0.43-0.54	18-19	18-19	21-22	12-13
Lean clay	Soft	50-55	1.00-1.22	13-14	15-18	18-19	8-9
	Slightly plastic	35-45	0.54-0.82	15-18	17-21	19-22	10-13
	Hard	30-35	0.43-0.54	18-19	18-22	21-22	12-13
Fat clay	Soft	60-70	1.50-2.33	9-15	12-18	16-22	6-12
	Slightly plastic	40-55	0.67-1.22	15-18	15-20	20-23	10-13
	Hard	30-40	0.43-0.67	18-20	17-22	22-24	12-14

$G_s = 2.7$. Determine the the bulk unit weight, water content, void ratio, porosity, and degree of saturation.

- For a given soil, the in situ void ratio e is 0.8 and the soil specific gravity G_s is 2.7. Calculate the porosity, dry unit weight, and saturated unit weight. What would the bulk unit weight be when the soil is 60% saturated?
- A base course for a highway is compacted to a unit weight of 18.25 kN/m³ at a water content of 14.6%. The specific gravity G_s of the soil is 2.81. Specifications require compaction to achieve a void ratio of no greater than 0.80. Has this specification been met?
- A soil sample has a mass of 129.1 g and a volume of 56.4 cm³. The mass of the soil grains is 121.5 g. The soil grains' specific gravity G_s is 2.7. Find the water content w , the void ratio e , and the degree of saturation S_r .
- A cylinder contains 500 cm³ of loose dry sand, which weighs 750 g. The volume is reduced by vibration to 10% of the original volume. Assume that the specific gravity of the sand grains is $G_s = 2.65$. For loose sand, compute the void ratio, porosity, and dry unit weight. Compute the same quantities for vibrated sand.
- The total volume of a soil specimen is 85 cm³. Its weight is 155 g. The dry weight of the specimen is 122 g. The density of the solid G_s is 2.75. Calculate the water content, void ratio, porosity, degree of saturation, bulk unit weight, and dry unit weight.
- A soil has a unit weight of 19.93 kN/m³, a specific density G_s of 2.67, and a water content w of 12.6%. Determine its dry unit weight, void ratio, porosity, and degree of saturation. What is the weight of water needed to fully saturate 1 m³ of this soil?
- Soil has been compacted in an embankment at a bulk unit weight of 21.09 kN/m³ and a water content of 12%. The value of soil specific gravity G_s is 2.65. Calculate the dry unit weight, void ratio, and degree of saturation. Would it be possible to compact this soil at a water content of 13.5% to a dry unit weight of 19.62 kN/m³? Justify your answer.

3-2 Unit Weight of Cohesive Soils

OBJECTIVE

The unit weight of cohesive soils is determined by either measuring the weight of sample trimmed to measurable volumes or by weighing in water. The latter method applies to specimens of irregular shapes that cannot be trimmed easily.

EQUIPMENT

The equipment for measuring the unit weight of cohesive soils (Fig. 1) by trimming is listed below.

- Balance accurate to 0.01 g.
- Ring with cutting edge (about 5 cm in diameter and 2 cm high).
- Calipers.
- Wire saw.
- Drying oven.
- Evaporating dish.

The following equipment is also required for weighing in water:

- Support frame for suspending the sample to a line attached to the balance.
- Wax and pan to melt wax. Blocks of solidified wax are readily available from most hardware stores.
- Container filled with about 1 L of water.

TEST PROCEDURE

Trimming

1. Measure the weight of the clean cutting ring, and determine its internal diameter and height by using a caliper.



Figure 1 Equipment for measurement of unit weight of cohesive soils. Balance accurate to 0.01 g, solidified wax block, and wax bath, container filled with water, and evaporating dish

2. Gently push the cutting ring completely into the cohesive soil. With the help of a knife, cut a larger block containing the cutting ring and the sample soil.
3. Cut the excess soil on both ends of the ring by using a wire saw as shown in Fig. 2. Also clean the sides of the cutting ring from any excess soil.
4. Weigh the ring with the soil inside.
5. Oven dry it and measure its dry weight.

Weighing in Water

1. Trim the specimen to a convenient bulky shape about 5 cm in size. Avoid having sharp corners or holes, as those create air pockets when coating the specimen with wax.
2. Attach the specimen to 50 cm of fishing line and weigh the specimen as shown in Fig. 3a.
3. Immerse the specimen in a bath of hot wax as shown in Fig. 4. The wax must be heated to just above its melting point. Repeat the immersion process several times to obtain a specimen continuously coated by wax. If the sample is fragile and has a tendency to disintegrate, use a brush to coat it with wax before immersing completely it in the wax bath.
4. After the wax has solidified on the sample, attach the waxed sample to the scale and weigh it again as shown in Figs. 3a and 5.
5. Lift the waxed specimen, put a bucket of water right under the scale, and immerse the specimen in the water as shown in Figs. 3b and 6. Record its immersed weight.

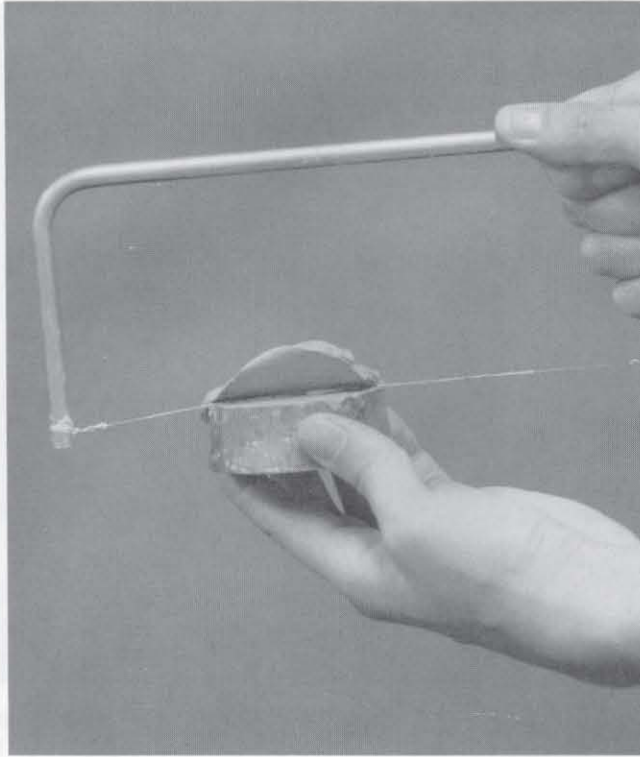


Figure 2 The unit weight of a cohesive soil can be determined by measuring the weight of a sample of measurable volume. The sample is cut using a ring with a cutting edge, then its ends are trimmed using a wire saw.

6. Remove the sample from the weighing bath, remove the excess water with a rag, and cut a smaller sample that is free of wax for water determination. Measure its weight, oven dry it, and measure its dry weight.

Determination of Wax Unit Weight

When weighing in water, the wax unit weight γ_p needs to be determined, but only once for a series of tests. Because wax is lighter than water, it does not sink into water and needs to be ballasted. As shown in Fig. 7, (a) measure the submerged weight W_1 of a metal block heavy enough to sink the wax piece in water, (b) measure the weight W_2 of the wax piece alone, and (c) measure the total buoyant unit weight W_3 of both metal and wax pieces. The wax unit weight is

$$\gamma_p = \gamma_w \frac{W_2}{W_1 + W_2 - W_3} \quad (1)$$

where γ_w is the water unit mass. A typical value for γ_w is 9.32 kN/m³.

COMPUTATION

Trimming

The total unit weight is calculated as follows:

$$\gamma = \frac{W - W_{\text{ring}}}{\pi/4 D^2 H} \quad (2)$$

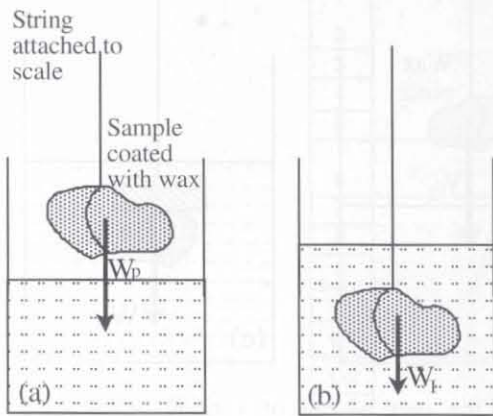


Figure 3 Use of buoyancy to measure volume.



Figure 4 The specimen is immersed in a bath of melted wax.

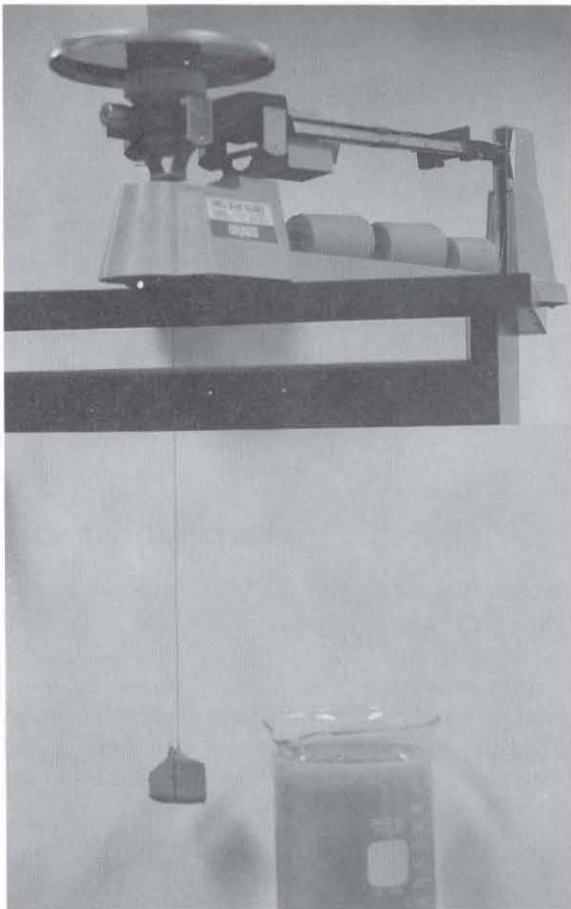


Figure 5 The sample is weighed by suspending it to a fishing line attached to the balance.

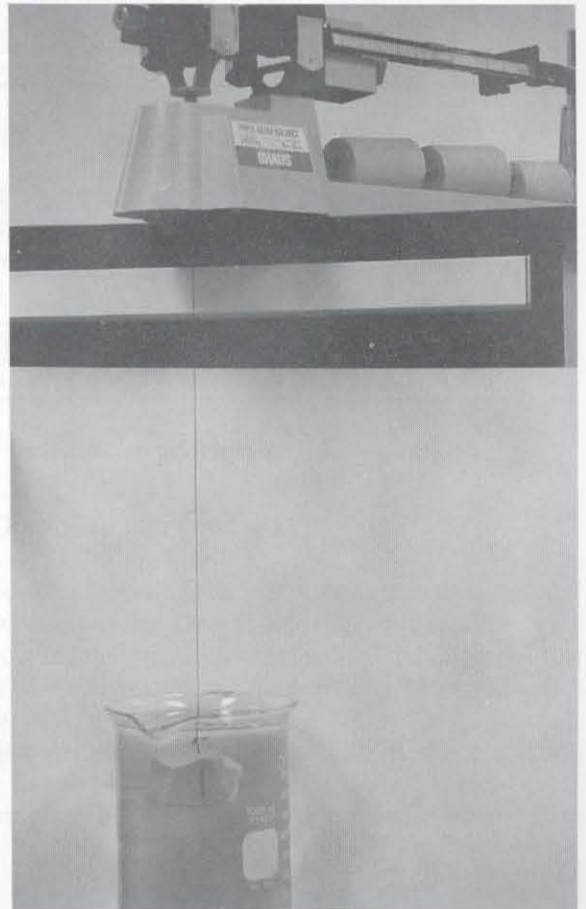


Figure 6 The waxed soil sample is immersed in water and its buoyant weight is measured.

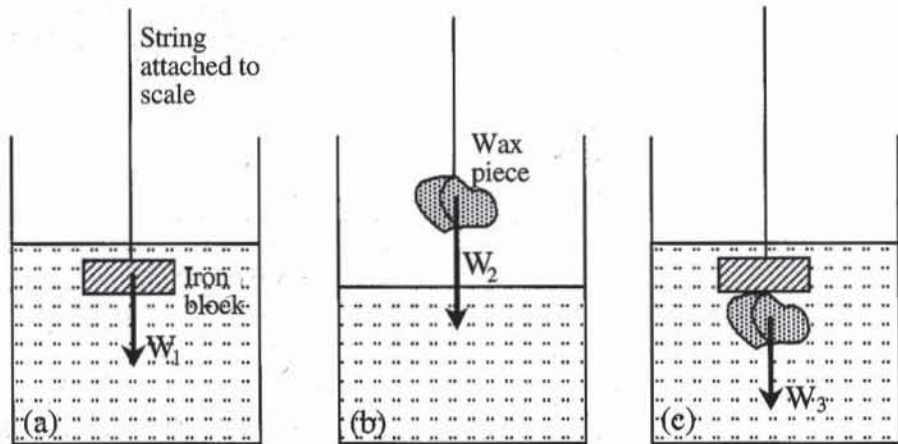


Figure 7 Steps to determine the unit weight of a body lighter than water.

where W is the weight of the sample and ring, W_{ring} the weight of the sampling ring, D the diameter of the ring, and H the height of the ring. The water content is

$$w = \frac{W_w - W_d}{W_d - W_{\text{dish}}} \times 100 \quad (\%) \quad (3)$$

where W_w is the weight of the soil sample and weighing dish, W_d the weight of the oven-dried soil sample and weighing dish, and W_{dish} the weight of the weighing dish. The soil dry unit weight is

$$\gamma_d = \frac{\gamma}{1 + w} \quad (4)$$

Weighing in Water

The total unit weight of the soil is calculated as follows:

$$\gamma = \gamma_w \frac{W}{W_p - W_I - (\gamma_w / \gamma_p) (W_p - W)} \quad (5)$$

where W is the weight of the soil sample, W_p the weight of the waxed soil sample, W_I the immersed weight of the waxed soil sample, γ_w the water unit weight, and γ_p the wax unit weight. The water content and dry unit weight are calculated using Eqs. 3 and 4.

EXAMPLE

Figure 8 shows an example for the measurement of soil unit weight by weighing in water. The formulas used in Fig. 8 are shown in Fig. 9.

	A	B	C	D
1	Unit weight of soils			
2	Analyst name: <i>J.P. Bardet</i>			
3	Test date: <i>11/13/90</i>			
4	Sample description: <i>Brown clay</i>			
5				
6	SOIL UNIT WEIGHT	Sample 1	Sample 2	Sample 3
7	Mass of soil sample (g) M	511.40		
8	Mass of waxed soil (g) M_p	519.50		
9	Mass of immersed soil (g) M_i	215.50		
10	Mass of trimmed sample (g) M_t	41.2		
11	Mass of dry sample (g) M_d	37.1		
12	Bulk unit weight $\gamma_{sat} =$	16.53 kN/m ³		
13	Water content $w =$	11.05%		
14	Dry unit weight $\gamma_d =$	14.89 kN/m ³		
15				
16	WAX UNIT WEIGHT	Sample 1	Sample 2	Sample 3
17	Mass of immersed iron block (g) M_{wi}	51.40	51.40	
18	Mass of wax block (g) M_{wb}	72.10	81.65	
19	Mass of immersed iron and wax blocks (g) M_{wbi}	48.50	47.56	
20	Unit weight of wax $\gamma_p =$	9.42 kN/m ³		

Figure 8 Example of data set for measurement of soil unit weight.

	A	B	C
12	Bulk unit weight $\gamma_{sat} = \text{=AVERAGE}(M/(M_p - M_i - (M_p - M)/B20) * 9.8)$		kN/m ³
13	Water content $w = \text{=AVERAGE}((M_t - M_d)/M_d)$		
14	Dry unit weight $\gamma_d = \text{=gsat}/(1+w)$		kN/m ³
20	Unit weight of wax $\gamma_p = \text{=AVERAGE}(9.8 * M_{wb}/(M_{wi} + M_{wb} - M_{wbi}))$		kN/m ³

Figure 9 Formulas used in Fig. 8.

REVIEW QUESTIONS

1. What is the simplest method for measuring the unit weight of cohesive soils? Under what conditions do we use weighing in water to determine unit weight?
2. What precaution should you take if you must measure the unit weight of soils with many air pockets? Should you or not fill and coat these holes with wax?
3. Can you apply the technique described in this chapter to measure the unit weight of sands? Why?
4. Derive Eq. 1, which determines the unit weight of a sample lighter than water.

EXERCISE

1. Calculate the unit weight of a cohesive soil sample by trimming and weighing in water, and compare the results.

3-3

Determination of Specific Gravity

OBJECTIVE

The specific gravity G_s of a soil is the ratio between the unit masses of soil particles and water. G_s is useful for determining weight-volume relationships.

$$G_s = \frac{\gamma_s}{\gamma_w}$$

EQUIPMENT

The equipment for determination of specific gravity includes:

- Volumetric flasks (250 or 500 mL) with stoppers, numbered and calibrated (Fig. 1).
- Vacuum pump.
- Balance accurate to 0.01 g.
- Distilled deaired water.
- Thermometer, ranging from 0 to 50°C, accurate to 0.5°C.
- Drying oven.
- Evaporating dish.

DEAIRING WATER AND FLASK CALIBRATION

The test water must be deaired and the volumetric flask calibrated. The flask calibration does not need to be repeated before each experiment.

1. As shown in Fig. 2, water is deaired in the flask which is three-fourths filled by applying vacuum through the stopper. While water is deaired, bubbles appear because the reduced air pressure causes the water to boil. Deaired water should be stored in airtight bottles.



Figure 1 Equipment for measurement of specific density. Balance sensitive to 0.01g, 500-mL volumetric flask, evaporating dish, supply of deaired water, and thermometer.

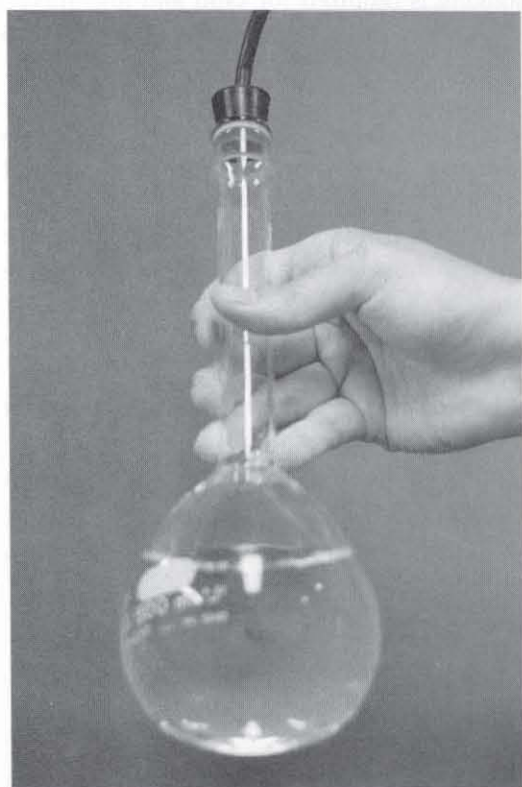


Figure 2 Water is deaired by filling the flask about three-fourths and applying vacuum through the stopper.

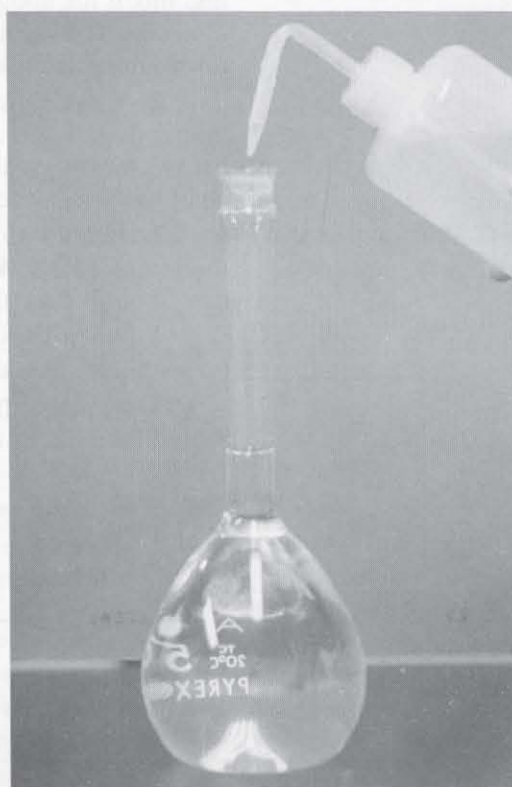


Figure 3 During the flask calibration, the flask is carefully filled with deaired water up to its mark.

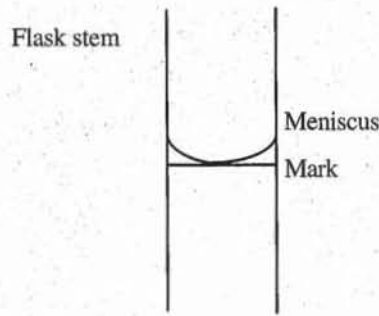


Figure 4 The volumetric flask is filled when the bottom of the water meniscus is aligned with the mark on its stem.

2. The volumetric flask is calibrated by measuring its weight when it is filled with deaired water. Wash the volumetric flask. As shown in Fig. 3, carefully fill it to the volume mark with deaired water, without splashing to introduce air bubbles. The flask is filled correctly when the mark on its stem is at the bottom of the water meniscus, as shown in Fig. 4. Put the stopper on the volumetric flask, and measure its weight W_{fw} . Measure the water temperature T . The bottle should be calibrated at the same temperature as during the test. Any change in water temperature modifies the flask volume.

TEST PROCEDURE

1. Take a sample of 100 to 120 g of air-dried soil. For fine-grained soils, mix the sample with water in an evaporating dish to make about 200 mL of soil-water mixture. For clays, transfer the soil-water mixture into a malt mixer container and mix it for about 5 to 10 min. No soaking is required for sand and fine gravel. However, the aggregates should be broken into pieces small enough to go into the volumetric flask.

2. Transfer the soil-water mixture from the evaporating dish into the volumetric flask. Wash any remaining soil into the flask using a wash bottle. Add sufficient water to fill the flask two-thirds to three-fourths full. Do not fill it completely, because its contents must be agitated under vacuum.

3. Attach the flask to a vacuum line and for at least 10 min gently agitate the mixture while keeping it away from the flask stopper. The reduced air pressure should cause the water to boil.

4. When the deairing process is complete, add deaired water to fill the calibrated flask volume (see Fig. 3).

5. Measure the weight of the flask. Measure the water temperature, which should be close to that of the temperature of flask calibration.

6. Empty the flask and its contents into a deep evaporating dish and oven dry. Measure the weight of dry soil.

7. Repeat the test to calculate additional values of G_s , until the values of G_s are within 2% of each other.

COMPUTATION

The specific gravity G_s of a soil is calculated as follows:

$$G_s = \frac{W_s}{W_s + W_{fw} - W_{fs}} \quad (1)$$

where W_s is the weight of the dry soil, W_{fs} the weight of the flask filled with soil and water, and W_{fw} the weight of the flask filled with deaired water only.

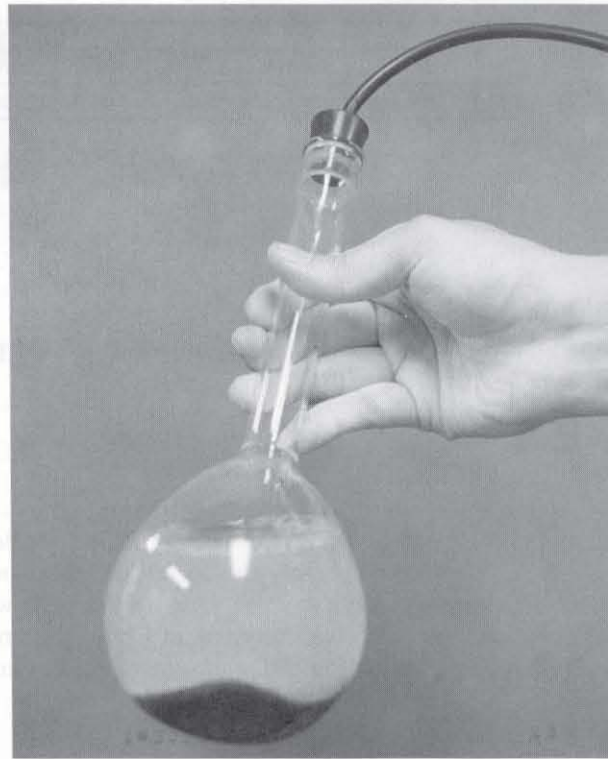


Figure 5 The flask is attached to a vacuum line, and its mixture is gently agitated by turning the flask for at least 10 min.

EXAMPLE

Figure 6 shows an example of a data set for the specific gravity of soils. The formulas used in Fig. 6 are shown in Fig. 7.

	A	B	C
1	Specific Gravity		
2	Analyst name: <i>J.E. Bowles</i>		
3	Test date: <i>11/13/90</i>		
4	Sample description:		
5			
6		Sample 1	Sample 2
7	Mass of flask and water (g) M_w	693.27	693.27
8	Mass of flask, soil and water (g) M_s	753.66	754.69
9	Mass of evaporating dish (g) M_c	254.52	270.52
10	Mass of evaporating dish and dry soil (g) M_d	350.11	368.49
11	Specific Gravity G_s	2.72	2.68
12	Average Specific Gravity $G_s =$	2.70	

Figure 6 Example of data set for measurement of specific gravity.

	A	B	C
11	Specific Gravity G_s	$= (M_d - M_c) / (M_d - M_c + M_{fw} - M_{fs})$	$= (M_d - M_c) / (M_d - M_c + M_{fw} - M_{fs})$
12	Average Specific Gravity G_s	$= \text{AVERAGE}(G_s)$	

Figure 7 Formulas used in Fig. 6.

REFERENCE

See Introduction for references to ASTM procedures (pages 4 to 6).

REVIEW QUESTIONS

1. Define *specific gravity of soil*.
2. What are typical values of the specific gravity for soils?
3. Can you apply the technique described in this section to measure the specific gravity of material lighter than water?
4. Why do we use vacuum while determining the specific gravity of soils?
5. What is the effect of water temperature on the determination of the specific gravity of soils?

3-4 The Principles of Compaction

INTRODUCTION

For many civil engineering projects, soils have to be compacted to a denser state to improve their engineering properties. They are compacted by mechanical means with rolling, ramming, or vibrating equipment. The soil density to be obtained by field compaction is defined by means of two basic laboratory compaction tests: the standard and modified compaction tests. In 1933, Proctor introduced a laboratory test to control soil compaction, which later became known as the standard Proctor compaction test. The other compaction test, the modified AASHTO test, was later introduced to simulate the compaction of heavy equipment, which produces higher compaction energy.

DEFINITIONS

Soil compaction consists of closely packing the soil particles together by mechanical means, thus increasing the soil dry unit weight. As illustrated in Fig. 1a, soils are made of solid grains with voids filled with air and water. The proportion of solid, liquid, and air is represented in Fig. 1b. As shown in Fig. 1c, compaction only reduces the air fraction. It barely changes the water content and has no effect on the solid volume. In theory, the most efficient compaction process should remove the air fraction completely. However, in practice, compaction cannot completely eliminate the air fraction, but only reduces it to a minimum, provided that appropriate techniques are used.

Compaction should not be confused with consolidation, which corresponds to the drainage of water from soils subjected to static loads. In most soils, compaction is too rapid to allow time for drainage.

As illustrated in the typical compaction curve of Fig. 2, water has an important effect on soil compaction. Even at low water content, the soil grains are surrounded by a thin film of water. A small increase in water content tends to increase the repulsion of particles and to facilitate their orderly arrangement. Un-

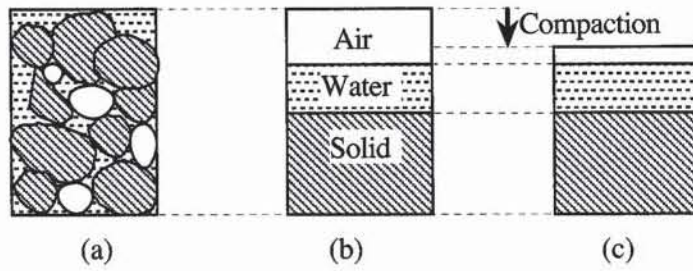


Figure 1 Principle of soil compaction.

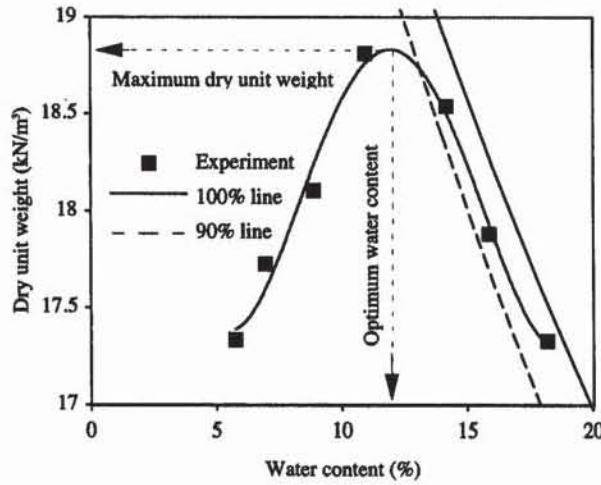


Figure 2 Typical compaction curve (after Lambe, 1951).

til the optimum water content is reached, the addition of water expels more air from soils, and enables to reach larger dry unit weight. The densest soil is obtained at the optimum water content. When the water content exceeds this optimum value, the water pushes the grains apart. Since water is much more incompressible than the grain assembly and has no time to drain, the dry unit weight starts to decrease.

Saturation Lines

The dry unit weight γ_d , total unit weight γ , water content w , degree of saturation S_r , and specific gravity G_s are related through

$$\gamma_d = \frac{\gamma}{1 + w} = \gamma_w \frac{G_s}{1 + G_s w / S_r} \tag{1}$$

When S_r , γ_w , and G_s are given, Eq. 1 defines the saturation lines. Figure 3 shows the saturation lines corresponding to $S_r = 100\%$, 90% and 70% for $G_s = 2.65$ and $\gamma_w = 9.8 \text{ kN/m}^3$. γ_d decreases with w but increases with S_r . Because $S_r \leq 100\%$, all measured points (w, γ_d) must be below the 100% saturation line. The 100% saturation line defines the upper limit of compaction curves. No data point can be beyond this line. As shown in Fig. 2, the descending branch of the measured compaction curve falls between the 100% and 90% saturation lines. The dry unit weight decreases with water content because water filled the soil voids before drying. The 100% saturation line is commonly plotted next to compaction curves while reporting the result of compaction tests.

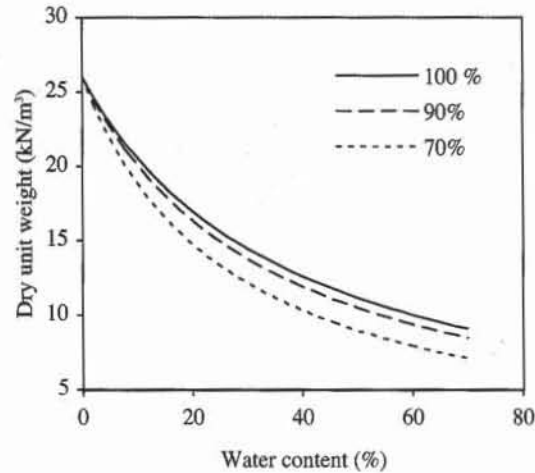


Figure 3 Variation of dry unit weight versus water content for constant degree of saturation $S_r = 100\%$, 90% , and 70% .

Compacting Efforts

The methods used for various standard types of compaction tests are summarized in Table 1. The compaction methods vary depending on the rammer weight, rammer drop, size and height of mold, and the number of layers and blows per layer. The work done E by the rammer per unit volume of soil is

$$E = W_r \frac{H}{V} N_B N_L \quad (2)$$

where W_r is the rammer weight, H the rammer drop, V the volume of compacted soil, N_B the number of blows per layer, and N_L the number of layers. As shown in Table 1, the work done E in the modified compaction test is about 4.5 times as much as that in the standard test. According to ASTM the larger mold is used for coarser soils having particles larger than 9.5 mm but smaller than 19 mm. As shown in Fig. 4, the relation between density and water content is influenced by the compactive

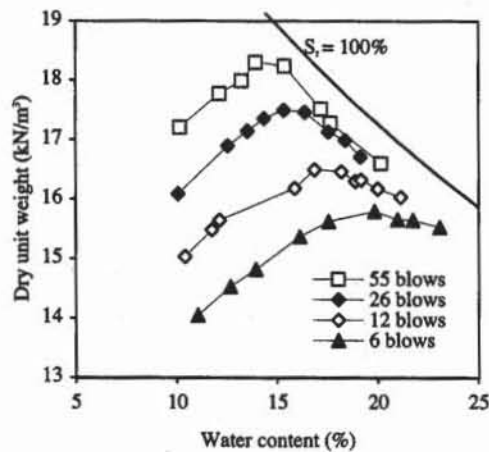


Figure 4 Compaction curves for a silty clay subjected to different numbers of blows per layer in modified compaction test (after Turnbull and Foster, 1956).

TABLE 1

Summary of compaction procedures (ASTM D698 and D1557)

Type of test	W_r Rammer weight (N)	H Hammer drop (mm)	N_L Number of layers	N_B Number of blows per Layer	D Diameter of mold (cm)	L Height of mold (cm)	E Work done per unit volume of soil (kJ/m ³)
Standard compaction	24.4	305	3	25	10.2	11.6	592
ASTM D 698	24.4	305	3	56	15.2	11.6	589
Modified compaction	44.5	457	5	25	10.2	11.6	2695
ASTM D 1557	44.5	457	5	56	15.2	11.6	2683

effort, higher compactive efforts giving denser soils. Modified compaction tests yield denser soils than standard compaction tests.

Influence of soil compaction on soil properties

The nature and magnitude of compaction in fine-grained soils significantly influences their mechanical behavior. A few effects are illustrated in Figs. 5 and 6. For additional information refer to Mitchell et al. (1965), and Hilf (1991).

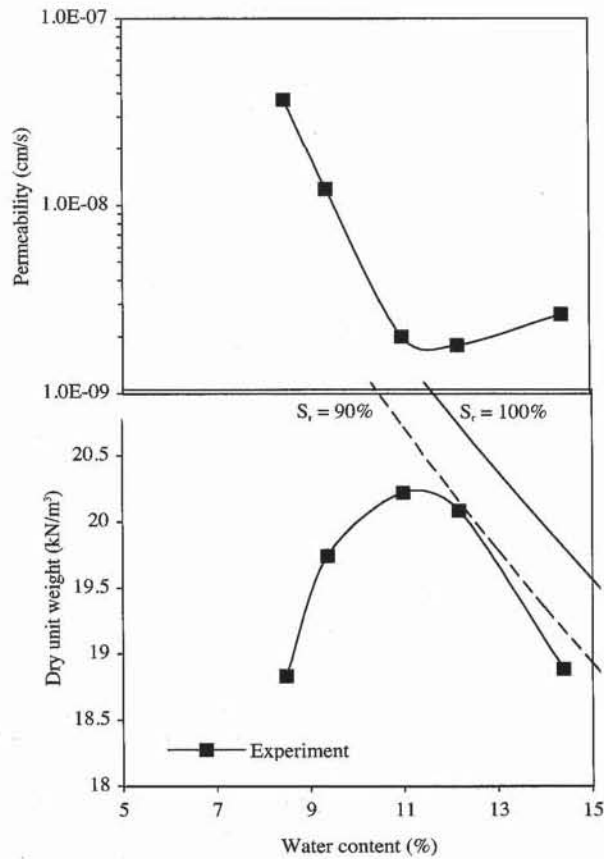


Figure 5 Compaction–permeability tests on Siburua clay (Lambe, 1962).

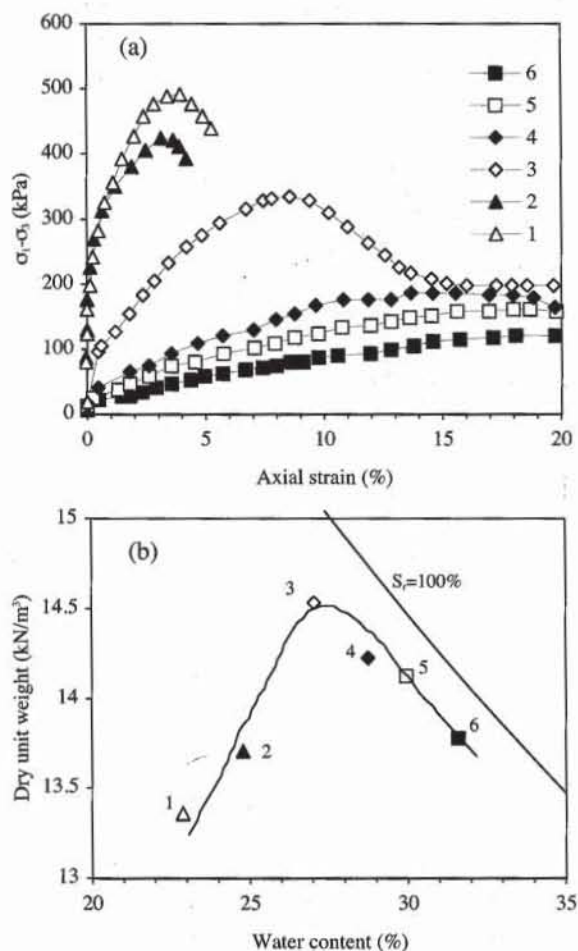


Figure 6 Influence of water content on the stress–strain relationship for compacted samples of kaolinite (a) stress versus strain relationships for compacted samples, (b) dry unit weight versus water content (from Seed and Chan, 1959).

As shown in Fig. 5, an increase in water content w during compaction causes a decrease in permeability k when w is smaller than the optimum water content w_{opt} , and a slight increase in k when $w > w_{opt}$. Compaction modifies the permeability by decreasing the voids available for flow, and reorienting soil particles.

Fig. 6 shows the influence of compaction water content w on the stress–strain response of compacted samples of kaolinite subjected to triaxial tests (see Chapter 7-6). Samples compacted with $w < w_{opt}$ tend to be more rigid and stronger than samples compacted with $w > w_{opt}$.

As pointed by Lambe and Whitman (1969), the engineer must consider the behavior of the soil not only as compacted. Many changes can occur in the compacted soil, such as changes in saturation due to permeating water, which ultimately determine its shear strength and compressibility.

REFERENCES

- See Introduction for references to ASTM procedures (pages 4 to 6).
- TURNBULL, W. J., and C. R. FOSTER, 1956, "Stabilization of material by compaction," *Journal of the Soil Mechanics and Foundations Division, ASCE*, Vol. 82, No. SM2, pp. 1-23.
- MITCHELL, J. K., D. R. HOOPER, and R. G. CAMPANELLA, 1965, "Permeability of compacted clay," *Journal of the Soil Mechanics and Foundations Division, ASCE*, Vol. 91, No. SM4, pp. 41-65.
- HILF, J. W., 1991, "Compacted Fill," in *Foundation Engineering Handbook, Second Edition, Chapter 8*, H.-Y. Fang ed., Chapman & Hall, New York, pp. 249-316.
- LAMBE, T. W., 1951, *Soil Testing for Engineers*, John Wiley & Sons, Inc., New York.
- LAMBE, T. W., 1962, "Soil Stabilization," in *Foundation Engineering, Chapter 4*, G.A. Leonards ed., McGraw-Hill, New York.
- LAMBE, T. W., and R. V. WHITMAN, 1979, "Soil Mechanics, SI Version," *John Wiley & Sons, New York*, pp. 514-524.
- SEED, H. B., and C. K. CHAN, 1959, "Structure and strength characteristics of compacted clay," *Journal of the Soil Mechanics and Foundations Division, ASCE*, Vol. 85, No. SM5, pp. 87-128.

REVIEW QUESTIONS

1. What is the compaction of soils? How is it different from consolidation? Illustrate your answer with a diagram showing the variation of air, water and soil fractions of soil samples during compaction and during consolidation.
2. Who introduced the standard compaction test?
3. What is the main difference between standard and modified compaction tests?
4. What is a compaction curve?
5. What is the 100% saturation line? How is it related to compaction curves?
6. What is the influence of compactive effort on compaction curve?
7. Why do we compact soils in civil engineering?

EXERCISES

1. Find the maximum dry unit weight and optimum water content for the compaction test results of Table E1 (data from Lambe, 1962). Plot the data points and the 100% and 90% saturation lines ($G_s = 2.65$ and $\gamma_w = 9.8 \text{ kN/m}^3$).

TABLE E1

Water content (%)	Dry unit weight (kN/m ³)
5.75	17.34
6.95	17.72
8.90	18.10
10.97	18.81
14.19	18.54
15.90	17.88
18.21	17.33

2. Find the maximum dry unit weight and optimum water content for the compaction test results of Table E2 on Siburua clay (data from Lambe, 1962). Plot the data points and the 100% and 90% saturation lines ($G_s = 2.85$ and $\gamma_w = 9.8 \text{ kN/m}^3$). Plot the variation of permeability versus water content, and comment on the effect of compaction on permeability.

TABLE E2

Water content (%)	Dry unit weight (kN/m^3)	Water content (%)	Permeability (cm/s)
8.47	18.83	8.27	3.7×10^{-8}
9.37	19.74	9.17	1.2×10^{-8}
10.99	20.22	10.98	2.0×10^{-9}
11.46	20.23	12.39	1.8×10^{-9}
11.85	20.08	14.34	2.6×10^{-9}
12.17	20.08		
13.32	19.74		
13.93	19.03		
14.22	19.03		
14.40	18.88		

3. Same as Exercise 1 for the results of Table E3.

TABLE E3

Water content (%)	Dry unit weight (kN/m^3)
22.87	13.36
24.78	13.70
27.04	14.53
28.75	14.22
29.96	14.12
31.62	13.78

4. Find the maximum dry unit weight and optimum water content for the results of four different compaction tests in Table E4. Plot the data points on the same graph, and draw the 100% saturation line ($G_s = 2.65$ and $\gamma_w = 9.8 \text{ kN/m}^3$).

TABLE E4

	Water content (%)	Dry unit weight (kN/m^3)
Modified 55 blows per layer	10.19	17.20
	12.14	17.77
	13.25	17.98
	13.95	18.30
	15.39	18.24
	17.20	17.52
	17.66	17.28
	20.17	16.60
Modified 26 blows per layer	10.09	16.09
	12.55	16.89
	13.53	17.14
	14.37	17.36
	15.34	17.50
	16.41	17.46
	17.57	17.13
	18.41	16.99

TABLE E4 (CONT.)

	Water content (%)	Dry unit weight (kN/m ³)
	19.15	16.71
Modified	10.42	15.04
6 blows per layer	11.76	15.48
	12.14	15.64
	15.90	16.19
	16.87	16.50
	18.22	16.46
	18.92	16.30
	19.20	16.32
	20.03	16.17
	21.15	16.03
Modified	11.07	14.04
12 blows per layer	12.69	14.53
	13.95	14.82
	16.13	15.37
	17.57	15.62
	19.85	15.80
	21.01	15.66
	21.75	15.64
	23.10	15.52

3-5

Compaction Tests

OBJECTIVE

Laboratory compaction tests are used to determine the relation between water content and dry unit weight and to find the maximum dry unit weight and optimum water content.

EQUIPMENT

The equipment used in compaction tests includes:

- Cylindrical metal mold, internal dimension 105 mm in diameter and 115 mm high (volume 1000 cm³). The mold is fitted with a detachable base plate and a removable extension collar (Figs. 1 to 3). A split mold (Fig. 4) may be used when an extractor is not available.
- For the standard compaction test, metal rammer with 50-mm-diameter face, weighing 24.4 kN, sliding freely in a tube that controls the height of drop to 300 mm (Fig. 5). For the modified compaction test, the rammer weight is 44.5 kN and the height of drop is 460 mm.
- Extractor apparatus for removing compacted material from the mold (see Figs. 11 and 12).
- Scoop or trowel.
- Steel straightedge, 30 cm long.
- No. 4 sieve.
- Balance, 10 kg capacity, accurate to 1.0 g.
- Drying oven, and evaporating dishes for moisture content determination.
- Ruler and vernier caliper.

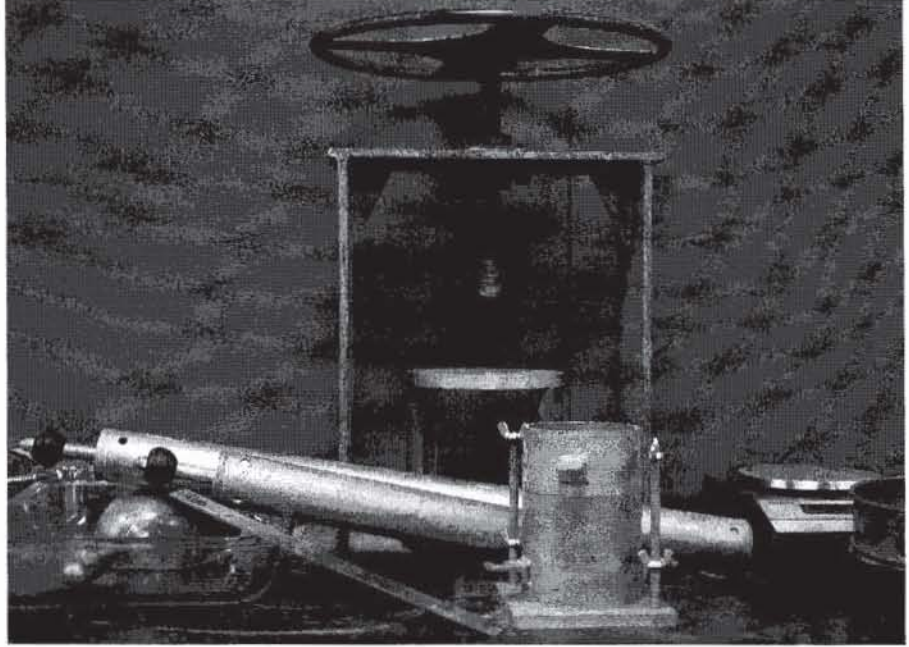


Figure 1 Equipment for compaction test. Cylindrical mold, rammer, scoop, steel straightedge, 10 kg capacity scale, and extractor.

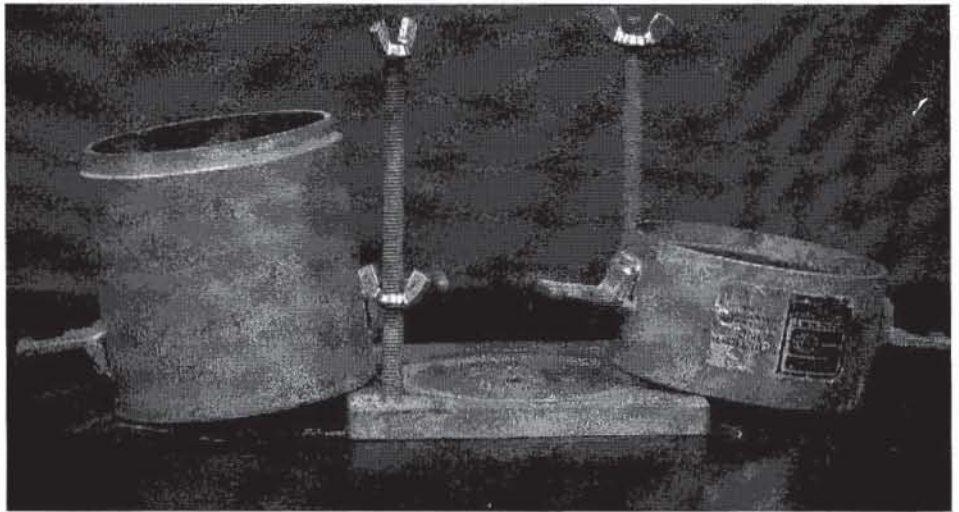


Figure 2 Base, mold body, and extension collar of cylindrical mold for compaction test.

PREPARATION OF EQUIPMENT

The exact volume of the standard compaction mold is measured before the compaction test. Clean and dry the mold, extension collar, and base plate. Weigh the mold body without the base plate and extension collar. Measure the internal diameter D and height H of the mold body. The mold volume V is

$$V = \frac{\pi}{4} D^2 H \quad (1)$$

Check the rammer to ensure that it falls freely through the correct height of drop (Table 1 of Chapter 3-4).

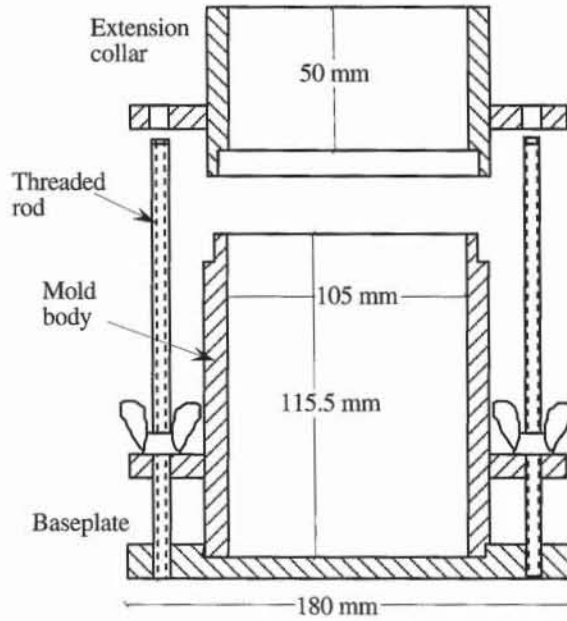


Figure 3 Dimensions and parts of a standard compaction mold.

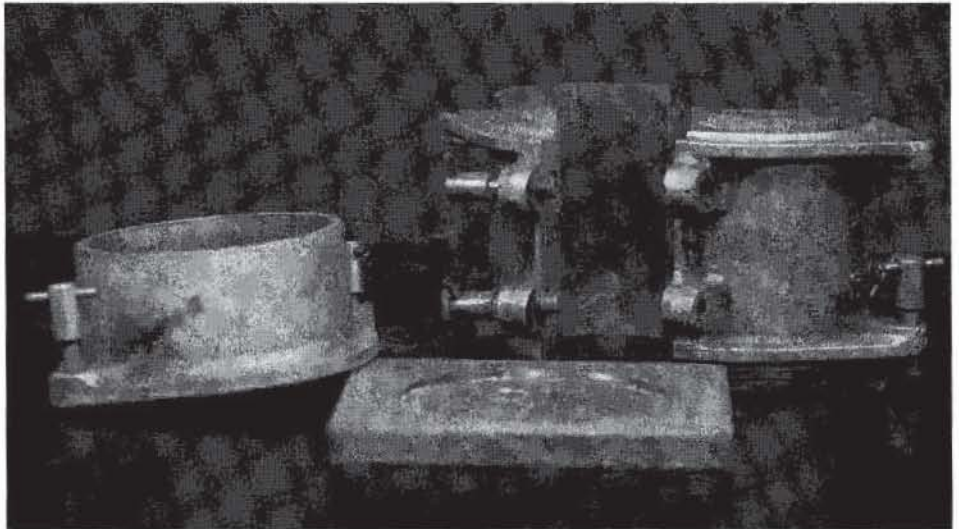


Figure 4 Split mold for compaction test. In contrast to the standard mold, the split mold can be split open to remove the compacted soil sample, and does not require the use of an extruding device.

PREPARATION OF SOIL SAMPLE

The original bulk sample is air dried and weighed. The large particles are removed by passing the sample through a No. 4 sieve. The mass of material required for the test is about 3 kg when the same soil is used in all the test points. ASTM recommends using a fresh soil sample for each test point, which requires about 15 kg of soils for five test points.

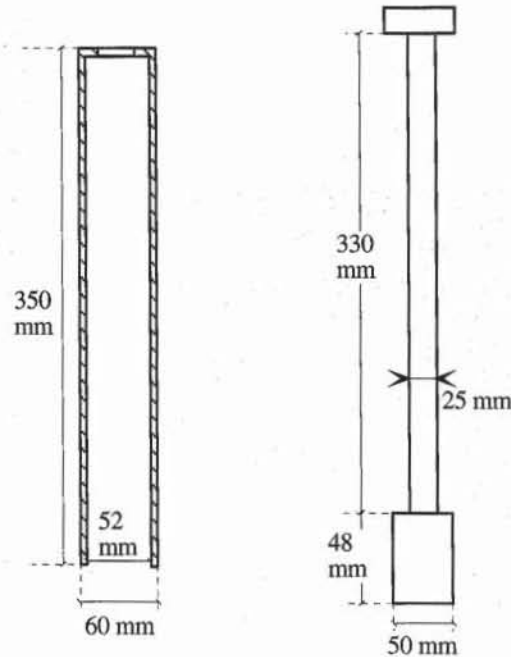


Figure 5 Rammer for standard compaction test.

TEST PROCEDURE

Standard compaction test

1. To obtain five well-placed points on the compaction curve, the water content is selected low for the first test point and is gradually increased for the other points. It should be about 4 to 5% below the optimum water content for the first point, and 4 to 5% above the optimum water content for the fifth and last point.

2. Add a suitable amount of water and mix thoroughly. Thorough mixing of soil and water is essential. The weight of water W_w to be added to achieve the water content w in percent may be estimated as follows:

$$W_w = \frac{W_s(w - w_0)}{100} \quad (2)$$

where w_0 is the previous water content (%) and W_s is the weight of dry soil.

3. Place the mold assembly on a solid base such as a concrete floor. Add loose soil to the mold so that it is about half full (Fig. 6). Compact the soil by applying 25 blows of the rammer dropped from the controlled height of 300 mm (Fig. 7). The rammer should be positioned properly before releasing. The guide tube must be held vertically. Place the tube gently on the soil surface; the rammer does the compaction, not the tube. To avoid injury, the hand that holds the tube must be kept clear from the falling hammer. As shown in Fig. 8, the rammer should be positioned to evenly distribute the compaction energy into the soil.

4. Place a second, approximately equal layer of soil in the mold, and compact it with 25 blows as before. Repeat with a third layer, which should bring the

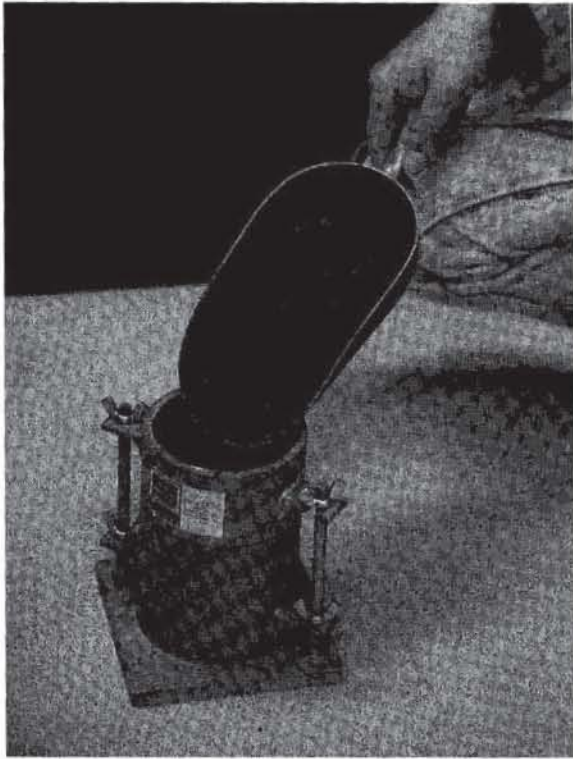


Figure 6 The compaction mold is half-filled with loose soil.



Figure 7 The soil is compacted by applying 25 blows with the rammer.

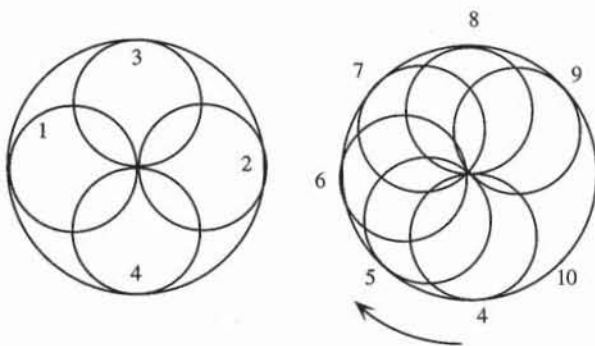


Figure 8 Sequence of blows using hand rammer.

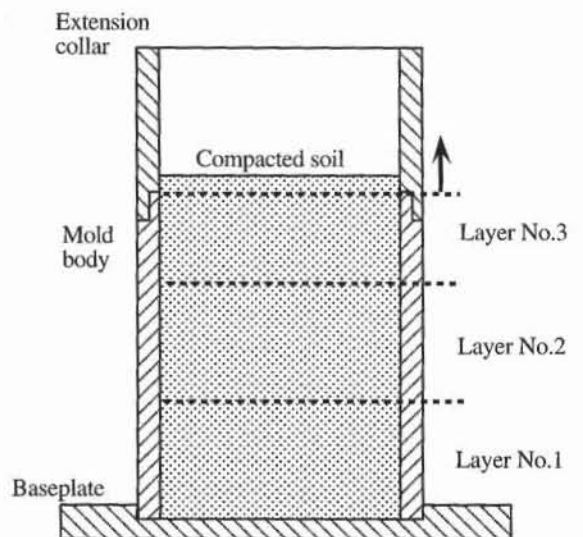


Figure 9 At the end of the compaction phases, the compacted soil level should be just above the mold body.

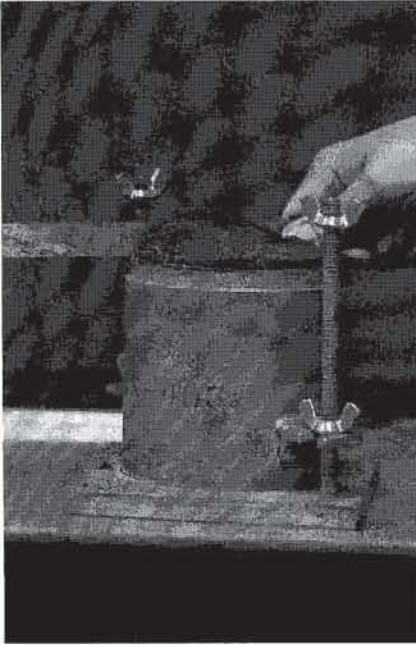


Figure 10 The excess soil is cut away by leveling off the top of the mold.

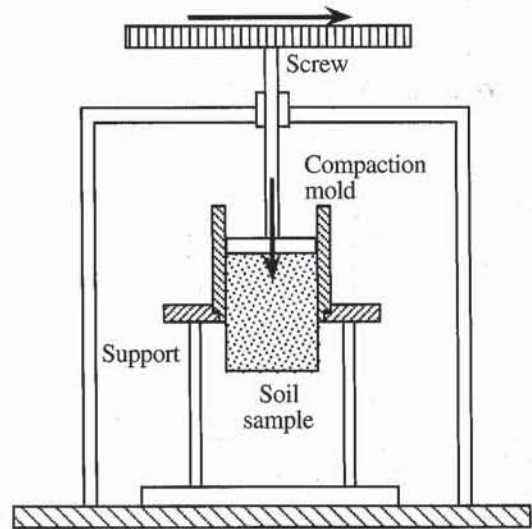


Figure 11 Extractor for removing compacted soil samples.

compacted soil level in the extension collar to about 6 mm above the level of the mold body, as shown in Fig. 9. If the compacted soil level in the extension collar is much higher, the test becomes inaccurate because the compacting energy per unit volume of soil is no longer constant.

5. Remove the extension collar carefully. Cut away the excess soil and level off to the top of the mold (Fig. 10). Any small cavity resulting from the removal of stones should be filled with fine materials.

6. Remove the base plate carefully, and weigh soil and mold.

7. Fit the mold on the extractor and extract the soil from the mold (Figs. 11 and 12).

8. Immediately take up to three representative samples to determine the sample water content (Fig. 13).

9. Break up the material on the tray and add an increment of water to achieve a desirable water content (refer to Eq. 2).

10. Go to step 2 and repeat to obtain five compaction points.

Modified compaction test

Follow the same procedure as the standard compaction test, but use the heavier rammer (44.5 kN instead of 24.4 kN) with a larger height of drop (457 mm instead of 305 mm). Also compact the soil in 5 layers (instead of 3) by applying 56 blows per layer (instead of 25).

COMPUTATION

The bulk unit weight γ is calculated as follows:

$$\gamma = \frac{W - W_m}{V} \quad (3)$$

where W is the weight of the soil and mold, W_m the weight of the empty mold, and V the volume of the mold. The dry unit weight γ_d is

$$\gamma_d = \frac{\gamma}{1 + w/100} \quad (4)$$

where w is the water content (%).

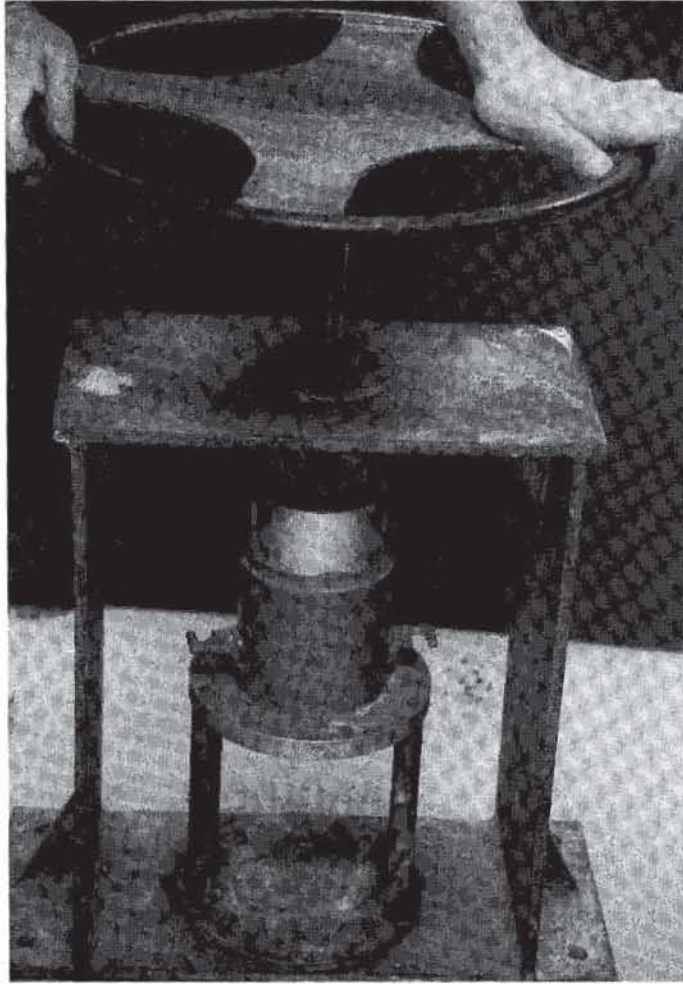


Figure 12 The compacted soil may become very hard; it is removed from the compaction mold by using an extractor.

EXAMPLE

Figures 14 and 15 show an example of a compaction test. The results are presented in the form of a compaction curve: dry unit weight γ_d versus water content w (%). This curve is obtained by plotting the data points for each compacted sample and connecting these points by a smooth curve. The 100% and 90% saturation lines are also plotted next to the compaction curve. They are obtained by using Eq. 1 of Chapter 3-4 for $G_s = 2.65$. All the experimental data points fall under the 100% saturation line, and some fall on the 90% saturation line. Figure 16 shows the formulas used in Figs. 14 and 15, and Fig. 17 shows the user-defined functions used in Fig. 15. These user-defined functions use functions FIT2 and FIT3, which are defined in Chapter 8-1. FIT2

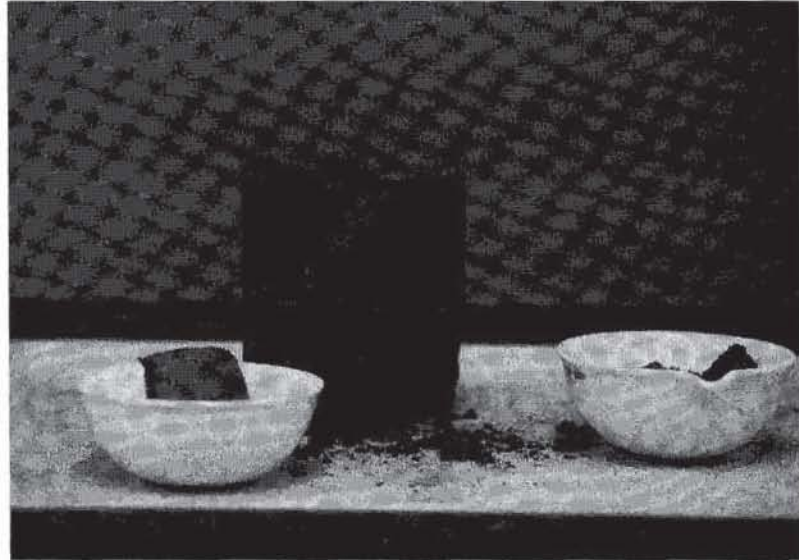


Figure 13 Take up to three representative samples to determine the moisture content of the sample.

and FIT3 perform a quadratic and a polynomial regression, respectively. The maximum unit weight and optimum water content are determined by using two different methods, referred to as A and B. Method A uses the user-defined function OPTIMUM3, which returns the maximum dry unit weight and optimum water content by fitting all data points with the cubic polynomial regression of function FIT3. The optimum of method A is plotted as a solid triangle in Fig. 14. Method B uses the user-defined function OPTIMUM2, which returns the maximum dry unit weight and optimum water content by fitting only three data points with the quadratic polynomial regression of function FIT2. The three data points are selected close to the maximum. The optimum of method B is plotted as a solid circle. Method B is equivalent to the one specified by ASTM D 5080. In the example of Fig. 14, method B probably gives a better optimum than method A.

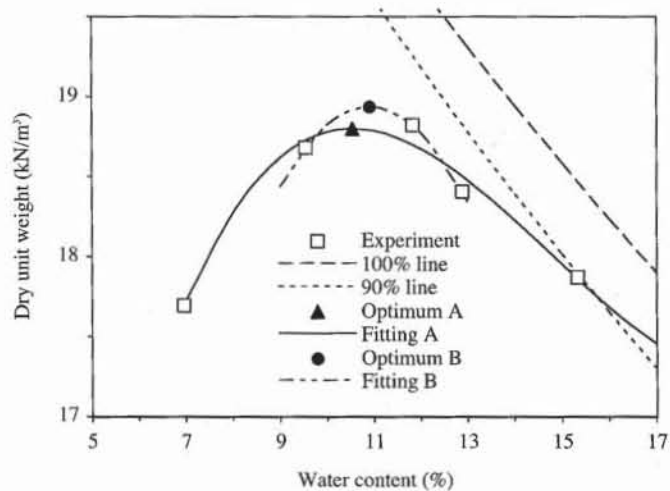


Figure 14 Example of compaction curve with 100% and 90% saturation lines.

	A	B	C	D	E
1	Compaction test				
2	Analyst name: K. Tiel				
3	Test date: 3/1/1993				
4	Sample description: Kaprielian soil				
5					
6	Diameter of mold $d = 10.14$ cm				
7	Height of mold $h = 11.67$ cm				
8	Mass of mold $M_m = 4250.00$ g				
9	Specific gravity $G_s = 2.65$				
10					
11	Mass of soil and mold (g)	Mass of can and wet soil (g)	Mass of can and dry soil (g)	Mass of can (g)	Water content (%)
12		M_w	M_d	M_c	
13	6070.00	81.42	79.18	46.58	6.87
14		95.56	92.19	45.50	7.22
15		90.20	87.49	47.44	6.77
16	6274.00	185.76	177.10	104.90	11.99
17		171.66	164.54	104.20	11.80
18		165.30	156.63	82.46	11.69
19	6218.00	94.21	90.07	46.58	9.52
20		106.93	101.50	45.50	9.70
21		85.04	81.80	47.44	9.43
22	6248.00	169.50	162.56	104.90	12.04
23		214.50	201.79	104.20	13.02
24		163.45	153.75	82.46	13.61
25	6232.00	82.80	78.27	46.58	14.29
26		90.33	84.22	45.50	15.78
27		85.45	80.23	47.44	15.92
28					
29	Mass of soil and mold (g)	Average water content (%)	Dry unit weight (kN/m^3)		
30	M	w	γ_d		
31	6070.00	6.95	17.70		
32	6274.00	11.83	18.82		
33	6218.00	9.55	18.68		
34	6248.00	12.89	18.40		
35	6232.00	15.33	17.87		
36				Method A	Method B
37	Optimum moisture (%) =			10.55	10.91
38	Maximum dry unit weight (kN/m^3) =			18.80	18.93

Figure 15 Example of data set.

REVIEW QUESTIONS

1. How many data points are necessary to construct a standard compaction curve?
2. Why is it important for the final level of compacted soil to be just above the mold body?
3. How do you select the water content for the five samples in the compaction test?

			B	C
			Average water content (%)	Dry unit weight (kN/m ³)
	E	29		
	Water content (%)	30	w	g _d
11		31	=AVERAGE(E13:E15)	=(M-Mm)/(PI()*d ² /4*h)/(1+w/100)*9.8
12		32	=AVERAGE(E16:E18)	=(M-Mm)/(PI()*d ² /4*h)/(1+w/100)*9.8
13		33	=AVERAGE(E19:E21)	=(M-Mm)/(PI()*d ² /4*h)/(1+w/100)*9.8
14	=(Mw-Md)/(Md-Mc)*100	34	=AVERAGE(E22:E24)	=(M-Mm)/(PI()*d ² /4*h)/(1+w/100)*9.8
	=(Mw-Md)/(Md-Mc)*100	35	=AVERAGE(E25:E27)	=(M-Mm)/(PI()*d ² /4*h)/(1+w/100)*9.8
	C		D	E
36			Method A	Method B
37	Optimum moisture (%)	=	OPTIMUM3(w,gd)	=OPTIMUM2(B32:B34,C32:C34)
38	Maximum dry unit weight (kN/m ³)	=	OPTIMUM3(w,gd)	=OPTIMUM2(B32:B34,C32:C34)

Figure 16 Formulas used in Fig. 15.

	A	B
1	OPTIMUM3	Optimum water content and Maximum unit weight with a cubic fitting
2	=RESULT(64)	A0
3	=ARGUMENT("W",64)	5.15634642049554
4	=ARGUMENT("GD",64)	
5	=SET.VALUE(B5:E5,TRANSPOSE(FIT3(W,GD)))	
6	=(-D5+SQRT(D5^2-3*E5*C5))/3/E5	
7	=(-D5-SQRT(D5^2-3*E5*C5))/3/E5	
8	=IF(AND(A6>=MIN(W),W<=MAX(W)),SET.VALUE(B9,A6))	
9	=IF(AND(A7>=MIN(W),W<=MAX(W)),SET.VALUE(B9,A7))	10.5521567377323
10	=SET.VALUE(B10,E5*B9^3+D5*B9^2+C5*B9+B5)	18.7974176689729
11	=RETURN(B9:B10)	
12		
13	GDFIT3	Unit weight corresponding to water content with a cubic fitting
14	=RESULT(1)	A0
15	=ARGUMENT("Wnew",1)	5.15634642049554
16	=ARGUMENT("W",64)	
17	=ARGUMENT("GD",64)	
18	=SET.VALUE(B18:E18,TRANSPOSE(FIT3(W,GD)))	
19	=RETURN(E18*Wnew^3+D18*Wnew^2+C18*Wnew+B18)	
20		
21	OPTIMUM2	Optimum water content and Maximum unit weight with a quadratic fitting
22	=RESULT(64)	A0
23	=ARGUMENT("W",64)	2.74895896163071
24	=ARGUMENT("GD",64)	
25	=SET.VALUE(B25:D25,TRANSPOSE(FIT2(W,GD)))	
26	=-C25/2/D25	
27	=D25*A26^2+C25*A26+B25	
28	=RETURN(A26:A27)	
29		
30	GDFIT2	Unit weight corresponding to water content with a quadratic fitting
31	=RESULT(1)	A0
32	=ARGUMENT("Wnew",1)	2.74895896163071
33	=ARGUMENT("W",64)	
34	=ARGUMENT("GD",64)	
35	=SET.VALUE(B35:D35,TRANSPOSE(FIT2(W,GD)))	
36	=RETURN(D35*Wnew^2+C35*Wnew+B35)	

Figure 17 User-defined functions OPTIMUM3 and GDFIT3 for cubic fitting, and OPTIMUM2 and GDFIT2 for quadratic fitting.

- Will you obtain the same optimum water content and maximum density for the standard and modified compaction tests? How would you expect the values to be different?

EXERCISE

1. Calculate the optimum water content and the maximum dry unit weight from the data

Diameter of mold (cm)	10.07		
Height of mold (cm)	11.54		
Mass of mold (g)	4258.00		
Mass of soil and mold (g)	Mass of can and wet soil (g)	Mass of can and dry soil (g)	Mass of can (g)
6070.00	98.03	94.65	46.67
	95.13	91.56	45.67
	105.80	101.67	45.61
6274.00	88.29	84.76	46.69
	72.27	70.07	45.67
	79.00	76.08	45.61
6218.00	73.22	70.29	46.69
	77.32	73.73	45.67
	84.36	77.84	45.61
6248.00	62.62	60.46	46.69
	75.95	71.64	45.67
	62.68	60.33	45.61
6232.00	90.35	83.68	46.69
	82.73	77.09	45.67
	86.33	80.34	45.61
Diameter of mold (cm)	10.16		
Height of mold (cm)	11.65		
Mass of mold (g)	4256.00		
Mass of soil and mold (g)	Mass of can and wet soil (g)	Mass of can and dry soil (g)	Mass of can (g)
6178.00	171.79	166.2	104.87
	129.50	126.14	89.05
	145.91	142.32	104.17
6318.00	145.00	140.93	104.87
	148.26	142.21	89.05
	141.11	137.42	104.17
6318.00	161.02	154.46	104.87
	133.16	128.06	89.05
	135.69	132.06	104.17
6274.00	162.90	155.53	104.87
	131.99	126.53	89.05
	164.55	156.93	104.17
6212.00	169.49	160.41	104.87
	147.39	139.33	89.05
	171.19	162.02	104.17

REFERENCES

See Introduction for references to ASTM procedures (pages 4 to 6).

3-6

The Sand Cone Method

PRINCIPLE

The sand cone method is used to determine soil density in the field and to control the results of field compaction in earth embankments, road fill, and structural backfill. Figure 1 illustrates the principle of the sand cone method and two other techniques: balloon density and nuclear methods. In the sand cone method shown in Fig. 1a, a soil sample is excavated manually and its weight W measured (Fig. 2). The volume V of excavated soil is determined from the volume of fine sand required to fill the hole. The bulk unit weight γ and dry unit weight γ_d of the in-place soil is

$$\gamma = \frac{W}{V}, \quad \text{and} \quad \gamma_d = \frac{\gamma}{1 + w/100} \quad (1)$$

where w is the water content (%), which is usually determined in the laboratory. The volume of fine sand is determined by measuring its weight, which assumes that it has a well-known density.

As shown in Fig. 1b, the rubber balloon method is based on the same principle as the sand cone method but uses a balloon inflated with water to fill the excavated hole. The volume of the hole, which is equal to the volume of injected water, is measured directly on the graduated cylinder of the rubber balloon device.

As shown in Fig. 1c, the nuclear density method measures both soil density and water content by using two types of radioactive sources. The radium or cesium isotope source generates gamma radiation, which is scattered by soil particles, whereas the americium-beryllium isotopes source emits neutrons that are scattered by the hydrogen atoms of the soil water. In the field, the radioactive sources, which are stored in a protective container during transport, are pushed at the end of a rod into the soil. The amounts of scatter between sources and detectors are measured by a Geiger counter and are related to soil density and water content after calibration. Nuclear methods have increased in popularity during

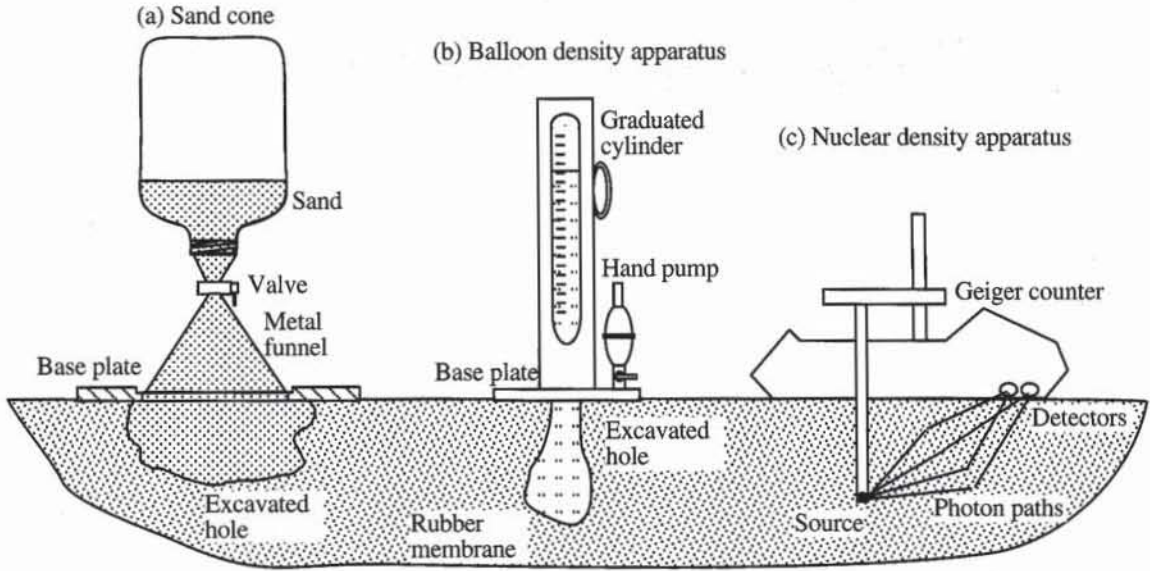


Figure 1 Three methods of determining the unit weight of soils in the field.

the past twenty years, owing to their advantages over traditional techniques. They are conducted rapidly and yield results within minutes. However, their disadvantages include high initial cost and potential danger of radioactive exposure. Strict radiation safety standards, such as carrying safety badges with radiation-sensitive films, must be enforced for these methods.

Only the sand cone method is described hereafter. Although it is not the most efficient and rapid test method, this basic test illustrates well the principle of the determination of density of soil in the field.

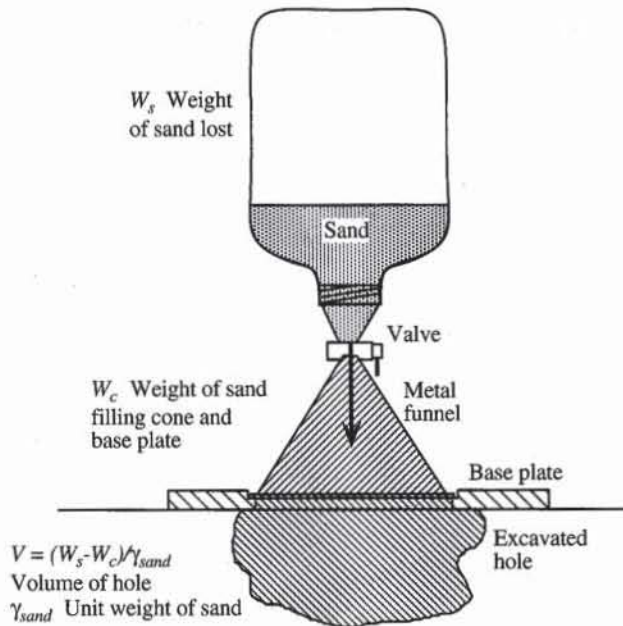


Figure 2 Principle of sand cone method.

EQUIPMENT

The equipment for the sand cone method includes:

- Sand cone with fitted valve (Fig. 3). The metal funnel is screwed on a 3.83-L plastic jar. (Fig. 4).
- Base plate about 30 cm wide.
- Uniform fine sand. About 1 kg of sand is required for each field measurement.

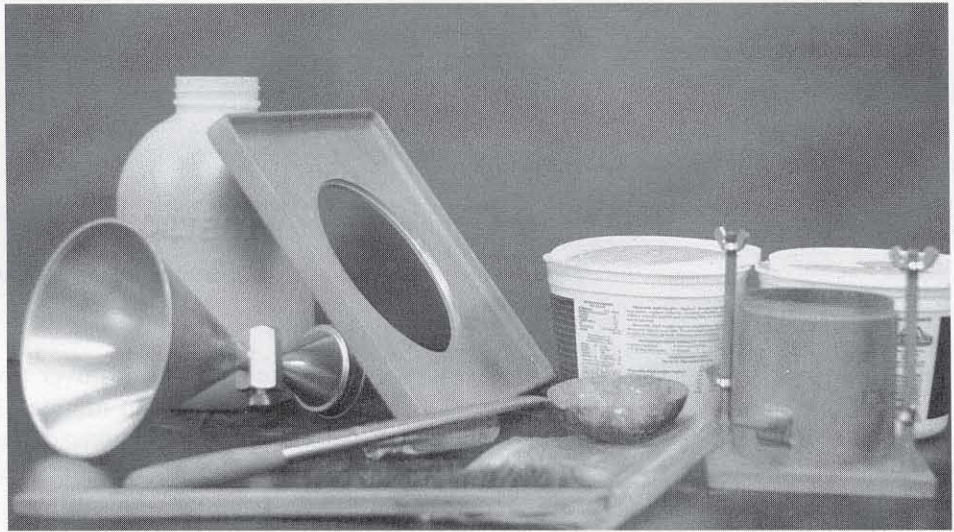


Figure 3 Equipment for sand cone method. Sand cone, 3.83-L plastic jar, digging tools, airtight container, base plate, brush, and compaction mold.

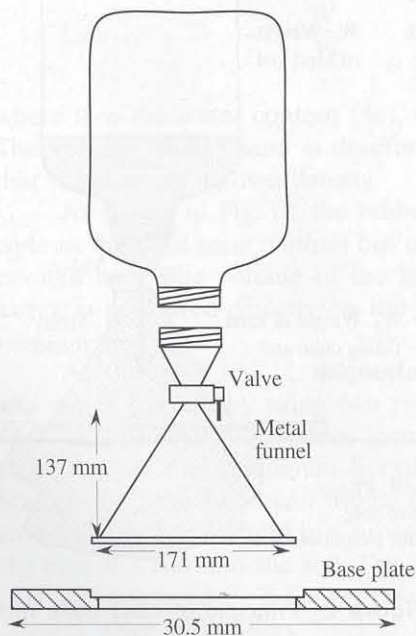


Figure 4 Sand cone (ASTM dimension)

- Digging tools (large spoons and screwdriver) to dig a hole in the soil.
- Airtight plastic bag or container to collect soil samples.
- Balance, 10 to 25 kg capacity, accurate to 1.0 g. A rugged field balance with leveling capabilities is recommended.
- Drying oven and evaporating dishes for moisture content determination.

CALIBRATION OF EQUIPMENT

The sand cone method uses a fine uniform sand that passes through a No.20 sieve but is retained on a No. 30 sieve. The sand grain size ranges from 0.85 to 0.6 mm. Its uniformity helps to keep a constant density, which is a requirement when volumes are to be determined from weight measurements. ASTM requires a coefficient of uniformity C_u smaller than 2, all particle sizes smaller than 2.0 mm, and no more than 3% smaller than 0.25 mm. The sand cone equipment is calibrated as follows.

Determination of Sand Unit Weight

1. Measure the weight W_m of a standard compaction mold, which includes the mold body and base plate but not its extension collar. Calculate its internal volume V after having measured its internal height and diameter.
2. As shown in Fig. 5, pour sand into the mold by using a scoop. Ideally, the pouring of sand in the laboratory should be similar to that in the field. Do not shake or vibrate the mold, which may increase the sand density. Fill the mold completely and strike off the excess sand with a straightedge, as shown in Fig. 6. Measure the weight W of the mold and sand.
3. Repeat step 2 until two weight readings are in good agreement, within 10 g. The sand unit weight γ_{sand} is

$$\gamma_{\text{sand}} = \frac{W - W_m}{V} \quad (2)$$

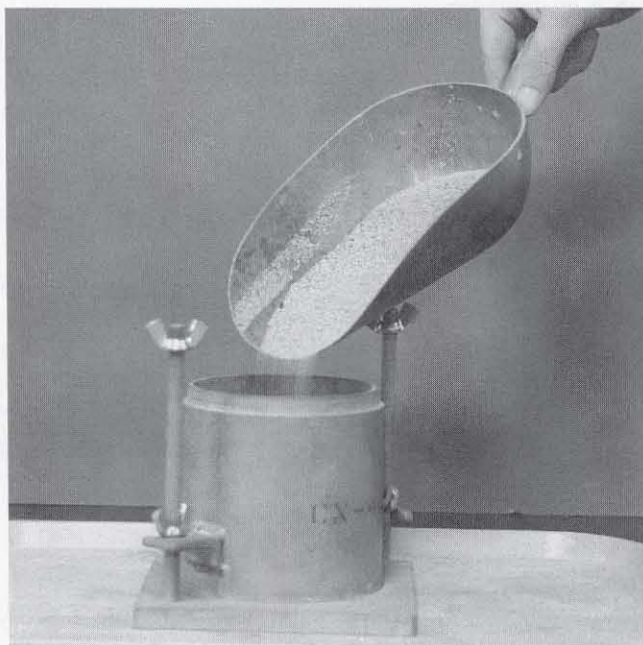


Figure 5 Filling the mold with sand using a scoop to determine the sand unit weight.

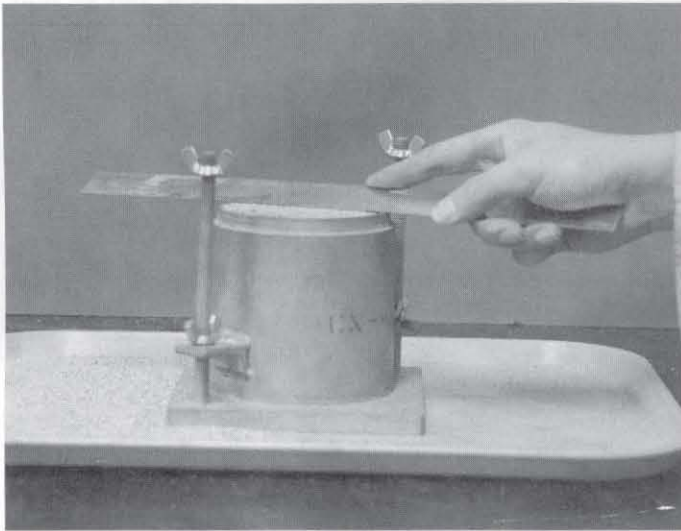


Figure 6 After filling the mold completely, strike off the excess sand with a straightedge.

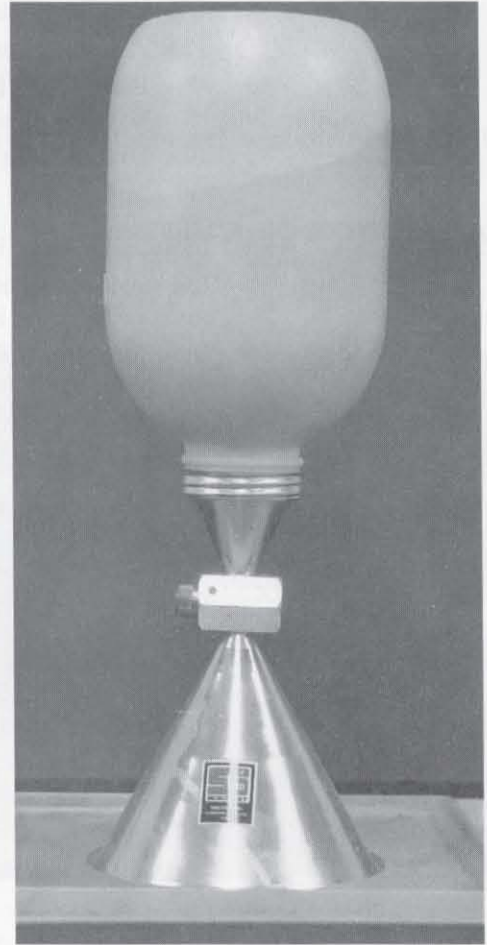


Figure 7 The sand weight required to fill the volumes of cone and base plate is measured in the laboratory.

Determination of Weight of Sand to Fill Jar, Cone, and Base

1. Fill the jar completely with sand, and measure its weight W_f .
2. Place the base plate on a flat tray. The groove along the circular hole of the base plate should be facing up, as shown in Fig. 7. Turn the sand cone upside down with the valve closed, and position the metal funnel on the base plate. Open the valve to let the sand fill the funnel. Close it when the sand stops flowing. Measure the weight W_b of the partially empty bottle. The difference $W_f - W_b$ is the sand weight W_c required to fill the cone and base plate.
3. Repeat steps 1 and 2 until two weight readings are in good agreement.

TEST PROCEDURE

1. At the location where the density is to be determined, level off the ground surface and position the baseplate horizontally. By using a screwdriver, mark the base plate opening on the ground as shown in Fig. 8. Remove the base plate, and dig a hole with an opening size slightly larger than the base plate open-

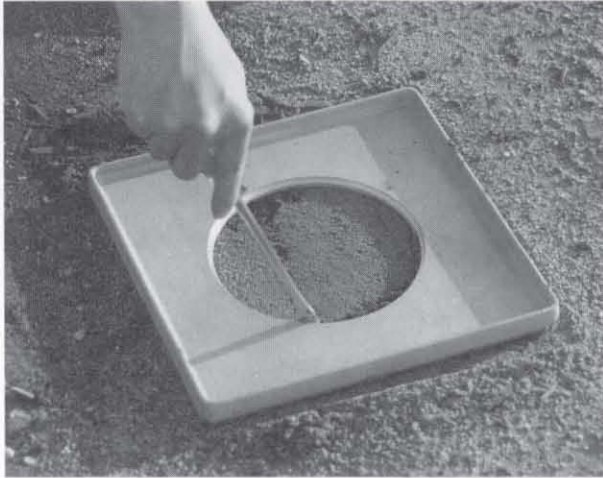


Figure 8 In the field, level off the ground surface, position the base plate, and mark the base plate opening using a screwdriver.



Figure 9 A hole is excavated with an opening size slightly larger than the base plate opening.

ing as shown in Fig. 9. The volume of the excavated hole should be smaller than 3830 cm^3 , the full capacity of the sand cone jar. As a guide, ASTM suggests the following volumes for the holes:

Maximum grain size (mm)	Volume of test hole (cm^3)
4.75	700
12.7	1400
25.0	2100
50.0	2800

2. Carefully place all the soil removed from the hole into the airtight plastic bag or container. It is important not to lose any material. A loss of material would introduce substantial error in the determination of the unit weight for such a relatively small sample.

3. Measure the weight W_f of the full jar on the field scale.

4. Center the base plate above the hole (see Fig. 10). The base plate opening should be facing up. If necessary, brush soil off the base plate. Turn the sand cone upside down with the valve closed, and position the metal funnel on the groove of the base plate (see Fig. 11). Open the valve to let the sand fill the hole. Close it when the sand stops flowing. Measure the weight W_e of the partially empty jar and the weight W of the soil sample.

5. Salvage as much sand from the hole as possible.

6. After returning from the field, determine the water content of the soil samples.

COMPUTATION

As shown in Fig. 2, the volume V of the sampling hole is calculated as follows:

$$V = \frac{W_f - W_e - W_c}{\gamma_{\text{sand}}} \quad (3)$$

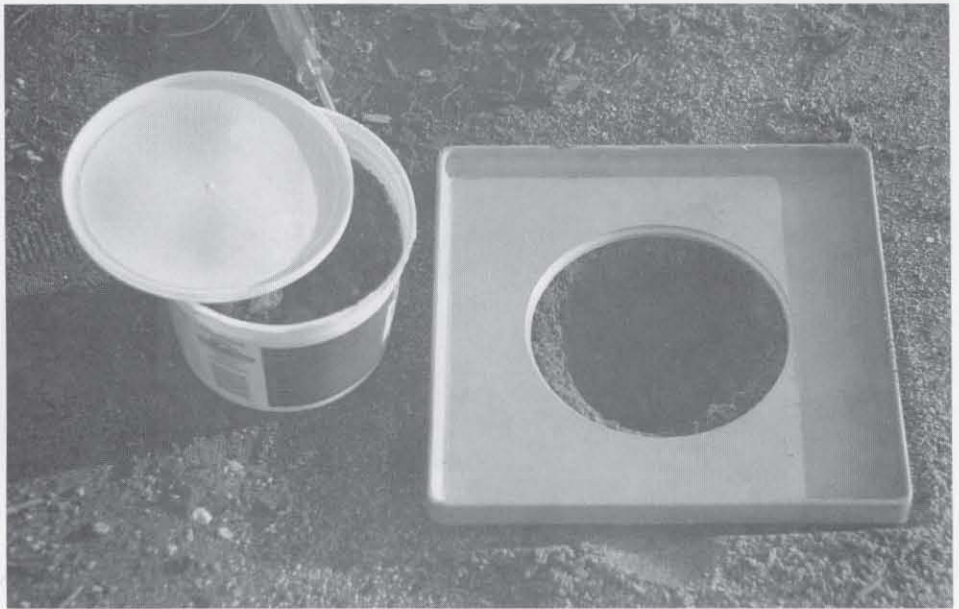


Figure 10 Face up, the base plate is centered above the hole and cleaned up by using a brush.



Figure 11 During the actual field test, the valve of the the sand cone is opened and the sand flows down to fill the excavated hole.

jar partially empty, W_c the sand weight required to fill the cone and base plate, and γ_{sand} the sand unit weight. The bulk unit weight γ and dry unit weight γ_d of the field sample are calculated as follows:

$$\gamma = \frac{W}{V} \quad \text{and} \quad \gamma_d = \frac{\gamma}{1 + w/100} \tag{4}$$

where W is the weight of the sample collected and w is the water content of the sample (%).

EXAMPLE

The reported test results of the sand cone method should clearly indicate the bulk unit weight γ , dry unit weight γ_d , and water content w (%). The point (w, γ_d) should be plotted on the compaction curve obtained in a laboratory compaction test to compare the field values to the optimum water content and maximum dry unit weight. Then one can easily verify whether or not the compacted soil in the field meets the compaction requirement. Figure 12 shows an example of the sand cone method test, and Fig. 13 shows the formulas used in Fig. 12.

	A	B	C
1	Sand cone method		
2			
3	Analyst name: <i>Kary P. Tiel</i>		
4	Test date: <i>3/1/1993</i>		
5	Sample description: <i>Sample from Kaprielian Hall</i>		
6	Measurement in the field		
7	Mass of jar and sand before use $M_j =$	6804.00	g
8	Mass of jar and sand after use $M_e =$	4384.00	g
9	Mass of collected soil $M_s =$	1181.69	g
10			
11	Water content in the laboratory	Sample 1	Sample 2
12	Mass of can and wet soil (g) $M_w =$	169.81	189.70
13	Mass of can and dry soil (g) $M_d =$	165.52	184.05
14	Mass of can (g) $M_t =$	104.79	104.19
15	Water content $w =$	7.06%	7.07%
16	Average water content $w =$	7.07%	
17	Bulk unit weight $\gamma =$	20.12 kN/m ³	
18	Dry unit weight $\gamma_d =$	18.79 kN/m ³	
19			
20	Calibration in the laboratory		
21	Diameter of mold $D =$	10.14 cm	
22	Height of mold $H =$	11.67 cm	
23			
24		Sample 1	Sample 2
25	Mass of mold and sand (g) $M_{ms} =$	5570.0	5580.0
26	Mass of empty mold (g) $M_m =$	4242.0	4256.0
27	Mass of jar and sand before filling cone	4946.0	
28	Mass of jar and sand after filling cone (g)	3336.0	
29	Unit weight of sand (kN/m ³) $\gamma_{sand} =$	13.81	13.77
30	Average unit weight of sand $\gamma_{sand} =$	13.79 kN/m ³	
31	Sand mass required to fill cone $M_c =$	1610.0 g	

Figure 12 Example of data set.

	A	B	C
15	Water content w	$= (Mw - Md) / (Md - Mt)$	$= (Mw - Md) / (Md - Mt)$
16	Average water content $w = \text{=AVERAGE}(B15:C15)$		
17	Bulk unit weight γ	$= M / (Mf - Me - Mc) * g_{\text{sand}}$	kN/m^3
18	Dry unit weight γ_d	$= g / (1 + w)$	kN/m^3

	A	B	C
29	Unit weight of sand (kN/m^3) γ_{sand}	$= 9.8 * (Mms - Mm) / (\text{PI}() * D^2 * H / 4)$	$= 9.8 * (Mms - Mm) / (\text{PI}() * D^2 * H / 4)$
30	Average unit weight of sand $\gamma_{\text{sand}} = \text{=AVERAGE}(B29:C29)$		kN/m^3
31	Sand mass required to fill cone $M_c = \text{=AVERAGE}(Mjb - Mja)$		g

Figure 13 Formulas used in Fig. 12.

REVIEW QUESTIONS

1. State the objective and principle of the sand cone method.
2. Why is it important not to lose any soil from the excavated hole during the sand cone method?
3. Why do we use a particular sand for the sand cone method? Why not use any sand?
4. Can you name two other test methods that are used to define soil density in the field?

EXERCISES

1. Measure the internal dimension of the cone and base plate and calculate the volumes of the cone and base plate. Compare with the weight found during the equipment calibration.
2. Measure exactly the volume of the 1-gallon jar by measuring its weight empty and filled with water. After drying the jar, fill it with sand and weigh it. Verify that the sand unit weight is approximately equal to the sand density determined during the equipment calibration.
3. Calculate the in situ density from the following results obtained from a sand cone test.

Determination of sand unit mass in the laboratory	Diameter of mold (cm)	10.13			
	Height of mold (cm)	11.65			
	Mass of mold and sand (g)	5602			
	Mass of mold (g)	4252			
Determination of sand mass to fill cone	Mass of jar and sand before filling cone (g)	3516			
	Mass of jar and sand after filling cone (g)	1934			
In place measurement	Mass of jar and sand before use (g)	6542			
	Mass of jar and sand after use (g)	4334			
	Mass of collected soil (g)	865.52			
			Trial 1	Trial 2	Trial 3
Determination of water content in the laboratory	Mass of can and wet soil (g)	146.54	142.52	147.32	
	Mass of can and dry soil (g)	144.63	140.27	144.83	
	Mass of can (g)	113.65	104.89	104.18	

4. Calculate the in situ density from the following results obtained from a sand cone test.

Determination of sand unit mass in the laboratory	Diameter of mold (cm)	10.16		
	Height of mold (cm)	11.65		
	Mass of mold and sand (g)	5596		
	Mass of mold (g)	4246		
Determination of sand mass to fill cone	Mass of jar and sand before filling cone (g)	6122		
	Mass of jar and sand after filling cone (g)	4460		
In place measurement	Mass of jar and sand before use (g)	6314		
	Mass of jar and sand after use (g)	3594		
	Mass of collected soil (g)	1552		
		Trial 1	Trial 2	Trial 3
Determination of water content in the laboratory	Mass of can and wet soil (g)	106	130	122
	Mass of can and dry soil (g)	104	128	120
	Mass of can (g)	82	104	104

4

Permeability and Seepage

- 4-1 Principles of permeability tests
- 4-2 Constant head permeability test
- 4-3 Falling head permeability test
- 4-4 Electrical analogy of seepage problems
- 4-5 Finite difference solutions of seepage problems

4-1

Principles of Permeability Tests

INTRODUCTION

Soils are permeable to water because the voids between soil particles are interconnected. The degree of permeability is characterized by the permeability coefficient k , also referred to as hydraulic conductivity. In the laboratory, k is measured by using either the constant head test for soils of high permeability (e.g., sands), or the falling head test for soils of intermediate and low permeability (e.g., silts and clays). Before describing the test procedures, the basic concepts of seepage are reviewed.

DEFINITIONS

Fluid Velocity

Figure 1 illustrates a flow of water through an inclined tube filled with soil. The water molecules moving from cross sections A to B follow a tortuous path around the soil particles and through the voids. As shown in the cross section of Fig. 2, the velocity of water, denoted by the vector \mathbf{v}_f , is only defined in the voids through which water travels, and it varies from void to void.

Seepage Quantity

In Fig. 2, the seepage quantity q is the volume of water passing through a tube cross section during a unit time interval. q is the flux of water:

$$q = \int_S v_f dS \quad (1)$$

where v_f is the component of \mathbf{v}_f parallel to the tube axis and S is the total cross-sectional area of the tube. v_f is assumed equal to zero at the particle locations.

Discharge Velocity

The discharge velocity v parallel to the tube axis is defined as

$$v = \frac{q}{S} \tag{2}$$

It is smaller than the average fluid velocity \bar{v}_f on cross-sectional area S_f only occupied by water. v and \bar{v}_f are related through

$$v = n\bar{v}_f, \quad \bar{v}_f = \frac{1}{S_f} \int_{S_f} v_f dS_f, \quad \text{and} \quad n = \frac{V_v}{V} \tag{3}$$

where n is the porosity and V_v is the volume of voids in volume V between cross sections A and B of Fig. 1. As shown in Figs. 1 and 2, v averages the real water flow. The smoothed trajectory of water particles, which is tangent to the discharge velocity, is called a *flow line*.

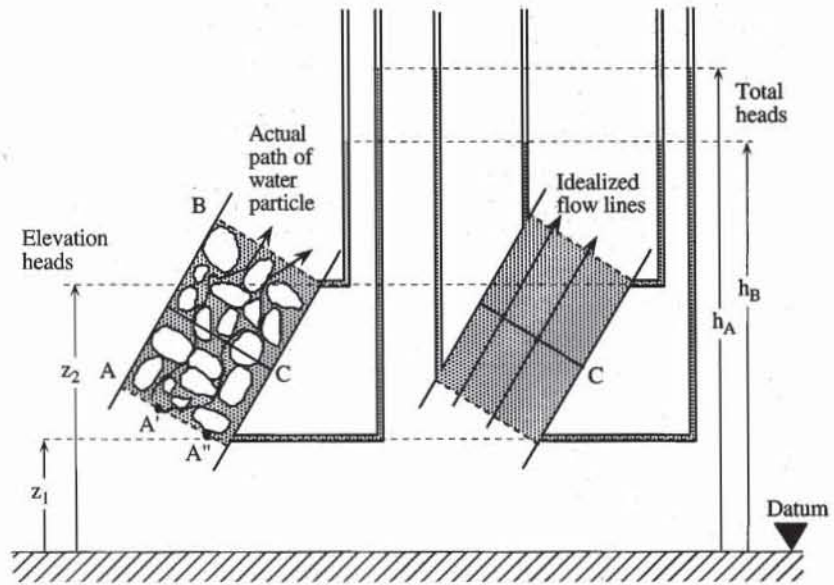


Figure 1 Flow of water through soil.

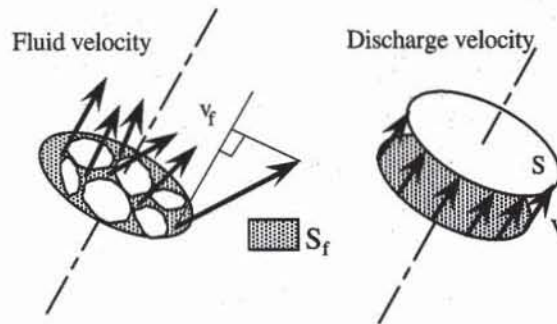


Figure 2 Fluid velocity and discharge velocity.

Total Head

In hydrostatics (i.e., when the water does not move), the total head h is the sum of the pressure head u/γ_w , and the elevation head z :

$$h = \frac{u}{\gamma_w} + z \quad (4)$$

where u is the pore water pressure, γ_w is the fluid unit weight, and z the elevation above a given datum. As shown in Fig. 1, pressure, elevation, and total heads must always have the same datum. When water moves at velocity v_f , the total head is defined using the Bernoulli equation:

$$h = \frac{v_f^2}{2g} + \frac{u}{\gamma_w} + z \quad (5)$$

where g is the earth gravity. For most soil flow problems, $v_f^2/2g$ is negligible compared to the pressure and elevation head, because v_f is much smaller than 1 m/s. Therefore, the total head in soils is given by Eq. 4.

Piezometric Head

In hydrostatics, the total head h is equal to the elevation of the free surface of water above the datum. This elevation is called the *piezometric head*. In Fig. 1, the total (or piezometric) head is the elevation above the datum of the water level in the pipes. The total head is constant at all points of the same cross section in Fig. 1 (e.g., points A , A' , and A'' of Fig. 1).

Hydraulic Gradient

The hydraulic gradient i is the gradient of total head. In Fig. 1, the hydraulic gradient between sections A and B is equal to the head drop $h_B - h_A$ divided by the distance $L = AB$ where the head drop takes place:

$$i = \frac{h_B - h_A}{L} \quad (6)$$

where h_A is the total head in section A and h_B is the total head in section B . The hydraulic gradient i is a dimensionless number because h and L have the same dimension. In Fig. 3, i is the slope of the variation of h versus distance x .

Darcy's Law

As described in Chapter 1-3, fluid flows can be laminar, turbulent, or transitional, depending on the Reynolds number. In laminar flows, the fluid flows in parallel layers without mixing. In turbulent flows, random velocity fluctuations result in mixing and internal energy dissipation. In transitional flows, the flows are between the laminar and turbulent regimes. These different flow regimes are also found in soils and influence the relation between discharge velocity and hydraulic gradient. As shown in Fig. 4, i varies linearly with v in the laminar regime but varies nonlinearly and irreversibly with v in the transitional and turbulent zones.

For most flows in soils, v is so small that v is proportional to i ; that is, Darcy's law (Darcy, 1856) applies:

$$v = k i \quad (7)$$

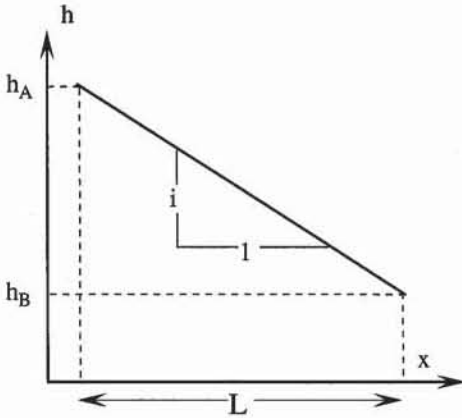


Figure 3 Variation of total head h versus distance x .

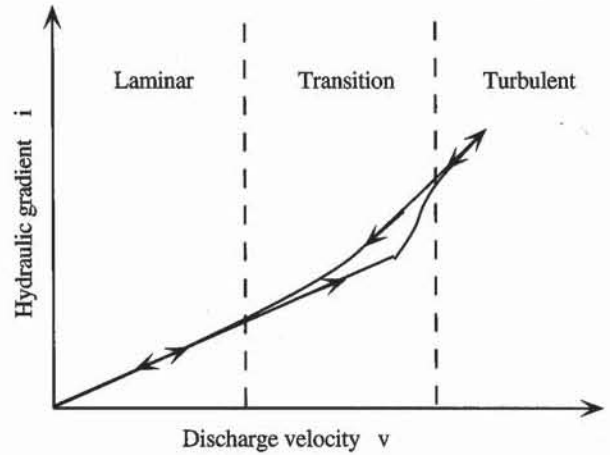


Figure 4 Zones of laminar and turbulent flows (after Taylor, 1948).

where k is the coefficient of permeability. The coefficient of permeability k is defined as the rate of discharge of water under conditions of laminar flow through a unit cross-sectional area of a soil subjected to a unit hydraulic gradient. The dimension of k is velocity (i.e., $[k] = LT^{-1}$), and its unit is usually cm/s.

Experiments have shown that Darcy's law (Eq. 7) is valid for a wide range of soil types and hydraulic gradients. However, Darcy's law no longer applies for large hydraulic gradients in clean gravels and rock fills where flows may be turbulent. It also breaks down for very small hydraulic gradients in clays. As shown in Fig. 5, in Swedish clays, Hansbo (1960) found a nonlinear relation between v and i for very small hydraulic gradients (i.e., $i < i_0$), and a linear relation with an offset for larger hydraulic gradients (i.e., $i \geq i_0$).

Critical Hydraulic Gradient

When the water flows upward, frictional drag tends to lift the particles and force them apart. The hydraulic gradient that breaks contact between particles is the

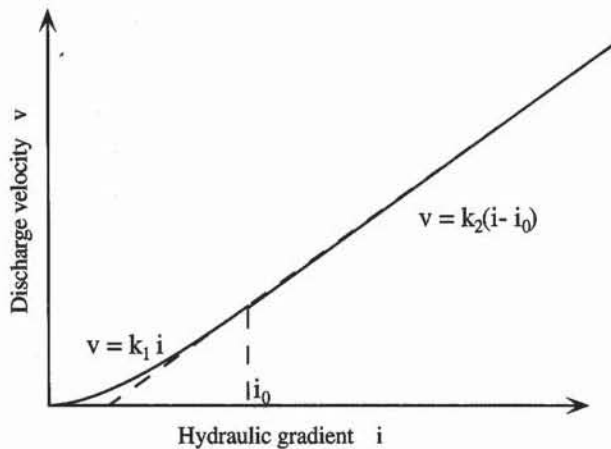


Figure 5 Deviation from Darcy's law observed in Swedish clays (after Hansbo, 1960).

critical hydraulic gradient i_c :

$$i_c = \frac{\gamma_b}{\gamma_w} \quad (8)$$

where $\gamma_b = \gamma_{\text{sat}} - \gamma_w$ is the submerged (or buoyant) unit weight of the soil, γ_w the unit weight of the water, and γ_{sat} the saturated unit weight of the soil. For most soils, $\gamma_b \approx \gamma_w$; therefore, $i_c \approx 1$. The loss of contact between soil grains results in the *quick condition*, in which soils behave as liquids. A quick condition can occur in any cohesionless soil when the upward hydraulic gradient exceeds i_c . A hydraulic gradient in excess of i_c is also responsible for the *boiling* of sand at the bottom of excavations and subsurface erosion known as *pipng*.

EMPIRICAL RELATIONSHIPS

The permeability of a soil depends primarily on the size and shape of grains, shape and arrangement of voids, void ratio, degree of saturation, and temperature. Several equations were proposed to calculate the permeability of soils, especially sands, from their physical characteristics. Two correlations are given below.

Hazen's Formula

Based on experimental work with fine uniform sand, Hazen (1892) related permeability k and effective particle size D_{10} (cm) as follows:

$$k = C_1 D_{10}^2 \quad (\text{cm/s}) \quad (9)$$

where $C_1 \approx 100$ for fine uniform sand. As shown in Table 1, C_1 is not a constant but varies with soil types. Its average value in Table 1 is 16. Figure 6 suggests that k is related to not only the particle size D_{10} but also the void ratio e .

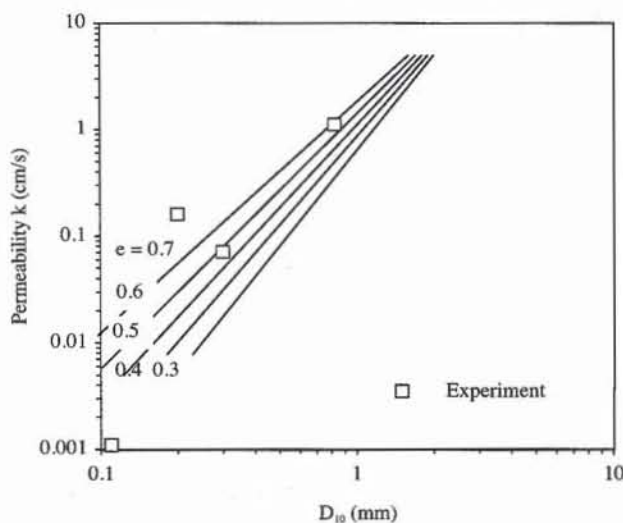


Figure 6 Variation of coefficient of permeability with particle size D_{10} (after NAVFAC, 1982).

TABLE 1
Permeability test data (after Lane and Washburn, 1946;
and Lambe and Whitman, 1979)

Soil type	Particle size D_{10} (cm)	Permeability ($\mu\text{m/s}$)	$C_1 = k/D_{10}^2$ ($\text{cm}^{-1}\text{s}^{-1}$)
Coarse gravel	0.0820	1100	17
Sandy gravel	0.0200	160	40
Fine gravel	0.0300	71	8
Silty gravel	0.0060	4.6	13
Coarse sand	0.0110	1.1	1
Medium sand	0.0020	0.29	7
Fine sand	0.0030	0.096	1
Silt	0.0006	0.15	42

Kozeny–Carman Formula

The Kozeny–Carman formula (Kozeny, 1927; and Carman, 1939) is

$$k = \frac{\gamma_w}{5f\eta S^2} \frac{e^3}{1+e} \quad (10)$$

where e is the void ratio, and η the dynamic viscosity of water. The coefficient f depends on pore shape: $f = 1.1$ for rounded grains, $f = 1.25$ for subrounded grains, and $f = 1.4$ for angular grains (Loudon, 1952). The specific surface area S (i.e., the surface area per unit volume of grains) is obtained from the equation

$$S = \frac{6}{\sqrt{d_{\max} d_{\min}}} \text{ (mm}^{-1}\text{)} \quad (11)$$

where d_{\max} is the maximum grain diameter (mm) and d_{\min} is the minimum grain diameter (mm).

Effect of Temperature on Permeability Coefficient

Equation 10 shows that k is not a constant for a given soil but varies with η , which in turn varies with temperature T . The permeability at temperature T , k_T , is reduced to that at 20°C , $k_{20^\circ\text{C}}$, by using

$$k_{20^\circ\text{C}} = \frac{\eta_T}{\eta_{20^\circ\text{C}}} k_T = Rk_T \quad (12)$$

where $\eta_{20^\circ\text{C}}$ is the viscosity of water at 20°C , η_T the viscosity of water at temperature T , and $R = \eta_T/\eta_{20^\circ\text{C}}$. The variation of R with temperature is shown in Fig. 7.

TYPES OF TESTS

There are two main types of laboratory permeability tests: constant head test and falling head test.

Constant Head Test

As schematized in Fig. 8, in the constant head test, a constant head drop is ap-

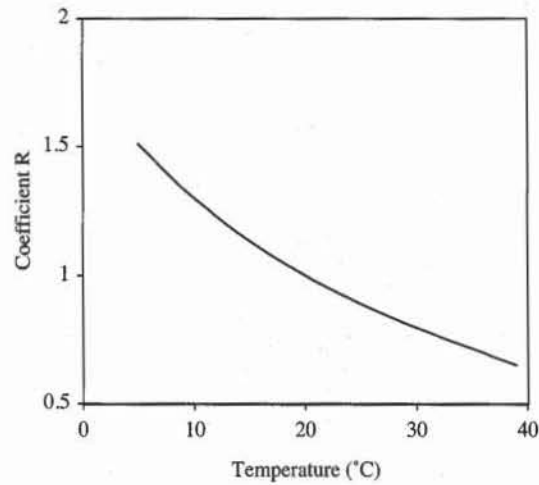


Figure 7 Variation of correction factor R versus temperature T .

plied to the soil sample, and the resulting seepage quantity is measured. The constant head test is used primarily for coarse-grained soils (clean sands and gravels) with $k \geq 10^{-3}$ cm/s. For fine-grained soils, the seepage quantity becomes too small to be measured accurately.

The coefficient of permeability k_T at temperature T is

$$k_T = \frac{qL}{(h_1 - h_2)At} \quad (13)$$

where q is the volume of water collected in a burette during time interval t , L the length of the specimen, h_1 the head at the left end of the specimen, h_2 the head at the right end of the specimen, and A the cross-sectional area of the specimen.

Falling Head Test

As illustrated in Fig. 9, the falling head test does not fix the total head. It lets it fall in the standpipe connected to the upper part of the specimen. The falling

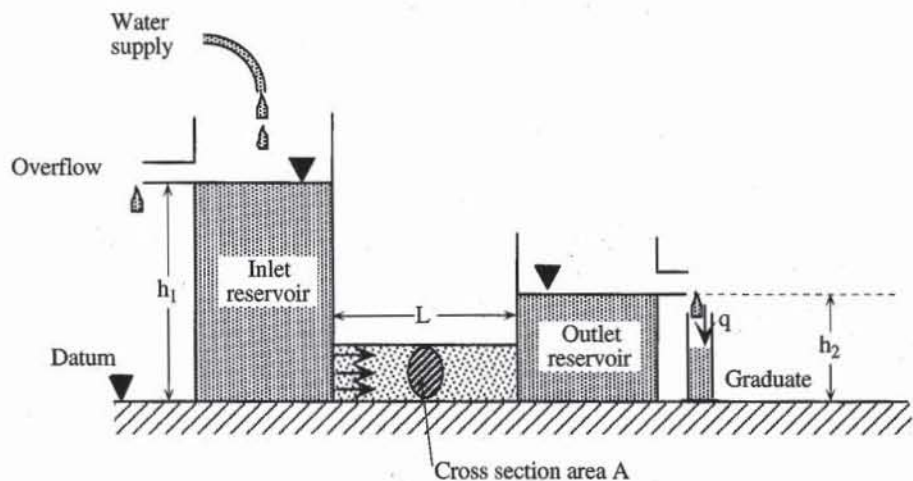


Figure 8 Principle of constant head test.

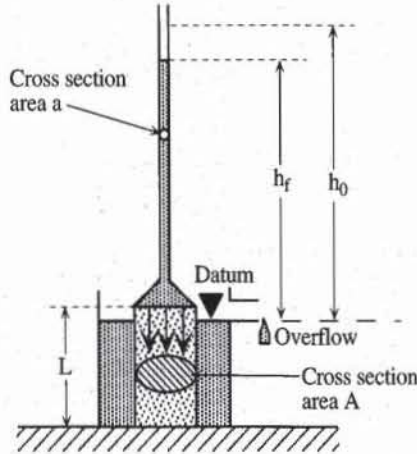


Figure 9 Principle of falling head test.

head test is generally used for less permeable soils (fine sands to fat clays) with $k \leq 10^{-3}$ cm/s. It is not practical for soils with $k > 10^{-3}$ cm/s because the head falls too rapidly to be measured. The coefficient of permeability k_T at temperature T is calculated as follows:

$$k_T = \frac{aL}{At} \log \frac{h_0}{h_f} \tag{14}$$

where a is the cross-sectional area of the standpipe, A the cross-sectional area of the specimen, L the length of the specimen, h_0 the elevation above the datum of water in the standpipe at the beginning of the experiment ($t = 0$), and h_f the elevation above the datum of water in the standpipe at time t .

TYPICAL VALUES FOR PERMEABILITY

Table 2 gives some typical values of permeability for various types of soil, and classify them on the basis of permeability. Figures 10 and 11 present permeability data on a variety of soils with different void ratios. The range of permeability covered by Figs. 10 and 11 is 1 cm/s to 10^{-10} cm/s. As shown in Fig. 12, the permeability of clay vary with void ratio, plasticity index PI , and clay fraction CF . As shown in Fig. 13, the permeability coefficient is almost isotropic in most clays (i.e., the horizontal permeability k_h is practically equal to the vertical permeability k_v) except for varved clay and stratified deposits where the ratio k_h/k_v) can exceed 10.

TABLE 2

Classification of soils according to their coefficients of permeability (after Kulhawy and Mayne, 1990; and Terzaghi and Peck, 1967)

Soil	Coefficient of permeability k (cm/s)	Degree of permeability
Gravel	Over 10^{-1}	High
Sandy gravel, clean sand, fine sand	10^{-1} to 10^{-3}	Medium
Sand, dirty sand, silty sand	10^{-3} to 10^{-5}	Low
Silt, silty clay	10^{-5} to 10^{-7}	Very low
Clay	Less than 10^{-7}	Practically impermeable

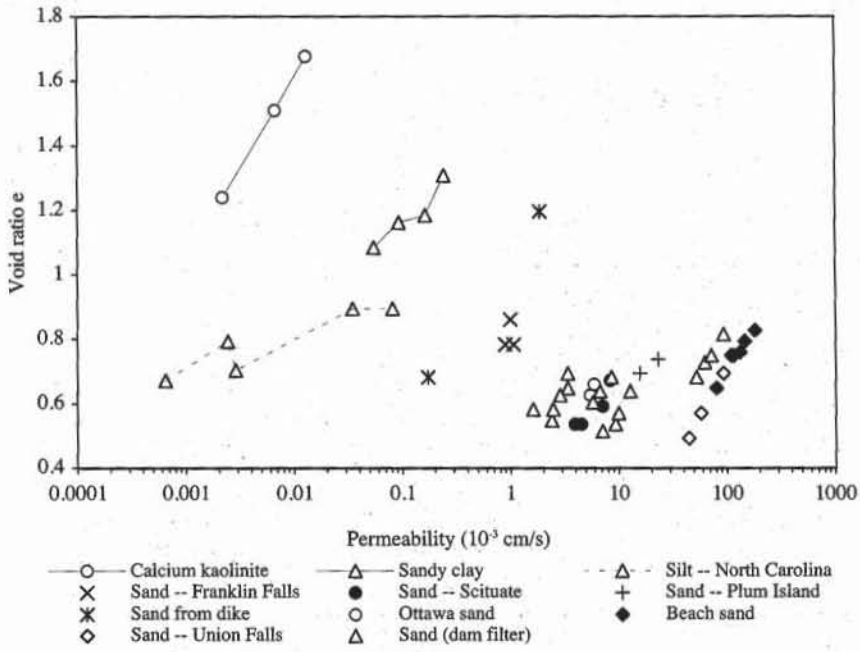


Figure 10 Permeability data on various soils in range 1 to 10^{-7} cm/s (data after Lambe and Whitman, 1979).

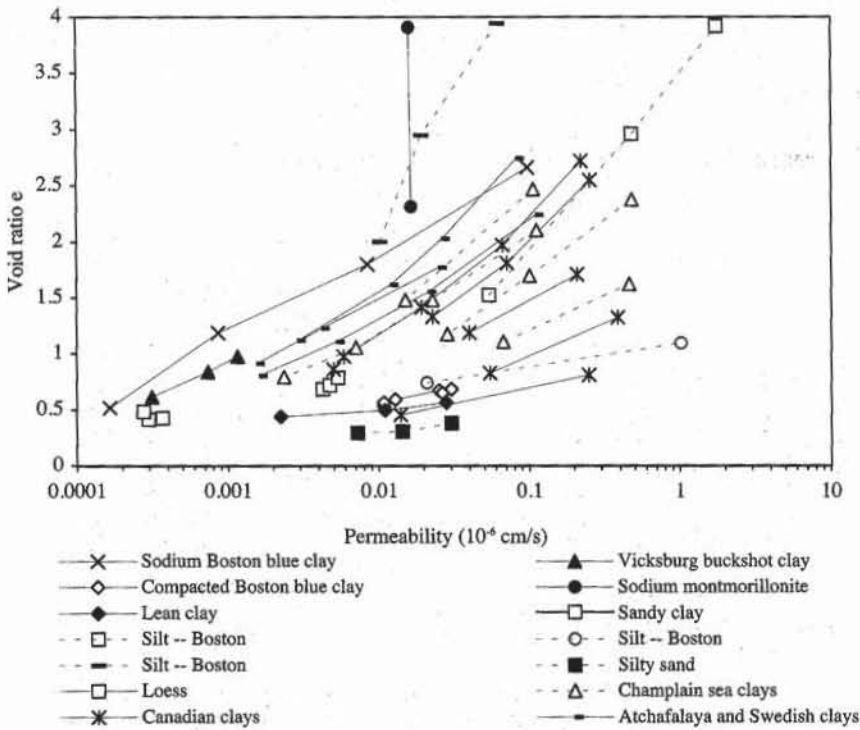


Figure 11 Permeability data on various soils in range 10^{-5} to 10^{-10} cm/s (data after Lambe and Whitman, 1979; and Tavenas et al., 1983).

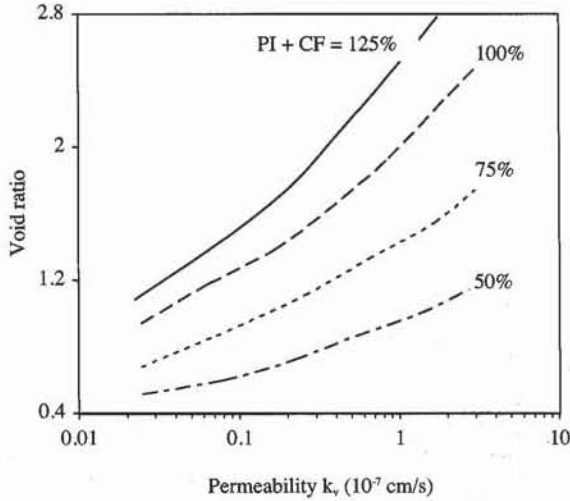


Figure 12 Variation of vertical coefficient of permeability with void ratio, plasticity index PI, and clay fraction CF for clay (after Tavenas et al., 1983).

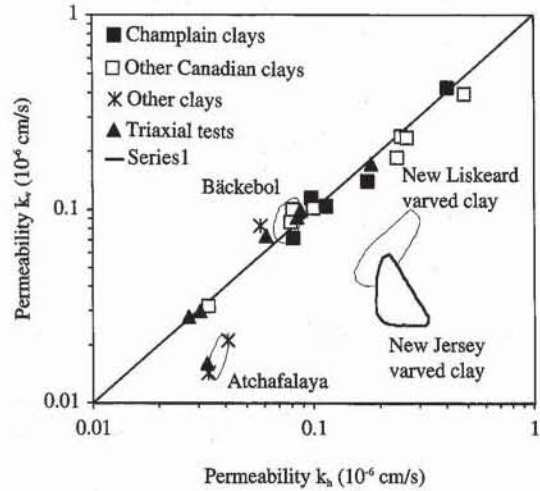


Figure 13 Permeability anisotropy for various natural clays (Tavenas and Leroueil, 1987).

REFERENCES

- CARMAN, P. S., 1939, "Permeability of saturated sands, soils, and clays," *J. Agric. Sci.*, Vol. XXIX, No. 11.
- DARCY, H., 1856, *Les Fontaines Publiques de la Ville de Dijon*, Dalmont, Paris.
- HANSBO, S., 1960, "Consolidation of clay with special reference to influence of vertical sand drains," *Proceedings No.18, Swedish Geotechnical Institute*, pp. 45-50.
- HAZEN, A., 1892, "Some physical properties of sands and gravels with special reference to their use in filtration," *24th annual report*, Massachusetts State Board of Health, USA.
- KULHAWY, F. H., and P. W. MAYNE, 1990, *Manual on Estimating Soil Properties for Foundations Design*, Report EL-9800 to Electric Power Research Institute, Cornell University, Ithaca, New York.
- KOZENY, J., 1927, "Über kapillare leitung des wassers in boden," *Ber. Wien. Akad.*, pp. 136-271.
- LAMBE, T. W., and R. V. WHITMAN, 1979, *Soil Mechanics, SI Version*, John Wiley & Sons, Inc., New York, 553 p.
- LANE, K. S., and D. E. WASHBURN, 1946, "Capillary tests by capillarimeter and by soil filled tubes," *Proceedings of Highway Research Board*.
- LOUDON, A. G., 1952, "The computation of permeability from simple soil tests," *Géotechnique*, Vol. 28, No. 3.
- NAVFAC, 1982, *Soil Mechanics (Design Manual 7.1)*, Naval Facilities Engineering Command, Alexandria, 355 p.
- TAVENAS, F., P. JEAN, P. LEBLOND, and S. LEROUÉIL, 1983, "The permeability of natural soft clays. Part II, Permeability characteristics," *Canadian Geotech. J.*, Vol. 20, No. 4, pp. 645-660.
- TAVENAS, F., and S. LEROUÉIL, 1987, "State-of-the-Art on laboratory and in-situ stress-strain-time behavior of soft clays," *Proceedings of the International Symposium on Geotechnical Engineering of Soft Soils, Mexico City*, pp. 1-46.

- TAYLOR, D. W., 1948, *Fundamentals of Soil Mechanics*, John Wiley & Sons, New York, 700 p.
- TERZAGHI, K., and R. B. PECK, 1967, *Soil Mechanics in Engineering Practice*, 2nd Ed., John Wiley & Sons, New York, 729 p.

REVIEW QUESTIONS

1. Define the total head in terms of water pressure, elevation, and unit weight of water. What is the physical meaning of total head?
2. Why do we use the hydrostatic definition of total head instead of the Bernoulli definition of total head?
3. Why do we neglect the term $v^2/2g$ in defining the total head in soil? (v is the fluid velocity and g is the earth gravity.) Justify your answer with numbers.
4. Define *soil permeability*. What are the dimensions and units of permeability?
5. Does the permeability increase or decrease with temperature?
6. Name two laboratory tests used for determining soil permeability. For which types of soils are they used?
7. Is the fluid velocity larger or smaller than the discharge velocity? What is the relationship between these velocities?
8. What is the critical hydraulic gradient?
9. Can you name several empirical relationships that relate soil permeability to physical parameters?
10. Derive the expression for permeability in a constant head test.
11. Derive the expression for permeability for a falling head test.
12. What is a typical range of permeability for gravels, sands, silts, and clays?

EXERCISES

1. Plot permeability versus void ratio for the silts of Table E1, and define the coefficient of the Kozeny-Carman equation.

TABLE E1

Soil type	k (cm/s)	Void ratio e
Silty sand	7.E-09	0.29
	1.E-08	0.30
	3.E-08	0.38
Silt, Boston	2.E-08	0.74
	1.E-06	1.09
	1.E-08	2.00
	2.E-08	2.95
	6.E-08	3.94
	5.E-08	1.52
	5.E-07	2.96
	2.E-06	3.92
Silt, North Carolina	6.E-07	0.67
	2.E-06	0.79
	3.E-06	0.70
	3.E-05	0.89
	8.E-05	0.89

2. Same as Exercise 1 but for Table E2.
3. Same as Exercise 1 but for Table E3.

TABLE E2

Soil type	k (cm/s)	Void ratio e
Beach sand	8.E-02	0.65
	1.E-01	0.75
	1.E-01	0.75
	1.E-01	0.76
	1.E-01	0.79
	2.E-01	0.83
Ottawa sand	5.E-03	0.63
	6.E-03	0.66
Sand, Franklin Falls	9.E-04	0.78
	1.E-03	0.86
	1.E-03	0.78
Sand, Scituate	4.E-03	0.54
	5.E-03	0.54
	7.E-03	0.59
	8.E-03	0.67
Sand, Plum Island	2.E-02	0.69
	2.E-02	0.74
Sand, Fort Peck	2.E-03	0.63
	3.E-03	0.65
	3.E-03	0.67
	3.E-03	0.67
Sand, Union Falls	4.E-02	0.49
	6.E-02	0.57
	9.E-02	0.69
Sand from dike	2.E-04	0.68
	2.E-03	1.20

TABLE E3

Soil type	k (cm/s)	Void ratio e
Sandy clay	3.E-10	0.41
	4.E-10	0.42
	3.E-10	0.48
Compacted Boston blue clay	1.E-08	0.53
	1.E-08	0.56
	1.E-08	0.59
	3.E-08	0.67
Vicksburg buckshot clay	3.E-08	0.68
	3.E-08	0.65
	1.E-09	0.97
Sandy clay	7.E-10	0.84
	3.E-10	0.61
	5.E-05	1.08
	9.E-05	1.16
Loess	2.E-04	1.18
	2.E-04	1.31
	4.E-09	0.68
	5.E-09	0.72
Lean clay	5.E-09	0.78
	2.E-09	0.44
	1.E-08	0.49
Sodium Boston blue clay	3.E-08	0.56
	2.E-10	0.51
	9.E-10	1.18
	8.E-09	1.80
Calcium kaolinite	1.E-07	2.66
	2.E-06	1.24
	7.E-06	1.51
Sodium montmorillonite	1.E-05	1.68
	2.E-08	2.31
	2.E-08	3.91

4-2

Constant Head Permeability Test

SCOPE

The constant head permeability test (Fig. 1) is used for determining the permeability of samples of coarse-grained soils. Here we describe the constant head permeability test for sand and gravel samples.

EQUIPMENT

The equipment for the constant head permeability test includes:

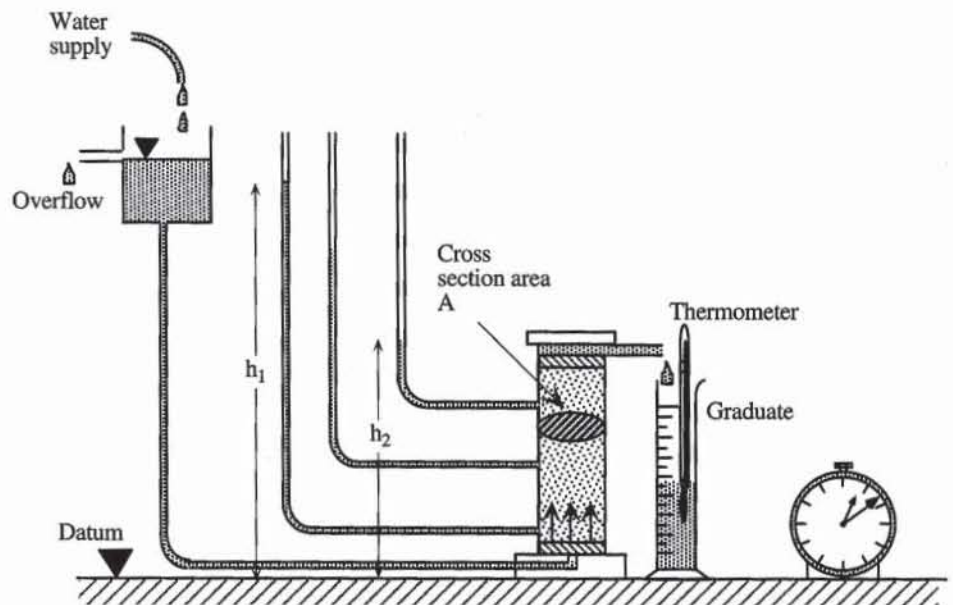


Figure 1 Experimental setup for constant head permeability test.

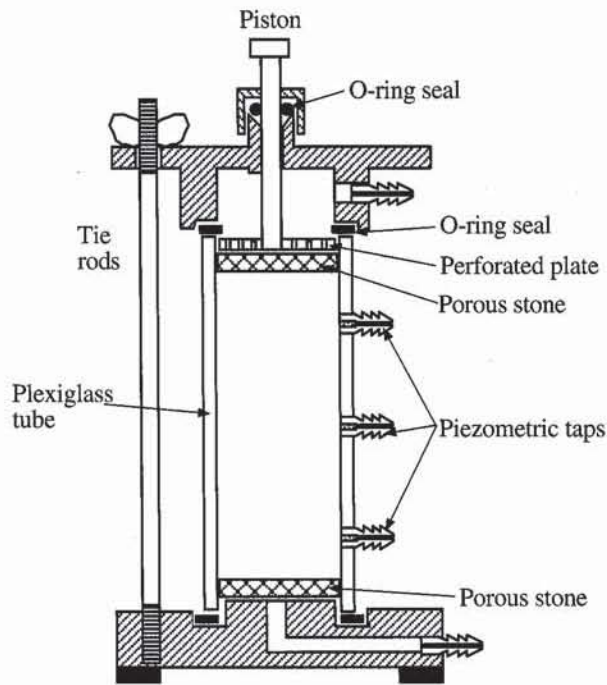


Figure 2 Permeameter cell.

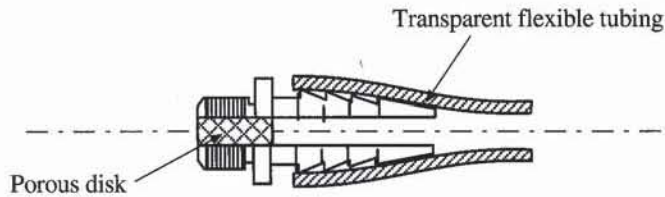


Figure 3 Piezometric tap of Fig. 1.

- Permeameter cell similar to that shown schematically in Fig. 2. Its cylinder is transparent to allow observation of the sample and to permit checking the saturation. As shown in Fig. 3, piezometer taps are located along the side of the permeameter cell for measuring the total head loss along a given sample length. This type of permeameter which encases the soil sample in a rigid cylinder is called a fixed wall permeameter. There is also another type of permeameter with a flexible wall to examine the effect of confining pressure on permeability. Its experimental setup is similar to the one of the triaxial test (see Chapter 7-6).
- Perforated metal or plastic disks, porous stones, or circular wire screens, cut for a close fit inside the permeameter.
- Glass tubing 2 to 4 mm in diameter (piezometer) mounted on a panel.
- Flexible transparent hoses and screw clamps necessary to connect piezometers and water supply.
- Constant-pressure supply device for water supply, as described later.
- Deaired distilled water prepared as described later.
- Timing device.
- Graduated cylinder, 100 mL.
- Thermometer, range 0 to 50°C, accurate to 0.1°C.
- Silicon or vacuum grease.

- Balance sensitive to 0.1 g.
- Oven.
- Ruler.

PREPARATION OF WATER FOR PERMEABILITY TEST

Ideally, the water used in the permeability test should be identical to that of the soils in the field. Since such water is rarely available, deaired tap water is generally used. When flowing between soil particles, untreated tap water would release air bubbles that would impede the flow of water, thereby giving erroneously low measurements of permeability. Figure 4 shows an arrangement for deairing water. A fine spray of water is sent into the vessel under internal vacuum. The vacuum pump is protected from water inflow by a water trap. Deaired water can also be prepared by boiling it on a heat source, and cooling it in a vessel sealed from the atmosphere to prevent it from dissolving air again.

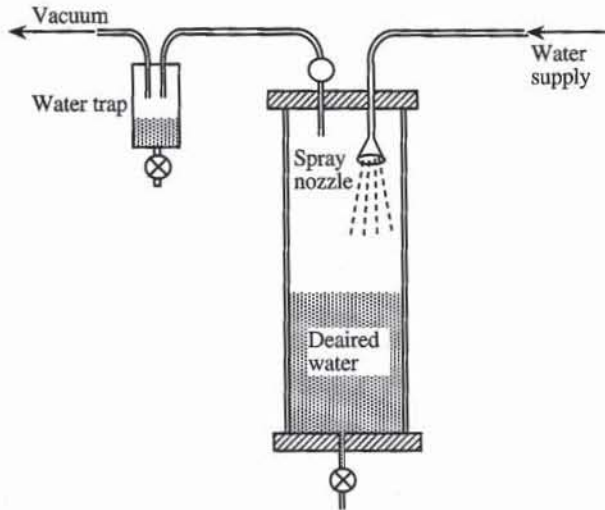


Figure 4 Deairing water with vacuum.

WATER SUPPLY AT CONSTANT PRESSURE

Figures 5 and 6 show two types of devices which can be used to supply water to the permeameter cell at a constant pressure. As shown in Fig. 5, the overflow maintains the level *A* constant, and therefore the pressure at *B* does not depend on the water level in the main supply tank.

As shown in Fig. 6, a tube is inserted and lowered to a selected depth in the container, which is hermetically sealed. When the water attempts to flow, the water level goes down in the tube and stops at point *A*. The water pressure at point *A* stays at atmospheric pressure, independently of the water level in the rest of the tank, provided that this level remains above point *A*. Therefore, the tank delivers water at constant pressure, which is controlled by the position of point *A*. Point *A* is chosen as low as possible to maximize the tank capacity. A constant pressure tank uses less deaired water than the device of Fig. 5.

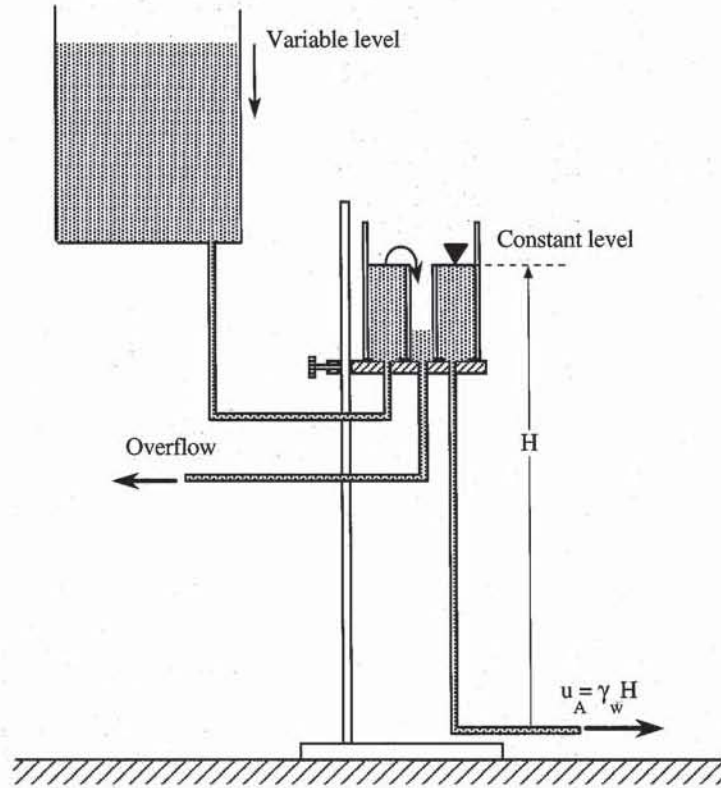


Figure 5 Suspended tank with constant water level for supplying water at constant pressure.

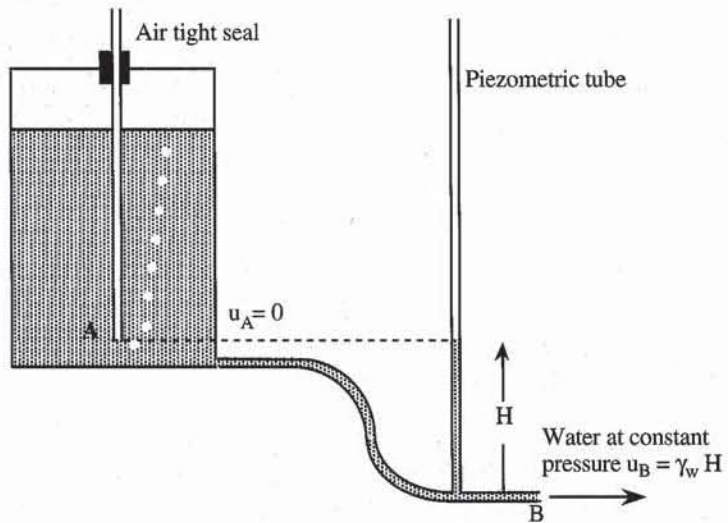


Figure 6 Constant-pressure tank.

PROCEDURE

1. Measure the inside diameter of the permeameter cell and the distance between piezometer taps.
2. Clean the cell base, apply silicon or vacuum grease on the lower gasket, place a porous stone on the base, and mount the permeameter cylinder.



Figure 7 A loose specimen is obtained by using a funnel and a flexible nozzle. Denser specimens are obtained by tapping or vibrating loose samples.

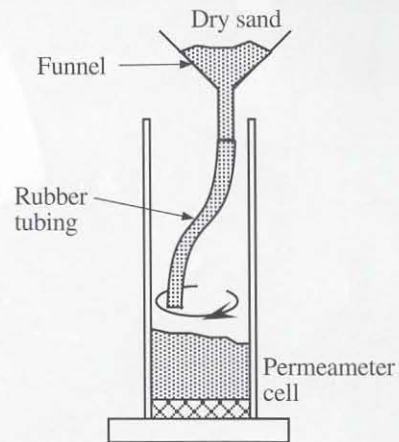


Figure 8 Dry, loose specimens are prepared by using a funnel and flexible tubing.

3. Mix the dry soil material to be tested in a large pan, and measure its weight. The specimen can be prepared using dry or wet pluviation. In the *dry pluviation method* the soil is poured in the permeameter as shown in Figs 7 and 8. It falls from a constant height through the flexible tubing and funnel system, making a specimen of uniformly low density. The specimen density may be controlled by measuring its height and weight of soil left over in the pan. Denser specimens are obtained by tapping the sample sides. In the *wet pluviation method*, the permeameter cell is first filled with a few centimeters of water. Then by using a spoon, the soil is gently poured a few centimeters away from the water surface, which is gradually raised. Wet pluviation produces saturated specimens of uniformly low density, the density of which can be controlled and increased as in the dry pluviation method.

4. Measure the weight of material left over in the pan to compute the specimen weight.

5. Apply vacuum or silicon grease to the top rubber gasket, mount the permeameter cap, and tighten its bolts. As shown in Fig. 9, lower the permeameter piston so that it slightly touches the specimen. During the test, the piston will maintain the sample in place and fix its height.

6. As shown in Figs. 10 and 11, connect the permeameter inlet valve to the constant pressure tank with a flexible hose, and attach a 50-cm-long transparent hose to each permeameter tap. Two permeameter taps are usually sufficient.

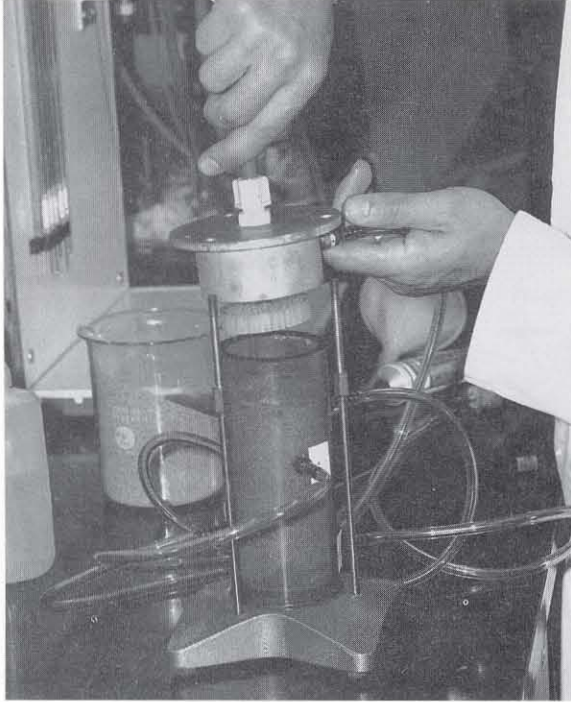


Figure 9 The permeater cell is closed.

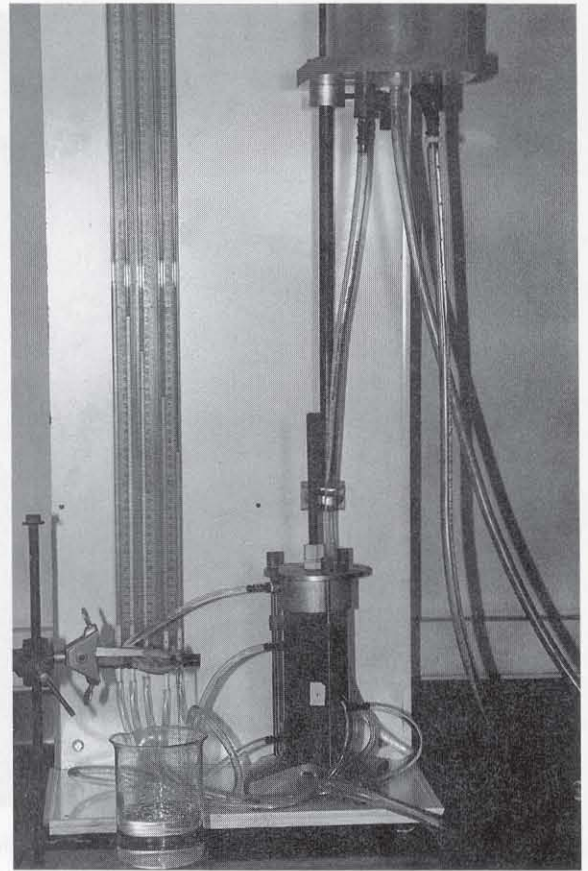


Figure 10 Constant head permeability test in progress.

Open the inlet valve to create a gentle upward flow of water inside the sample. The water flow should displace and flush the air within the sample and piezometer hoses. When there are no more air bubbles in the hoses, connect them to the piezometric tubes. The piezometric tubes are glass tubes with an internal diameter of 2 to 4 mm. The sand specimen should be fully saturated, and no air bubbles should be seen in the transparent hoses. After saturation, measure the sample height through the transparent cylinder.

7. When the permeameter outlet valve is closed, there should be no flow inside the sample, and the water levels in all the piezometric tubes should be identical. The elevation of their water column gives the total heads at the permeameter taps. When the outlet is opened, the piezometric levels should first fall, then stabilize. When the piezometer levels stop moving, measure the vertical distance between their meniscus bottoms. This distance is equal to the total head drop.

8. Adjust the outlet valve and/or the water pressure of the supply tank to obtain the desired head drop. While the water flows at a steady rate and the piezometer levels are constant, collect water in a container at convenient intervals. Measure the water temperature and the weight of the water collected to determine its volume.

9. Repeat step 8 for various head drops. Compute the coefficient of permeability for each measurement.

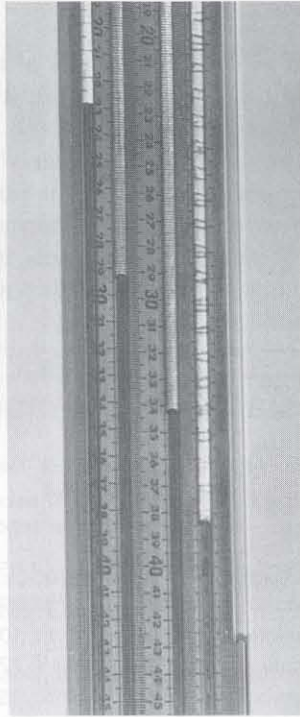


Figure 11 Close-up view of piezometric tubes of Fig. 10.

COMPUTATIONS

The dry unit weight γ_d and void ratio e of the soil specimen are

$$\gamma_d = \frac{W}{(\pi/4) D^2 H} \quad \text{and} \quad e = \frac{G_s \gamma_w}{\gamma_d} - 1 \quad (1)$$

where H is the sample height, D the sample diameter, W the dry sample weight, G_s the soil specific density, and γ_w the water unit weight. The discharge velocity v , hydraulic gradient i , and coefficient of permeability k_T at temperature T are

$$v = \frac{Q}{A_t}, \quad i = \frac{\Delta h}{L}, \quad \text{and} \quad k_T = \frac{v}{i} \quad (2)$$

where L is the distance between piezometer taps, Δh the distance between free surfaces in the piezometer tubes, $A = \pi D^2/4$ is the cross-sectional area of the specimen, and Q the volume of water collected during time t . The coefficient of permeability k at 20°C is

$$k_{20^\circ\text{C}} = \frac{\eta_T}{\eta_{20^\circ\text{C}}} k_T \quad (3)$$

where $\eta_{20^\circ\text{C}}$ is the viscosity of water at 20°C and η_T is the viscosity of water at temperature T .

EXAMPLE

Figures 12 and 14 show the results of a constant head permeability test. As shown in Fig. 12, the input data are italicized. Figure 13 lists the formulas used in Fig. 12, and Fig. 14 shows the variation of the discharge velocity v versus the hydraulic gradient i . Darcy's law is verified in the range of applied hydraulic gradient, because v varies linearly with i . The slope of the linear $v-i$ relation is equal to the permeability coefficient k at ambient temperature. The permeability coefficient is then calculated at 20°C to compensate for the change in water viscosity with temperature.

	A	B	C	D	E	F
1	Constant Head Permeability					
2	Analyst Name: <i>Kary P. Tiel, J. S. Tkach, E. Davidson, and H. Guapo</i>					
3	Test Date: <i>3/1/93</i>					
4	Soil Sample: <i>Loose sand mixture</i>					
5	Specific gravity $G_s =$ <i>2.65</i>					
6	Specimen dry mass $M_d =$ <i>674.00</i> g					
7	Specimen height $H =$ <i>14.50</i> cm					
8	Specimen diameter $D =$ <i>6.22</i> cm					
9	Piezometer tap distance $L =$ <i>10.35</i> cm					
10	Initial void ratio $e =$ <i>0.73</i>					
11	Dry unit weight $\gamma_d =$ <i>14.99</i> kN/m ³					
13	Trial	1	2	3	4	
14	Piezometer level distance (cm) Δh	<i>4.75</i>	<i>13.60</i>	<i>25.30</i>	<i>36.10</i>	
15	Duration of sampling (s) t	<i>60</i>	<i>60</i>	<i>60</i>	<i>60</i>	
16	Mass of water collected & container (g) M_{wc}	<i>484.0</i>	<i>630.0</i>	<i>782.0</i>	<i>964.0</i>	
17	Mass of container (g) M_c	<i>398.0</i>	<i>396.0</i>	<i>390.0</i>	<i>398.0</i>	
18	Water temperature (°C) T_e	<i>21.8</i>	<i>22</i>	<i>21.5</i>	<i>21.5</i>	
19	Hydraulic gradient i	0.5	1.3	2.4	3.5	
20	Discharge velocity (cm/s) v	0.047	0.128	0.215	0.310	
21	Permeability at ambient temperature (cm/s) k_T	0.103	0.098	0.088	0.089	
22	Permeability at 20°C (cm/s) k	0.098	0.093	0.085	0.086	
23	Average permeability at ambient =	0.094 cm/s				
24	Average permeability at 20°C =	0.090 cm/s				

Figure 12 Example of data set for the constant head permeability test.

	A	B	C
10	Initial void ratio $e = =Gs/gd*9.81-1$		
11	Dry unit weight $\gamma_d = =Md/H/PI()*4/D^2*9.81$		kN/m ³
19	Hydraulic gradient i	$=Dh/L$	$=Dh/L$
20	Discharge velocity (cm/s) v	$=(Mwc-Mc)/t/(PI()*D^2/4)$	$=(Mwc-Mc)/t/(PI()*D^2/4)$
21	Permeability at ambient temperature (cm/s) k_T	$=v/i$	$=v/i$
22	Permeability at 20°C (cm/s) k	$=kT*VISCO(Te)/VISCO(20)$	$=kT*VISCO(Te)/VISCO(20)$
23	Average permeability at ambient =	$=AVERAGE(kT)$	cm/s
24	Average permeability at 20°C =	$=AVERAGE(k)$	cm/s

Figure 13 Formulas used in Fig. 12.

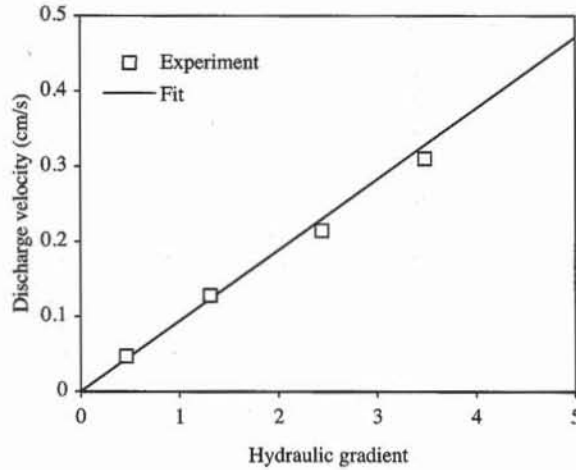


Figure 14 Variation of discharge velocity versus hydraulic gradient.

Indirect Calculation of Permeability from Grain Size Distribution Curve

Figures 15 and 16 show the variation of the permeability coefficient k versus the void ratio e for the same material. The permeability decreases with the void ratio.

A grain size distribution is required to calculate k with Hazen’s or Kozeny–Carman’s equations (Eqs. 9 and 10 of Chapter 4-1). The grain size analysis results for the soil tested in Fig. 16 are reported in Figs. 17 and 18 (see Chapter 1-2 for details). Hazen’s formula neglects the effect of void ratio on k , which corresponds to a vertical dashed line in Fig. 16, and overestimates the measured values. For Kozeny–Carman’s formula, as shown in Fig. 17, we assume that grains larger than 0.25 are subrounded (i.e., $f = 1.25$) and those smaller than 0.25 mm are rounded (i.e., $f = 1.1$). The total value of fS^2 is the weighed sum of fS^2 which is calculated independently for each grain size range. Figure 19 shows the details of these calculations. Kozeny–Carman’s formula is slightly in better agreement with measured values than is Hazen’s formula. It accounts for the decrease in permeability with void ratio.

k (cm/s)	e
0.0943	0.73
0.0428	0.61
0.0140	0.75
0.0045	0.44
0.1934	0.77
0.1033	0.62

Figure 15 Measured variation of permeability with void ratio.

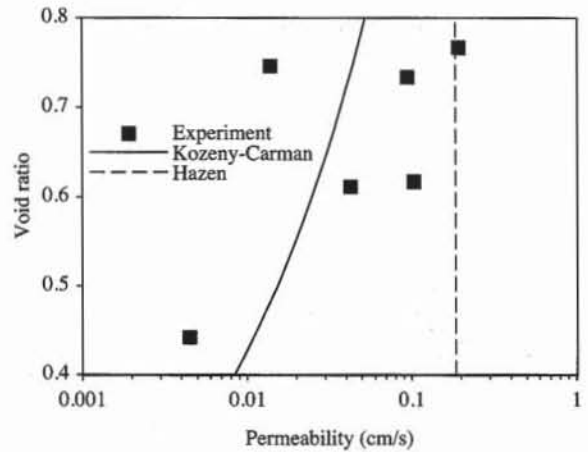


Figure 16 Measured variation of permeability with void ratio and values of permeability predicted by Hazen’s and Kozeny–Carman’s equations.

	A	B	C	D	E	F	G
1	Calculation of permeability coefficient with empirical relations						
2							
3	Analyst: <i>J. S. Tkach</i>						
4	Test date: <i>2-Feb-93</i>						
5	Soil type: <i>Sand Mixture</i>						
6							
7	Grain size (mm)	Percent finer by weight	Frequency	Specific surface	Angularity		
8	<i>d</i>	<i>pf</i>	<i>p</i>	(mm^{-1}) <i>S</i>	factor <i>f</i>		
9	<i>0.42</i>	100.0	35.0%	16.90	1.25		
10	<i>0.3</i>	65.2	11.0%	21.91	1.25		
11	<i>0.25</i>	53.9	22.0%	28.52	1.10		
12	<i>0.177</i>	32.0	7.0%	36.82	1.10		
13	<i>0.15</i>	25.2	16.0%	56.57	1.10		
14	<i>0.075</i>	9.2	9.0%				
15	$D_{10} = 0.078 \text{ mm}$		$C_u = 3.558$				
16	$D_{30} = 0.169 \text{ mm}$		$C_c = 1.328$				
17	$D_{60} = 0.276 \text{ mm}$		Kozeny-Carman $C_k = 0.185 \text{ cm/s}$				
18	Permeability coefficient						
19	Hazen, <i>k</i> (cm/s)	0.006					
20	Void ratio <i>e</i>	0.730	0.610	0.440	0.750	0.770	0.620
21	Kozeny-Carman, <i>k</i> (cm/s)	0.042	0.026	0.011	0.045	0.048	0.027

Figure 17 Results of grain size analysis and calculation of permeability coefficient with Hazen's and Kozeny-Carman's equations.

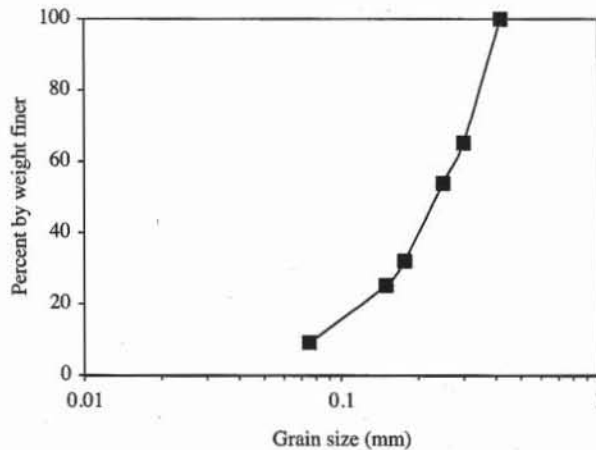


Figure 18 Grain size distribution curve of materials tested in Fig. 16.

REVIEW QUESTIONS

1. What is the purpose of the constant head permeability test?
2. What is the smallest value of permeability coefficient that can be measured in the constant head permeability test? What other test do you apply to the soils of smaller permeability?
3. Is the permeability coefficient of sands influenced by their void ratio? What is the trend?

	C	D				
7	Frequency	Specific surface (mm ⁻¹)				
8	p	S				
9	=(B9-B10)/100	=6/SQRT(A9*A10)				
10	=(B10-B11)/100	=6/SQRT(A10*A11)				
11	=(B11-B12)/100	=6/SQRT(A11*A12)				
12	=(B12-B13)/100	=6/SQRT(A12*A13)				
13	=(B13-B14)/100	=6/SQRT(A13*A14)				
14	=(B14/100)					

	A	B	C	D
19	Hazen, k (cm/s)	=100*(D_10/10)^2		
20	Void ratio e	0.73	0.61	0.44
21	Kozeny-Carman, k (cm/s)	=Ck*e^3/(1+e)	=Ck*e^3/(1+e)	=Ck*e^3/(1+e)

	A	B	C	D	E
15		D ₁₀ = =INTER(10,pf,d)	C _u = =D_60/D_10		
16		D ₃₀ = =INTER(30,pf,d)	C _c = =D_30^2/D_10/D_60		
17		D ₆₀ = =INTER(60,pf,d)	Kozeny-Carman C _k = =(9.81/(5*VISCO(20)*SUMPRODUCT(p,f,S,S)))		

Figure 19 Formulas used in Fig. 17.

- Can you give a relation that accounts for permeability change versus void ratio?
- Explain the principle of the constant-pressure tank shown in Fig. 6.
- Why do you use deaired water instead of tap water for the permeability test?
- How do you remove air from water?
- Does the measurement of permeability increase or decrease with the air content of the test water?
- What technique do you use to get a loose specimen of sand in the permeameter cell?
- Does the permeability coefficient increase or decrease with water temperature? Why?

EXERCISES

- Calculate the void ratio and average permeability coefficient from the test results in Table E1. Verify that the discharge velocity varies linearly with the hydraulic gradient.

TABLE E1

Specific gravity	2.65				
Specimen dry mass (g)	674.00				
Specimen height (cm)	13.48				
Specimen diameter (cm)	6.22				
Piezometer tap distance (cm)	10.35				
	Trial	1	2	3	4
Piezometer reading, inlet (cm)		89.90	57.40	44.90	22.00
Piezometer reading, outlet (cm)		42.70	27.70	23.00	15.50
Duration of sampling (sec)		60	60	60	60
Mass of water collected and container (g)		766.0	614.0	560.0	438.0
Mass of container (g)		396.0	390.0	398.0	390.0
Water Temperature (°C)		21.8	21.9	21.9	22.2

2. Same as Exercise 1 but for Table E2.

TABLE E2

Specific gravity	2.65				
Specimen dry mass (g)	712.00				
Specimen height (cm)	15.50				
Specimen diameter (cm)	6.21				
Piezometer tap distance (cm)	10.33				
	Trial	1	2	3	4
Piezometer reading, inlet (cm)		54.60	16.60	63.90	74.80
Piezometer reading, outlet (cm)		9.10	5.50	10.20	11.30
Duration of sampling (s)		150	150	90	90
Mass of water collected and container (g)		670.0	470.0	594.0	620.0
Mass of container (g)		396.8	396.8	396.8	396.8
Water temperature (°C)		22.5	22.5	22.5	22.5

3. Same as Exercise 1 but for Table E3.

TABLE E3

Specific gravity	2.65				
Specimen dry mass (gr)	712.00				
Specimen height (cm)	12.80				
Specimen diameter (cm)	6.21				
Piezometer tap distance (cm)	10.33				
	Trial	1	2	3	4
Piezometer reading, inlet (cm)		86.90	67.20	48.40	25.40
Piezometer reading, outlet (cm)		6.40	5.90	5.70	5.50
Duration of sampling (s)		90	90	180	180
Mass of water collected and container (g)		494.0	468.0	492.0	448.0
Mass of container (g)		396.8	396.8	396.8	396.8
Water temperature (°C)		22	22	22	22

4. Same as Exercise 1 but for Table E4.

TABLE E4

Specific gravity	2.65				
Specimen dry mass (g)	698.00				
Specimen height (cm)	15.30				
Specimen diameter (cm)	6.22				
Piezometer tap distance (cm)	10.30				
	Trial	1	2	3	4
Piezometer reading, inlet (cm)		19.10	46.40	62.40	72.20
Piezometer Reading, outlet (cm)		11.50	30.00	41.80	48.70
Duration of sampling (s)		60	90	60	60
Mass of water collected and container (g)		656.0	1214.0	1094.0	1174.0
Mass of container (g)		390.0	390.0	390.0	390.0
Water temperature (°C)		21	21	21	21

5. Same as Exercise 1 but for Table E5.

TABLE E5

Specific gravity	2.65				
Specimen dry mass (g)	698.00				
Specimen height (cm)	14.00				
Specimen diameter (cm)	6.22				
Piezometer tap distance (cm)	10.30				
	Trial	1	2	3	4
Piezometer reading, inlet (cm)		18.20	52.10	64.80	80.40
Piezometer reading, outlet (cm)		7.20	22.10	28.30	35.90
Duration of sampling (s)		60	60	60	60
Mass of water collected and container (g)		608.0	936.0	1034.0	1146.0
Mass of container (g)		390.0	390.0	390.0	390.0
Water temperature (°C)		21	21	21	21

4-3

Falling Head Permeability Test

OBJECTIVE

The falling head permeability test is used for determining the permeability of soil samples that have a permeability less than about 10^{-3} cm/s.

EQUIPMENT

The equipment for the falling head permeability test includes:

- Permeameter similar to that shown schematically in Fig. 1.
- Perforated metal or plastic disks, circular wire screens, or porous stones.
- Glass standpipe with its support.
- Transparent flexible hoses, screw clamps, and so on.
- Deaired distilled water.
- Watch or clock.
- Thermometers, range 0 to 50°C, accurate to 0.1°C.
- Balance sensitive to 0.1 g.
- Oven.
- Ruler.

PROCEDURE

1. Dry specimens are prepared as for the constant head test. Wet specimens may be trimmed and fitted into the permeameter mold as described in Chapter 7-2.
2. Measure the specimen height, diameter, and dry weight. Determine the standpipe internal diameter by measuring the volume of water contained in a standpipe section of given height.

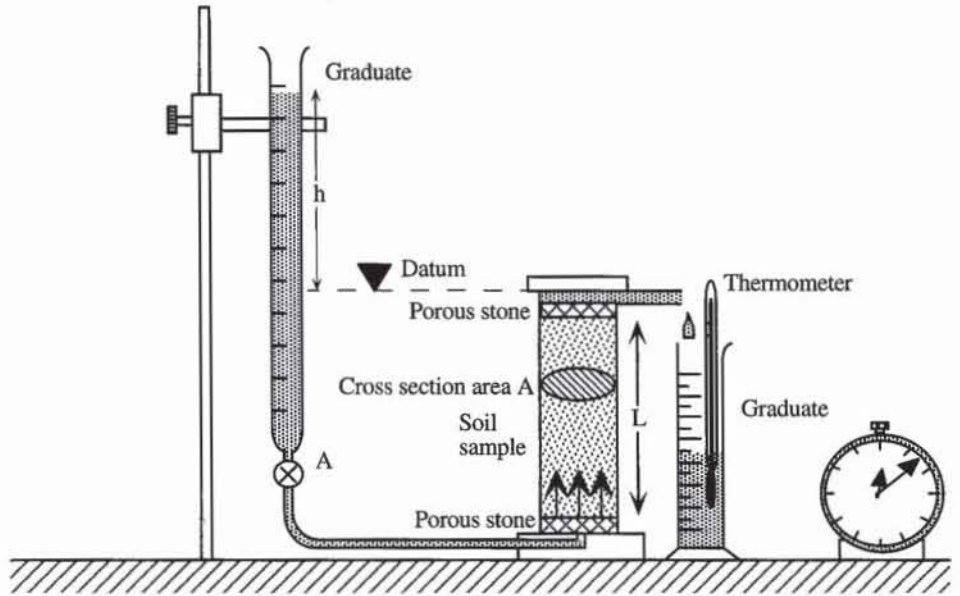


Figure 1 Setup of falling head permeability device.

3. Saturate the specimen by immersing it in water for several days. It is important that the specimen be fully saturated; otherwise, the falling head test will give erroneous results.

4. Fill the standpipe with deaired water well above the discharge level of the permeameter cell. If the water level falls slowly and the test lasts a few days, it is recommended that a few drops of oil be added on the water surface in the standpipe to prevent water from evaporating.

5. Begin the test by opening the inlet valve A simultaneously and starting the timer. As the water flows through the specimen, measure the water elevation above the datum and the water temperature at various times *t*.

PERMEABILITY TEST WITH CONSOLIDOMETER

Soil permeability can also be measured during the consolidation test by using either the falling head method or the rate of settlement. The former method is described below, the latter in Chapter 7-2.

Figure 2 shows the falling head permeability test during a consolidation test. The specimen in the rigid container is squeezed by a constant vertical load. The standpipe is attached to the consolidation cell and forces water through the specimen. The specimen is subjected to the falling head test after being consolidated. The permeability is computed using Eq. 1.

COMPUTATIONS

For dry samples, the void ratio and dry unit weight are calculated as for the constant head test. For wet samples, the water content is and dry sample weight is obtained as in Chapter 7-2.

The coefficient of permeability k_T is calculated as follows:

$$k_T = \frac{aL}{At} \log \frac{h_0}{h_f} \tag{1}$$

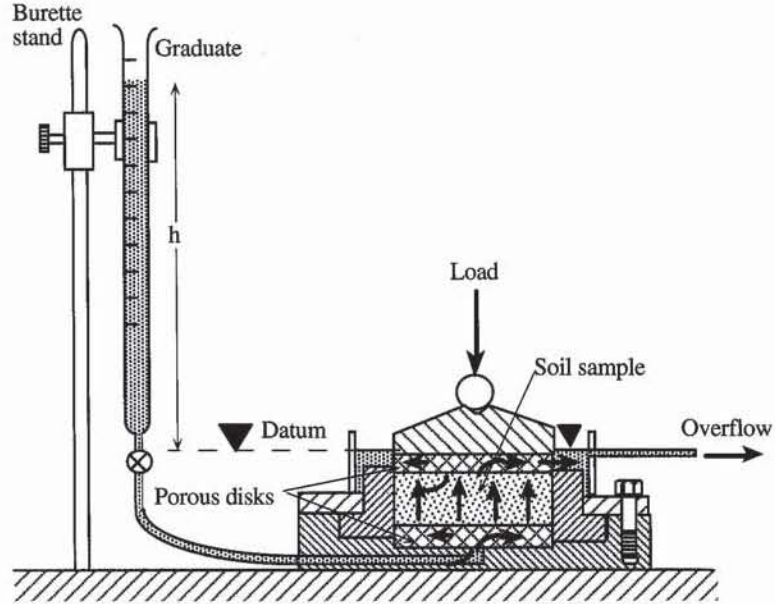


Figure 2 Falling head permeability test during consolidation test.

where $a = \pi d^2/4$ is the inside area of the standpipe, $A = \pi D^2/4$ is the cross-sectional area of the specimen, L the length of the specimen, d the internal diameter of the standpipe, D the diameter of the sample, h_0 the elevation of water in the standpipe above the discharge level at time $t = 0$, and h_f the elevation of water in the standpipe above the discharge level at time t . The coefficient of permeability $k_{20^\circ\text{C}}$ is calculated as for the constant head test.

For small-diameter standpipes, the capillary rise h_c may not be neglected compared to h_0 and h_f . In this case, Eq. 1 becomes

$$k_T = \frac{aL}{At} \log \frac{h_0 - h_c}{h_f - h_c} \tag{2}$$

EXAMPLE

Figure 3 shows the results of a falling head permeability test. The formulas used in Fig. 3 are listed in Fig. 4. Figure 5 shows the variation of k computed by using Eq. 1 for different times and also shows the mean value of k calculated by using average and linear regression. The average method consists of averaging the values of k calculated at each sampling time. The linear regression method consists of fitting the variation of water height for the complete test duration. By using Eq. 1, the water column height h_t varies with time t as follows:

$$\ln(h_t) = \ln(h_0) - \frac{kA}{aL}t \tag{3}$$

The value of k can therefore be computed from the slope S of the linear regression passing through the data points $(t_i, \ln(h_i))$, $i = 1, \dots, n$:

$$k = -\frac{SaL}{A} = -\frac{d^2}{D^2}SL \tag{4}$$

where d is the diameter of the standpipe and D is the diameter of the sample. As shown in Fig. 6, the average and regression methods give similar results.

	A	B	C	D	E	F	G
1	Falling Head Permeability						
2	Analyst Name: <i>Kate Allison, Paul Murphy, Francis Chin, L.P Chua</i>						
3	Test Date: <i>6/8/95</i>						
4	Soil Sample: <i>Sample 4, Westport sand, New Brighton sand and silica flour 100</i>						
5	Specific gravity $G_s = 2.65$						
6	Specimen dry mass $M = 1756.00$ g						
7	Specimen height $H = 12.18$ cm						
8	Specimen diameter $D = 10.09$ cm						
9	Diameter of standpipe $d_s = 0.95$ cm						
10	Initial height in standpipe $h_0 = 141.90$ cm						
11	Initial void ratio $e = 0.47$						
12	Dry unit weight $\gamma_d = 17.69$ kN/m ³						
13							
	Time (min)	Height of water in standpipe (cm)	Temperature θ (°C)	Permeability (cm/s)	Permeability at 20 °C (cm/s)	Height predicted by average (cm)	Height predicted by regression (cm)
14	t	h_t	T_θ	k_T	k		
15							
16	1	134.1	16.5	1.02E-04	1.11E-04	134.47	134.66
17	2	127.3	16.5	9.77E-05	1.07E-04	127.43	127.79
18	3	120.7	16.5	9.71E-05	1.06E-04	120.76	121.27
19	4	114.3	16.5	9.73E-05	1.06E-04	114.44	115.08
20	5	108.3	16.5	9.73E-05	1.06E-04	108.44	109.21
21	6	102.8	16.5	9.67E-05	1.06E-04	102.77	103.64
22	7	97.7	16.5	9.60E-05	1.05E-04	97.39	98.35
23	8	92.7	16.5	9.58E-05	1.05E-04	92.29	93.33
24	9	88.2	16.5	9.51E-05	1.04E-04	87.46	88.57
25	10	83.7	16.5	9.50E-05	1.04E-04	82.88	84.05
26	11	79.4	16.5	9.50E-05	1.04E-04	78.54	79.76
27	Permeability calculated by average $k_{Ta} = 9.68E-05$ cm/s						
28	Permeability calculated by regression $k_{Tr} = 9.43E-05$ cm/s						
29	Permeability calculated by average $k_{20^\circ C} = 1.06E-04$ cm/s						

Figure 3 Example of data set for the falling head permeability test.

	C	D	E
11	Initial void ratio $e = G_s/gd \cdot 9.81 - 1$		
12	Dry unit weight $\gamma_d = M/H/PI() \cdot 4/D^2 \cdot 9.81$		kN/m ³

	D	E	F	G
14	Permeability (cm/s)	Permeability at 20 °C (cm/s)	Height predicted by average (cm)	Height predicted by regression (cm)
15	k_T	k		
16	$=ds^2 \cdot H/D^2 / (t \cdot 60) \cdot LN(h_0/ht)$	$=kT \cdot VISCO(T_\theta) / VISCO(20)$	$=h_0 \cdot EXP(-kTa \cdot D^2/ds^2/H \cdot t \cdot 60)$	$=h_0 \cdot EXP(-kTr \cdot D^2/ds^2/H \cdot t \cdot 60)$
17	$=ds^2 \cdot H/D^2 / (t \cdot 60) \cdot LN(h_0/ht)$	$=kT \cdot VISCO(T_\theta) / VISCO(20)$	$=h_0 \cdot EXP(-kTa \cdot D^2/ds^2/H \cdot t \cdot 60)$	$=h_0 \cdot EXP(-kTr \cdot D^2/ds^2/H \cdot t \cdot 60)$

	D	E	F
27	Permeability calculated by average $k_{Ta} =$	$=AVERAGE(kT)$	cm/s
28	Permeability calculated by regression $k_{Tr} =$	$=-SLOPE(LN(ht), t) \cdot ds^2/D^2 \cdot H/60$	cm/s
29	Permeability calculated by average $k_{20^\circ C} =$	$=AVERAGE(k)$	cm/s

Figure 4 Formulas used for the falling head test.

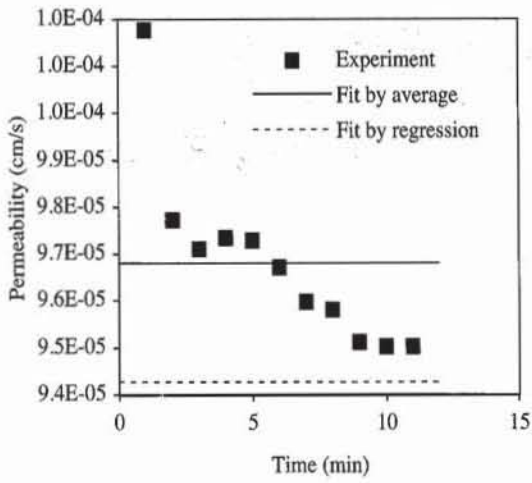


Figure 5 Permeability coefficient computed at various time intervals, and average permeability coefficient calculated by average and linear regression.

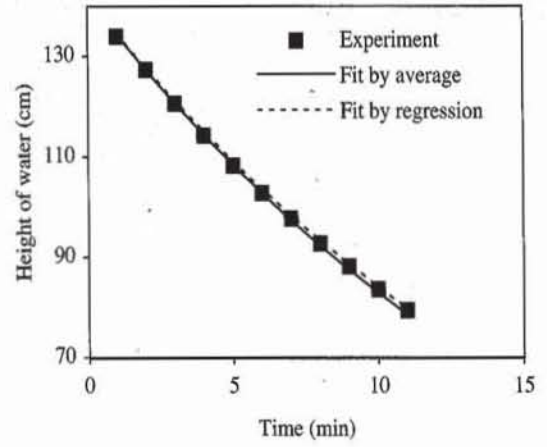


Figure 6 Variation of height of water column versus time predicted by the average and linear regression methods.

4-4

Electrical Analogy of Seepage Problems

DEFINITION

The steady-state flow of a fluid through a porous medium is analogous to the steady-state flow of an electric current through a current-conducting medium. The electrical analogy method solves seepage problems by constructing an analog problem with resistive papers and by measuring voltage instead of total head.

ELECTRICAL ANALOGY OF WATER FLOW

Seepage Theory

When water flows steadily through a two-dimensional saturated soil of isotropic permeability, the distribution of total head $h(x,y)$ obeys Laplace's equation:

$$\frac{\partial^2 h}{\partial x^2} + \frac{\partial^2 h}{\partial y^2} = 0 \quad \text{or} \quad \nabla^2 h = 0 \quad (1)$$

where x and y are spatial coordinates. Laplace's equation is not only found in the steady-state flow of water but in many other branches of engineering and physics. In particular, it describes the steady flow of electricity through resistive paper.

Conduction Theory

One-dimensional Ohm's law. As shown in Figs. 1 and 2, if two electrical potentials V_1 and V_2 are applied to the extremities of resistance R , the current i obeys Ohm's law:

$$i = -\frac{1}{R} (V_2 - V_1) \quad (2)$$

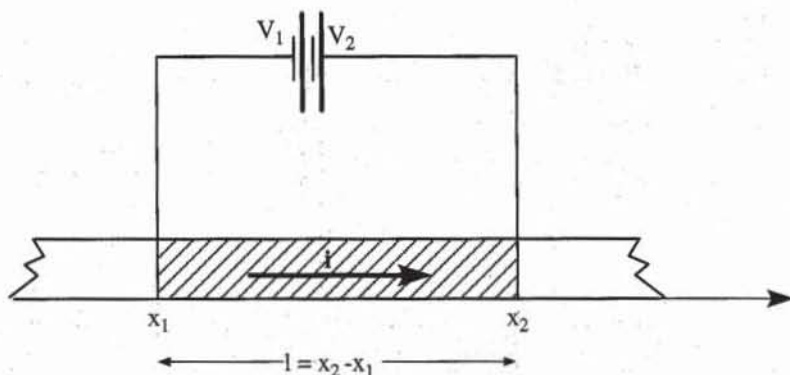


Figure 1 One-dimensional resistance of finite length.

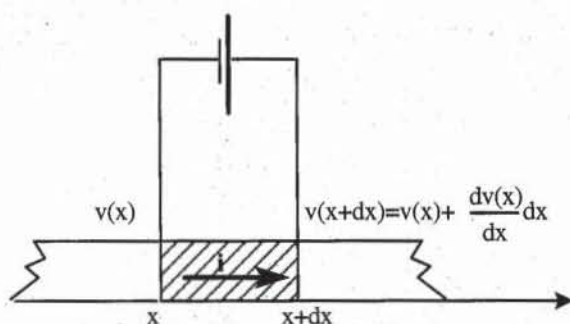


Figure 2 One-dimensional resistance of infinitesimal length.

The resistance r per unit of length is

$$r = \frac{R}{l} = \frac{R}{x_2 - x_1} \quad (3)$$

where $l = x_2 - x_1$ is the resistance length. The conductivity σ is the inverse of R (i.e., $\sigma = 1/R$). When $l \ll 1$;

$$\frac{V_2 - V_1}{x_2 - x_1} = \frac{dV(x)}{dx} \quad (4)$$

and Ohm's law becomes

$$i = -\frac{1}{r} \frac{dV}{dx} = -\sigma \frac{dV}{dx} = -\sigma \text{grad } V \quad (5)$$

Ohm's law for two-dimensional flow of electricity. For the two-dimensional flow of current in an isotropically resistive paper, Ohm's law becomes

$$i_x = -\sigma \frac{\partial V}{\partial x}, \quad i_y = -\sigma \frac{\partial V}{\partial y} \quad (6)$$

where i_x and i_y are components of current intensity in the x and y directions, σ is the conductivity of the resistive paper, and $V(x, y)$ is an electric potential depending on the x and y coordinates. When no electricity is stored or lost in the infinitesimal element of Fig. 3, the conservation of electricity implies that

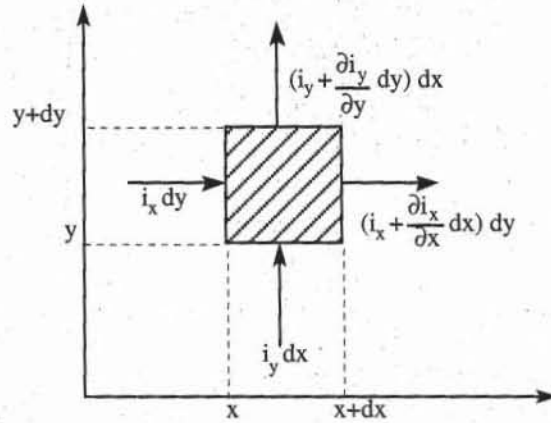


Figure 3 Flow of current through an infinitesimal element of two-dimensional resistance.

$$\left(i_y + \frac{\partial i_y}{\partial y} dy\right) dx - i_y dx + \left(i_x + \frac{\partial i_x}{\partial x} dx\right) dy - i_x dy = 0 \tag{7}$$

Equation 7 simplifies to

$$\frac{\partial i_x}{\partial x} + \frac{\partial i_y}{\partial y} = 0 \tag{8}$$

By substituting Eq. 6 into Eq. 8, $V(x, y)$ also satisfies Laplace's equation:

$$\frac{\partial^2 V}{\partial x^2} + \frac{\partial^2 V}{\partial y^2} = 0 \text{ or } \nabla^2 V = 0 \tag{9}$$

Analogy between Seepage and Conduction Theories

Table 1 presents the correspondence between the variables and relations of water seepage in soils and electric current flow in resistive papers. Although the flow of water through a porous medium and the flow of electrons through a resistive medium are different in nature, they are described by similar variables and governing equations. These two physical phenomena are said to be analogous. The analogy between seepage flow and current flow permits us to determine the total head $h(x,y)$ in soils by measuring $V(x, y)$ directly on resistive paper.

TABLE 1
Correspondence between seepage and flow of electrical current

Flow of water	Flow of electrical current
h total head	V voltage
k coefficient of permeability	σ conductivity ($\sigma = 1/r$)
v discharge velocity	i current
Darcy's law: $v = -k \text{ grad } h$	Ohm's law: $i = -\sigma \text{ grad } V$
$\nabla^2 h = 0$	$\nabla^2 V = 0$
Equipotential lines: $h = \text{constant}$	Equipotential lines: $V = \text{constant}$
Impervious boundary: $\frac{\partial h}{\partial n} = 0$	Insulated boundary: $\frac{\partial V}{\partial n} = 0$

APPLICATION OF ANALOGY TO SEEPAGE PROBLEM

Figures 4 to 6 show a seepage problem and its electrical analog. In Figs. 5 and 6, the electrical analog is cut out in a large sheet of resistive paper. Compared to the seepage problem of Fig. 4, the electrical analog has the same geometric proportions but is 100 times smaller. One meter in the field corresponds to 1 centimeter in the analog model. The thin slot in the resistive paper is an electric barrier representing the impervious sheet-pile wall. The conductive electrodes A and B represent the equipotential lines on the upstream and downstream boundaries of Fig. 4. The 6-V differential voltage applied between A and B corresponds to the total head drop of 6 m in Fig. 4. Each volt in Fig. 5 conveniently corresponds to 1 m of total head in Fig. 4. One voltmeter pin is connected to electrode B, which is equivalent to choosing the datum along the downstream surface of Fig. 4. The voltmeter indicates 6 V and 0 V on electrodes A and B, respectively. The equipotential line along which the total head is equal to 5 m can therefore be constructed point by point by tracking the places on the resistive paper where the voltmeter probe indicates 5 V. The equipotential lines for $h = 1, 2, 3,$ and 4 m can be drawn in a similar way.

The flow lines can be obtained either by sketching the flow net by hand or by using the complementary electrical analog. In the former case, the flow lines are sketched by hand over the equipotential lines by ensuring that equipotential and flow lines intersect at right angles and generate curvilinear squares. In the latter case, the complementary electrical analog must be defined. In the complementary problem, boundary flow lines become equipotential boundaries, while

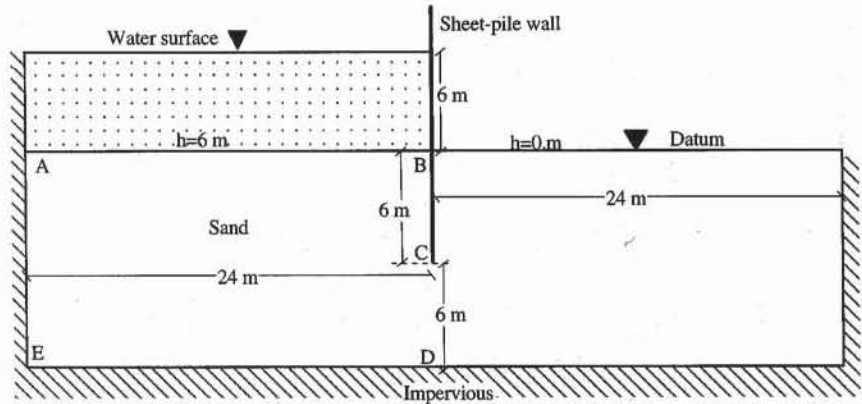


Figure 4 Definition of the geometry for the original seepage problem with a sheet-pile wall.

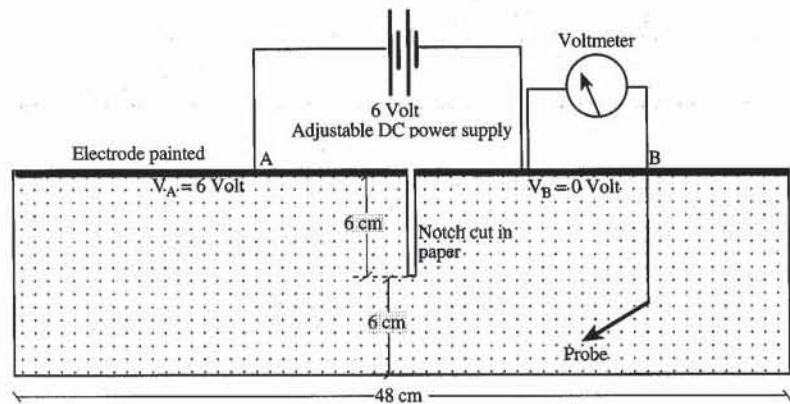


Figure 5 Electrical analogy of the problem in Fig. 4.

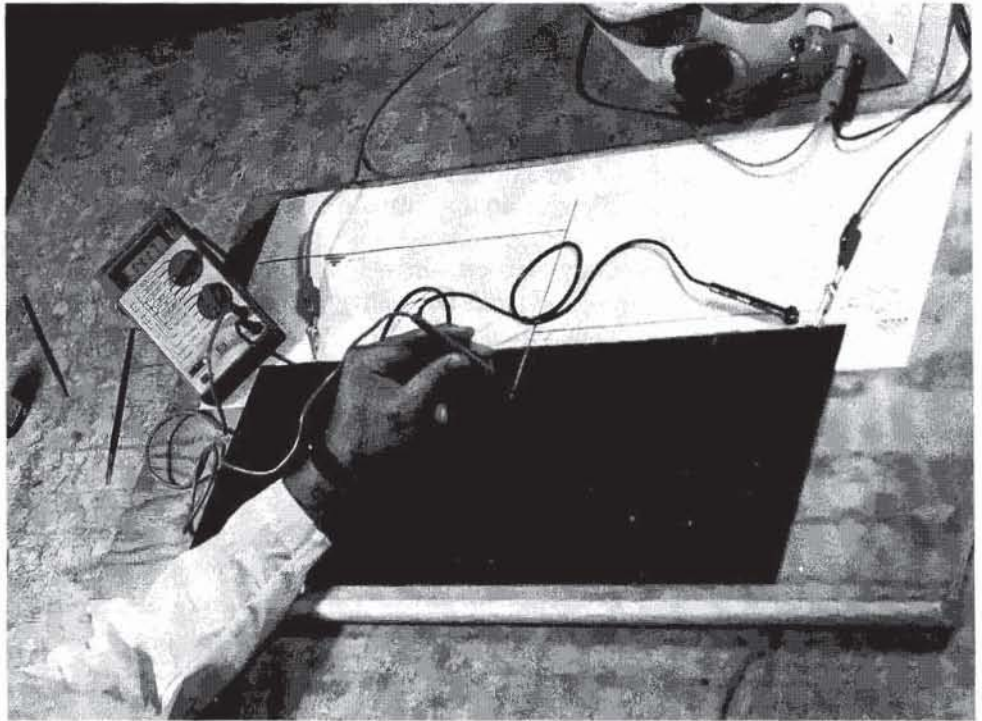


Figure 6 Electrical analogy setup. The resistive paper is cut as shown in Fig. 5. The notch in the paper represents the sheet-pile wall.

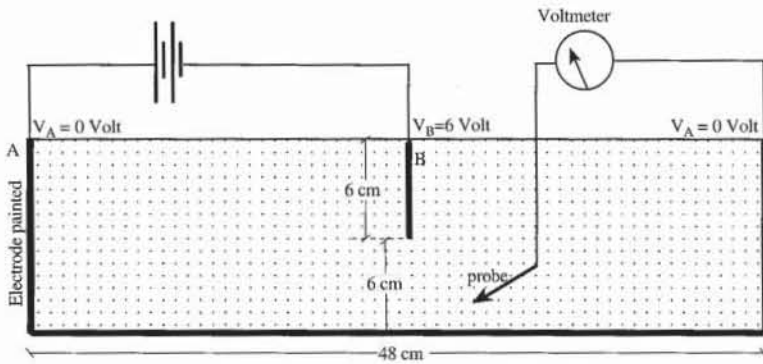


Figure 7 Complementary seepage problem to obtain flow lines and flow net.

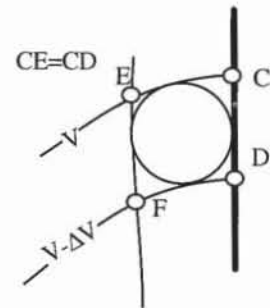


Figure 8 Determination of the differential voltage between two complementary flow lines for the construction of flow nets.

equipotential boundaries become flow lines. As shown in Fig. 7, the complementary analog has the same size as the original model but has complementary boundaries. The differential voltage between electrodes A and B is set arbitrarily to the same value as in Fig. 5. The differential voltage ΔV between two consecutive flow lines is determined as illustrated in Fig. 8. The distance CD between two consecutive equipotential lines is measured with a compass in the region of Fig. 5 where the equipotential lines are almost parallel. Point E is then drawn in Fig. 7 on the same equipotential line as C so that $CD = CE$. The differential voltage $\Delta V = V_C - V_E$ is measured. The flow lines are then traced for the differential volt-

ages that are multiples of ΔV . The flow net is finally obtained by superimposing equipotential and flow lines on the same piece of paper.

EQUIPMENT

The following equipment is needed:

- Voltmeter with high input impedance. The high input impedance prevents the voltage measurements from interfering with the flow of electricity in the analog model.
- DC voltage supply with an adjustable voltage between 0 and 15 V.
- Resistive paper. This graphite-coated paper is an excellent material for use as an electrical-analogy cutout. Although its conductivity may vary slightly between the x and y directions, these differences in conductivity are of negligible importance for the solution of most seepage problems. The resistive paper should be handled and stored carefully because its conducting qualities become erratic when it is perforated or crumpled.
- Silver- or nickel-based paint to make electrodes. The electrodes should be much more conductive than the resistive paper. These metallic paints are available from electronic supply stores. These paints are used to mend heat-sensitive printed circuit boards that cannot be soldered.
- Scissors and rulers.

TEST PROCEDURE

1. Identify the flow lines (impervious boundaries) and equipotential lines (prescribed total head) that form the boundaries of the confined seepage problem. Make a scaled cutout of the seepage problem with the resistive paper. Before cutting the paper, add a 3- to 5-mm-wide strip along the equipotential boundaries of the analog model. This strip will be reserved for painting electrodes.

2. Carefully paint the electrodes on the cutout with the conductive paint. The electrodes simulate the boundaries with a constant total head but are not part of the soil itself. The electrodes should be painted as straight as possible to form a continuous 3- to 5-mm-wide strip. The electrodes should be highly conductive with respect to the resistive paper. Their conductivity may be checked by measuring the voltage at several locations. The voltage should be almost constant along a highly conductive electrode. You may apply several coats of conductive paint to increase the electrode conductivity.

3. Apply a voltage across the upstream and downstream electrodes of the cutout. The voltage should be chosen to have a basic correspondence between voltage and total head. Trace at least 10 equipotential lines on the model by using the voltmeter probe. Lightly mark the points where the voltage is constant with a soft lead pencil. Do not perforate the paper since holes will change the model conductivity.

4. Make a tracing of the cutout and equipotential line locations and complete the flow net either by freehand sketching of the flow paths or by solving the complementary problem.

LIMITATIONS OF ELECTRICAL ANALOGY

Unconfined Seepage

In contrast to water, electrons are not affected by gravity. Hence the electrical analogy is limited to confined seepage problems and cannot be applied directly to unconfined seepage problems such as those found in earth dams. For instance, the earth dam of Fig. 9 must be represented by the cutout of Fig. 10, the upper boundary of which is constructed by the Casagrande method. Casagrande (1940) represents the top flow line with the following parabola:

$$y = -\frac{y^2}{2S} + \frac{S}{2} \quad \text{and} \quad S = \sqrt{d^2 + H^2} - d \quad (10)$$

where d is the horizontal distance between points A and G of Fig. 11. Point G is defined so that

$$EG = 0.3EF \quad (11)$$

For the seepage problem of Fig. 9, the calculation results are listed in Table 1. The toe drain correction corresponding to $\beta = 30^\circ$ is $\Delta a/a = 0.36$ (Fig. 12). The distance $a = AH$ is found by drawing the parabola of Eq. 10 in Fig. 10. The top flow line is corrected as shown in Fig. 10, and cut out as shown in Fig. 12.

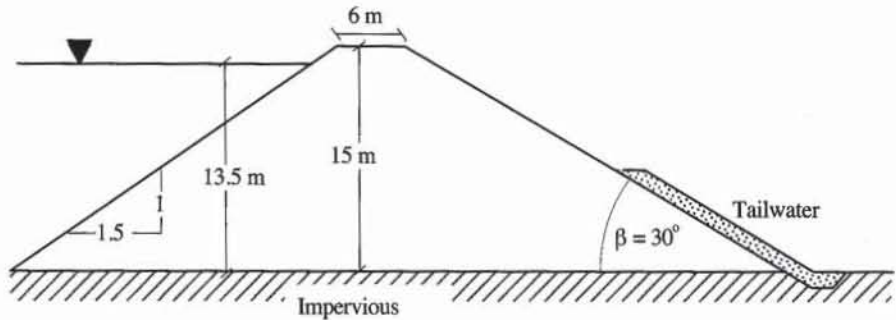
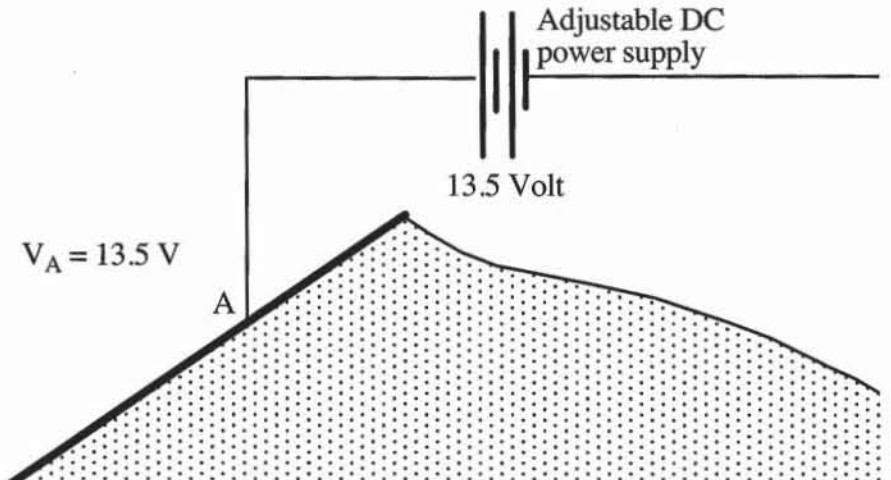


Figure 9 Seepage problem for an earth dam on an impervious base.



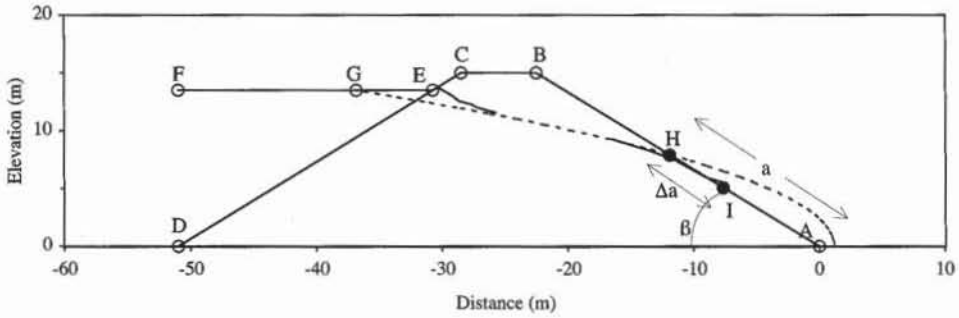


Figure 11 Construction of the top flow line by the Terzaghi-Casagrande method.

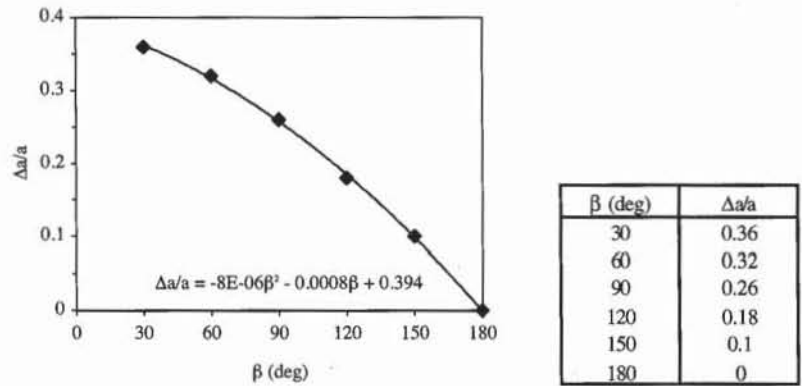


Figure 12 Toe-drain correction proposed by Casagrande (1937).

TABLE 2

Calculation for seepage problem of Fig. 9

Inclination of upstream slope = 1.5
 Inclination of downstream slope = 1.5
 Dam height = 15 m
 Water level = 13.5 m
 Crest width = 6 m
 Inclination of drain = 33.69°
 $d = 36.83$ m
 $S = 2.40$
 $a = 14.27$ m
 $\Delta a = 5.11$ m

	x (m)	y (m)
A	0.00	0.00
B	-22.50	15.00
C	-28.50	15.00
D	-51.00	0.00
E	-30.75	13.50
F	-36.83	13.50
G	-51.00	13.50
H	-11.87	7.92
I	-7.62	5.08

Seepage with Infinite Dimension and Anisotropic Permeability

The seepage problems with soil layers of infinite extent are difficult to model with an electrical analog of finite size. The effects of infinite size can be approximated by selecting a model three to six times longer than its height. It is recommended that this length, be varied to assess its effects on the solution of the seepage problem.

The electrical paper has an isotropic resistivity. When the electrical analog is to be used to model seepage problems with an anisotropic permeability (i.e., $k_x \neq k_y$), the electrical model must be defined after scaling either the x or y coordinates as follows:

$$x_t = x \sqrt{\frac{k_x}{k_y}} \quad \text{or} \quad y_t = y \sqrt{\frac{k_y}{k_x}} \quad (12)$$

REFERENCE

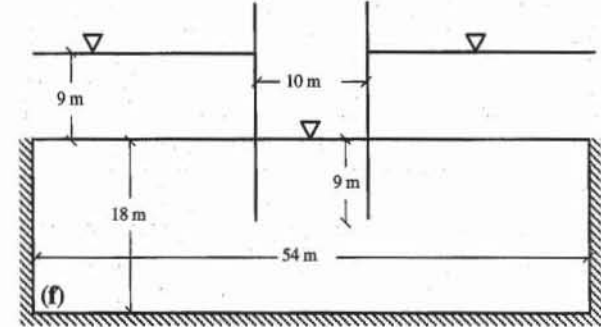
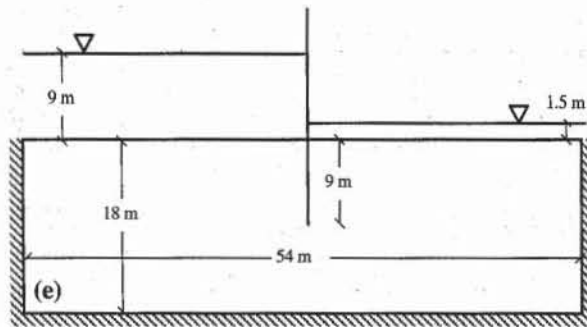
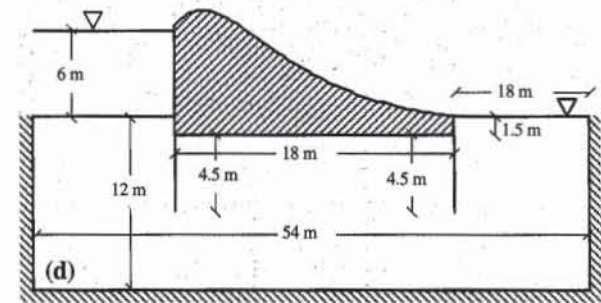
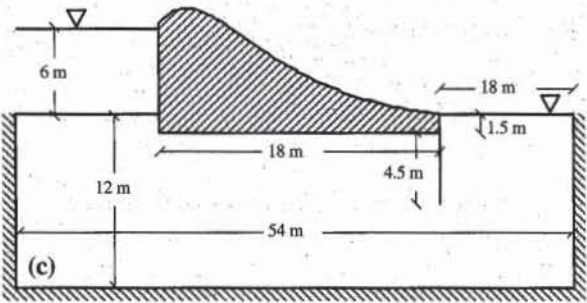
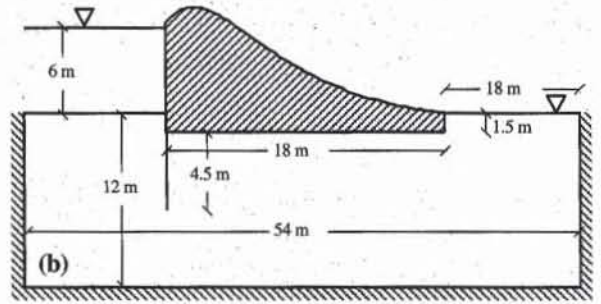
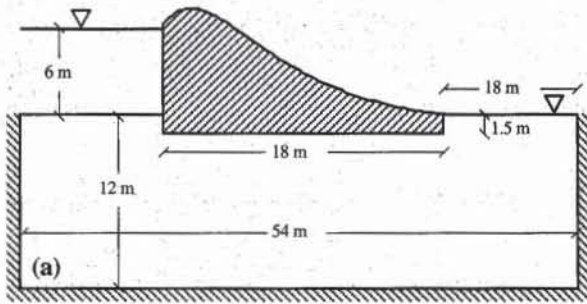
CASAGRANDE, A., 1937, "Seepage through dams," Contribution to Soil Mechanics, BSCE, 1925-1940 (Paper first published in J. New England Water Works Association, June 1937).

REVIEW QUESTIONS

1. What is the purpose of the electrical analogy test? On what analogy is this test based?
2. What quantities correspond to water head and permeability in the flow of electrical current? What physical law corresponds to Darcy's law?
3. Do painted electrodes represent flow lines or equipotential lines?
4. How can you check the high conductivity of painted electrodes?
5. Write down the partial differential equation that governs the steady-state flow of water in two-dimensional problems with isotropic permeability. What is the name of this partial differential equation? Can you name some other fields of physics and engineering where this equation is found?
6. Why is it important not to fold, perforate, or kink the resistive paper?
7. Does perforation increase or decrease the conductivity of resistive paper? Can you suggest an application for carefully perforated holes?
8. Should the nickel-based paint have low or high conductivity?
9. Are painted electrodes strictly parts of the soil where water flows?
10. Is it possible to obtain the top flow lines from the electrical analogy? How?
11. Is it possible to obtain the top flow lines of unconfined seepage problems by using the electrical analogy directly? How do you define the electrical analog of an unconfined seepage problem?
12. What technique do you use to model an anisotropic seepage problem with an electrical analog model?

EXERCISES

1. Determine the distribution of total head and flow net for one of the seepage problems [(a) to (f)] shown below using the electrical analogy method.
2. Determine the distribution of water pressure on the structure (cofferdam and/or sheet-pile wall) of one of the seepage problems shown below by using the electrical analogy method.



4-5

Finite Difference Solutions of Seepage Problems

DEFINITION

The finite difference method is a numerical approach to solving partial differential equations such as those governing the two-dimensional steady-state flow of a fluid through a porous medium. In the case of confined problems with simple geometry and boundary conditions, the finite difference method can easily be implemented in spreadsheet programs. The method can be applied to multiple layers and anisotropic cases.

FINITE DIFFERENCE SOLUTION OF SEEPAGE PROBLEMS

Seepage Theory

When water flows steadily through a two-dimensional porous soil with an anisotropic permeability ($k_x \neq k_y$), the distribution of total head $h(x,y)$ within the saturated soil obeys the following partial differential equation:

$$k_x \frac{\partial^2 h}{\partial x^2} + k_y \frac{\partial^2 h}{\partial y^2} = 0 \quad (1)$$

Equation 1. becomes Laplace's equation in the case of isotropic permeability ($k_x = k_y$):

$$\frac{\partial^2 h}{\partial x^2} + \frac{\partial^2 h}{\partial y^2} = 0 \quad (2)$$

In the case of confined seepage problems, the total head or the fluid velocity is prescribed on the boundaries. In mathematical terms, the boundary conditions are prescribed in either total head or gradients of total head.

Principles of Finite Differences

Discretization of function derivatives. As shown in Fig. 1, a continuous function $f(x)$ may be defined in terms of discrete values f_i corresponding to values x_i spaced along the x axis. Assuming that the function f is differentiable, the function may be expanded by using a Taylor expansion about x :

$$f(x + \Delta x) = f(x) + \frac{df}{dx}(x)\Delta x + \frac{1}{2!} \frac{d^2f}{dx^2}(x)\Delta x^2 + \frac{1}{3!} \frac{d^3f}{dx^3}(x)\Delta x^3 + \dots \quad (3)$$

Equation 3 may be written for $x = x_i$:

$$f_{i+1} = f_i + \left. \frac{df}{dx} \right|_i \Delta x + \frac{1}{2!} \left. \frac{d^2f}{dx^2} \right|_i \Delta x^2 + \frac{1}{3!} \left. \frac{d^3f}{dx^3} \right|_i \Delta x^3 + \dots \quad (4)$$

$$f_{i-1} = f_i - \left. \frac{df}{dx} \right|_i \Delta x + \frac{1}{2!} \left. \frac{d^2f}{dx^2} \right|_i \Delta x^2 - \frac{1}{3!} \left. \frac{d^3f}{dx^3} \right|_i \Delta x^3 + \dots \quad (5)$$

The first-order differential may be approximated from discrete values by subtracting Eq. 4 from Eq. 5:

$$\left. \frac{df}{dx} \right|_i \approx \frac{f_{i+1} - f_{i-1}}{2\Delta x} \quad (6)$$

The second-order derivative may be approximated by adding Eqs. 4 and 5:

$$\left. \frac{d^2f}{dx^2} \right|_i \approx \frac{f_{i+1} + f_{i-1} - 2f_i}{\Delta x^2} \quad (7)$$

Equations 6 and 7 are second-order approximations of the first- and second-order derivatives. The errors between the exact and approximate differentials are proportional to Δx^2 . When Δx tends toward zero, the approximated differential converges quadratically toward its exact values.

Discretization of two-dimensional problems. Equations 6 and 7 also apply to functions of two variables x and y , such as the two-dimensional distribution of total head over a spatial region. As shown in Fig. 2, the two-dimensional space is discretized with a grid of points, the coordinates of which are

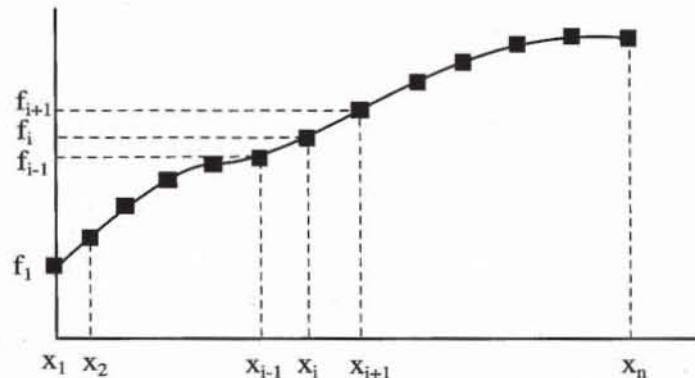


Figure 1 Discrete representation of a continuous function f .

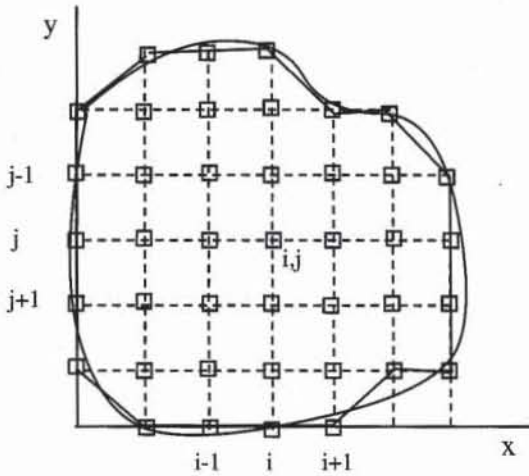


Figure 2 Discrete representation a two-dimensional region.

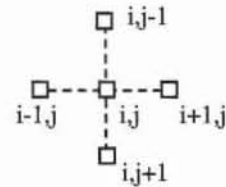


Figure 3 Nodes contributing to Eq. 8.

denoted by i and j . Curved boundaries have to be approximated with straight segments in order to be described with points.

If Δx and Δy are the nodes spacing in the x and y directions, respectively, the discretized form of Eq. 1 at point i, j is

$$\frac{k_x}{\Delta x^2} (h_{i+1,j} + h_{i-1,j} - 2h_{i,j}) + \frac{k_y}{\Delta y^2} (h_{i,j+1} + h_{i,j-1} - 2h_{i,j}) = 0 \quad (8)$$

As shown in Fig. 3, only the values of h at the nodes surrounding the node i, j contribute to Eq. 8. When $\Delta x = \Delta y$, Eq. 8 becomes

$$h_{i,j} = \frac{1}{2(1 + \alpha)} (\alpha h_{i+1,j} + \alpha h_{i-1,j} + h_{i,j+1} + h_{i,j-1}) \quad (9)$$

where $\alpha = k_x/k_y$. When $\Delta x = \Delta y$ and $k_x = k_y$ ($\alpha = 1$), Eq. 8 becomes

$$h_{i,j} = \frac{1}{4} (h_{i+1,j} + h_{i-1,j} + h_{i,j+1} + h_{i,j-1}) \quad (10)$$

Boundary conditions. In confined seepage, either the total head or the total flow is prescribed on the boundaries. For prescribed flow boundaries, we consider only impervious boundaries and exclude prescribed flux boundaries. For an impervious boundary, the seepage velocity is tangential to the boundary: that is,

$$\frac{\partial h}{\partial n} = 0 \quad (11)$$

where n is the coordinate normal to the boundary as shown in Fig. 4. In the case of a horizontal surface, $n = y$ and Eq. 11 becomes

$$\frac{\partial h}{\partial y} = 0 \quad (12)$$

The first-order differential is approximated by introducing a fictitious node, outside the seepage domain (see Fig. 4). Using Eq. 6, at node i, j ; we obtain

$$\frac{\partial h}{\partial y} \approx h_{i,j+1} - h_{i,j-1} = 0 \quad (13)$$

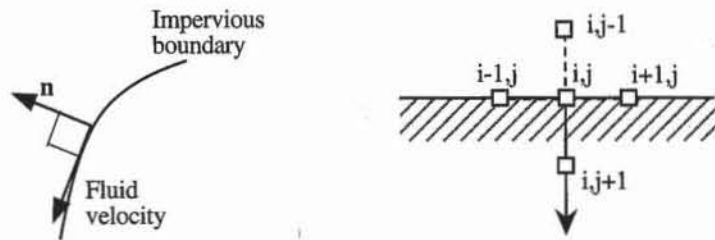


Figure 4 Impervious boundary conditions.

Therefore, $h_{i,j+1} = h_{i,j-1}$. The value of total head at the fictitious node $i, j + 1$ is eliminated by combining Eqs. 10 and 13:

$$h_{i,j} = \frac{1}{4} (h_{i+1,j} + h_{i-1,j} + 2h_{i,j-1}) \quad (14)$$

In summary, for a horizontal impervious boundary, it is not necessary to define fictitious nodes; however, it is necessary to replace Eq. 10 by Eq. 14. The coefficient 2 in Eq. 14 applies to the internal nodes, not to the nodes on the boundary. Thus Eq. 14 may easily be generalized to a vertical boundary. Figure 5 gives additional relations for the total head at grid points on inclined boundaries and at various types of corner boundaries. In all these cases, the sum of the coefficients is equal to 1.

Interfaces. The partial differential equations (Eqs. 1 or 2) do not hold on an interface between soils of different permeability because the permeability and the hydraulic gradient are not continuous there. In the case of the horizontal in-

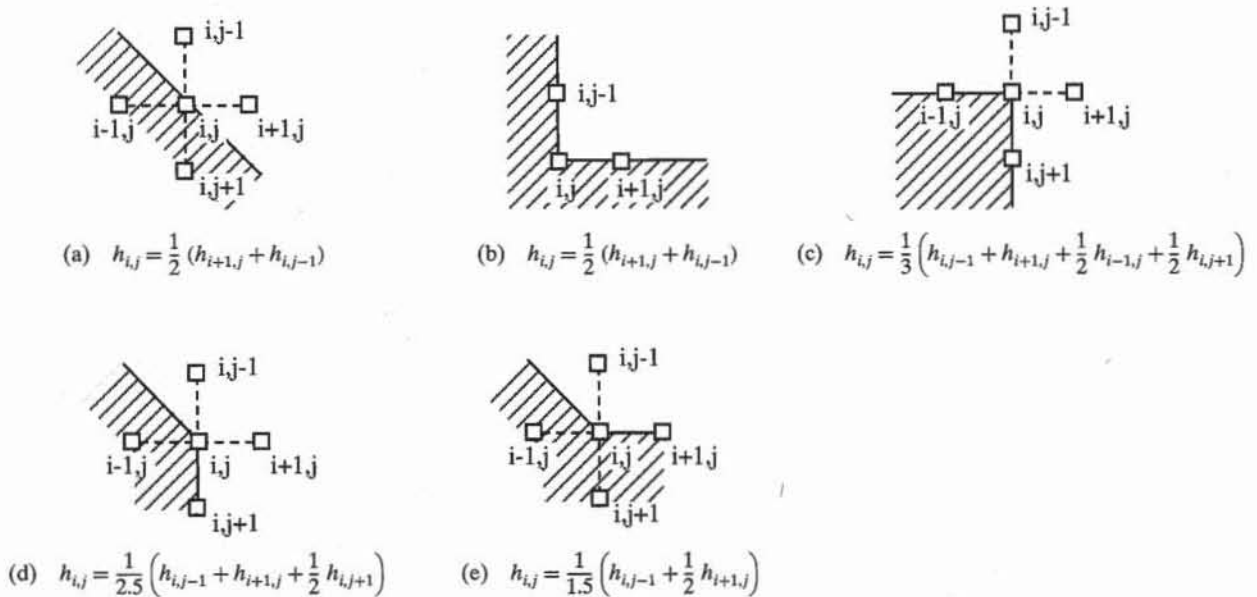


Figure 5 Relations for corners and 45° inclined surfaces of impervious boundaries.

interface shown in Fig. 6, the discharge velocity can only be defined on each side of the interface:

$$v_y^1 = k_1 \frac{h_{i,j} - h_{i,j-1}}{\Delta y} \quad \text{and} \quad v_y^2 = k_2 \frac{h_{i,j+1} - h_{i,j}}{\Delta y} \quad (15)$$

where v_y^1 and v_y^2 are the y-component of the discharge velocity in medium of permeability k_1 and k_2 , respectively. Due to the conservation of flux of water across the interface (i.e., $v_y^1 = v_y^2$), Eq. 15 becomes:

$$h_{i,j} = \frac{k_1}{k_1 + k_2} h_{i,j-1} + \frac{k_2}{k_1 + k_2} h_{i,j+1} \quad (16)$$

In the case of a vertical interface, Eq. 16 becomes:

$$h_{i,j} = \frac{k_1}{k_1 + k_2} h_{i-1,j} + \frac{k_2}{k_1 + k_2} h_{i+1,j} \quad (17)$$

It can be shown that the discharge velocity changes direction abruptly at the interface, and that its angle α_1 of incidence and angle α_2 of emergence are related through:

$$\frac{\tan \alpha_1}{\tan \alpha_2} = \frac{k_1}{k_2} \quad (18)$$

Seepage flow. The total quantity q of flow per unit of time may be calculated from the discrete values of total head, without drawing a flow net. q is obtained for any area A that cuts the flow completely:

$$q = \int_A (v_x n_x + v_y n_y) dA \quad (19)$$

where n_x and n_y = x and y components of a unit vector normal to surface A , and v_x and v_y = x and y components of seepage velocity (Fig. 7). If the surface A is vertical, then

$$q = \int_A v_x dA = \int_A k_x \frac{\partial h}{\partial x} dA \quad (20)$$

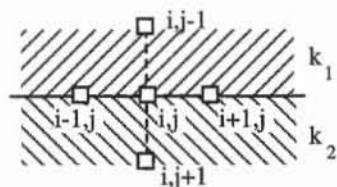


Figure 6 Interface between soils of different permeability.

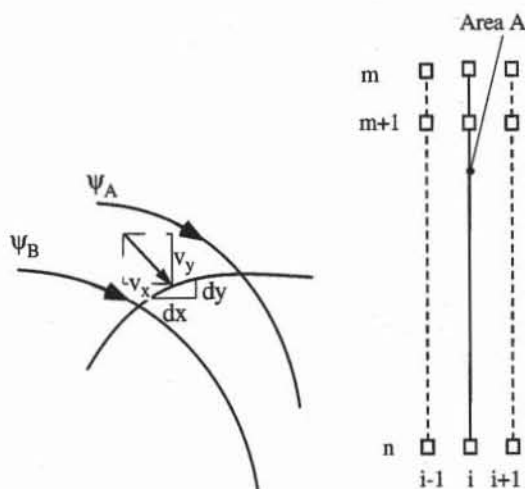


Figure 7 Flow lines and calculation of total quantity of seepage from discrete values of total head.

The area A of Eq. 20 may be selected arbitrarily, provided that it blocks the flow completely. In the case of the vertical section shown in Fig. 7 ($m < n$), Eq. 20 may be integrated by using a trapezoidal rule:

$$q = \frac{\Delta x}{2} v_{i,m} + \Delta x \sum_{j=m+1}^{n-1} v_{i,j} + \frac{\Delta x}{2} v_{i,n} \quad (21)$$

where

$$v_{i,j} = \frac{k_x}{2\Delta x} (h_{i+1,j} - h_{i-1,j}) \quad (22)$$

Finally, the total quantity of seepage is

$$q = \frac{k_x}{4} \left[h_{i+1,m} - h_{i-1,m} + 2 \sum_{j=m+1}^{n-1} (h_{i+1,j} - h_{i-1,j}) + h_{i+1,n} - h_{i-1,n} \right] \quad (23)$$

Stream function and flow lines. By definition, the stream function $\psi(x, y)$ is

$$v_x = \frac{\partial \psi}{\partial y} \quad \text{and} \quad v_y = -\frac{\partial \psi}{\partial x} \quad (24)$$

The quantity of seepage dq through the small element with sides dx and dy in Fig. 7 is

$$dq = v_x dy - v_y dx = \frac{\partial \psi}{\partial y} dy + \frac{\partial \psi}{\partial x} dx = d\psi \quad (25)$$

Using Eq. 23, the quantity of seepage Δq between two nodes (i, j) and $(i, j + 1)$ is

$$\begin{aligned} \Delta q &= \int_{i,j+1}^{i,j} v_x dy = \frac{k_x}{4} (h_{i+1,j} - h_{i-1,j} + h_{i+1,j+1} - h_{i-1,j+1}) \\ &= \Delta \psi = \psi_{i,j} - \psi_{i,j+1} \end{aligned} \quad (26)$$

The values of $\psi_{i,j}$ are usually set equal to zero along one of the flow lines on the external boundary. After the calculation of total head $h_{i,j}$, the values of $\psi_{i,j}$ in the interior are calculated with Eq. 26 by moving away from the flow line where $\psi_{i,j} = 0$. The stream function is constant on flow lines. To draw a flow net with equipotential and flow lines, it is useful to introduce the modified stream function $\psi'_{i,j} = \psi_{i,j}/k$. The flow net can be obtained by superimposing the contour lines of $h_{i,j}$ and $\psi'_{i,j}$ for identical value of contour interval.

Solutions of Finite Difference Problems

The values of the total head at the grid points may be found by using either a direct method or an iterative method. These methods will be illustrated by considering the example in Fig. 8, which has no direct relation to a seepage problem. The Laplace equation holds inside the square region $[0,1]$ by $[0,1]$. The function $h(x,y)$ is prescribed on the boundary. It is equal to zero on the left, bottom, and

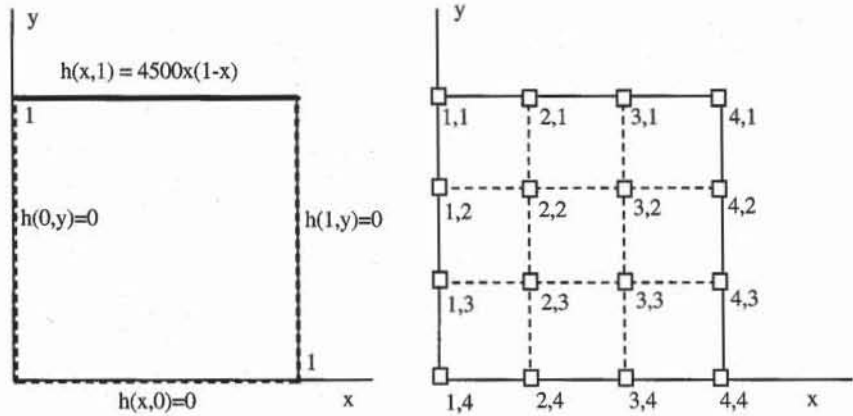


Figure 8 Example of boundary value problem.

right boundaries. It is equal to $h(x) = 4500(1 - x)$ on the top boundary. The problem is to find the distribution of h inside the square region.

As shown in Fig. 8, the region is coarsely discretized with a grid with 16 nodes. The value of h is known at the 12 nodes at the boundaries. There are only four unknown values: $h_{2,2}$, $h_{2,3}$, $h_{3,2}$, and $h_{3,3}$.

Direct method. There are only two unknowns, $h_{2,2}$ and $h_{2,3}$, owing to the symmetry about the line $x = \frac{1}{2}$, which implies that

$$h_{2,2} = h_{3,2} \quad \text{and} \quad h_{2,3} = h_{3,3} \quad (27)$$

These two unknowns $h_{2,2}$ and $h_{2,3}$ are found by solving the two linear equations

$$h_{2,2} = \frac{1}{4}(1000 + 0 + h_{2,3} + h_{2,2}) \quad \text{and} \quad h_{2,3} = \frac{1}{4}(0 + 0 + h_{2,2} + h_{2,3}) \quad (28)$$

The matrix equation corresponding to Eq. 28 is

$$\begin{pmatrix} 3 & -1 \\ -1 & 3 \end{pmatrix} \begin{pmatrix} h_{2,2} \\ h_{2,3} \end{pmatrix} = \begin{pmatrix} 1000 \\ 0 \end{pmatrix} \quad (29)$$

Its solutions are $h_{2,2} = 375$ and $h_{2,3} = 125$. They are found by forming and solving a matrix equation, which is a lengthy operation for more complicated grids.

Relaxation method. The relaxation method is one of the solution methods for finite difference equations which is the most suited to spreadsheet calculations. In the relaxation method, the unknowns are initially assigned an arbitrary value. Then new values are calculated from old ones by iteratively using Eq. 28 until their final values satisfy Eq. 28 within a specified error tolerance.

For instance, the problem of Fig. 8 can be solved by relaxation as shown in Figs. 9 and 10. Nodes (1,1), (1,2), ... are represented by cells A1, A2, ..., respectively. The specified values of h are entered in cells A1, B1, C1, D1, A2, A3, A4, B4, C4, D4, D3, and D2. Equations 27 and 28 are defined in cells B2, B3, C2, and C3, where the function h is unknown.

As shown in Fig. 10, the relaxation solution gradually converges toward the exact solution within 100 iterations. The iterative calculations are activated by Options Calculation and by clicking on the iteration box. The number of itera-

	A	B	C	D
1	0	1000	1000	0
2	0	$= (B1+B3+A2+C2)/4$	$= B2$	0
3	0	$= (B2+B4+A3+C3)/4$	$= B3$	0
4	0	0	0	0

Figure 9 Formulas used for solving Eqs. 27 and 28 by relaxation.

	A	B	C	D
1	0	1000	1000	0
2	0	250	250	0
3	0	250	250	0
4	0	0	0	0

1 iteration

	A	B	C	D
1	0	1000	1000	0
2	0	375.2	375.1	0
3	0	125.1	125.1	0
4	0	0	0	0

5 iterations

A	B	C	D	
1	0	1000	1000	0
2	0	375	375	0
3	0	125	125	0
4	0	0	0	0

100 iterations

Figure 10 Results of relaxation calculation after 1, 5, and 100 iterations.

tions and the error tolerance can also be defined in the Calculation dialog box. When the iteration option is not activated, the error message "Cannot resolve circular references" should be displayed, indicating that the formulas of Fig. 9 are referring to each other's values.

APPLICATION TO SEEPAGE PROBLEMS

Figure 11 defines a seepage problem with a sheet-pile wall. As shown in Fig. 12a, only the left half of the problem will be analyzed owing to the symmetry about the sheet-pile wall. The total head is $h = 6$ m on AB . Owing to the problem symmetry, $h = 3$ m on CD . In Fig. 12a the equipotential lines AB and CD , where the total head is constant, are dashed. The flow lines AED and BC which are followed by the water are solid. Figure 13 shows the spreadsheet representation of the seepage problem of Fig. 12a. The finite difference nodes are evenly spaced every 2 m in the x and y directions. There is a total of 91 nodes, 13 and 7 nodes in the x and y directions, respectively.

Figure 14 shows the formulas used in Fig. 12. The prescribed total head $h = 6$ m is copied into cell range A2:M2, while $h = 3$ m is copied into range M5:M8. The formulas for vertical impervious boundaries are entered in cell A3 and copied into range A4:A7. Those for right vertical boundaries are entered in cells M3 and M4. Equation 14 for horizontal impervious boundaries is entered in cell B8 and copied to C8:L8, Eq. 15 for a corner boundary is entered in cell A8 and Eq. 10 is entered in B3 and copied into range B3:L7.

The iterative calculations are turned on by using Options Calculations. The

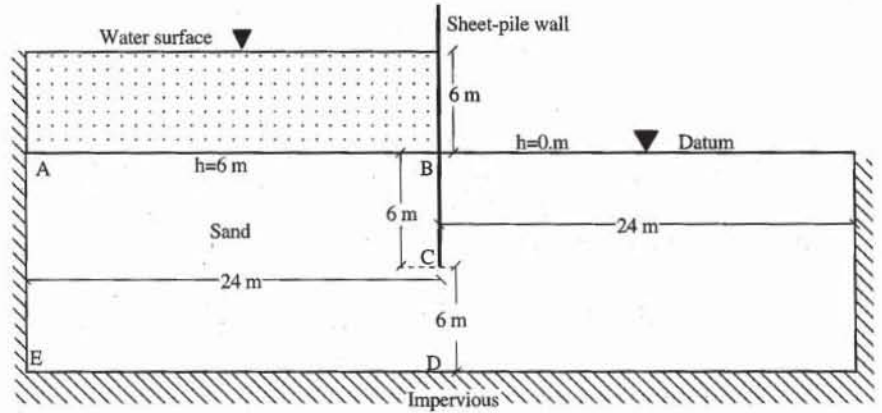


Figure 11 Definition of seepage problem with a sheet-pile wall.

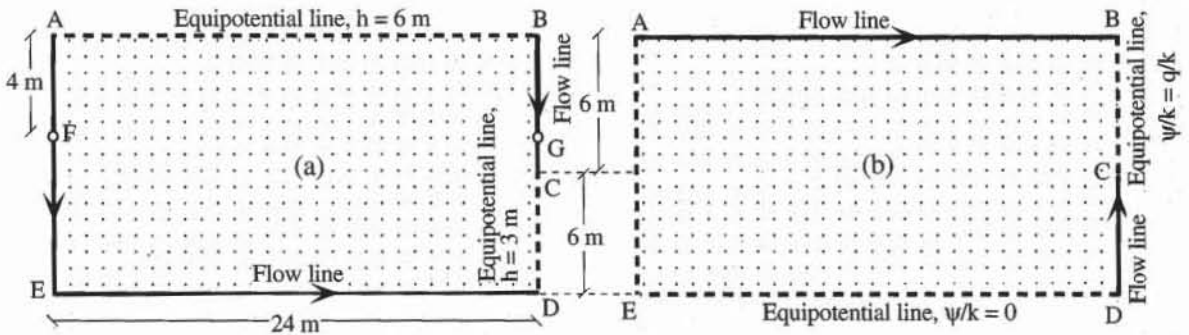


Figure 12 Boundary conditions for (a) original seepage problem and (b) complementary seepage problem.

	A	B	C	D	E	F	G	H	I	J	K	L	M
1	Total head (m)				Upstream head (m) = 6				Downstream head (m) = 3				
2	6.00	6.00	6.00	6.00	6.00	6.00	6.00	6.00	6.00	6.00	6.00	6.00	6.00
3	5.92	5.92	5.91	5.90	5.88	5.85	5.81	5.75	5.68	5.59	5.48	5.36	5.28
4	5.85	5.85	5.83	5.80	5.76	5.71	5.63	5.53	5.39	5.21	4.97	4.68	4.41
5	5.79	5.78	5.76	5.72	5.67	5.59	5.48	5.33	5.14	4.88	4.52	3.97	3.00
6	5.74	5.74	5.71	5.66	5.59	5.49	5.36	5.19	4.95	4.65	4.24	3.70	3.00
7	5.71	5.70	5.68	5.62	5.55	5.44	5.29	5.10	4.84	4.52	4.10	3.59	3.00
8	5.70	5.69	5.66	5.61	5.53	5.42	5.27	5.07	4.81	4.48	4.06	3.56	3.00
9	Quantity of flow per unit of time and unit of permeability = 3.2543												

Figure 13 Value of total head after 100 iterations.

results of the calculations after 100 iterations are shown in Fig. 13. The error after 100 iterations is less than 0.001 m. As shown in Figs. 13 and 14, the total quantity of seepage q (divided by permeability k) is calculated in cell E9 by adapting Eq. 23 for the horizontal line FG passing at 4 m depth. Line FG cuts and blocks the flow completely.

Excel has several two- and three-dimensional capabilities to represent the distribution of total head. Figure 15 shows a two-dimensional contour plot, and Fig. 16 shows a three-dimensional surface plot. To get those plots, select the range

	A	B	C	D	J	K	L	M
1	Total head (m)				3			
2	=\$F\$1	=\$F\$1	=\$F\$1	=\$F\$1	=\$F\$1	=\$F\$1	=\$F\$1	=\$F\$1
3	=(A2+A4+2*B3)/4	=(B2+A3+B4+C3)/4	=(C2+B3+C4+D3)/4	=(D2+C3+D4+E3)/4	=(J2+I3+J4+K3)/4	=(K2+J3+K4+L3)/4	=(L2+K3+L4+M3)/4	=(M2+M4+2*L3)/4
4	=(A3+A5+2*B4)/4	=(B3+A4+B5+C4)/4	=(C3+B4+C5+D4)/4	=(D3+C4+D5+E4)/4	=(J3+I4+J5+K4)/4	=(K3+J4+K5+L4)/4	=(L3+K4+L5+M4)/4	=(M3+M5+2*L4)/4
5	=(A4+A6+2*B5)/4	=(B4+A5+B6+C5)/4	=(C4+B5+C6+D5)/4	=(D4+C5+D6+E5)/4	=(J4+I5+J6+K5)/4	=(K4+J5+K6+L5)/4	=(L4+K5+L6+M5)/4	=\$J\$1
6	=(A5+A7+2*B6)/4	=(B5+A6+B7+C6)/4	=(C5+B6+C7+D6)/4	=(D5+C6+D7+E6)/4	=(J5+I6+J7+K6)/4	=(K5+J6+K7+L6)/4	=(L5+K6+L7+M6)/4	=\$J\$1
7	=(A6+A8+2*B7)/4	=(B6+A7+B8+C7)/4	=(C6+B7+C8+D7)/4	=(D6+C7+D8+E7)/4	=(J6+I7+J8+K7)/4	=(K6+J7+K8+L7)/4	=(L6+K7+L8+M7)/4	=\$J\$1
8	=(A7+B8)/2	=(A8+C8+2*B7)/4	=(B8+D8+2*C7)/4	=(C8+E8+2*D7)/4	=(I8+K8+2*J7)/4	=(J8+L8+2*K7)/4	=(K8+M8+2*L7)/4	=\$J\$1

	H	I
9	Quantity of flow per unit of time and unit of permeability = =(A3-A5+M3-M5+2*SUM(B3:L3)-2*SUM(B5:L5))/4	

Figure 14 Formulas used in Fig. 13.

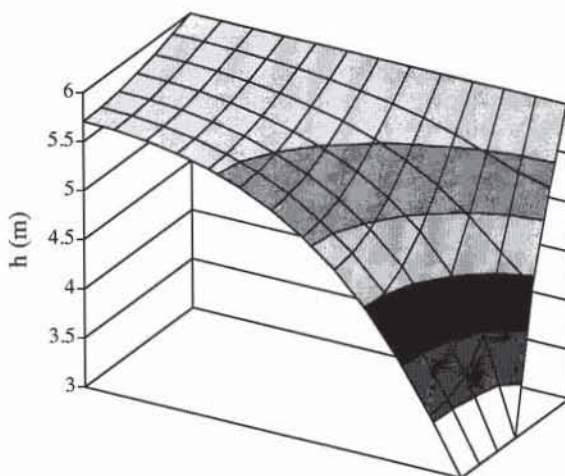
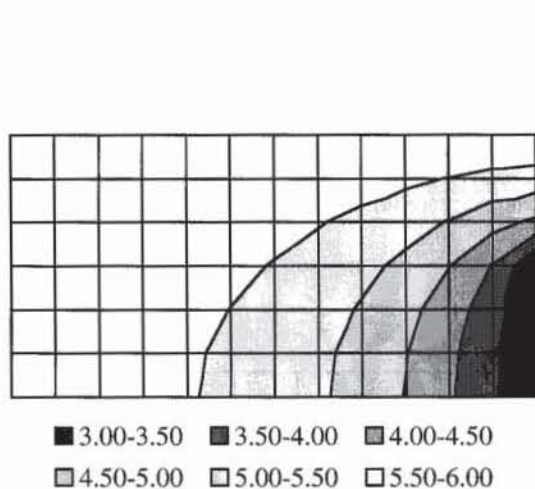


Figure 15 Two-dimensional contour representation of total head for seepage problem of Fig. 11.

Figure 16 Three-dimensional surface representation of total head for seepage problem of Fig. 11.

A2:M2 with the mouse, and select the appropriate three-dimensional chart type by using the Chart Wizard. Change the scale of the third axis to select the contour values. Inverse the second axis to display the contour in the right upward direction. Add the contour values by using the Insert Legend option. As shown in Fig. 17, the equipotential lines, which are the lines along which the total head is a constant, can be drawn using the three-dimensional chart type without the filling option.

The water pressure u is related to the total head h through

$$u = \gamma_w(h - y) \tag{30}$$

where γ_w is the water unit weight and y is the elevation with respect to the datum. The distribution of water pressure which corresponds to the total head in Fig. 15 is shown in Fig. 17. Figure 18 shows the formulas that are used to calculate the water pressure from the total head and the vertical mesh spacing. As shown in Fig. 17, the water pressure, which is hydrostatic away from the pile, becomes lower in the vicinity of the pile, owing to the water flow.

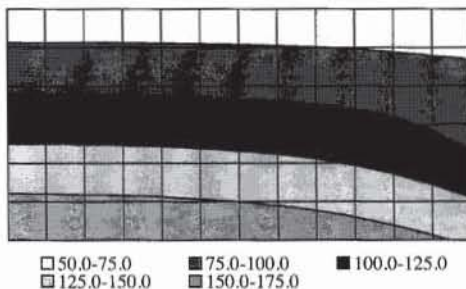


Figure 17 Distribution of water pressure (kPa) in seepage problem of Fig. 11.

	A	F	G
1 0	Water pressure (kPa) Vertical mesh spacing (m)= 2		
1 1	=9.8*(A2+(ROW(A11)-ROW(\$A\$11))*\$G\$10)	=9.8*(F2+(ROW(F11)-ROW(\$A\$11))*\$G\$10)	=9.8*(G2+(ROW(G11)-ROW(\$A\$11))*\$G\$10)
1 2	=9.8*(A3+(ROW(A12)-ROW(\$A\$11))*\$G\$10)	=9.8*(F3+(ROW(F12)-ROW(\$A\$11))*\$G\$10)	=9.8*(G3+(ROW(G12)-ROW(\$A\$11))*\$G\$10)
1 3	=9.8*(A4+(ROW(A13)-ROW(\$A\$11))*\$G\$10)	=9.8*(F4+(ROW(F13)-ROW(\$A\$11))*\$G\$10)	=9.8*(G4+(ROW(G13)-ROW(\$A\$11))*\$G\$10)
1 4	=9.8*(A5+(ROW(A14)-ROW(\$A\$11))*\$G\$10)	=9.8*(F5+(ROW(F14)-ROW(\$A\$11))*\$G\$10)	=9.8*(G5+(ROW(G14)-ROW(\$A\$11))*\$G\$10)
1 5	=9.8*(A6+(ROW(A15)-ROW(\$A\$11))*\$G\$10)	=9.8*(F6+(ROW(F15)-ROW(\$A\$11))*\$G\$10)	=9.8*(G6+(ROW(G15)-ROW(\$A\$11))*\$G\$10)
1 6	=9.8*(A7+(ROW(A16)-ROW(\$A\$11))*\$G\$10)	=9.8*(F7+(ROW(F16)-ROW(\$A\$11))*\$G\$10)	=9.8*(G7+(ROW(G16)-ROW(\$A\$11))*\$G\$10)
1 7	=9.8*(A8+(ROW(A17)-ROW(\$A\$11))*\$G\$10)	=9.8*(F8+(ROW(F17)-ROW(\$A\$11))*\$G\$10)	=9.8*(G8+(ROW(G17)-ROW(\$A\$11))*\$G\$10)

Figure 18 Formulas used to calculate the water pressure (kPa) of Fig. 17 from the total head of Fig. 13.

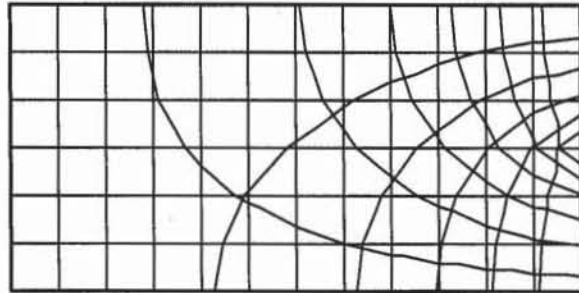


Figure 19 Flow net for seepage problem of Fig. 11.

As shown in Fig. 19, the flow lines, which represent the water trajectory, can be obtained by Eq. 26. They can also be obtained by using the same method as for the equipotential lines, but by solving the complementary seepage problem (Fig. 20). In the complementary seepage problem, boundary flow lines become equipotential boundaries, while equipotential boundaries become flow lines. The total head $h(x,y)$ is also replaced by the modified flow function $\psi' = \psi(x, y)/k$, which must also obey the Laplace equation (i.e., Eq. 2). Therefore, the flow lines of the initial problem are transformed into prescribed ψ' -value lines. It is convenient to set ψ' equal to zero on one of those lines and q/k on the other line, where q is the total seepage flow, calculated using Eq. 23.

Figure 20 shows the value of ψ' as calculated by the formulas of Fig. 21. As shown in Fig. 19, the flow lines, where ψ' is constant, can be plotted by using two-dimensional contours. The flow net is obtained by manually superimposing the two-dimensional contours of h and ψ' with identical interval values along the third axis. One can verify that the flow lines intersect the equipotential lines at right angles and that these lines form curvilinear squares. The ratio between the number N_f of flow channels and the number N_d of equipotential drops should also be equal to $q/(k \Delta h)$, where q is the seepage flow calculated from Eq. 23 and Δh is the total head drop.

The finite difference technique described earlier can be applied to solve many practical seepage problems. Some examples of seepage problems are given in the exercises. In the case of thin sheet piles as shown in Fig. 22, an extra column of nodes must be inserted at the location of the sheet pile. As shown in Fig. 23, this additional column is required to have different total head on the front and back of the sheet pile. Beneath the sheet pile, the nodes are set to have the same total head. As shown in Fig. 24, this additional row unfortunately distorts the flow net in the vicinity of the sheet pile. This distortion was removed in

	A	B	C	D	E	F	G	H	I	J	K	L	M	
19	Flow lines (complementary problem)				Upstream value (m) = 3.2543					Downstream value (m) = 0				
20	3.25	3.17	3.08	2.98	2.86	2.71	2.52	2.29	2.00	1.63	1.17	0.62	0.00	
21	3.25	3.17	3.09	2.99	2.87	2.73	2.55	2.32	2.04	1.67	1.21	0.65	0.00	
22	3.25	3.18	3.10	3.01	2.91	2.78	2.62	2.41	2.15	1.81	1.36	0.77	0.00	
23	3.25	3.19	3.13	3.06	2.97	2.87	2.73	2.56	2.34	2.05	1.66	1.06	0.00	
24	3.25	3.21	3.17	3.12	3.05	2.98	2.89	2.77	2.61	2.41	2.15	1.83	1.53	
25	3.25	3.23	3.21	3.18	3.15	3.11	3.06	3.00	2.92	2.82	2.70	2.56	2.48	
26	3.25	3.25	3.25	3.25	3.25	3.25	3.25	3.25	3.25	3.25	3.25	3.25	3.25	

Figure 20 Values of ψ' after 100 iterations.

	A	B	C	D	K	L	M
20	=\$H\$19	=(A20+C20+2*B21)/4	=(B20+D20+2*C21)/4	=(C20+E20+2*D21)/4	=(J20+L20+2*K21)/4	=(K20+M20+2*L21)/4	=\$L\$19
21	=\$H\$19	=(B20+A21+B22+C21)/4	=(C20+B21+C22+D21)/4	=(D20+C21+D22+E21)/4	=(K20+J21+K22+L21)/4	=(L20+K21+L22+M21)/4	=\$L\$19
22	=\$H\$19	=(B21+A22+B23+C22)/4	=(C21+B22+C23+D22)/4	=(D21+C22+D23+E22)/4	=(K21+J22+K23+L22)/4	=(L21+K22+L23+M22)/4	=\$L\$19
23	=\$H\$19	=(B22+A23+B24+C23)/4	=(C22+B23+C24+D23)/4	=(D22+C23+D24+E23)/4	=(K22+J23+K24+L23)/4	=(L22+K23+L24+M23)/4	=\$L\$19
24	=\$H\$19	=(B23+A24+B25+C24)/4	=(C23+B24+C25+D24)/4	=(D23+C24+D25+E24)/4	=(K23+J24+K25+L24)/4	=(L23+K24+L25+M24)/4	=(M23+M25+2*L24)/4
25	=\$H\$19	=(B24+A25+B26+C25)/4	=(C24+B25+C26+D25)/4	=(D24+C25+D26+E25)/4	=(K24+J25+K26+L25)/4	=(L24+K25+L26+M25)/4	=(M24+M26+2*L25)/4
26	=\$H\$19	=\$H\$19	=\$H\$19	=\$H\$19	=\$H\$19	=\$H\$19	=\$H\$19

Figure 21 Formulas used in Fig. 20.

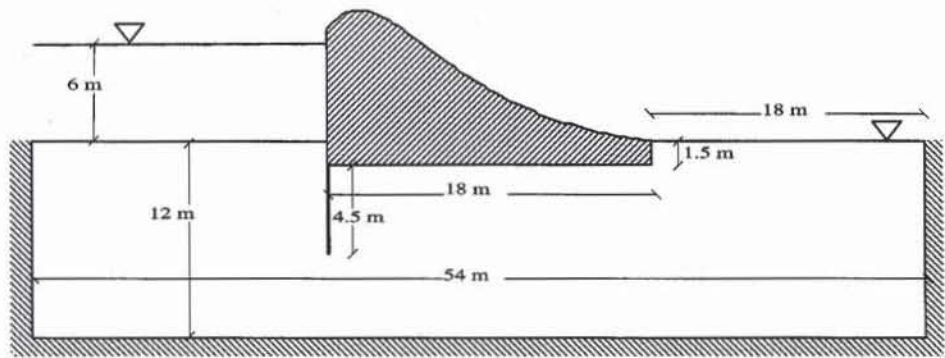


Figure 22 Seepage problem with a cofferdam and a sheet-pile wall.

Fig. 25 after replotting the numerical results of Fig. 24 with a more advanced contouring program. Figures 26 and 27 show the distributions of water pressure on the bottom surface of the cofferdam and on the front and back of the sheet pile wall.

LIMITATIONS

The present method is limited to confined seepage problems for which the boundary conditions have known positions. In its present form it does not apply to unconfined seepage problems such as those in earth dams, where the free surface is undefined. The determination of the position of unknown boundaries with finite difference is possible but requires that additional equations be solved.

One of the major limitations of the finite difference method is the difficulty encountered in describing curved boundary conditions and complicated layer geometries. For this reason, another numerical technique, referred to as the finite element method, is often preferred. Seepage problems of infinite size, such as cofferdams on soil strata extending to infinity, are also difficult to analyze by using a grid of finite size. In this case the infinite size can be approximated by taking a length equal to three to six times the stratum thickness. It is recommended this length be varied in order to assess its effects on the solution of the seepage problem.

REVIEW QUESTIONS

1. What is the purpose of the finite difference method? How is it applied to confined seepage problems?
2. What is the partial differential equation that controls the distribution of total head for anisotropic and isotropic permeability?
3. What is the principal numerical technique used to solve the equations of finite difference methods?
4. Why does the grid spacing control the accuracy of the solution of a seepage problem with finite difference?
5. How do you represent curved boundaries in finite difference methods?
6. What is the main limitation of finite difference when dealing with seepage problems?

	A	L	M	N	O	Z	AA	AL
2	=\$G\$1	=\$G\$1	=\$G\$1				=\$L\$1	=\$L\$1
3	=(A2+A4+2*B3)/4	=(L2+K3+L4+M3)/4	=(M2+M4+2*L3)/4	=(O3+N4)/2	=(N3+P3+2*O4)/4	=(Y3+AA3+2*Z4)/4	=(AA4+AB3+AA2/2+Z3/2)/3	=(AL2+AL4+2*AK3)/4
4	=(A3+A5+2*B4)/4	=(L3+K4+L5+M4)/4	=(M3+M5+2*L4)/4	=(N3+N5+2*O4)/4	=(O3+N4+O5+P4)/4	=(Z3+Y4+Z5+AA4)/4	=(AA3+Z4+AA5+AB4)/4	=(AL3+AL5+2*AK4)/4
5	=(A4+A6+2*B5)/4	=(L4+K5+L6+M5)/4	=(M4+M6+2*L5)/4	=(N4+N6+2*O5)/4	=(O4+N5+O6+P5)/4	=(Z4+Y5+Z6+AA5)/4	=(AA4+Z5+AA6+AB5)/4	=(AL4+AL6+2*AK5)/4
6	=(A5+A9+2*B6)/4	=(L5+K6+L7+M6)/4	=(M5+M7+2*L6)/4	=(N5+N7+2*O6)/4	=(O5+N6+O7+P6)/4	=(Z5+Y6+Z7+AA6)/4	=(AA5+Z6+AA7+AB6)/4	=(AL5+AL7+2*AK6)/4
7	=(A6+A10+2*B7)/4	=(L6+K7+L8+M7)/4	=(M7+L7+M8+O7)/4	=M7	=(O6+N7+O8+P7)/4	=(Z6+Y7+Z8+AA7)/4	=(AA6+Z7+AA8+AB7)/4	=(AL6+AL8+2*AK7)/4
8	=(A5+A9+2*B8)/4	=(L7+K8+L9+M8)/4	=(M7+L8+M9+O8)/4	=M8	=(O7+N8+O9+P8)/4	=(Z7+Y8+Z9+AA8)/4	=(AA7+Z8+AA9+AB8)/4	=(AL7+AL9+2*AK8)/4
9	=(A6+A10+2*B9)/4	=(L8+K9+L10+M9)/4	=(M8+L9+M10+O9)/4	=M9	=(O8+N9+O10+P9)/4	=(Z8+Y9+Z10+AA9)/4	=(AA8+Z9+AA10+AB9)/4	=(AL8+AL10+2*AK9)/4
10	=(A9+B10)/2	=(K10+M10+2*L9)/4	=(L10+O10+2*M9)/4	=M10	=(N10+P10+2*O9)/4	=(Y10+AA10+2*Z9)/4	=(Z10+AB10+2*AA9)/4	=(AL9+AK10)/2

Figure 23 Formulas used in solving the seepage problem of Fig. 22.

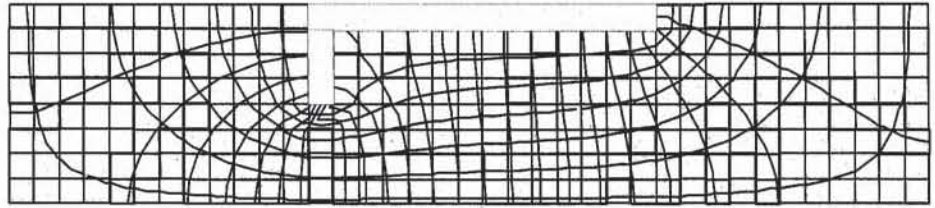


Figure 24 Flow net of the seepage problem in Fig. 22.

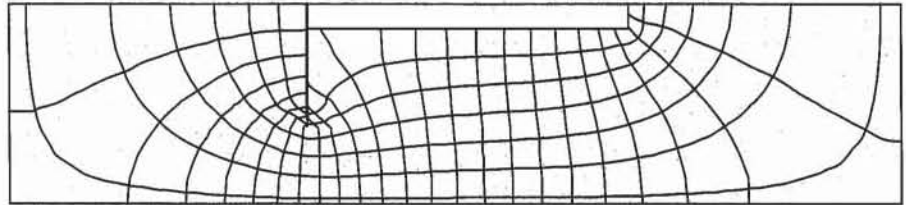


Figure 25 Flow net of Fig. 24 redrawn with a more sophisticated contouring package.

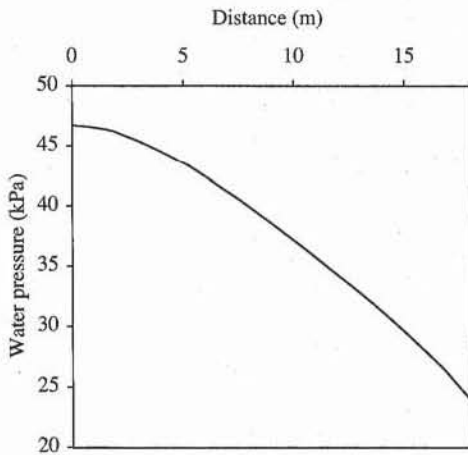


Figure 26 Distribution of water pressure along the horizontal surface of the cofferdam of Fig. 22.

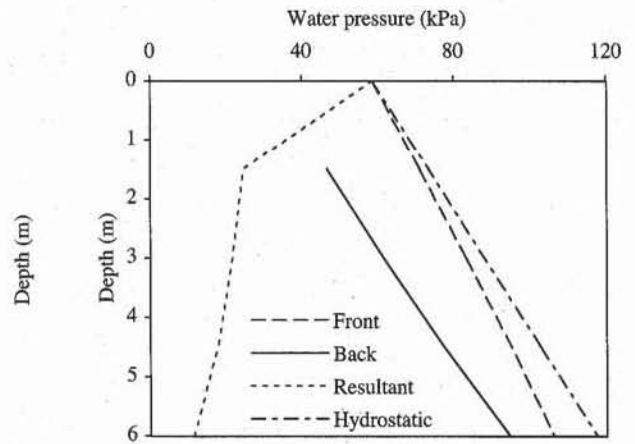
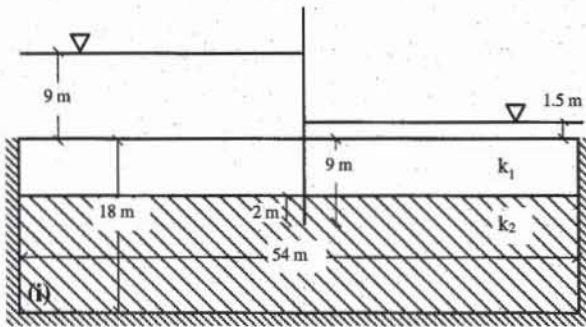
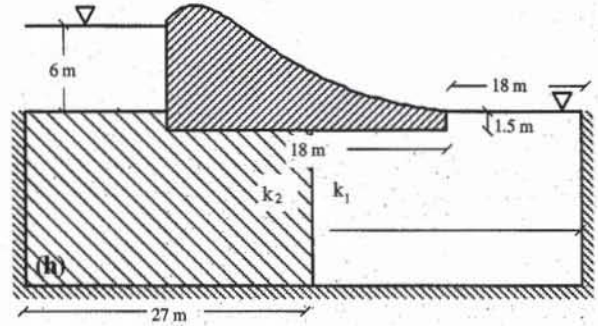
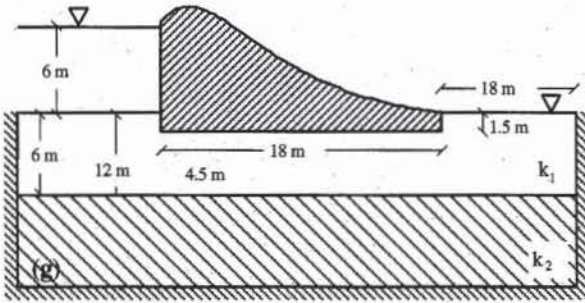


Figure 27 Distribution of water pressure on the front and back of the sheet pile of Fig. 22.

EXERCISES

1. Generalize Eq. 9 in the case of non-evenly spaced nodes.
2. Calculate the hydraulic gradient vector in terms of discrete head values.
3. Find the distribution of total head and flow net for one of the problems (a) to (f) in Exercise 2 of Chapter 4-4.
4. Find the distribution of total head and flow net for one of the problems (g), to (i) shown below.
5. Find the distribution of pressures on one of the structures (sheet-pile wall and/or cofferdam) defined in Exercises 3 and 4.
6. Plot the water pressure applied to the structure for one of the problems of Exercises 3 and 4.



7. Calculate the maximum hydraulic gradient and its location for one of the problems of Exercises 3 and 4.
8. Compare the distributions of total head obtained by using two different grid spacings for one of the problems of Exercises 3 and 4.
9. Compare the distribution of total head obtained by the electrical analogy methods and the finite difference method for one of the problems in Exercise 3.

5

Stress-Strain-Strength Properties

- 5-1** Stress in soils
- 5-2** Strain in soils
- 5-3** Stress-strain relations
- 5-4** Laboratory tests for determination of stress-strain-strength of soils
- 5-5** Elastic properties of soils

5-1 Stress in Soils

Departing from solid mechanics, soil mechanics defines the concept of stress in a slightly different way to consider the particulate structure of soils. Here we review the concepts of Cauchy and Mohr stresses for describing the stress-strain response of soils in laboratory experiments.

BODY FORCES AND CONTACT FORCES

As illustrated in Fig. 1a, a soil mass B is made of soil particles of various sizes. The voids between the grains may be partially or fully saturated with water. This solid-water-air system is considered to be homogeneous. The forces acting on element A of Fig. 1b are divided into two categories:

- The body forces acting on the volume of A
- The surface forces acting on the surface of A

Body Forces

In soils, body forces are created by earth gravity, buoyancy, and water seepage. Their intensity is proportional to the volume on which they act. The resultant body force \mathbf{F} acting on volume V is the volume integral of the body force \mathbf{X} per unit volume:

$$\mathbf{F} = \int_V \mathbf{X} dv \quad (1)$$

The X and Y components of \mathbf{X} have the dimension of force per unit volume. $[X] = [Y] = ML^{-2}T^{-2}$, where M , L , and T indicate the dimension of mass, length, and time, respectively. The body force of the earth gravity is

$$X = 0, \quad Y = -\rho g \quad (2)$$

where g is the earth gravitational acceleration (i.e., $g = 9.81 \text{ m/s}^2$) and ρ is the mass per unit volume. If the body is immersed in water, X for buoyancy is

$$X = 0, \quad Y = \rho_w g \tag{3}$$

where ρ_w is the unit mass of water. If water seeps through the soil interstices, X for seepage is

$$X = \rho_w g i_x, \quad Y = \rho_w g i_y \tag{4}$$

where i_x and i_y are the x and y components of hydraulic gradient i .

Contact Forces

The small element A of Fig. 1b is not only subjected to body forces, but also interacts with its exterior through its surface. Consider the surface ΔS_n of Fig. 1b with unit normal vector \mathbf{n} pointing inside the element. The exterior of A exerts the force $\Delta \mathbf{F}$ and moment $\Delta \mathbf{m}$ on surface ΔS_n . Both $\Delta \mathbf{F}$ and $\Delta \mathbf{m}$ are functions of ΔS_n and \mathbf{n} . As ΔS_n tends toward zero, $\Delta \mathbf{F}/\Delta S_n$ is assumed to tend toward the vector \mathbf{T}_n , whereas $\Delta \mathbf{m}/\Delta S_n$ is assumed to become negligible. The subscript n of ΔS_n and \mathbf{T}_n denotes the normal vector \mathbf{n} . \mathbf{T}_n , called the *stress* (or *traction*) vector, represents the force per unit area acting on surface ΔS_n .

As shown in Fig. 2, on the vertical surface ΔS_x with $(n_x, n_y) = (1,0)$, the components of the stress vector \mathbf{T}_x are σ_{xx} and τ_{xy} . On the horizontal surface ΔS_y with $(n_x, n_y) = (0,1)$, the components of the stress vector \mathbf{T}_y are τ_{yx} and σ_{yy} . These stress components are tabulated in the following matrix:

	Component of stress	
	x	y
Surface normal to x	σ_{xx}	τ_{xy}
Surface normal to y	τ_{yx}	σ_{yy}

The components σ_{xx} and σ_{yy} are called *normal stresses*, whereas τ_{xy} and τ_{yx} are called *shear stresses*. The dimension of σ_{xx} , σ_{yy} , τ_{xy} , and τ_{yx} is force per unit area (i.e., $[\sigma_{xx}] = [\sigma_{yy}] = [\tau_{xy}] = [\tau_{yx}] = ML^{-1}T^{-2}$). σ_{xx} and σ_{yy} are also denoted as σ_x and σ_y . The physical origins of contact forces in soils are discussed later.

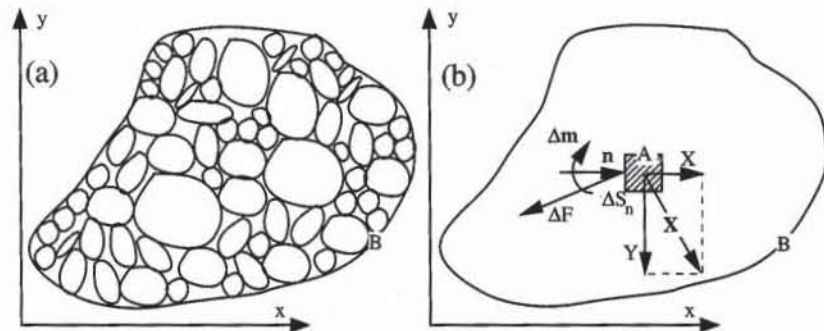


Figure 1 (a) Two-dimensional representation of a soil mass and (b) its idealization.

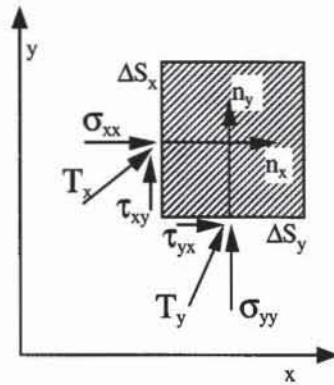


Figure 2 Stress vectors and their components on horizontal and vertical surfaces.

Equilibrium of Forces and Moments

If the soil mass *B* of Fig. 1b is in a static equilibrium, the total force that results from body forces on volume *V* and contact forces on the surface *S* enclosing volume *V* is equal to zero:

$$\int_S \mathbf{T}_n dS + \int_V \mathbf{X} dV = 0 \tag{5}$$

where \mathbf{T}_n is the stress vector acting on surface *dS* with normal vector **n**. The total torque about the space origin resulting from body and surface forces is also equal to zero:

$$\int_S \mathbf{r} \otimes \mathbf{T}_n dS + \int_V \mathbf{r} \otimes \mathbf{X} dV = 0 \tag{6}$$

where **r** is a position vector and \otimes is the cross product between two vectors.

Equations of Stress Equilibrium

In general, σ_x , σ_y , τ_{yx} , and τ_{xy} are not constant throughout the soil mass but vary with the *x* and *y* coordinates. By applying the equilibrium of forces (i.e., Eq. 5) and moments (i.e., Eq. 6) to the small element of Fig. 3, it can be shown that σ_x , σ_y , τ_{yx} , and τ_{xy} obey the following equations:

$$\frac{\partial \sigma_x}{\partial x} + \frac{\partial \tau_{xy}}{\partial y} = X \tag{7}$$

$$\frac{\partial \tau_{yx}}{\partial x} + \frac{\partial \sigma_y}{\partial y} = Y \tag{8}$$

$$\tau_{xy} = \tau_{yx} \tag{9}$$

Equations 7 to 9 are called the *stress-equilibrium equations*. Equation 9 implies that there are only three independent stress components: σ_x , σ_y , and τ_{xy} . The stress-equilibrium equations are widely used in soil mechanics.

CAUCHY REPRESENTATION OF STRESS

In the Cauchy representation, the stress vector is defined in a fixed x - and y -coordinate system. The stress vector has the same sign convention as the coordinates. In contrast to solid mechanics, soil mechanics imposes that the unit vector \mathbf{n} normal to the surface points inward to the material surface (see Fig. 4).

Stress Acting on an Inclined Surface

Consider the uniform stress state within the material element of Fig. 4. By definition, the uniform stress state implies that σ_x , σ_y , and τ_{xy} are independent of x and y . There are no body forces (i.e., $X = Y = 0$) in Eqs. 7 and 8. As shown in Fig. 4, the stresses σ_{nx} and σ_{ny} acting on surface AB inclined at angle θ with respect to the x axis can be calculated from σ_x , σ_y , and τ_{xy} by writing the equilibrium of forces acting on element AOB in the x and y directions:

$$\sigma_x AB \sin \theta + \tau_{xy} AB \cos \theta + AB \sigma_{nx} = 0 \tag{10}$$

$$\sigma_y AB \cos \theta + \tau_{xy} AB \sin \theta + AB \sigma_{ny} = 0 \tag{11}$$

Because the unit vector pointing inside the surface AB is $\mathbf{n} = (n_x, n_y) = (-\sin \theta, -\cos \theta)$, the stresses σ_{nx} and σ_{ny} acting on the surface with unit vector \mathbf{n} can be obtained by multiplying the stress matrix by \mathbf{n} :

$$\begin{pmatrix} \sigma_{nx} \\ \sigma_{ny} \end{pmatrix} = \begin{pmatrix} \sigma_x & \tau_{xy} \\ \tau_{xy} & \sigma_y \end{pmatrix} \begin{pmatrix} n_x \\ n_y \end{pmatrix} \tag{12}$$

Note that the orientation of \mathbf{n} with respect to the surface implies that σ_x and σ_y are positive for compression and negative for tension. This sign convention eliminates a lot of negative signs in soils, which, in contrast to metals, undergo mostly compressive stress.

Principal Stress

By definition, the principal surfaces are free of shear stress. The stress vector acting on principal surfaces is thus collinear to their normal unit vector (n_x, n_y) .

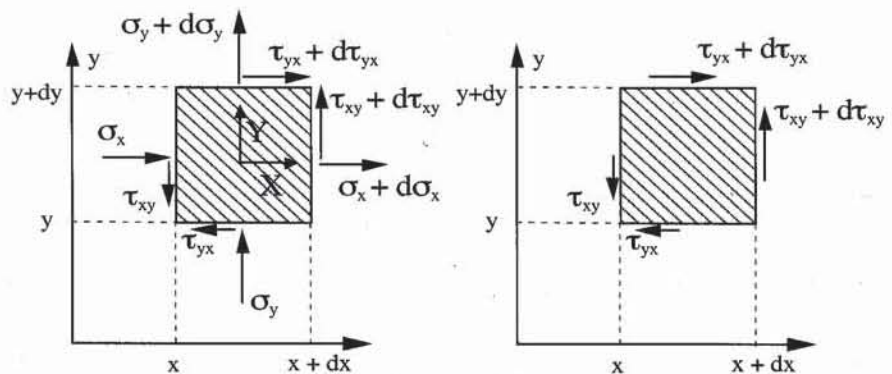


Figure 3 Small element used for the calculation of equilibrium of (a) forces and (b) moment.

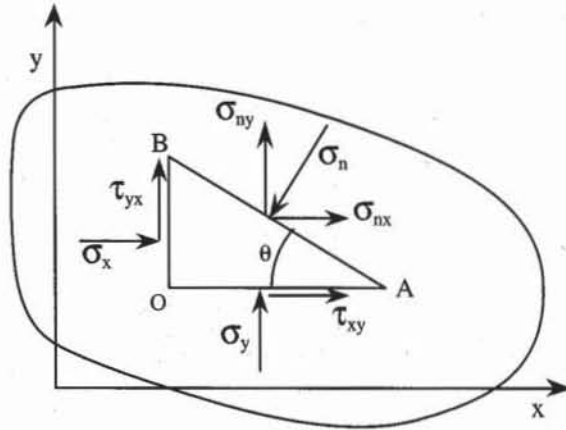


Figure 4 Determination of stress acting on segment AB.

Their direction is found by solving the following eigenvalue problem:

$$\begin{pmatrix} \sigma_x & \tau_{xy} \\ \tau_{xy} & \sigma_y \end{pmatrix} \begin{pmatrix} n_x \\ n_y \end{pmatrix} = \sigma \begin{pmatrix} n_x \\ n_y \end{pmatrix} \quad (13)$$

where σ is the principal stress value. σ is obtained by solving the following quadratic equation:

$$\sigma^2 - \sigma(\sigma_x + \sigma_y) + \sigma_x\sigma_y - \tau_{xy}^2 = 0 \quad (14)$$

There are always two principal stresses: the major and minor principal stresses:

$$\sigma_1 = \frac{1}{2}(\sigma_x + \sigma_y) + \sqrt{\frac{1}{4}(\sigma_x - \sigma_y)^2 + \tau_{xy}^2} \quad (15)$$

$$\sigma_2 = \frac{1}{2}(\sigma_x + \sigma_y) - \sqrt{\frac{1}{4}(\sigma_x - \sigma_y)^2 + \tau_{xy}^2}$$

The principal stresses are equal when $\sigma_x = \sigma_y$ and $\tau_{xy} = 0$, which is the hydrostatic pressure case. The orientation of the principal surfaces is found by setting σ equal to σ_1 or σ_2 in Eq. 13 and by solving for n_x and n_y :

$$\frac{n_y}{n_x} = \tan \theta = \frac{\sigma_x - \sigma}{\tau_{xy}} \quad (16)$$

where θ is the inclination of \mathbf{n} with respect to the horizontal direction. Equation 16 does not apply to hydrostatic pressure, for which any direction is principal.

MOHR REPRESENTATION OF STRESS

Mohr and Cauchy represent stresses in different ways. The Mohr representation, which is the most commonly used in geotechnical engineering, provides us with a graphical determination of stresses. In contrast to Cauchy, who uses fixed axes, Mohr defines the stresses in reference to the surface on which they act.

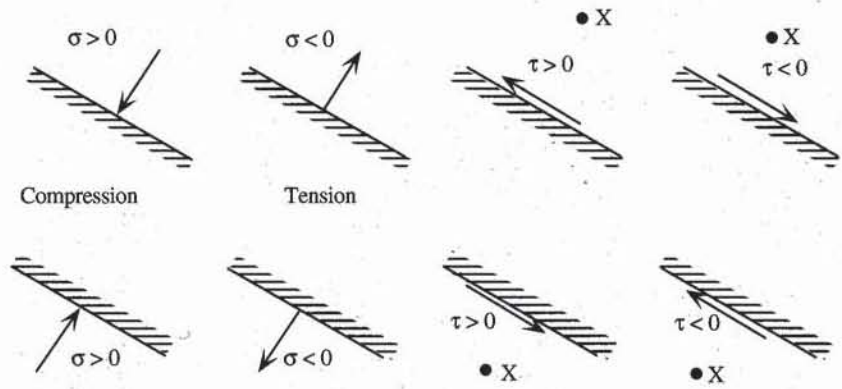


Figure 5 Sign convention for Mohr representation of stresses in soil mechanics.

Sign Convention for Stress

Figure 5 defines the sign convention of Mohr in soil mechanics. This sign convention is different from that of solid mechanics. Because normal stresses are usually compressive in soils, they are assigned a positive sign to avoid the profusion of negative signs. As shown in Fig. 5, compressive normal stresses are positive and tensile normal stresses are negative. The sign convention for shear stress τ is more arbitrary than for normal stress. As shown in Fig. 5, if τ acting on the surface produces a clockwise moment about a point X located at the exterior of the material surface, τ is positive. If the moment about the point X is counterclockwise, τ is negative. As shown in Fig. 5, the Mohr stresses on surfaces facing each other are identical, although the corresponding stress vectors have opposite direction.

Stress Acting on an Inclined Surface

Consider the uniform state of stress within the element of Fig. 6. The stresses σ and τ acting on AB can be calculated from σ_x , σ_y , and τ_{xy} , by writing the equilib-

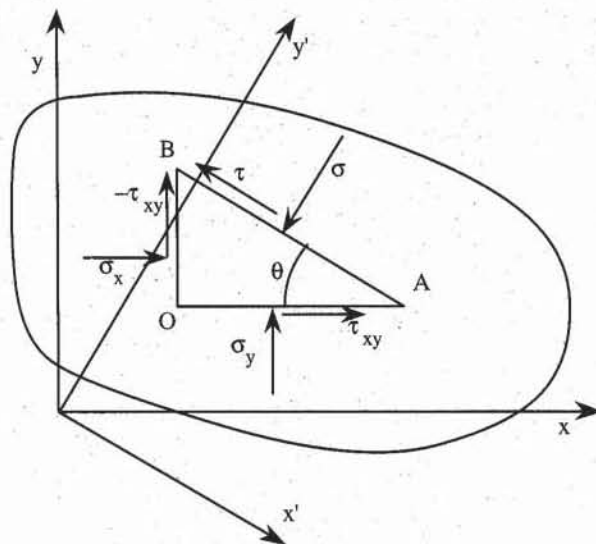


Figure 6 Determination of stress acting on segment AB .

rium of forces in the x' and y' directions, which are parallel and normal to segment AB , respectively. As shown in Fig. 6, in the Mohr representation, the shear stresses acting on surfaces OA and OB must have opposite signs. The equilibrium of forces acting on element AOB in the y' direction is

$$\sigma_x OB \sin \theta + \tau_{xy} OB \cos \theta + \sigma_y OA \cos \theta + \tau_{xy} OA \sin \theta - AB\sigma = 0 \quad (17)$$

Note that the shear stress acting on the vertical surface is negative in the Mohr representation but produces a positive force in the y' direction. The equilibrium of forces in the x' direction implies that

$$\sigma_x OB \cos \theta - \tau_{xy} OB \sin \theta - \sigma_y OA \sin \theta + \tau_{xy} OA \cos \theta - AB\tau = 0 \quad (18)$$

From Fig. 6 we have

$$AO = AB \cos \theta \quad \text{and} \quad BO = AB \sin \theta \quad (19)$$

Using Eq. 19, Eqs. 17 and 18 become

$$\sigma = \sigma_x \sin^2 \theta + \sigma_y \cos^2 \theta + 2\tau_{xy} \sin \theta \cos \theta \quad (20)$$

$$\tau = \sigma_x \sin \theta \cos \theta - \sigma_y \sin \theta \cos \theta + \tau_{xy} (\cos^2 \theta - \sin^2 \theta)$$

Using the relations:

$$\sigma_x = \frac{1}{2}(\sigma_x + \sigma_y) + \frac{1}{2}(\sigma_x - \sigma_y) \quad \text{and} \quad \sigma_y = \frac{1}{2}(\sigma_x + \sigma_y) - \frac{1}{2}(\sigma_x - \sigma_y) \quad (21)$$

Eq. 20 becomes

$$\sigma = \frac{1}{2}(\sigma_x + \sigma_y) + \frac{1}{2}(\sigma_x - \sigma_y) \cos 2\theta + \tau_{xy} \sin 2\theta \quad (22)$$

$$\tau = \frac{1}{2}(\sigma_x - \sigma_y) \sin 2\theta + \tau_{xy} \cos 2\theta$$

Mohr Circle

When θ varies from -90° to 90° , σ and τ of Eq. 22 describe a circle in the space (σ, τ) , which has the equation

$$\left[\sigma - \frac{1}{2}(\sigma_x + \sigma_y)\right]^2 + \tau^2 = \frac{1}{4}(\sigma_x - \sigma_y)^2 + \tau_{xy}^2 \quad (23)$$

The (σ, τ) space is called the *Mohr stress space*. As shown in Fig. 7, the circle of Eq. 23 is called the *Mohr circle*. It is centered at position $(\sigma_m, 0)$ on the σ axis and has radius R :

$$\sigma_m = \frac{1}{2}(\sigma_x + \sigma_y) \quad \text{and} \quad R = \sqrt{\frac{1}{4}(\sigma_x - \sigma_y)^2 + \tau_{xy}^2} \quad (24)$$

The stress states $(\sigma_x, -\tau_{xy})$ and (σ_y, τ_{xy}) are represented by points B and A in the Mohr space of Fig. 7, respectively. Points A and B are diametrically opposite on the Mohr circle and are used to construct the Mohr circle. The circle diameter is AB , and its center is the intersection between the σ axis and the segment AB . In conclusion, given a uniform stress state, the stresses acting on inclined surfaces are located on the circle of radius R centered at position $(0, \sigma_m)$.

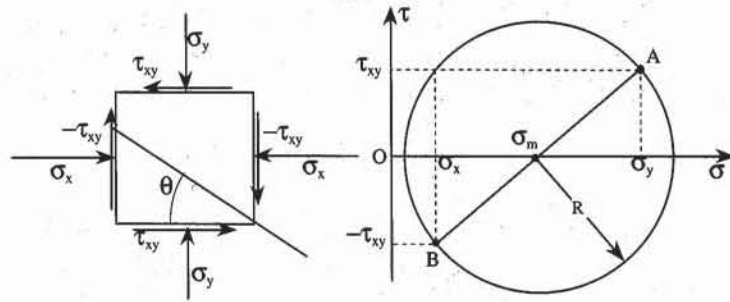


Figure 7 Construction of the Mohr circle in the Mohr space.

Principal Stress

Using Eq. 22, the shear stress becomes zero for the following surface inclination θ :

$$\tan 2\theta = \frac{2\tau_{xy}}{\sigma_x - \sigma_y} \quad (25)$$

For every set of σ_x , σ_y , and τ_{xy} , there are two values of θ that satisfy Eq. 25. These two angles characterize the principal directions. By substituting Eq. 25 into Eq. 22, the principal stresses are

$$\sigma_1 = \frac{1}{2}(\sigma_x + \sigma_y) + \sqrt{\frac{1}{4}(\sigma_x - \sigma_y)^2 + \tau_{xy}^2} \quad (26)$$

$$\sigma_2 = \frac{1}{2}(\sigma_x + \sigma_y) - \sqrt{\frac{1}{4}(\sigma_x - \sigma_y)^2 + \tau_{xy}^2}$$

where σ_1 is the major principal stress and σ_2 is the minor principal stress, as for the Cauchy representation. In the Mohr space, the principal stresses are the intersections of the Mohr circle with the σ axis.

Relation between Stress and Surface Orientation

Equation 22, which gives the stresses σ and τ acting on an inclined surface, may be rewritten

$$\sigma - \sigma_m = R \left(-\frac{\sigma_x - \sigma_y}{2R} \cos 2\theta + \frac{\tau_{xy}}{2R} \sin 2\theta \right) \quad (27)$$

$$\tau = R \left(\frac{\sigma_x - \sigma_y}{2R} \sin 2\theta + \frac{\tau_{xy}}{2R} \cos 2\theta \right)$$

After introducing the angle α shown in Fig. 8, Eq. 27 becomes

$$\sigma - \sigma_m = R(\cos \alpha \cos 2\theta + \sin \alpha \sin 2\theta) = R \cos(\alpha - 2\theta) \quad (28)$$

$$\tau = R(-\cos \alpha \sin 2\theta + \sin \alpha \cos 2\theta) = R \sin(\alpha - 2\theta) \quad (29)$$

By using Eqs. 28 and 29, σ and τ on any inclined surface can be calculated from R and α , provided that the surface inclination θ is known.

Pole of the Mohr Circle

In contrast to the physical stress states, which have three independent components— σ_x , σ_y , and τ_{xy} —the Mohr circle has only two variables— R and σ_m . Therefore, there is no unique correspondence between the Mohr circle and physical stresses. In fact, a particular Mohr circle corresponds to an infinite number of stress states. This problem is solved by adding a third variable, the pole.

The pole is constructed as shown in Fig. 8. (1) Draw points B and A with coordinates $(\sigma_x, -\tau_{xy})$ and (σ_y, τ_{xy}) , respectively. (2) Draw the Mohr circle centered on the σ axis and passing through A and B . (3) Through A , draw the line parallel to the surface on which (σ_y, τ_{xy}) acts. This horizontal line intersects the circle at points A and P . (4) Through B , draw the line parallel to the surface on which $(\sigma_x, -\tau_{xy})$ acts. This vertical line intersects the circle at points B and P . Lines AP and BP intersect at point P on the Mohr circle. Point P is the pole.

The pole is used to determine stresses on inclined surfaces graphically. Draw a straight line passing through the pole and parallel to the surface on which stresses need to be defined. This line intersects the Mohr circle at the desired normal and shear stresses. The pole can also be used to find the orientation of a surface on which is acting a given stress state σ and τ . Draw the line through the pole and point (σ, τ) on the Mohr circle. That line is parallel to the surface on which σ and τ are acting.

The pole property derives from Eqs. 28 and 29. The graphical pole construction uses θ instead of 2θ as in Eq. 27. As shown in Fig. 8, both angles AQM and APM intersect chord AM , and therefore $AQM = 2\theta = 2APM$.

The pole may be used to calculate the principal stress directions as shown in Fig. 9. The Mohr circle and its pole are first constructed from points A and B , as explained in Fig. 8. The line passing through P and $(\sigma_1, 0)$ gives the orientation θ_1 of the surface on which σ_1 is acting. The line passing through P and $(\sigma_2, 0)$ gives the orientation θ_2 of the surface on which σ_2 is acting. The orientation of surfaces where the shear stress is maximum (i.e., $\tau = \tau_{max}$) is found by drawing the two lines passing through the pole and points $(\sigma_m, \pm \tau_{max})$ on the Mohr circle.

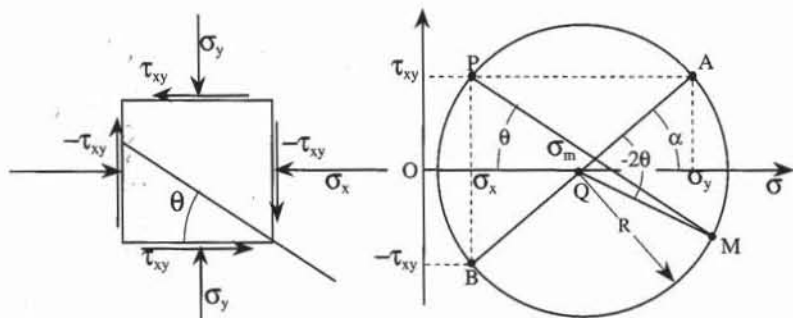


Figure 8 Construction of the Mohr circle and its pole in the Mohr space.

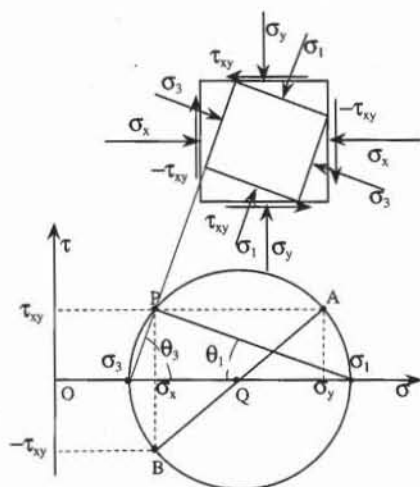


Figure 9 Determination of principal stress direction by using the pole.

TOTAL AND EFFECTIVE STRESSES

Stresses in soils are more difficult to describe than in other materials because soils are a mixture of solid, water, and air. We restrict our presentation of stresses to two-phase (i.e., fully saturated) soils. Three-phase (i.e., unsaturated) soils are beyond the scope of this book.

Fillunger-Terzaghi Postulate

In saturated soils, the contact forces are distributed on soil grains and interstitial water. Fillunger (1915) and Terzaghi (1943) introduced the concept of effective stress to distinguish the contact forces acting on the soil grains from those acting on water. They postulated that the total stress vector \mathbf{T}_n acting on a surface with unit normal vector \mathbf{n} is the sum of the *effective stress* \mathbf{T}'_n and *porewater pressure* u :

$$\mathbf{T}_n = \mathbf{T}'_n + u\mathbf{n} \tag{30}$$

In the Mohr representation, Eq. 30 is written as

$$\sigma = \sigma' + u \quad \text{and} \quad \tau = \tau' \tag{31}$$

where σ and τ are the normal and shear components of \mathbf{T}_n and σ' and τ' are normal and shear components of \mathbf{T}'_n . The physical meaning of \mathbf{T}'_n and σ' is explained as follows. As shown in Fig. 10, the total normal stress acting on surface A is

$$\sigma = \frac{A_s}{A_w + A_s} \sigma_s + \frac{A_w}{A_w + A_s} u \tag{32}$$

where A_s is the solid–solid contact area, A_w the water–water contact area, σ_s the average normal stress on A_s (i.e., *granular stress*), and u the average pore pressure on A_w . $A = A_s + A_w$ because the material has only two phases. The tangential total force acting on surface A is transmitted only through the solid–solid contact because water does not transmit any shear:

$$\tau = \frac{A_s}{A_w + A_s} \tau_s \tag{33}$$

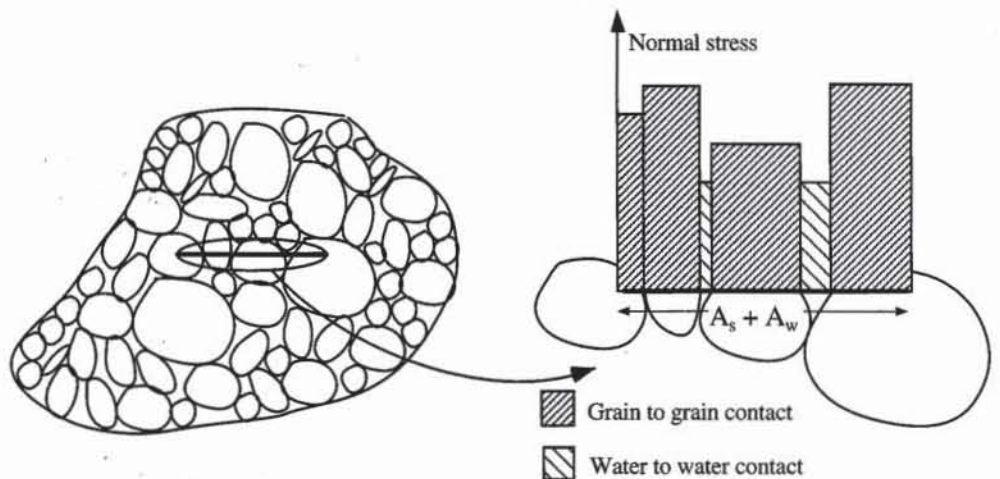


Figure 10 Grain–grain and water–water contacts in soils.

where τ_s is the average shear stress on A_s . If surfaces A_w and A_s are the same for all cross sections, then

$$\frac{A_w}{A} = 1 - \frac{A_s}{A} = \frac{V_w}{V} = n \tag{34}$$

where n is the porosity. Therefore,

$$\sigma = (1 - n) \sigma_s + nu \quad \text{and} \quad \tau = (1 - n) \tau_s \tag{35}$$

Using Eqs. 31 and 35,

$$\sigma = \sigma' + u = (1 - n) \sigma_s + nu \tag{36}$$

Therefore, the effective stress is related to σ_s and u through

$$\sigma' = (1 - n) (\sigma_s - u) \quad \text{and} \quad \tau' = \tau = (1 - n) \tau_s \tag{37}$$

As shown in Eq. 37, the effective stress σ' depends on σ_s and u . In the case when $\sigma_s \gg u$, σ' becomes equal to the *distributed granular stress* $(1 - n)\sigma_s$.

Cauchy Representation of Total and Effective Stresses

In the Cauchy representation, Eq. 30 becomes

$$\begin{pmatrix} \sigma_x & \tau_{xy} \\ \tau_{xy} & \sigma_y \end{pmatrix} = \begin{pmatrix} \sigma'_x & \tau'_{xy} \\ \tau'_{xy} & \sigma'_y \end{pmatrix} + \begin{pmatrix} u & 0 \\ 0 & u \end{pmatrix} \tag{38}$$

where the first matrix represents the *total stress*, and the second matrix, the *effective stress*.

Mohr Representation of Total and Effective Stresses

Like total stresses, effective stresses have a Mohr circle. As shown in Fig. 11, the Mohr circles of effective and total stresses have the same diameter because of Eq. 31. The center and pole of the Mohr circle of effective stress are obtained from those of total stress by a translation in the amount $-u$ along the σ axis.

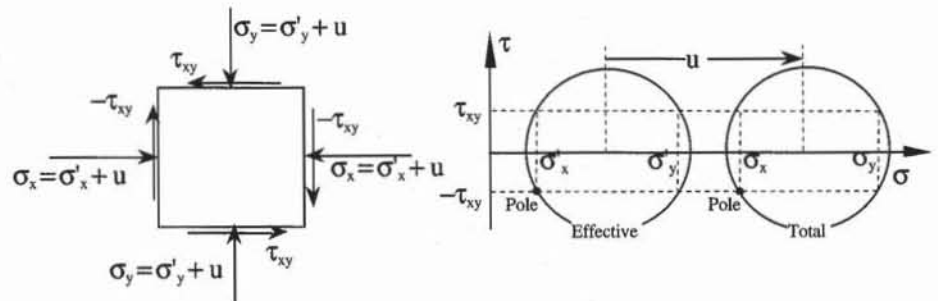


Figure 11 Mohr circles and poles of effective and total stresses.

S-T REPRESENTATION

The evolution of the Mohr circle during a loading process can be defined in terms of s and t , where s is the σ -coordinate of the Mohr circle center and t is the Mohr circle radius:

$$s = \frac{1}{2}(\sigma_1 + \sigma_3) \quad \text{and} \quad t = \frac{1}{2}(\sigma_1 - \sigma_3) \tag{39}$$

where σ_1 is the major principal stress and σ_3 is the minor principal stress. The effective coordinates s' and t' are:

$$s' = \frac{1}{2}(\sigma'_1 + \sigma'_3) \quad \text{and} \quad t' = \frac{1}{2}(\sigma'_1 - \sigma'_3) \tag{40}$$

The s - t and s' - t' components are referred to as the *MIT stress system*. Using Eq. 31, s , t , s' , and t' are related through

$$s = s' + u \quad \text{and} \quad t = t' \tag{41}$$

Figure 12 schematizes the evolution of the effective and total Mohr circles during an arbitrary loading process. The Mohr circles of total and effective stress and their corresponding points in the s - t and s' - t' spaces are shown in Fig. 12. The Mohr circles A and A' have the same radius, but their centers are separated by pore pressure u_A . Points A' and A have identical t (i.e., $t_A = t'_A$), but different s (i.e., $s_A = s'_A + u_A$).

THREE-DIMENSIONAL STRESS

Stresses are three-dimensional in the field and in the laboratory. We discuss briefly the three-dimensional representations of Cauchy and Mohr. Additional information can be found in Chen and Saleeb (1982).

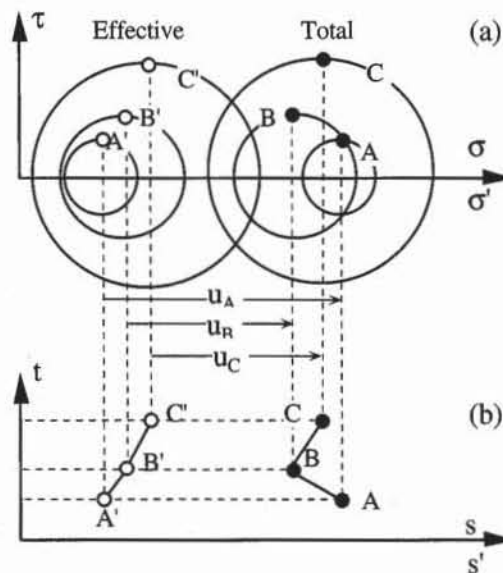


Figure 12 Evolution of the Mohr circle of effective and total stresses, and their representation in the s - t and s' - t' spaces.

Cauchy Representation

In three dimensions, the stress vector $(\sigma_{nx}, \sigma_{ny}, \sigma_{nz})$ acting on the surface with normal unit vector (n_x, n_y, n_z) is given by the Cauchy stress tensor

$$\begin{pmatrix} \sigma_{nx} \\ \sigma_{ny} \\ \sigma_{nz} \end{pmatrix} = \begin{pmatrix} \sigma_x & \tau_{xy} & \tau_{xz} \\ \tau_{xy} & \sigma_y & \tau_{yz} \\ \tau_{xz} & \tau_{yz} & \sigma_z \end{pmatrix} \begin{pmatrix} n_x \\ n_y \\ n_z \end{pmatrix} \quad (42)$$

The principal stresses σ_1 , σ_2 , and σ_3 are found by solving the following eigenvalue problem:

$$\begin{pmatrix} \sigma_x & \tau_{xy} & \tau_{xz} \\ \tau_{xy} & \sigma_y & \tau_{yz} \\ \tau_{xz} & \tau_{yz} & \sigma_z \end{pmatrix} \begin{pmatrix} n_x \\ n_y \\ n_z \end{pmatrix} = \sigma \begin{pmatrix} n_x \\ n_y \\ n_z \end{pmatrix} \quad (43)$$

which is equivalent to solving the following cubic equation:

$$\sigma^3 - I_1\sigma^2 + I_2\sigma - I_3 = 0 \quad (44)$$

where I_1 , I_2 , and I_3 are the stress invariants

$$I_1 = \sigma_x + \sigma_y + \sigma_z$$

$$I_2 = \sigma_x\sigma_y + \sigma_y\sigma_z + \sigma_z\sigma_x - \tau_{xy}^2 - \tau_{yz}^2 - \tau_{zx}^2 \quad (45)$$

$$I_3 = \sigma_x\sigma_y\sigma_z - \sigma_x\tau_{yz}^2 - \sigma_y\tau_{zx}^2 - \sigma_z\tau_{xy}^2 + 2\tau_{xy}\tau_{yz}\tau_{zx}$$

Equation 44 can be solved analytically as follows:

$$\sigma_1 = \frac{I_1}{3} + \frac{2}{3}\sqrt{I_1^2 - 3I_2} \cos \theta$$

$$\sigma_2 = \frac{I_1}{3} + \frac{2}{3}\sqrt{I_1^2 - 3I_2} \cos \left(\frac{2\pi}{3} - \theta \right) \quad (46)$$

$$\sigma_3 = \frac{I_1}{3} + \frac{2}{3}\sqrt{I_1^2 - 3I_2} \cos \left(\frac{2\pi}{3} + \theta \right)$$

where θ is given by

$$\cos 3\theta = \frac{2I_1^3 - 9I_1I_2 + 27I_3}{2(I_1^2 - 3I_2)^{3/2}} \quad (47)$$

The stress invariants of Eq. 45 can also be expressed in terms of principal stresses:

$$I_1 = \sigma_1 + \sigma_2 + \sigma_3, \quad I_2 = \sigma_1\sigma_2 + \sigma_2\sigma_3 + \sigma_1\sigma_3, \quad \text{and} \quad I_3 = \sigma_1\sigma_2\sigma_3 \quad (48)$$

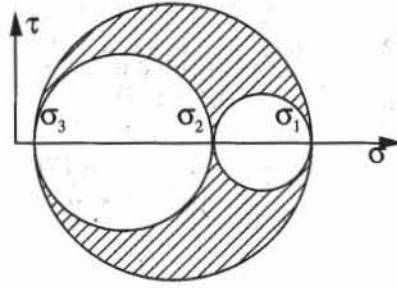


Figure 13 Mohr representation of three-dimensional stresses.

The principal stress directions are found by setting σ equal to σ_1 , σ_2 , or σ_3 in Eq. 43.

Mohr Representation

As shown in Fig. 13, in three dimensions, the stress point (σ, τ) describes the shaded area between the three circles passing through points $(\sigma_1, 0)$, $(\sigma_2, 0)$, and $(\sigma_3, 0)$ where σ_1 , σ_2 , and σ_3 are the principal stresses. The geometrical determination of point (σ, τ) in this area is impractical because it is much more complicated than in two dimensions. When the intermediate principal stress σ_2 is equal to the major or minor principal stress (i.e., $\sigma_2 = \sigma_1$, or $\sigma_2 = \sigma_3$), the shaded area becomes a circle, and the three-dimensional Mohr representation coincides with the two-dimensional representation. This is the case of axisymmetric stresses, for which

$$\sigma_x = \sigma_y \quad \text{and} \quad \tau_{xy} = \tau_{yz} = \tau_{zx} = 0 \quad (49)$$

Therefore, axisymmetric stresses can be described by using the Mohr representation.

P-Q REPRESENTATION

In the case of axisymmetric stress states (Eq. 49), it is convenient to introduce the mean effective pressure p' and the deviator stress q

$$p' = \frac{1}{3}(\sigma'_1 + 2\sigma'_3) \quad \text{and} \quad q = \sigma_1 - \sigma_3 = \sigma'_1 - \sigma'_3 \quad (50)$$

where σ'_1 are σ'_3 the axial and radial effective stress, respectively, and σ_1 and σ_3 are their total stress counterparts. The total mean pressure p corresponding to p' is $p = \frac{1}{3}(\sigma_1 + 2\sigma_3) = p' + u$. The p - q and p' - q components are referred to as the *Cambridge stress system*. Using Eq. 39,

$$s' = p' + \frac{q}{6} \quad \text{and} \quad t = \frac{q}{2} \quad (51)$$

Note that $s' = p'$ and $t = q = 0$ when $\sigma'_1 = \sigma'_3$, and that $s' \neq p'$ and $t \neq q$ otherwise. Table 1 summarizes the definitions of the MIT and Cambridge stress systems. p and q are also related to the stress invariants through

$$p = \frac{1}{3} I_1 \quad \text{and} \quad q = \sqrt{I_1^2 - 3I_2} \quad (52)$$

TABLE 1
The MIT and Cambridge stress notations

Principal stresses	MIT notation s - t and s' - t' stresses	Cambridge notation p - q and p' - q' stresses
$\sigma_1 = \sigma'_1 + u$	$s = \frac{1}{2}(\sigma_1 + \sigma_3) = s' + u$	$p = \frac{1}{3}(\sigma_1 + 2\sigma_3) = p' + u$
$\sigma'_1 = \sigma_1 - u$	$s' = \frac{1}{2}(\sigma'_1 + \sigma'_3) = s - u$	$p' = \frac{1}{3}(\sigma'_1 + 2\sigma'_3) = p - u$
$\sigma_3 = \sigma'_3 + u$	$t = \frac{1}{2}(\sigma_1 - \sigma_3)$	$q = \sigma_1 - \sigma_3$
$\sigma'_3 = \sigma_3 - u$	$t' = t = \frac{1}{2}(\sigma'_1 - \sigma'_3)$	$q' = q = \sigma'_1 - \sigma'_3$
σ'_1	$\sigma'_1 = s' + t$	$\sigma'_1 = p' + \frac{2}{3}q$
σ'_3	$\sigma'_3 = s' - t$	$\sigma'_3 = p' - \frac{1}{3}q$

REFERENCES

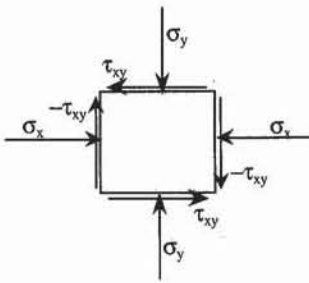
- CHEN, W. F., and A. F. SALEEB, 1982, *Constitutive Equations for Engineering Materials*, Vol. 1, John Wiley & Sons, New York, pp. 48–108.
- FILLUNGER, P., 1915, Versuche über die Zugfestigkeit bei Allseitigem Wasserdruk, *Österr. Wochenschr. Öffentl. Baudienst*, Vol. H.29, pp. 443–448.
- TERZAGHI, K., 1943, *Theoretical Soil Mechanics*, John Wiley & Sons, New York.

REVIEW QUESTIONS

1. What are the main types of force acting on a soil element?
2. Define three different types of body forces acting in soils.
3. What is the physical dimension of stress?
4. Define the Cauchy representation of stresses. How does it relate stress matrix and stress vector on an inclined surface?
5. Define *principal stresses*.
6. Define the sign convention for the Cauchy and Mohr representations of stress.
7. What does the Mohr circle represent?
8. Define the radius and center position of the Mohr circle from arbitrary stresses acting on a square element.
9. Define the pole of the Mohr circle. Why do we introduce the pole of the Mohr circle?
10. What is the principle of the pole of the Mohr circle?
11. What are the effective stress and total stress?
12. What is the difference between effective stress and distributed granular stress? Under what conditions are these stresses equal?
13. Define the s and t coordinates. Why are they useful?
14. Why does the Mohr circle have a limited use in three dimensions?
15. What are the stress invariants?

EXERCISES

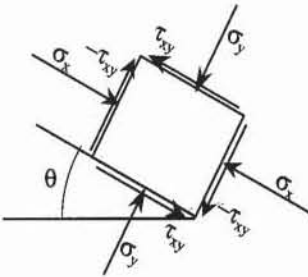
1. Derive the stress equilibrium equations (Eqs. 7 to 9) by using Fig. 3.
2. (a) Draw the Mohr circle and its pole for the following stress state.



(b) Find the stresses acting on a surface inclined at 30° with respect to the horizontal direction.

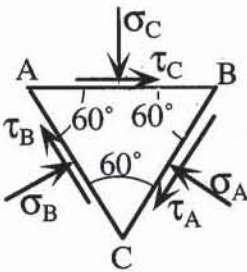
$$\sigma_x = 20 \text{ kPa}, \quad \sigma_y = 100 \text{ kPa}, \quad \tau_{xy} = 10 \text{ kPa}$$

3. (a) Draw the Mohr circle and its pole for the following stress state.
- (b) Find the stresses acting on a surface inclined at 30° with respect to the horizontal direction.
- (c) Find the values and inclinations of the principal stresses by using the pole.



$$\sigma_x = 20 \text{ kPa}, \quad \sigma_y = 100 \text{ kPa}, \quad \tau_{xy} = 10 \text{ kPa}, \quad \theta = 30^\circ$$

4. (a) Find stress σ_C , σ_A , and τ_A on the triangular element in order to have an equilibrium.
- (b) Plot the Mohr circle and its pole.
- (c) Verify that the stress points (σ_A, τ_A) , (σ_B, τ_B) , and (σ_C, τ_C) are on the Mohr circle and are obtained by using the pole.



$$\tau_B = 20 \text{ kPa}, \quad \sigma_B = 100 \text{ kPa}, \quad \tau_C = 10 \text{ kPa}$$

5. In a triaxial test at constant confining pressure, only the major principal stress σ_1 varies from 50 to 100 kPa, whereas stresses σ_2 and σ_3 remain equal to 50 kPa. Draw the corresponding s - t stress path.

5-2 Strain in Soils

INTRODUCTION

In the following section we review the concepts of strain for describing the stress-strain response of soils in laboratory experiments. Strains are first presented in two dimensions, using the tensor and Mohr representations, and then in three dimensions.

TWO-DIMENSIONAL DISPLACEMENT AND STRAIN IN SOILS

As shown in Fig. 1, the soil mass H deforms from its initial to final positions when it is subjected to external loads (e.g., weight of a building) or internal forces (e.g., the soil's own weight). The small element $OACB$ located within soil mass H deforms as shown in Fig. 2. Like stresses, strains are defined by assuming that soils are continuous materials. Figure 2 shows the initial position of element $OACB$ and its final position $O'A'C'B''$.

The displacement of point O from its initial position (x, y) is characterized by the displacement vector (u, v) . The components u and v are assumed to be continuous functions of x and y . Therefore, in the close proximity of point O , u and v may be approximated by using Taylor expansions:

$$u(x + dx, y + dy) = u(x, y) + \frac{\partial u}{\partial x}(x, y) dx + \frac{\partial u}{\partial y}(x, y) dy + \dots \quad (1)$$

$$v(x + dx, y + dy) = v(x, y) + \frac{\partial v}{\partial x}(x, y) dx + \frac{\partial v}{\partial y}(x, y) dy + \dots \quad (2)$$

As listed in Table 1, the coordinates of the displacement vectors of points A , B , and C may be calculated by using Eqs. 1 and 2 and their position relative to point O . The displacements of O , A , B , and C are represented in Fig. 3. The element $O'A'C'B'$ is obtained by translating $OACB$ purely, without deforming or rotating it.

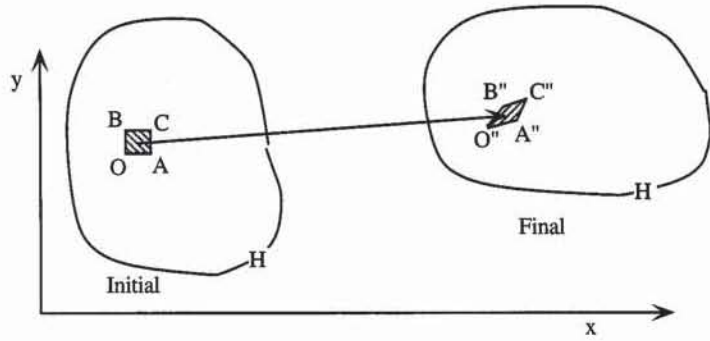


Figure 1 Initial and final positions of a soil mass during a deformation process.

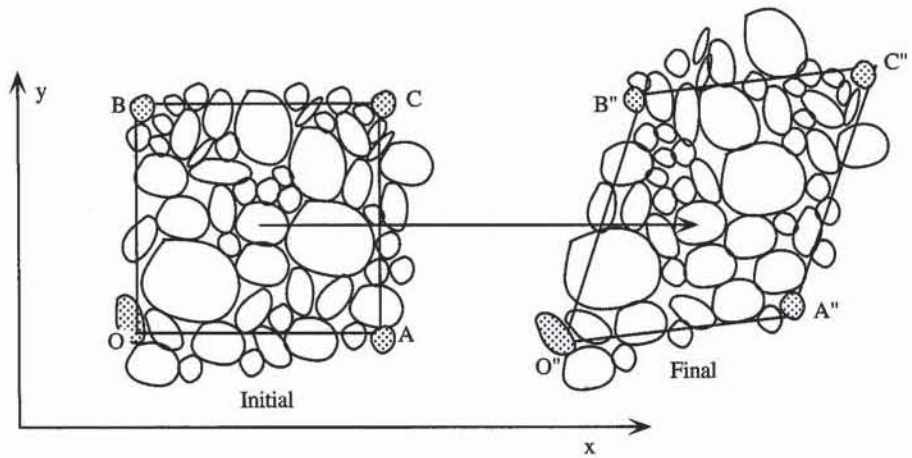


Figure 2 Deformation of the small element of Fig. 1 from initial to final positions.

TABLE 1

Coordinates of initial positions of points *O*, *A*, *B*, and *C* and coordinates of their displacement

Initial position			Final position		Displacement	
Point	<i>x</i>	<i>y</i>	Point	<i>x</i>	<i>y</i>	
<i>O</i>	<i>x</i>	<i>y</i>	<i>O''</i>	<i>u</i>	<i>v</i>	
<i>A</i>	<i>x + dx</i>	<i>y</i>	<i>A''</i>	$u + \frac{\partial u}{\partial x} dx$	$v + \frac{\partial v}{\partial x} dx$	
<i>B</i>	<i>x</i>	<i>y + dy</i>	<i>B''</i>	$u + \frac{\partial u}{\partial y} dy$	$v + \frac{\partial v}{\partial y} dy$	
<i>C</i>	<i>x + dx</i>	<i>y + dy</i>	<i>C''</i>	$u + \frac{\partial u}{\partial x} dx + \frac{\partial u}{\partial y} dy$	$v + \frac{\partial v}{\partial x} dx + \frac{\partial v}{\partial y} dy$	

Axial Strain

The material fiber *OA*, which is made of the soil particles between *O* and *A*, becomes *O''A''* after the deformation process. The elongation of *OA* in the *x* direction is

$$O''D - OA = u + \frac{\partial u}{\partial x} dx - u = \frac{\partial u}{\partial x} dx \quad (3)$$

Because OA is equal to dx , the elongation of OA per unit length in the x direction is

$$\frac{O''D - OA}{OA} = \frac{\partial u}{\partial x} = -\epsilon_x \quad (4)$$

where ϵ_x is the axial strain in the x direction, by definition. Owing to the sign convention of soil mechanics, ϵ_x is positive in compression, which justifies the negative sign in Eq. 4. Similarly, the elongation of fiber OB per unit length in the y direction per unit length is

$$\frac{O''E - OB}{OB} = \frac{\partial v}{\partial y} = -\epsilon_y \quad (5)$$

where ϵ_y is the axial strain in the y direction, by definition.

Shear Strain

As shown in Fig. 3, the rotations of fibers OA and OB are equal to the angles $\overline{A'O''A''}$ and $\overline{B'O''B''}$, respectively. $\overline{A'O''A''}$ can be approximated by using Fig. 3:

$$\overline{A'O''A''} \approx \tan(\overline{A'O''A''}) = \frac{\frac{\partial v}{\partial x} dx}{dx + \frac{\partial u}{\partial x} dx} \approx \frac{\partial v}{\partial x} \quad (6)$$

where $|\partial u/\partial x|$ is assumed much smaller than 1. $\overline{B'O''B''}$ is

$$\overline{B'O''B''} \approx \tan(\overline{B'O''B''}) = \frac{\frac{\partial u}{\partial y} dy}{dy + \frac{\partial v}{\partial y} dy} \approx \frac{\partial u}{\partial y} \quad (7)$$

where $|\partial v/\partial y|$ is also assumed much smaller than 1. The angular distortion of \overline{AOB} is

$$\overline{AOB} - \overline{A''O''B''} \approx \frac{\partial u}{\partial y} + \frac{\partial v}{\partial x} = -\gamma_{xy} = -2\epsilon_{xy} \quad (8)$$

where ϵ_{xy} is the shear strain and γ_{xy} is the engineering shear strain, by definition. From a physical point of view, the shear strain γ_{xy} is the angular distortion of two fibers that are initially perpendicular.

Volumetric Strain

As shown in Fig. 3, the area $OABC = S = dx dy$ becomes the area $O''A''B''C'' = S''$. It can be shown that the area change per unit of area is

$$\frac{S - S''}{S} = \epsilon_x + \epsilon_y = \epsilon_v \quad (9)$$

where ϵ_v is the volumetric strain. Eq. 9 assumes that the absolute values of $\partial u/\partial x$ and $\partial v/\partial y$ are much smaller than 1. The volumetric strain ϵ_v is positive when S decreases, and negative when S increases.

Rigid-Body Rotation

As shown in Fig. 3, OC transforms into $O''C''$ and rotates by the angle $\overline{C'O''C''}$, where

$$\overline{C'O''C''} = \frac{1}{2} \overline{A'O''A''} - \frac{1}{2} \overline{B'O''B''} \tag{10}$$

Therefore,

$$\overline{C'O''C''} \approx \frac{1}{2} \left(\frac{\partial u}{\partial y} - \frac{\partial v}{\partial x} \right) = -\omega \tag{11}$$

where ω is the angle of rigid-body rotation about point O'' , by definition. In general, a rigid rotation ω about the origin creates the following displacement:

$$\begin{pmatrix} u \\ v \end{pmatrix} = \begin{pmatrix} \cos\omega - 1 & -\sin\omega \\ \sin\omega & \cos\omega - 1 \end{pmatrix} \begin{pmatrix} x \\ y \end{pmatrix} \tag{12}$$

In the case of infinitesimal rotations (i.e., $|\omega| \ll 1$), Eq. 12 becomes

$$\begin{pmatrix} u \\ v \end{pmatrix} = \begin{pmatrix} 0 & -\omega \\ \omega & 0 \end{pmatrix} \begin{pmatrix} x \\ y \end{pmatrix} \tag{13}$$

which implies that points A , B , and C are subjected to rigid-body rotation of angle ω about point O'' . As the translation for O to O'' , the rigid-body rotation creates no axial and shear strain in the element $OACB$.

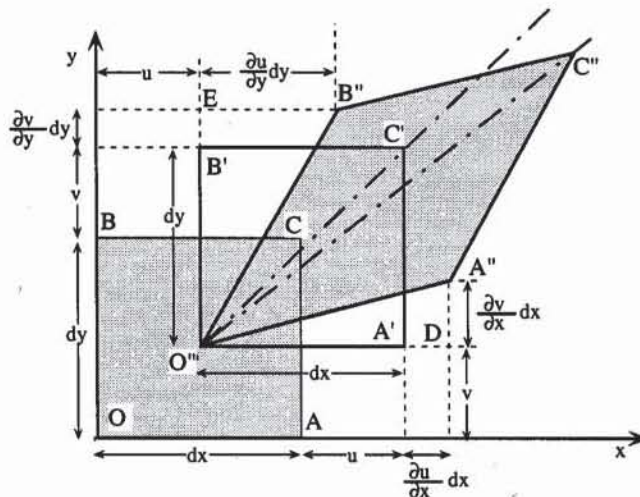


Figure 3 Infinitesimal displacement of points A , B , and C , neighbors of O .

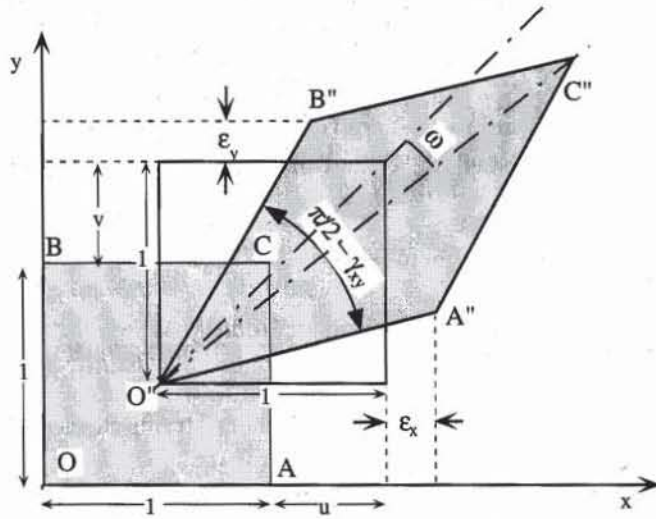


Figure 4 Physical interpretation of strains ϵ_x , ϵ_y , γ_{xy} , and rotation ω .

Summary

As shown in Fig. 4, ϵ_x and ϵ_y represent the length change per unit length in the horizontal and vertical directions, respectively, whereas γ_{xy} represents the angular distortion of two segments that are initially perpendicular. The angle ω of rigid-body rotation represents the rotation of the diagonals about O'' . Note that the foregoing relations between strain and displacement are valid only for infinitesimal deformation (i.e., $|\partial u/\partial x|$, $|\partial v/\partial y|$, $|\partial u/\partial y|$, and $|\partial v/\partial x| \ll 1$). The description of large strain is beyond the scope of this book.

VARIATION OF STRAIN WITH DIRECTION

Axial and shear strains may be calculated for elements oriented in any direction. As shown in Fig. 5, when the x' and y' axes are obtained from the x and y axes by a $-\theta$ rotation, the x - y and x' - y' coordinates are related through

$$\begin{pmatrix} x' \\ y' \end{pmatrix} = \begin{pmatrix} \cos \theta & -\sin \theta \\ \sin \theta & \cos \theta \end{pmatrix} \begin{pmatrix} x \\ y \end{pmatrix} \quad \text{or} \quad \begin{pmatrix} x \\ y \end{pmatrix} = \begin{pmatrix} \cos \theta & \sin \theta \\ -\sin \theta & \cos \theta \end{pmatrix} \begin{pmatrix} x' \\ y' \end{pmatrix} \quad (14)$$

Equation 14 applies also to the displacement vectors:

$$\begin{pmatrix} u' \\ v' \end{pmatrix} = \begin{pmatrix} \cos \theta & -\sin \theta \\ \sin \theta & \cos \theta \end{pmatrix} \begin{pmatrix} u \\ v \end{pmatrix} \quad (15)$$

The small element $oacb$ within $OACB$ is aligned along the x' and y' axes. The deformed element is $o''a''c''b''$. By using the previous definitions, the axial strain in the x' and y' directions and the shear strain are

$$\epsilon_{x'} = -\frac{\partial u'}{\partial x'}, \quad \epsilon_{y'} = -\frac{\partial v'}{\partial y'}, \quad \text{and} \quad \gamma_{x'y'} = -\frac{\partial u'}{\partial y'} - \frac{\partial v'}{\partial x'} \quad (16)$$

Using Eqs. 14 and 15, the following relations are obtained:

$$\frac{\partial x}{\partial x'} = \frac{\partial y}{\partial y'} = \frac{\partial u}{\partial u'} = \frac{\partial v}{\partial v'} = \cos \theta \quad \text{and} \quad \frac{\partial x}{\partial y'} = -\frac{\partial y}{\partial x'} = -\frac{\partial u'}{\partial v} = \frac{\partial v'}{\partial u} = \sin \theta \quad (17)$$

Using Eq. 17 and the chain rule of differentiation yields

$$\begin{aligned} \epsilon_{x'} &= -\frac{\partial u'}{\partial x} \frac{\partial x}{\partial x'} - \frac{\partial u'}{\partial y} \frac{\partial y}{\partial x'} = -\frac{\partial u'}{\partial x} \cos \theta + \frac{\partial u'}{\partial y} \sin \theta \\ &= -\left(\frac{\partial u'}{\partial x} \frac{\partial u}{\partial x} + \frac{\partial u'}{\partial y} \frac{\partial v}{\partial x}\right) \cos \theta + \left(\frac{\partial u'}{\partial u} \frac{\partial u}{\partial y} + \frac{\partial u'}{\partial v} \frac{\partial v}{\partial y}\right) \sin \theta \end{aligned} \quad (18)$$

Finally, the axial and shear strains of element *oabc* are

$$\begin{aligned} \epsilon_{x'} &= \epsilon_x \cos^2 \theta + \epsilon_y \sin^2 \theta - \gamma_{xy} \sin \theta \cos \theta \\ \epsilon_{y'} &= \epsilon_x \sin^2 \theta + \epsilon_y \cos^2 \theta + \gamma_{xy} \sin \theta \cos \theta \\ \gamma_{x'y'} &= 2\epsilon_x \sin \theta \cos \theta - 2\epsilon_y \sin \theta \cos \theta + \gamma_{xy} (\cos^2 \theta - \sin^2 \theta) \end{aligned} \quad (19)$$

Equation 19 is similar to Eq. 20.5-1 defining the stresses on an inclined surface. The variation of strain with direction may be described by using two different approaches: strain tensor and Mohr circle.

Tensor Representation of Strain

The strain tensor is defined as the stress tensor. It gives the projections ϵ_{nx} and ϵ_{ny} of the strains $\epsilon_{x'}$, $\epsilon_{y'}$, and $\epsilon_{x'y'}$ on the *x* and *y* axes.

Strain Tensor

As shown in Fig. 6, the unit vector normal to the surface *bc* is $\mathbf{n} = (n_x, n_y)$, and the unit vector tangent to *bc* is $\mathbf{t} = (n_y, -n_x)$. The strains ϵ_{nx} and ϵ_{ny} along the direction \mathbf{n} are obtained from the strain matrix:

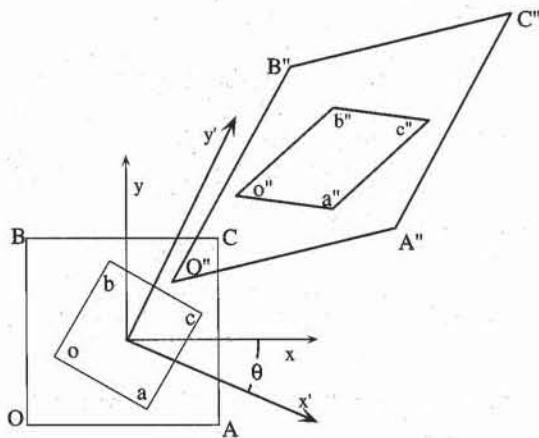


Figure 5 Initial and deformed elements.

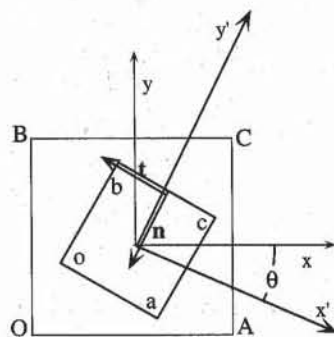


Figure 6 Strain on an inclined element.

$$\begin{pmatrix} \epsilon_{nx} \\ \epsilon_{ny} \end{pmatrix} = \begin{pmatrix} \epsilon_x & \epsilon_{xy} \\ \epsilon_{xy} & \epsilon_y \end{pmatrix} \begin{pmatrix} n_x \\ n_y \end{pmatrix} \quad (20)$$

The unit vector \mathbf{n} points inside the surface bc to obtain positive axial strain in compression and negative axial strain in tension. The normal strain ϵ_n along the \mathbf{n} direction is obtained by projecting $(\epsilon_{nx}, \epsilon_{ny})$ onto the \mathbf{n} direction:

$$\epsilon_n = \epsilon_{nx}n_x + \epsilon_{ny}n_y = \epsilon_x n_x^2 + \epsilon_y n_y^2 + 2\epsilon_{xy}n_x n_y = \epsilon_x n_x^2 + \epsilon_y n_y^2 + \gamma_{xy}n_x n_y \quad (21)$$

and the corresponding shear strain γ_t by projecting $(\epsilon_{nx}, \epsilon_{ny})$ onto the \mathbf{t} direction:

$$\gamma_t = 2\epsilon_t = 2(\epsilon_{nx}n_y - \epsilon_{ny}n_x) = 2\epsilon_x n_x n_y - 2\epsilon_y n_x n_y + \gamma_{xy}(n_y^2 - n_x^2) \quad (22)$$

When \mathbf{n} is normal to surface ac [i.e., $(n_x, n_y) = (-\cos \theta, \sin \theta)$], Eqs. 21 and 22 become

$$\begin{aligned} \epsilon_n &= \epsilon_x \cos^2 \theta + \epsilon_y \sin^2 \theta - \gamma_{xy} \sin \theta \cos \theta = \epsilon_{x'} \\ \gamma_t &= -2\epsilon_x \sin \theta \cos \theta + 2\epsilon_y \sin \theta \cos \theta - \gamma_{xy}(\cos^2 \theta - \sin^2 \theta) = -\gamma_{x'y'} \end{aligned} \quad (23)$$

and when \mathbf{n} is normal to surface bc [i.e., $(n_x, n_y) = (-\sin \theta, -\cos \theta)$]:

$$\begin{aligned} \epsilon_n &= \epsilon_x \sin^2 \theta + \epsilon_y \cos^2 \theta + \gamma_{xy} \sin \theta \cos \theta = \epsilon_{y'} \\ \gamma_t &= 2\epsilon_x \sin \theta \cos \theta - 2\epsilon_y \sin \theta \cos \theta + \gamma_{xy}(\cos^2 \theta - \sin^2 \theta) = \gamma_{x'y'} \end{aligned} \quad (24)$$

Equations 23 and 24 give the same strains as Eq. 19. The strain tensor therefore represents strain along various directions.

Principal Strain

By definition, the principal surfaces remain perpendicular to each other during a deformation process. Therefore, their normals (n_x, n_y) are found by solving the following eigenvalue problem:

$$\begin{pmatrix} \epsilon_x & \epsilon_{xy} \\ \epsilon_{xy} & \epsilon_y \end{pmatrix} \begin{pmatrix} n_x \\ n_y \end{pmatrix} = \epsilon \begin{pmatrix} n_x \\ n_y \end{pmatrix} \quad (25)$$

where ϵ is the principal strain values. ϵ is obtained by solving the following quadratic equation:

$$\epsilon^2 - \epsilon(\epsilon_x + \epsilon_y) + \epsilon_x \epsilon_y - \epsilon_{xy}^2 = 0 \quad (26)$$

The major and minor principal strains are

$$\begin{aligned} \epsilon_1 &= \frac{1}{2}(\epsilon_x + \epsilon_y) + \sqrt{\frac{1}{4}(\epsilon_x - \epsilon_y)^2 + \epsilon_{xy}^2} \\ \epsilon_3 &= \frac{1}{2}(\epsilon_x + \epsilon_y) - \sqrt{\frac{1}{4}(\epsilon_x - \epsilon_y)^2 + \epsilon_{xy}^2} \end{aligned} \quad (27)$$

The principal strains are equal when $\epsilon_x = \epsilon_y$ and $\epsilon_{xy} = 0$, which is the case of

purely volumetric deformation. The principal surface directions are found as for the principal stress directions.

MOHR REPRESENTATION OF STRAIN

Like stresses, strains can be represented by using the Mohr circle.

Sign Conventions for Strain

Figure 7 defines the sign convention of strains for Mohr representation. As shown in Fig. 7, compressive strains are positive and tensile strains are negative. The sign of angular distortion is defined as that of shear stress.

Mohr Circle

Because strain components obey Eq. 23, when θ varies from -90° to 90° , the point $(\epsilon, \gamma/2)$ describes the following circle in the space $(\epsilon, \gamma/2)$:

$$[\epsilon - \frac{1}{2}(\epsilon_x + \epsilon_y)]^2 + \frac{1}{4}\gamma^2 = \frac{1}{4}(\epsilon_x - \epsilon_y)^2 + \epsilon_{xy}^2 \tag{28}$$

The $(\epsilon, \gamma/2)$ space is called the *Mohr strain space*. As shown in Fig. 8, the Mohr circle of Eq. 28 is centered on the ϵ axis at position ϵ_m and has radius R :

$$\epsilon_m = \frac{1}{2}(\epsilon_x + \epsilon_y) \quad \text{and} \quad R = \sqrt{\frac{1}{4}(\epsilon_x - \epsilon_y)^2 + \epsilon_{xy}^2} \tag{29}$$

The strains $(\epsilon_x, -\epsilon_{xy})$ and $(\epsilon_y, \epsilon_{xy})$ are represented by points B and A in the Mohr plane of Fig. 8, respectively. Given a uniform strain state, the normal and shear strains along any direction are located on the circle with center position $(0, \epsilon_m)$ and radius R . The principal strains are the intersections of the Mohr circle with the ϵ axis (Eq. 27).

The definition and properties of the pole of strain are identical to that of stress (see Fig. 8). The pole can be used to calculate the principal strain directions and to find the orientation of the element undergoing the maximum angular distortion.

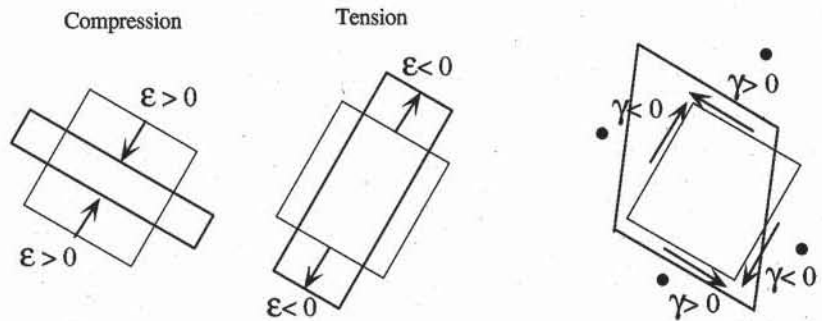


Figure 7 Sign conventions for Mohr representations of strains in soil mechanics.

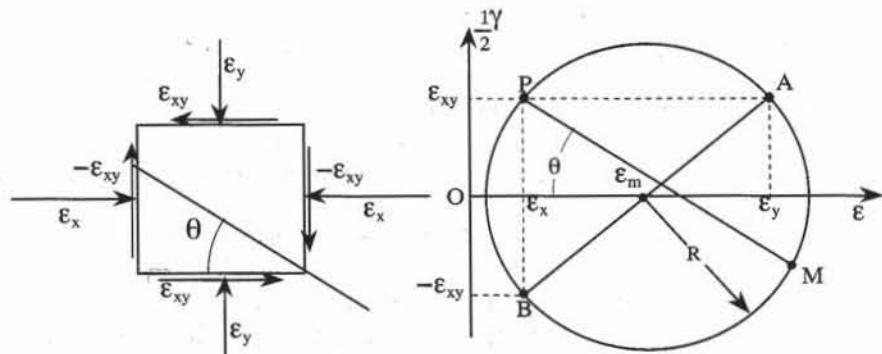


Figure 8 Construction of Mohr circle of strain in Mohr space.

THREE-DIMENSIONAL STRAIN

As mentioned previously, soils undergo three-dimensional strains in the field and the laboratory. We discuss briefly the three-dimensional representations. In three dimensions, the strain tensor gives the x , y , and z projections (ϵ_{nx} , ϵ_{ny} , ϵ_{nz}) of strain along the unit vector (n_x , n_y , n_z):

$$\begin{pmatrix} \epsilon_{nx} \\ \epsilon_{ny} \\ \epsilon_{nz} \end{pmatrix} = \begin{pmatrix} \epsilon_x & \epsilon_{xy} & \epsilon_{xz} \\ \epsilon_{xy} & \epsilon_y & \epsilon_{yz} \\ \epsilon_{xz} & \epsilon_{yz} & \epsilon_z \end{pmatrix} \begin{pmatrix} n_x \\ n_y \\ n_z \end{pmatrix} \quad (30)$$

The strain components are defined from the derivatives of the displacement components u , v , and w , in the x , y , and z directions:

$$\epsilon_x = -\frac{\partial u}{\partial x}, \quad \epsilon_y = -\frac{\partial v}{\partial y}, \quad \epsilon_z = -\frac{\partial w}{\partial z} \quad (31)$$

$$\gamma_{xy} = 2\epsilon_{xy} = -\frac{\partial u}{\partial y} - \frac{\partial v}{\partial x}, \quad \gamma_{yz} = 2\epsilon_{yz} = -\frac{\partial v}{\partial z} - \frac{\partial w}{\partial y}, \quad \gamma_{xz} = 2\epsilon_{xz} = -\frac{\partial w}{\partial x} - \frac{\partial u}{\partial z}$$

The principal strains ϵ_1 , ϵ_2 , and ϵ_3 are found by solving the following eigenvalue problem:

$$\begin{pmatrix} \epsilon_x & \epsilon_{xy} & \epsilon_{xz} \\ \epsilon_{xy} & \epsilon_y & \epsilon_{yz} \\ \epsilon_{xz} & \epsilon_{yz} & \epsilon_z \end{pmatrix} \begin{pmatrix} n_x \\ n_y \\ n_z \end{pmatrix} = \epsilon \begin{pmatrix} n_x \\ n_y \\ n_z \end{pmatrix} \quad (32)$$

which leads to the same cubic equation and invariants as for stress.

As in the case of stress, the three-dimensional Mohr representation of strain is complicated. When two principal strains coincide, it becomes identical to the two-dimensional Mohr representation.

The volumetric strain which is equal to $(V_0 - V)/V_0$, where V_0 is the initial volume and V the deformed volume, can be related to the strain components as follows

$$\epsilon_v = \frac{V_0 - V}{V_0} = \epsilon_x + \epsilon_y + \epsilon_z \quad (33)$$

REVIEW QUESTIONS

1. What is the sign convention for strain in soil mechanics?
2. What are the relations between strain and displacement? In what range do these equations apply?
3. What are the physical meanings of axial strain and shear strain?
4. What is the relation between volumetric strain and normal strain in two and three dimensions?
5. Do rigid-body rotation and translation create strain?
6. What is the physical meaning of principal strains?
7. What are the two representations that are used for strains?
8. Calculate the center and radius of the Mohr circle of two-dimensional strain in terms of ϵ_x , ϵ_y , and ϵ_{xy} .
9. Define the pole of the Mohr circle of strain. What is the use of the pole?
10. Under which condition is the Mohr representation useful in three dimensions?

EXERCISE

1. Show that the area change ϵ_v of a unit area is equal to $\epsilon_x + \epsilon_y$, where ϵ_x and ϵ_y are axial strains in the x and y directions.

INTRODUCTION

When soils are subjected to stress changes in the laboratory and in the field, they deform in complicated ways which can be represented in terms of stress-strain relationships. To describe the stress-strain relations of soils, we first survey some basic models.

FUNDAMENTALS OF STRESS-STRAIN RELATIONS

Figure 1 shows three major types of idealized stress-strain curves for materials subjected to loading and unloading. In the one-dimensional case, loading corresponds to an increase in applied strain or stress, while unloading is associated with a removal of strain or stress. Figure 1a shows identical responses during loading OA and unloading AO . The strain is fully recovered when the stress is removed. This reversibility characterizes *elastic* materials. The elastic material is *linear* when the stress-strain curve is straight (Fig. 1b), and *nonlinear* when it is curved (Fig. 1a). As shown in Fig. 1c, when a significant amount of strain is not recovered upon unloading, the material behavior is *irreversible* (or *elastoplastic*). The responses of nonlinear-elastic and elastoplastic models are different during unloading, but may be identical during loading. In one-dimension, the elastic and irreversible behaviors are distinguishable only after an unloading.

Figure 2 shows several types of irreversible behavior that are observed for soils. In all cases, the behavior is considered elastic below the yield stress σ^* and irreversible beyond σ^* . The yield stress σ^* marks the transition between reversible and irreversible behaviors. The determination of σ^* is not always trivial and may be subject to interpretations. In Fig. 2a, the material is *strain hardening*—it is stronger during the reloading BC than during the previous loading OA . The loading OA has hardened the material, thus the term *strain hardening*. In Fig. 2c, the material is *strain softening*—it is softer during the reloading BC than during loading OA . The previous loading OA has weakened the material of Fig. 2c. In Fig.

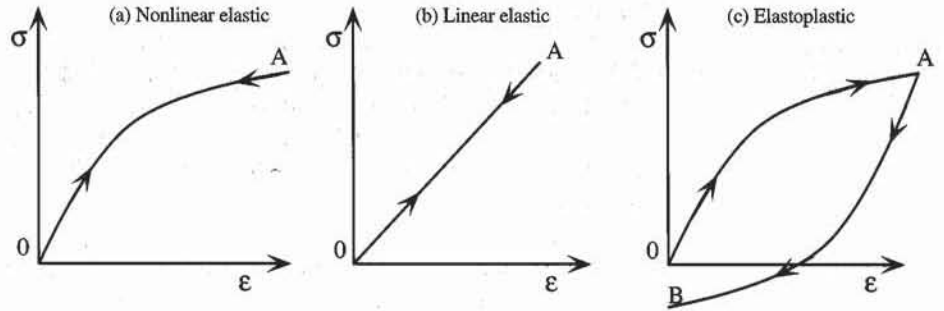


Figure 1 Idealized types of stress-strain behaviors: (a) nonlinear elastic model, (b) linearly elastic model, and (c) elastoplastic model.

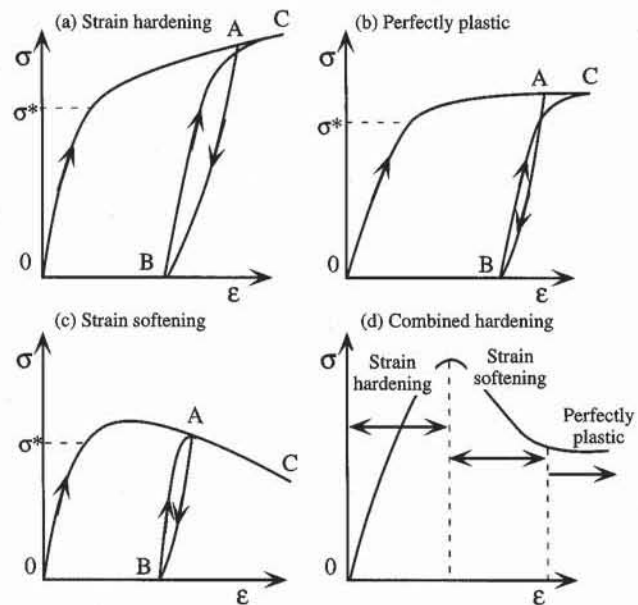


Figure 2 Various types of elastoplastic behaviors: (a) strain hardening, (b) perfectly plastic, (c) strain softening, and (d) combination of a to c.

2b, the material does not harden or soften—it is *perfectly plastic*. The stress remains constant as the strain becomes very large. The curves *OA* and *BC* are similar, and are not influenced by previous loadings. As shown in Fig. 2d, soils may be strain hardening, strain softening, then perfectly plastic. This behavior, which is complicated to describe and to measure in the laboratory, is generally simplified for engineering purposes.

Figure 3 shows three simplified models used in soil mechanics: (a) rigid-perfectly plastic, (b) elastic-perfectly plastic, and (c) elastic-strain hardening. The *rigid-perfectly plastic* model of Fig. 3a is useful in stability analysis, to calculate the maximum load sustainable by a soil mass. However, this model provides only the failure stress, and cannot be used to calculate strain or displacement. The failure stress of soils, also referred to as *shear strength*, is described in Chapter 7-1. As shown in Fig. 3b, the *elastic-perfectly plastic* model first behaves elastically for stress σ smaller than σ^* , then becomes perfectly plastic when σ reaches σ^* (i.e.,

σ remains constant with strain). The rigid-perfectly plastic model is a particular case of elastic-perfectly plastic model with a very stiff elastic response. As shown in Fig. 3c, in contrast to perfectly-plastic models, the *elastic-strain hardening* model has a yield stress that depends on the loading history. Initially, the yield stress is equal to σ_0^* , and becomes σ_A^* after the loading OA . Strain hardening is used in Chapter 6-1 to describe the irreversible behavior of clays during consolidation tests.

The behaviors in Figs. 1 to 3 are *rate independent* (or *inviscid*): they do not depend on the rate of loading or unloading. Rate dependency is generally neglected in most practical applications, except for the long-term settlement of fine-grained soils. In contrast to inviscid materials, *rate-dependent* (or *viscous*) materials depend on the rate of loading. As shown in Fig. 4, when the applied stress is constant, the strain increases with time (creep) for a viscous material but remains constant for an inviscid material. As shown in Fig. 5, when the applied strain is constant, the stress decreases with time (relaxation) for a viscous material but re-

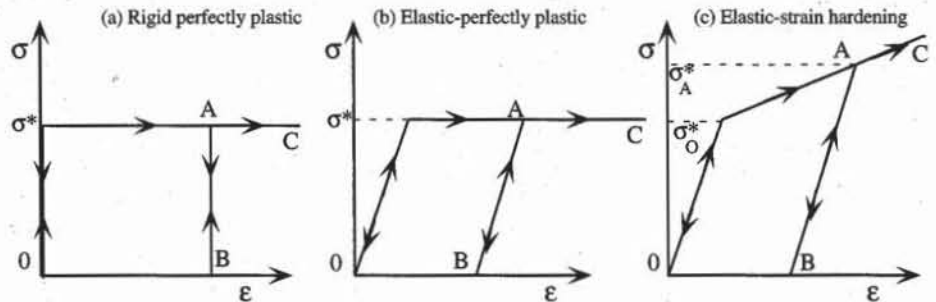


Figure 3 Idealized behaviors commonly used in soil mechanics.

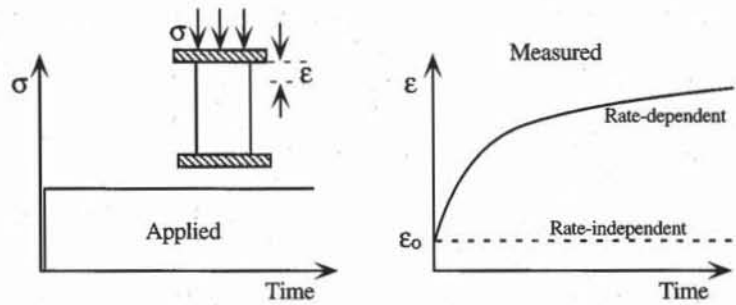


Figure 4 Creep effect in rate-dependent materials.

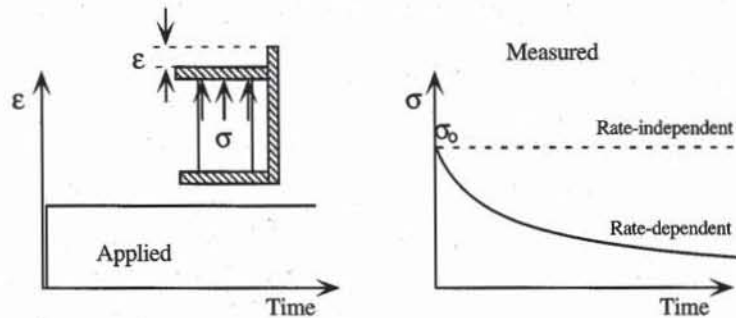


Figure 5 Stress-relaxation effect in rate-dependent materials.

mains constant for an inviscid material. Some features of the rate dependent behavior of soils are presented in Chapter 6-1.

CONSTITUTIVE EQUATIONS FOR SOILS

The most accurate and general representation of soil behavior is based on constitutive equations. These advanced methods are capable of describing the nonlinear, irreversible, and rate-dependent stress-strain response of soils under various loadings including cyclic and dynamic conditions. Various types of constitutive equations have been proposed for soils (e.g., Bardet, 1986; Dafalias and Herrmann, 1985; Lade, 1977; and Schofield and Wroth, 1968). Refer to Chen and Saleeb (1982) for more information. When these constitutive equations are implemented in finite element programs, they can be used to solve geotechnical engineering problems such as boundary value problems. Examples of finite element applications to geotechnical engineering can be found in Zienkiewicz and Taylor (1991).

REFERENCES

- BARDET, J. P., 1986, Bounding surface plasticity model for sands, *J. Eng. Mechanics*, ASCE, Vol. 112, No. 11, pp. 1198-1217.
- CHEN, W. F., and A. F. SALEEB, 1982, *Constitutive Equations for Engineering Materials*, John Wiley & Sons, New York, pp. 441-559.
- DAFALIAS, Y. F., and L.R. HERRMANN, 1985, Bounding surface plasticity: II. Applications to isotropic cohesive soils, *J. Eng. Mechanics*, ASCE, Vol. 111, No. 12, pp. 1263-1291.
- LADE, P. V., 1977, Elasto-plastic stress-strain theory for cohesionless soil with curved yield surfaces, *Int. J. Solids Structures*, Vol. 113, pp. 1019-1035.
- SCHOFIELD, A. N., and C. P. WROTH, 1968, *Critical State Soil Mechanics*, McGraw-Hill, London, U.K.
- ZIENKIEWICZ, O. C., and R. L. TAYLOR, 1991, *The Finite Element Method*, McGraw-Hill, London, U.K.

5-4 Laboratory Tests for Determination of Stress–Strain–Strength of Soils

STRESSES IN THE FIELD

Most geotechnical engineering analyses have to determine: (1) the initial stress state and stress history of the soil prior to any construction activity, and (2) the deformation and stability of soils resulting from the changes in stresses imposed by construction.

Initial Stresses

The initial stresses in the field, also referred to as *in-situ* stresses, must first be defined due to their effects on nonlinear soil behavior. As shown in Fig. 1, for horizontal ground conditions, the in-situ stresses are expressed in terms of the effective vertical stress σ'_{z0} and effective horizontal stresses σ'_{x0} and σ'_{y0} :

$$\sigma'_{z0} = \gamma z - u_0 \quad \text{and} \quad \sigma'_{x0} = \sigma'_{y0} = K_0 \sigma'_{z0} \quad (1)$$

where γ is the average total unit weight of soil above depth z , u_0 the water pressure at depth z , and K_0 the coefficient of lateral earth pressure at rest. The value of K_0 depends on soil properties and loading history. The stress caused by the weight of soils above a given depth is called *overburden* stress. As shown in Fig. 1, the initial stress state can be represented in terms $\sigma' - \tau$ and $s' - t$. Point A is on the line passing through the origin and having for slope $(1 - K_0)/(1 + K_0)$. The total vertical stress σ_{z0} and total horizontal stresses σ_{x0} and σ_{y0} corresponding to σ'_{z0} , σ'_{x0} and σ'_{y0} are

$$\sigma_{z0} = \gamma z = \sigma'_{z0} + u_0 \quad \text{and} \quad \sigma_{x0} = \sigma_{y0} = K_0 \sigma'_{z0} + u_0 \quad (2)$$

Stress Changes Applied by Engineered Constructions

As illustrated in Fig. 1, various types of constructions impose different stress changes to soils in the field. For all these loadings, the approximate changes in total and effective stresses are represented in $\sigma' - \tau$ and $s' - t$ spaces. In $s' - t$

space, point A represents the initial effective stress state before construction. Segments AB and AB' represent the change in total stress and effective stress due to construction, respectively. Points B and B' have the same t component, but their s components are related through $s_B = s_{B'} + u_B$ where u_B is the excess pore pressure induced by external loading. Points B and B' coincide when $u_B = 0$, but differ otherwise. Figure 1 shows the effective stress Mohr circles corresponding to points A and B , assuming that $u_B = 0$. Point B indicates a change in total stress, and not an absolute value of total stress; it does not account for the initial water pressure u_0 .

The position of points B and B' varies depending on the type of construction and the location of the soil element. As shown in Fig. 1b, the soil element beneath the tank is subjected to an increase in vertical stress $\Delta\sigma_z$, which is represented by AB in $s - t$ space. If the loading generates an excess pore pressure, the effective stress change is represented by AB' instead of AB . When the stress increment $\Delta\sigma_z$ remains constant, point B' will move toward point B as the excess pore pressure dissipates with time. Behind the retaining wall of Fig. 1c (active case), the soil element is subjected to an increase in lateral stress $\Delta\sigma_x$ while the vertical stress σ'_z remains constant. In front of the anchor of Fig. 1d (passive case), the soil element endures an increase in lateral stress $\Delta\sigma_x$. Beneath the center of the excavation of Fig. 1e, the soil is subjected to a decrease in vertical stress $\Delta\sigma_z$. As shown in Fig. 1f, the change in stress on a soil element depends on its position. Element C is subjected to an increase in vertical stress $\Delta\sigma_z$, element D to an increase in shear stress $\Delta\tau_{xz}$, and element E to a decrease in vertical stress $\Delta\sigma_z$.

LABORATORY TESTING OF SOILS

Figure 1 illustrates the variety of loadings which constructions apply to soils. The objective of laboratory soil testing is to determine the stress-strain response and shear strength of soil samples by subjecting them to stress paths with direction and initial state similar to those in the field. The initial state of soil samples is generally altered after they have been removed from the field, transported to the laboratory, and cut into laboratory specimens. Reliable laboratory tests attempt first to reproduce the initial state, especially density, then to recreate the initial stresses and loading history by performing an isotropic or K_0 consolidation.

We now briefly introduce the laboratory tests for determining the stress-strain-strength properties of soils, and describe the loading they apply to soil samples in terms of stress paths.

Isotropic Test

The *isotropic test* simulates approximately the effects of overburden pressure on soils in the field by assuming $K_0 = 1$. As shown in Fig. 2, the isotropic test applies pressure σ_c to soil samples, generally in the triaxial cell (Fig. 8). The effective stresses are

$$\sigma'_x = \sigma'_y = \sigma'_z = \sigma_c \quad \text{and} \quad \tau_{xy} = \tau_{yz} = \tau_{zx} = 0 \quad (3)$$

Figure 2 shows the stress path of the isotropic loading in $\sigma' - \tau$ and $s' - t$ spaces. In $\sigma' - \tau$ space, the Mohr circle is reduced to a point. In $s' - t$ space, $s' = \sigma_c$ and $t = 0$. In both spaces, the stress path is horizontal and the stress point moves with σ_c .

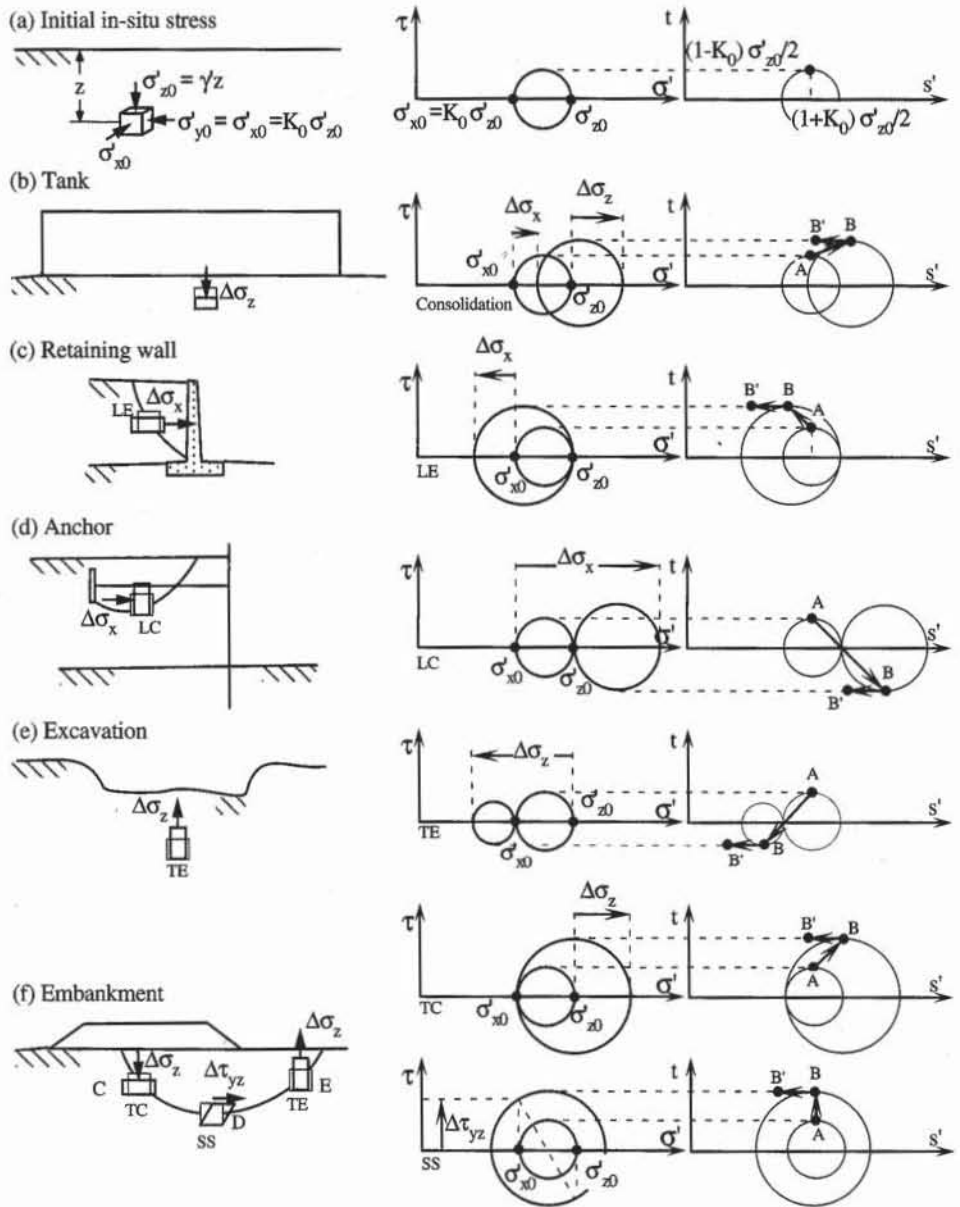


Figure 1 Initial in-situ stresses, and stress changes resulting from some typical constructions in geotechnical engineering.

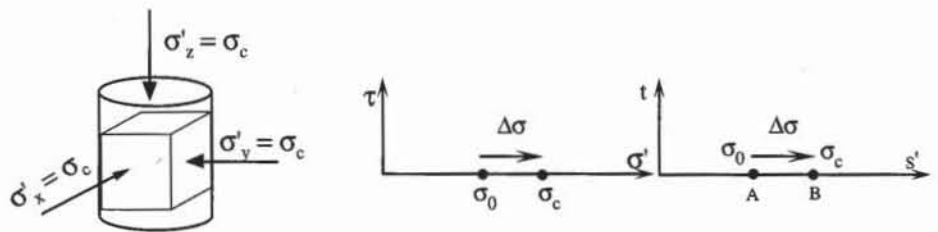


Figure 2 Stresses acting on samples, and stress paths in $\sigma' - \tau$ and $\sigma' - t$ spaces during an isotropic test.

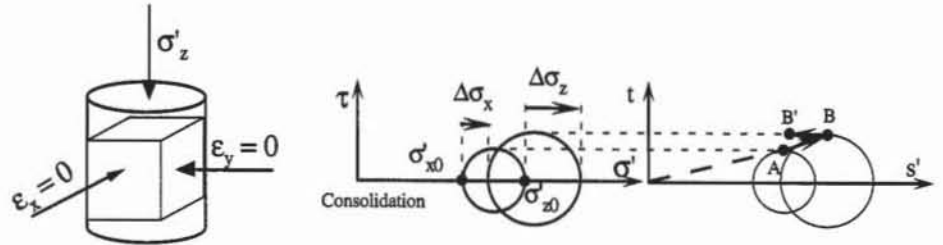


Figure 3 Stresses and strains applied to sample, and stress paths in $\sigma' - \tau$ and $s' - t$ spaces during a K_0 test.

K_0 Test

The K_0 test simulates an increase of overburden, and recreates the loading history and initial stress states of soils in the field. The loading conditions are

$$\sigma'_x = \sigma'_y, \tau_{xy} = \tau_{yz} = \tau_{zx} = 0, \text{ and } \epsilon_x = \epsilon_y = 0 \tag{4}$$

In contrast to the isotropic test, the K_0 test applies different lateral and vertical stresses (i.e., $\sigma'_z \neq \sigma'_x$). This anisotropic loading can be performed in the triaxial test (Fig. 8) by controlling simultaneously the variation of axial stress σ_z and confining pressure σ_x so that the soil sample does not deform laterally.

Confined Compression Test

The *confined compression test*, also referred to as *oedometer* and *consolidation test* (see Chapter 6-1), is used to calculate the settlement of footings, tanks and embankments. It simulates the vertical loading applied to soils in the field, including the overburden and changes in vertical stress due to constructions. As shown in Fig. 4, the soil sample, which is confined in a stiff ring, is loaded axially. The stiff ring prevents the sample from expanding radially, a condition which prevails for the soil element under the tank of Fig. 1b. Except for the axial strain ϵ_z , all strain components are assumed to be equal to zero:

$$\epsilon_x = \epsilon_y = \gamma_{xy} = \gamma_{yz} = \gamma_{zx} = 0 \tag{5}$$

During the consolidation test, the axial stress σ_z is varied in abrupt steps, and the resulting variation of ϵ_z is measured with time. The excess pore pressure generated by these abrupt loads dissipates gradually with time. The effective stress path, which cannot be represented exactly because the effective lateral stress is not measured, is assumed to be similar to the K_0 stress path.



Figure 4 Consolidation cell, and strains and stresses applied to samples during the confined compression test.

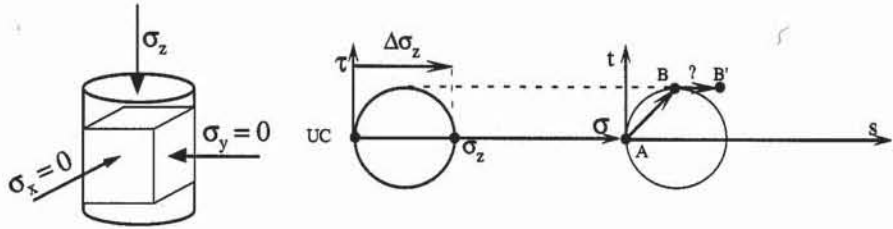


Figure 5 Stresses acting on sample, and stress paths in $\sigma - \tau$ and $s - t$ spaces during unconfined compression tests.

Unconfined Compression Test

The *unconfined compression test* (see Chapters 7-2 and 7-3) is a rapid means to obtain approximate values of the shear strength of fine-grained soils. As shown in Fig. 11, the total axial stress σ_z is applied to the sample which has no radial confinement. The total stresses are all equal to zero, except for axial stress σ_z :

$$\sigma_x = \sigma_y = \tau_{xy} = \tau_{yz} = \tau_{zx} = 0 \tag{6}$$

Figure 5 shows the stress paths in $\sigma - \tau$ and $s - t$ spaces. The Mohr circle expands about A with σ_z . The effective stress path cannot be represented because the initial and excess pore pressures are undefined.

Direct Shear Test

The *direct shear test* (see Chapters 7-4 and 7-5) simulates the effects of shear loads acting on a predetermined failure surface (e.g., the circular failure surface under the embankment of Fig. 1f). As shown in Fig. 6, the soil sample which is confined by two rigid boxes is subjected to the normal load N , and is sheared by the shear force T . If A is the area of surface CD , the shear stress acting on CD is $\tau_{xz} = T/A$, and the normal stress is $\sigma_z = N/A$. The stress path or Mohr circle cannot be drawn because σ_x is not defined. The strains are not uniform, and cannot be measured. The direct shear test is useful to determine the shear strength of soils, but not their stress-strain response.

As shown in Fig. 7a, the predecessor of the direct shear device—the double direct shear apparatus—was initially devised by Collin in 1846. The soil is placed in a split box, the central part of which is sheared by hanging weights. In the torsional direct shear test of Fig. 7b, the soil sample fills an annulus confined between two hollow annular caps. The torsional direct shear device allows us to apply larger shear displacement than the direct shear apparatus because the area of the shear surface remains constant.

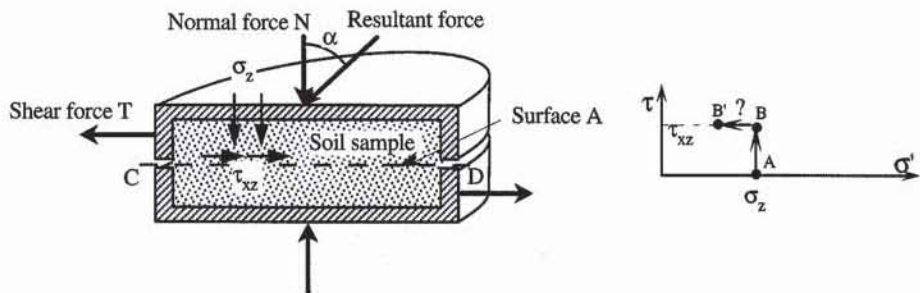


Figure 6 Direct shear cell and variation of stress on surface CD .

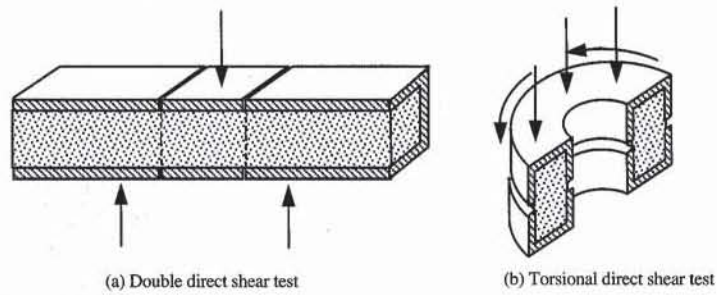


Figure 7 Double and torsional direct shear devices.

Triaxial Test

The *triaxial test* (see Chapters 7-6 and 7-8) is one of the most reliable and useful laboratory tests for determining the stress-strain-strength characteristics of soils. It is more reliable than the unconfined compression test and direct shear test.

As shown in Fig. 8, the cylindrical soil specimen is encased within a rubber sleeve. The lower and upper caps are equipped with porous disks, and are connected to the drainage system. The lateral stress σ_3 is applied by adjusting the confining pressure inside the triaxial chamber, and the axial stress σ_1 is applied by pushing the piston.

The triaxial test is *unconsolidated* or *consolidated*, depending on whether the soil sample is consolidated or not before being sheared. During the consolidation phase, the stresses are increased gradually to recreate the initial stresses of specimens in the field. The samples can be isotropically or K_0 consolidated.

During the shear phase following the consolidation phase, the stresses are varied to simulate the loadings applied to soils by constructions. The shear phase may be either drained or undrained. The test is *drained* when the drainage valves (*A* and *B* in Fig. 8) are open, so that water can drain without change in pore pressure. The test is *undrained* when the drainage valves are closed, so no water is allowed to drain from the sample. During undrained tests, there is excess pore pressure, and the total and effective stresses do not coincide. During drained tests, there is no pore pressure, and effective and total stresses are equal.

To summarize the consolidation and shear phases, the triaxial tests are labeled by using several letters including C or U for the consolidation phase (*Consolidated* or *Unconsolidated*), and D or U for drainage conditions during the shear phase (*Drained* or *Undrained*). Table 1 identifies additional tests, which combine several possible types of consolidation (none, isotropic, or K_0), drainage conditions (drained or undrained), and variation of axial and lateral stresses (constant, increasing or decreasing). Drained tests are always consolidated.

The axial stress σ_1 and lateral stress σ_3 acting on the triaxial sample can be decreased, increased, or kept constant separately. This produces the $s - t$ stress paths of Fig. 9 which are referred to as *Triaxial Compression* (TC), *Lateral Extension* (LE), *Triaxial Extension* (TE), and *Lateral Compression* (LC). Hereafter we describe only the stress paths during triaxial tests with isotropic consolidation. Those with K_0 consolidated triaxial tests have already been shown in Fig. 1.

During the isotropically consolidated triaxial compression (TC), the axial stress σ_z is increased while the radial stress $\sigma_x = \sigma_y$ is kept constant:

$$\sigma_x = \sigma_y = \sigma_c, \quad \text{and} \quad \tau_{xy} = \tau_{yz} = \tau_{zx} = 0 \quad (7)$$

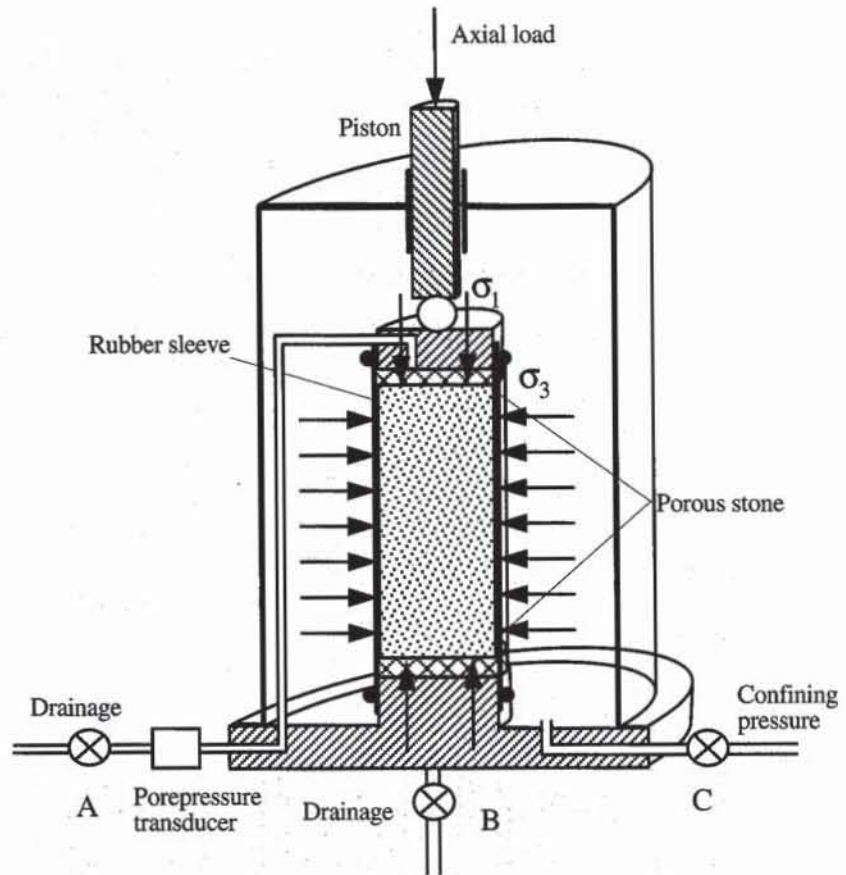


Figure 8 Experimental setup of triaxial test.

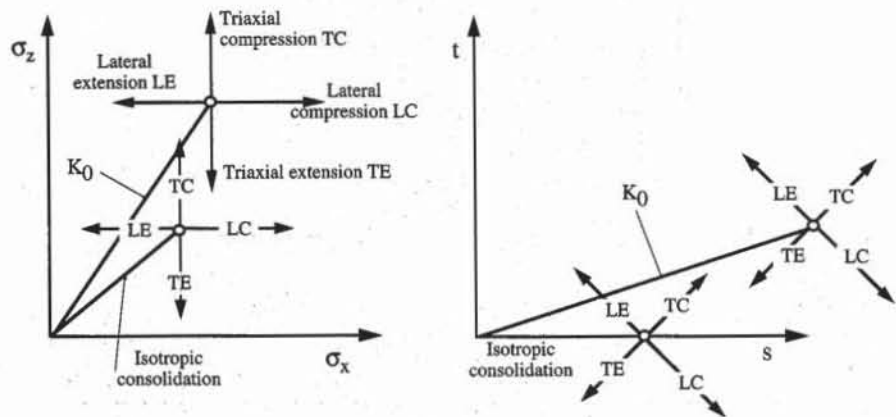


Figure 9 Stress paths in $\sigma_x - \sigma_z$ and $s - t$ spaces during isotropically and K_0 consolidated triaxial compression (TC), triaxial extension (TE), lateral triaxial compression (LC), and lateral triaxial extension (LE).

TABLE 1

Various types of triaxial test

Appellations	Type of consolidation	Drainage conditions	Axial stress	Lateral stress	Full name
CD, CID, or CIDC	Isotropic	Drained	Increasing	Constant	Consolidated drained triaxial compression
CDE, or CIDE	Isotropic	—	Decreasing	—	Consolidated drained triaxial extension
CK ₀ DC	K ₀	—	Increasing	—	K ₀ consolidated drained triaxial compression
CK ₀ DE	K ₀	—	Decreasing	—	K ₀ consolidated drained triaxial extension
CDLC or CIDLC	Isotropic	—	Constant	Increasing	Consolidated drained lateral triaxial compression
CDLE or CIDLE	Isotropic	—	—	Decreasing	Consolidated drained lateral triaxial extension
CK ₀ DLC	K ₀	—	—	Increasing	K ₀ consolidated drained lateral triaxial compression
CK ₀ DLE	K ₀	—	—	Decreasing	K ₀ consolidated drained lateral triaxial extension
CU, CIU, or CIUC	Isotropic	Undrained	Increasing	Constant	Consolidated undrained triaxial compression
CK ₀ U or CK ₀ UC	K ₀	—	Increasing	Constant	K ₀ consolidated undrained triaxial compression
CUE or CIUE	Isotropic	—	Decreasing	Constant	Consolidated undrained triaxial extension
CK ₀ UE	K ₀	—	Decreasing	Constant	K ₀ consolidated undrained triaxial extension
CULC or CIULC	Isotropic	—	Constant	Increasing	Consolidated undrained lateral triaxial compression
CULE or CIULE	Isotropic	—	—	Decreasing	Consolidated undrained lateral triaxial extension
CK ₀ ULC	K ₀	—	—	Increasing	K ₀ consolidated undrained lateral triaxial compression
CK ₀ ULE	K ₀	—	—	Decreasing	K ₀ consolidated undrained lateral triaxial extension
UU or UUC	None	—	Increasing	Constant	Unconsolidated undrained triaxial compression
UUE	None	—	Decreasing	Constant	Unconsolidated undrained triaxial extension

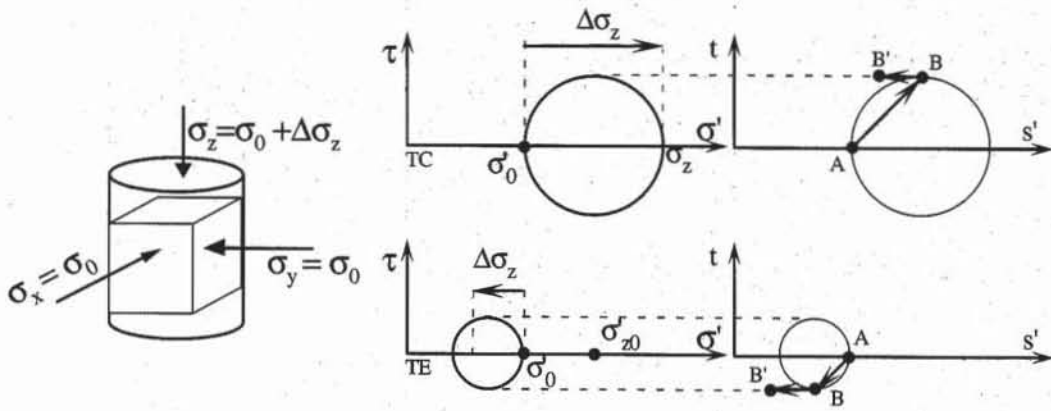


Figure 10 Stress changes applied to samples and stress paths in $\sigma' - \tau$ and $s' - t$ spaces during isotropically consolidated drained and undrained triaxial compression (TC) and extension (TE) tests.

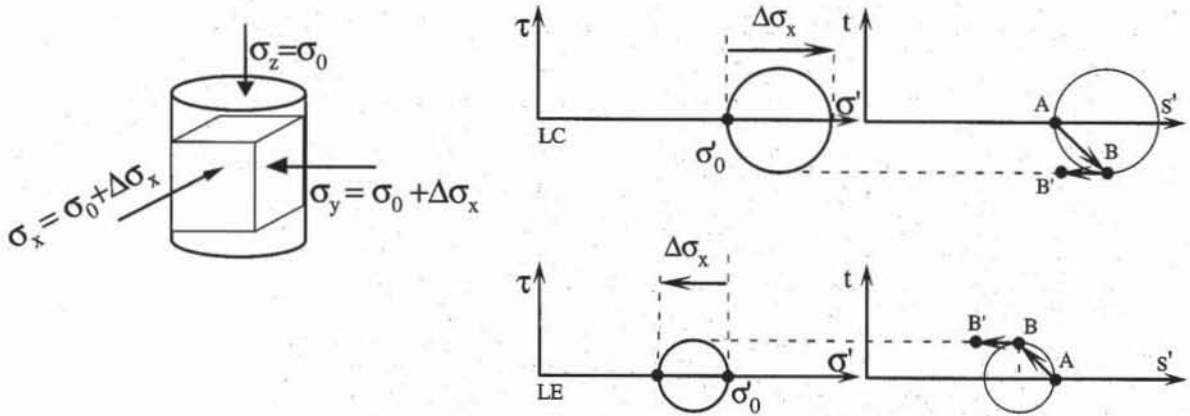


Figure 11 Stress changes applied to samples and stress paths in $\sigma' - \tau$ and $s' - t$ spaces during isotropically consolidated drained and undrained lateral triaxial compression (LC) and extension (LE) tests.

Equation 7 also holds during triaxial extension (TE), in which the axial stress σ_z is decreased. Figure 10 shows the TC and TE stress paths in $\sigma' - \tau$ and $s' - t$ spaces. Point A represents the initial stress state, segment AB the change in total stress, and segment AB' the change in effective stress. B and B' coincide for drained tests, but differ for undrained tests due to excess pore pressure. For both loadings, the Mohr circle varies with σ'_z but keeps a fixed point (i.e., $\sigma'_x = \sigma'_y = \sigma_0$). The $s' - t$ stress paths follow a straight line inclined at 45° .

Equation 7 applies also to lateral triaxial extension (LE) and lateral triaxial compression (LC), in which the axial stress σ_z is kept constant while the radial stress $\sigma_x = \sigma_y$ varies. Figure 11 shows the LC and LE stress paths in $\sigma' - \tau$ and $s' - t$ spaces. The $s' - t$ stress paths follow a straight line inclined at -45° .

Simple Shear Test

The *simple shear test* is an improved version of the direct shear test, which generates uniform stress and strain and is suitable for determining the stress-strain re-

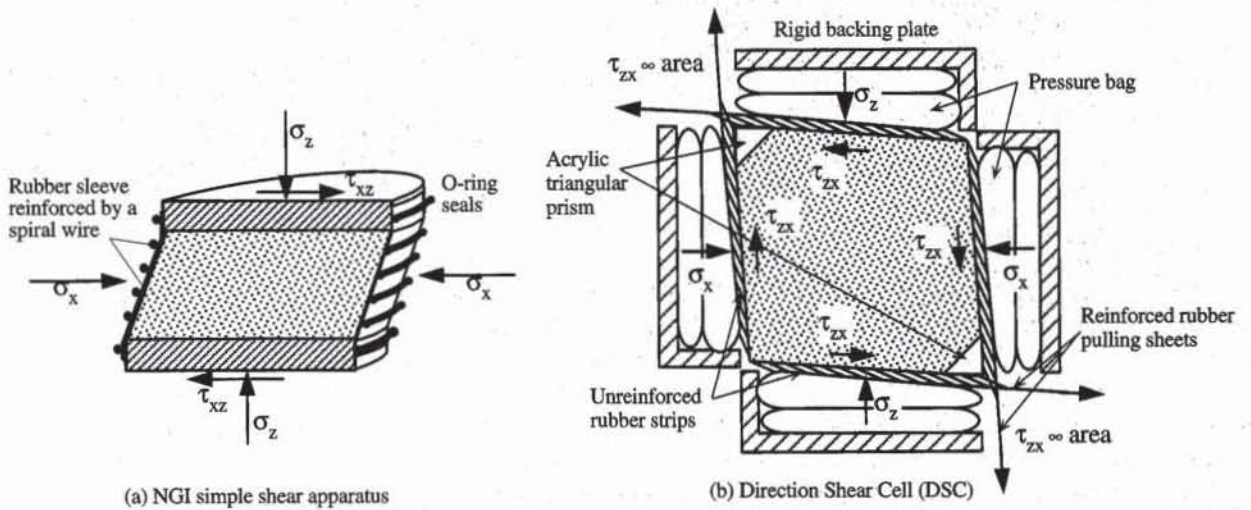


Figure 12 Simple shear devices.

sponse of soils. In the simple shear apparatus of Fig. 12a, the cylindrical sample is confined in a rubber sleeve reinforced by a spiral wire. The confining pressure is transmitted to the soil sample through the rubber sleeve. The spiral wire prevents the sample from expanding radially, but not from being sheared.

Like the triaxial test, the simple shear test has a consolidation and shear phase. During the shear phase, σ_x , σ_y , and σ_z are kept equal to σ_0 and the shear stress τ_{yz} is increased:

$$\sigma_x = \sigma_y = \sigma_z = \sigma_0, \text{ and } \tau_{xy} = \tau_{xz} = 0 \tag{8}$$

Figure 13 shows the corresponding stress path in $\sigma - \tau$ and $s - t$ spaces.

In the simple shear device of Fig. 12b, also referred to as direct simple shear (Arthur et al., 1981), the rectangular sample is confined between two rigid boundaries, and four flexible boundaries. The normal stresses σ_x and σ_z are applied by pressure bags. The shear stress τ_{xz} is applied by rubber strips attached to pulling sheets. There is no deformation in the y direction (i.e., $\epsilon_y = 0$), a condition which is known as plane strain. As shown in Fig. 12b, the controlled variation of lateral and shear stresses allows one to vary the orientation of the principal stresses.

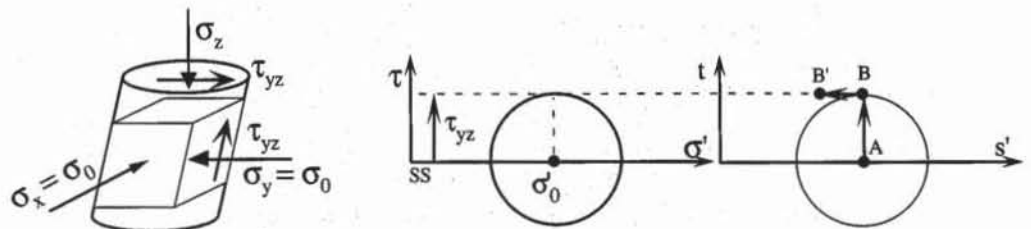


Figure 13 Strains applied to samples, and stress paths in $\sigma - \tau$ and $s' - t$ spaces during the simple shear test of Fig. 12a.

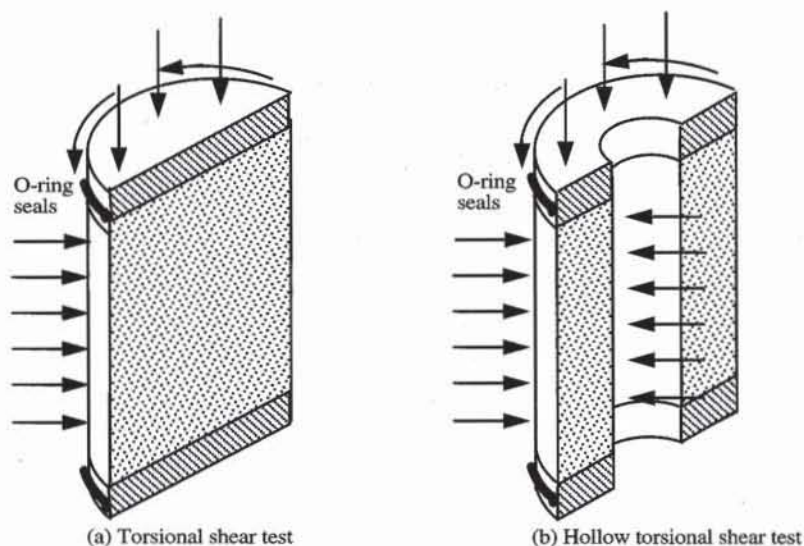


Figure 14 Torsional shear devices.

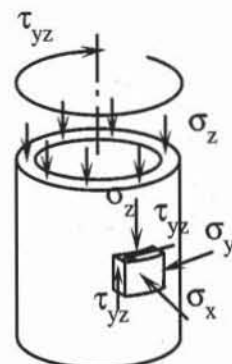


Figure 15 State of stress in hollow torsional apparatus (after Saada and Townsend, 1981).

Torsional Test

In the *torsional shear test* of Fig. 14a, the soil cylinder is subjected to a twisting moment, which is applied through the ribbed top and bottom caps. The lateral confining pressure is applied to the specimen through the flexible rubber sleeve. The *hollow torsional device* of Fig. 14b is an improved version of the torsional device which maintains uniform strain across the specimen. There are inner and outer rubber sleeves that transmit the lateral pressure to both sides of the hollow soil specimen. As shown in Fig. 15, the axial and lateral stress and shear stress can be controlled in the hollow cylinder, which allows one to incline the orientation of the principal stresses. (Saada and Townsend, 1981).

Plane Strain Compression Test

Plane strain experiments (e.g., Fig. 12b) are used to determine the properties of soils under plane-strain conditions (i.e., $\epsilon_y = 0$), which are found in the analysis of very long structures. Figure 16 shows another example of a plane strain apparatus where the soil sample which is encased in a flexible membrane is confined between two parallel glass plates and two loading platens.

True Triaxial Apparatus

The *true triaxial apparatus* allows one to control independently the *three* normal stresses applied to cubical samples of soils. The term "true" is used to avoid confusion with the triaxial test which controls only stresses along two axes. Figure 17 shows the principle of a true triaxial apparatus with rigid platens. The cubical soil sample is encased in a rubber membrane. The six platens are activated by mechanical means so that they generate a rectangular shape. There is also an apparatus with a flexible membrane and a combination of both (e.g., Lade and Duncan, 1973). The true triaxial apparatus is a research tool which has been used to investigate three-dimensional soil behavior. It is rarely used in the practice of geotechnical engineering.

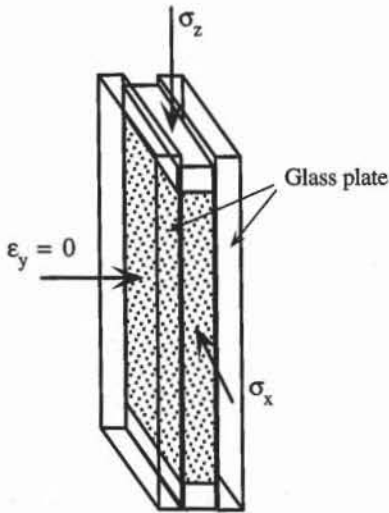


Figure 16 Plane strain compression apparatus.

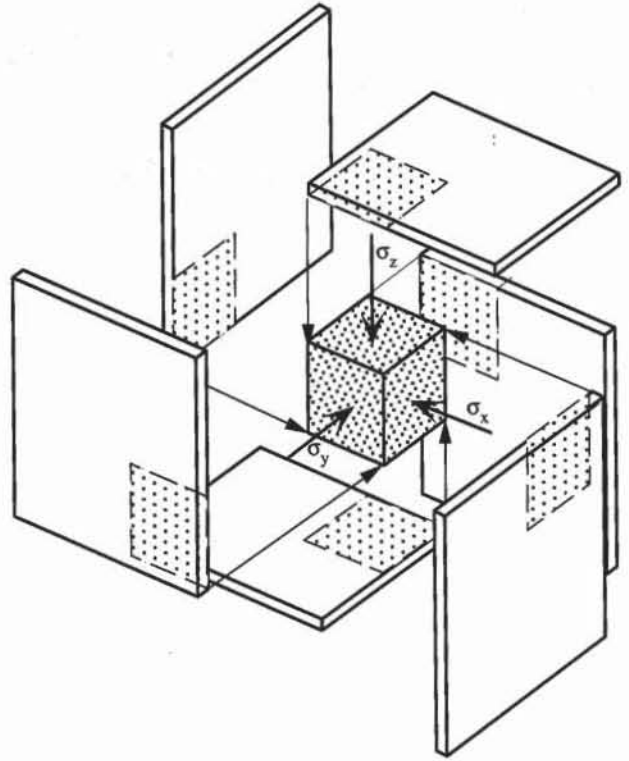


Figure 17 True triaxial apparatus with rigid platens.

REFERENCES

- ARTHUR, J. R. F., S. BEKENSTEIN, J. T. GERMAINE, and C. C. LADD, 1981, Stress path with controlled rotation of principal stress directions, in *Laboratory Shear Strength of Soils, ASTM Special Technical Publication 740*, R. N. Yong and F. C. Townsend, eds., American Society for Testing and Materials, Philadelphia, PA.
- COLLIN, A., 1856, *Experimental Investigation on Sliding in Clay Slopes*, Translated from French by W. R. Schriever, University of Toronto Press, 1956, Toronto, Canada.
- LADE, P. V., and J. M. DUNCAN, 1973, Cubical triaxial tests on cohesionless soils, *J. Soil Mech. Found. Eng. Div., ASCE*, Vol. 99, No. 10, pp. 793-812.
- SAADA, A. S., and F. C. TOWNSEND, 1981, State-of-the-Art: Laboratory strength testing of soils, in *Laboratory Shear Strength of Soils, ASTM Special Technical Publication 740*, R. N. Yong and F. C. Townsend, eds., American Society for Testing and Materials, Philadelphia, PA, pp. 7-77.

5-5

Elastic Properties of Soils

Many constitutive models have been proposed to describe the behavior of soils observed in the laboratory. Linear isotropic elasticity is certainly the most elementary and convenient stress-strain relationship to use for describing the deformation of soils before they fail.

ELASTICITY AND ELASTIC PROPERTIES

The isotropic linearly-elastic stress-strain relationship (or generalized Hooke's law) is defined as follows:

$$\begin{aligned}\varepsilon_x &= \frac{1}{E}(\sigma_x - \nu(\sigma_y + \sigma_z)) & \varepsilon_{xy} &= \frac{\tau_{xy}}{2G} \\ \varepsilon_y &= \frac{1}{E}(\sigma_y - \nu(\sigma_z + \sigma_x)) & \text{and } \varepsilon_{yz} &= \frac{\tau_{yz}}{2G} \\ \varepsilon_z &= \frac{1}{E}(\sigma_z - \nu(\sigma_x + \sigma_y)) & \varepsilon_{xz} &= \frac{\tau_{xz}}{2G}\end{aligned}\quad (1)$$

where E is Young's modulus, ν the Poisson ratio, and G the shear modulus $= \frac{E}{2(1+\nu)}$. Equation 1 can be inverted so that the stresses are functions of strains:

$$\begin{aligned}\sigma_x &= \lambda \varepsilon_v + 2G\varepsilon_x & \tau_{xy} &= 2G\varepsilon_{xy} \\ \sigma_y &= \lambda \varepsilon_v + 2G\varepsilon_y & \text{and } \tau_{yz} &= 2G\varepsilon_{yz} \\ \sigma_z &= \lambda \varepsilon_v + 2G\varepsilon_z & \tau_{xz} &= 2G\varepsilon_{xz}\end{aligned}\quad (2)$$

where ε_v is the volumetric strain ($\varepsilon_v = \varepsilon_x + \varepsilon_y + \varepsilon_z$), and λ is Lamé's modulus $\left(\lambda = \frac{\nu E}{(1+\nu)(1-2\nu)}\right)$. Using Eq. 1, the mean pressure p is proportional to ε_v :

$$p = \frac{1}{3}(\sigma_x + \sigma_y + \sigma_z) = B\epsilon_v \tag{3}$$

where B is the bulk modulus ($B = \frac{E}{3(1-2\nu)}$). An additional elastic constant—the constrained modulus M —relates axial strain and stress during a confined compression test where $\epsilon_x = \epsilon_y = 0$:

$$\sigma_z = M\epsilon_z \quad \text{and} \quad M = \frac{E(1-\nu)}{(1+\nu)(1-2\nu)} \tag{4}$$

For isotropic linearly elastic materials, there are six material constants: E , ν , G , λ , B , and M . However, there are only two independent constants. The moduli E , ν , G , λ , B and M can be expressed in terms of two other moduli as given in Table 1.

TABLE 1
Relations among elastic moduli E , G , B , ν , λ , and M

	Shear modulus G	Young's modulus E	Constrained modulus M	Bulk modulus B	Lame modulus λ	Poisson ratio ν
G, E	G	E	$\frac{G(4G-E)}{3G-E}$	$\frac{GE}{9G-3E}$	$\frac{G(E-2G)}{3G-E}$	$\frac{E-2G}{2G}$
G, M	G	$\frac{G(3M-4G)}{M-G}$	M	$M - \frac{4}{3}G$	$M - 2G$	$\frac{M-2G}{2(M-G)}$
G, B	G	$\frac{9GB}{3B+G}$	$B + \frac{4}{3}G$	B	$B - \frac{2}{3}G$	$\frac{3B-2G}{2(3B+G)}$
G, λ	G	$\frac{G(3\lambda+2G)}{\lambda+G}$	$\lambda + 2G$	$\lambda + \frac{2}{3}G$	λ	$\frac{\lambda}{2(\lambda+G)}$
G, ν	G	$2G(1+\nu)$	$\frac{2G(1-\nu)}{1-2\nu}$	$\frac{2G(1+\nu)}{3(1-2\nu)}$	$\frac{2G\nu}{1-2\nu}$	ν
E, B	$\frac{3BE}{9B-E}$	E	$\frac{B(9B+3E)}{9B-E}$	B	$\frac{B(9B-3E)}{9B-E}$	$\frac{3B-E}{6B}$
E, ν	$\frac{E}{2(1+\nu)}$	E	$\frac{E(1-\nu)}{(1+\nu)(1-2\nu)}$	$\frac{E}{3(1-2\nu)}$	$\frac{\nu E}{(1+\nu)(1-2\nu)}$	ν
B, λ	$\frac{3}{2}(B-\lambda)$	$\frac{9B(B-\lambda)}{3B-\lambda}$	$3B - 2\lambda$	B	λ	$\frac{\lambda}{3B-\lambda}$
B, M	$\frac{3}{4}(M-B)$	$\frac{9B(M-B)}{3B+M}$	M	B	$\frac{3B-M}{2}$	$\frac{3B(2M-1)+M}{3B(2M+1)-M}$
B, ν	$\frac{3B(1-2\nu)}{2(1+\nu)}$	$3B(1-2\nu)$	$\frac{3B(1-\nu)}{1+\nu}$	B	$\frac{3B\nu}{1+\nu}$	ν

Homogeneity and Isotropy

Equation 1 assumes that the samples are homogeneous and isotropic. *Homogeneity* specifies that the elastic properties are the same everywhere in the laboratory samples. This assumption holds for uniform samples with particles relatively small compared to the whole sample, but not for those with heterogeneous composition containing a few large particles. *Isotropy* postulates that the elastic properties are the same in all directions. This assumption applies to remolded laboratory samples constructed under isotropic conditions, but not to the soil samples which acquired directional, laminated and varved structures during their natural

deposition and stress history in the field. In this case, it may be preferable to use anisotropic, instead of isotropic, elasticity (see Chen and Seeb, 1982) to describe their directional behavior, at the cost of determining additional soil properties. Hereafter, we only use the isotropic linearly-elastic model and assume homogeneous samples. Homogeneity and isotropy are convenient assumptions to characterize the deformation properties of soils with a minimum number of parameters.

ELASTIC RESPONSES IN CONVENTIONAL LABORATORY TESTS

The relations of elasticity can be simplified in the case of soil laboratory tests introduced in Chapter 5-3, namely, the isotropic, consolidation, triaxial, unconfined compression, and simple shear tests.

Isotropic Test

For the isotropic test (Eq. 3.5-4), Eq. 1 gives the following elastic strains:

$$\epsilon_x = \epsilon_y = \epsilon_z = \frac{1 - 2\nu}{E} \sigma_c \quad (5)$$

where σ_c is the applied pressure. Equation 5 implies that ϵ_v and σ_c are linearly related through

$$\epsilon_v = \epsilon_x + \epsilon_y + \epsilon_z = \frac{3(1 - 2\nu)}{E} \sigma_c = \frac{1}{B} \sigma_c \quad (6)$$

where B is the bulk modulus. As shown in Fig. 1, Eq. 6 predicts a linear relation between σ_c and ϵ_v , while experiments generally produce nonlinear relations. The experimental response can be fitted with straight lines, either tangent at the origin, which produces the initial bulk modulus B_i , or over a larger range of pressure, which gives the secant bulk modulus B_s . Only B can be measured in the isotropic test. E and ν cannot be defined individually.

Figure 2 shows the experimental response of the dense Sacramento River sand during an isotropic loading ABD, and two cycles of unloading - reloading BCB and DED. The response during loading is softer than that during the cycles of unloading and reloading. The straight lines defined by B_i and B_s crudely approximate the nonlinear stress-strain response. As shown in Fig. 3, B_s is calculated at points A, C and E of Fig. 2 for the loading and unloading - reloading cycles. B_s approximately increases with the square root of pressure.

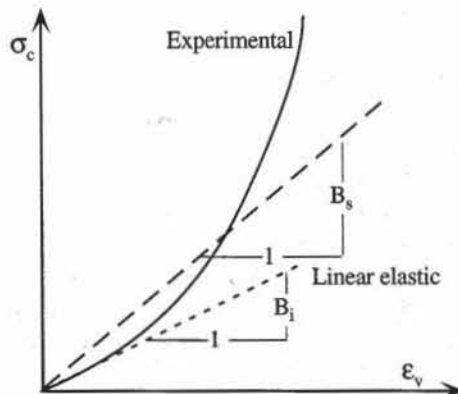


Figure 1 Experimental response, and initial and secant bulk moduli during an isotropic test.

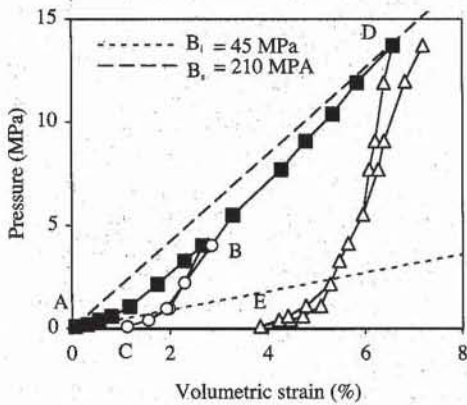


Figure 2 Experimental stress-strain response, initial and secant bulk moduli during isotropic loading (solid points) and two cycles of unloading - reloading (hollow points) on dense Sacramento River sand (data after Lee and Seed, 1967).

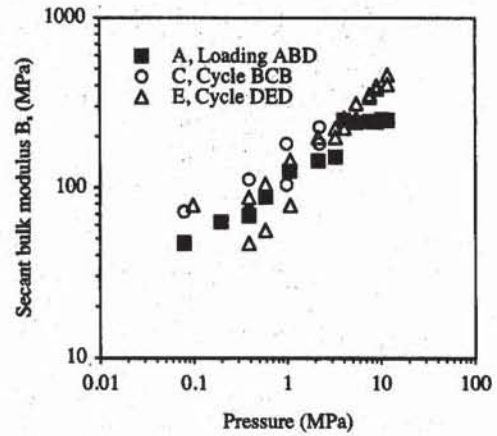


Figure 3 Variation of secant bulk modulus B_s with pressure at points A, C, and E for the test of Fig. 2.

Unconfined Compression Test

For the unconfined compression test (Eq. 6.5-4), Eq. 1 implies that σ_z and ϵ_z are linearly related and gives the following elastic strains,

$$\epsilon_z = \frac{1}{E} \sigma_z, \epsilon_x = \epsilon_y = -\frac{\nu}{E} \sigma_z = -\nu \epsilon_z \tag{7}$$

As shown in Fig. 4, the experimental response may be approximated by drawing a straight line through the origin to obtain the initial Young's modulus E_i , or over a larger strain range to get a secant Young's modulus E_s . Figure 5 shows the measured response of a remolded clay during the unconfined compression test ($E_i = 4$ MPa, and $E_s = 0.5$ MPa at $\epsilon_z = 16\%$). As shown in Fig. 6, E_s decreases gradually from E_i to zero with ϵ_z . The Poisson ratio ν cannot be calculated from the unconfined compression test.

Drained Triaxial Compression Test

It is convenient to reset the stresses and strains to zero at the beginning of shear, and to introduce the stress changes $\Delta\sigma_x$, $\Delta\sigma_y$, and $\Delta\sigma_z$:

$$\Delta\sigma_x = \sigma'_x - \sigma_0, \Delta\sigma_y = \sigma'_y - \sigma_0, \text{ and } \Delta\sigma'_z = \sigma'_z - \sigma_0 \tag{8}$$

where σ_0 is the confining pressure. Equation 9.5-4 implies that $\Delta\sigma_x = \Delta\sigma_y = 0$. Using Eq. 8, the triaxial test gives the same elastic strain and linear relations as the unconfined compression:

$$\epsilon_z = \frac{1}{E} \Delta\sigma_z, \epsilon_x = \epsilon_y = -\frac{\nu}{E} \Delta\sigma_z = -\nu \epsilon_z \tag{9}$$

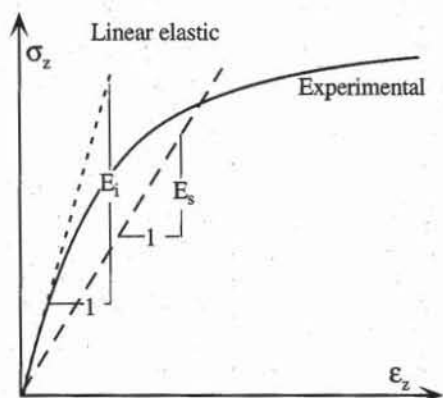


Figure 4 Experimental stress-strain response, and initial and secant Young's moduli during an unconfined compression test.

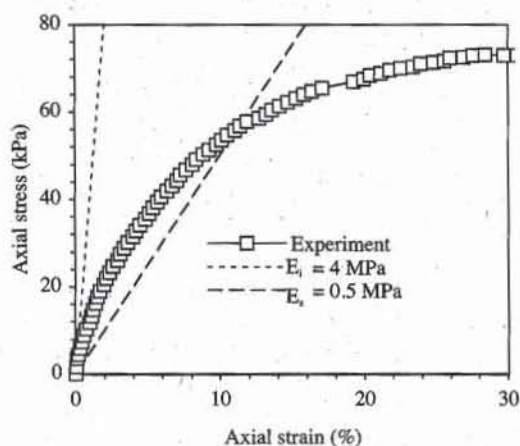


Figure 5 Measured stress-strain response, initial and secant Young's moduli during unconfined compression of remolded Aardvack clay.

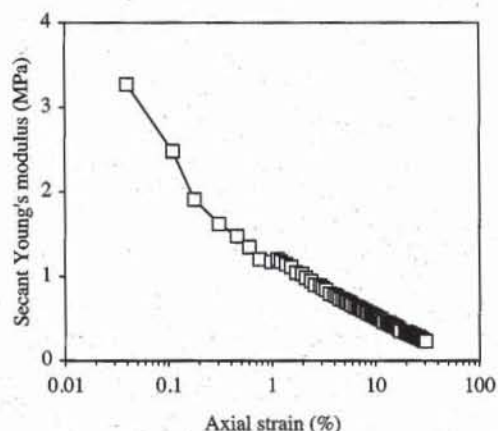


Figure 6 Variation of secant Young's modulus E_s versus axial strain in the test of Fig. 5.

and $\epsilon_v = \epsilon_x + \epsilon_y + \epsilon_z = (1 - 2\nu) \epsilon_z$. As shown in Fig. 7, the slope of the theoretical straight line is E for the stress-strain response and $1-2\nu$ for the volumetric response. The experimental response may be approximated with straight lines either tangent at the origin, which produces the initial moduli E_i and ν_i , or over a larger strain range, which gives the secant moduli E_s and ν_s . The volume change of the soil sample is measured directly in the drained triaxial test. For theoretical and practical reasons, the values of ν must be kept between 0 and 0.5.

Figures 8 and 9 show the stress-strain and volumetric responses of dense Sacramento River sand during a drained triaxial compression test at constant confining pressure σ'_3 . As shown in Fig. 9, the axial stress σ'_1 is divided by σ'_3 . The initial moduli are $E_i = 375$ MPa and $\nu_i = 0.25$; and the secant moduli are $E_s = 50$ MPa and $\nu_s = 0.6$ for axial strain $\epsilon_z = 5\%$. As shown in Figs. 10 and 11, E_s decreases from its maximum value E_i with ϵ_z , while ν_s increases from ν_i and exceeds 0.5 when $\epsilon_z > 2\%$. The fact that $\nu_i > 0.5$ is caused by the dilatation of the soil specimen during shear. Due to theoretical considerations, the values of ν_s larger than 0.5 cannot be used in engineering analysis; they would produce negative values for the secant bulk modulus, constrained modulus, and Lamé's modulus (see Table 1).

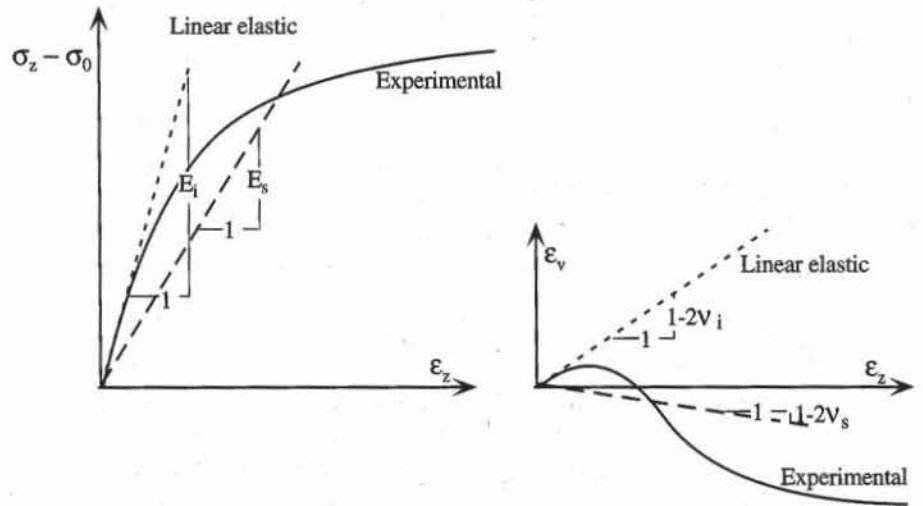


Figure 7 Experimental responses, and initial and secant Young's modulus and Poisson ratio during a drained triaxial compression test.

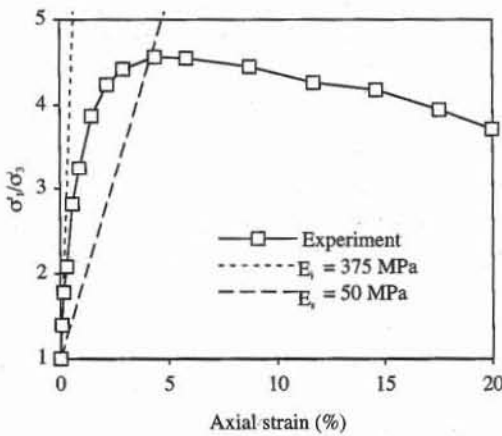


Figure 8 Measured stress-strain response of dense Sacramento River sand, initial and secant Young's moduli during drained triaxial compression at 588 kPa confining pressure (data after Lee and Seed, 1967).

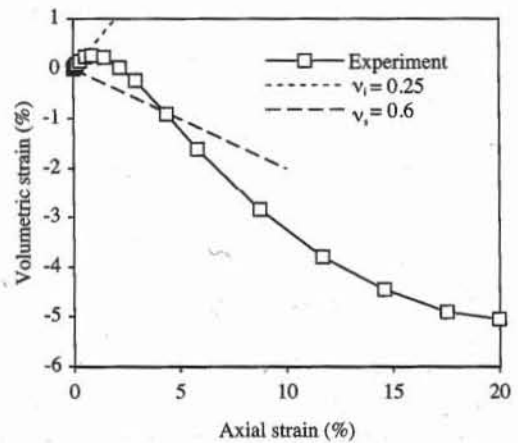


Figure 9 Measured volumetric response of dense Sacramento River sand, initial and secant Poisson ratios during the test of Fig. 8.

Confined Compression Test

For the confined compression test (Eq. 5.5-4), Eq. 1 gives the following elastic strain and linear relations:

$$\epsilon_v = \epsilon_z = \frac{1}{M} \sigma'_z \quad \text{and} \quad M = \frac{E(1 - \nu)}{(1 + \nu)(1 - 2\nu)} \tag{10}$$

$$\sigma'_x = \sigma'_y = K_0^e \sigma'_z \quad \text{and} \quad K_0^e = \frac{\nu}{1 - \nu}$$

where K_0^e is the elastic coefficient of lateral earth pressure at rest, and M is the constrained modulus.

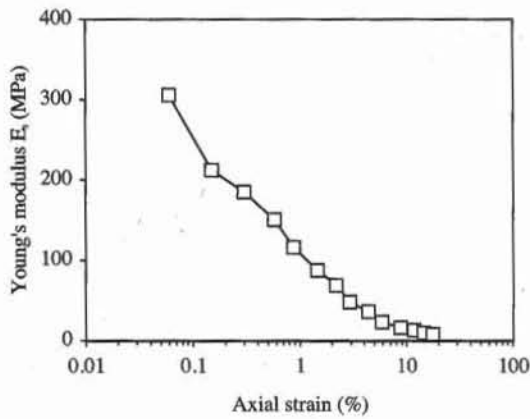


Figure 10 Variation of secant Young's modulus with axial strain in the test of Fig. 8.

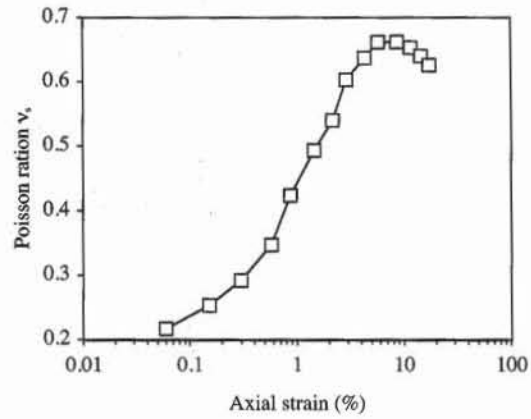


Figure 11 Variation of secant Poisson ratio with axial strain in the test of Fig. 8.

As shown in Fig. 12, the initial constrained modulus M_i and secant modulus M_s approximate the experimental response at the origin, and over a larger strain range, respectively. Figure 13a shows the measured stress-strain response of San Francisco Bay mud subjected to confined compression test. $M_i = 0.14$ MPa, and $M_s = 0.09$ MPa at $\epsilon_z = 25\%$. As shown in Fig. 13b, M_s first decreases then increases with axial strain, due to an increase in radial stress.

Simple Shear Test

For the simple shear test (Eq. 8.5-4), Eq. 1 gives the following elastic strain and linear relations:

$$\gamma_{yz} = \frac{1}{G} \tau_{yz}, \quad \text{and} \quad \epsilon_x = \epsilon_y = \epsilon_z = \gamma_{xz} = \gamma_{xy} = 0 \quad (11)$$

where G is the elastic shear modulus.

As shown in Fig. 14, the initial shear modulus G_i and secant shear modulus G_s approximate the experimental response at the origin, and over a larger strain range, respectively.

TYPICAL VALUES OF ELASTIC CONSTANTS

Tables 2 to 4 list typical ranges of values of Young's modulus E and Poisson ratio ν for various soils, rocks, and other materials.

The values of E for rocks in Table 2 are computed at confining pressures between 300 and 500 MPa. E varies from 7 GPa for partially decomposed granite to 200 GPa for steel. In contrast to rocks and metals, soils have a much broader range of E values. In Table 3, the lowest values for E (0.4 MPa) are observed for soft clay and peat; the largest (1.4 GPa) for dense gravels and glacial till. Loose sands, silts and clays have generally smaller values of E than rocks. However, dense gravels and hard clays may have values of E similar to those of weathered and decomposed sedimentary rocks. The values of elastic properties listed in Tables 2 and 3 should be considered as estimates that may vary widely from actual values. The elastic properties of soils are influenced by a number of factors, which

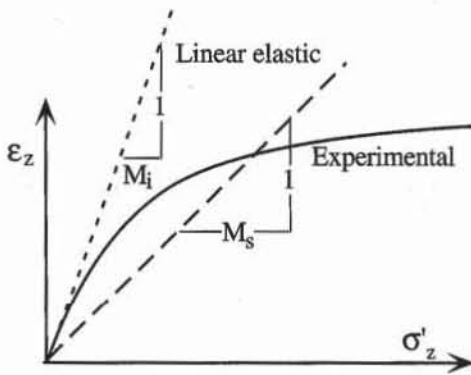


Figure 12 Experimental responses, initial and secant constrained moduli during a confined compression test.

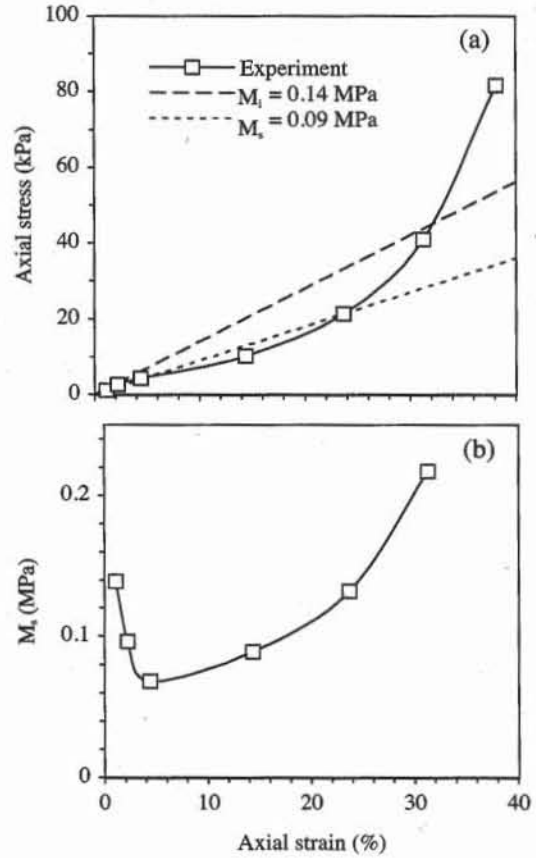


Figure 13 Results of confined compression of San Francisco Bay mud: (a) measured stress-strain response, initial and secant constrained moduli, and (b) variation of secant constrained modulus M_s with axial strain (data after Holtz and Kovacs, 1981).

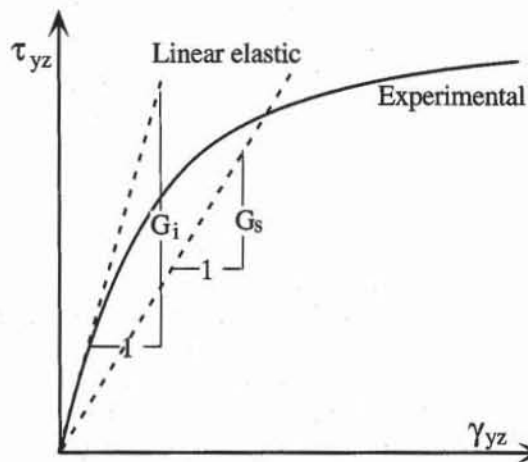


Figure 14 Experimental responses, initial and secant shear moduli during a simple shear test.

TABLE 2

Values of Young's modulus and Poisson ratio for various materials.

Material	Young's modulus (GPa)	Poisson ratio	References
Amphibolite	93-121	0.28-0.30	Lambe and Whitman (1979)
Anhydrite	68	0.30	—
Diabase	87-117	0.27-0.30	—
Diorite	75-108	0.26-0.29	—
Dolomite	110-121	0.30	—
Dunite	149-183	0.26-0.28	—
Feldspathic Gneiss	83-118	0.15-0.20	—
Gabbro	89-127	0.27-0.31	—
Granite	73-86	0.23-0.27	—
Limestone	87-108	0.27-0.30	—
Marble	87-108	0.27-0.30	—
Mica Schist	79-101	0.15-0.20	—
Obsidian	65-80	0.12-0.18	—
Oligoclaseite	80-85	0.29	—
Quartzite	82-97	0.12-0.15	—
Rock salt	35	0.25	—
Slate	79-112	0.15-0.20	—
Ice	7.1	0.36	—
Aluminium	55-76	0.34-0.36	—
Steel	200	0.28-0.29	—
Granite sound	31-57	0.15-0.24	Converse (1962)
Granite partially decomposed	7-14	0.15-0.24	—
Limestone	21-48	0.16-0.23	—
Sound, intact igneous and metamorphics	57-96	0.25-0.33	Hunt (1986)
Sound, intact sandstone and limestone	38-76	0.25-0.33	—
Sound intact shale	10-40	0.25-0.33	—
Coal	10-20	—	—

include type of soil, water content, density, void ratio, fabric anisotropy, temperature, time, stress history, consolidation stress, applied shear stress, initial stress state, rate of strain, degree of sample disturbance, testing conditions, amplitude, and direction of stress changes.

As shown in Table 3, the Poisson ratio ν has a small range of variation (i.e., 0 to 0.45). When $\nu = 0.5$, the material is incompressible, $G = E/3$ and $B \rightarrow \infty$.

Variation of Initial Shear Modulus with Pressure, Overconsolidation Ratio and Void Ratio

Figure 15 shows the variation of secant shear modulus G_s with shear strain amplitude γ which was obtained from resonant column tests on Nevada sand. Resonant column tests are dynamic tests which are described in Kramer (1996). During these dynamic tests, G_s is first equal to the initial modulus G_i , which is also referred to as G_{\max} , then decreases when γ exceeds 0.001%.

As shown in Fig. 16, G_{\max} varies with the mean effective pressure p' [$p' = (\sigma'_1 + \sigma'_2 + \sigma'_3)/3$]. Several empirical models have been proposed for the initial shear modulus G_{\max} . Hardin and Drnevich (1972) and Hardin (1978) proposed that

$$G_{\max} = \frac{198}{0.3 + 0.7e^2} OCR^k \sqrt{p'} \quad (\text{MPa}) \quad (11)$$

TABLE 3

Approximate values of Young's modulus in MPa for various soils

Soil group	Soil type	Bowles (1988)	Cernica (1995)	Converse (1962)	Hallam et al. (1978)	Hunt (1986)
Organic soil	Muck	—	—	0.5–3.5	—	—
	Peat	—	—	—	0.4–1	—
		—	—	—	0.8–2	—
Clay	Very soft	2–15	—	—	—	—
	Soft	2–25	3	—	1–3	2–4
	Medium	15–50	7	—	—	—
	Stiff	—	—	—	2.5–5	8–19
	Weak plastic	—	—	1.4–4	—	—
	Stiff plastic	—	—	4.2–8	—	—
	Semi-firm	—	—	—	5–10	—
	Semi-solid	—	—	6.9–14	—	—
	Hard	50–100	14	—	—	8–19
	Sandy	25–250	36	—	—	—
	Boulder clay, solid	—	—	—	30–100	—
Silt	Silt	2–20	—	—	3–10	2–19
	Soft, slightly clayey sea silt	—	—	—	2–5	—
	Soft, very strongly clayey silt	—	—	—	0.5–3	—
	Soft	—	—	—	4–8	—
	Semi-firm	—	—	—	5–20	—
Sand	Loose	10–25	15	10–21	20–80	10–29
	Medium	—	—	—	50–150	29–48
	Dense	50–81	80	52–83	49–78	48–77
	Silty	5–20	—	—	—	—
Gravel	Loose	50–150	100	—	—	29–77
	Dense	100–200	150	102–204	—	96–192
Gravel	Gravel without sand	—	—	—	100–200	—
	Coarse gravel, sharp edged	—	—	—	150–300	—
Loess		14–60	—	—	—	14–58
Glacial till	Loose	10–150	—	—	—	—
	Dense	150–720	—	—	—	—
	Very dense	500–1440	—	—	—	—

Note: Actual values may vary widely from those shown.

TABLE 4

Approximate values of Poisson ratio for various soils

Soil group	Soil type	Bowles (1988)	Cernica (1995)	Converse (1962)	Hunt (1986)	Poulos (1975)
Clay	Soft	—	0.4	—	—	—
	Medium	—	0.3	—	—	0.3–0.35
	Hard	—	0.25	—	—	—
	Stiff plastic	—	—	0.4–0.45	—	—
	Saturated	0.4–0.5	—	—	—	—
	Unsaturated	0.1–0.3	—	—	—	—
	Soft normally consolidated	—	—	—	—	0.35–0.45
	Stiff overconsolidated	—	—	—	—	0.1–0.3
	Sandy	0.2–0.3	0.25	—	—	—
Silt		0.3–0.35	—	—	0.3–0.35	—
Loess		0.1–0.3	—	—	0.1–0.3	—
Sand	Loose	—	0.2	—	0.2–0.35	0.35–0.4
	Medium	—	—	—	—	0.3–0.35
	Dense	0.3–0.4	0.3	0.3–0.36	0.3–0.4	0.25–0.3
Gravel	Loose	—	0.2	—	—	—
	Dense	—	0.3	—	—	—

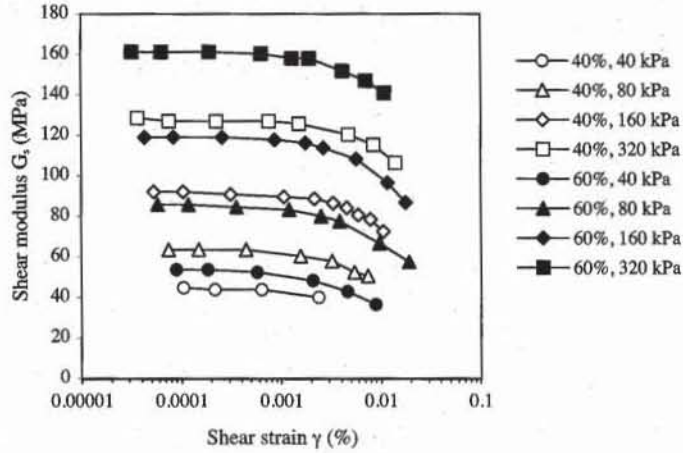


Figure 15 Variation of secant shear modulus G_s with shear strain amplitude during resonant column tests at various confining pressures for Nevada sand at 40 and 60% relative density (data after Arulmoli et al., 1992).

where e is the void ratio, OCR the overconsolidation ratio, k an overconsolidation ratio exponent given in Table 5, and p' the mean effective pressure in MPa. $OCR = p'_{max}/p'$ where p'_{max} is the largest value of p' that the soil underwent in its past. $OCR = 1$ for normally consolidated clay and $OCR > 1$ for overconsolidated soils (see Chapter 6-1). Jamiolkowski et al (1991) suggested that

$$G_{max} = \frac{198}{e^{1.3}} OCR^k \sqrt{p'} \text{ (MPa)} \tag{12}$$

Seed and Idriss (1970) proposed that

$$G_{max} = K \sqrt{p'} \text{ (MPa)} \tag{13}$$

where K is given in Table 6. As shown in Fig. 16, Eqs. 11 to 13 are equally capable of describing the variation of G_{max} for Nevada sand at relative density $D_r = 40$ and 60% ($e = 0.736$ and 0.661), respectively.

TABLE 5
Overconsolidation ratio exponent k (after Hardin and Drnevich, 1972).

Plasticity index (%)	k
0	0.00
20	0.18
40	0.30
60	0.41
80	0.48
≥ 100	0.50

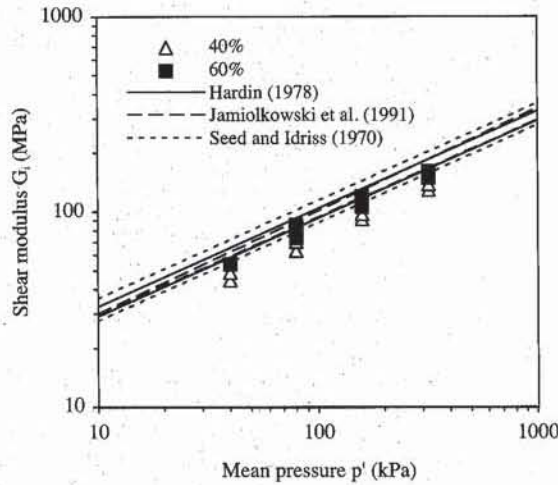


Figure 16 Variation of initial shear modulus G_i with mean effective pressure p' measured in the tests of Fig. 15.

TABLE 6
Estimation of K (adapted from Seed and Idriss, 1970).

e	K	D_r (%)	K
0.4	484	30	235
0.5	415	40	277
0.6	353	45	298
0.7	304	60	360
0.8	270	75	408
0.9	235	90	484

Variation of Elastic Properties with Strain

The variation of shear modulus G with shear strain can also be represented in the static triaxial test conditions by introducing the equivalent shear strain $\epsilon_z - \epsilon_x$. During the triaxial test, Eq. 1 becomes:

$$\frac{1}{2}(\sigma_z - \sigma_x) = G(\epsilon_z - \epsilon_x), \quad \epsilon_x = \epsilon_y, \quad \text{and} \quad \gamma_{xy} = \gamma_{yz} = \gamma_{zx} = 0 \quad (14)$$

where ϵ_x is related to volumetric strain ϵ_v through

$$\epsilon_x = \epsilon_y = \frac{1}{2}(\epsilon_v - \epsilon_z) \quad (15)$$

Based on this definition of equivalent shear strain, the stress-strain relations of Figs. 17a and b have identical slope G and maximum stress. Figure 18 shows the variation of G_s / G_i with axial strain during drained triaxial tests at constant mean pressure p' where G_i is obtained from Fig. 16. The static values of G_s / G_i are not represented for $\epsilon_z - \epsilon_x < 0.02\%$ due to the scatter in data caused by inaccurate measurement of small strain, but are replaced by the dynamic values of G_s / G_i measured during the resonant column test of Fig. 15. The results of Fig. 18 fall within the range of typical values obtained by Seed and Idriss (1970).

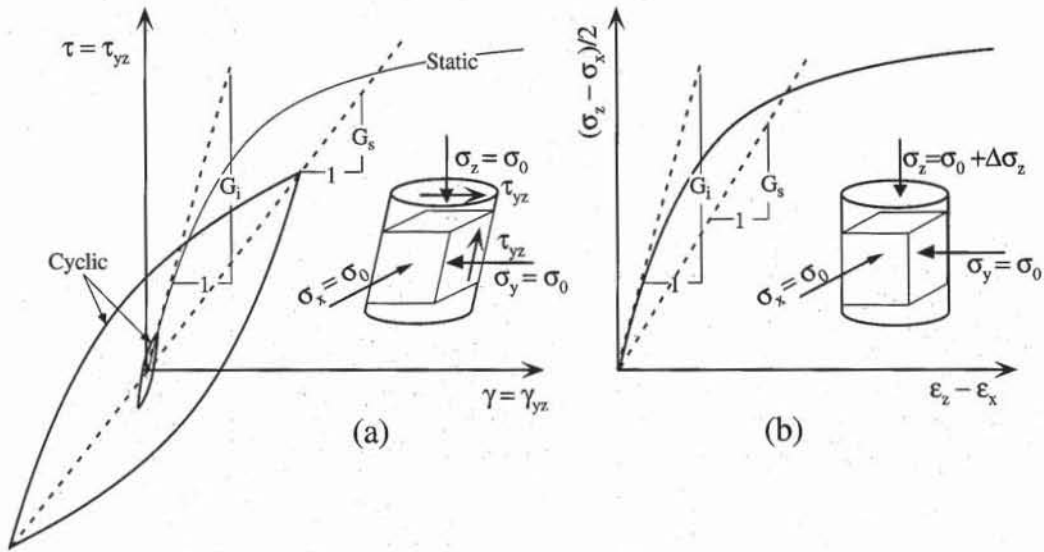


Figure 17 Determination of initial shear modulus G_i and secant shear modulus G_s during (a) cyclic or dynamic simple shear tests, and (b) static triaxial tests.

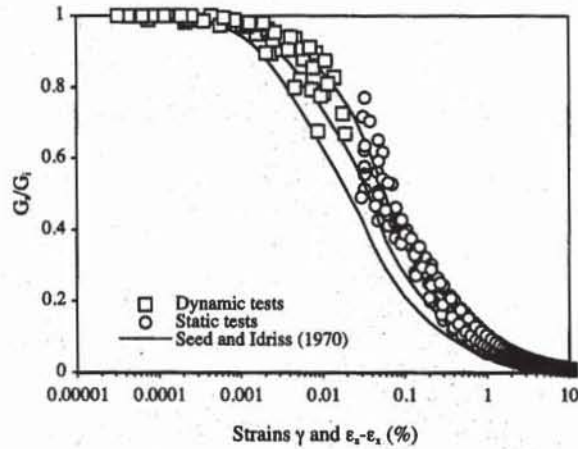


Figure 18 Variation of G_s/G_i versus shear strain calculated from dynamic resonant column test, and static drained triaxial test at constant mean pressures on Nevada sand at 40 and 60% relative density (data after Arulmoli et al., 1992).

The determination of the elastic properties of soils and soft rocks during static tests requires measuring strain smaller than 0.001%, which can only be accomplished by using local strain measurement, away from the loading platens where displacement transducers are usually located (e.g., Jardine et al., 1984; Kim et al., 1994; LoPresti et al., 1993; Tatsuoka et al., 1994; and Tatsuoka and Kohata, 1996). As shown in Fig. 19, the axial strain ϵ_z during the triaxial test is usually equal to $\Delta H/H_0$ where ΔH is the displacement measured by the external displacement transducer, and H_0 is the initial sample height. In contrast to ϵ_z , the local strain ϵ'_z , is taken equal to $\Delta H'/H'_0$ where $\Delta H'$ is the local displacement

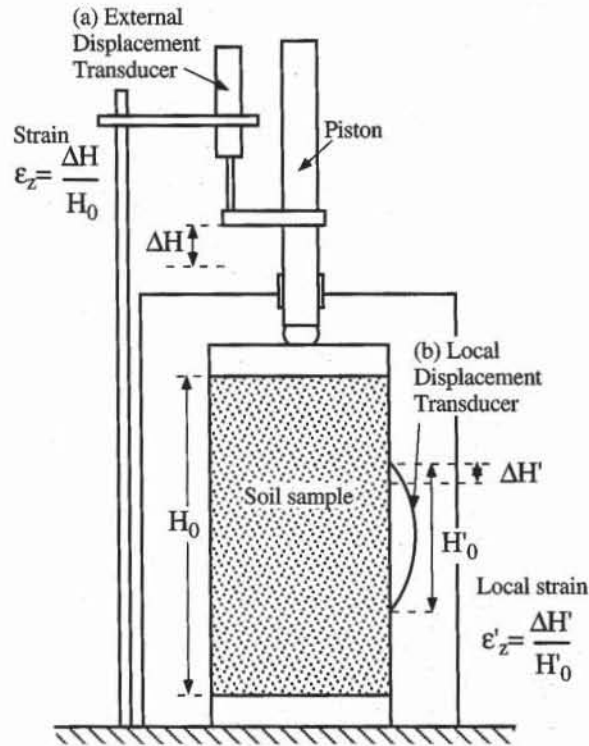


Figure 19 Measurement of axial strain of soil samples (a) with external displacement transducer, and (b) local displacement transducer (after Tatsuoka and Kohata, 1995)

measured by the flexible bending element of initial length H'_0 which is attached to the soil specimen.

Figure 20 shows an example of local strain measurement during a drained triaxial test at 300 kPa confining pressure on normally consolidated white clay. The strain-strain response and secant Young's modulus E_s were represented by using linear and logarithmic scales to emphasize the small strain behavior. As shown in Fig. 20d, when $\epsilon_z < 0.003\%$, E_s is constant and equal to E_i , and the material is linear elastic. As shown in Fig. 21, in fine-grained soils, the typical variation of G_s/G_i with shear strain depends on plasticity index PI , and is bounded by the variation of G_s/G_i for sands for which $PI = 0$.

Local strain measurements in static tests reveal that soils are much stiffer at small strains than previously obtained from conventional strain measurement. Such a finding closes the gap between the dynamic and static measurement of ground stiffness. In the past, dynamic measurement of Young's modulus, or shear modulus, have given results so much higher than static values determined in the laboratory that the dynamic values have been discounted. However in a number of recent cases, the accurately determined static small-strain values of stiffness have been found to be very close to the values measured by dynamic methods (Burland, 1989).

REFERENCES

- ARULMOLI, K., K. K. MURALEETHARAN, M. M. HOSSAIN, and L. S. FRUTH, 1992, VELACS: Verification of Liquefaction Analyses by Centrifuge Studies. Labora-

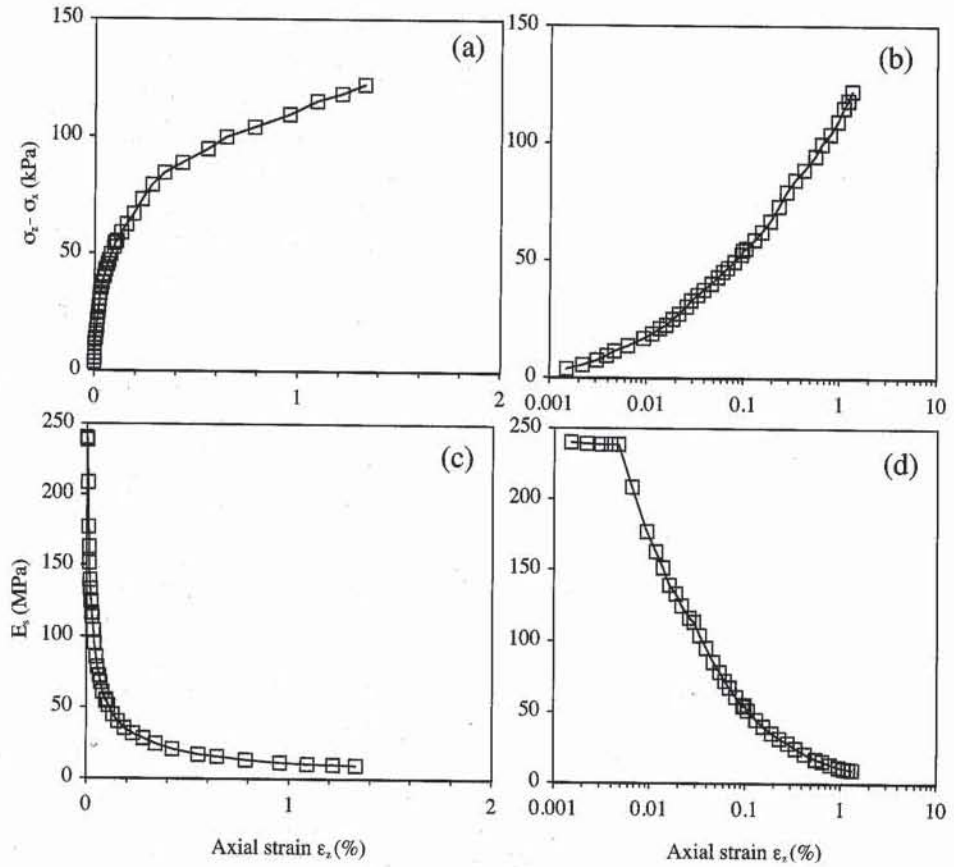


Figure 20 Example of local strain measurement during drained tri-axial test at 300 kPa confining pressure on normally consolidated white clay, $w = 61\%$ and $PI = 30\%$ (after Biarez and Hicher, 1994).

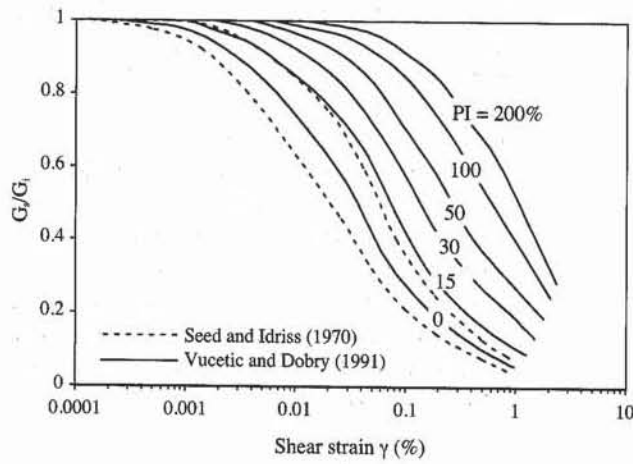


Figure 21 Variation of shear modulus ratio G_s/G_i with shear strain amplitude for sands (after Seed and Idriss, 1970) and fine grained soils of different plasticity index PI (after Vucetic and Dobry, 1991).

- tory testing program. Soil data report, *The Earth Technology Corporation*, Project No. 90-0562, Irvine, CA.
- BIAREZ, J., and P.-Y. HICHER, 1994, *Elementary Mechanics of Soil Behavior, Saturated Remoulded Soils*, A. A. Balkema, Rotterdam, Netherlands, pp. 30-32.
- BOWLES, J. E., 1988, *Foundation Analysis and Design*, 4th ed., McGraw-Hill, New York, pp. 99-100.
- BURLAND, J. B., 1989, Ninth Laurits Bjerrum Memorial Lecture, Small is beautiful - The stiffness of soils at small strains, *Canadian Geotech. J.*, Vol. 26, pp. 499-516.
- CERNICA, J. N., 1995, *Geotechnical Engineering, Soil Mechanics*, John Wiley & Sons, New York, p. 241.
- CONVERSE, F. J., 1962, Foundations subjected to dynamic forces, Chapter 8 of *Foundation Engineering*, G.A. Leonards ed., McGraw-Hill, New York, pp. 769-825.
- DJOENAI, W. J., 1985, A compendium of soil properties and correlations, *Master of Engineering Science in Geotechnical Engineering*, University of Sydney, Sydney, Australia.
- HALLAM, M. G., N. J. HEAF, and L. R. WOOTTON, 1978, Dynamic of marine structures, *Report UR 8, 2nd edition*, CIRIA Underwater Engineering Group.
- HARDIN, B. O., 1978, The nature of stress-strain behavior of soils, *Proceedings of the ASCE Geotechnical Engineering Division, Specialty Conference, Earthquake Engineering and Soil Dynamics*, Pasadena, CA, Vol. 1, pp. 3-89.
- HARDIN, B. O., and V. P. DRNEVICH, 1972, Shear modulus and damping in soils: design equations and curves, *J. Soil Mech. Found. Div.*, ASCE, Vol. 98, No. SM7, pp. 667-692.
- HOLTZ, R. D., and W. D. KOVACZ, 1981, *An Introduction to Geotechnical Engineering*, Prentice-Hall, Englewoods Cliffs, NJ.
- HUNT, R. E., 1986, *Geotechnical Engineering Techniques and Practices*, McGraw-Hill, New York, p. 134.
- JAMIOLKOWSKI, M., S. LEROUÉIL, and D. C. F. LOPRESTI, 1991, Theme lecture: Design parameters from theory to practice, *Proceedings of Geo-Coast 1991*, Yokohama, Japan, pp. 1-41.
- JARDINE, R. J., M. J. SYMES, and J. B. BURLAND, 1984, The measurement of soil stiffness in the triaxial apparatus, *Geotechnique*, Vol. 34, pp. 323-340.
- KIM, D.-S., F. TATSUOKA, and K. OCHI, 1994, Deformation characteristics at small strains of sedimentary soft rocks by triaxial compression tests, *Geotechnique*, Vol. 44, No. 3, pp. 461-478.
- KRAMER, S. L., 1996, *Geotechnical Earthquake Engineering*, Prentice Hall, Upper Saddle River, NJ, pp. 184-253.
- LAMBE, T. W. and R. V. WHITMAN, 1979, *Soil Mechanics, SI Version*, John Wiley & Sons, New York, p. 161.
- LEE, K. L., and H. B. SEED, 1967, Drained Strength Characteristics of Cohesionless Soils, *J. Soil Mech. Found. Div.*, ASCE, Vol. 93, No. SM6, pp. 117-141.
- LOPRESTI, D. C. F., O. PALLARA, R. LANCELOTTA, M. ARMANDI, and R. MANISCALCO, 1993, Monotonic and cyclic loading behaviour of two sands at small strains, *Geotech. Testing J.*, ASTM, Vol. 16, No. 4, pp. 409-424.
- POULOS, H. G., 1975, Settlement of isolated foundations, *Proceedings of the Symposium on Soil Mechanics - Recent Developments*, Sydney, Australia, pp. 181-212.
- SEED, H. B. and K. L. LEE, 1967, Undrained Strength Characteristics of Cohesionless Soils, *J. Soil Mech. Found. Div.*, ASCE, Vol. 93, No. SM6, pp. 333-360.

- SEED, H. B., and I. M. IDRIS, 1970, Soil moduli and damping factors for dynamic response analyses, *Report EERC 70-10*, Earthquake Engineering Research Center, University of California, Berkeley, CA.
- TATSUOKA, F., and Y. KOHATA, 1995, Stiffness of hard soils and soft rocks in engineering applications, *Report of the Institute of Industrial Science, The University of Tokyo*, Vol. 38, No. 5, Serial No. 242, 140 p.
- TATSUOKA, F., T. SATO, C. S. PARK, Y. S. KIM, J. N. MUKABI, and J. KOHATA, 1994, Measurements of elastic properties of geomaterials in laboratory compression tests, *Geotech. Testing J.*, ASTM, Vol. 17, No. 1, pp. 80-94.
- VUCETIC, M. and R. DOBRY, 1991, Effects of soil plasticity on cyclic response, *J. Geotech. Eng.*, ASCE, Vol. 117, No. 1, pp. 89-107.

REVIEW QUESTIONS

1. Define nonlinear-elastic, linear-elastic, and elastoplastic materials by using stress-strain curves.
2. Define strain hardening, perfectly plastic, and strain softening materials by using stress-strain curves.
3. Define rigid-perfectly plastic, and elastic-perfectly plastic materials by using stress-strain curves.
4. What is the yield stress for an elastoplastic material?
5. What is a viscous material?
6. Define *creep* and *relaxation*.
7. What is the number of independent material constants in the isotropic linear theory of elasticity?
8. What is the relation between the bulk modulus, Young's modulus, and the Poisson ratio?
9. What is the relation between the shear modulus, Young's modulus, and the Poisson ratio?
10. What is the constrained modulus?
11. What are the theoretical constraints on Young's modulus and the Poisson ratio?
12. What is the state of stress during the isotropic test? What is the elastic relation between volumetric strain and pressure?
13. What is the state of stress during the unconfined compression test? What is the elastic relation between axial strain and axial stress?
14. What is the state of stress during the drained triaxial test? What are the elastic relations between axial strain and axial stress, and between volumetric stress and axial strain?
15. What is the state of stress during the confined compression test?

EXERCISES

1. From the results of the isotropic test on dense Sacramento River sand in Table E1, plot the volumetric strain versus pressure. Calculate the initial bulk modulus at 78 kPa, and plot the variation of secant bulk modulus versus pressure.

TABLE E1

1			2		
Pressure (kPa)	Void ratio	Volumetric strain (%)	Pressure (kPa)	Void ratio	Volumetric strain (%)
78	0.608	0.06	11925	0.506	6.40
196	0.604	0.31	9081	0.509	6.22
392	0.600	0.56	7708	0.511	6.09
588	0.596	0.81	5531	0.513	5.97
1069	0.590	1.18	4119	0.518	5.66
2167	0.581	1.74	3285	0.521	5.47
3285	0.572	2.30	2157	0.524	5.28
4021	0.566	2.67	1079	0.527	5.10
2216	0.572	2.30	588	0.533	4.72
981	0.577	1.99	392	0.537	4.47
392	0.584	1.55	98	0.547	3.85
78	0.591	1.12	392	0.541	4.23
392	0.584	1.55	588	0.538	4.41
981	0.578	1.93	1079	0.532	4.79
2216	0.572	2.30	2157	0.524	5.28
4021	0.563	2.86	3285	0.521	5.47
5492	0.556	3.29	4119	0.518	5.66
7708	0.540	4.29	5531	0.513	5.97
9081	0.532	4.79	7708	0.508	6.28
10395	0.523	5.34	9081	0.506	6.40
11925	0.515	5.84	11964	0.499	6.84
13729	0.503	6.59	13729	0.493	7.21

Initial void ratio = 0.609

2. From the results of the unconfined compression of a remolded clay in Table E2, calculate the initial Young's modulus. Plot the variation of secant Young's modulus versus axial strain.

TABLE E2

Axial strain (%)	Axial stress (kPa)
0.0	0.0
1.0	8.7
1.9	13.8
2.9	20.2
5.0	31.6
5.8	35.2
6.9	40.6
7.8	45.5
8.8	50.2
9.9	56.1
11.0	58.3
12.0	60.8
13.4	63.0
14.1	64.7
15.0	65.3
16.0	66.7
18.0	67.3
20.1	69.7
21.1	70.1

3. From the results of the confined compression test on San Francisco Bay mud in Table E3, calculate the initial constrained modulus. Plot the variation of secant constrained modulus versus axial strain.

TABLE E3

Axial stress (kPa)	Axial strain (%)
1	1.1
3	2.2
4	4.4
10	14.3
21	23.7
41	31.3
82	38.2
22	37.0
6	34.2

4. From the results of the drained triaxial compression test of a sand in Table E4, calculate the initial Young's modulus and Poisson ratio. Plot the variation of secant Young's modulus and Poisson ratio versus axial strain.

TABLE E4

σ'_1 / σ'_3	$\sigma_1 - \sigma_3$ (kPa)	Axial strain (%)	Volumetric strain (%)
1.00	0.0	0.00	0.00
1.39	229.5	0.06	0.03
1.78	459.0	0.15	0.09
2.08	635.5	0.30	0.15
2.82	1070.9	0.58	0.24
3.25	1323.9	0.88	0.27
3.87	1688.7	1.46	0.22
4.24	1906.4	2.19	0.03
4.42	2012.3	2.92	-0.24
4.56	2094.7	4.38	-0.91
4.55	2088.8	5.85	-1.61
4.45	2030.0	8.77	-2.85
4.26	1918.2	11.70	-3.80
4.18	1871.1	14.60	-4.46
3.94	1729.9	17.55	-4.91
3.72	1600.5	20.00	-5.05

Confining Pressure = 588 kPa
Initial void Ratio = 0.596



6

Consolidation

- 6-1** Principles of consolidation
- 6-2** Consolidation test

6-1

Principles of Consolidation

INTRODUCTION

When fine-grained soils are subjected to changes in load due to construction, they deform in a way different from that of coarse-grained materials. Their deformation takes place not only at the time of the load application, but also continues for very long time periods which may last several years. The long-term settlement of fine-grained soil layers is primarily controlled by *consolidation*, a physical process in which the interstitial water that is under excess pressure slowly diffuses through the compressible matrix of soil particles. After the excess pore pressure has completely dissipated, fine-grained soils can also deform due to their viscous nature. The properties that characterize the amplitude and rate of deformation for fine-grained soils are determined in the consolidation test.

NONLINEAR AND IRREVERSIBLE COMPRESSIBILITY

One-Dimensional Tests

The basic setup of the consolidation test is shown in Fig. 1. The soil sample is inside a stiff ring which blocks its lateral expansion, and between two porous disks, which drains its porewater. The sample is completely immersed in water and remains fully saturated during the test. When the axial stress σ is applied, the sample of initial height h_0 deforms vertically with time. It ultimately settles the amount Δh when the excess porewater pressure is completely dissipated (i.e., when the internal effective stress σ' becomes equal to the externally applied stress σ). The corresponding axial strain ϵ_z is

$$\epsilon_z = \frac{\Delta h}{h_0} \quad (1)$$

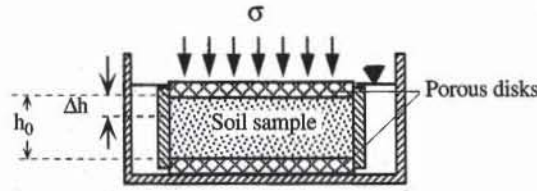


Figure 1 Basic experimental setup of consolidation cell.

Because the stiff ring prohibits lateral strain (i.e., $\epsilon_x = \epsilon_y = 0$), the volumetric strain ϵ_v is equal to the axial strain:

$$\epsilon_v = \epsilon_x + \epsilon_y + \epsilon_z = \epsilon_z = \frac{\Delta h}{h_0} \tag{2}$$

The volumetric strain is also

$$\epsilon_v = \frac{V_0 - V}{V_0} = \frac{V_0/V_s - V/V_s}{V_0/V_s} = \frac{e_0 - e}{1 + e_0} \tag{3}$$

where e is the present void ratio, e_0 the initial void ratio, V the present volume, V_0 the initial volume, and V_s the total volume of soil particles alone. Therefore, e is related to Δh through

$$e = e_0 - \epsilon_v(1 + e_0) = e_0 - \frac{\Delta h}{h_0} (1 + e_0) \tag{4}$$

Figure 2 shows an experimental result that is representative of the response of fine-grained soils subjected to a loading-unloading cycle in the consolidation test. The same experimental results are plotted in two different ways: vertical strain ϵ_z versus effective stress σ' and void ratio e versus σ' . The σ' axis has a linear scale in Fig. 2a but a logarithmic scale in Fig. 2b. As shown in Fig. 2b, e decreases from the initial state A as σ' is increased. From point A to B, the relation between e and σ' is nonlinear. The material behaves differently during loading (from A to B) and unloading (from B to C), which indicates that the nonlinear $e-\sigma'$ relation is also irreversible.

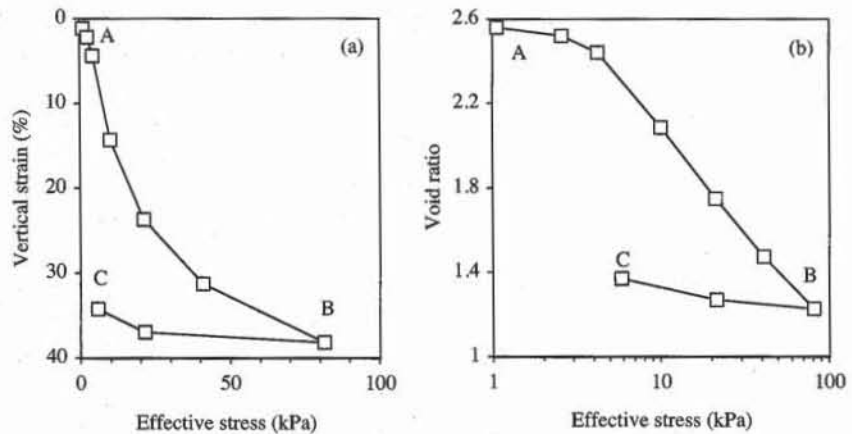


Figure 2 Consolidation test results on San Francisco bay mud: (a) vertical strain versus effective stress in linear scale, and (b) void ratio versus effective stress in semilogarithmic scale (after Holtz and Kovacs, 1981).

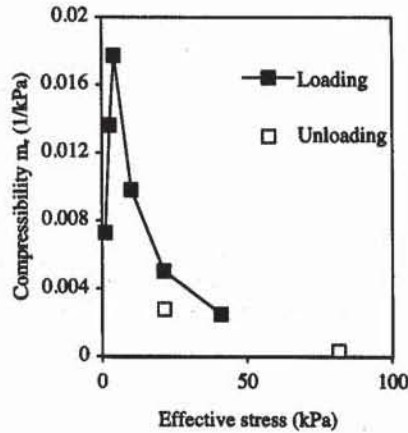


Figure 3 Variation of the compressibility of Fig. 2 with stress level and loading direction.

Coefficient of Compressibility

Within the small stress interval from σ'_1 to σ'_2 , the ϵ_z - σ' curve is characterized by the coefficient of compressibility m_v :

$$m_v = \frac{\epsilon_{v1} - \epsilon_{v2}}{\sigma'_2 - \sigma'_1} \tag{5}$$

where ϵ_{v1} is the volumetric strain at effective stress σ'_1 and ϵ_{v2} is the volumetric strain at σ'_2 . Since $\epsilon_z = \epsilon_v$, $m_v = 1/M$, where M is the constrained modulus of elasticity (see Chapter 5-5). m_v is inversely proportional to stress [m_v] = $F^{-1}L^2$, where L and F represent the dimension of length and force, respectively. m_v is also computed from the e - σ' curve using Eq. 4:

$$m_v = \frac{e_1 - e_2}{1 + e_1} \frac{1}{\sigma'_2 - \sigma'_1} \tag{6}$$

where e_1 is the void ratio at σ'_1 and e_2 is the void ratio at σ'_2 . As shown in Fig. 3, m_v varies with the stress level and the loading direction. m_v is generally used to calculate the vertical settlement s of a layer of initial thickness h_0 subjected to the increased $\Delta\sigma'$ in vertical effective stress:

$$s = m_v h_0 \Delta\sigma' \tag{7}$$

Caution should be exercised in the calculation and use of m_v . The value of m_v depends not only on the stress level but also on the loading direction (i.e., loading or unloading). Equation 7 applies provided that the soils in the laboratory and the field undergo a similar stress level, stress increment, and loading direction.

e - σ' Curves for Clays

Figure 2b shows that e varies linearly with $\log \sigma'$ in some parts, whereas Fig. 2a displays a complicated nonlinear relation between ϵ_z and σ' . The void ratio e is therefore more convenient than ϵ_z to represent consolidation results.

Figures 4 to 6 show a few examples of consolidation results covering a wide variety of soils. Figure 4 shows the consolidation curves for glacial lake silty clays (Rutledge, 1944). Sample CP1 is an undisturbed sample taken from the field, sample CP2 is artificially remolded from sample CP1, and sample CP3 is in turn remolded from sample CP2. As shown in Fig. 4, the consolidation curves of samples CP1, CP2, and CP3, although they retained a similar shape, are influenced by remolding.

Figure 5 shows the consolidation curves that are typical of soils from the lower Mississippi River Valley near Baton Rouge, Louisiana (Kaufman and Sherman, 1964). These soils are made of silts and sandy silts with clay strata and are classified as CH and CL-clay of high and low plasticity, respectively. During the deposition process in the Mississippi River Valley, they have been subjected to wetting and drying cycles. The consolidation curves of these clays are also compared to that of a poorly graded sand. As shown in Fig. 5, sand is much less compressible than clay and undergoes smaller changes in void ratio.

Figure 6 shows the consolidation curves of Mexico City clay (Rutledge, 1944). This soil was previously thought to be a volcanic ash that had been weathered and had become an allophane clay mineral. Indeed, Mexico City clay is not really a clay mineral, but is composed primarily of porous microfossils and diatoms, which are responsible for very high void ratio, water content, and compressibility (Holtz and Kovacs, 1981). As shown in Fig. 6, the solid and dashed lines represent the response of undisturbed and remolded samples taken from different locations. The difference in undisturbed responses illustrates the difficulty in obtaining reproducible results on clays having such a large void ratio. As expected, remolding almost completely destroys the preconsolidation effects.

Elastoplastic Modeling of $e-\sigma'$ Responses

Figure 7 shows the consolidation curve of clay tills (MacDonald and Sauer, 1970), a typical response for fine-grained soils. The relation between e and σ' is nonlinear and irreversible. The material behaves differently during loading (A to C , or

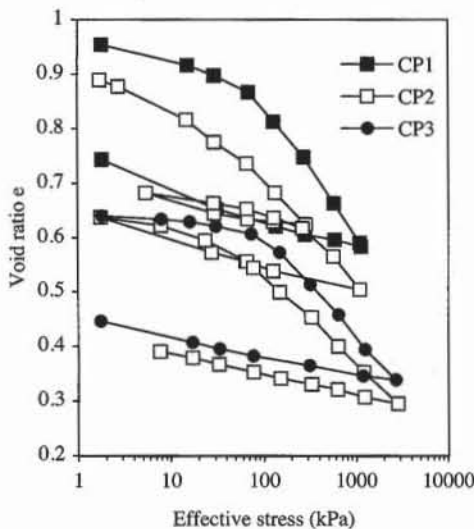


Figure 4 Consolidation test results on Chicago and Indiana clays (after Rutledge, 1944).

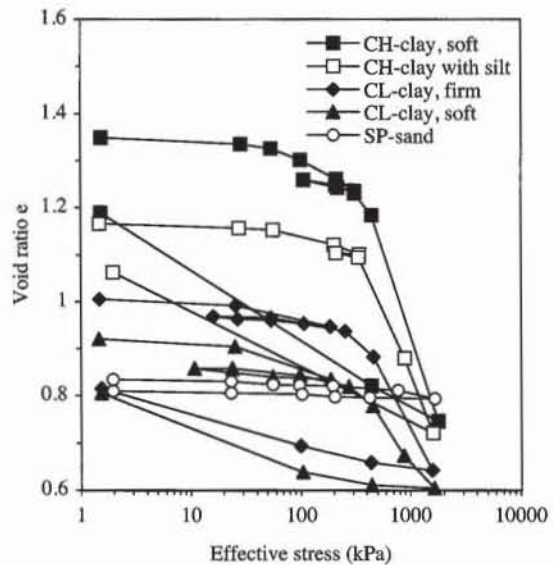


Figure 5 Consolidation test results on nearly normally consolidated clays and silts (after Kaufman and Sherman, 1964).

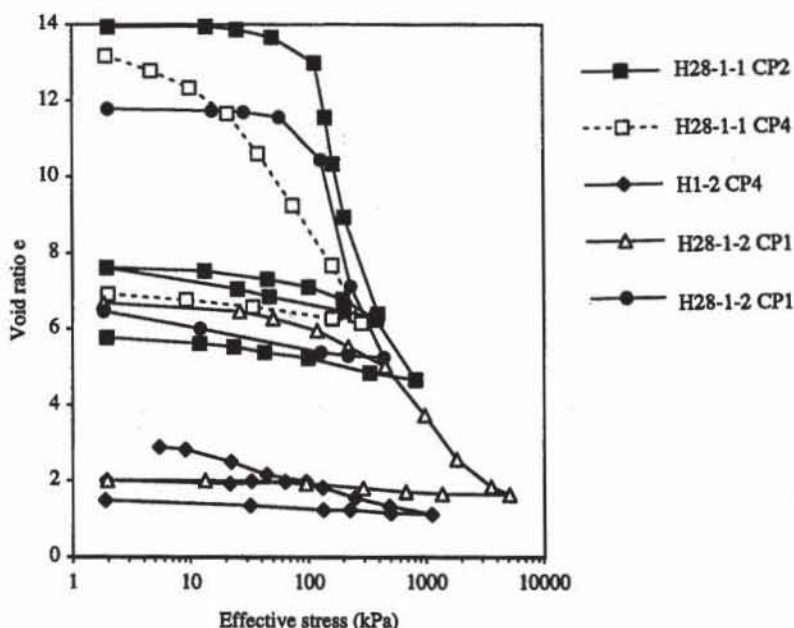


Figure 6 Consolidation test results on Mexico City clay (after Rutledge, 1944).

D to *E*) and unloading (*C* to *D*, or *E* to *F*). The material response of Fig. 7 is not elastic but is elastoplastic.

Figure 8 illustrates the elastoplastic modeling of the response $e-\log \sigma'$ of Fig. 7. Starting from point *A*, e varies linearly with $\log \sigma'$ when σ' is increased from σ'_A to σ'_B :

$$e = e_A - C_s \log \frac{\sigma'}{\sigma'_A} \tag{8}$$

where C_s is the swelling index, e_A the void ratio at point *A*, and σ'_A the effective stress at point *A*. Equation 8 is valid until σ' reaches stress σ'_B , at which point the $e-\sigma'$ curve abruptly becomes steeper than the branch *AB*. When $\sigma' > \sigma'_B$, e varies again linearly with $\log \sigma'$ but with a steeper slope:

$$e = e_B - C_c \log \frac{\sigma'}{\sigma'_B} \tag{9}$$

where C_c is the compression index, e_B the void ratio at point *B* and σ'_B the effective stress at point *B*. When σ' is decreased from σ'_C to σ'_D , the point ($e-\log \sigma'$) follows the unloading branch *CD*, which is parallel to *AB* and has the same swelling index. But Eq. 8 is now referenced about *C* instead of *A*:

$$e = e_C - C_s \log \frac{\sigma'}{\sigma'_C} \tag{10}$$

When σ' is increased again, the point ($e-\log \sigma'$) follows the branch *CD* in the opposite direction and moves toward *E* on the branch that extends *BC*. When σ' is finally decreased from *E* to *F*, the point ($e-\log \sigma'$) follows the branch *EF* parallel to *AB* and *CD*. The branch *BCE* is called the *virgin compression line* (VCL). The

branches AB , CD , and EF are *swelling lines*. A particular clay has only one virgin consolidation curve but an indefinite number of swelling branches. The swelling branches are always to the left of VCL. The point $(e-\log \sigma')$ cannot go to the right of VCL.

The stress-strain relations specified by Eqs. 8 to 10 are nonlinear because e is a logarithmic function of σ' . They are also irreversible because it is not possible to return to point A once σ' has exceeded σ'_B . The threshold of irreversibility is defined by the largest effective stress applied, which is also referred to as the *preconsolidation pressure* σ'_p . When the stress state is smaller than σ'_p , the response is described by a swelling branch. When the stress state is equal to σ'_p , the response follows the VCL for loading and a swelling line for unloading. The preconsolidation pressure σ'_p either increases or remains constant but never decreases. During the loading ABC of Fig. 8, σ'_p moves from σ'_B to σ'_C . σ'_p is constant during the unloading CD and reloading DC but increases again during the loading CE .

Compression and Swelling Indices and Compressibility

The compression index C_c is the slope of the virgin consolidation line (VCL) in the $e-\log \sigma'$ axes, whereas the swelling index C_s is the slope of a swelling curve. These indices are

$$C_c = \frac{e_B - e_C}{\log(\sigma'_C / \sigma'_B)} \quad \text{and} \quad C_s = \frac{e_D - e_C}{\log(\sigma'_C / \sigma'_D)} \quad (11)$$

where B and C are two points on the VCL, and C and D are two points on a swelling line as shown in Fig. 8. Both C_c and C_s are positive dimensionless number, and C_s is always smaller than C_c . In contrast to m_v , C_c and C_s are constant for a soil. As mentioned previously, m_v depends on the loading direction and the position relative to the VCL. For very small loading steps, the compressibility coefficient m_v is related to C_c and C_s through

$$m_v = - \frac{1}{(1+e) \ln(10)} \frac{de}{d\sigma'} = \begin{cases} \frac{0.435 C_c}{1+e} \frac{1}{\sigma'} & \text{for loading on VCL} \\ \frac{0.435 C_s}{1+e} \frac{1}{\sigma'} & \text{otherwise} \end{cases} \quad (12)$$

Overconsolidation Ratio, Normally Consolidated and Overconsolidated Clays

The overconsolidation ratio OCR characterizes the position of the present state (e, σ') relative to the preconsolidation pressure σ'_p :

$$OCR = \frac{\sigma'_p}{\sigma'} \quad (13)$$

When the excess pore pressure is dissipated completely, OCR is always larger or equal than 1. Based on the overconsolidation ratio, clays are divided into normally consolidated and overconsolidated.

Normally consolidated clays have never been subjected to an effective stress greater than the present effective stress ($OCR = 1$). Examples of normally con-

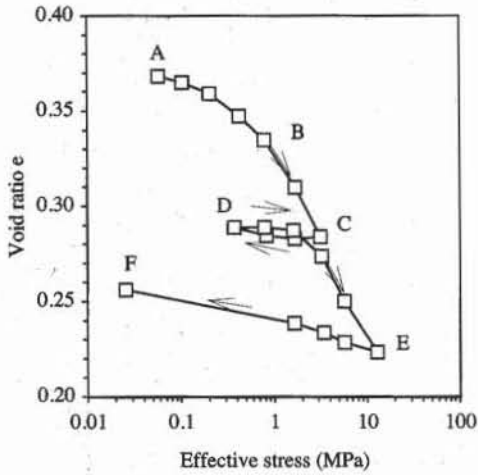


Figure 7 Typical experimental results during one-dimensional compression tests on clay tills (data after MacDonald and Sauer, 1970).

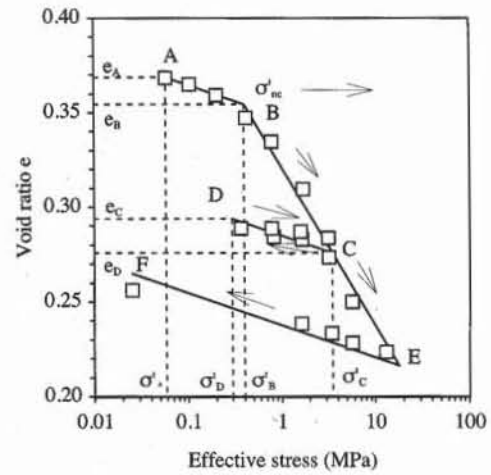


Figure 8 Idealized representation of stress-strain response of Fig. 7.

solidated clays are geologically recent alluvial deposits which have never been eroded. Normally consolidated clays are sensitive to the effects of disturbances, which influence the $e-\sigma'$ relationship.

Overconsolidated clays have been subjected to an effective stress greater than the present effective stress ($OCR > 1$). This past loading could have been the result of deposits of soils and rocks, perhaps 2 to 3 km thick, which were subsequently eroded away in the course of geological time or by a great thickness of ice during periods of glaciation. Other factors such as aging, dessication, and fluctuation in water level, may also contribute to modify the mechanical behavior of clays.

Determination of Preconsolidation Pressure

There are primarily two ways to determine the preconsolidation pressure σ'_p , which is the largest effective stress undergone by the soil. Both methods detect σ'_p from the $e-\log \sigma'$ curve.

Method a (Casagrande, 1936; and ASTM 2435)

- Choose the point of minimum curvature on the consolidation curve (point A in Fig. 9).
- Draw the horizontal line AB from point A.
- Draw the line AC tangent to the curve at point A.
- Draw the line AD so that the angles BAD and DAC are equal.
- Extend the straight portion EF of the virgin compression curve as shown in Fig. 9.
- The preconsolidation stress σ'_p is the intersection point M between EF and AD.

Method b

- Extend the straight portion EF of the virgin compression curve as shown in Fig. 9.

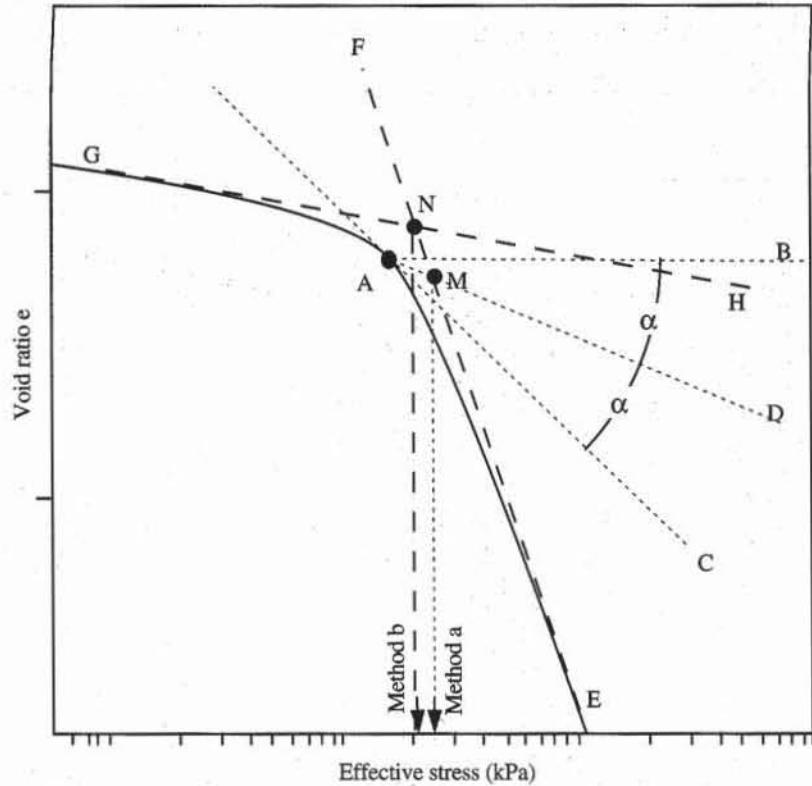


Figure 9 Determination of preconsolidation pressure with methods a and b.

- Extend the straight portion GH of the compression curve as shown in Fig. 9.
- The preconsolidation stress σ'_p is the intersection point N between EF and GH .

As shown in Fig. 9, methods a and b predict only slightly different preconsolidation pressure. They give similar results for practical purposes.

Typical Values and Correlations for Compressibility Indices

Table 1 lists the values of compression index C_c , swelling index C_s , and Atterberg limits for various clays. The values of C_c vary from 2.6 for montmorillonite (Na^-) to 0.08 for clay till, whereas those of C_s range from 0.01 to 0.51.

Many different correlations have been published for correlating C_c and C_s to the index properties of soils (Djoenaidi, 1985). Figure 10 shows three types of correlations between C_c and the liquid limit, initial void ratio, and natural water content. The correlations between C_c and the natural water content appear to be more consistent than the others. One of these correlations still in use today is due to Terzaghi and Peck (1967):

$$C_c = 0.009 (LL - 10) \quad (14)$$

where LL is the liquid limit in percent. As shown in Fig. 11, Eq. 14 describes the measured values of C_c for some, but not all clays. Based on the critical state model (see Chapter 7-1), Wroth and Wood (1978) showed that:

$$C_c = G_s \frac{PI}{200} \quad \text{and} \quad C_s = C_c(1 - \Lambda) \quad (15)$$

TABLE 1

Values of compression and swelling indices and Atterberg limit for various clay minerals and natural soils.

Type of clays	Undisturbed C_c	Remolded C_c	Swelling C_s	Liquid limit (%)	Plastic limit (%)	Plasticity index (%)	References
Boston blue clay	0.32	0.21	0.07	41	20	21	1
Chicago clay	0.42	0.22	—	58	21	37	1,2
Louisiana clay	0.33	0.29	0.05	74	26	48	1,2
New Orleans clay	0.29	0.26	0.04	79	26	53	1,2
Fort Union clay	0.26	—	0.04	89	20	69	1
Delaware organic silty clay	0.95	—	—	84	46	38	1
Indiana silty clay	0.21	0.12	—	36	20	16	1
Fore River clay	0.36	0.25	0.09	49	21	28	1
Beauharnois clay	0.55	—	0.01	56	22	34	1
Cincinnati clay	0.17	—	0.02	30	12	18	1
St Lawrence clay	0.84	—	0.04	55	22	33	1
Siburua clay	0.21	—	0.08	70	26	44	1
CL-clay, soft	0.34	—	—	41	24	17	4
CL-clay, firm	0.44	—	—	50	23	27	4
ML-sandy silt	0.16	—	—	31	25	6	4
CH-clay, soft	0.84	—	—	81	25	56	4
CH-clay with silt strata	0.52	—	—	71	28	43	4
Montmorillonite, Na ⁺	2.6	—	—	710	54	656	3
Montmorillonite, K ⁺	1	—	—	660	98	562	3
Montmorillonite, Ca ²⁺	2.2	—	0.51	510	81	429	3
Montmorillonite, H ⁺	1.9	—	0.34	440	55	385	3
Montmorillonite, Mg ²⁺	1.9	—	0.44	410	60	350	3
Montmorillonite, Fe ³⁺	1.6	—	0.03	290	75	215	3
Illite, Na ⁺	1.1	—	0.15	120	53	67	3
Illite, K ⁺	0.62	—	0.27	120	60	60	3
Illite, Ca ²⁺	0.86	—	0.21	100	45	55	3
Illite, H ⁺	0.61	—	0.10	100	51	49	3
Illite, Mg ²⁺	0.56	—	0.18	94	46	48	3
Illite, Fe ³⁺	—	—	0.15	110	49	61	3
Kaolinite, Na ⁺	0.26	—	—	53	32	21	3
Kaolinite, K ⁺	—	—	0.06	49	29	20	3
Kaolinite, Ca ²⁺	0.21	—	0.06	38	27	11	3
Kaolinite, H ⁺	0.23	—	0.05	53	25	28	3
Kaolinite, Mg ²⁺	0.24	—	0.08	54	31	23	3
Kaolinite, Fe ³⁺	0.24	—	0.06	59	37	22	3
Attapulgite, Mg ²⁺	0.77	—	0.24	270	150	120	3
Clay till	0.08	—	—	24	12	12	5

References

¹Winterkorn and Wang, 1975

²Mitchell, 1976

³Lambe and Whitman, 1979

⁴Kaufman and Sherman, 1964

⁵MacDonald and Sauer, 1970

where G_s is the soil specific density and Λ a critical state material constant. For $G_s = 2.7$ and $\Lambda = 0.8$, Eq. 15 becomes

$$C_c = \frac{PI}{74} \quad \text{and} \quad C_s = \frac{PI}{370} \quad (16)$$

As shown in Fig. 12, there is a general agreement between the measured values of C_c and C_s and those calculated from Eq. 16. The measured values of the swelling index C_s are generally about 5 times smaller than C_c , as predicted by Eq. 16. As shown in Fig. 13, Lambe and Whitman (1979) suggest that the representa-

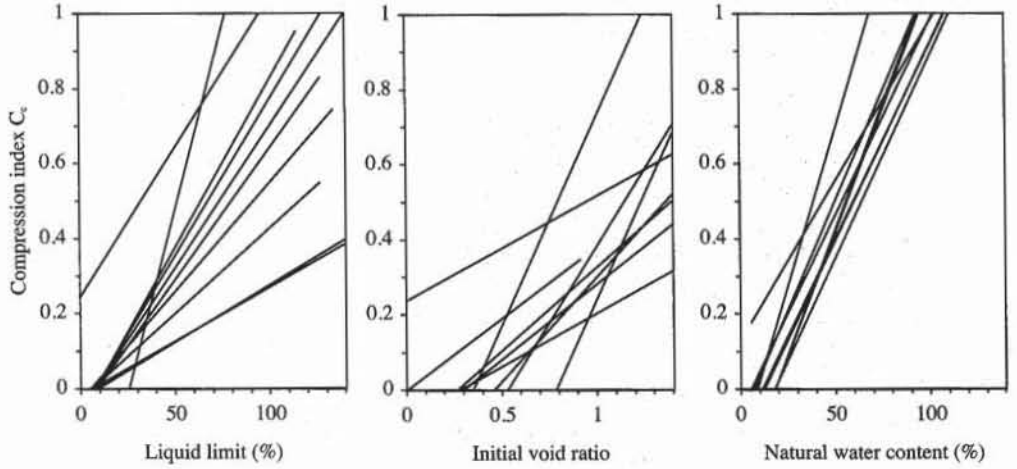


Figure 10 Empirical relations between compression index C_c , liquid limit, initial void ratio, and natural water content (after Djoenaidi, 1985).

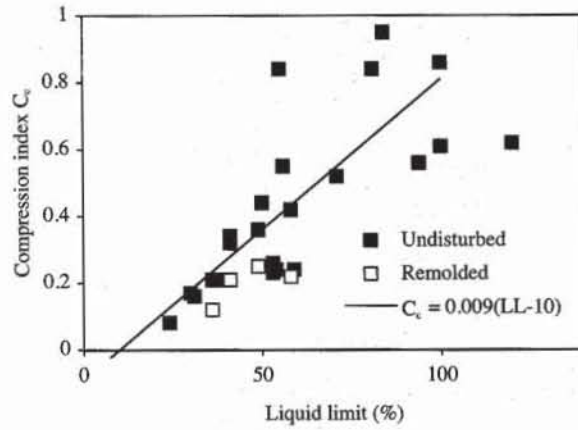


Figure 11 Relation between compression index C_c and liquid limit for clays (experimental data of Table 1).

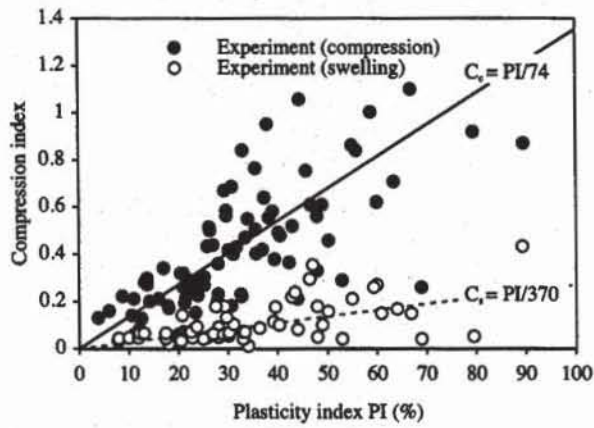


Figure 12 Variation of compression index C_c and swelling index C_s with plasticity index (experimental data from Table 1 and Kulhawy and Mayne, 1990).

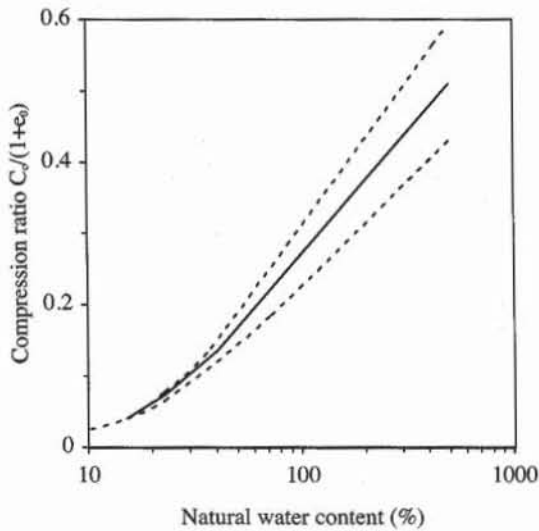


Figure 13 Range of variation of $C_c/(1 + e_0)$ with natural water content (Lambe and Whitman, 1979).

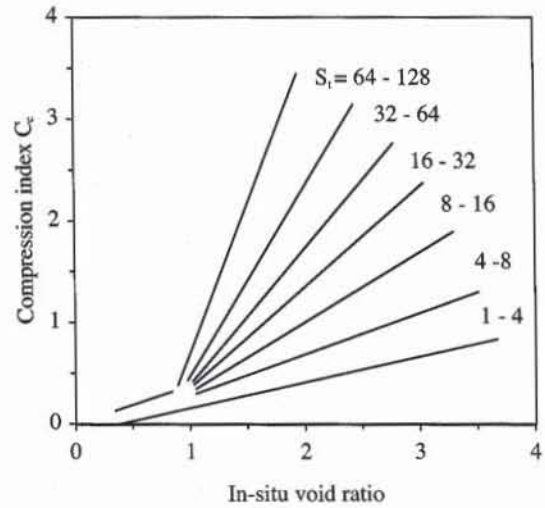


Figure 14 Influence of sensitivity S_t on compression index (Leroueil et al., 1983).

tion of $C_c/(1 + e_0)$ versus the natural water content reduces the data scatter, where e_0 is the initial void ratio.

As shown in Fig. 14, the sensitivity S_t of clays, which is the ratio between their undrained shear strengths in undisturbed and remolded states (see Chapter 7-1), influences strongly the compressibility index of clays, especially marine clays (Leroueil et al., 1983). An example of the effect of disturbance on the compressibility of sensitive soils can also be found in Fig. 6.

RATE OF CONSOLIDATION

Definition

When a load is applied to a specimen of saturated soil in the consolidation test, it is initially carried by the porewater, which is much less compressible than the assembly of soil particles. The resulting porewater pressure, in excess of the hydrostatic water pressure, is termed *excess porewater pressure*. When water drains from the soil pores, the load is gradually shifted from water to soil particles. For fully saturated soils, the load transfer is accompanied by a volume change equal to the volume of drained water. This process is known as *consolidation*.

The consolidation process is illustrated with the spring analogy of Fig. 15. As shown in Fig. 15a, the assembly of soil grains is modeled with a spring. If the weight W is placed on the model with the valve closed, W is carried entirely by the water, which is stiffer than the spring. If the valve is opened and the water is allowed to escape, the load will eventually be carried entirely by the spring (Fig. 15c). The time required to transfer W from water to spring depends on how rapidly the water escapes through the valve. In soils, the rate of volume change and porewater diffusion is related to the soil permeability. In most sands the permeability is so large that the consolidation time is negligible, whereas in

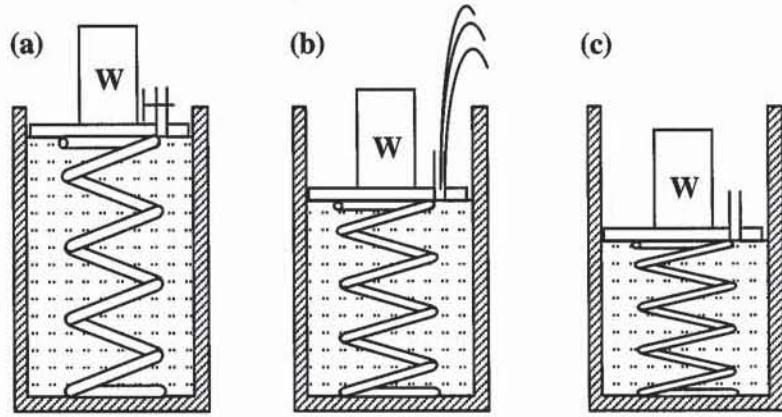


Figure 15 Spring analogy to soil consolidation.

clays, the permeability is small and slows down the rate of consolidation considerably.

Consolidation Theory

Figure 16 shows a layer of soil which is consolidating. The soil layer of thickness H is loaded by two porous boundaries which allow water to drain. The soil layer is infinitely wide so that the soil deformation and flow of water can be assumed one-dimensional and in the vertical y direction.

When the water flows only in the y direction, there is no discharge velocity in the x and z directions (i.e., $v_x = v_z = 0$). If the flow obeys Darcy's law, the discharge velocity v_y in the y direction is

$$v_y = -k \frac{\partial h}{\partial y} \tag{17}$$

where k is the permeability coefficient, $h = \frac{u}{\gamma_w} + y$ the total head, u the water

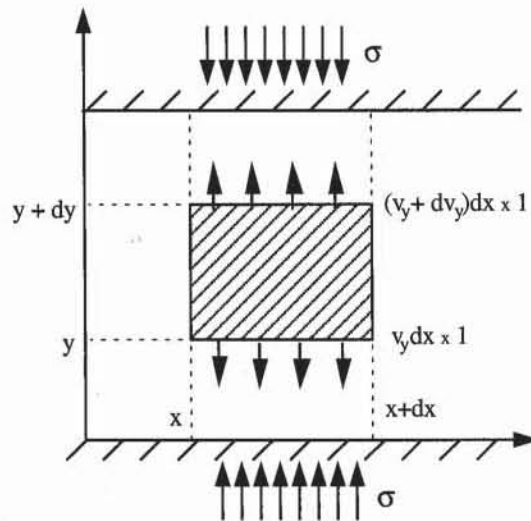


Figure 16 Small element of a soil layer undergoing consolidation.

pressure, and γ_w the unit weight of water. For the small element shown in Fig. 16, the incoming and outgoing volume of water during a unit time interval is $v_y dx \times 1$, and $(v_y + \frac{\partial v_y}{\partial y} dy) dx \times 1$, respectively. Therefore the volume of water V_w stored or lost by the element per unit of time is

$$\frac{dV_w}{dt} = \left(v_y + \frac{\partial v_y}{\partial y} dy \right) dx \times 1 - v_y dx \times 1 = \frac{\partial v_y}{\partial y} dy dx = -k \frac{\partial^2 h}{\partial y^2} dx dy \quad (18)$$

The water pressure u can be defined as the sum of static pore pressure u_s and excess pore pressure u_e (i.e., $u = u_s + u_e$). The second-order derivative of u_s is equal to 0 (i.e., $\frac{\partial^2 u_s}{\partial y^2} = 0$) because u_s varies linearly with respect to y . Eq. 18 becomes

$$\frac{dV_w}{dt} = \frac{k}{\gamma_w} \left(\frac{\partial^2 u_s}{\partial y^2} + \frac{\partial^2 u_e}{\partial y^2} \right) dx dy = -\frac{k}{\gamma_w} \frac{\partial^2 u_e}{\partial y^2} dx dy \quad (19)$$

If the soil behaves elastically, the change in void ratio resulting from the change in effective stress $d\sigma'$ is

$$\frac{de}{1 + e_0} = m_v d\sigma' \quad (20)$$

where e_0 is the initial void ratio and m_v the soil compressibility. The change in void ratio is related to the initial volume V_0 , solid volume V_s and void volume V_v through

$$\frac{de}{1 + e_0} = \frac{d(V_v + V_s)}{V_0} = \frac{dV_v}{V_0} = \frac{dV_v}{dx \times dy \times 1} \quad (21)$$

where the soil particles are assumed incompressible (i.e., $dV_s = 0$). The change in the void volume dV_v per time dt is

$$\frac{dV_v}{dt} = m_v \frac{\partial \sigma'}{\partial t} dx dy \quad (22)$$

If the total stress σ is constant (i.e., $\frac{\partial \sigma}{\partial t} = \frac{\partial \sigma'}{\partial t} + \frac{\partial u}{\partial t} = 0$), the time derivative of effective stress is

$$\frac{\partial \sigma'}{\partial t} = -\frac{\partial u}{\partial t} \quad (23)$$

because u_s is time independent (i.e., $\frac{\partial u_s}{\partial t} = 0$). Equation 22 becomes:

$$\frac{dV_v}{dt} = -m_v \frac{\partial u}{\partial t} dx dy \quad (24)$$

When the soil element remains fully saturated, the volume of voids and interstitial water changes at the same rate:

$$\frac{dV_v}{dt} = \frac{dV_w}{dt} \quad (25)$$

Equations 19, 24 and 25 give the consolidation equation:

$$\frac{\partial u_e}{\partial t} = C_v \frac{\partial^2 u_e}{\partial y^2} \quad (26)$$

where C_v is the coefficient of consolidation:

$$C_v = \frac{k}{\gamma_w m_v} \quad (27)$$

C_v has the dimension of $L^2 T^{-1}$ and its units are generally m^2/yr . The assumptions of the consolidation theory are summarized as follows:

- The layer of soil is homogeneous and is laterally confined.
- The soil is fully saturated.
- Soil particles and water are incompressible.
- The flow of water is one-dimensional.
- Darcy's law describes the flow of water through soil.
- The permeability coefficient k remains constant.
- The relationship between e and σ' is linear during a stress increment.
- The soil's own weight has negligible effects.

Consolidation of a Soil Layer under Constant Load

Equation 26 is a partial differential equation with two variables, time t and position y . The unknown function is the excess pore water pressure, noted hereafter as $u(y, t)$. Equation 26 can be solved for the particular boundary and initial conditions of Fig. 17, which represents the consolidation test. As shown in Fig. 17b, when the layer is drained at the top and bottom, the boundary conditions are

$$u(0, t) = u(H, t) = 0 \text{ for } t \geq 0 \quad (28)$$

When the initial excess pressure is uniform in the layer at time $t = 0$, the initial conditions are

$$u(y, 0) = u_i \text{ for } 0 < y < H \quad (29)$$

The analytical solution of Eqs. 26 to 29 is

$$u(y, t) = u_i \sum_{n=0}^{\infty} \frac{4}{(2n+1)\pi} \sin \left[(2n+1)\pi \frac{y}{H} \right] e^{-(2n+1)^2 \pi^2 T_v / 4} \quad (30)$$

where $T_v = \frac{C_v t}{d^2}$ is the dimensionless time factor, and $d = H/2$ is the drainage distance. Equation 30 applies when the water drains at both top and bottom surfaces

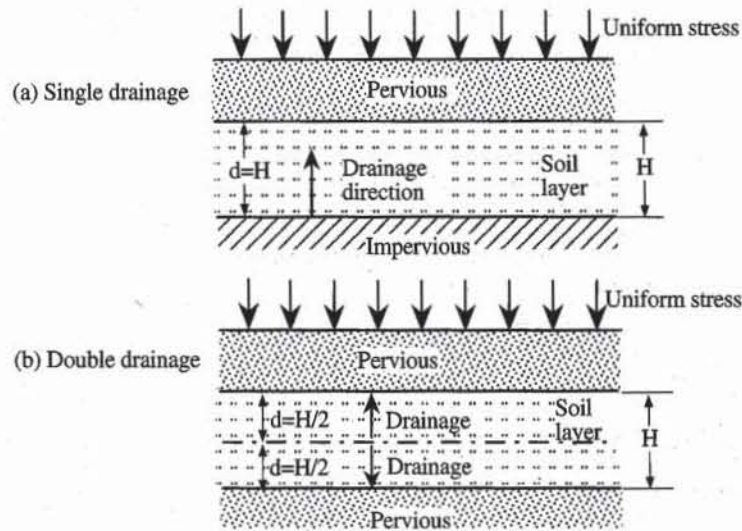


Figure 17 Definition of (a) single- and (b) double-drainage consolidation problems.

(double drainage, Fig. 17a). When the water drains at only one surface (single drainage, Fig. 17b). Eq. 30 can also be applied by using $d = H$. In the standard consolidation test, the sample is between two porous disks (i.e., $d = H/2$).

When the change in total stress $\Delta\sigma$ applied to the layer is kept constant, the change in effective stress $\Delta\sigma'(y, t)$ and excess pore pressure $u(y, t)$ in the layer are related through

$$\Delta\sigma = u_i = \Delta\sigma'(y, t) + u(y, t) \quad (31)$$

At the beginning of consolidation, $\Delta\sigma'(y, t) = 0$ and $u(y, t) = u_i$. At the end of consolidation, $\Delta\sigma'(y, t) = \Delta\sigma$ and $u(y, t) = 0$. The progress of consolidation at position y and time t is then characterized by introducing the degree U_y of consolidation

$$U_y = \frac{u_i - u(y, t)}{u_i} = \frac{\Delta\sigma'(y, t)}{\Delta\sigma} \quad (32)$$

where $U_y = 0$ at the beginning of consolidation and $U_y = 1$, at the end of consolidation. The settlement of a small element of thickness dy is ds_f after consolidation, and $ds(t)$ at time t during consolidation

$$ds_f = m_v \Delta\sigma dy \quad \text{and} \quad ds(t) = m_v \Delta\sigma'(y, t) dy = m_v \Delta\sigma U_y dy \quad (33)$$

Using Eq. 33, the total settlement of the layer of thickness H after and during consolidation are

$$s_f = \int_0^H ds_f = m_v H \Delta\sigma \quad \text{and} \quad s(t) = \int_0^H ds(t) = \frac{s_f}{H} \int_0^H U_y dy = s_f U \quad (34)$$

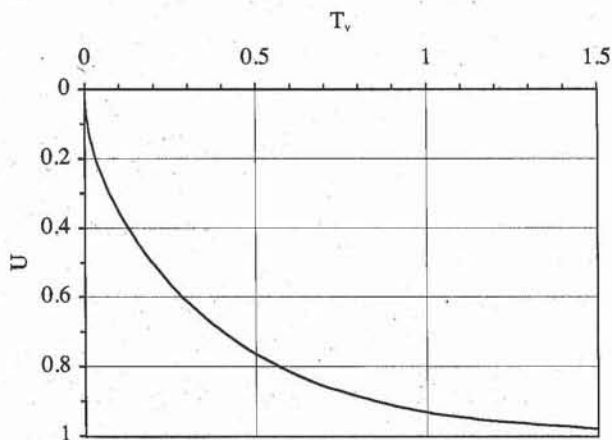


Figure 18 Relation between U and T_v .

where U is the average degree of consolidation of the entire layer,

$$U = \frac{1}{H} \int_0^H U_y dy \quad (35)$$

Using Eq. 30, Eq. 35 becomes:

$$U = 1 - \frac{8}{\pi^2} \sum_{\substack{m=1 \\ \text{odd}}}^{+\infty} \frac{e^{-m^2\pi^2 T_v/4}}{m^2} \quad (36)$$

Figure 18 shows the variation of U with T_v which is given by Eq. 36. U varies from 0 at the beginning of consolidation ($T_v = 0$) and tends toward 1 at the end of consolidation ($T_v \rightarrow \infty$). Eq. 36 can be approximated as follows:

$$U(T_v) = \begin{cases} U_1(T_v) = \sqrt{\frac{4}{\pi} T_v} & \text{for } T_v < 0.2827 \\ U_2(T_v) = 1 - \frac{8}{\pi^2} \exp\left(-\frac{\pi^2}{4} T_v\right) & \text{for } T_v \geq 0.2827 \end{cases} \quad (37)$$

or inversely,

$$T_v(U) = \begin{cases} T_1(U) = \frac{\pi}{4} U^2 & \text{for } U < 0.6 \\ T_2(U) = -0.085 - 0.933 \log(1 - U) & \text{for } U \geq 0.6 \end{cases} \quad (38)$$

Several methods for determining the coefficient of consolidation from experimental results are based on Eqs. 34 to 38. These methods are described later in this chapter.

Initial, Primary, and Secondary Compressions, and Compression Ratios

Equation 26 describes the time-dependent deformation of soils that results from the diffusion of water. However, this phenomenon, hereafter referred to as the *primary consolidation* or *primary compression*, is not the only phenomenon taking place during the consolidation test; it is accompanied by initial and secondary compressions. Figure 19 introduces these different compressions by using a typical variation of dial reading with time during consolidation test. The dial reading indicates the settlement of the soil sample.

As shown in Fig. 19, the dial reading d_0 at the beginning of primary consolidation (i.e., $U = 0\%$) is different from the dial reading d_c at $t = 0$, due to the *initial compression*, which takes place before the primary consolidation, almost instantaneously with the load application. The initial compression corresponds to an abrupt settlement unexplained by the primary consolidation, and is due partly to the compression of small pockets of gas within the pore spaces, and partly to the elastic compression of soil grains.

As shown in Fig. 19, the *secondary compression*, also referred to as creep, continues after the primary consolidation is completed and the excess pore pressure is dissipated. The final dial reading d_f is larger than d_{100} corresponding to $U = 100\%$. The secondary compression is caused by the particle movements and readjustments without a change in effective stress. For most soils, it also takes place during primary compression to a negligible extent, and becomes only noticeable near the completion of the primary compression. The secondary compression phenomenon will be covered in more detail later.

The relative magnitude of initial, primary and secondary phases is expressed in terms of the *initial compression ratio* r_i , *primary compression ratio* r_p , and *secondary compression ratio* r_s :

$$r_i = \frac{d_c - d_0}{d_c - d_f}, \quad r_p = \frac{d_0 - d_{100}}{d_c - d_f}, \quad \text{and} \quad r_s = \frac{d_{100} - d_f}{d_c - d_f} \quad (39)$$

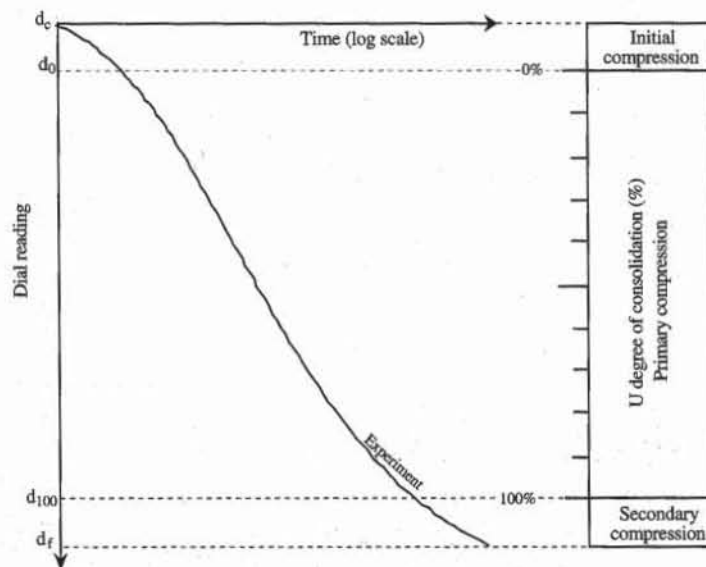


Figure 19 Initial, primary, and secondary compressions during the consolidation test.

where d_c is the initial dial reading, d_f the final dial reading, d_0 the dial reading at the beginning of primary consolidation, and d_{100} the dial reading at the end of primary consolidation. The compression ratios r_i , r_p , and r_s are the proportions of initial (i.e., $d_c - d_0$), primary (i.e., $d_0 - d_{100}$), and secondary (i.e., $d_{100} - d_f$) compressions to the total compression (i.e., $d_c - d_f$). r_i , r_p , and r_s are dimensionless, and $r_i + r_p + r_s = 1$. For most inorganic clays, the primary compression ratio r_p is larger than r_i and r_s . Several methods for determining the compression ratios are described later in this chapter.

Typical Values and Correlations for Consolidation Coefficients

Table 2 lists the values of consolidation coefficients C_v for various soils and indicates their range of variation. The smallest value for C_v is equal to 0.1 m²/yr in the case of sensitive Swedish clay, whereas the largest value is about 30,000 m²/yr which implies a very rapid rate of consolidation. Sands and gravels may have even larger consolidation coefficients due to their large permeability coefficient. Figure 20 shows the approximate relation between the coefficient of consolidation with the liquid limit in cases of undisturbed and remolded samples of fine-grained soils.

TABLE 2

Values of consolidation coefficient for various soils.

Type of soil	Coefficient of consolidation (m ² /yr)	Coefficient of consolidation (10 ⁻⁴ cm ² /s)	References
Mexico City clay (MH)	0.9-1.5	0.28-0.47	Leonards and Girault (1961)
Boston blue clay (CL, marine deposit glacial clay, illite)	6-18	1.89-5.68	Ladd and Lusher (1965)
Organic silt (OH)	0.6-3.0	0.19-0.95	Lowe et al. (1964)
Glacial lake clays (CL)	2.0-2.7	0.63-0.85	Wallace and Otto (1964)
Chicago silty clay (CL)	2.70	0.85	Terzaghi and Peck (1967)
Swedish medium-sensitive clays (CL-CH)	0.1-0.2	0.03-0.06	Holtz and Broms (1972)
San Francisco Bay mud (CL)	0.6-1.2	0.19-0.38	
Maine clay (silty, glacial clay, partially illite)	6.3-13	1.99-3.97	
Normally consolidated stuarine silty clay	3.17-32	1-10	Lee et al. (1983)
Stiff red clay	3.17	1	
Sandy clay	32-317	10-100	
Silt	317-31710	100-10000	
London clay	1.90-6.34	0.6-2.0	Skempton and Henkel (1957)
Shellhaven postglacial clay	1.27-3.81	0.4-1.2	Skempton and Henkel (1953)
Tilbury postglacial clay	2.85-3.49	0.9-1.1	
Calcareous silt (normally consolidated)	1015	320	Poulos (1980)
Carbonate silt	222	70	
Marine clay	634-6342	200-2000	Bishop and Henkel (1962)
Boulder clay	63-634	20-200	
Boulder clay and residual clay	3.17-630	1-20	

ALTERNATE CONSOLIDATION TESTS

One of the major disadvantages of the consolidation test is the length of time required for completion. A typical test can take up to two weeks (see Chapter 6-2). To reduce the testing period, several alternate methods have been proposed.

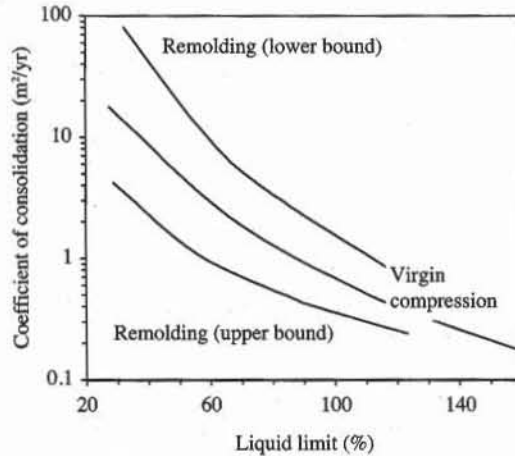


Figure 20 Approximate correlation of the coefficient of consolidation with liquid limit (after NAVFAC, 1982).

Summary of Alternate Tests

The principles of the alternate consolidation test can be explained by using the experimental setup of Fig. 21. The soil sample in the consolidation cell is subjected to the total stress σ which is applied by the piston moving at a control rate of either displacement or load. The water is allowed to drain through the upper face of the sample, and is kept at the back pressure u_B . On the lower side of the sample, there is no drainage and a pore pressure transducer records the pore pressure u_A . The settlement Δh of the sample is recorded by a displacement transducer.

Using Figs. 21 and 22, the various consolidation methods can be summarized as follows:

- (a) *Conventional incremental loading*: the total stress σ is kept constant during each loading segment.
- (b) *Constant rate of strain (CRS)*: the vertical deformation Δh is applied at a constant rate.
- (c) *Constant rate of loading*: the applied total stress σ is increased at a constant rate.
- (d) *Constant pore pressure gradient*: the difference in pore pressure $u_A - u_B$ between the upper and lower faces of the sample is kept constant.
- (e) *Constant ratio of pore pressure to load*: the loading is applied such that the pore pressure u_A is always a fixed proportion of the total stress σ .
- (f) *Consolidation with back pressure control*: the back pressure u_B is initially equal to the pore pressure u_A in the sample and is steadily reduced to a constant final value.

We will only briefly summarize the constant rate of strain consolidation, which is covered by ASTM 4186. The description of other procedures can be found in Head (1986) and Lowe et al. (1969).

Constant Rate of Strain Consolidation

During the *constant rate of strain (CRS) consolidation* tests, the vertical deformation Δh is applied at a constant rate, and the pore pressure u_A and total stress σ

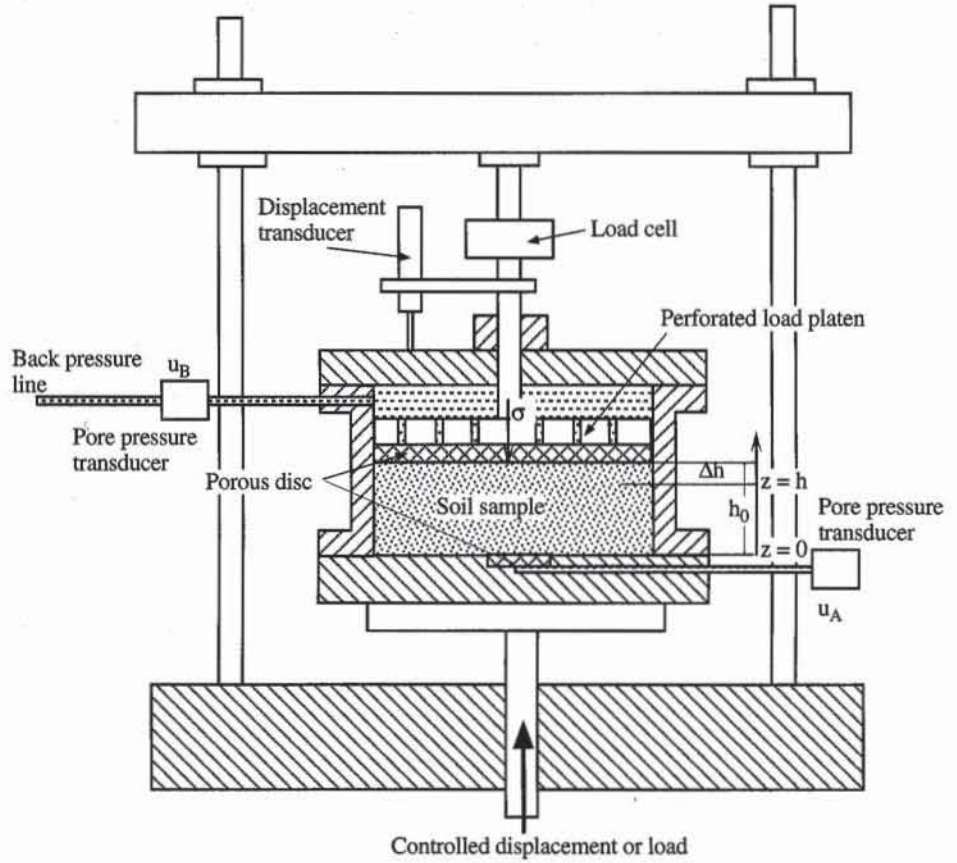


Figure 21 Experimental setup for alternate consolidation test (after Head, 1986).

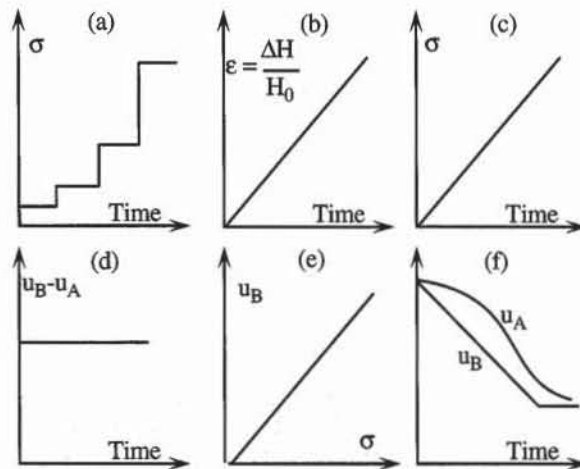


Figure 22 Representation of loading patterns for consolidation tests: (a) conventional incremental loading, (b) constant rate of strain, (c) constant rate of loading, (d) constant pore pressure gradient, (e) constant pore pressure ratio, and (f) back pressure control.

are measured at specified time intervals. The back pressure u_B is set equal to zero. The spatial distribution of pore pressure within the layer of thickness h is assumed to be parabolic, that is

$$u(z, t) = u_A(t) \left(1 - \frac{z^2}{h^2}\right) \quad (40)$$

and obeys the following boundary conditions

$$u(0, t) = u_A(t), \quad u(h, t) = u_B = 0, \quad \text{and} \quad \frac{\partial u}{\partial z}(0, t) = 0 \quad (41)$$

The layer thickness is h_0 at time $t = 0$, and decreases at the constant rate r specified during the test. The average pore pressure excess in the layer is

$$\bar{u}(t) = \frac{1}{h} \int_0^h u(z, t) dz = \frac{2}{3} u_A(t) \quad (42)$$

The rate of change in volume of water is

$$\frac{dV_w}{dt} = \frac{k}{\gamma_w} \frac{\partial^2 u}{\partial z^2} A = -\frac{2k}{\gamma_w} \frac{u_A(t)}{h^2} A = -rA \quad (43)$$

where A is the surface area of the soil sample. The average effective stress in the layer is:

$$\bar{\sigma}'(t) = \sigma(t) - \bar{u}(t) = \sigma(t) - \frac{2}{3} u_A(t) \quad (44)$$

The rate of change in volume of solid is

$$\frac{dV_v}{dt} = -m_v \frac{\partial \bar{\sigma}'}{\partial t} A = -m_v \left(\frac{d\sigma}{dt} - \frac{2}{3} \frac{du_A}{dt} \right) A = -rA \quad (45)$$

Therefore the consolidation coefficient is:

$$C_v(t) = \frac{k}{\gamma_w m_v} = \frac{1}{2} \left(\frac{d\sigma}{dt} - \frac{2}{3} \frac{du_A}{dt} \right) \frac{h^2}{u_A(t)} \quad (46)$$

Replacing the time derivative by small increment, Eq. 46 becomes

$$C_v \approx \frac{\bar{h}^2}{2\bar{u}_A \delta t} \left(\delta\sigma - \frac{2}{3} \delta u_A \right) \quad (47)$$

where δt is the time interval between two measurements, \bar{h} the average height during δt , \bar{u}_A the average excess pore pressure during δt , $\delta\sigma$ the change in applied total stress during δt , and δu_A the change in excess pore pressure during δt . The average coefficient of consolidation in a time interval can also be calculated as follows (ASTM 4186)

$$C_v \approx \frac{\bar{h}^2 \log \left(\frac{\sigma_2}{\sigma_1} \right)}{2(t_2 - t_1) \log \left(1 - \frac{\bar{u}_A}{\bar{\sigma}} \right)} \quad (48)$$

where σ_1 is the total stress at time t_1 , σ_2 the total stress at time $t_2 = t_1 + \delta t$, \bar{h} the average height during δt , and $\bar{\sigma}$ the average total stress during δt . The average effective stress $\bar{\sigma}'$ in the layer during δt is

$$\bar{\sigma}' = \bar{\sigma} - \frac{2}{3} \bar{u}_A \quad (49)$$

and the corresponding void ratio e is

$$e = e_0 - \frac{\Delta h}{h_0} (1 + e_0) \quad (50)$$

where e_0 is the initial void ratio and h_0 the initial sample height.

Like the conventional consolidation test, the CRS consolidation test gives the variation of effective stress and coefficient of consolidation with void ratio. However, the CRS consolidation does not last as long as the conventional test because it does not wait for the complete dissipation of pore pressure. The duration of the test is controlled by the strain rate. ASTM 4186 recommends to select a strain rate so that the excess pore pressure remains between 3 and 30% of the applied stress at any time during the test. One of the disadvantages of the CRS consolidation test is to require the measurement of pore pressure and force.

Figure 23 shows the results of a CRS consolidation test at constant strain rates of 0.024 and 0.06% per min on Masena clay (Smith and Wahls, 1969). The CRS consolidation results are in good agreement with those of conventional tests, especially at lower strain rate.

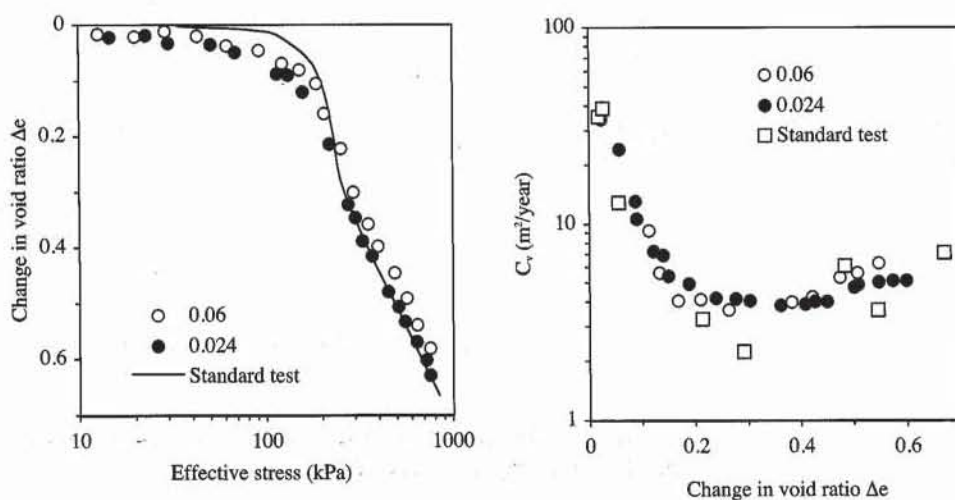


Figure 23 Results of constant rate of strain consolidation tests at 0.024 and 0.06% per min on Masena clay and comparison with standard tests (after Smith and Wahls, 1969).

SECONDARY COMPRESSION

As mentioned previously, the settlement of fine-grained soils in the consolidation test is caused not only by primary consolidation but also by secondary compression. In contrast to primary consolidation, secondary compression takes place at constant effective stress and without a diffusion of excess pore pressure.

Theory

In general, while the excess pore pressure is still dissipating, both primary and secondary compressions take place simultaneously, which complicates interpretation of the consolidation test results. Hereafter, secondary compression is assumed to be negligible during primary compression, and is identified after primary consolidation is completed.

Secondary compression is reported by using expressions similar to those used for primary compression. The change in void ratio Δe_s resulting from secondary compression from time t_s to time t is described as follows (Mesri and Godlewski, 1977):

$$\Delta e_s = C_\alpha \log_{10} \left(\frac{t}{t_s} \right) \quad (51)$$

where C_α is the secondary compression index. The secondary compression axial strain ϵ_s corresponding to Δe_s is

$$\epsilon_s = C_{\alpha e} \log_{10} \left(\frac{t}{t_s} \right) \quad (52)$$

where $C_{\alpha e}$ is the modified secondary compression index, which is related to C_α using Eq. 4:

$$C_{\alpha e} = \frac{C_\alpha}{1 + e_s} \quad (53)$$

e_s is the void at the beginning of the secondary compression. e_s may also be set equal to e_0 without introducing substantial errors. Using Eq. 41, the secondary compression settlement is

$$s_s = h_s C_{\alpha e} \log_{10} \left(\frac{t}{t_s} \right) \quad (54)$$

where h_s is the sample height at the beginning of secondary compression.

Typical Values and Correlations for Coefficient of Secondary Compression

Table 3 lists values of the ratio between the coefficient C_α of secondary compression and the compression index C_c . Values of C_α may be obtained by using the values of C_c listed in Table 1. As shown in Table 3, the ratio C_α/C_c is almost constant for a given soil, and varies from 0.025 to 0.1 for all soils.

As shown in Fig. 24, $C_{\alpha e}$ has been correlated to the natural water content

for a wide variety of clays. Based on Fig. 24, the following relation was suggested for normally consolidated clays

$$C_{\alpha\epsilon} = 0.0001 w_n \quad (55)$$

where w_n is the natural water content in percent.

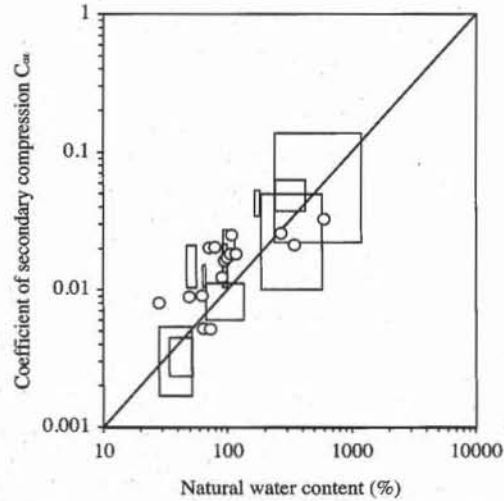


Figure 24 Variation of coefficient of secondary compression $C_{\alpha\epsilon}$ with natural water content (Mesri, 1973).

TABLE 3

Values of secondary consolidation coefficient for various soils (after Mesri and Godlewski, 1977).

Type of soil	C_{α}/C_c
Whangamarino clay	0.03–0.04
Norfolk organic silts	0.03
Calcareous organic silt	0.035–0.06
Amorphous and fibrous peat	0.035–0.083
Canadian Muskeg	0.09–0.10
Leda clay (Canada)	0.03–0.06
Peat	0.075–0.085
Post glacial organic clay	0.05–0.07
Soft blue clay	0.026
Organic clays and silts	0.04–0.06
Sensitive clay, Portland	0.025–0.055
San Francisco Bay Mud	0.04–0.06
New Liskeard varved clay (Canada)	0.03–0.06
Mexico City clay	0.03–0.035
Hudson River silt	0.03–0.06
New Haven organic clay silt	0.04–0.075

DETERMINATION OF CONSOLIDATION COEFFICIENTS

As derived in Eq. 34, during primary consolidation, the settlement $s(t)$ of soil samples at time t is

$$s(t) = s_f U(T_v) \quad \text{and} \quad T_v = \frac{C_v t}{d_m^2} \quad (56)$$

where s_f is the final settlement, C_v the coefficient of consolidation, d_m the average drainage distance, T_v the dimensionless time factor, and $U(T_v)$ the function of T_v given in Eqs. 36 to 38. During the consolidation test, the settlement $s(t)$ is continuously monitored by the displacement dial reading $d(t)$. In this case, Eq. 56 becomes

$$s(t) = d(t) - d_0 = s_f U(T_v) = (d_{100} - d_0) U(T_v) \quad (57)$$

where d_0 is the dial reading at the beginning of consolidation ($U = 0\%$), and d_{100} is the dial reading after completion of consolidation ($U = 100\%$). The dial reading $d(t)$ at time t is therefore

$$d(t) = d_0 + (d_{100} - d_0) U\left(\frac{C_v t}{d_m^2}\right) \quad (58)$$

The average drainage distance $d_m = h/2$ for samples between two porous disks (double drainage), and $d_m = h$ for single drainage where h is the average sample height during consolidation. In the case of double drainage, the average drainage distance d_m is

$$d_m = \frac{1}{2} \left(h_0 + d_i - \frac{1}{2} (d_{100} + d_0) \right) \quad (59)$$

where h_0 is the initial sample height corresponding to dial reading d_i . d_m also corresponds to $U = 50\%$.

The coefficient of consolidation C_v is determined by matching Eq. 58 with the data points that are relevant only to the primary consolidation. Four methods for determining C_v are presented, including two traditional procedures—the log-time and square-root-time methods—and two other methods based on regression analysis.

Log-Time Method

In the log-time method, the theoretical curve $U(T_v)$ is plotted by using a logarithmic scale for T_v , as shown in Fig. 25, and is matched with the experimental data points of primary consolidation by determining C_v , d_0 , and d_{100} . As shown in Fig. 26, d_0 is determined by selecting two experimental data points A and B that are both on the theoretical curve $T_v = T_1(U)$ for $U < 0.6$:

$$\frac{t_B}{t_A} = \frac{T_v^B}{T_v^A} = \frac{U_B^2}{U_A^2} = \frac{(d_B - d_0)^2}{(d_A - d_0)^2} \quad (60)$$

where d_A is the dial reading time at point A , t_A the time at point A , T_v^A the time factor at point A , and U_A the degree of consolidation at point A . Similar definitions apply for points B . By using Eq. 60, d_0 is

$$d_0 = \frac{d_A \sqrt{t_B} - d_B \sqrt{t_A}}{\sqrt{t_B} - \sqrt{t_A}} \quad (61)$$

It is a common practice to choose $t_A \approx 1$ min and $t_B \approx 4 t_A$ so that Eq. 61 becomes $d_0 = 2d_A - d_B$.

d_{100} is calculated by determining the end of primary consolidation (i.e., $U =$

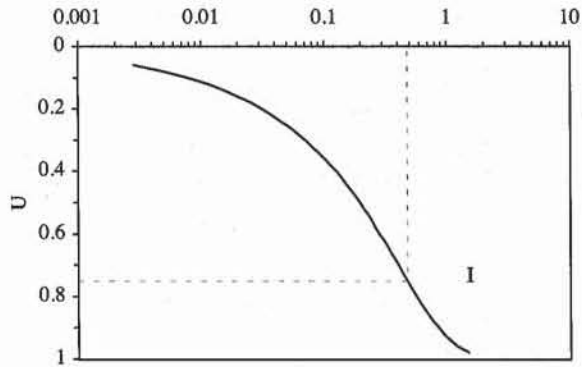


Figure 25 Theoretical relation $U(T_v)$ plotted with a logarithmic scale for T_v .

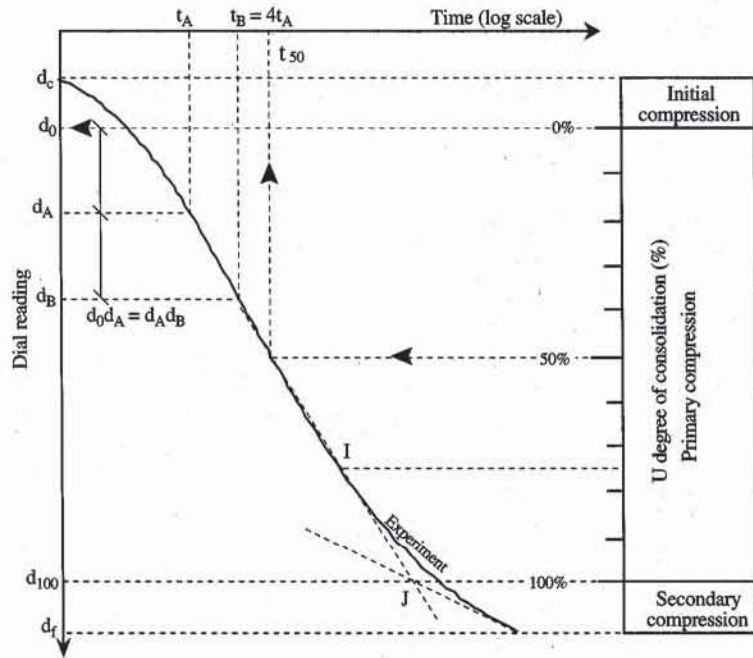


Figure 26 Determination of C_v with-log-time method.

100%). As shown in Fig. 25, the theoretical curve has a point of inflection I at $U \approx 75\%$. At point I , the curve has a different curvature and the steepest slope. As shown in Fig. 26, the intersection point J of the tangent point I with the backward extension of the secondary compression line defines the point where $U = 100\%$. The middle d_{50} of segment $d_0 d_{100}$ is

$$d_{50} = \frac{1}{2} (d_0 + d_{100}) \tag{62}$$

and corresponds to $U = 50\%$ and time t_{50} , which is thus obtained from the experimental curve. By using Eq. 17 with $U = 50\%$, $T_v = 0.197$ and C_v is

$$C_v = 0.197 \frac{d_m^2}{t_{50}} \tag{63}$$

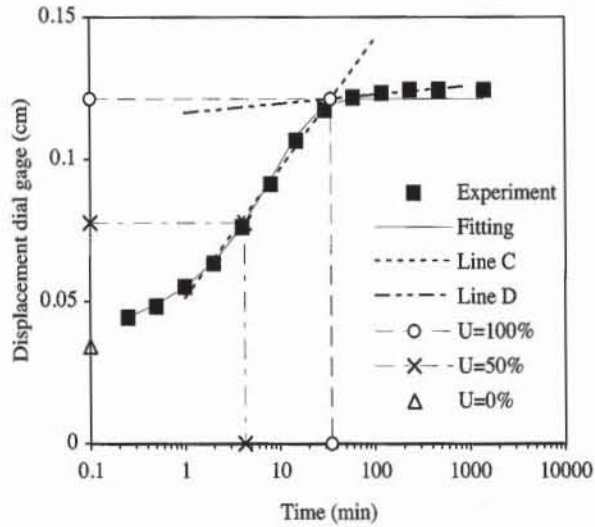


Figure 27 Determination of C_v with log-time method.

Example of C_v Determination with Log-Time Method

Figure 27 to 30 show the experimental and fitted results, the calculation details, and the formulas used for the consolidation test. The straight lines *C* and *D* of Fig. 27 are tangent to the experimental curve on each side of the inflection point. They are determined by using a linear regression through selected data points and give the intersection point (t_{100}, d_{100}) , which corresponds to $U = 100\%$. The time t_{50} corresponding to d_{50} is calculated by using the user-defined function INTER, which performs a linear interpolation on the points $(\log_{10} t_i, d_i)$ (see Chapter 8-1). The fitted data points are determined by using Eq. 58. $U(T_v)$ is implemented in the user-defined function *U* of Fig. 30. As shown in Fig. 27, there is a very good agreement between the experimental and fitted points, which implies that C_v is defined correctly.

Square-Root-Time Method

The function $U(T_v)$ is plotted in Fig. 31 versus the square root of T_v . The square-root-time method determines d_0, d_{100} , and C_v so that the theoretical curve of Fig. 31 falls as closely as possible to the experimental data points relevant to the primary consolidation. The dial reading is plotted against the square root of time as shown in Fig. 32. d_0 is given by the intercept *D* of line *DB* passing through the straight part of the experimental curve.

The next step is to find t_{90} and d_{90} corresponding to $U = 90\%$. Using Eq. 38 for $U = U_s$, we obtain

$$\sqrt{\frac{t_2(U_s)}{t_1(U_s)}} = \sqrt{\frac{T_2(U_s)}{T_1(U_s)}} = \frac{2}{U_s \sqrt{\pi}} \sqrt{-0.085 - 0.933 \log_{10}(1 - U_s)} = \alpha(U_s) \quad (64)$$

When $U_s = 0.9$, Eq. 64 becomes

$$\alpha(0.9) = 1.1545 \quad (65)$$

	A	B	C	D	E	F
1	Log-time method					
2	Time (min)	Displacement dial gage (cm)	Fitted displacement (cm)		line C	line D
3	t	d			Slope s_C or $s_D =$	0.0454 0.0032
4	0.0	0.0000	0.0340		Intercept i_C or $i_D =$	0.0512 0.1163
5	0.3	0.0445	0.0446		Time $t_A =$	1.0 min
6	0.5	0.0483	0.0490		Dial reading at time t_A , $d_A =$	0.0551 cm
7	1.0	0.0551	0.0552		Time $t_B =$	4.0 min
8	2.0	0.0635	0.0639		Dial reading at time t_B , $d_B =$	0.0762 cm
9	4.0	0.0762	0.0763	Dial reading at beginning of primary consolidation $d_0 =$	0.0340 cm	
10	8.0	0.0912	0.0928		Initial height $h_0 =$	1.905 cm
11	15.0	0.1067	0.1084		Initial dial reading $d_i =$	0 cm
12	30.0	0.1173	0.1189	Time at 100% of primary consolidation $t_{100} =$	34.79 min	
13	60.0	0.1217	0.1212	Dial reading at 100% of primary consolidation $d_{100} =$	0.1212 cm	
14	120.0	0.1232	0.1212	Dial reading at 50% of primary consolidation $d_{50} =$	0.0776 cm	
15	240.0	0.1245	0.1212	Time at 50% of primary consolidation $t_{50} =$	4.27 min	
16	480.0	0.1245	0.1212	Average drainage distance $d_m =$	0.9137 cm	
17	1440.0	0.1245	0.1212	Coefficient of consolidation $C_v =$	0.0385 cm ² /min	
18				Initial compression ratio $r_i =$	27.3%	
19				Primary compression ratio $r_p =$	70.1%	
20				Secondary compression ratio $r_s =$	2.6%	

Figure 28 Example of data set for determination of C_v with log-time method.

	D	E	F
3		Slope s_C or $s_D = \text{=SLOPE}(B10:B12, \text{LOG}(A10:A12))$	$\text{=SLOPE}(B13:B16, \text{LOG}(A13:A16))$
4		Intercept i_C or $i_D = \text{=INTERCEPT}(B10:B12, \text{LOG}(A10:A12))$	$\text{=INTERCEPT}(B13:B16, \text{LOG}(A13:A16))$
5		Time $t_A = \text{=A7}$	min
6		Dial reading at time t_A , $d_A = \text{=B7}$	cm
7		Time $t_B = \text{=A9}$	min
8		Dial reading at time t_B , $d_B = \text{=B9}$	cm
9		Dial reading at beginning of primary consolidation $d_0 = \text{=(dA*SQRT(tB)-dB*SQRT(tA))/(SQRT(tB)-SQRT(tA))}$	cm
10		Initial height $h_0 = 1.905$	cm
11		Initial dial reading $d_i = 0$	cm
12		Time at 100% of primary consolidation $t_{100} = \text{=10}^{((iD-iC)/(sC-sD))}$	min
13		Dial reading at 100% of primary consolidation $d_{100} = \text{=sC*LOG}(t_{100})+iC$	cm
14		Dial reading at 50% of primary consolidation $d_{50} = \text{=(d0+d_{100})/2}$	cm
15		Time at 50% of primary consolidation $t_{50} = \text{=INTER}(d_{50}, d, t)$	min
16		Average drainage distance $d_m = \text{=(h0+di-(d0+d_{100})/2)/2}$	cm
17		Coefficient of consolidation $C_v = \text{=0.197*dm}^2/t_{50}$	cm^2/min
18		Initial compression ratio $r_i = \text{=(B4-d0)/(B4-B17)}$	
19		Primary compression ratio $r_p = \text{=(d0-d_{100})/(B4-B17)}$	
20		Secondary compression ratio $r_s = \text{=1-r_i-r_p}$	

	C
2	Fitted displacement (cm)
3	
4	$\text{=d0+(d_{100}-d0)*U}(Cv*t/dm^2)$
5	$\text{=d0+(d_{100}-d0)*U}(Cv*t/dm^2)$

Figure 29 Formulas used in Fig. 28.

	B	C
2	U	Degree of consolidation
3	=RESULT(1)	
4	=ARGUMENT("T",1)	Dimensionless time factor
5	=IF(T>0.2827,RETURN(1-8/PI()*^2/EXP(PI()*^2*T/4)),RETURN(SQRT(4*T/PI())))	

Figure 30 User-defined function U used in Fig. 29.

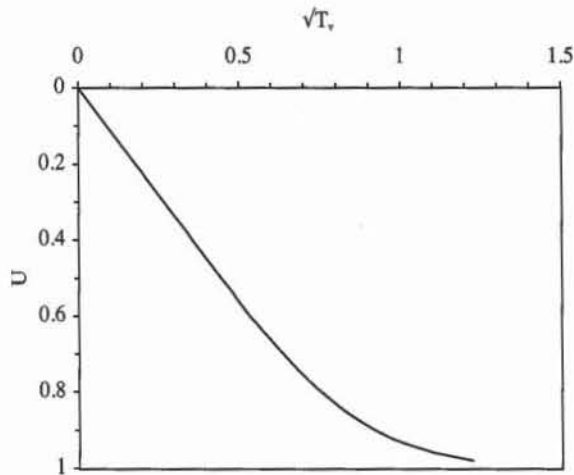


Figure 31 Theoretical relation $U(T_v)$ plotted versus the square root of T_v .

The time t_{90} corresponding to $U = 90\%$ is found by drawing the straight line DC , the slope of which is $1/1.1545$ times the slope of line DB . The straight line DC cuts the experimental consolidation curve at point E , which corresponds to $U = 90\%$ and has for coordinates d_{90} and $\sqrt{t_{90}}$. Using Eqs. 37 and 51, C_v and d_{100} are

$$C_v = 0.848 \frac{d^2}{t_{90}} \quad \text{and} \quad d_{100} = d_0 - \frac{10}{9}(d_0 - d_{90}) \quad (66)$$

Generalized Square-Root-Time Method

The square-root method can be generalized to values of U_s between 0.6 and 1. The slope of line DC is now $1/\alpha(U_s)$ times the slope of line DB . This generalized square-root method is implemented in the user-defined function CONSO. The first step is to select m data points and to fit them by linear regression with line DB :

$$d = d_0 + \beta \sqrt{t} \quad (67)$$

where d_0 is the intercept and β is the slope. The second step is to find the intersection between the data points and line DC :

$$d = d_0 + \beta' \sqrt{t} \quad \text{with} \quad \beta' = \frac{\beta}{\alpha(U_s)} \quad (68)$$

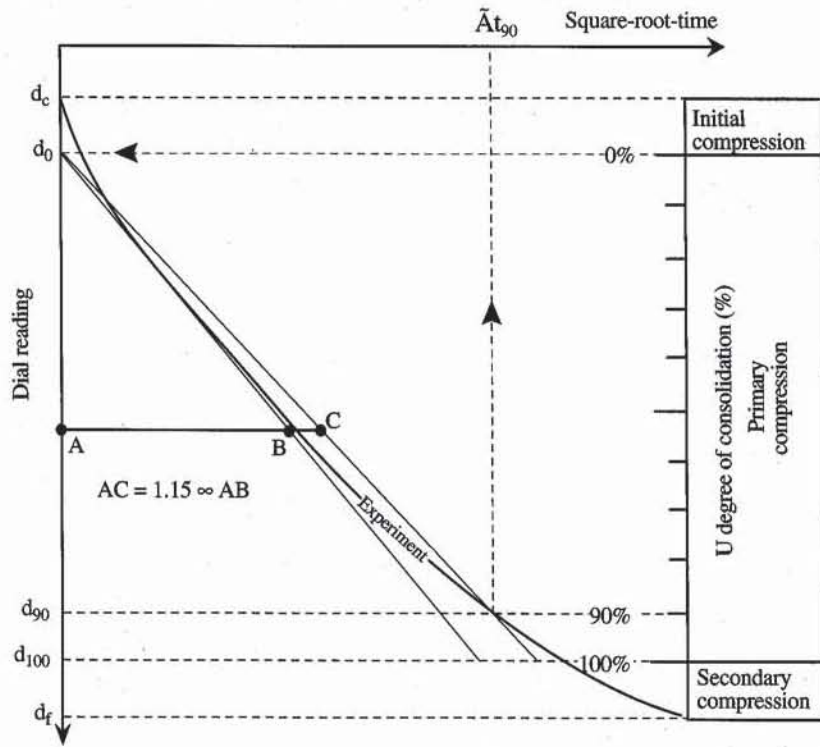


Figure 32 Determination of C_v with square-root-time method.

The n data points $(d_i, \sqrt{t_i})$ form jointed segments, each having the equation

$$d = d_i + \frac{d_{i+1} - d_i}{\sqrt{t_{i+1}} - \sqrt{t_i}} (\sqrt{t} - \sqrt{t_i}) \tag{69}$$

The segment connecting points i and $i + 1$ is intersected by line DC when

$$(d_i - d_0 - \beta' \sqrt{t_i}) (d_{i+1} - d_0 - \beta' \sqrt{t_{i+1}}) \leq 0 \tag{70}$$

The coordinates of the intersection point are

$$\sqrt{t_s} = \frac{(d_0 - d_i) (\sqrt{t_{i+1}} - \sqrt{t_i}) + (d_{i+1} - d_i) \sqrt{t_i}}{d_{i+1} - d_i - \beta' (\sqrt{t_{i+1}} - \sqrt{t_i})} \quad \text{and} \quad d_s = d_0 + \beta' \sqrt{t_s} \tag{71}$$

Therefore, the consolidation coefficient C_v and d_{100} are

$$C_v = T_v(U_s) \frac{d^2}{t_s} \quad \text{and} \quad d_{100} = d_0 + \frac{1}{U_s} (d_s - d_0) \tag{72}$$

User-Defined Function CONSO

Figure 33 lists the user-defined function CONSO for the generalized square-root-time method. CONSO determines the following quantities: t_s is the time at $U = U_s$, d_s the dial reading at $U = U_s$, d_0 the dial reading at $U = 0\%$, d_{100} the dial

A	B	C
12	Conso	User-defined function
13	=RESULT(64)	Input
14	=ARGUMENT("T";64)	t , time series
15	=ARGUMENT("D";64)	d , dial reading series
16	=ARGUMENT("H0";1)	h_0 , height of sample at beginning of time series
17	=ARGUMENT("TB";1)	t_b , time at beginning of square root time fitting
18	=ARGUMENT("TE";1)	t_e , time at end of square root time method
19	=ARGUMENT("US";1)	U_s , variable ($0.6 < U_s < 1$)
20	=IF(OR(ROWS(T)<>ROWS(D));RETURN(#VALUE!))	Arrays T and D must be in columns
21	n=ROWS(T)	Number of input data points
22	=SET.VALUE(D25:D29;(0,0,0,0,0))	Find slope b by using a
23	=FOR("I";1;n)	linear regression for square root time
24	= IF(AND(INDEX(T;I)>=TB;INDEX(T;I)<=TE))	with points such that $T_S \leq T \leq T_E$
25	m = SET.VALUE(m;m+1)	number of selected points
26	ax = SET.VALUE(ax;ax+SQRT(INDEX(T;I)))	sum of \sqrt{t}
27	ay = SET.VALUE(ay;ay+INDEX(D;I))	sum of d
28	axy = SET.VALUE(axy;axy+INDEX(D;I)*SQRT(INDEX(T;I)))	sum of $\sqrt{t} \cdot d$
29	axx = SET.VALUE(axx;axx+INDEX(T;I))	sum of t
30	= END.IF()	
31	=NEXT()	
32	aUs = 2*SQRT((-0.085-0.933*LOG(1-US))/PI())/US	$a(U_s)$
33	bp = (m*axy-ax*ay)/(m*axx-ax^2)/aUs	b' slope of straight line
34	d0 = (ay*axx-ax*axy)/(m*axx-ax^2)	d_0 , intercept of straight line
35	=FOR("I";1;n-1)	Find the intersection of straight line
36	= IF(INDEX(T;I)>TE)	with data segments
37	= IF((INDEX(D;I+1)-d0-bp*SQRT(INDEX(T;I+1)))*(INDEX(D;I)-d0-bp*SQRT(INDEX(T;I)))<=0)	
38	Dx = SQRT(INDEX(T;I+1))-SQRT(INDEX(T;I))	
39	Dd = INDEX(D;I+1)-INDEX(D;I)	
40	ts = ((d0-INDEX(D;I))*Dt+Dd*SQRT(INDEX(T;I))^2/(Dd-bp*Dl)^2	t_s , time at $U=U_s$
41	ds = d0+bp*SQRT(ts)	d_s , dial reading at $U=U_s$
42	= d0	d_0 , dial reading at $U=0\%$
43	d_100 = (ds-d0)/US+d0	d_{100} , dial reading at $U=100\%$
44	dm = (H0+INDEX(D;1)-(d0+d_100)/2)/2	d_m , average drainage length
45	Ov = Tv(US)*dm^2/ts	C_v , consolidation coefficient
46	ri = (INDEX(D;1)-d0)/(INDEX(D;1)-INDEX(D;n))	r_i , initial compression ratio
47	rp = (d0-d_100)/(INDEX(D;1)-INDEX(D;n))	r_p , primary compression ratio
48	rs = 1-ri-rp	r_s , secondary compression ratio
49	= RETURN(B40:B48)	Note:
50	= END.IF()	h_0 is not the initial sample height, but
51	= END.IF()	the height at beginning of time series
52	=NEXT()	
53	=RETURN(#VALUE!)	

Figure 33 User-defined function CONSO for determination of consolidation coefficient and compression ratios.

reading at $U = 100\%$, d_m the average drainage length, C_v the consolidation coefficient, r_i the initial compression ratio, r_p the primary compression ratio, and r_s the secondary compression ratio. The input data are: ($t_i, i = 1, \dots, n$) is the time series, ($d_i, i = 1, \dots, n$) the dial reading series, h_0 the sample height at dial reading d_i , t_b the starting time for fitting line DB , t_e the ending time for fitting line DB , and U_s the fitting degree of consolidation ($0.6 < U_s < 1$). All input data with the same dimension should have the same unit. The time series should be increasing and starting at $t_1 = 0$. Times t_b and t_e select the data points for fitting line DB . In general, t_b is selected equal to 1 min to eliminate initial compression. t_e is selected large enough to have at least three data points between t_b and t_e .

Example of C_v Determination with Square-Root-Time Methods

Figures 34 and 36 show the experimental results of Fig. 27 which are fitted by using the square-root-time method for $U_s = 90\%$ and 99% . Figures 35 to 38 compare the experimental and fitted curves, and list the formulas used in the calculation. The calculations are performed by the user-defined function CONSO. Times t_b and t_e select the data points for fitting line DB . Both square-root-time methods give similar results for C_v , r_i , r_p , and r_s . These values are also close to those found by the log-time method. The generalized method ($U_s = 99\%$) fits the data points slightly better than the conventional method ($U_s = 90\%$).

Nonlinear Optimization with Constraints

Nonlinear optimization with constraints (see Chapter 8-1) can be applied to optimize the following three variables: d_0 , d_{100} , and $C'_v = C_v/d_m^2$ with the following constraints:

$$d_0 \geq d_1, \quad d_{100} \leq d_n, \quad d_{100} \geq d_0, \quad \text{and} \quad C'_v \geq 0 \tag{73}$$

where d_1 is the first dial reading, and d_n is the last dial reading. The function to minimize is the error E between the experimental dial reading d_i and fitted dial reading $d_i^p = d_0 + (d_{100} - d_0)U(C'_v t_i)$ at time t_i :

$$E = \sum_{i=1}^n (d_i - d_i^p)^2 \tag{74}$$

	A	B	C	D	E	F	G
1	Square root-time method						
2	Elapsed (min)	Displacement dial gage (cm)	\sqrt{t} (√min)	Fitted displacement (cm)			
3	t	d					
4	0.0	0.0000	0.0	0.0336			
5	0.3	0.0445	0.5	0.0442	Initial height $h_n =$		1.905 cm
6	0.5	0.0483	0.7	0.0486	Starting time for fitting, $t_b =$		0.3 min
7	1.0	0.0551	1.0	0.0549	Ending time for fitting, $t_e =$		4.0 min
8	2.0	0.0635	1.4	0.0637	Degree of consolidation of method $U_s =$		99%
9	4.0	0.0762	2.0	0.0761	Time corresponding to U_s , $t_s =$		36.86 min
10	8.0	0.0912	2.8	0.0926	Dial reading corresponding to U_s , $d_s =$		0.1185 cm
11	15.0	0.1067	3.9	0.1077	Dial reading at beginning of primary consolidation $d_0 =$		0.0336 cm
12	30.0	0.1173	5.5	0.1174	Dial reading at 100% of primary consolidation $d_{100} =$		0.1193 cm
13	60.0	0.1217	7.7	0.1193	Average drainage distance $d_n =$		0.9143 cm
14	120.0	0.1232	11.0	0.1193	Coefficient of consolidation $C_v =$		0.0404 cm ² /min
15	240.0	0.1245	15.5	0.1193	Initial compression ratio $r_i =$		27.0%
16	480.0	0.1245	21.9	0.1193	Primary compression ratio $r_p =$		68.9%
17	1440.0	0.1245	37.9	0.1193	Secondary compression ratio $r_s =$		4.1%
18		initial slope = 0.021		0.00			0.0336
19				10.00			0.2463
20		modified slope = 0.014		0.00			0.0336
21				10.00			0.1734
22		intersection point		0.00			0.1185
23				6.07			0.1185

Figure 34 Data set for square-root-time method ($U_s = 90\%$).

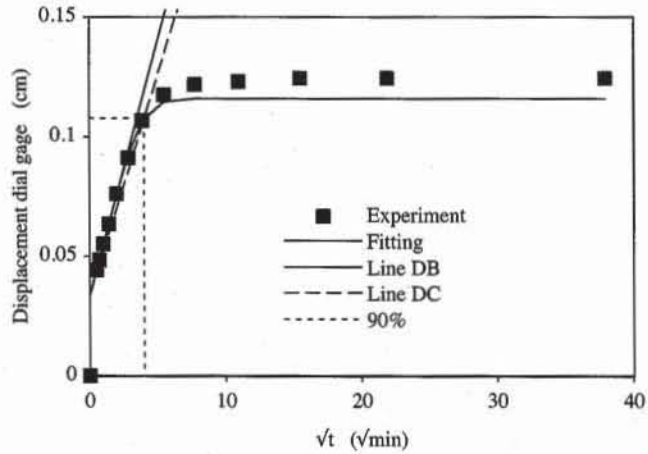


Figure 35 Experimental and fitted data points for the square-root-time method ($U_s = 90\%$).

	E	F	G
3			
4	Initial height $h_0 =$	1.905 cm	
5	Starting time for fitting, $t_b =$	0.3 min	
6	Ending time for fitting, $t_e =$	4.0 min	
7	Degree of consolidation of method $U_s =$	99%	
8	Time corresponding to U_s , $t_s =$	36.86 min	
9	Dial reading corresponding to U_s , $d_s =$	0.1185 cm	
10	Dial reading at beginning of primary consolidation $d_o =$	0.0336 cm	
11	Dial reading at 100% of primary consolidation $d_{100} =$	0.1193 cm	
12	Average drainage distance $d_m =$	0.9143 cm	
13	Coefficient of consolidation $C_v =$	0.0404 cm^2/min	
14	Initial compression ratio $r_i =$	27.0%	
15	Primary compression ratio $r_p =$	68.9%	
16	Secondary compression ratio $r_s =$	4.1%	

Figure 36 Data set for determination of consolidation coefficient and compression ratios with the generalized square-root-time method ($U_s = 99\%$).

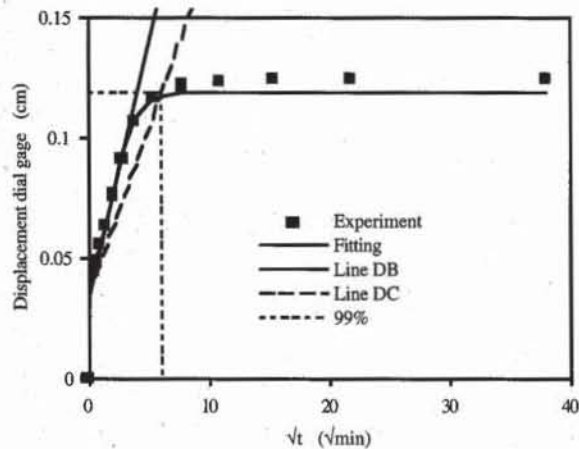


Figure 37 Experimental and fitted data points for the generalized square-root-time method ($U_s = 99\%$).

	C	D
	\sqrt{t} ($\sqrt{\text{min}}$)	Fitted displacement (cm)
2		
3		
4	=SQRT(t)	=d0+(d_100-d0)*U(Cv*t/dm^2)
5	=SQRT(t)	=d0+(d_100-d0)*U(Cv*t/dm^2)

	E	F	G
8	Time corresponding to U_s , $t_s =$	=Conso(t,d,h0,tb,te,Us)	min
9	Dial reading corresponding to U_s , $d_s =$	=Conso(t,d,h0,tb,te,Us)	cm
10	Dial reading at beginning of primary consolidation $d_0 =$	=Conso(t,d,h0,tb,te,Us)	cm
11	Dial reading at 100% of primary consolidation $d_{100} =$	=Conso(t,d,h0,tb,te,Us)	cm
12	Average drainage distance $d_m =$	=Conso(t,d,h0,tb,te,Us)	cm
13	Coefficient of consolidation $C_v =$	=Conso(t,d,h0,tb,te,Us)	cm ² /min
14	Initial compression ratio $r_i =$	=Conso(t,d,h0,tb,te,Us)	
15	Primary compression ratio $r_p =$	=Conso(t,d,h0,tb,te,Us)	
16	Secondary compression ratio $r_s =$	=Conso(t,d,h0,tb,te,Us)	

Figure 38 Formulas used in Figs. 34 and 36.

Once the optimal values of d_0 , d_{100} , and C'_v are found, d_m is given by Eq. 59, and $C_v = C'_v d_m^2$. Equation 73 applies when the dial readings increase with time, and for a decreasing series becomes

$$d_0 \leq d_1, \quad d_{100} \geq d_n, \quad d_{100} \leq d_0, \quad \text{and} \quad C'_v \geq 0 \quad (75)$$

Figures 39 and 40 show the same data set as that used for the square-root-time and log-time methods, and Fig. 41 lists the formulas used in Fig. 39. In Excel, the nonlinear optimization with constraints is performed by using SOLVER (see Chapter 8-1). Note that the first point is omitted in calculating E in order to remove the initial compression. At the beginning of the calculations, C'_v , d_0 , and d_{100} were set equal to 0.01, d_1 , and d_n . As shown in Fig. 39, SOLVER generally produces results that are more accurate than the log-time and square-root-time methods. In most cases the optimization converges without a problem when the variables C'_v , d_0 , and d_{100} are properly constrained and initialized.

Comparison of Methods

As shown in Table 4, all methods for determining C_v work well and give similar results. Compared to the log-time method, the square-root-time method can detect the beginning and end of primary compression during the consolidation test. It can also be used to start the next loading step automatically as soon as the primary consolidation is almost completed.

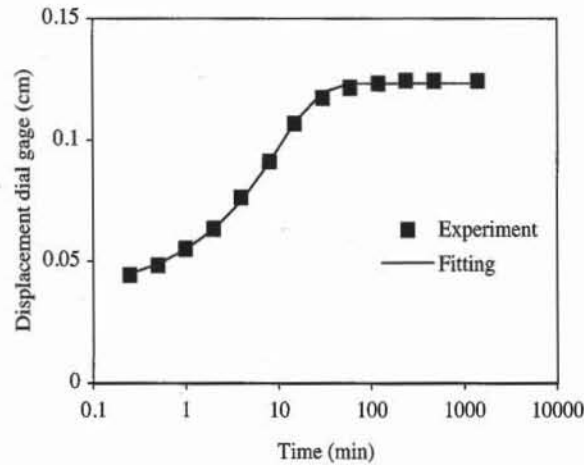


Figure 39 Experimental data points and fitting for nonlinear optimization with constraints.

	A	B	C	D	E	F
1	Solver method (only primary consolidation)					
2	Time (min)	Displacement dial gage (cm)	Fitted displacement (cm)			
3	t	d	d ^p	Dial reading at beginning of primary consolidation d ₀ = 0.0350 cm		
4	0.0	0.0000	0.0350	Dial reading at 100% of primary consolidation d ₁₀₀ = 0.1234 cm		
5	0.3	0.0445	0.0449	Coefficient C _v /d _m ² = 0.0400 1/min		
6	0.5	0.0483	0.0491	Error E = 0.0012 cm ²		
7	1.0	0.0551	0.0549	Initial height h ₀ = 1.905 cm		
8	2.0	0.0635	0.0632	Coefficient of consolidation C _v = 0.0333 cm ² /min		
9	4.0	0.0762	0.0748	Average drainage distance d _m = 0.9129 cm		
10	8.0	0.0912	0.0908	Initial compression ratio r _i = 28.1%		
11	15.0	0.1067	0.1070	Primary compression ratio r _p = 71.0%		
12	30.0	0.1173	0.1196	Secondary compression ratio r _s = 0.9%		
13	60.0	0.1217	0.1232			
14	120.0	0.1232	0.1234			
15	240.0	0.1245	0.1234			
16	480.0	0.1245	0.1234			
17	1440.0	0.1245	0.1234			

Figure 40 Data set and results of nonlinear optimization with constraints.

TABLE 4

Comparison of results obtained by log-time, square-root-time ($U_s=90\%$ and 99%), and SOLVER methods

	Method			
	Log	$U_s=90\%$	$U_s=99\%$	SOLVER
Dial reading at beginning of primary consolidation (cm) d ₀	0.0340	0.0336	0.0336	0.0350
Dial reading at 100% of primary consolidation (cm) d ₁₀₀	0.1212	0.1159	0.1193	0.1234
Coefficient of consolidation (cm ² /min) C _v	0.038	0.044	0.040	0.033
Initial compression ratio r _i (%)	27.3	27.0	27.0	28.1
Primary compression ratio r _p (%)	70.1	66.1	68.9	71.0
Secondary compression ratio r _s (%)	2.6	6.9	4.1	0.9

		C	
	2	Fitted displacement (cm)	
	3	d^p	
	4	$=d_0+(d_{100}-d_0)*U(C_v*t/d_m^2)$	
	5	$=d_0+(d_{100}-d_0)*U(C_v*t/d_m^2)$	
		D	E
6		Error E = =SUMPRODUCT(d-dp,d-dp)	cm ²
7		Initial height $h_0 = 1.905$	cm
8		Coefficient of consolidation $C_v = =E5*dm^2$	cm ² /min
9		Average drainage distance $d_m = =(h_0+B4-(d_0+d_{100})/2)/2$	cm
10		Initial compression ratio $r_i = =(B4-d_0)/(B4-B17)$	
11		Primary compression ratio $r_p = =(d_0-d_{100})/(B4-B17)$	
12		Secondary compression ratio $r_s = =1-ri-rp$	

Figure 41 Formulas used in Fig. 40.

Determination of Coefficient of Secondary Compression

Figures 42 and 43 show an example of consolidation test results obtained on a silt. Figure 44 lists the formulas used in Fig. 43. SOLVER is first used to define the primary compression parameters C_v , d_0 , and d_{100} . The first and last five data points are excluded from the SOLVER optimization, because they are attributed to the initial and secondary compressions. Using Eq. 54, the dial reading during the secondary compression is written as

$$d = d_s + h_s C_{\alpha\epsilon} \log_{10} \frac{t}{t_s} = A \log_{10}(t) + B \tag{76}$$

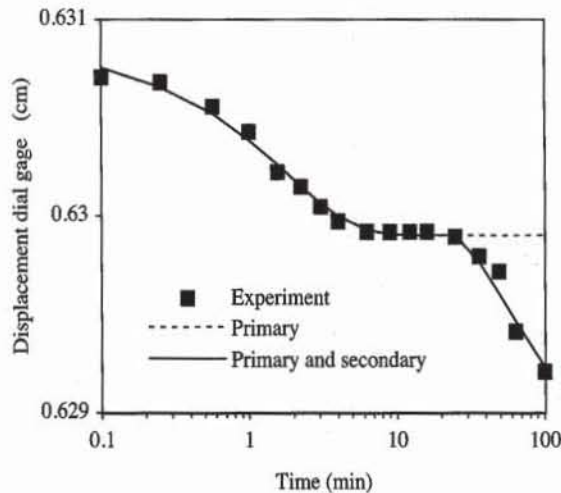


Figure 42 Experimental data and fittings for primary compression alone, and primary with secondary compressions.

	A	B	C	D	E	F	G
1	Solver method (primary and secondary consolidations)						
2	Measured		Fitted				
3	Time (min)	Displacement dial gage (cm)	Fitted displacement (cm)	Primary and secondary (cm)			
4	t	d	d ^p				
5	0.00	0.6312	0.6309	0.6309	Primary compression		
6	0.10	0.6307	0.6308	0.6308	Dial reading at beginning of primary consolidation d ₀ =	0.6309	cm
7	0.25	0.6307	0.6307	0.6307	Dial reading at 100% of primary consolidation d ₁₀₀ =	0.6299	cm
8	0.57	0.6306	0.6305	0.6305	Coefficient C _v = C _v /d _m ² =	0.2164	1/min
9	1.00	0.6304	0.6304	0.6304	Error E =	0.8579	
10	1.57	0.6302	0.6303	0.6303	Initial compression ration r _i =	14.5%	
11	2.25	0.6301	0.6302	0.6302	Primary compression ratio r _p =	51.0%	
12	3.07	0.6300	0.6301	0.6301	Secondary compression ratio r _s =	34.5%	
13	4.00	0.6300	0.6300	0.6300	Initial height h ₀ =	1.899	cm
14	6.25	0.6299	0.6299	0.6299	Dial reading at sample height h ₀ , d _i =	0.635	cm
15	9.00	0.6299	0.6299	0.6299	Average drainage distance d _m =	0.9518	cm
16	12.25	0.6299	0.6299	0.6299	Coefficient of consolidation C _v =	0.1961	cm ² /min
17	16.00	0.6299	0.6299	0.6299	Secondary compression		
18	25.00	0.6299	0.6299	0.6299	Slope s =	-0.0012	
19	36.00	0.6298	0.6299	0.6298	Intercept i =	0.6316	
20	49.00	0.6297	0.6299	0.6296	Sample height at beginning of secondary compression h _s =	1.9041	cm
21	64.00	0.6294	0.6299	0.6295	Starting time for secondary compression t _s =	27.73	min
22	100.00	0.6292	0.6299	0.6292	Modified secondary compression index C _{cs} =	0.063%	

Figure 43 Example of consolidation data set for determination of C_{cs}.

	E	F	G
8	Error E = =SUMPRODUCT(d-dp,d-dp)*1000000		
9	Initial compression ratio $r_i = =(B5-d0)/(B5-B22)$		
10	Primary compression ratio $r_p = =(d0-d_{100})/(B5-B22)$		
11	Secondary compression ratio $r_s = =1-r_i-r_p$		
12	Initial height $h_0 = 1.899$		cm
13	Dial reading at sample height h_0 , $d_1 = 0.635$		cm
14	Average drainage distance $d_m = =(h0+di-(d0+d_{100})/2)/2$		cm
15	Coefficient of consolidation $C_v = =Cvp*dm^2$		cm ² /min
16	Secondary compression		
17	Slope $s = =SLOPE(B18:B22,LOG(A18:A22))$		
18	Intercept $i = =INTERCEPT(B18:B22,LOG(A18:A22))$		
19	Sample height at beginning of secondary compression $h_s = =h0+di-d_{100}$		cm
20	Starting time for secondary compression $t_s = =10^((d_{100}-i)/s)$		min
21	Modified secondary compression index $C_{\alpha\epsilon} = =ABS(s/ha)$		

	C	D
	Fitted displacement (cm)	Primary and secondary (cm)
3		
4	d^p	
5	$=d0+(d_{100}-d0)*U(Cv*t/dm^2)$	$=IF(t>ta,dp-ha*Cae*LOG(t/ta),dp)$
6	$=d0+(d_{100}-d0)*U(Cv*t/dm^2)$	$=IF(t>ta,dp-ha*Cae*LOG(t/ta),dp)$

Figure 44. Formulas used in Fig. 43.

where d_s is the dial reading at time t_s when the secondary compression starts, and the coefficients A and B are

$$A = h_s C_{\alpha\epsilon} \quad \text{and} \quad B = d_s - A \log_{10}(t_s) \quad (77)$$

In the formulas of Fig. 44, the secondary compression is assumed negligible when $t < t_s$. The slope A and intercept B were calculated by linear regression. The dial reading at the beginning of secondary compression was set equal to d_{100} and the time t_s was calculated as follows:

$$t_s = 10 \frac{d_s - B}{A} \quad (78)$$

As shown in Fig. 42, there is a good agreement between the experimental and fitted data points.

REFERENCES

- See Introduction for references to ASTM procedures (pages 4 to 6).
- ARMOUR, D. W., Jr., and V. P. DRNEVITCH, 1986, Improved techniques for the constant-rate-of-strain consolidation for soils: Testing and evaluation, *ASTM Special Technical Publication No. 892*, Yong R. N. and F. C. Townsend, eds., American Society for Testing and Materials, Philadelphia, pp. 170-183.
- BISHOP, A. W., and D. J. HENKEL, 1962, *The Measurement of Soil Properties in the Triaxial Test*, 2nd ed., Edward Arnold, London, 228 p.
- CASAGRANDE, A., 1936, The determination of pre-consolidation load and its prac-

- tical significance, *Discussion D-34, Proceedings of the First International Conference on Soil Mechanics and Foundation Engineering*, Cambridge, Vol. III, pp. 60-64.
- DJOENAI, W. J., 1985, A Compendium of soil properties and correlations, *Master of Engineering Science Thesis*, School of Civil and Mineral Engineering, University of Sydney, Sydney, Australia.
- HEAD, K. H., 1986, *Manual of Soil Laboratory Testing, Vol. 3 Effective Stress Tests*, John Wiley & Sons, New York, pp. 1197-1225.
- HOLTZ, R. D., and B. B. Broms, 1972, Long-term loading tests at Skå-Edeby, Sweden: relation of undisturbed sampling to laboratory testing, *Proceedings of the ASCE Specialty Conference on Performance of Earth and Earth-Supported Structures*, Purdue University, West Lafayette, IN, Vol. 1, Part 1, pp. 435-464.
- HOLTZ, R. D., and W. D. KOVACS, 1981, *An Introduction to Geotechnical Engineering*, Prentice Hall, Englewoods Cliffs, NJ, pp. 283-423.
- KAUFMAN, R. I., and W. C. SHERMAN, Jr., 1964, Engineering measurements for Port Allen Lock, *J. Soil Mech. Found. Eng. Div.*, ASCE, Vol. 90, No. SM5, pp. 221-247.
- KULHAWY, F. H., and P. W. MAYNE, 1990, *Manual on Estimating Soil Properties for Foundations Design*, Report EL-9800 to Electric Power Research Institute, Cornell University, Ithaca, New York.
- LADD, C. C., and U. LUSCHER, 1965, Engineering properties of the soils underlying the M.I.T campus, *Research Report R65-68, Soil Publication 185*, Department of Civil Engineering, Massachusetts Institute of Technology, Cambridge, MA.
- LAMBE, T. W., and R. V. WHITMAN, 1979, *Soil Mechanics, SI Version*, John Wiley & Sons, New York, 553 p.
- LEE, I. K., W. WHITE, and O. G. INGLES, 1983, *Geotechnical Engineering*, Pitman Publishing, Marsfield, MA, 508 p.
- LEONARDS, G. A., and P. GIRAULT, 1961, A study of the one-dimensional consolidation test, *Proceedings of the Ninth International Conference on Soil Mechanics and Foundation Engineering*, Paris, Vol. 1, pp. 116-130.
- LEROUÉIL, S., F. TAVENAS, and J. P. LEBIHAN, 1983, Propriétés caractéristiques des argiles de l'est du Canada, *Can. Geotech. J.*, Vol. 20, No. 4, pp. 681-705.
- LOWE, J. III., P. F. ZACHEO, and H. S. FELDMAN, 1964, Consolidation testing with back pressure, *J. Soil Mech. Found. Eng. Div.*, ASCE, Vol. 90, No. SM5, pp. 69-86.
- LOWE, J. III., E. JONA, and V. OBRICIAN, 1969, Controlled gradient consolidation test, *J. Soil Mech. Found. Eng. Div.*, ASCE, Vol. 95, No. SM1, pp. 77-98.
- MACDONALD, A. B., and E. K. SAUER, 1970, The engineering significance of Pleistocene stratigraphy in the Saskatoon area, Saskatchewan, Canada, *Can. Geotech. J.*, Vol. 7, No. 2., pp. 116-126.
- MESRI, G., and P. M. GODLEWSKI, 1977, Time- and stress-compressibility interrelationship, *J. Geotech. Eng.*, ASCE, Vol. 103, No. 5, pp. 417-430.
- MESRI, G., Coefficients of secondary compression, *J. Soil Mech. Found. Eng. Div.*, ASCE, Vol. 99, No. SM1, pp. 123-137.
- MITCHELL, J. K., 1976, *Fundamentals of Soil Behavior*, John Wiley & Sons, New York, 422 p.
- NAVAFAC, 1982, *Soil Mechanics (Design Manual 7.1)*, Naval Facilities Engineering Command, Alexandria, 355 p.
- POULOS, H. G., 1980, A review of the behavior and engineering properties of car-

- bonate soils, *Research Report R381*, School of Civil Engineering, University of Sydney, Sydney, Australia, 46 p.
- RUTLEDGE, P. C., 1944, Relation of undisturbed sampling to laboratory testing, *Trans., ASCE*, Vol. 109, pp. 1162–1163.
- SKEMPTON, A. W., 1944, Notes on the compressibility of clays, *Q. J. Geol. Soc. London*, Vol. C, pp. 119–135.
- SKEMPTON, A. W., and D. J. HENKEL, 1953, The post-glacial clays of the Thames Estuary at Tillbury and Shellhaven, *Proceedings of the Third International Conference on Soil Mechanics and Foundation Engineering*, Zurich, Vol. 1, pp. 302–308.
- SKEMPTON, A. W., and D. J. HENKEL, 1957, Test on London clay from deep boring at Paddington, Victoria and the South Bank, *Proceedings of the Fourth International Conference on Soil Mechanics and Foundation Engineering*, London, Vol. 1, pp. 100–106.
- SMITH, R. E. and H. E. WAHL, 1969, Consolidation under constant rate of strain, *J. Soil Mech. Found. Eng. Div.*, ASCE, Vol. 95, No. SM2, pp. 519–538.
- TERZAGHI, K., and R. B. PECK, 1967, *Soil Mechanics in Engineering Practice*, 2nd Ed., John Wiley & Sons, New York, 729 pp.
- WALLACE, G. B., and W. C. OTTO, 1964, Differential settlement at Selfridge Air Force base, *J. Soil Mech. Found. Eng. Div.*, ASCE, Vol. 90, No. 5, pp. 197–220.
- WINTERKORN, H. F., and H. Y. FANG, 1975, Soil technology and engineering properties of soils, Chap. 2 of *Foundation Engineering Handbook*, H. F. Winterkorn and H. Y. Fang, eds., Van Nostrand Reinhold, New York, pp. 67–120.
- WISSA, A. E. Z., J. T. CHRISTIAN, E. H. DAVIS, and S. HEIBERG, 1971, Consolidation at constant rate of strain, *J. Soil Mech. Found. Eng. Div.*, ASCE, Vol. 97, No. SM10, pp. 1393–1421.
- WROTH, C. P., and D. M. WOOD, 1978, The correlation of index properties with some basic engineering properties of soils, *Can. Geotech. J.*, Vol. 15, No. 2, pp. 137–145.

REVIEW QUESTIONS

1. Which soil properties are measured during a consolidation test?
2. To what kinds of soils is the consolidation test applicable?
3. Which strain and stress components vary during a consolidation test?
4. What is the relation between volumetric strain and void ratio? Derive this relation.
5. Which is the most common system of coordinates to report the compressibility of soils?
6. Define *coefficient of compressibility* (m_v).
7. Why does m_v depend on the size and direction of the load increment?
8. How does m_v relate to the calculation of settlement?
9. What are the preconsolidation pressure and overconsolidation ratio?
10. Define *virgin consolidation line*.
11. What is a swelling line?
12. Define *compression index* (C_c) and *swelling index* (C_s).
13. What are two ways to define the preconsolidation pressure?
14. What are normally and overconsolidated clays?
15. Are there approximate relations to calculate the compression index in terms of the liquid limit?
16. What are the minimum and maximum values for C_c and swelling index C_s in soils?

17. Write the consolidation equation. Which variables does it relate? Which material parameters control the porewater pressure diffusion?
18. What is the dimensionless time factor T_v ?
19. What is the average degree of consolidation U ?
20. Which basic relation relates T_v and U when $U < 0.6$?
21. How many phases are distinguished during the consolidation tests? Which parameters characterize the relative importance of these phases?
22. What are primary and secondary compressions? What is their primary difference?
23. Define the initial, primary, and secondary compression ratios in terms of dial reading. What is the meaning of these ratios?
24. What methods are commonly used to determine the consolidation coefficient C_v ?
25. Briefly explain the log-time method.
26. Briefly explain the square-root-time method.
27. On which mathematical principle is the SOLVER method based?
28. How do you detect the secondary compression during the consolidation test?
29. What are log-time and square-root-time methods? What are the corrections introduced in these methods? Why do we need to introduce these corrections?
30. What are typical values for the coefficient of consolidation? In what units is it generally expressed?
31. Is there a relation between C_α and C_c ?
32. What is the relation between coefficients of consolidation and permeability? Does the coefficient of consolidation increase or decrease with permeability?

EXERCISES

1. For the data of Table E1, plot the $e-\sigma'$ curve and determine the preconsolidation pressure and compression and swelling indices. Plot the variation of compressibility m_v versus effective stress.
2. Same as Exercise 1 but for the data of Table E2.

TABLE E1

Effective stress (kPa)	Vertical strain (%)	Void ratio
1	1.1	2.56
3	2.2	2.52
4	4.4	2.44
10	14.3	2.08
21	23.7	1.75
41	31.3	1.47
82	38.2	1.22
22	37.0	1.27
6	34.2	1.37

Initial void ratio, 2.6.

TABLE E2

Soil type	Liquid limit (%)	Effective stress (kPa)	Void ratio e
CH-clay with silt	71	1.5	1.167
		27.5	1.157
		56.0	1.153
		202.2	1.121
		344.5	1.100
		210.3	1.103
		337.7	1.095
		888.3	0.879
		1605.9	0.722
		2.0	1.062

3. Same as Exercise 1 but for the data of Table E3.
4. Same as Exercise 1 but for the data of Table E4.
5. Same as Exercise 1 but for the data of Table E5.
6. Same as Exercise 1 but for the data of Table E6.
7. Same as Exercise 1 but for the data of Table E7.

TABLE E3

Soil type	Liquid limit (%)	Effective stress (kPa)	Void ratio e
CH-clay, soft	41	1.5	1.350
		28.7	1.335
		53.9	1.326
		101.3	1.301
		214.5	1.260
		312.1	1.236
		218.8	1.242
		107.5	1.259
		210.3	1.248
		312.1	1.231
		445.2	1.184
		1772.4	0.746
		445.2	0.821
		1.5	1.189

TABLE E4

Soil type	Liquid limit (%)	Effective stress (kPa)	Void ratio e
CL-clay, firm	50	1.5	1.005
		26.0	0.991
		186.8	0.947
		107.5	0.953
		53.9	0.960
		27.0	0.963
		16.2	0.968
		53.9	0.966
		256.2	0.937
		463.1	0.882
		1574.5	0.643
		436.5	0.658
		101.3	0.694
		1.5	0.815

TABLE E5

Soil type	Liquid limit (%)	Effective stress (kPa)	Void ratio e
CL-clay, soft	81	1.5	0.920
		25.5	0.905
		190.5	0.835
		56.0	0.839
		10.9	0.858
		24.0	0.858
		99.3	0.842
		277.2	0.820
		454.1	0.779
		871.0	0.674
		1637.9	0.604
		445.2	0.611
		105.4	0.638
		1.5	0.805

TABLE E7

Soil type	Effective stress (kPa)	Void ratio e
H28-1-1 CP2	2.0	13.926
	13.7	13.946
	25.4	13.864
	49.9	13.659
	114.9	12.982
	140.2	11.547
	164.3	10.337
	204.4	8.942
	393.6	6.399
	385.9	6.296
	204.4	6.460
	47.0	6.850
	25.4	7.055
	2.0	7.609
	13.2	7.527
	45.2	7.301
	102.0	7.096
	200.4	6.789
	378.3	6.235
	820.7	4.656
	335.8	4.840
	100.0	5.230
	42.6	5.373
23.5	5.537	
11.9	5.620	
2.0	5.763	

TABLE E6

Soil type	Liquid limit (%)	Effective stress (kPa)	Void ratio e
ML-sandy silt	31	1.5	0.841
		1.9	0.835
		9.5	0.821
		24.5	0.810
		53.9	0.794
		99.3	0.780
		202.2	0.760
		256.2	0.750
		107.5	0.752
		65.6	0.754
		190.5	0.752
		271.8	0.745
		436.5	0.723
		1605.9	0.623
		436.5	0.637
		91.8	0.645
		1.3	0.718

TABLE E8

Soil type	Effective stress (kPa)	Void ratio e
H28-1-2 CP1	2.0	11.772
	15.5	11.731
	28.6	11.690
	57.3	11.547
	129.5	10.439
	230.3	7.117
	443.4	5.250
	221.3	5.291
	129.5	5.373
	12.2	6.009
	1.8	6.460

TABLE E9

Soil type	Effective stress (kPa)	Void ratio e
H28-1-2 CP1	1.8	6.686
	26.4	6.460
	50.9	6.276
	119.6	5.948
	221.3	5.537
	452.3	5.004
	981.3	3.733
	1816.1	2.564
	3567.5	1.846
	5100.3	1.641
	1375.3	1.661
	672.9	1.702
	292.2	1.805
	96.1	1.928
	13.2	2.010
	2.0	2.010

8. Same as Exercise 1 but for the data of Table E8.
9. Same as Exercise 1 but for the data of Table E9.
10. By using the equations of linear isotropic elasticity, derive the elastic relation between void ratio and effective stress for the one-dimensional loading of the consolidation test. What is the relation between the compressibility coefficient, Young's modulus, and the Poisson ratio?
11. Plot the following $e-\sigma'$ curves and determine the preconsolidation pressures and compression and swelling indices. CP3 is a remolded sample from CP1. What is the effect of remolding on the consolidation properties?

Soil type	Effective stress (kPa)	Void ratio e
CP1	1.8	0.954
	15.3	0.916
	29.5	0.898
	69.6	0.867
	129.8	0.812
	272.1	0.748
	580.3	0.663
	1099.8	0.590
	1137.4	0.583
	590.1	0.596
	281.5	0.605
	136.5	0.620
	31.1	0.653
	1.8	0.743

Soil type	Effective stress (kPa)	Void ratio e
CP3	1.8	0.639
	7.9	0.634
	16.1	0.629
	30.5	0.620
	74.5	0.607
	151.0	0.573
	322.0	0.513
	652.8	0.459
	1258.2	0.394
	2728.4	0.340
	1196.3	0.346
	316.6	0.365
	78.4	0.382
	33.8	0.396
17.2	0.408	
1.7	0.447	

12. Plot the following $e-\sigma'$ curve and determine the preconsolidation pressures and compression and swelling indices. By using the Casagrande method, determine the preconsolidation pressure in the reloading section of the $e-\sigma'$ curve and compare it to the stress where unloading took place.
13. Plot the compression index versus liquid limit for the data in Table 1, and

Effective stress (kPa)	Void ratio e
58.3	0.368
105.0	0.365
203.5	0.359
424.3	0.347
792.4	0.335
1714.1	0.310
3201.3	0.284
1682.9	0.283
837.3	0.285
373.1	0.289
792.4	0.289
1622.2	0.287
3260.6	0.274
5762.9	0.250
12933.1	0.223
5762.9	0.228
3445.4	0.233
1652.3	0.238
25.5	0.256

compare the data points to the approximate relations between compression index and liquid limit.

14. For the data of Table E10, calculate the consolidation coefficient C_v and secondary compression coefficient $C_{\alpha e}$. The initial height is 1.899 cm and corresponds to the dial reading equal to 0.6350. Use the both square-root-time and log-time methods.
15. Same as Exercise 14 but for the data set of Table E11.
16. For the data of Table E12, calculate the consolidation coefficient C_v and secondary compression coefficient $C_{\alpha e}$. The initial height is 1.899 cm and corresponds to a dial reading of 0.6350. Use the generalized square-root-time method with $U_s = 90\%$ and 99% .
17. Same as Exercise 16 but for the data set of Table E13.

TABLE E10

Elapsed time (min)	Displacement dial gage (cm)
0.00	0.6350
0.10	0.6342
0.25	0.6340
0.57	0.6337
1.00	0.6335
1.57	0.6333
2.25	0.6332
3.07	0.6330
4.00	0.6328
6.25	0.6327
9.00	0.6325
12.25	0.6324
16.00	0.6323
25.00	0.6322
36.00	0.6320
49.00	0.6318
64.00	0.6315
100.00	0.6312

TABLE E11

Elapsed time (min)	Displacement dial gage (cm)
0.00	0.5288
0.25	0.5161
0.57	0.5118
1.00	0.5077
1.57	0.5033
2.25	0.4994
3.07	0.4959
4.00	0.4931
6.25	0.4883
9.00	0.4851
12.25	0.4826
16.00	0.4806
25.00	0.4778
36.00	0.4757
49.00	0.4737
64.00	0.4722
100.00	0.4700

TABLE E12

Elapsed time (min)	Displacement dial gage (cm)
0.00	0.6312
0.10	0.6307
0.25	0.6307
0.57	0.6306
1.00	0.6304
1.57	0.6302
2.25	0.6301
3.07	0.6300
4.00	0.6300
6.25	0.6299
9.00	0.6299
12.25	0.6299
16.00	0.6299
25.00	0.6299
36.00	0.6298
49.00	0.6297
64.00	0.6294
100.00	0.6292

TABLE E13

Elapsed time (min)	Displacement dial gage (cm)
0.00	0.6292
0.10	0.6279
0.25	0.6276
0.57	0.6271
1.00	0.6266
1.57	0.6261
2.25	0.6259
3.07	0.6256
4.00	0.6252
6.25	0.6248
9.00	0.6246
12.25	0.6243
16.00	0.6241
25.00	0.6238
36.00	0.6229
49.00	0.6228
64.00	0.6227
100.00	0.6227
900.00	0.6224

TABLE E14

Elapsed time (min)	Displacement dial gage (cm)
0	0.6224
0.25	0.6199
0.57	0.6193
1.00	0.6186
1.57	0.6181
2.25	0.6175
3.07	0.6172
4.00	0.6167
6.25	0.6161
9.00	0.6157
12.25	0.6152
16.00	0.6149
25.00	0.6144
36.00	0.6142
49.00	0.6140
64.00	0.6139
100.00	0.6137
120.00	0.6137
200.00	0.6131

TABLE E15

Elapsed time (min)	Displacement dial gage (cm)
0.00	0.5983
0.25	0.5921
0.57	0.5916
1.00	0.5906
1.57	0.5895
2.25	0.5880
3.07	0.5872
4.00	0.5867
6.25	0.5860
9.00	0.5853
12.25	0.5850
16.00	0.5847
25.00	0.5843
36.00	0.5838
49.00	0.5835
64.00	0.5834
100.00	0.5829

18. Same as Exercise 16 but for the data set of Table E14.
19. Same as Exercise 16 but for the data set of Table E15.
20. For the data of Table E16, calculate the consolidation coefficient C_v and secondary compression coefficient $C_{\alpha e}$ for the following data set. The initial height is 1.899 cm and corresponds to a dial reading of 0.6350. Calculate the compression ratios.
21. Same as Exercise 20 but for the data of Table E17.
22. Same as Exercise 20 but for the data of Table E18.

TABLE E16

Elapsed time (min)	Displacement dial gage (cm)
0.00	0.5829
0.25	0.5867
0.57	0.5872
1.00	0.5871
1.57	0.5878
2.25	0.5880
3.07	0.5883
4.00	0.5884
6.25	0.5886
9.00	0.5887
12.25	0.5887
16.00	0.5888
25.00	0.5890
36.00	0.5890
49.00	0.5891
64.00	0.5891
100.00	0.5892
900.00	0.5892

TABLE E17

Elapsed time (min)	Displacement dial gage (cm)
0.00	0.5916
0.25	0.5875
0.57	0.5861
1.00	0.5848
1.57	0.5838
2.25	0.5829
3.07	0.5824
4.00	0.5820
6.25	0.5814
9.00	0.5810
12.25	0.5834
16.00	0.5806
25.00	0.5804
36.00	0.5801
49.00	0.5799
64.00	0.5799
100.00	0.5797
110.00	0.5796
940.00	0.5789

TABLE E18

Elapsed time (min)	Displacement dial gage (cm)
0.00	0.2986
0.10	0.2796
0.25	0.2764
0.57	0.2690
1.00	0.2619
1.57	0.2553
2.25	0.2494
3.07	0.2440
4.00	0.2398
6.25	0.2337
9.00	0.2298
12.25	0.2272
16.00	0.2254
25.00	0.2228
36.00	0.2210
49.00	0.2190
64.00	0.2178
100.00	0.2161
1000.00	0.2060

6-2

Consolidation Test

OBJECTIVE

The consolidation (oedometer) test is used to determine the compression index C_c , swelling index C_s , and preconsolidation pressure σ'_p , which define the soil compressibility; the coefficient of consolidation C_v , which characterizes the rate of primary compression; and the secondary compression coefficient C_α , which defines the creep properties. We present only the conventional consolidation test (ASTM 2435).

EQUIPMENT

The equipment for the consolidation test includes:

- Consolidation loading device (see Figs. 1 and 2)
- Consolidation cell (see Figs. 3 and 4).
- Specimen trimmer and accessories (miter box, wire saw, and knives).
- Device for placing specimen in container.
- Balance sensitive to 0.1 g.
- Drying oven.
- Dial indicator or displacement transducer with a range of 10 mm and an accuracy of 0.002 mm.
- Timer.
- Moisture content cans.

Loading Devices

The most commonly used loading devices are the beam-and-weight mechanism and the pneumatic device (Fig. 1). Both devices apply a sudden axial load to the specimen and maintain it constant after that. Figure 2 shows the operating princi-

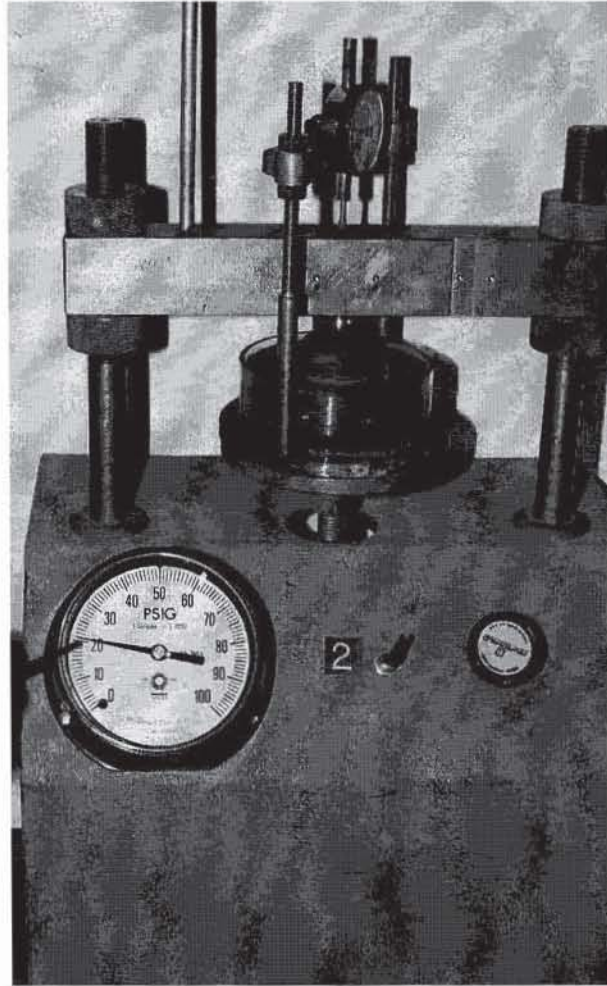


Figure 1 Equipment for the consolidation test.

ple of the pneumatic device of Fig. 1. The pressurized piston squeezes the sample against the reaction beam. The air pressure is adjusted with the pressure regulator and is controlled with the pressure gage. The toggle valve is useful to control the load increments. When the toggle valve is closed, the incoming air pressure is adjusted to the desired value with the air regulator, while the air pressure inside the piston remains constant. Then the toggle valve is released to transmit the new pressure to the sample.

Consolidation Cells

As shown in Figs. 3 and 4, there are two commonly used types of consolidation cells: fixed-ring and floating-ring cells. In the fixed-ring cell of Fig. 3, the specimen moves downward in relation to the ring, which generates friction drag on the sidewall. As described in Chapter 4-3, the fixed-ring cell may also be used as a falling head permeameter for measuring the soil permeability. In the floating-ring container of Fig. 4, compression occurs toward the middle from both top and bottom. The effect of friction between the container wall and the soil specimen is smaller than that of the fixed-ring container. However, unlike the fixed-ring container, the floating-ring cell cannot be used for permeability tests.

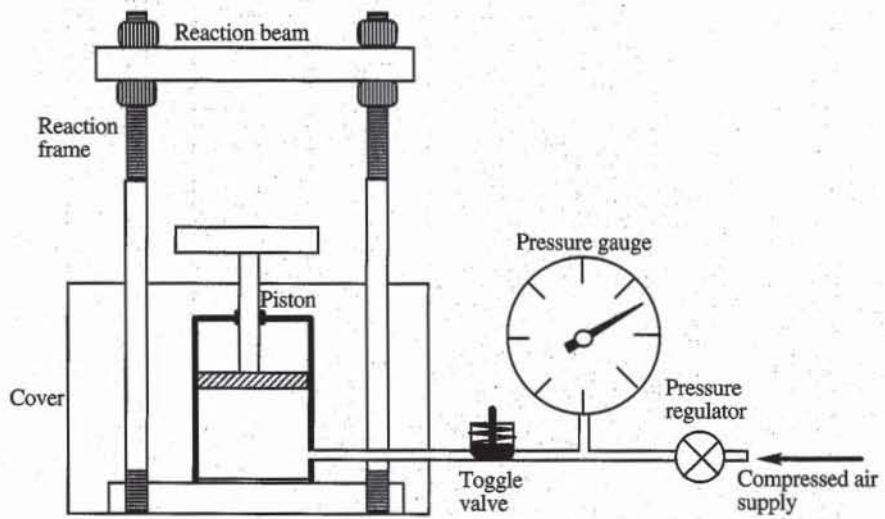


Figure 2 Pneumatic loading device for the consolidation test.

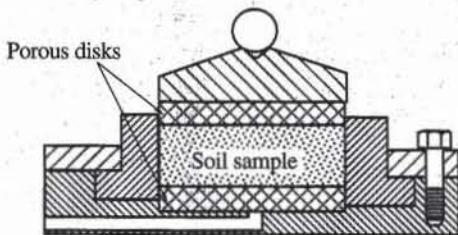


Figure 3 Fixed-ring consolidation cell.

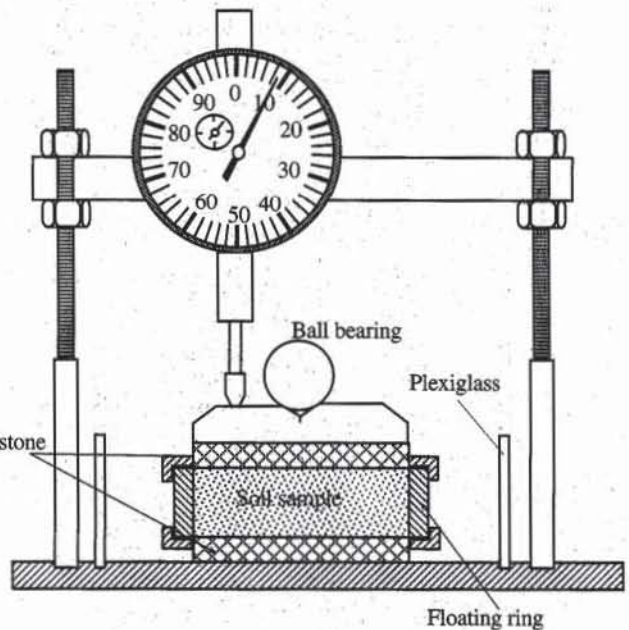


Figure 4 Floating-ring consolidation cell. The dial indicator can also be replaced by a displacement transducer.

PREPARATION OF SPECIMENS

Several types of devices may be used to trim and place the test specimen in the consolidation cell. Figures 5 to 8 show an example of sample preparation.

Measuring Devices

Dial indicators can be replaced by displacement transducers (e.g., LVDT) with similar or even better range and accuracy. Displacement transducers are usually



Figure 5 A stack of rings of identical diameter is pushed into the soil mass. The lowest ring has a cutting edge. The other cylinders are oedometer floating rings.



Figure 6 After removing the stack of rings filled with soil, the wire saw is inserted in the interstices between two rings, and the soil excess is cut off.



Figure 7 A small coating of vacuum or silicon grease is applied to the upper and lower edges of the ring, and the two external rings are added.



Figure 8 Filter papers are added to the top and bottom surfaces of the specimen. Then the floating ring is placed on the bottom porous stone and the top porous stone is positioned.

connected to a signal conditioner which supplies and processes electrical signals, and a readout unit which displays the transducer output. They can also be connected to an Analog/Digital (A/D) converter for computer data acquisition. It is very important that displacement transducers be calibrated and positioned in their normal working range. Their output must vary linearly with the displacement that is measured from a dial indicator. When a readout unit or A/D converter is available, it is recommended to scale the displacement transducers output so it can easily be interpreted in terms of length (e.g., 1 output unit = 1 mm).

SELECTION OF LOADING SEQUENCE

The loading sequence of the consolidation test depends not only on the soils tested but also on the types of engineering applications. As shown in Fig. 9, a typical loading sequence generally has a low initial value, which increases logarithmically to a maximum value and then decreases rapidly toward zero. For the particular sequence of Fig. 9, the applied stresses are 50, 100, 200, 400, 800, 1600, 400, and 50 kPa. In general, the range of applied stress should completely cover the effective stresses that are needed for settlement calculations. This range should encompass the smallest and largest effective stresses in the field, which depend on depth, foundation loads, and excavations.

The duration of each load application depends on the rate of consolidation of the soil. Ideally, the load should only be changed after the degree of consolidation U reaches 100%. In practice, the load is changed at convenient times provided that U exceeds 90%. When the soil exhibits a large amount of secondary compression, the load should be sustained even longer to determine the secondary compression coefficient.

PROCEDURE

1. Measure the weight W_{ring} and diameter D of consolidation ring.
2. Measure the initial height h_0 of the specimen and the weight W_{w0} of the initial specimen and ring.

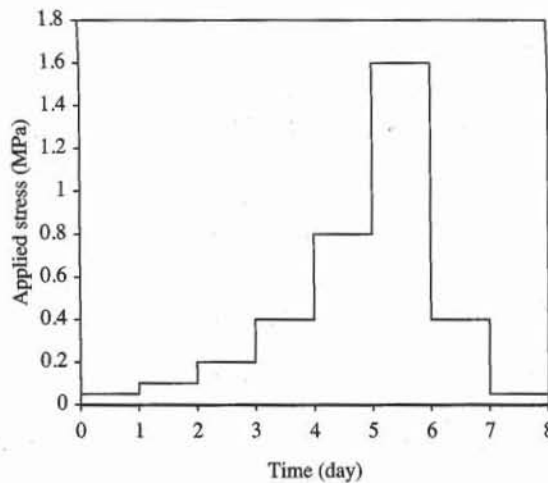


Figure 9 Example of loading sequence for consolidation test.

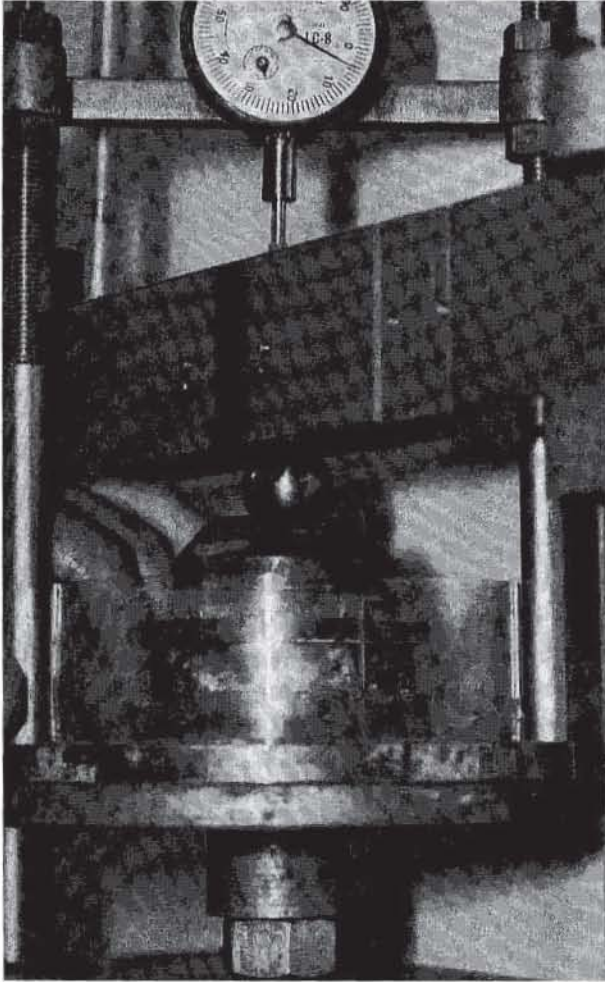


Figure 10 The floating-ring cell is mounted on the loading plate. A rigid cap and a steel ball are added on top of the porous stone. The plate of the pneumatic oedometer is raised very slowly by increasing the air pressure and is adjusted so that the ball slightly touches the reaction beam.

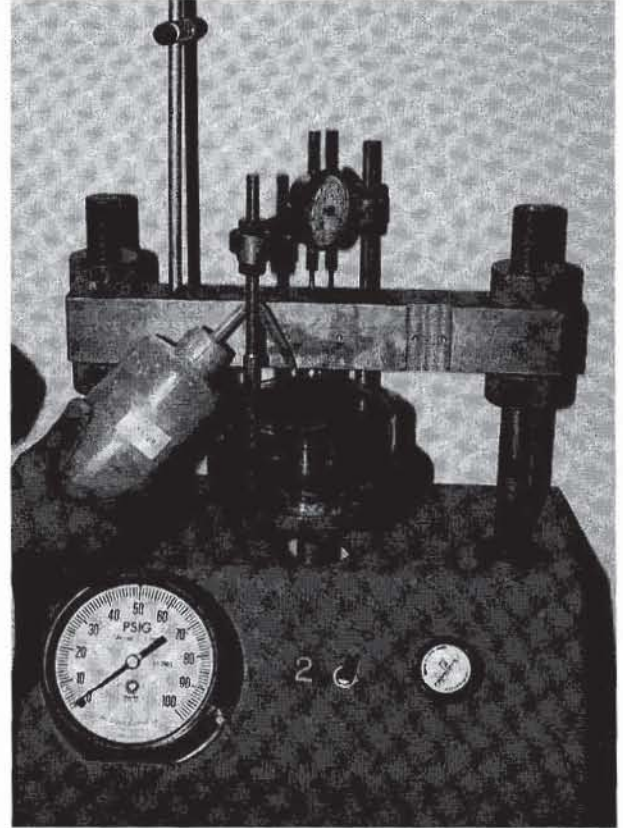


Figure 11 The load on the sample is changed by closing the toggle valve, adjusting the air pressure to the desired value with the pressure regulator, and then releasing the toggle valve.

3. Mount the consolidation cell in the loading unit. Set the vertical displacement dial so that its full range is available during compression (see Fig. 10).

4. Adjust the loading pressure to the first value of the pressure series (see Fig. 11) and measure the vertical displacement at selected time intervals. The vertical displacement gage should be measured at time intervals of 0, 0.1, 0.25, 0.5, 1, 2, 4, 8, 15, 30, 60 min and 2, 4, 8, and 24 h after application of the load increment. In practice, readings can be stopped when the degree of consolidation U exceeds 90% ($U = 90\%$ may be detected by using the square-root-time method).

5. After 24 h, or after U exceeds 90%, the applied load can be changed to its next value, and the vertical displacement is measured as in step 4.

6. Repeat step 5 until all the loading steps are completed.

7. After unloading the specimen completely, record the final dial reading.

8. Quickly dismantle the consolidometer cell and weigh the wet sample.

9. Dry the specimen in the oven and measure its dry weight W_d .

COMPUTATIONS**Soil Characteristics**

The initial state of the soil is characterized by its initial water content w_0 , void ratio e_0 , degree of saturation S_{r0} , and dry unit weight γ_{d0} . The initial dry unit weight γ_{d0} and initial void ratio e_0 are

$$\gamma_{d0} = \frac{W_d - W_{\text{ring}}}{V_0} \quad \text{and} \quad e_0 = \frac{G_s \gamma_w}{\gamma_{d0}} - 1 \quad (1)$$

where W_d is the weight of the dry sample and ring, W_{ring} the weight of the ring, $V_0 = \pi D^2 h_0 / 4$ the initial sample volume, D the sample diameter, h_0 the initial sample height, G_s the soil specific gravity, and γ_w the unit weight of water. The initial water content w_0 is

$$w_0 = \frac{W_{w0} - W_d}{W_d - W_{\text{ring}}} \times 100 \quad (\%) \quad (2)$$

where W_{w0} is the weight of initial wet sample and ring. The initial degree of saturation S_{r0} is

$$S_{r0} = \frac{G_s w_0}{e_0} \quad (3)$$

S_{r0} should be close to 100% for fully saturated specimens. If S_{r0} is much smaller than 100%, the results for the first consolidation loading steps are doubtful.

The water content w_f and void ratio e_f after the consolidation test are calculated similarly to the initial quantities by using the sample height h and weight W_{wf} of wet sample after the test. h_f is obtained after completely removing the load, and letting the sample expand freely while keeping it covered with water.

The specific gravity G_s is calculated by assuming that the sample is completely saturated after the test (i.e., $S_{rf} = 100\%$):

$$G_s = \frac{\gamma_{df}}{\gamma_w - w_f \gamma_{df}} \quad (4)$$

where $\gamma_{df} = \gamma_{d0} h_0 / h_f$ is the final dry unit weight.

Amplitude of Settlement

The sample height h at time t is

$$h = h_0 - d_0 + d(t) - h_c(\sigma) \quad (5)$$

where h_0 is the initial height of sample, d_0 the dial reading corresponding to the sample height h_0 , $d(t)$ the dial reading at time t , and h_c the correction due to loading-frame compliance. $h_c(\sigma)$, which accounts for the deformation of the loading frame when the applied load varies, is obtained by loading a very rigid steel block and recording the variation of dial reading h_c with pressure σ . For rigid loading frames and small pressures, h_c is negligible compared to $d(t)$.

The void ratio e of the specimen of height h is

$$e = e_0 - \frac{h_0 - h}{h_0} (1 + e_0) \tag{6}$$

where e_0 is the initial void ratio for $h = h_0$.

Rate of Settlement

The coefficient of primary consolidation C_v and secondary compression $C_{\alpha e}$ are calculated for a few selected steps by using one of the procedures (e.g., square-root-time or log-time method) described in Chapter 6-1.

Determination of Permeability

As described in Eq. 27.6-1, the permeability k is related to m_v and C_v through

$$k = C_v m_v \gamma_w \tag{7}$$

Therefore, k can be determined from the measured values of C_v , and the compression and swelling indices C_c and C_s . However, this indirect method for determining k gives less accurate values of k than the falling-head permeability test (see Chapter 4-3).

PRESENTATION OF RESULTS

The consolidation test report presents the $\log \sigma' - e$ curve, the swelling index C_s , the compression index C_c , the preconsolidation pressure σ'_p , and the variation of the consolidation coefficient C_v versus effective stress σ' . The compression ratios r_i , r_p , and r_s are also reported to indicate the relative proportion of the initial, primary, and secondary compressions. When the secondary compression ratio r_s is large, the secondary compression coefficient C_{α} is also reported. The calculations of C_s , C_c , σ'_p , C_v , r_i , r_p , r_s , and C_{α} are detailed in Chapter 6-1. The compressibility m_v and permeability coefficient k may also be reported for particular stresses.

EXAMPLES

Figures 12 to 24 cover parts of a complete data set of the consolidation test of a silty clay. The rest of the data set is unprocessed in Table E1. Figure 14

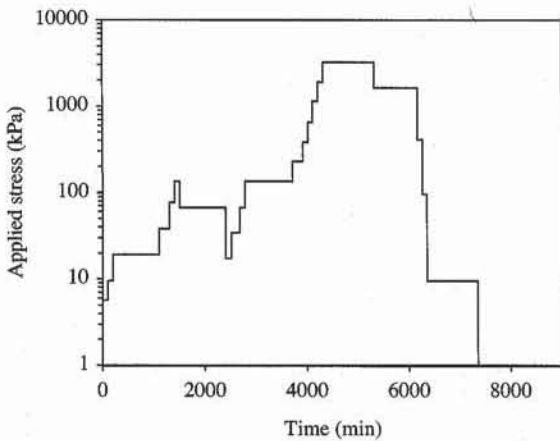


Figure 12 Loading sequence of consolidation test of Fig. 14.

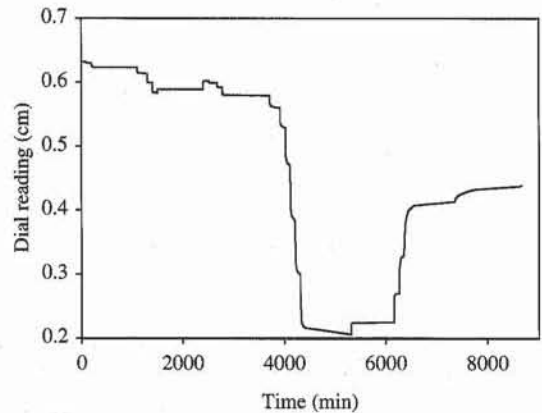


Figure 13 Dial reading corresponding to the loading sequence of Fig. 14.

	A	B	C	D	E	F	G	H	I
1	Consolidation test								
2	Analyst : <i>Shiva Karimi</i>								
3	Test date: <i>11-12-1986</i>								
4	Sample description: <i>Boston gray silty gray (13.5 m depth)</i>								
5	Initial sample height $h_0 =$								
6	Sample diameter $d_0 =$								
7	Initial sample weight $W_{w0} =$								
8	Final sample weight $W_w =$								
9	Final weight of dry sample $W_d =$								
10	Initial dial reading $d_i =$								
11	Final dial reading $d_f =$								
12	Initial water content $w_0 =$								
13	Initial dry unit weight $\gamma_{d0} =$								
14	Initial void ratio $e_0 =$								
15	Initial degree of saturation $S_{r0} =$								
16	Assumed final degree of saturation $S_r =$								
17	Estimated specific gravity $G_s =$								
18	Final water content $w =$								
19	Final dry unit weight $\gamma_d =$								
20	Final void ratio $e =$								
21	Liquid limit LL =								
22	Plastic limit PL =								
23	Preconsolidation pressure $\sigma_p =$								
24	Compression index $C_c =$								
25	Swelling index $C_s =$								
26									
27	Load number	Vertical stress (kPa)	Dial reading (cm)	System deflection (cm)	Vertical strain (%)	Void ratio	C_v (cm ² /sec)	$C_{\alpha\alpha}$ (%)	Elapsed time (min)
28			d	hc	eps				
29	1	5.7	0.63122	0.00025	0.21	1.311	0.00208	0.07	100
30	2	9.6	0.62921	0.00040	0.33	1.309	0.00309	0.05	100
31	3	19.2	0.62243	0.00080	0.70	1.300	0.00218	0.04	900
32	4	38.3	0.61311	0.00135	1.22	1.288	0.00189	0.07	200
33	5	76.6	0.59830	0.00230	2.05	1.269	0.00166	0.09	100
34	6	134.1	0.58293	0.00325	2.91	1.249	0.00208	0.10	100
35	7	67.0	0.58918	0.00270	2.56	1.257	0.00231	0.01	900
36	8	17.2	0.60201	0.00225	1.86	1.273	0.00199	0.07	120
37	9	34.5	0.59888	0.00222	2.02	1.270	0.00220	0.02	160
38	10	67.0	0.59157	0.00194	2.39	1.261	0.00240	0.04	100
39	11	134.1	0.57887	0.00282	3.10	1.244	0.00281	0.05	940
40	12	229.8	0.56007	0.00445	4.18	1.220	0.00183	0.17	200
41	13	383.0	0.52883	0.00550	5.88	1.180	0.00159	0.27	100
42	14	651.2	0.47003	0.00705	9.06	1.107	0.00124	0.69	100
43	15	1149.1	0.38354	0.00915	13.72	0.998	0.00131	0.83	100
44	16	1915.2	0.29972	0.01150	18.26	0.893	0.00154	0.66	100
45	17	3255.8	0.20599	0.01500	23.38	0.775	0.00220	0.65	1000
46	18	1627.9	0.22492	0.01205	22.23	0.801	0.00246	0.03	840
47	19	407.0	0.27064	0.00795	19.61	0.862	0.00171	0.13	100
48	20	95.8	0.32896	0.00540	16.40	0.936	0.00067	0.49	100
49	21	9.6	0.41351	0.00340	11.84	1.042	0.00014	0.44	1000
50	22	1.0	0.43818	0.00290	10.52	1.073	0.00003	0.62	1315
51	Preconsolidation pressure with Casagrande method								
52	Slope = 0.07								
53	Preconsolidation pressure = 409.4 kPa								

Figure 14 Example of data set for the consolidation test.

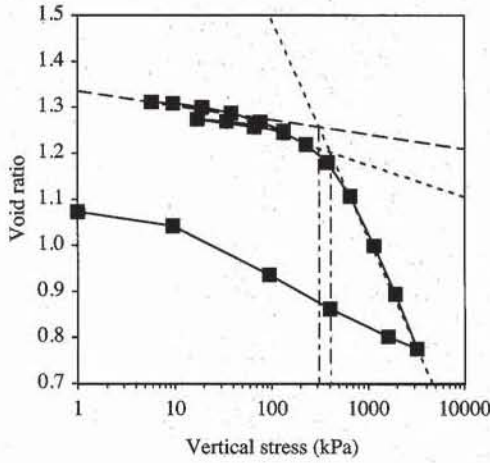


Figure 15 Consolidation curve for Fig. 14.

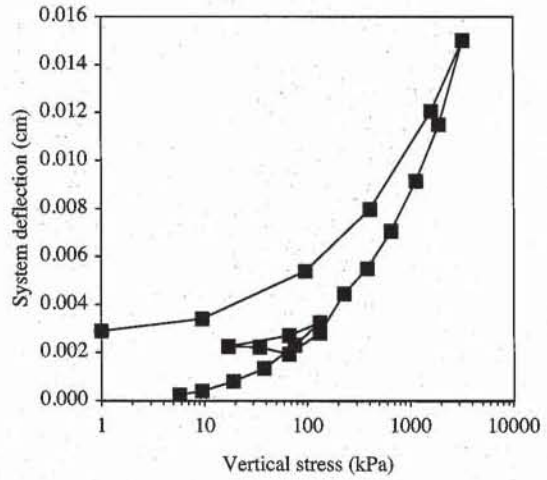


Figure 16 System deflection versus applied pressure.

	C	D	E
12	Initial water content $w_0 = (Ww_0 - Wd)/Wd$		
13	Initial dry unit weight $\gamma_{d0} = Wd / (h_0 \cdot \pi \cdot (d_0^2 / 4)) \cdot 9.8$		kN/m ³
14	Initial void ratio $e_0 = G_s \cdot \pi \cdot (d_0^2 / 4) \cdot h_0 / Wd - 1$		
15	Initial degree of saturation $S_{r0} = G_s \cdot w_0 / e_0$		
16	Assumed final degree of saturation $S_r = 1$		
17	Estimated specific gravity $G_s = gd / (9.8 - w \cdot gd)$		
18	Final water content $w = (Ww - Wd) / Wd$		
19	Final dry unit weight $\gamma_d = gd \cdot h_0 / (h_0 - d_i + d_f)$		kN/m ³
20	Final void ratio $e = G_s \cdot w$		
21	Liquid limit $LL = 0.553$		
22	Plastic limit $PL = 0.242$		
23	Preconsolidation pressure $\sigma_p = 10^{((F45 + C_c \cdot \text{LOG}(B45) - F29 - C_s \cdot \text{LOG}(B29)) / (C_c - C_s))}$		
24	Compression index $C_c = -\text{SLOPE}(F42:F45, \text{LOG}(B42:B45))$		
25	Swelling index $C_s = -\text{SLOPE}(F34:F39, \text{LOG}(B34:B39))$		

	E	F
27	Vertical strain (%)	Void ratio
28	eps	
29	$= (d_i - d + hc) / h_0 \cdot 100 = e_0 - \text{eps} / 100 \cdot (1 + e_0)$	
30	$= (d_i - d + hc) / h_0 \cdot 100 = e_0 - \text{eps} / 100 \cdot (1 + e_0)$	

	C	D
51	Preconsolidation pressure with Casagrande method	
52	Slope = $-\text{SLOPE}(F39:F41, \text{LOG}(B39:B41)) / 2$	
53	Preconsolidation pressure = $10^{((F45 + C_c \cdot \text{LOG}(B45) - F40 - D52 \cdot \text{LOG}(B40)) / (C_c - D52))}$	

Figure 17 Formulas used in Fig. 14.

summarizes the experimental measurements and processed results. The liquid and plastic limits were obtained from tests which are not reported here.

As shown in Fig. 12, the consolidation test lasted for about 6 days and had 22 loading steps (i.e., more steps than usual tests). The soil sample was taken from the field at a depth of 13.5 m. Assuming that the water table in the field is at the ground surface, the initial vertical effective stress σ'_v at

	A	B	C	D	E	F	G	H
1	Measured		Fitted displacement					
2	Load (kPa)	Time (min)	Displacement dial gage (cm)	Primary only (cm)	Primary and secondary (cm)			
3		t	d	dp	dps			
4	5.7	0.00	0.6350	0.6344	0.6344	Primary consolidation		
5		0.10	0.6342	0.6341	0.6341	Initial height $h_0 =$	1.899	cm
6		0.25	0.6340	0.6340	0.6340	Starting time for fitting, $t_b =$	0.3	min
7		0.57	0.6337	0.6337	0.6337	Ending time for fitting, $t_e =$	1.6	min
8		1.00	0.6335	0.6335	0.6335	Degree of consolidation of method $U_s =$	99.0%	
9		1.57	0.6333	0.6333	0.6333	Time corresponding to U_s , $t_s =$	11.86	min
10		2.25	0.6332	0.6331	0.6331	Dial reading corresponding to U_s , $d_s =$	0.6324	cm
11		3.07	0.6330	0.6329	0.6329	Dial reading at beginning of primary consolidation $d_0 =$	0.6344	cm
12		4.00	0.6328	0.6328	0.6328	Dial reading at 100% of primary consolidation $d_{100} =$	0.6324	cm
13		6.25	0.6327	0.6326	0.6326	Average drainage distance $d_m =$	0.9503	cm
14		9.00	0.6325	0.6325	0.6325	Coefficient of consolidation $C_v =$	0.1356	cm ² /min
15		12.25	0.6324	0.6324	0.6324	Initial compression ratio $r_1 =$	16.1%	
16		16.00	0.6323	0.6324	0.6324	Primary compression ratio $r_p =$	52.1%	
17		25.00	0.6322	0.6324	0.6321	Secondary compression ratio $r_s =$	31.8%	
18		36.00	0.6320	0.6324	0.6319	Secondary consolidation		
19		49.00	0.6318	0.6324	0.6317	Slope of secondary compression $ss =$	-0.0014	
20		64.00	0.6315	0.6324	0.6316	Intercept of secondary compression $is =$	0.6341	
21		100.00	0.6312	0.6324	0.6313	Height at beginning of secondary compression $h_s =$	1.8964	cm
22						Time at beginning of secondary compression $t_s =$	15.29	min
						Coefficient of secondary compression $C_{\alpha s} =$	0.073%	

Figure 18 Experimental and calculated data for the first loading step of the consolidation test in Fig. 14.

	B	C	D	E	F	G	H
1	Measured		Fitted displacement				
2	Time (min)	Displacement dial gage (cm)	Primary only (cm)	Primary and secondary (cm)			
3	t	d	dp	dps			
4	0.00	0.5892	0.5910	0.5910	Primary consolidation		
5	0.10	0.5921	0.5923	0.5923	Initial height $h_0 =$	1.8532	cm
6	0.25	0.5929	0.5930	0.5930	Starting time for fitting, $t_b =$	0.3	min
7	0.57	0.5942	0.5940	0.5940	Ending time for fitting, $t_e =$	1.6	min
8	1.00	0.5949	0.5950	0.5950	Degree of consolidation of method $U_s =$	99.0%	
9	1.57	0.5959	0.5960	0.5960	Time corresponding to U_s , $t_s =$	13.09	min
10	2.25	0.5968	0.5969	0.5969	Dial reading corresponding to U_s , $d_s =$	0.6004	cm
11	3.07	0.5975	0.5978	0.5978	Dial reading at beginning of primary consolidation $d_0 =$	0.5910	cm
12	4.00	0.5981	0.5985	0.5985	Dial reading at 100% of primary consolidation $d_{100} =$	0.6005	cm
13	6.25	0.5990	0.5996	0.5996	Average drainage distance $d_m =$	0.9233	cm
14	9.00	0.5997	0.6001	0.6002	Coefficient of consolidation $C_v =$	0.1159	cm ² /min
15	12.25	0.6003	0.6004	0.6006	Initial compression ratio $r_1 =$	14.5%	
16	16.00	0.6008	0.6005	0.6008	Primary compression ratio $r_p =$	73.9%	
17	25.00	0.6012	0.6005	0.6012	Secondary compression ratio $r_s =$	11.6%	
18	36.00	0.6015	0.6005	0.6014	Secondary consolidation		
19	49.00	0.6016	0.6005	0.6016	Slope of secondary compression $ss =$	0.0014	
20	64.00	0.6018	0.6005	0.6017	Intercept of secondary compression $is =$	0.5992	
21	100.00	0.6020	0.6005	0.6020	Height at beginning of secondary compression $h_s =$	1.8646	cm
22	120.00	0.6020	0.6005	0.6021	Time at beginning of secondary compression $t_s =$	8.79	min
					Coefficient of secondary compression $C_{\alpha s} =$	0.077%	

Figure 19 Experimental and calculated data for the first unloading step of the consolidation test in Fig. 14.

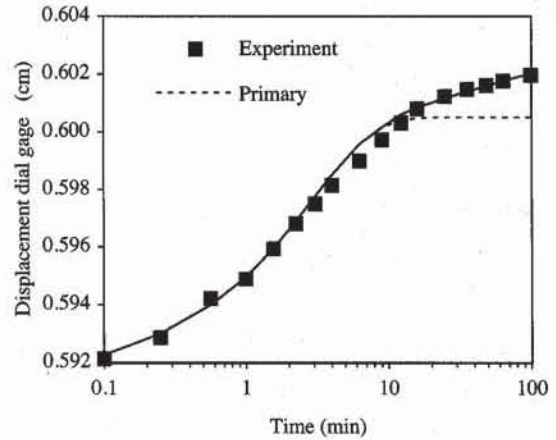
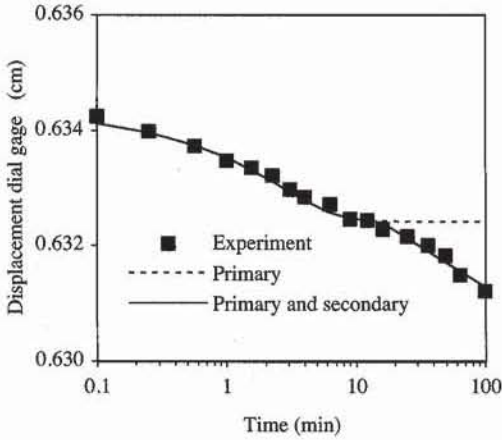


Figure 20 Experimental and fitted data for the first loading step.

Figure 21 Experimental and fitted data for the first unloading step.

	F	G	H
3	Primary consolidation		
4	Initial height $h_0 = 1.899$		cm
5	Starting time for fitting, $t_b = =B6$		min
6	Ending time for fitting, $t_e = =B9$		min
7	Degree of consolidation of method $U_s = 0.99$		
8	Time corresponding to U_s , $t_s = =Conso(t,d,h_0,t_b,t_e,U_s)$		min
9	Dial reading corresponding to U_s , $d_s = =Conso(t,d,h_0,t_b,t_e,U_s)$		cm
10	Dial reading at beginning of primary consolidation $d_0 = =Conso(t,d,h_0,t_b,t_e,U_s)$		cm
11	Dial reading at 100% of primary consolidation $d_{100} = =Conso(t,d,h_0,t_b,t_e,U_s)$		cm
12	Average drainage distance $d_m = =Conso(t,d,h_0,t_b,t_e,U_s)$		cm
13	Coefficient of consolidation $C_v = =Conso(t,d,h_0,t_b,t_e,U_s)$		cm ² /min
14	Initial compression ratio $r_i = =Conso(t,d,h_0,t_b,t_e,U_s)$		
15	Primary compression ratio $r_p = =Conso(t,d,h_0,t_b,t_e,U_s)$		
16	Secondary compression ratio $r_s = =Conso(t,d,h_0,t_b,t_e,U_s)$		
17	Secondary consolidation		
18	Slope of secondary compression $ss = =SLOPE(C16:C21,LOG(B16:B21))$		
19	Intercept of secondary compression $is = =INTERCEPT(C16:C21,LOG(B16:B21))$		
20	Height at beginning of secondary compression $h_s = =h_0-INDEX(d,1)+d_{100}$		cm
21	Time at beginning of secondary compression $t_s = =10^{((d_{100}-is)/ss)}$		min
22	Coefficient of secondary compression $C_{\alpha s} = =ABS(ss/h_s)$		

	D	E
1	Fitted displacement	
2	Primary only (cm)	Primary and secondary (cm)
3	dp	dps
4	$=d_0+(d_{100}-d_0)*U(C_v*t/d_m^2)$	$=IF(t>t_s,dp-Cae*hs*LOG(t/t_s),dp)$
5	$=d_0+(d_{100}-d_0)*U(C_v*t/d_m^2)$	$=IF(t>t_s,dp-Cae*hs*LOG(t/t_s),dp)$

Figure 22 Formulas used in Fig. 18.

13.5 m depth is about 123 kPa for this soil, which has a saturated unit weight of 18.9 kN/m³. In the consolidation test, the lowest pressure was 5.7 kPa and the largest pressure was 3256 kPa. A small unloading was performed at 134.1 kPa. Each load was maintained for at least 100 min and for a few loading steps was kept constant during 1000 min (≈ 17 h).

Figure 13 shows the variation of dial reading during the entire test.

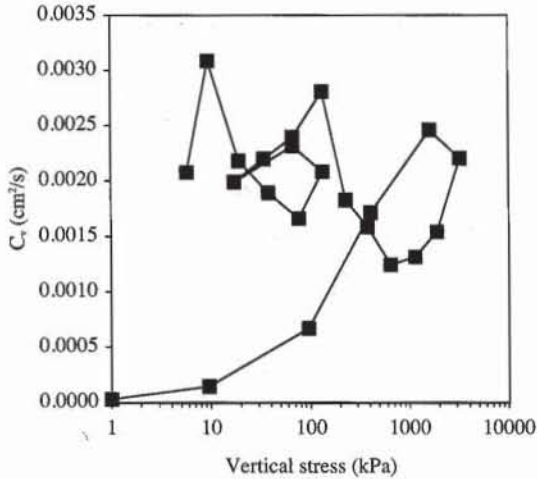


Figure 23 Variation of consolidation coefficient versus effective stress.

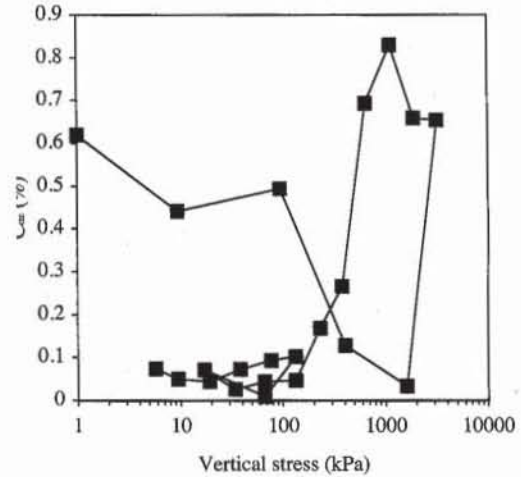


Figure 24 Variation of secondary compression coefficient C_{oe} versus effective stress.

Figure 15 shows the consolidation curve corresponding to the data points of Fig. 13. Each point corresponds to the dial readings after each loading step. The system deflection $h_c(\sigma)$ shown in Fig. 16 was obtained by subjecting a very stiff dummy sample to the same loading sequence as the soil sample. $h_c(\sigma)$ is nonlinear and slightly irreversible. Figure 17 lists the formulas used in Fig. 14 to calculate the compression and swelling indices C_c and C_s and the preconsolidation pressure σ'_p . σ'_p was calculated using methods a and b described in Chapter 6-1. Method a gives $\sigma'_p = 409$ kPa, whereas method b yields $\sigma'_p = 314$ kPa. Both values are higher than the estimated vertical effective stress $\sigma'_v = 123$ kPa.

The coefficient of consolidation C_v was calculated for each loading step (i.e., 22 times). Figures 18 to 21 show only two particular determinations of C_v , at the first loading and unloading. C_v and the initial, primary, and secondary compression ratios are calculated by using the generalized square-root-time method with $U_s = 99\%$ and the user-defined function CONSO. The secondary compression coefficient C_{oe} is calculated using linear regression after the end of the primary compression. The dial reading d_s at the beginning of the secondary compression is assumed to be equal to d_{100} . In Figs. 18 and 19, the fitted dial readings include the primary consolidation only and the cumulated primary and secondary compressions. As shown in Figs. 20 and 21, there is very good agreement between the experimental and fitted values, which indicates that the coefficients C_v and C_{oe} are determined completely. As shown in Fig. 23, C_v varies from 0.0013 to 0.003 cm^2/s during loading and becomes as small as 0.0003 cm^2/s during unloading. As shown in Fig. 24, C_{oe} varies from 0.01 to 0.82%. The secondary compression cannot be neglected for this particular silty clay.

REFERENCES

See Introduction for references to ASTM procedures (pages 4 to 6).

REVIEW QUESTIONS

1. Which material parameters are measured in the consolidation test?
2. What are the log-time and square-root-time methods?
3. Describe two different types of consolidation cells. What are their respective advantages and shortcomings?
4. Name two common types of loading devices used in the consolidation test.
5. On which basis should a loading sequence in the consolidation test be defined?
6. What is the typical time distribution of readings for determining the consolidation coefficient? Why such a sequence?
7. Why do we measure the final height of the sample after the consolidation test?
8. Why do we have to keep the sample fully saturated during the consolidation test?
9. What is the effect of the system deflection during the consolidation test?

EXERCISES

1. Calculate the coefficients of consolidation and secondary compression for one of the loading steps in the data set of Table E1. This data set completes the one in Fig. 14. Refer to Fig. 14 for additional data.
2. By using the square-root-time and log-time methods, calculate the coefficient of consolidation for one of the loading steps in the data set of Table E1. This data set completes the one in Fig. 14. Compare your results.

TABLE E1

Load (kPa)	Elapsed time (min)	Displacement dial gage (cm)	Load (kPa)	Elapsed time (min)	Displacement dial gage (cm)	Load (kPa)	Elapsed time (min)	Displacement dial gage (cm)
5.7	0.00	0.6350	9.6	0.00	0.6312	19.2	0.00	0.6292
	0.10	0.6342		0.10	0.6307		0.10	0.6279
	0.25	0.6340		0.25	0.6307		0.25	0.6276
	0.57	0.6337		0.57	0.6306		0.57	0.6271
	1.00	0.6335		1.00	0.6304		1.00	0.6266
	1.57	0.6333		1.57	0.6302		1.57	0.6261
	2.25	0.6332		2.25	0.6301		2.25	0.6259
	3.07	0.6330		3.07	0.6300		3.07	0.6256
	4.00	0.6328		4.00	0.6300		4.00	0.6252
	6.25	0.6327		6.25	0.6299		6.25	0.6248
	9.00	0.6325		9.00	0.6299		9.00	0.6246
	12.25	0.6324		12.25	0.6299		12.25	0.6243
	16.00	0.6323		16.00	0.6299		16.00	0.6241
	25.00	0.6322		25.00	0.6299		25.00	0.6238
36.00	0.6320	36.00	0.6298	36.00	0.6229			
49.00	0.6318	49.00	0.6297	49.00	0.6228			
64.00	0.6315	64.00	0.6294	64.00	0.6227			
100.00	0.6312	100.00	0.6292	100.00	0.6227			
						900.00	0.6224	

TABLE E1 (cont.)

Load (kPa)	Elapsed time (min)	Displacement dial gage (cm)	Load (kPa)	Elapsed time (min)	Displacement dial gage (cm)	Load (kPa)	Elapsed time (min)	Displacement dial gage (cm)
38.3	0.00	0.6224	67.0	0.00	0.5829	67.0	0.00	0.5989
	0.25	0.6199		0.25	0.5867		0.25	0.5964
	0.57	0.6193		0.57	0.5872		0.57	0.5959
	1.00	0.6186		1.00	0.5871		1.00	0.5950
	1.57	0.6181		1.57	0.5878		1.57	0.5944
	2.25	0.6175		2.25	0.5880		2.25	0.5939
	3.07	0.6172		3.07	0.5883		3.07	0.5933
	4.00	0.6167		4.00	0.5884		4.00	0.5931
	6.25	0.6161		6.25	0.5886		6.25	0.5928
	9.00	0.6157		9.00	0.5887		9.00	0.5926
	12.25	0.6152		12.25	0.5887		12.25	0.5924
	16.00	0.6149		16.00	0.5888		16.00	0.5923
	25.00	0.6144		25.00	0.5890		25.00	0.5921
	36.00	0.6142		36.00	0.5890		36.00	0.5919
	49.00	0.6140		49.00	0.5891		49.00	0.5918
	64.00	0.6139		64.00	0.5891		64.00	0.5918
	100.00	0.6137		100.00	0.5892		100.00	0.5916
	120.00	0.6137		900.00	0.5892			
	200.00	0.6131						
Load (kPa)	Elapsed time (min)	Displacement dial gage (cm)	Load (kPa)	Elapsed time (min)	Displacement dial gage (cm)	Load (kPa)	Elapsed time (min)	Displacement dial gage (cm)
76.6	0.00	0.6131	17.2	0.00	0.5892	134.1	0.00	0.5916
	0.25	0.6074		0.10	0.5921		0.25	0.5875
	0.57	0.6063		0.25	0.5929		0.57	0.5861
	1.00	0.6053		0.57	0.5942		1.00	0.5848
	1.57	0.6045		1.00	0.5949		1.57	0.5838
	2.25	0.6035		1.57	0.5959		2.25	0.5829
	3.07	0.6027		2.25	0.5968		3.07	0.5824
	4.00	0.6022		3.07	0.5975		4.00	0.5820
	6.25	0.6012		4.00	0.5981		6.25	0.5814
	9.00	0.6005		6.25	0.5990		9.00	0.5810
	12.25	0.6001		9.00	0.5997		12.25	0.5834
	16.00	0.5998		12.25	0.6003		16.00	0.5806
	25.00	0.5994		16.00	0.6008		25.00	0.5804
	36.00	0.5991		25.00	0.6012		36.00	0.5801
	49.00	0.5989		36.00	0.6015		49.00	0.5799
	64.00	0.5987		49.00	0.6016		64.00	0.5799
	100.00	0.5983		64.00	0.6018		100.00	0.5797
				100.00	0.6020		110.00	0.5796
				120.00	0.6020		940.00	0.5789
Load (kPa)	Elapsed time (min)	Displacement dial gage (cm)	Load (kPa)	Elapsed time (min)	Displacement dial gage (cm)	Load (kPa)	Elapsed time (min)	Displacement dial gage (cm)
134.1	0.00	0.5983	34.5	0.00	0.6020	229.8	0.00	0.5789
	0.25	0.5921		0.25	0.6013		0.25	0.5745
	0.57	0.5916		0.57	0.6010		0.57	0.5729
	1.00	0.5906		1.00	0.6006		1.00	0.5715
	1.57	0.5895		1.57	0.6003		1.57	0.5699
	2.25	0.5880		2.25	0.6001		2.25	0.5689
	3.07	0.5872		3.07	0.5999		3.07	0.5676
	4.00	0.5867		4.00	0.5997		4.00	0.5669
	6.25	0.5860		6.25	0.5995		6.25	0.5655
	9.00	0.5853		9.00	0.5994		9.00	0.5648
	12.25	0.5850		12.25	0.5994		12.25	0.5644
	16.00	0.5847		16.00	0.5992		16.00	0.5639
	25.00	0.5843		25.00	0.5992		25.00	0.5631
	36.00	0.5838		36.00	0.5992		36.00	0.5624
	49.00	0.5835		49.00	0.5991		49.00	0.5620
	64.00	0.5834		64.00	0.5990		64.00	0.5617
	100.00	0.5829		100.00	0.5989		100.00	0.5609
				120.00	0.5989		200.00	0.5601
				140.00	0.5989			
				160.00	0.5989			

TABLE E1 (cont.)

Load (kPa)	Elapsed time (min)	Displacement dial gage (cm)	Load (kPa)	Elapsed time (min)	Displacement dial gage (cm)	Load (kPa)	Elapsed time (min)	Displacement dial gage (cm)
383.0	0.00	0.5601	1915.2	0.00	0.3835	407.0	0.00	0.2249
	0.25	0.5527		0.25	0.3660		0.25	0.2457
	0.57	0.5502		0.57	0.3556		0.57	0.2464
	1.00	0.5476		1.00	0.3518		1.00	0.2497
	1.57	0.5453		1.57	0.3477		1.57	0.2530
	2.25	0.5432		2.25	0.3401		2.25	0.2560
	3.07	0.5413		3.07	0.3325		3.07	0.2586
	4.00	0.5398		4.00	0.3284		4.00	0.2607
	6.25	0.5377		6.25	0.3213		6.25	0.2638
	9.00	0.5357		9.00	0.3165		9.00	0.2659
	12.25	0.5344		12.25	0.3131		12.25	0.2672
	16.00	0.5335		16.00	0.3106		16.00	0.2680
	25.00	0.5321		25.00	0.3073		25.00	0.2689
	36.00	0.5310		36.00	0.3051		36.00	0.2695
	49.00	0.5302		49.00	0.3034		49.00	0.2698
	64.00	0.5293		64.00	0.3022		64.00	0.2701
	100.00	0.5288		100.00	0.2997		100.00	0.2706
651.2	0.00	0.5288	3255.8	0.00	0.2986	95.8	0.00	0.2706
	0.25	0.5161		0.10	0.2796		0.25	0.2823
	0.57	0.5118		0.25	0.2764		0.57	0.2840
	1.00	0.5077		0.57	0.2690		1.00	0.2870
	1.57	0.5033		1.00	0.2619		1.57	0.2901
	2.25	0.4994		1.57	0.2553		2.25	0.2932
	3.07	0.4959		2.25	0.2494		3.07	0.2963
	4.00	0.4931		3.07	0.2440		4.00	0.2992
	6.25	0.4883		4.00	0.2398		6.25	0.3047
	9.00	0.4851		6.25	0.2337		9.00	0.3094
	12.25	0.4826		9.00	0.2298		12.25	0.3134
	16.00	0.4806		12.25	0.2272		16.00	0.3168
	25.00	0.4778		16.00	0.2254		25.00	0.3200
	36.00	0.4757		25.00	0.2228		36.00	0.3246
	49.00	0.4737		36.00	0.2210		49.00	0.3265
	64.00	0.4722		49.00	0.2190		64.00	0.3276
	100.00	0.4700		64.00	0.2178		100.00	0.3290
				100.00	0.2161			
				1000.00	0.2060			
1149.1	0.00	0.4700	1627.9	0.00	0.2060	9.6	0.00	0.3290
	0.25	0.4470		0.25	0.2202		0.25	0.3376
	0.57	0.4412		0.57	0.2212		0.57	0.3383
	1.00	0.4382		1.00	0.2220		1.00	0.3403
	1.57	0.4298		1.57	0.2225		1.57	0.3424
	2.25	0.4239		2.25	0.2228		2.25	0.3444
	3.07	0.4191		3.07	0.2230		3.07	0.3467
	4.00	0.4145		4.00	0.2231		4.00	0.3489
	6.25	0.4079		6.25	0.2234		6.25	0.3534
	9.00	0.4026		9.00	0.2235		9.00	0.3581
	12.25	0.4006		12.25	0.2236		12.25	0.3627
	16.00	0.3980		16.00	0.2238		16.00	0.3666
	25.00	0.3928		25.00	0.2240		25.00	0.3744
	36.00	0.3903		36.00	0.2240		36.00	0.3815
	49.00	0.3882		49.00	0.2242		49.00	0.3876
	64.00	0.3866		64.00	0.2242		64.00	0.3927
	100.00	0.3835		100.00	0.2243		100.00	0.3999
				200.00	0.2245		200.00	0.4074
				840.00	0.2249		1000.00	0.4135

TABLE E1 (cont.)

Load (kPa)	Elapsed time (min)	Displacement dial gage (cm)
1.0	0.00	0.4135
	0.25	0.4141
	0.57	0.4144
	1.00	0.4146
	1.57	0.4149
	2.25	0.4151
	3.07	0.4153
	4.00	0.4155
	6.25	0.4161
	9.00	0.4166
	12.25	0.4171
	16.00	0.4178
	25.00	0.4191
	36.00	0.4199
	49.00	0.4211
	64.00	0.4219
	100.00	0.4242
	300.00	0.4300
	400.00	0.4324
	1275.00	0.4372
seating	1315.00	0.4382

7

Shear Strength

- 7-1** Shear strength of soils
- 7-2** Principles of the unconfined compression test
- 7-3** Unconfined compression test
- 7-4** Principles of direct shear tests
- 7-5** Direct shear test
- 7-6** Principles of triaxial tests
- 7-7** Triaxial tests on coarse-grained soils
- 7-8** Triaxial tests on fine-grained soils

7-1

Shear Strength of Soils

INTRODUCTION

Soils like any other materials fail at some point when they are subjected to increasing shear stresses. They cannot withstand a shear stress larger than their shear strength and deform extensively when the applied shear stress approaches their shear strength. Shear strength is a very important soil property to determine the stability of foundations, retaining walls, slopes, and embankments.

FAILURE THEORY

Peak and Residual Failures of Soils

Figure 1 illustrates the typical stress-strain response of soils during the unconfined compression test (Chapter 7-3). The sample, which has no lateral support, is compressed by gradually increasing the axial displacement (*displacement-controlled loading*). When the axial strain ϵ is increased, the axial stress σ first increases, reaches a maximum value, and then decreases to a residual value. From this stress-strain curve, two types of failure are defined: peak failure and residual failure. The *peak failure* corresponds to the *peak strength* σ_p at point *A*. The *residual failure* corresponds to the *residual strength* σ_r at point *B* sustainable at large strain.

If the axial load, instead of the axial displacement, is gradually increased (*load-controlled loading*), the sample of Fig. 1 becomes unstable at the peak failure (segment AC). For instance, when subjected to the increasing weight of Fig. 1c, the sample cannot withstand the applied load and collapses at peak failure. The soil residual strength cannot be measured with such a load-controlled system.

The strength of soils is usually described in terms of the Mohr-Coulomb theory, which originates from the Coulomb friction theory (Coulomb, 1776).

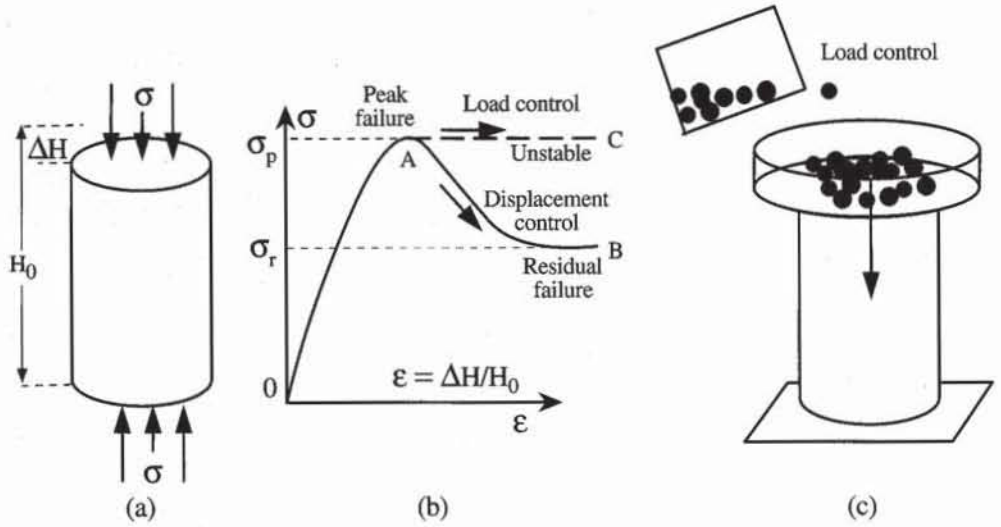


Figure 1 Typical stress-strain responses of soil sample during the unconfined compression test with displacement control and load control.

Coulomb Friction Theory

Figure 2a illustrates the Coulomb friction theory by considering two wooden blocks subjected to the normal force N and the shear force T . N is a constant force applied by a dead weight, and T is gradually increased. At first, the top block does not move when T is small; then starts to slide when T exceeds some particular value T_{max} . The experiment can be repeated for various values of N , and the corresponding T_{max} can be measured. As shown in Fig. 2b, the points (N, T_{max}) are aligned along a straight line that intercepts the T axis at C and makes the slope μ with the N axis:

$$T_{max} = C + \mu N \tag{1}$$

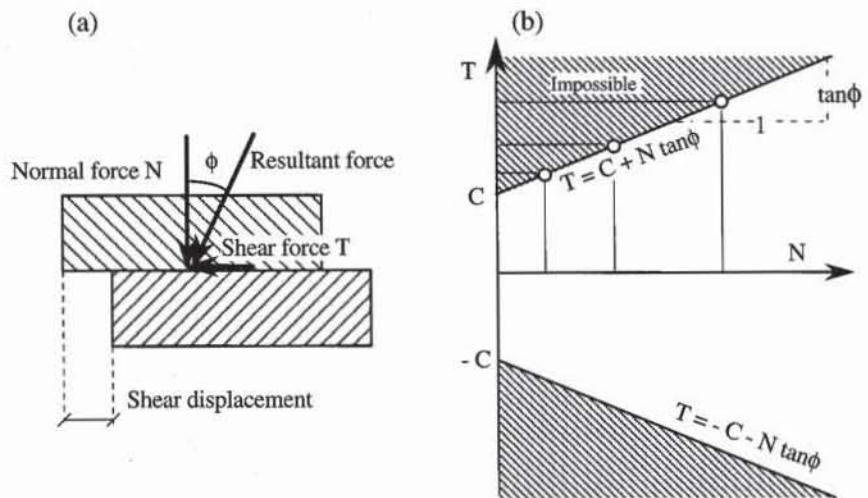


Figure 2 Coulomb friction theory with (a) sliding blocks and (b) possible states in N - T space.

The *cohesive force* C is the value of T that is required to obtain sliding when $N = 0$. The *friction coefficient* μ is dimensionless and characterizes the increase in T_{\max} with N . The *friction angle* ϕ is defined as $\phi = \tan^{-1}(\mu)$.

Both parameters C and ϕ depend on the material and the surface texture of the sliding blocks. In general, large values of C and ϕ correspond to rough surfaces and hard materials, whereas low values of C and ϕ are associated with smooth surfaces and weak materials. The largest absolute value of T is independent of the loading direction; $|T|$ never exceeds $T_{\max} = C + N \tan \phi$. The point (N, T) always stays between the lines $T = C + N \tan \phi$ and $T = -C - N \tan \phi$. The impossible domain for point (N, T) is shaded in Fig. 2b. When $C = 0$, the vertical inclination of the resultant force acting on the block is always smaller or equal to ϕ (i.e., $\tan^{-1}(T/N) \leq \phi$).

Mohr-Coulomb Failure Theory

The Mohr-Coulomb failure theory generalizes the Coulomb friction theory in σ - τ space. The normal stress σ and shear stress τ are

$$\sigma = \frac{N}{A} \text{ and } \tau = \frac{T}{A} \quad (2)$$

where A is the contact area. Using stresses instead of forces, Eq. 1 becomes

$$\tau_{\max} = c + \sigma \tan \phi \quad (3)$$

where τ_{\max} is the *shear strength*, $c = C/A$ is the *cohesion*, or *cohesion intercept*, and ϕ is the *friction angle*. The Mohr-Coulomb failure theory requires that $|\tau| \leq \tau_{\max}$. As shown in Chapter 5-1, the point (σ, τ) generates the Mohr circle when the surface inclination varies. Therefore, $|\tau| \leq \tau_{\max}$ is verified on any surface, provided that the Mohr circle is entirely located between the lines $\tau = \pm(c + \sigma \tan \phi)$.

As shown in Fig. 3, when the Mohr circle is strictly included between the failure lines, there is no surface on which τ is large enough to create a slip (i.e., $|\tau| < \tau_{\max}$). When the Mohr circle intersects the failure lines, there are several surfaces on which $|\tau| \geq \tau_{\max}$, which is unacceptable in the Mohr-Coulomb theory.

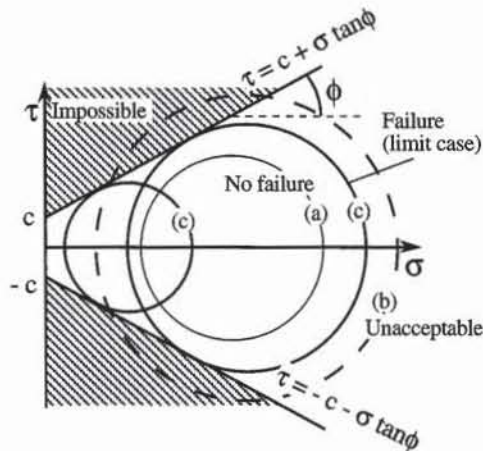


Figure 3 Acceptable, failure, and unacceptable Mohr circles in Mohr-Coulomb failure theory.

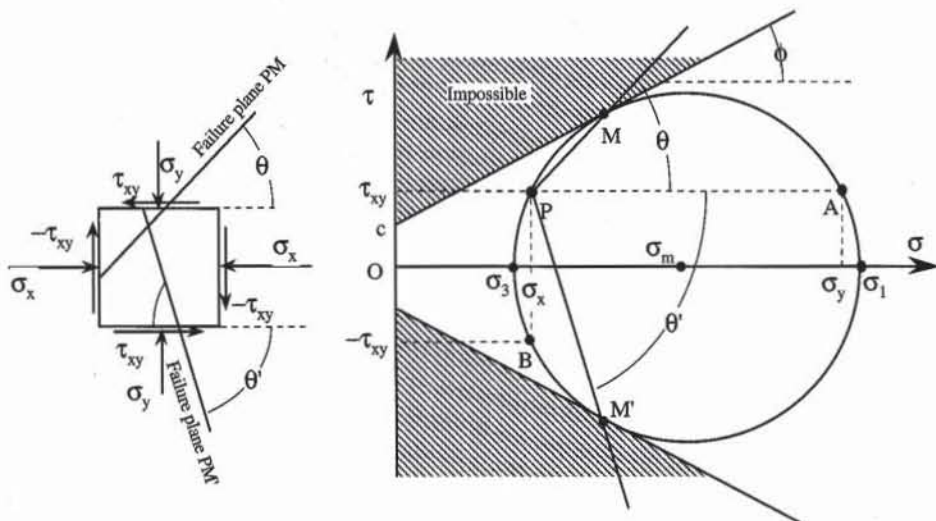


Figure 4 Inclination of failure planes in Mohr-Coulomb failure theory.

As shown in Fig. 4, in the limiting case when the Mohr circle is tangent to the failure lines at points M and M' (i.e., $|\tau| = \tau_{max}$), the failure takes place on surfaces parallel to PM and PM' , where P is the pole of the Mohr circle.

The failure line (Eq. 3) can also be expressed in terms of the major and minor principal stresses σ_1 and σ_3 as follows

$$\sigma_1(1 - \sin \phi) - \sigma_3(1 + \sin \phi) - 2c \cos \phi = 0 \tag{4}$$

When $c = 0$, Eq. 4 becomes

$$\sin \phi = \frac{\sigma_1 - \sigma_3}{\sigma_1 + \sigma_3} \tag{5}$$

MOHR-COULOMB FAILURE IN s - t SPACE

As described in Chapter 5-1, the Mohr circle is also defined in s - t space. Therefore, the failure line (Eq. 3) can be represented in s - t space as well. As shown in Fig. 5, the failure envelope is defined by points D and E in s - t space, and by points A and B in σ - τ space. In s - t space the failure line is

$$|t| = a + s \tan \xi \tag{6}$$

where

$$\tan \xi = \sin \phi \quad \text{and} \quad a = c \cos \phi \tag{7}$$

The s - t and σ - τ failure lines have different slopes and intercepts but have a common intersection point F with the horizontal axis.

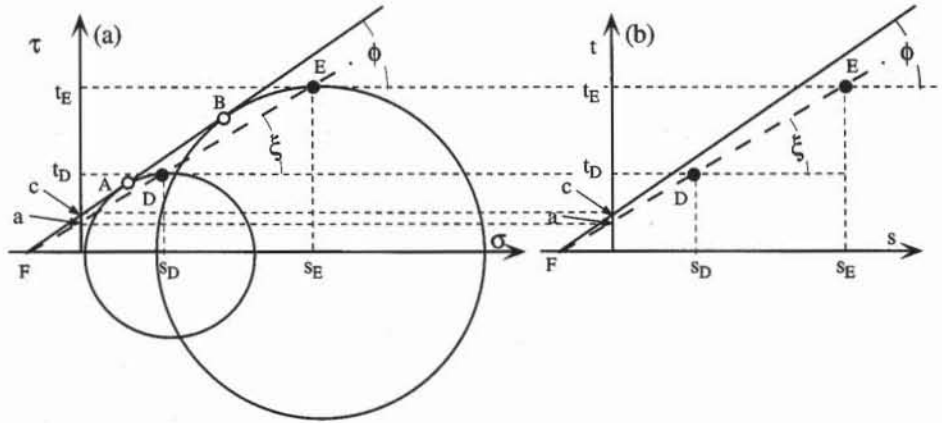


Figure 5 Mohr-Coulomb failure line in (a) σ - τ space and (b) s - t space.

Mohr-Coulomb Failure in p - q Space

As described in Chapter 5-1, stresses can be represented in terms of p and q under axisymmetric conditions. In p - q space, the Mohr-Coulomb failure line becomes

$$q = \frac{6 \sin \phi}{3 - \sin \phi} p + \frac{6 \cos \phi}{3 - \sin \phi} c \quad \text{if } q > 0 \tag{8}$$

$$q = -\frac{6 \sin \phi}{3 + \sin \phi} p - \frac{6 \cos \phi}{3 + \sin \phi} c \quad \text{if } q < 0$$

In contrast to σ - τ and s - t failure lines, the p - q failure lines in compression ($q > 0$) and tension ($q < 0$) are not symmetric about the p axis.

Three-dimensional Mohr-Coulomb Failure Surface

The Mohr-Coulomb failure line (Eq. 4) can be generalized into a failure surface for three-dimensional stress states which are difficult to represent with the Mohr circle (see Chapter 5-1). The shear strength is assumed to be independent of the intermediate principal stress σ_2 . After expressing the major and minor principal stresses σ_1 and σ_3 in terms of the stress invariants I_1, I_2 and I_3 (see Eq. 46.5-1), the Mohr-Coulomb surface is

$$\sqrt{I_1^2 - 3I_2} \left(\sqrt{3} \sin(\theta + \pi/3) - \sin \phi \cos(\phi + \pi/3) \right) - I_1 \sin \phi = 3c \cos \theta \tag{9}$$

where θ is given in Eq. 47.5-1. In the case of purely cohesive materials with $\phi = 0$, Eq. 9 becomes

$$\sqrt{I_1^2 - 3I_2} \sin(\theta + \pi/3) = \sqrt{3}c \tag{10}$$

which is referred to as the Tresca failure surface. The von Mises surface is another failure surface for purely cohesive materials

$$\sqrt{I_1^2 - 3I_2} = 2c \tag{11}$$

Figure 6 shows the surfaces of Eqs. 9 to 11 in the principal stress space of coordinates σ_1, σ_2 and σ_3 . The Mohr-Coulomb surface is a cone with six faces when $\phi \neq 0$, and becomes the Tresca hexagonal cylinder centered on the axis $\sigma_1 = \sigma_2 = \sigma_3$ when $\phi = 0$. The von Mises surface is a circular cylinder centered on

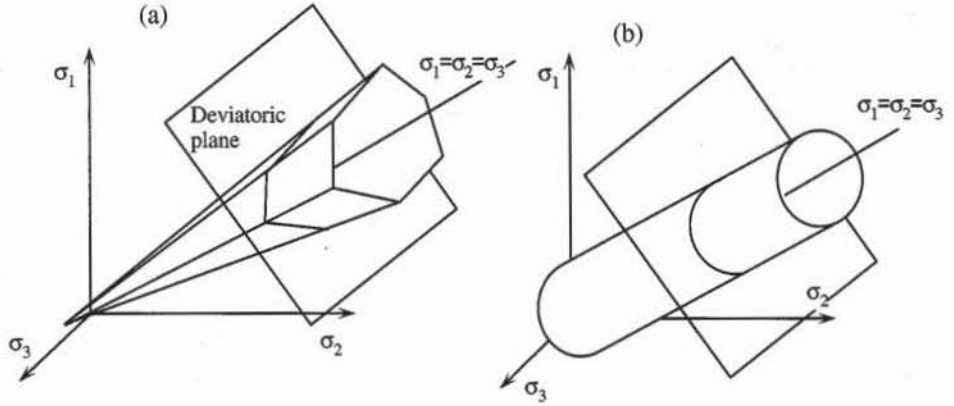


Figure 6 Failure surfaces in principal stress space: (a) Mohr-Coulomb and (b) von Mises.

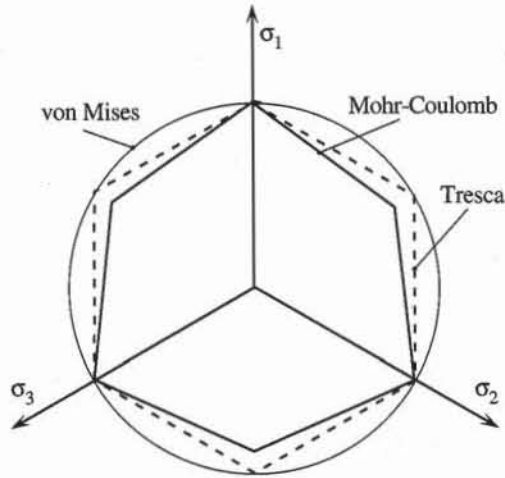


Figure 7 View of Mohr-Coulomb, Tresca and von Mises failure surfaces in deviatoric plane.

the axis $\sigma_1 = \sigma_2 = \sigma_3$ and contains the Tresca surface. Figure 7 shows a deviatoric view of these three surfaces (i.e., their intersection with a plane perpendicular to the axis $\sigma_1 = \sigma_2 = \sigma_3$).

Failure Envelope of Soils

The *failure envelope* (or *shear strength envelope*) of a soil describes the boundary between the stress states it can sustain and those it cannot sustain. This envelope can be expressed in terms of total and effective stresses (see Chapter 5-1). Hereafter, it is defined in terms of effective stress; this approach is more versatile and reliable than the total stress description presented at the end of this section. To avoid confusion between effective and total stresses, we denote the *effective cohesion intercept* by c' , and the *effective friction angle* by ϕ' . The effective shear strength envelope is defined in $s'-t$ space by introducing the parameter a' and ξ' which are related to c' and ϕ' through Eq. 7. We also introduce the *peak friction angle* ϕ'_p and the *residual friction angle* ϕ'_r which corresponds to the peak and residual failures, respectively, as defined in Fig .1.

The shear strength envelope of soils can be determined by using various types of laboratory experiments, including direct shear tests, triaxial tests, simple

TABLE 1
Relations between MIT, Cambridge and principal stress notations.

Parameter or function	Principal stress space	MIT notation <i>s-t</i> and <i>s'-t</i> space	Cambridge notation <i>p-q</i> and <i>p'-q</i> space
First component of total stress	$\sigma_1 = \sigma'_1 + u$	$s = \frac{1}{2}(\sigma_1 + \sigma_3) = s' + u$	$p = \frac{1}{3}(\sigma_1 + 2\sigma_3) = p' + u$
- effective stress	$\sigma'_1 = \sigma_1 - u$	$s' = \frac{1}{2}(\sigma'_1 + \sigma'_3) = s - u$	$p' = \frac{1}{3}(\sigma'_1 + 2\sigma'_3) = p - u$
Second component of total stress	$\sigma_3 = \sigma'_3 + u$	$t = \frac{1}{2}(\sigma_1 - \sigma_3)$	$q = \sigma_1 - \sigma_3$
- effective stress	$\sigma'_3 = \sigma_3 - u$	$t' = t = \frac{1}{2}(\sigma'_1 - \sigma'_3)$	$q' = q = \sigma'_1 - \sigma'_3$
Major principal effective stress	σ'_1	$\sigma'_1 = s' + t$	$\sigma'_1 = p' + \frac{2}{3}q$
Minor principal effective stress	σ'_3	$\sigma'_3 = s' - t$	$\sigma'_3 = p' - \frac{1}{3}q$
Mohr-Coulomb failure line in compression	$\sigma'_1(1 - \sin \phi')$ $-\sigma'_3(1 + \sin \phi') = 2c' \cos \phi'$	$t = c' \cos \phi' + s' \sin \phi'$ $t = a' + s' \tan \xi'$	$q = Mp' + q_c$ $q = \frac{6 \sin \phi'}{3 - \sin \phi'} p' + \frac{6 \cos \phi'}{3 - \sin \phi'} c'$
Stress path during K_0 consolidation	$\sigma'_3 = K_0 \sigma'_1$	$t' = \frac{1 - K_0}{1 + K_0} s'$	$q = 3 \frac{1 - K_0}{1 + 2K_0} p'$
Stress path during isotropic test	$\sigma'_1 = \sigma'_3$	$t' = 0$	$q = 0$
Stress path during drained triaxial compression	$\sigma'_3 = \sigma'_0$	$t' = s'_0 + s'$	$p = p_0 + \frac{1}{3}q$

shear, cubical, and torsional tests (see Chapter 5-4). It can be represented in the $\sigma'-\tau$, $s'-t$, and $p'-q$ spaces. Table 1 summarizes some useful relations between $s'-t$ and $p'-q$ notations.

Failure Envelope in $\sigma'-\tau$ Space

Figure 8 shows the effective shear strength envelopes of various types of soils in $\sigma'-\tau$ space. As illustrated in Fig. 9a for the particular case of London clay, the

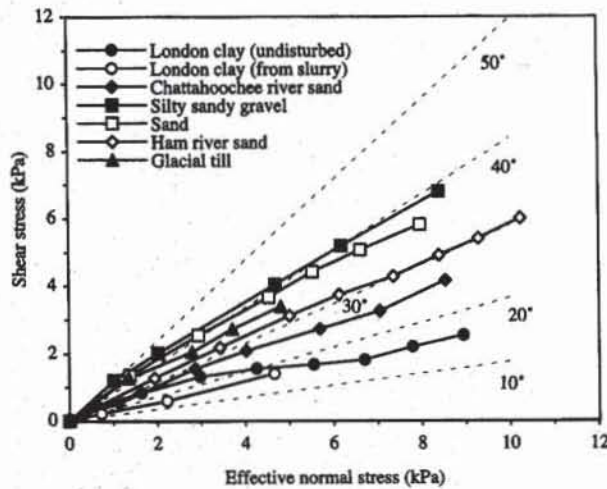


Figure 8 Failure envelopes in $\sigma'-\tau$ space for various soils (Bishop, 1966).

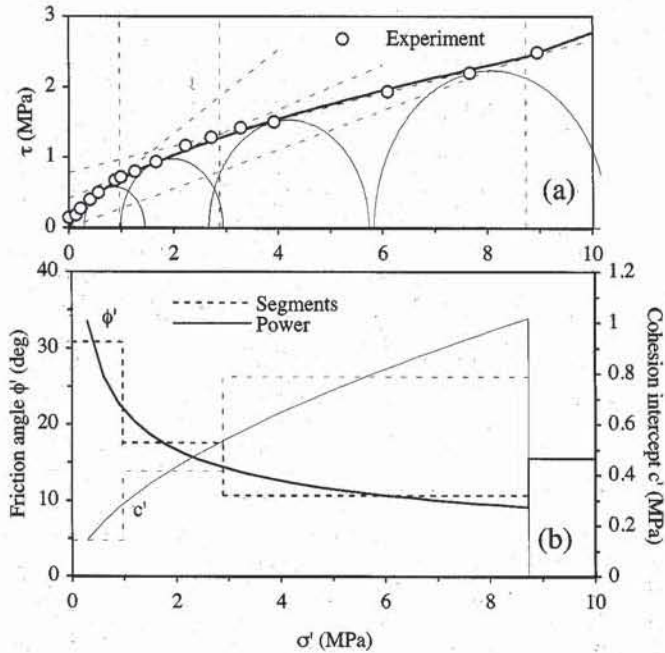


Figure 9 Shear strength envelope of undisturbed London clay in σ' - τ space: (a) approximation of curved envelope with segments and power relation, and (b) corresponding variations of c' and ϕ' with σ' (data after Bishop, 1966).

σ' - τ failure line is constructed as the envelope of the Mohr circles at failure for various ranges of effective normal stress σ' .

As shown in Fig. 8, over a large range of σ' , the failure envelope is curved, and not straight as assumed in Eq. 3. The curved failure line can be approximated by several straight segments, each having a different slope (i.e., $\tan \phi'$) and cohesion intercept c' . As shown in Fig. 9b and Table 1, in the case of London clay, c' and ϕ' must vary abruptly with σ' to fit the curved envelope.

TABLE 2

Variation of cohesion c' , friction angle ϕ' , and parameters ξ' and a' with normal effective stress σ' , for undisturbed London clay (data after Bishop, 1966)

σ' (MPa)	c' (MPa)	ϕ' (deg)	a' (MPa)	ξ' (deg)
$0 < \sigma' < 1$	0.14	30.8	0.12	27.1
$1 < \sigma' < 2.9$	0.42	17.5	0.40	16.8
$2.9 < \sigma' < 8.7$	0.79	10.6	0.77	10.4
$8.7 < \sigma'$	0.00	15.5	0.00	15.0

An alternate way to approximate curved failure envelope is to use nonlinear relations such as the power relation

$$\tau = A\sigma'^m \tag{12}$$

As shown in Fig. 9, Eq. 12 applies to London clay with $m = 0.6$, and $A = 0.69$. In this case, ϕ' and c' over a small stress range about σ' are

$$\tan \phi' = \frac{d\tau}{d\sigma'} = Am\sigma'^{m-1} \quad \text{and} \quad c' = \tau - \frac{d\tau}{d\sigma'} \sigma' = A(1 - m)\sigma'^m \tag{13}$$

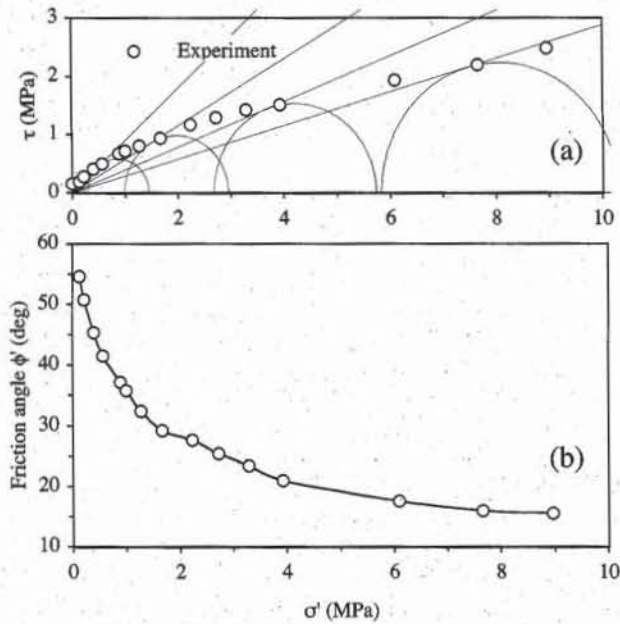


Figure 10 Shear strength envelope of undisturbed London clay in σ' - τ space: (a) approximation of curved envelope with segments originating from stress origin and (b) corresponding variations of ϕ' with σ' (data after Bishop, 1966).

As shown in Fig. 9b, in contrast to c' and ϕ' obtained by linear interpolation, c' and ϕ' calculated from Eq. 13 varies continuously with σ' .

A third way to describe curved failure surfaces is to introduce the friction angle ϕ' as follows

$$\tan \phi' = \frac{\tau}{\sigma'} \tag{14}$$

and to assume that $c' = 0$. Figure 10 shows the variation of ϕ' with σ' which Eq. 14 gives for London clay. The variation of ϕ' with σ' is comparable to those in Fig. 9b, except for small values of σ' at which ϕ' becomes excessively large.

In summary, the shear strength of soils varies nonlinearly with the effective normal stress σ' . There are different ways to define the friction angle ϕ' and cohesion intercept c' , which yield similar failure σ' - τ envelopes. Over a large range of σ' , ϕ' and c' vary with σ' to approximate the nonlinear shear strength of soils. It is only in a limited range of σ' that constant values of ϕ' and c' can be used to describe nonlinear shear strength envelopes.

Soils are *cohesionless* when their curved failure envelope goes through the stress origin (i.e., $\sigma' = \tau = 0$), and *cohesive* when their curved failure envelope intercepts the τ axis above the origin. Coarse grained soils without plastic fines are usually cohesionless. For most cohesive soils, at the exception of cemented soils, partially saturated soils, and heavily consolidated clays, the intercept of the curved failure envelope with the τ axis is generally small.

Failure Envelope in s' - t Space

Like the σ' - τ failure envelope, the s' - t failure envelope is also curved. As shown in Fig. 11, it is constructed from points B which are obtained from the Mohr cir-

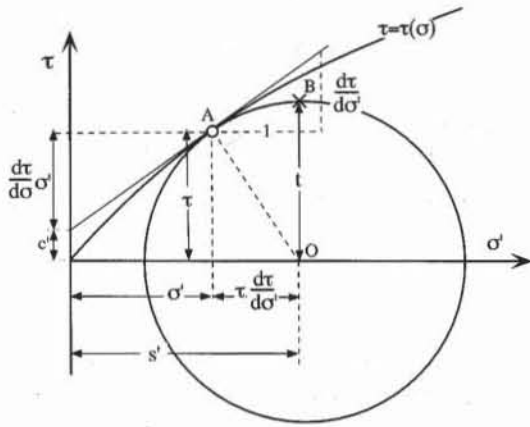


Figure 11 Definition of failure envelope in s' - t space based on failure line in σ' - τ space.

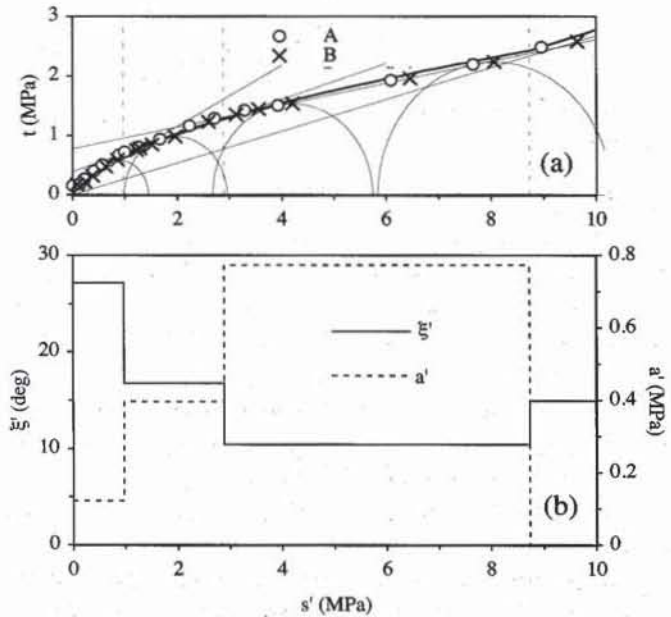


Figure 12 Shear strength envelope of undisturbed London clay in s' - t space: (a) construction of curved envelope from data points B , and (b) corresponding variations of a' and ξ' with s' (data after Bishop, 1966).

cles at failure. If the σ' - τ failure envelope is given by the relation $\tau = \tau(\sigma')$, then the s' - t envelope is generated by varying σ' as follows

$$s' = \sigma' + \tau(\sigma') \frac{d\tau}{d\sigma'}, \quad \text{and} \quad t = \tau(\sigma') \sqrt{1 + \left(\frac{d\tau}{d\sigma'}\right)^2} \quad (15)$$

In a few cases such as a straight failure line (Eq. 3), σ' can be eliminated from Eq. 15 to yield an explicit relation between s' and t . Figure 12a shows the construction of the failure line by using points B in s' - t space, and its approximation with segments for London clay. The corresponding values of a' and ξ' are listed in Table 2 and plotted in Fig. 12b.

Failure Envelope in p' - q Space

The failure envelope of soils can be constructed in the p' - q space. As shown in Fig. 13 for London clay, it is curved like the failure lines in σ' - τ and s' - t spaces. The friction angle ϕ' , can be computed from the p' - q failure envelope by using Eq. 8.

SHEAR STRENGTH OF COARSE-GRAINED SOILS

The shear strength characteristics of coarse-grained soils (e.g., sands and gravels) are introduced by examining the stress-strain response of a particular sand—Sacramento river sand—which was extensively tested in the laboratory under CD and CU triaxial compressions.

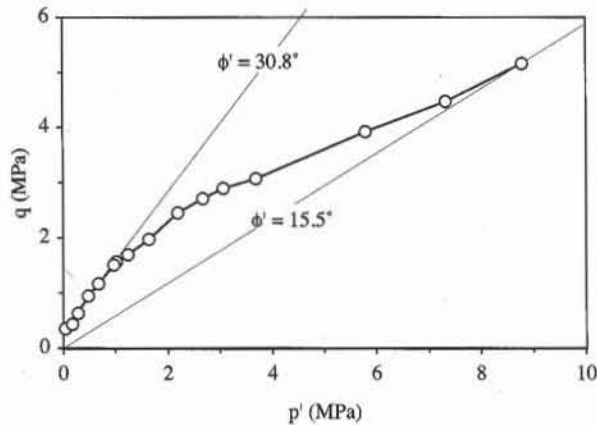


Figure 13 Shear strength envelope of undisturbed London clay in p' - q (data after Bishop, 1966).

Isotropic Compression on Sacramento River Sand

In the triaxial tests, the shear loading is usually preceded by a consolidation phase such as an isotropic loading to recreate in the laboratory the initial stresses in the field (see Chapter 5-4). Figure 11 shows the change in void ratio of loose and dense Sacramento River sands subjected to loading-unloading cycles of isotropic pressure. The sand response is nonlinear and irreversible like that of fine-grained soils subjected to consolidation tests (see Chapter 6-1).

CD Triaxial Compression on Sacramento River Sand

Figures 15 and 16 show the results of CD triaxial compression tests on loose and dense samples of Sacramento River sand. The initial void ratio e_0 and relative density D_r of the dense sand samples are $e_0 = 0.61$ and $D_r = 100\%$, and those of the loose sand samples are $e_0 = 0.87$ and $D_r = 38\%$. Each test has a different confining pressure σ'_3 ranging from 0.1 to 11.8 MPa, a very large range of pressure which corresponds to depths from 10 to 1000 m.

The peak failure, which is noticeable in all dense samples, appears only in loose samples for $\sigma'_3 < 1.9$ Mpa. The value of σ'_1/σ'_3 at peak failure depends on density and decreases with σ'_3 . However, the value of σ'_1/σ'_3 at residual failure is independent of σ'_3 and density. The loose and dense specimens share the same residual strength.

The loose samples except for those at 0.1 and 0.2 MPa compact in contrast to the dense samples which all dilate. This compaction and dilation is caused by shear and depends on the initial density and confining pressure. The dilatation is the largest in dense sand at low confining pressure, while the compaction is the largest in loose sands at high confining pressure. Figure 17 shows another representation of the variation of void ratio during triaxial compressions. At the beginning of each test, the state (p' - e) is initially on the isotropic compression curves of Fig. 14. During shear, the points (p' - e) move away from the isotropic compression line and tend toward a common line, which is referred to as the *critical state line* or *steady state line*. In Fig. 7, the complete convergence to the critical state line is not observed due to the inaccuracy in the measurement of volume changes in sands. Recent experimental results (e.g., Biarez and Hicher, 1994; and Ishihara,

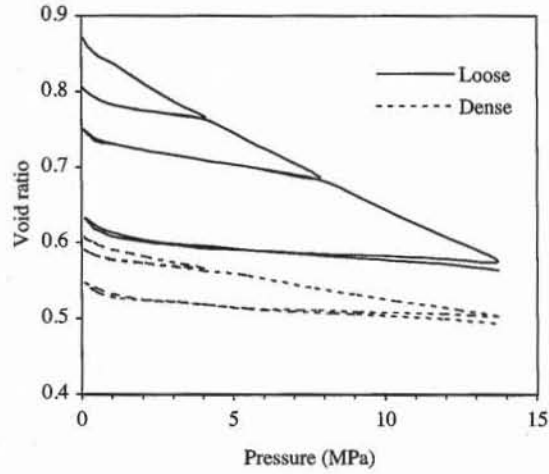


Figure 14 Variation of void ratio versus confining pressure during isotropic test on loose and dense Sacramento River sand (Lee and Seed, 1967).

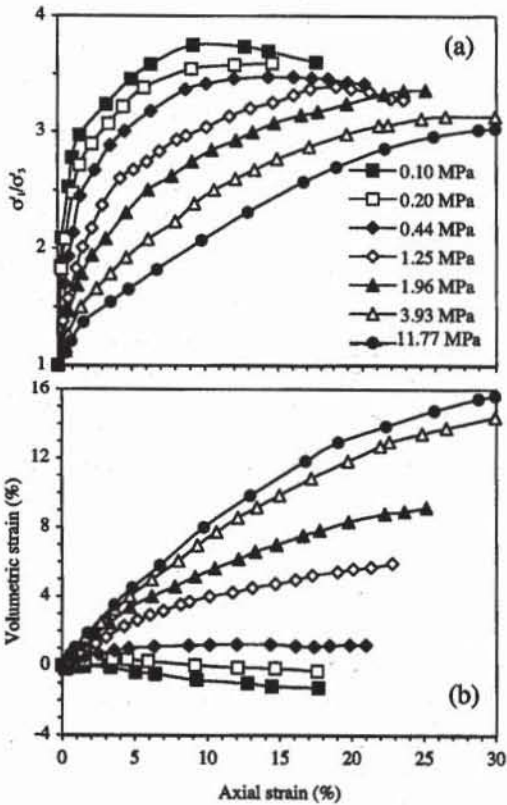


Figure 15 Results of CD triaxial compression tests on loose ($D_r = 38\%$) Sacramento River sand at various confining pressures: (a) variation of effective stress ratio versus axial strain, and (b) variation of volumetric strain with axial strain (Lee and Seed, 1967).

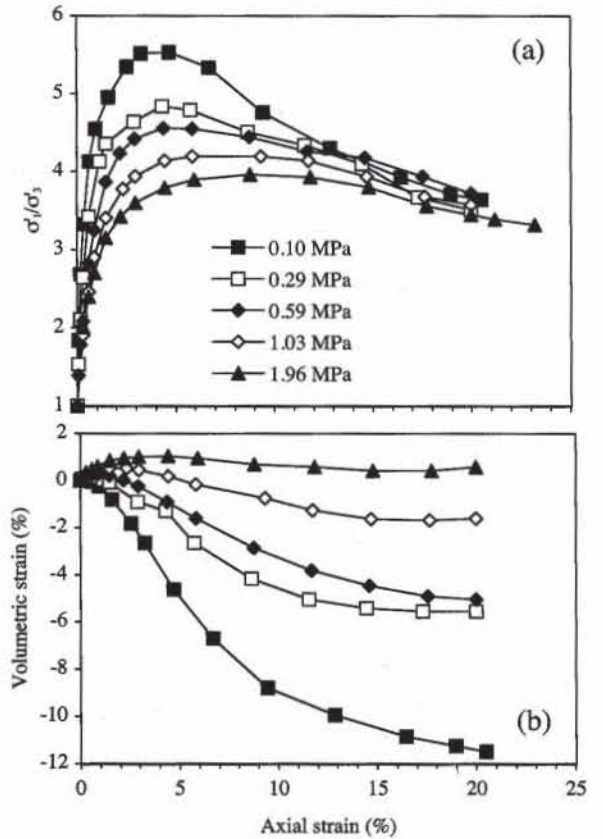


Figure 16 Results of CD triaxial compression tests on dense ($D_r = 100\%$) Sacramento River sand at various confining pressures: (a) variation of effective stress ratio versus axial strain, and (b) variation of volumetric strain with axial strain (Lee and Seed, 1967).

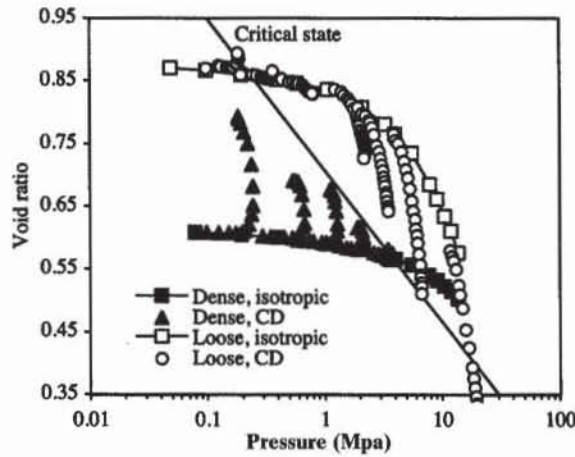


Figure 17 Variation of void ratio with mean effective pressure during the drained triaxial compression tests of Figs. 15 and 16.

As shown in Figs. 18, the failure envelopes of dense and loose Sacramento River sand are generated by the Mohr circles at the peak failure states of Figs. 15 and 16. These failure envelopes are both curved over a large range of normal effective stress σ' , but can be approximated by straight segments in smaller ranges of σ' . The values of cohesion intercept c' , friction angle ϕ'_p and stress ranges σ' are listed in Table 3. For $6.5 < \sigma' < 35$ MPa, c' is equal to 0.2 MPa to fit the curved failure envelope, which does not imply that the sand is cohesive as fine-grained materials. The dense sand has a larger and more curved failure envelope than loose sand in the lower σ' range, but about the same strength in the higher σ' range, as loose sands become denser under large pressure.

The failure envelope of Sacramento River sand can also be defined in s' - t space. This envelope is curved and can be approximated by straight segments defined by the values of ξ' and a' in Table 3. As shown in Fig. 19, the failure envelope in p' - q space is also slightly curved, and is larger for dense sand than for loose sand for $p' < 4$ MPa. Figure 20 represents the variation of ϕ'_p calculated by using Eq. 5 with the mean pressure p'_f at peak failure for the dense and loose sands. For $p'_f < 10$ MPa, ϕ'_p linearly varies with the logarithm of p'_f and depends on the sand density. However, for $p'_f > 10$ MPa, ϕ'_p coincides for dense and loose sands.

TABLE 3

Variation of cohesion c' , friction angle ϕ'_p , and parameters ξ' and a' with normal effective stress σ' for loose and dense Sacramento River sand.

State	Effective normal stress (MPa)	Friction angle ϕ'_p (deg)	Cohesion c' (kPa)	ξ' (deg)	a' (kPa)
Loose	0.0–6.5	33.0	0	28.6	0
	6.5–35.0	29.7	207	26.4	180
Dense	0.0–3.0	37.2	0	31.2	0
	3.0–10.0	30.2	393	26.7	340
	10.0–35.0	32.7	0	28.4	0

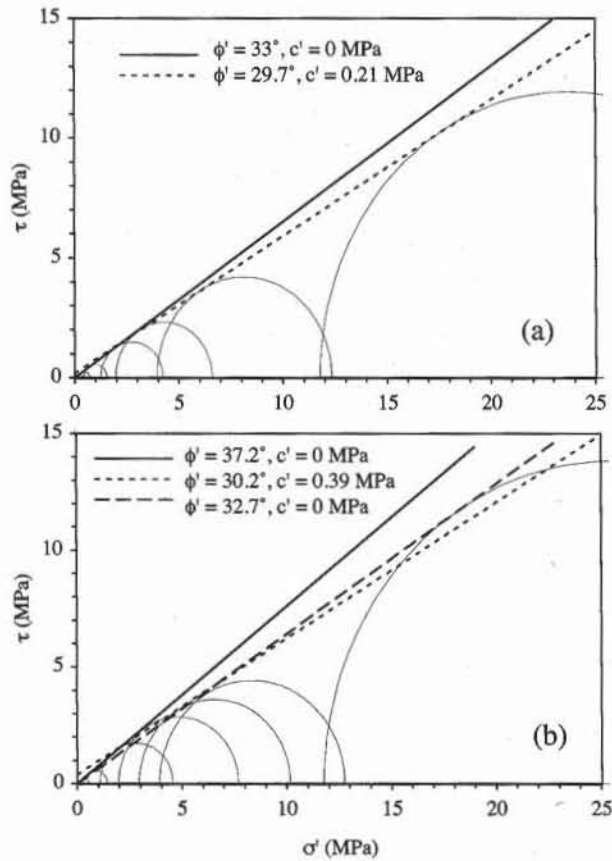


Figure 18 Peak failure envelope of (a) dense and (b) loose Sacramento River sand obtained from the results of Figs. 15 and 16.

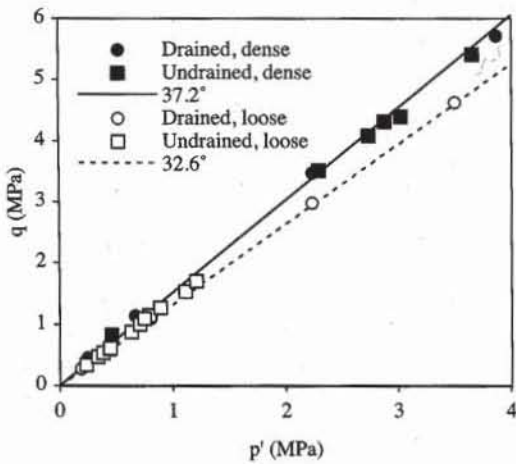


Figure 19 Peak failure envelope in p' - q space obtained for loose and dense Sacramento River sand from CD and CU triaxial compression tests at various confining pressures.

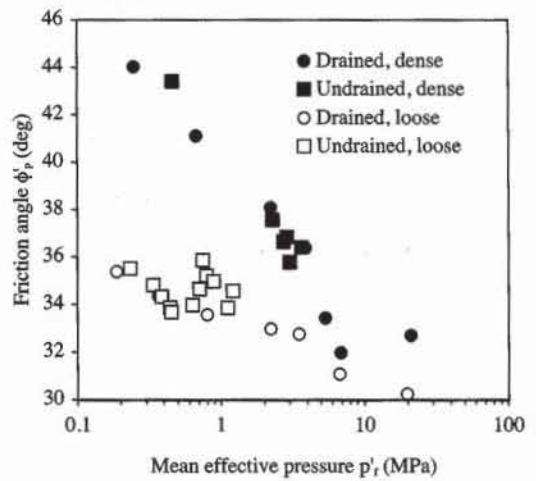


Figure 20 Variation of peak friction angle with mean effective pressure at failure for loose and dense Sacramento River sand during drained and undrained triaxial compression tests.

Undrained Triaxial Tests on Sacramento River Sand

Figures 21 and 23 show the stress-strain response, variation of excess pore pressure, and effective $p'-q$ stress paths for the loose and dense Sacramento River sand subjected to CU triaxial compression tests at various confining pressures σ_3 .

As shown in Figs. 15 and 21, the stress-strain responses of loose Sacramento River sand are quite different during CU and CD tests performed at the same cell pressure. For instance, for CD and CU tests at $\sigma_3 = 1.2$ MPa, the maximum value of q is about 2.9 and 1.1 MPa, respectively. As shown in Fig. 22, this reduction in strength in CU tests is caused by the increase in pore pressure and decrease in p' , compared to CD tests in which there is no pore pressure and p' increases.

As shown in Fig. 23, in the case of dense sands, the $p'-q$ effective stress paths are also curved due to changes in pore pressure. However, the shear strength increases because p' increases due to a decrease in pore pressure. During the undrained tests at $\sigma_3 = 0.1, 1.,$ and 1.5 MPa, the pore pressure becomes equal to minus atmospheric pressure (i.e., -0.1 MPa), which puts the water under vac-

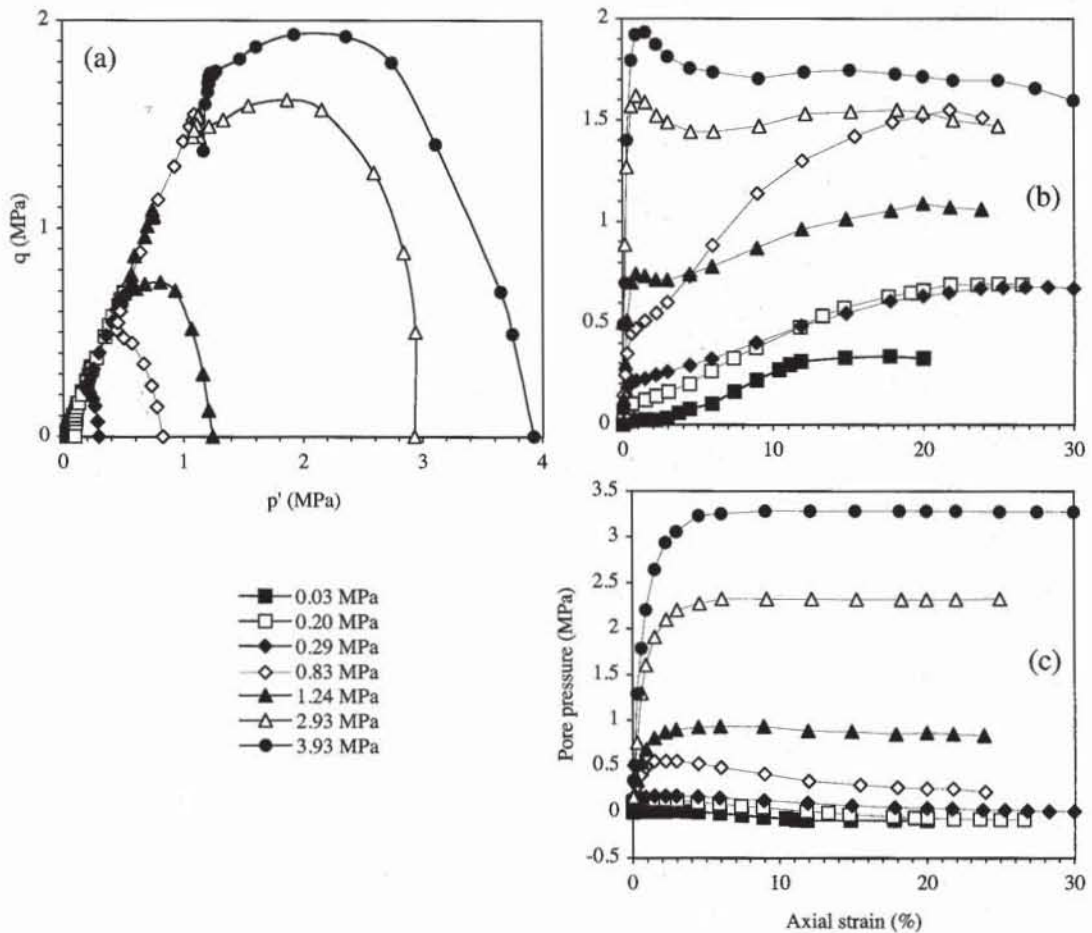


Figure 21 Results of CU triaxial compression tests on loose Sacramento River sand at various confining pressures: (a) effective stress paths, (b) variation of deviator stress q versus axial strain, and (c) variation of pore pressure versus axial strain (data after Seed and Lee, 1967).

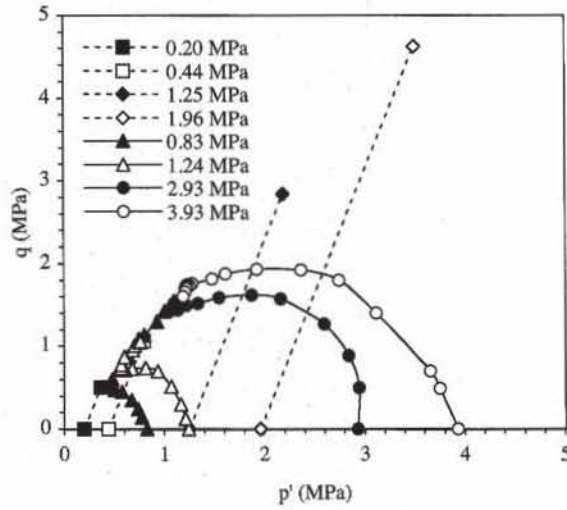


Figure 22 Effective stress path during the CD (dashed) and CU (solid) triaxial tests of Figs. 15 and 21.

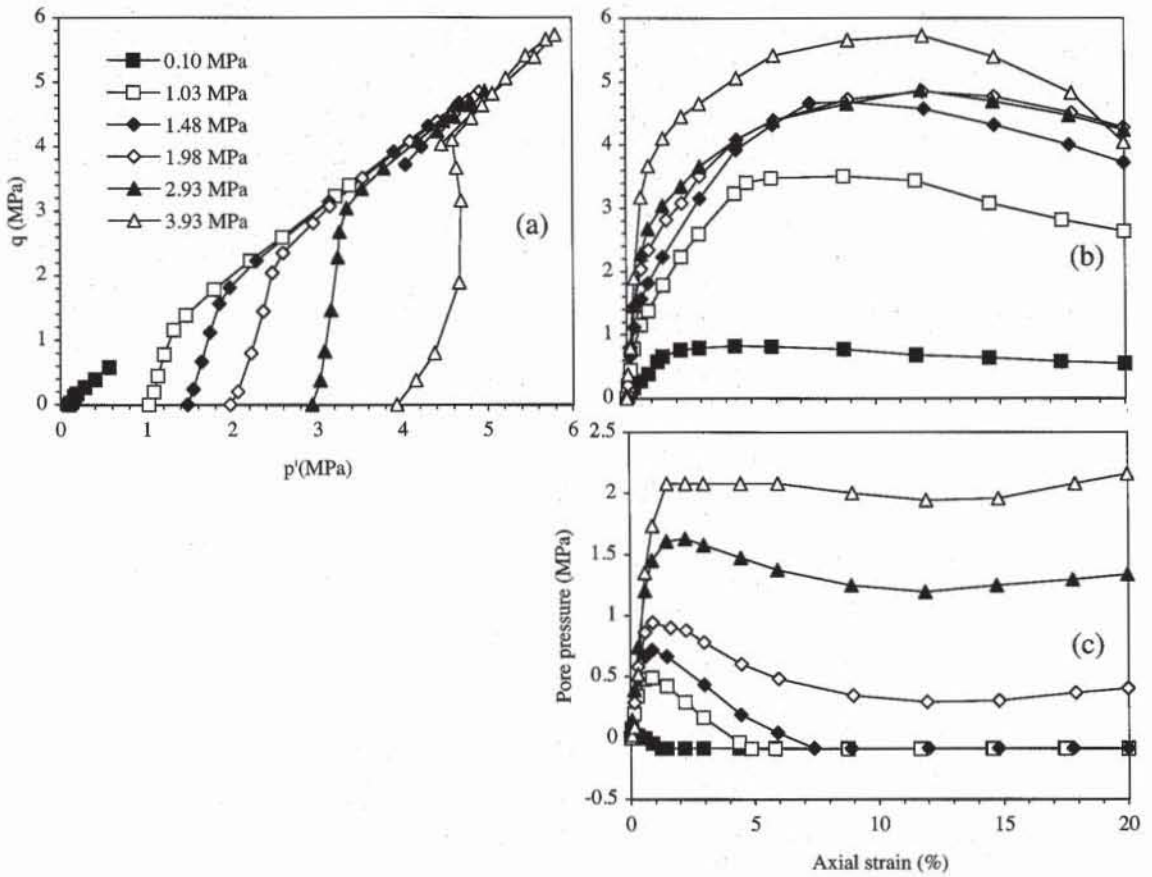


Figure 23 Results of CU triaxial compression tests on dense Sacramento River sand at various confining pressures: (a) effective stress paths, (b) variation of deviator stress q versus axial strain, and (c) variation of pore pressure versus axial strain (data after Seed and Lee, 1967).

uum. The pore pressure can no longer decrease because air bubbles form in water due to cavitation. When the pore pressure reaches -0.1 MPa, the CU triaxial test is no longer undrained, but drained as cavitation allows for volume changes. Cavitation may be avoided by increasing the back pressure (see Chapter 7-6).

Figures 19 and 20 compare the peak failure envelope obtained from CD and CU triaxial tests for the loose and dense Sacramento River sands. Both drained and undrained failure envelopes coincide. In term of effective stress, the failure envelopes of the Sacramento River sand are identical during drained and undrained conditions. This remark reconciles the apparent difference between the drained and undrained shear strength of sands, and demonstrates the advantage of expressing the failure of soils in terms of effective stress.

Undrained Triaxial Tests on Banding Sand

Figure 24 shows the stress-strain response and pore-pressure response of Banding sand subjected to CU triaxial compression tests, and compare them to drained responses during CD tests. The CU tests are performed at three different relative densities $D_r = 30\%$, 44% , and 47% , and the CD test at $D_r = 30\%$. All tests are performed at the same confining pressure $\sigma_3 = 400$ kPa. The undrained shear strength is smaller than the drained shear strength for $D_r = 30\%$ and 44% , but becomes larger for $D_r = 47\%$. For $D_r = 30\%$, the residual undrained shear strength is very small, which corresponds to the catastrophic phenomenon of liquefaction. Additional information on liquefaction can be found in Ishihara (1993).

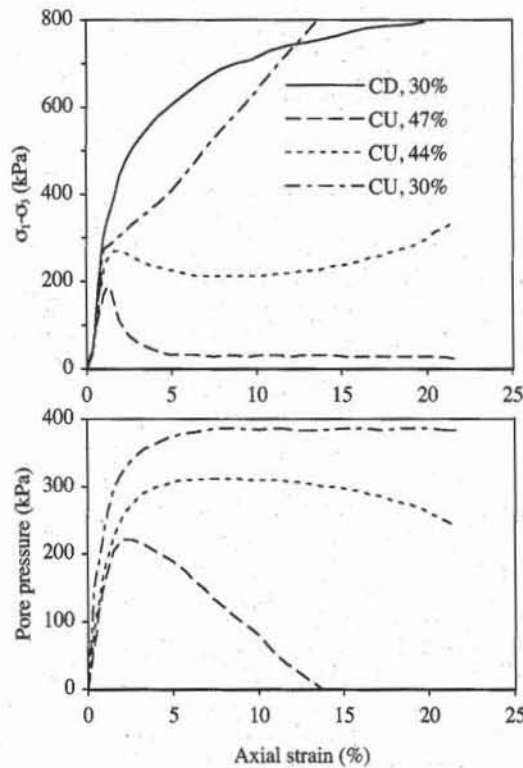


Figure 24 Stress-strain and pore pressure responses of three CU tests and one CD test on Banding sand with various relative density D_r , but identical confining pressure $\sigma_3 = 400$ kPa (after Castro, 1969).

Typical Characteristics for Shear Strength of Coarse-Grained Soils

The shear strength of sands and gravels are influenced by many factors, including mean effective pressure, void ratio, particle shape, grain size distribution, water, particle size, intermediate principal stress, and overconsolidation pressure.

Table 4 shows an early attempt to tabulate the variation of friction angle with density. The peak friction angle ϕ'_p varies from 28 to 48° depending on density. The residual friction angle ϕ'_r varies from 26 to 36°, independently of density. Table 5 includes the additional effects of void ratio, grain angularity, grain size and coefficient of uniformity on ϕ'_p for various soils, and extends the range of variation of ϕ'_p from 28 and 60°. Well-graded soils have a larger ϕ'_p than poorly-graded soils. In Tables 3 and 4, ϕ'_p increases with the grain angularity and density.

TABLE 4

Peak and residual friction angle of cohesionless soils (after Hough, 1957).

Classification	Friction angle ϕ'_p at peak strength (deg)		Friction angle ϕ'_r at ultimate strength (deg)
	Medium dense	Dense	
Silt (nonplastic)	28-32	30-34	26-30
Uniform fine to medium sand	30-34	32-36	26-30
Well-graded sand	34-40	38-46	30-34
Sand and gravel	36-42	40-48	32-36

TABLE 5

Friction angle of cohesionless soils (Holtz and Kovacs, 1981).

Soil type	Grain shape	D_{10} (mm)	C_u	Loose		Dense	
				e	ϕ'_p (deg)	e	ϕ'_p (deg)
Ottawa standard sand	Well rounded	0.56	1.2	0.7	28	0.5	35
Sand from St Peter sandstone	Rounded	0.16	1.7	0.69	31	0.5	37
Beach sand from Plymouth, MA	Rounded	0.18	1.5	0.89	29		
Silty sand from Franklin Falls dam site, NH	Subrounded	0.03	2.1	0.85	33	0.7	37
Silty sand from vicinity of John Martin dam, CO	Subangular to subrounded	0.04	4.1	0.65	36	0.5	40
Slightly silty sand, Ft. Peck dam, MT	Subangular to subrounded	0.13	1.8	0.84	34	0.5	42
Screened glacial sand, Manchester, NH	Subangular	0.22	1.4	0.85	33	0.6	43
Beach sand of hydraulic fill dam, Quabbin Project, MA	Subangular	0.07	2.7	0.81	35	0.5	46
Artificial, well-graded mixture of gravel with sands	Subangular to subrounded	0.16	68	0.41	42	0.1	57
Sand from Great Salt Lake fill (dust gritty)	Angular	0.07	4.5	0.82	38	0.5	47
Well-graded, compacted crushed rock	Angular					0.2	60

Figures 25 to 27 show that ϕ'_p is significantly influenced by void ratio e . As shown in Fig. 25, ϕ'_p decreases from 40 to 32° when e increases, but remains larger than the friction angle between particles (e.g., $\phi_\mu = 26^\circ$). Similar influence of void ratio on ϕ'_p is observed for various types of granular soils including grav-

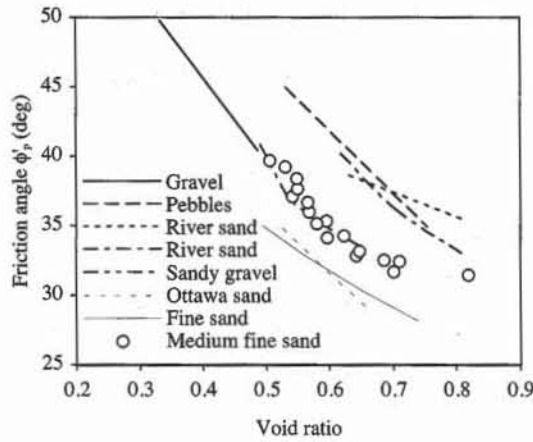


Figure 25 Variation of friction angle versus void ratio for several granular soils (data after Lambe and Whitman, 1979; and Rowe, 1962).

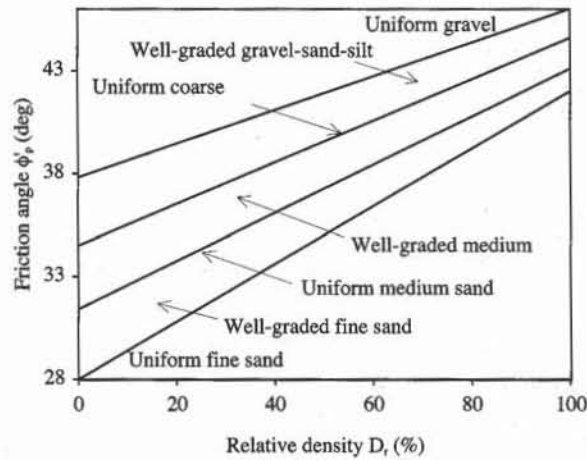


Figure 26 Variation of friction angle ϕ'_p with relative density D_r (Schertmann, 1978)

els and fine sands. As shown in Fig. 26, ϕ'_p varies with relative density D_r and coefficient of uniformity. As shown in Fig. 27, ϕ'_p can be correlated to dry unit weight, relative density, and USCS classification.

Figure 28 shows the effects of confining pressure σ'_3 on ϕ'_p in coarse-grained soils subjected to triaxial compression tests. These effects which were noticed for loose and dense Sacramento River sand are also observed in other sands, and can account for a decrease in ϕ'_p from 45 to 32°.

Using a database of clean sands, Bolton (1986) shows that the peak and residual friction angles ϕ'_p and ϕ'_r are related through

$$\phi'_p = \phi'_r + \alpha \max\{0, D_r[Q - \ln(p'_f)] - R\} \tag{16}$$

where α depends on the type of loading (3 triaxial compression, and 5 for plane strain compression), D_r is the relative density, Q the soil mineralogy and compressibility coefficient (10 for quartz and feldspar, 8 for limestone, 7 for anthra-

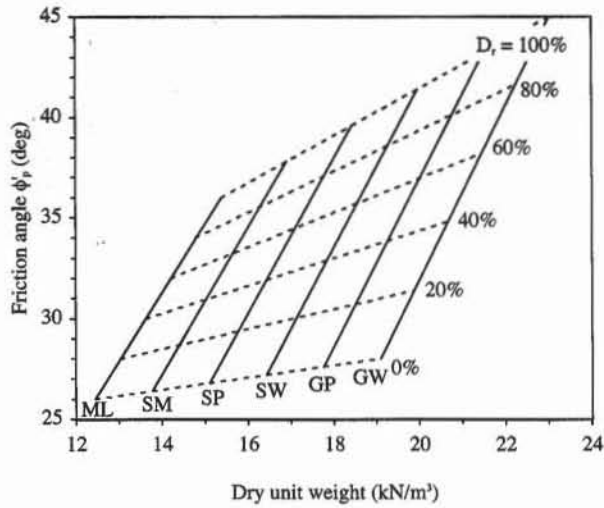


Figure 27 Correlation between friction angle, dry unit weight, relative density, and USCS classification for coarse-grained soils without plastic fines (NAVFAC, 1982).

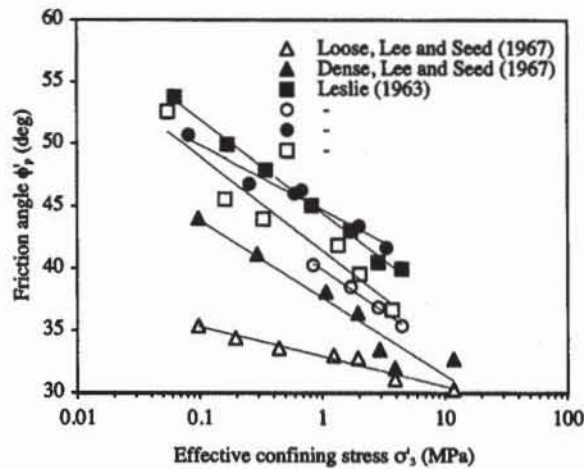


Figure 28 Variation of friction angle with confining pressure in tri-axial compression test (data after Leslie, 1963).

cite, 5.5 for chalk), R a fitting coefficient (equal to 1 for the data of Fig. 29), and $p'_f = (\sigma'_1 + \sigma'_2 + \sigma'_3)/3$ the mean effective pressure at failure. As shown in Fig. 29, Eq. 16 is capable of describing the variation of $\phi'_p - \phi'_r$ with density and mean pressure for loose and dense Sacramento River sands.

The residual friction angle ϕ'_r in Eq. 16 can be evaluated from the relation proposed by Koerner (1970):

$$\phi'_r = 36^\circ + \Delta\phi_1 + \Delta\phi_2 + \Delta\phi_3 + \Delta\phi_4 + \Delta\phi_5 \tag{17}$$

where $\Delta\phi_1, \Delta\phi_2, \Delta\phi_3, \Delta\phi_4,$ and $\Delta\phi_5$ depend on the grain shape, grain size, gradation, density and mineral hardness as specified in Table 6. By decreasing order of importance, the factors influencing ϕ'_r are particle size, particle shape, mineral hardness, density, and gradation.

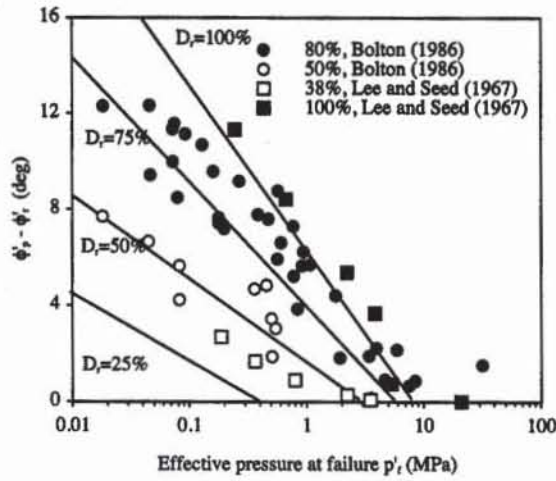


Figure 29 Variation of $\phi'_p - \phi'_r$ with effective mean pressure p'_f at failure (Bolton, 1986).

TABLE 6

Variation of friction angle ϕ'_r with particle shape, grain size, gradation, density, and mineral (Koerner, 1970).

Factor	Description	Correction factor (deg)				
		$\Delta\phi_1$	$\Delta\phi_2$	$\Delta\phi_3$	$\Delta\phi_4$	$\Delta\phi_5$
Particle shape	Low sphericity and angular shape	2				
	High sphericity and subrounded shape	-6				
Grain size	Fine sand, $0.2 > D_{10} > 0.06$ mm		0			
	Medium sand, $0.6 > D_{10} > 0.2$ mm		-4			
	Coarse sand, $2.0 > D_{10} > 0.6$ mm		-9			
	Gravel, $D_{10} > 2$ mm		-11			
Gradation	Poorly-graded soil, $C_u < 2$			0		
	Medium uniformity, $C_u = 10$			-1		
	Well-graded soil, $C_u > 2$			-2		
Density	Loosest packing, $0 < D_r < 50\%$				-1	
	Medium density, $50 < D_r < 75\%$				0	
	Denset packing, $D_r > 75\%$				4	
Mineral	Quartz					0
	Feldspar, calcite, chlorite					4
	Muscovite, mica					6

Influence of intermediate principal stress. The effect of intermediate principal stress σ'_2 on shear strength can be characterized by introducing the parameter b

$$b = \frac{\sigma'_2 - \sigma'_3}{\sigma'_1 - \sigma'_3} \tag{18}$$

where σ'_1 and σ'_3 are the major and minor principal effective stress, respectively. b varies from 0 to 1 when σ'_2 varies from σ'_3 to σ'_1 , $b = 0$ in triaxial compression tests ($\sigma'_2 = \sigma'_3$), and $b = 1$ in triaxial extension tests ($\sigma'_2 = \sigma'_1$).

The investigation of the effect of σ'_2 on friction angle ϕ'_p requires advanced testing apparatus, some of which are described in Chapter 5-4. As shown in Fig. 30 for various sands, b influences the friction angle ϕ'_p calculated from the measured values of σ'_1 and σ'_3 (Eq. 5). It is minimum for $b = 0$, sharply increases for

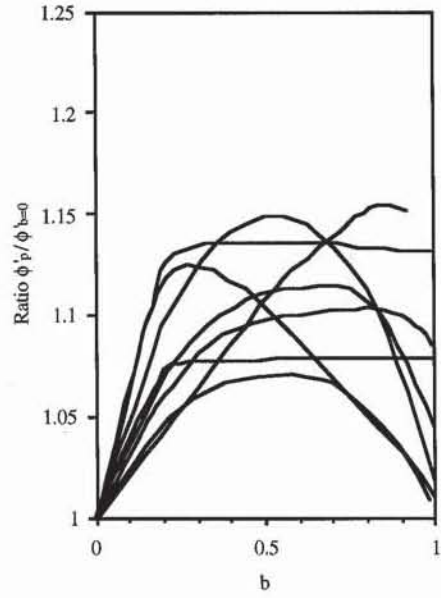
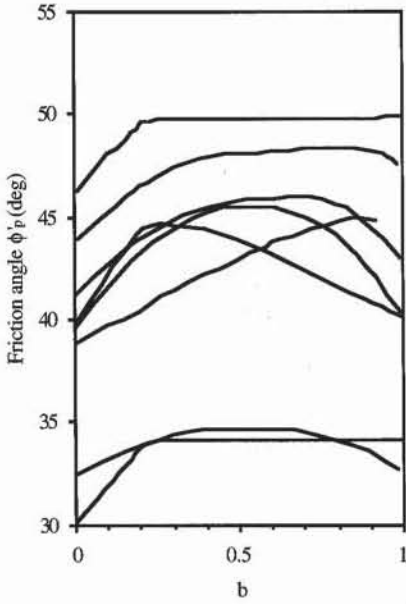


Figure 30 Variation of friction angle ϕ'_p with parameter b measured on various sands (after Biarez and Hicher, 1994).

Figure 31 Variation of normalized friction angle $\phi'_p / \phi'_{b=0}$ with parameter b corresponding to Fig. 30.

$0 < b < 0.3$, then keeps increasing or start to decrease depending on data sets. Biarez and Hicher (1994) attributed this scatter in experimental results to the diversity of testing conditions. In most cases, ϕ'_p is larger in extension ($b = 1$) than in compression ($b = 0$). Figure 31 shows the variation of $\phi'_p / \phi'_{b=0}$ with b , in which ϕ'_p is normalized by its values $\phi'_{b=0}$ in triaxial compression ($b = 0$). ϕ'_p can be 15% larger than $\phi'_{b=0}$.

The effect of intermediate principal stress σ'_2 on ϕ' is not accounted for in the three-dimensional Mohr–Coulomb failure surface (Eq. 9). To account for this effect, Lade and Duncan (1975) suggested the following failure envelope:

$$I_1^3 - \eta_1 I_3 = 0 \quad \text{and} \quad \eta_1 = \frac{(3 - \sin \phi')^3}{(1 - \sin \phi') \cos^2 \phi'} \quad (19)$$

while Matsuoka and Nakai (1974) proposed:

$$I_1 I_2 - \eta_2 I_3 = 0 \quad \text{and} \quad \eta_2 = \frac{9 - \sin^2 \phi'}{1 - \sin^2 \phi'} \quad (20)$$

where I_1 , I_2 and I_3 are the stress invariants defined in Chapter 5-1, and ϕ' is calculated for $b = 0$. In the $\sigma_1 - \sigma_2 - \sigma_3$ principal stress space of Fig. 6a, the failure surfaces of Eqs. 19 and 20 are smooth cones which encompass the angular Mohr–Coulomb surface. As shown in the deviatoric plane of Fig. 32, these failure surfaces have similar cross-sections.

Figure 33 and 34 shows the variations of ϕ' and $\phi'_p / \phi'_{b=0}$ with b which are calculated by introducing b in Eqs. 19 and 20. The variations corresponding to Mohr–Coulomb are not represented; they are horizontal lines. Equation 20 predicts the measured variation of ϕ' better than Eq. 19. However, Eq. 20 does not describe the change in ϕ' observed between triaxial compression and extension. In

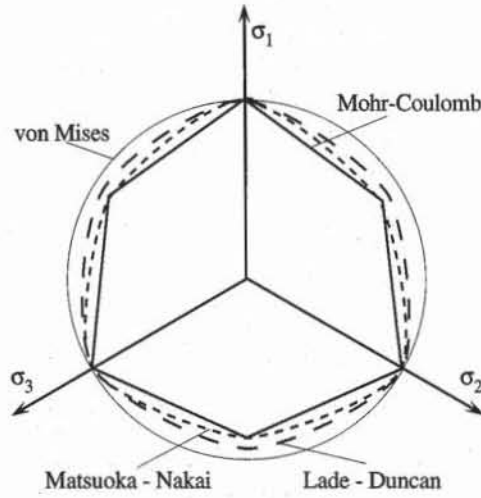


Figure 32 Failure surfaces in deviatoric plane: Mohr-Coulomb, von Mises, Lade-Duncan, and Matsuoka-Nakai.

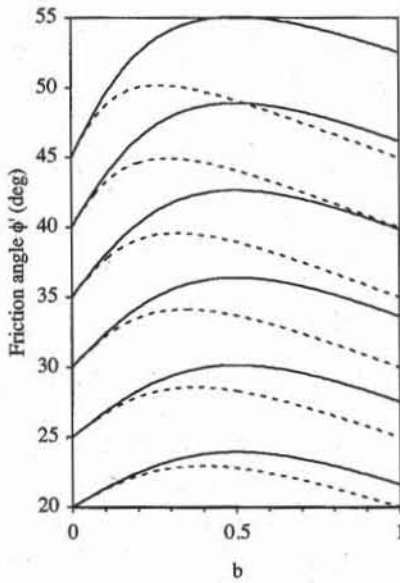


Figure 33 Variation of friction angle ϕ' with parameter b predicted by Lade and Matsuoka-Nakai failure surface for various friction angle in triaxial compression.

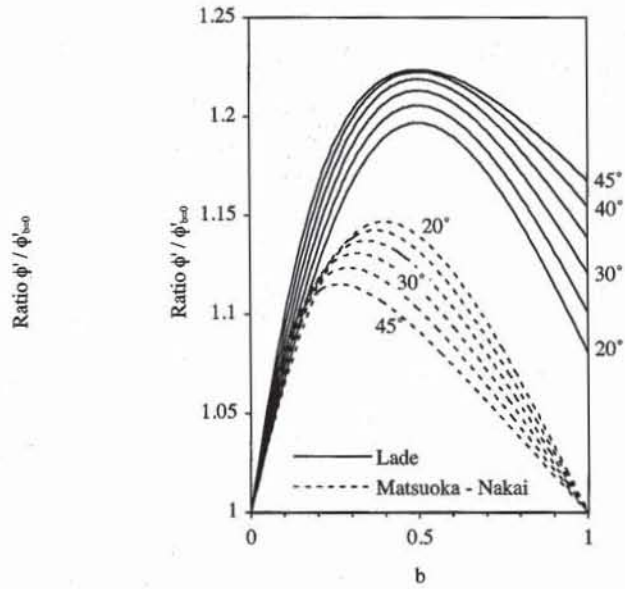


Figure 34 Variation of normalized friction angle $\phi'/\phi'_{b=0}$ with parameter b corresponding to Fig. 33.

addition to Eqs. 19 and 20, there are other failure envelopes (e.g., Bardet, 1990) which can account for the effects of b on ϕ' .

SHEAR STRENGTH OF FINE-GRAINED SOILS

The shear strength characteristics of fine-grained soils (e.g., clays and silts) are introduced by examining the stress-strain response of a particular clay—Weald clay—which was extensively tested under CD and CU triaxial compressions.

Isotropic Consolidation of Weald Clay

Figure 35 shows the result of an isotropic consolidation test on Weald clay. Starting from the value 0.8, the void ratio e decreases linearly with the logarithm of effective mean pressure p' . The point (p', e) moves on the *virgin consolidation line* (VCL), which has the equation

$$e = X - \lambda \ln(p') \quad (21)$$

where λ is the VCL slope, and X is the void ratio at $p' = 1$ kPa. As described in Chapter 6-1, the soil response is irreversible after a loading reversal. When p' is decreased from p'_1 , the point (p', e) moves away from the VCL along a swelling line defined by

$$e = e_1 - \kappa \ln \frac{p'}{p'_1} \quad (22)$$

where κ is the average swelling slope, and e_1 is the void ratio at $p' = p'_1$. The parameter λ and κ are related to the compression indices C_c and C_s defined in Chapter 6-1 through

$$\lambda = 0.434 C_c \quad \text{and} \quad \kappa = 0.434 C_s \quad (23)$$

where the coefficient 0.434 results from the conversion from decimal to natural logarithm. For Weald clay, $\lambda = 0.092$ and $\kappa = 0.032$.

The degree of overconsolidation of a clay is characterized by the overconsolidation ratio OCR which is

$$OCR = \frac{p'_p}{p'_0} \quad (24)$$

where p'_0 is the present mean effective pressure, and p'_p is the preconsolidation pressure, which is the largest effective pressure applied in the past. OCR is always larger or equal to 1. When the point (p'_0, e) is on the VCL, the clay is normally consolidated and $OCR = 1$. When it is on a swelling line, the clay is overconsoli-

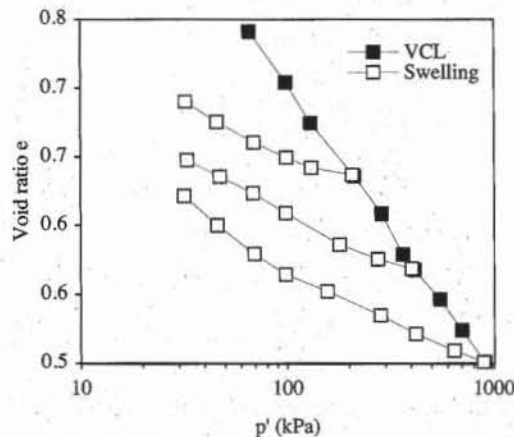


Figure 35 Results of isotropic consolidation on Weald clay (data after Parry, 1960).

dated and $OCR > 1$. For instance, a clay with an $OCR = 30$ and $p'_0 = 30$ kPa was first isotropically loaded to 900 kPa, before being unloaded to 30 kPa.

CD Triaxial Compression Tests on Weald Clay

Figure 36 shows the results of CD triaxial tests on normally consolidated and overconsolidated samples of Weald clay. At 69 kPa confining pressure, the shear strength of the overconsolidated ($OCR = 12$) sample is almost twice that of the normally consolidated sample. The overconsolidated samples initially compact then dilate during shear, whereas the normally consolidated samples compact until they fail. A similar behavior was observed for dense and loose Sacramento River sands. As shown in Fig. 36a, the failure envelope is not straight, but curved at small pressures.

CU Triaxial Compression Tests on Weald Clay

Figure 37 shows the results of CU triaxial tests on normally and over-consolidated samples of Weald clay at two different total confining pressures σ_3 . In p' - q space, the normally consolidated stress-path moves toward the origin, whereas the overconsolidated stress-path goes away from the origin, which increases p' , and makes the overconsolidated sample at $\sigma_3 = 35$ kPa almost as strong as the normally consolidated sample at $\sigma_3 = 207$ kPa.

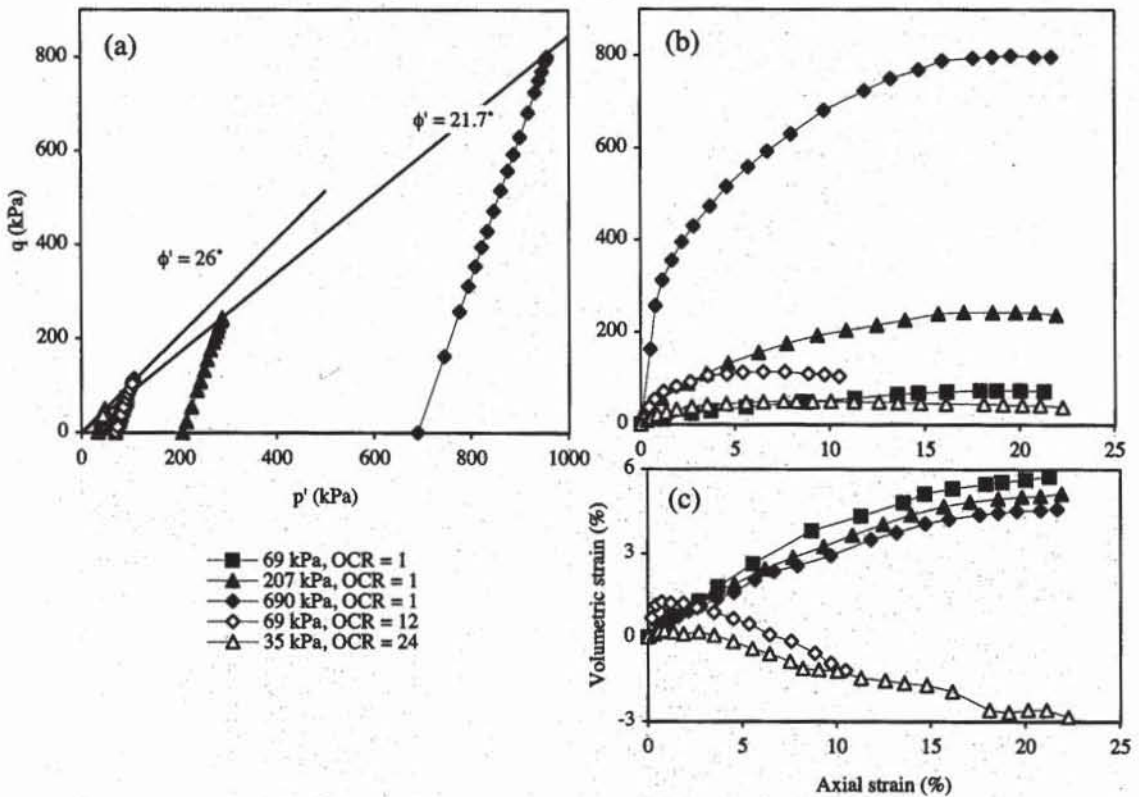


Figure 36 Results of CD triaxial tests at various confining pressures on normally consolidated ($OCR = 1$) and overconsolidated ($OCR = 12$ and 24) samples of Weald clay; (a) effective p' - q stress paths, (b) stress-strain response, and (c) volumetric response (data after Parry, 1960).

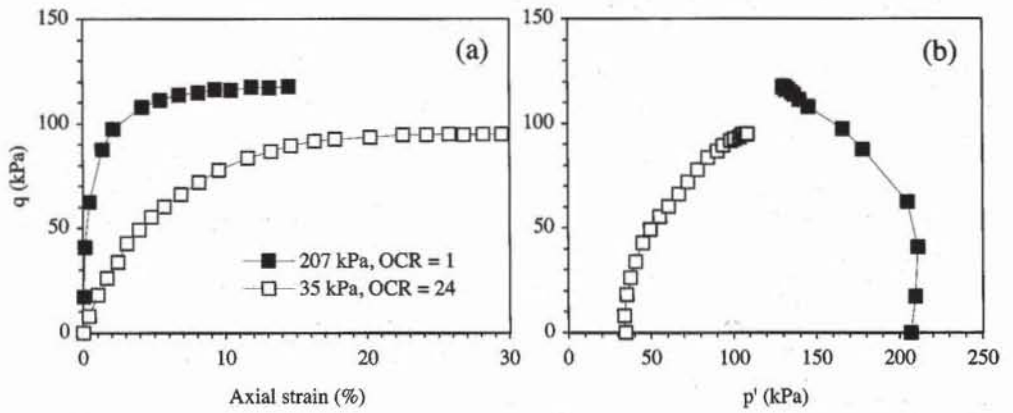


Figure 37 Results of CU triaxial tests on normally consolidated (207 kPa, OCR = 1) and overconsolidated sample (35 kPa, OCR = 24) of Weald clay: (a) stress-strain response, and (b) effective p' - q stress path (data after Parry, 1960).

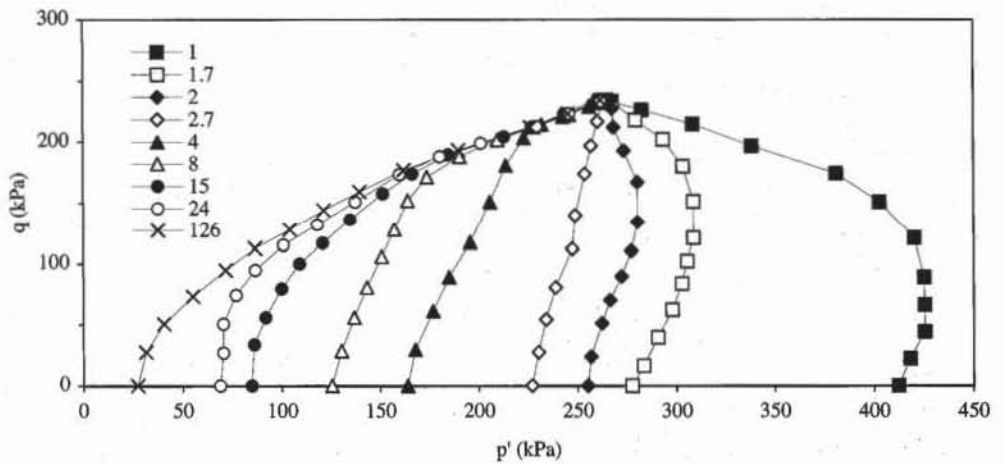


Figure 38 Effective p' - q stress paths for samples of Weald clay with the same void ratio but different overconsolidation ratios (data after Parry, 1960).

As shown in Fig. 38, the p' - q stress paths that are associated with the same void ratio but different overconsolidation ratios from 1 to 126 converge toward a common point. The undrained shear strength of Weald clay is largely determined by its initial void ratio.

Critical State Theory for Clays

The critical state theory (Schofield and Wroth, 1968) extends the Mohr-Coulomb failure theory by describing the variation of shear strength with void ratio. One of its major achievement is to relate the drained and undrained behaviors of fine-grained soils, and to predict their undrained shear strength.

In the critical state theory, soils reach their critical state when they undergo a residual failure at constant volume. The critical state is associated with residual failure, but not with peak failure, which is generally accompanied with a volume

change. The projection of the *critical state line (CSL)* onto the $p'-q$ space is

$$q = M p' \tag{25}$$

where M is related to the residual friction angle through:

$$\phi'_r = \sin^{-1}\left(\frac{3M}{6+M}\right), \text{ and } M = \frac{6 \sin \phi'_r}{3 - \sin \phi'_r} \tag{26}$$

The projection of the critical state line in the $p'-e$ space is parallel to the virgin compression line

$$e = \Gamma - \lambda \ln(p') \tag{27}$$

where Γ is the critical void ratio at $p' = 1$ kPa. The *CSL* void ratio Γ and *VCL* void ratio X at $p' = 1$ kPa are related through

$$\Gamma = X - (\lambda - \kappa) \ln(r) \tag{28}$$

where the parameter r is usually selected equal to 2.

As shown in Figs. 39 and 40, the critical state is identical for the drained and undrained responses of normally consolidated and overconsolidated samples of Weald clay. The point (p', q, e) tends to move closer to the critical state during shear loading. A material denser than the critical void ratio dilates to reach the critical state, whereas a material looser than the critical void ratio compacts to reach the critical state.

The critical state theory has four material constants: λ , κ , ϕ' and Γ . The values of these constants are listed in Table 7 for London clay, Weald clay, and kaolin, along with their liquid and plastic limits, specific gravity and the void ratios corresponding to plastic and liquid limits.

Undrained Shear Strength from Critical State Theory

By definition, the undrained shear strength S_u is the shear stress at failure during undrained loadings. During undrained triaxial compression tests, S_u is

$$S_u = \frac{1}{2} q_f = \frac{1}{2} (\sigma_1 - \sigma_3)_f = t_f \tag{29}$$

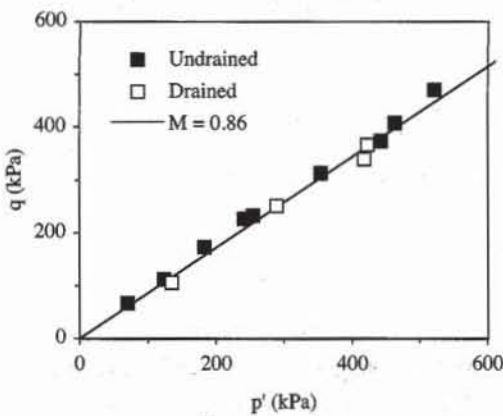


Figure 39 Critical state in $p'-q$ space from drained and undrained triaxial test results on Weald clay (data after Parry, 1960).

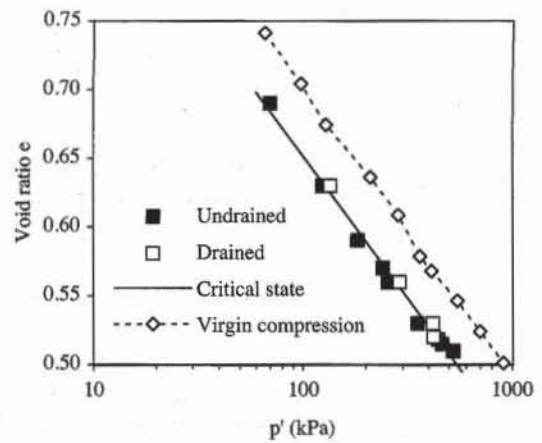


Figure 40 Critical state in $p'-e$ space from drained and undrained triaxial test results on Weald clay (data after Parry, 1960).

TABLE 7

Critical state parameters and plasticity indices for London clay, Weald clay, and kaolin (Schofield and Wroth, 1968)

Material constants	London clay	Weald clay	Kaolin
Slope of critical state line (CSL), λ	0.161	0.093	0.260
Void ratio on CSL at 1 kPa, Γ	1.759	1.060	2.767
Slope of critical state in p' - q space, M	0.88	0.95	1.02
Friction angle ϕ' at critical state (deg)	22.6	24.2	25.8
Slope of swelling line, κ	0.062	0.035	0.050
Parameter $\Lambda = (\lambda - \kappa)/\lambda$	0.615	0.624	0.808
Liquid limit LL (%)	78	43	74
Plastic limit PL (%)	26	18	42
Plasticity index PI (%)	52	25	32
Specific gravity G_s	2.75	2.75	2.61
Void ratio at LL	2.145	1.183	1.931
Void ratio at PL	0.715	0.495	1.096

At the critical state, S_u is therefore related to the effective mean pressure p'_f through

$$S_u = \frac{1}{2} M p'_f \quad (30)$$

During undrained tests, the void ratio e is constant (i.e., $e = e_0$) and is related to p'_f through Eq. 27, that is

$$e_0 = \Gamma - \lambda \ln(p'_f) \quad (31)$$

Therefore Eq. 30 becomes

$$S_u = \frac{M}{2} \exp\left(\frac{\Gamma - e_0}{\lambda}\right) \quad (32)$$

S_u can also be expressed in terms of the liquidity index LI . By definition, the liquidity index LI is

$$LI = \frac{w - PL}{PI} \quad (33)$$

where w is the water content, PL the plastic limit, PI the plasticity index ($PI = LL - PL$), and LL the liquid limit. $LI = 1$ when $w = LL$ and $LI = 0$ when $w = PL$. For saturated soils, the void ratio e_0 is related to the water content through

$$e_0 = w_0 G_s = G_s(PL + PI \times LI) \quad (34)$$

Therefore Eq. 32 becomes

$$S_u = \frac{M}{2} \exp\left[\frac{\Gamma - G_s(PL + PI \times LI)}{\lambda}\right] \quad (35)$$

The undrained shear strength S_u becomes the following function of plasticity index LI

$$S_u = S_{uPL} \left(\frac{S_{uLL}}{S_{uPL}}\right)^{LI} \quad (36)$$

where S_{uPL} and S_{uLL} are the undrained shear strength at plastic limit PL and liquid limit LL , respectively:

$$S_{uPL} = \frac{M}{2} \exp[(\Gamma - G_s PL)/\lambda] \quad \text{and} \quad S_{uLL} = S_{uPL} \exp[-G_s PI/\lambda] \quad (37)$$

Schofield and Wroth (1968) observed that the ratio S_{uPL}/S_{uLL} is practically equal to 100, which implies that the slope of the critical can approximately be related to specific gravity and plasticity index

$$\lambda = \frac{G_s PI}{\text{Ln}[S_{uPL}/S_{uLL}]} \approx 0.217 G_s PI \quad (38)$$

S_u can also be expressed in terms of OCR. An overconsolidated clay with the initial state (p'_0, e_0) corresponds to the normally consolidated state (p'_p, e_p) which is on the VCL

$$e_p = e_0 - \kappa \ln \frac{p'_p}{p'_0} = e_0 - \kappa \ln OCR = X - \lambda \ln(OCR p'_0) \quad (39)$$

Therefore e_0 is

$$e_0 = X - (\lambda - \kappa) \ln OCR - \lambda \ln p'_0 \quad (40)$$

Eq. 32 becomes

$$\frac{S_u}{p'_0} = \frac{M}{2} \exp\left(\frac{\Gamma - X}{\lambda}\right) OCR^{\frac{\lambda - \kappa}{\lambda}} \quad (41)$$

and using Eq. 28,

$$\frac{S_u}{p'_0} = \frac{M}{2} \left(\frac{OCR}{r}\right)^\Lambda \quad (42)$$

where the parameter Λ is

$$\Lambda = \frac{\lambda - \kappa}{\lambda} \quad (43)$$

The value of Λ is limited to be between 0 and 1, and is typically about 0.8. As mentioned previously, r depends on Γ and X and is usually selected equal to 2. The undrained shear strengths of overconsolidated and normally consolidated clays are therefore related through

$$\frac{S_u}{p'_0} = \left(\frac{S_u}{p'_0}\right)_{OCR=1} OCR^\Lambda \quad (44)$$

The undrained shear strength of normally consolidated clays can be approximated as

$$\left(\frac{S_u}{p'_0}\right)_{OCR=1} \approx 0.29 M = \frac{1.72 \sin \phi'_r}{3 - \sin \phi'_r} \quad (45)$$

The undrained shear strength predicted by Eqs. 36, 42, 44, and 45 is compared to experimental results later.

The normalization of Eq. 44 sets the basis of the *SHANSEP* procedure (Ladd and Foott, 1974). *SHANSEP*, which is the acronym for Stress History and Normalized Soil Engineering Properties, assumes the normalization of the undrained stress-strain response and undrained shear strength of normally and overconsolidated soils. This normalization is convenient to determine the undrained shear strength at various initial stresses p'_0 and overconsolidation ratios *OCR* by performing a relatively small number of tests with different values of p'_0 and *OCR*. Additional information on *SHANSEP* can be found in Jamiolkowski et al. (1985) and Ladd (1991).

Drained Shear Strength of Fine-grained Soils

As shown in Fig. 41, at low effective normal stress σ' , the failure envelope of overconsolidated fine-grained soils is usually more curved and larger than the failure envelope of normally consolidated material which is practically linear. As illustrated in Fig. 42, this bump *EDC* in the failure envelope originates from overconsolidation, which is represented by unloading *CDE* in the σ' -*e* space. *ABCF* represents the failure envelope of normally consolidated clays, while *EDCF* denotes that of overconsolidated clays.

Table 8 gives typical values of effective cohesion intercept c' and effective friction angle ϕ' for various fine-grained soils. The values of c' range from 0 to 150 kPa, and those of ϕ' from 5 to 38°. As described previously, the failure envelope of fine-grained soils is curved, and the cohesion intercept c' varies with the range of σ' . For normally consolidated clays, c' is practically equal to zero (see Fig. 41). For overconsolidated clays, c' depends nonlinearly on σ' and *OCR*. In most fine-grained soils, at the exception of cemented soils, partially saturated soils, and heavily consolidated clays, the intercept of the curved failure envelope with the τ axis is small.

As shown in Figs. 43 and 44, the friction angle ϕ' of fine-grained soils decreases from 40° to 20° when the plasticity index *PI* varies from 20% to 100%. In the particular case on montmorillonite clay with extremely large water content (1000%), ϕ' decreases to the low value of 5°. As shown in Fig. 44, the residual friction angle ϕ'_r decreases from 33 to 5° with the clay fraction (percent by weight finer than 2 μm obtained from grain-size distribution curve). Figures 45 and 46

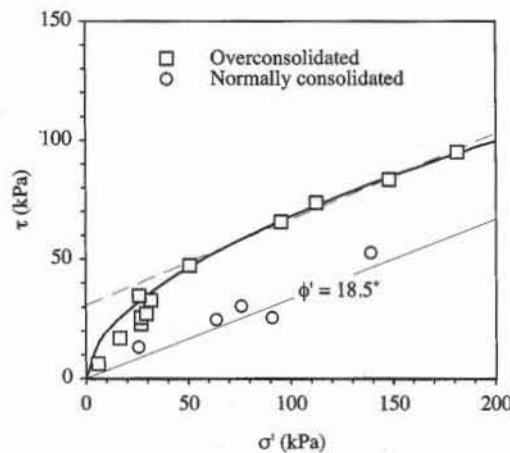


Figure 41 Failure envelopes of normally consolidated and overconsolidated clays (data from Singh et al., 1973).

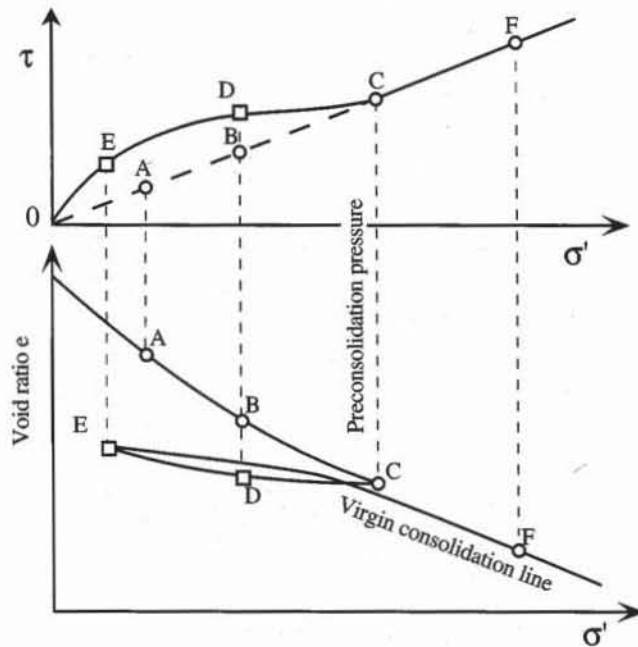


Figure 42 Effect of overconsolidation on failure envelope of fine-grained soils.

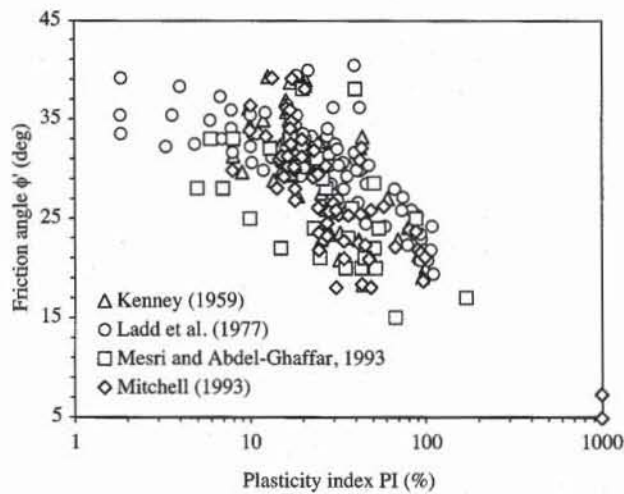


Figure 43 Relation between friction angle ϕ' and plasticity index PI on fine-grained soils (data after Kenney, 1959; Ladd et al., 1977; Mesri and Abdel-Ghaffar, 1993; and Mitchell, 1993).

show the effect of the intermediate principal stress on ϕ' . Like coarse grained soils, fine grained soils have a friction angle ϕ' that depends on the coefficient b , and may vary as much as 20% with b .

Undrained Shear Strength of Fine-grained Soils

The undrained shear strength S_u is a widely used soil parameters in geotechnical engineering. However, S_u is not a fundamental soil property like the effective

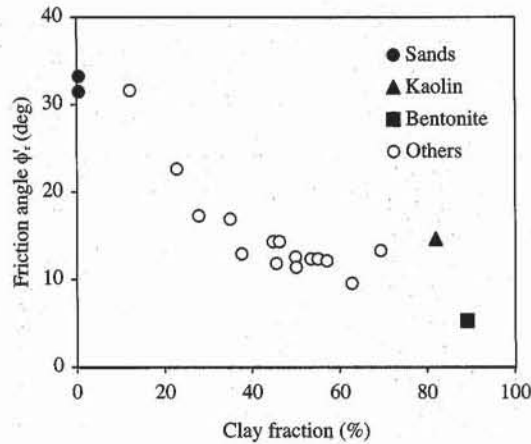


Figure 44 Relation between residual friction angle ϕ'_r and clay fraction from ring shear tests and field studies (Skempton, 1985).

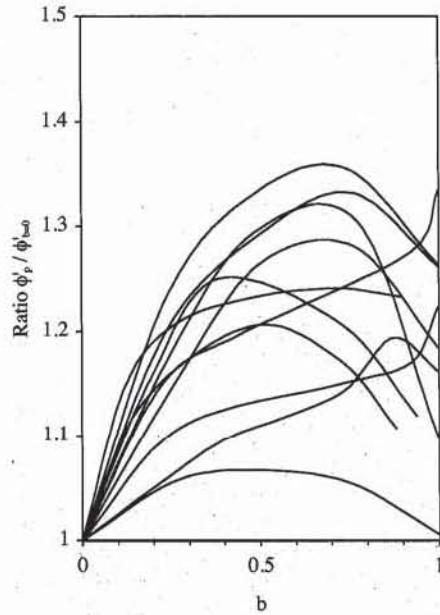
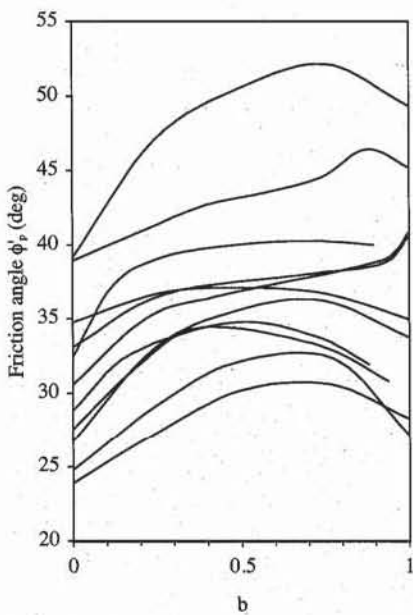


Figure 45 Variation of friction angle ϕ'_p with parameter b measured on various clays (after Biarez and Hicher, 1994).

Figure 46 Variation of normalized friction angle $\phi'_p / \phi'_{b=0}$ with parameter b corresponding to Fig. 45.

friction angle ϕ . S_u is influenced by many factors including the mode of testing, rate of loading, confining stress level, initial stress states, and other variables. Hereafter, we present typical values of S_u obtained in a standard or reference test—CU triaxial tests with isotropic consolidation—and examine the relations between S_u and plasticity index, overconsolidation ratio, liquidity index, and sensitivity.

Table 9 lists values of S_u for various soils as well as additional properties, including liquid and plastic limits and water content. The values for S_u in Table 9 range from 10 to 300 kPa.

TABLE 8

Values of cohesion intercept c' and friction angle ϕ' obtained for various soils (Mesri and Abdel-Ghaffar, 1993)

Case record	Water content (%)	Plasticity index PI (%)	Liquidity index LI	c' (kPa)	ϕ' (deg)
Kimola Canal	53	27	1	4.9	28
Lake Michigan bluffs	—	2–14	Stiff	8–20	31–35
Trondheim embankment	22–25	3–7	>1	22	28
Selnes landslide	34	5	3.4	4.9	28
Selnes landslide	—	7	1	14.9	28
Voitagio landslide	8	10	-1.1	20	25
Slope failure in China	22	20	0.05	11.8	38
Saguling power station	—	15	Stiff	26	22
Slope failure in Sri-Lanka	—	24	Stiff	10.4	31
Slope failures in varigated clay shale	20	24	-0.58	7.4	24
Slope failures in varigated clay shale	—	—	—	5.3	25
Jackfield landslide	30	25	0.4	7.2	21
Selset landslide	12	13	-0.8	8.6	32
Lodalén slide	31	17	0.75	9.8–12	27–32
Drammen River slide	32–38	17	1	0–2	33
Ullensaker landslide	30	6	1.3	1.5–2.3	32–34
S. Barbara coal mine	43	35	-0.6	150	20
Carsington Dam	40	43	0.19	10	20
Shellmouth test fill	39	38	0.48	12.4	26
Seven Sisters Dikes	48	67	0.27	13.8	15
North Ridge Dam	37	51	0.31	24.8	22
London clay failures	31	52	0	12	20
Lias clay failures, weathered	18–28	31–41	<0	17	23
Field test in Oslo clay	30–38	23	>0.5	8.8	24
Lesueur landslide	—	170	Stiff	29	17
Failure at Wetteren	—	88	0	8	25
Amuay slides	15–20	40	0.15	6.9	38
Bosse-Galine test cut	55	51	0.61	10–12	26–31
River Albedosa slide	29	26	0.17	55	29
Genesse embankment	20–45	45	0.2–0.4	10–20	21
Otford test embankment	31	54	0	10	24

Influence of Test Conditions

As mentioned in Chapter 5-4, the soil samples are not consolidated before being sheared in UU triaxial tests. In Table 9, the undrained shear strength measured from UU tests is denoted $S_u(UU)$, and that measured from CU tests is denoted by S_u , assuming that the CU tests are the reference laboratory tests to determine the undrained shear strength. As shown in Fig. 47, at the exception of a few cases, $S_u(UU)$ is systematically smaller than S_u . Detailed studies (e.g., Ladd et al., 1977) have shown that the UU tests are often in gross error because of sampling disturbance effects and omission of reconsolidation phase.

Influence of PI . Various empirical correlations were proposed to relate the undrained shear strength S_u and plasticity index PI . The most common correlation for normally consolidated clays (Skempton, 1957) is

$$\frac{S_u}{\sigma'_0} = 0.11 + 0.0037 PI \quad (46)$$

where σ'_0 is the effective vertical stress, and PI the plasticity index. As shown in Fig. 48, Eq. 46 applies to the soils tested by Bjerrum (1954) and Leonards (1962), but not to those of Osterman (1960) which have large plasticity index, and are difficult to sample in the field and test in the laboratory.

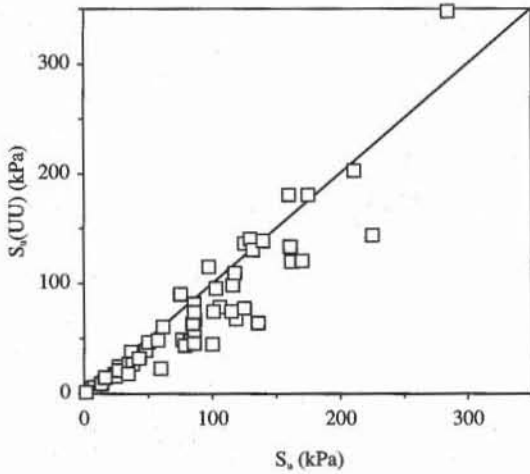


Figure 47 Relation between undrained shear strength $S_u(UU)$ measured in UU triaxial tests and undrained shear strength S_u measured in CU triaxial tests on various soils (data after Chen and Kulhawy, 1993).

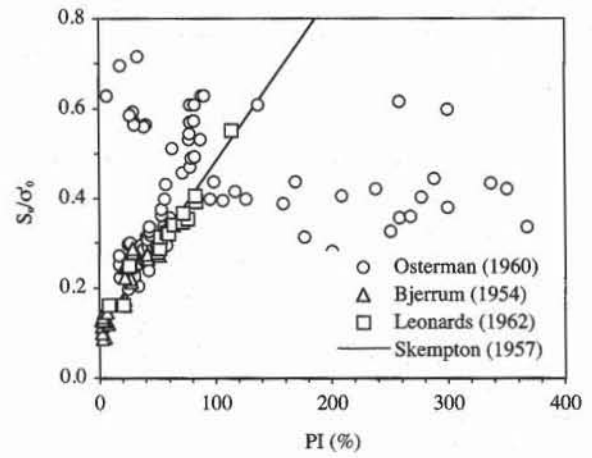


Figure 48 Variation of S_u/σ'_0 with plasticity index PI for normally consolidated clays (after Holtz and Kovacs, 1981).

TABLE 9

Database for undrained shear strength of various clays from CU and UU tests (Chen and Kulhawy, 1993)

Site	Soil description	LL (%)	PL (%)	w (%)	Total unit weight (kN/m ³)	Sensitivity	Depth (m)	OCR	S_u (kPa)	$S_u(UU) / S_u$	S_u / σ'_0
Boston	Medium blue clay	49	25	35	18.7		12.2	4	106	0.74	0.8
		49	26	38	18.4		18.3	1.8	86.6	0.77	0.48
		39	21	36	19.3		27.4	1	84.5	0.58	0.32
Lagunillas	High plasticity clay	61	24				6.2	1.3	23.5	0.75	0.4
		61	24				6.4	1.3	24.3	0.64	0.41
Kawasaki	High plasticity clay	65	34		15.1		20.5	1.2	76.6	0.64	0.49
		68	32		15.1		25	1.2	82.8	0.58	0.45
		70	27		15.6		35	1.2	118.7	0.57	0.48
Beau-mont	High plasticity clay with fissures and slickensides	61	21	25	19.8		0-8	7.5	75	1.2	1.58
Mont-gomery	Light grey sandy clay with dessication	31	15	20	20.9		9-17		162	0.74	1.14
Hamilton	Firm to stiff grey silty clay	32	18	30			3-6	3.2	47.8	0.82	1.16
		44	24	31			6-9	2.2	50.2	0.93	0.73
		39	22	33			11	1.2	78.9	0.55	0.78
Lackland	Expansive black to gray clay	60	18				0-3	5	57.4	0.84	1.48
		73	24	30			3-6	4.8	86.	0.95	1.12
		86	28	29			6-9	6.5	160	1.13	1.6
Rio de Janero Guana-bara bay	Fissured expansive Clay shale Soft gray clay	95	27	29			9-12	8.5	211	0.96	1.47
		135	50	170	13.2	2.6	2-4	2.1	6.2	0.83	0.62
		125	60	140	13.2	2.6	4-6	2	8.1	0.73	0.1
South Padre	Medium to stiff clay	110	45	125	13.2	2.6	6-8	1.7	13.5	0.69	0.46
		90	35	110	13.2	2.6	8-10	1.7	13.2	0.65	0.44
South Padre	Medium to stiff clay	57	26	29			6-12	1.2	86.1	0.61	0.6

TABLE 9 (CONT.)

Database for undrained shear strength of various clays from CU and UU tests (Chen and Kulhawy, 1993)

Site	Soil description	LL (%)	PL (%)	w (%)	Total unit weight (kN/m ³)	Sensitivity	Depth (m)	OCR	S _u (kPa)	S _u (UU)/S _u	S _u / σ' ₀
Island		55	27	25			15-18	1.1	136	0.47	0.51
St Alban	Soft to medium silty clay	48	23	100	15.3		2.1	2.1	16.3	0.89	0.99
		40	18	62	17		55	2.3	27.4	0.89	0.85
		30	14	48	16.8		7.2	2.4	37	1.02	0.93
Boston	Lean and moderately sensitive blue clay	38	18			5-10		18		0.87	1.7
		38	18			5-10		12		1.07	1.4
		38	18			5-10		3.2		0.75	0.72
		38	18			5-10		1		0.56	0.32
Laboratory results	Overconsolidated kaolinite	45	35					9	125	1.09	1.28
Hackensack Valley	Varved clay	44	9				7.9-15	1.8	61.6	0.98	0.6
Santa Barbara	Firm Pleistocene clay	63	28	45			20-60	1.6	85	0.75	0.36
channel	Hard silty clay	55	27	30			100-140	1.2	225	0.64	0.26
Lakeland	Cohesive slimes	32	22	32	18.8		0-33	1.1	100	0.45	0.41
San Francisco	Soft gray clay (new)	88	43	92	14		6-10	1.4	27	0.77	0.43
Bay mud	Bay mud	90	45	95	14.7		10-15	1.3	35	0.77	0.44
San Francisco	Sandy clay	83	45	92	14.5		6-9	1.4	38	0.71	0.55
Boston	Soft gray clay	70	40	72	15		9-12	1.2	43	0.75	0.49
	Marine illitic blue clay	41	20					4		0.68	0.91
		41	20					2		0.65	0.55
		41	20					1		0.61	0.31
Anacostia	Dark organic silty clay	67	32	60	15.7		4-6	2.1	34.2	0.53	0.46
		83	57	80	13.6		6-9	2.1	59.7	0.38	0.32
Tuckerton	Dark gray plastic clay	42	22	42			16	8	130	1.08	2.03
		57	37	55			17	5.2	86	0.86	1.17
	Dark gray plastic clay	78	28	58			18-23	4	116	0.85	1.16
Ottawa	Leda clay - moderately preconsolidated clay with high plasticity and sensitivity	46	14	72		26	6-9	3.1	97.5	1.18	1.08
		33	8	68		80	9-12	2.2	117.5	0.93	1.02
		34	9	51		114	2-15	2	125	0.62	0.95
		27	5	36		128	15-18	2	1.5	0.73	0.7
		38	28	52		84	18-21	1.6	115	0.65	0.68
Madingley	Gray fissure Gault clay with heavily overconsolidated clay	67	23	31	18.4		3-4	20	103	0.93	2.33
		68	26	30	18.6		4-6	18	132	0.99	2.27
		74	29	29	18.8		6-7	14	140	0.99	2
South-eastern Texas	Very stiff clay with high plasticity	67	30	30			15.2	6.5	175.5	1.03	0.87
		64	23	23			18.3	5.8	170	0.71	0.75
		61	12	26			21.3	2.9	161	0.83	0.64
Empire Chicago	Fine gray clay	83	26	45			36.6	12	86.1	0.53	0.27
	Hard silty clay	29	16	13	19.6		10	22	285	1.22	2.35

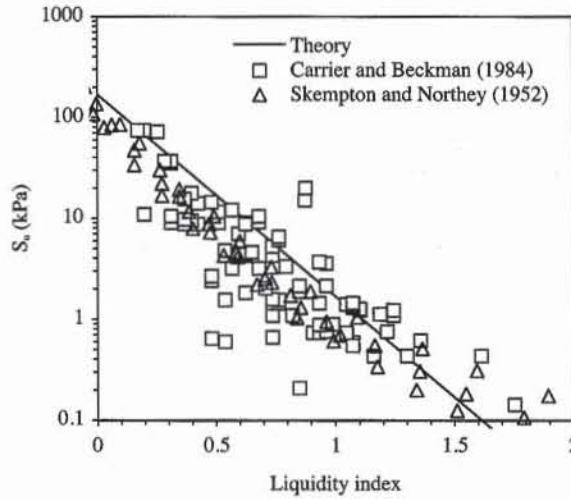


Figure 49 Relation between liquidity index and undrained shear strength S_u of clays (experimental data after Skempton and Northey, 1952; and Carrier and Beckman, 1984).

Influence of LI. As shown in Fig. 49, S_u decreases from about 100 to 0.1 kPa when LI increases from 0 to 2. Remarkably, S_u is almost 100 times larger at the plastic limit ($LI = 0$) than at the liquid limit ($LI = 1$). S_u is practically smaller than 1 kPa when $LI > 1$. The critical state theory (Eq. 36) describes the variation of S_u with LI as follows

$$S_u = S_{uPL} 10^{-2LI} \quad (47)$$

where S_{uPL} is the undrained shear strength at plastic limit, which is selected equal to 170 kPa in Fig. 49. As shown in Fig. 49, the values of S_u predicted by Eq. 47 are in agreement with measured values.

Influence of OCR. Figure 50 shows the variation of S_u/σ'_0 with overconsolidation ratio OCR . Jamiolkowski et al. (1985) suggested the following relation

$$\frac{S_u}{\sigma'_0} = (0.23 \pm 0.04) OCR^{0.8} \quad (48)$$

where σ'_0 is the initial vertical effective stress in the field. Eq. 48 can be obtained from Eq. 44 when $\Lambda = 0.8$, ϕ'_r varies from 17 to 24°, and σ'_0 is assumed equal to the mean effective pressure p'_0 . As shown in Fig. 50, Eq. 48 slightly overpredicts the measured variation of S_u/σ'_0 with OCR . As shown in Fig. 51, assuming that $\sigma'_0 = p'_0$, Eq. 44 predicts well the measured variation of normalized undrained shear strength with OCR .

Influence of Sensitivity. As shown in Fig. 52, the undrained shear strength is lower for remolded samples than for undisturbed samples. This change in S_u is characterized by the sensitivity S_t , which is the ratio of undrained shear strengths in the undisturbed and remolded states at the same water content:

$$S_t = \frac{S_u^{(undisturbed)}}{S_u^{(remolded)}} \quad (49)$$

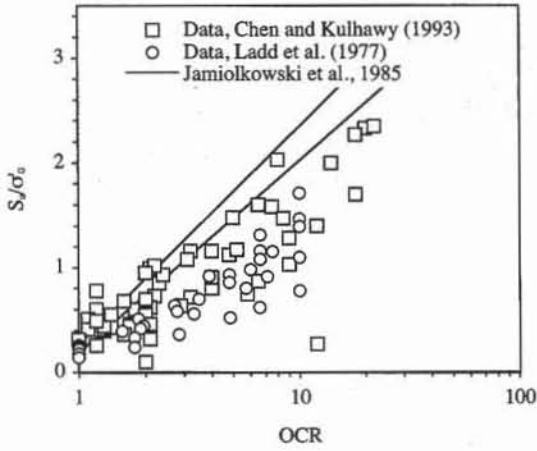


Figure 50 Variation of S_u/σ'_0 with overconsolidation ratio OCR for overconsolidated clays (data from Chen and Kulhawy, 1993, and Ladd et al., 1977).

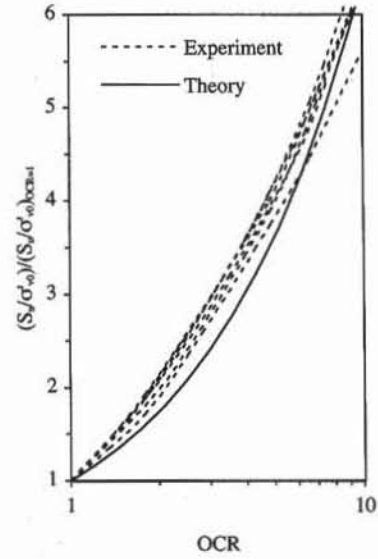


Figure 51 Variation of normalized S_u/σ'_0 with overconsolidation ratio OCR (data from Ladd et al., 1977; and theory of Eq. 44).

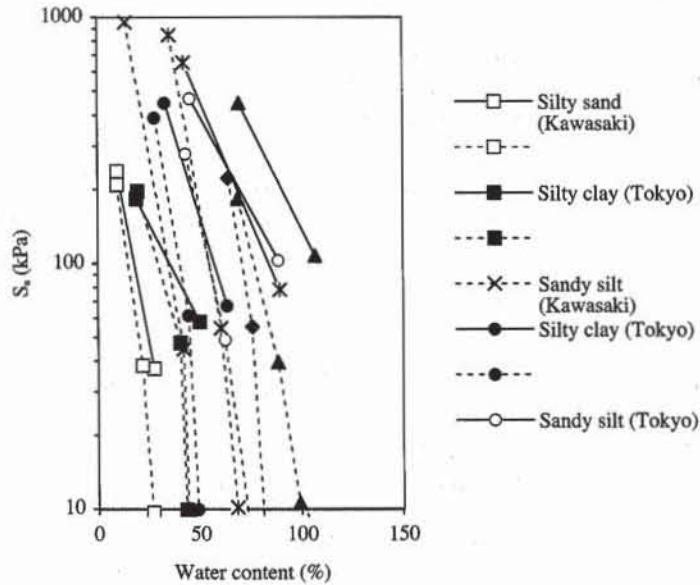


Figure 52 Relation between undrained shear strength S_u and water content for various undisturbed (solid lines) and remolded (dashed lines) samples of Japanese clays (Yoshinari, 1967).

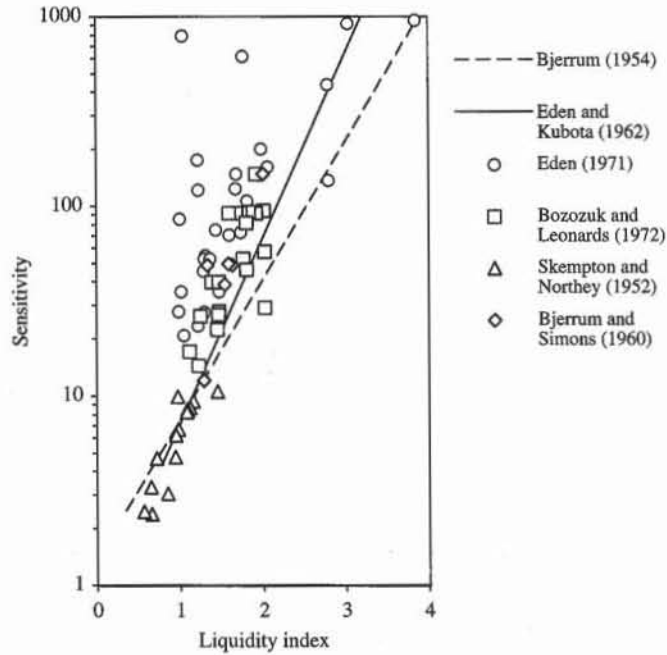


Figure 53 Relation between sensitivity and liquidity index for Scandinavian, British, Canadian, and some U.S. clays (after Holtz and Kovacs, 1981).

As shown in Fig. 53, S_t increases rapidly with liquidity index LI . S_t is generally less than 10 when LI is less than 1. Table 10 indicates the ranges of S_t commonly found in the United States, where highly sensitive clays are rare, and in eastern Canada and Scandinavia, where sensitive clays are more common.

TABLE 10

Typical values of sensitivity S_t
(after Holtz and Kovacs, 1981)

Condition	Range of S_t	
	United States	Sweden
Low sensitive	2-4	< 10
Medium sensitive	4-8	10-30
Highly sensitive	8-16	> 30
Quick	16	> 50
Extra quick		> 100

Relation between Elastic modulus and Undrained Shear Strength

The elastic Young's modulus can be compared to the undrained shear strength. As shown in Fig. 54, the ratio E_{max}/S_u for four different clays varies between 2500 and 500, where E_{max} is the elastic Young's modulus obtained for strain amplitudes smaller than 0.001%. The ratio E_{max}/S_u may become smaller than 500 when Young's modulus is determined for larger strain amplitude (see Chapter 5-5).

TOTAL STRESS FAILURE CRITERION

The failure envelopes of soils, which have been described in terms of effective stress until now, can also be represented in terms of total stress. In this case they

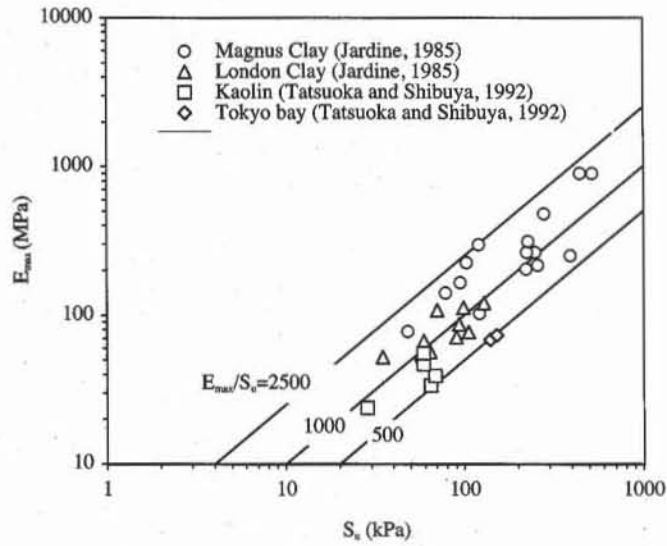


Figure 54 Relation between Young's modulus E_{max} measured at small strain amplitude ($< 10^{-3}\%$) and undrained shear strength S_u for several clays (after Tatsuoka and Shibuya, 1992).

are referred to as apparent. The apparent failure envelope in σ - τ space are constructed by enveloping the Mohr circles of total stress at failure during undrained tests, for instance as shown in Fig. 55 by enveloping circles A, B and C.

As shown in Fig. 55, in the case of CU tests, the apparent failure envelope has an apparent cohesion c_a and apparent friction angle ϕ_a which characterizes the increase in undrained shear strength S_u with the total normal stress σ (i.e., $S_u = c_a + \sigma \tan \phi_a$). When the pore pressures u_A , u_B , and u_C are known at failure, the effective failure envelope can also be constructed by drawing the effective stress circles A', B' and C' from the total stress Mohr circles A, B, and C. This construction is impossible without pore pressure measurement.

In the case of UU tests, the apparent failure envelope can be constructed in the same way as for CU tests, for instance by using the circles A, D and E of Fig. 56. The apparent UU failure envelope is generally a straight horizontal line, and S_u is independent of σ . In the UU tests, the external pressure, which is applied to the saturated soil samples, is entirely taken by the pore pressure, and not by the

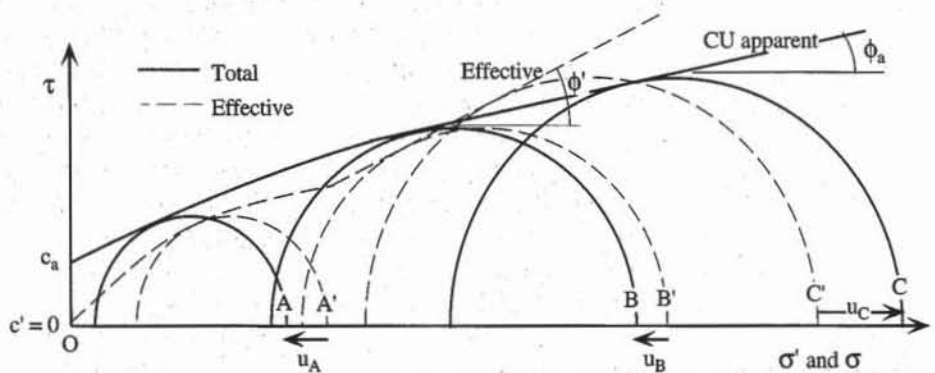


Figure 55 Apparent failure envelope constructed from CU tests, and effective failure envelope.

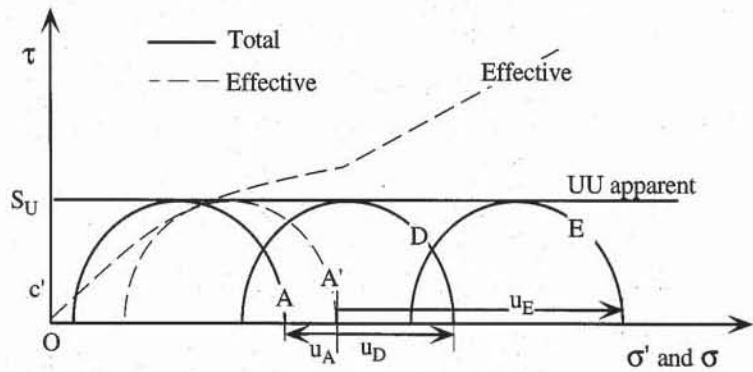


Figure 56 Apparent failure envelope constructed from UU tests, and effective failure envelope.

soil grains. At failure, the total stress Mohr circles *A*, *D*, and *E* have the same size because they correspond to the same effective stress Mohr circle *A'*, which is unfortunately unknown as the pore pressure is not measured.

REFERENCES

- BARDET, J. P., 1990, Lode dependences for isotropic pressure-sensitive elastoplastic materials, *J. Applied Mech.*, ASME, Vol. 57, pp. 498–506.
- BISHOP, A. W., 1966, The strength of soils as engineering materials, *Géotechnique*, Vol. 16, No. 2, pp. 91–128.
- BOLTON, M. D., 1986, The strength and dilatancy of soils, *Géotechnique*, Vol. 36, No. 1, pp. 65–78.
- CARRIER, W. D. III, and J. F. BECKMAN, 1984, Correlations between index tests and the properties of remoulded clays, *Géotechnique*, Vol. 34, No. 2, pp. 211–218.
- CHEN, Y. J. and F. H. KULHAWY, 1993, Undrained strength interrelationships among CIUC, UU, and UC tests, *J. Geotech. Eng.*, ASCE, Vol. 119, No. 11, pp. 1732–1750.
- CHEN, W. F., and A. F. SALEEB, 1982, *Constitutive Equations for Engineering Materials*, John Wiley & Sons, New York, pp. 441–559.
- COULOMB, C. A., 1776, Essai sur une application des règles de maximus et minimus à quelques problèmes de statique, relatifs à l'architecture, *Mémoires de Mathématique et de Physique, Présentés à l'Académie Royale des Sciences, par divers savants, et lûs dans ses Assemblées*, Paris, Vol. 7, pp. 343–382.
- GOLDER, H. Q., and A. W. SKEMPTON, 1948, The angle of shearing resistance in cohesive soils for tests at constant water content, *Proceedings of the Second International Conference on Soil Mechanics and Foundation Engineering*, Rotterdam, Netherlands, Vol. 1, pp. 185–192.
- HOLTZ, R. D., W. D. KOVACS, 1981, *An Introduction to Geotechnical Engineering*, Prentice-Hall, Englewood Cliffs, NJ, pp. 449–519.
- HOUGH, B. K., 1957, *Basic Soil Engineering*, The Ronald Press Company, New York.
- ISHIHARA, K., 1993, Liquefaction and flow failure during earthquakes, The 33rd Rankine lecture, *Géotechnique*, Vol. 43, No. 3, pp. 351–415.
- JAMIOLKOWSKI, M., C. C. LADD, J. T. GERMAINE, and R. LANCELLOTTA, 1985,

- New developments in field and laboratory testing of soils, *Proceedings of the 11th International Conference on Soil Mechanics and Foundation Engineering*, San Francisco, CA, Vol. 1, pp. 57-154.
- JARDINE, R. J., 1985, *Investigations of pile-soil behaviour with special reference to the foundation of offshore structures*, Ph. D. thesis, University of London, UK.
- KENNEY, T. C., 1959, Discussion of "Geotechnical properties of glacial lake clays," by T. H. Wu, *J. Soil Mech. Found. Div.*, ASCE, Vol. 85, No. SM3, pp. 67-79.
- KEZDI, A., 1974, *Handbook of Soil Mechanics, Volume 2: Soil Testing*, Elsevier Publishing, Hungary, 258 p.
- KOERNER, R. M., 1970, Effect of particle characteristics on soil strength, *J. Soil Mech. Found. Eng. Div.*, ASCE, Vol. 96, No. SM4, pp. 1221-1234.
- LADD, C. C., R. FOOTT, K. ISHIHARA, F. SCHLOSSER, and H. G. POULOS, 1977, Stress-deformation and strength characteristics, State-of-the-Art report, *Proceedings of the Ninth International Conference on Soil Mechanics and Foundation Engineering*, Tokyo, Vol. 2, pp. 421-494.
- LADD, C. C., and R. FOOTT, 1974, New design procedures for stability of soft clays, *J. Geotech. Eng.*, ASCE, Vol. 100, No. 7, pp. 763-786.
- LADD, C. C., 1991, Stability evaluation during staged construction (the twenty-second Karl Terzaghi lecture), *J. Geotech. Eng.*, ASCE, Vol. 117, No. 4, pp. 540-615.
- LADE, P. V., and J. M. DUNCAN, 1973, Cubical triaxial tests on cohesionless soils, *J. Soil Mech. Found. Eng. Div.*, ASCE, Vol. 99, No. 10, pp. 793-812.
- LADE, P. V., and J. M. DUNCAN, 1975, Elasto-plastic stress strain theory for cohesionless soils, *J. Geotech. Eng.*, ASCE, Vol. 101, No. 10, pp. 1037-1053.
- LAMBE, T. W., and R. V. WHITMAN, 1979, *Soil Mechanics*, John Wiley & Sons, pp. 116-121 and 135-150.
- LEE, K. L. and H. B. SEED, 1967, Drained strength characteristics of sands, *J. Soil Mech. Found. Eng. Div.*, ASCE, Vol. 93, No. SM6, pp. 117-141.
- LESLIE, D. D., 1963, Large-scale triaxial tests on gravelly soils, *Proceedings of the 2nd Pan American Conference on Soil Mechanics and Foundation Engineering*, Brazil, Vol. 1, pp. 181-202.
- MATSUOKA, H., and T. NAKAI, 1974, Stress-deformation and strength characteristics of soil under three different principal stresses, *Proceedings of the Japanese Society of Civil Engineers*, Vol. 32, pp. 59-70.
- MESRI, G., and M. E. M. ABDEL-GHAFFAR, 1993, Cohesion intercept in effective stress-stability analysis, *J. Geotech. Eng.*, ASCE, Vol. 119, No. 8, pp. 1229-1249.
- NAVFAC, 1982, *Soil Mechanics*, Naval Facilities Engineering Command, Design Manual DM-71, Alexandria, 355 p.
- PARRY, R. H. G., 1960, Triaxial compression and extension tests on remoulded saturated clay, *Géotechnique*, Vol. 10, pp. 166-180.
- ROWE, 1962, The stress-dilatancy relation for static equilibrium of an assembly of particles in contacts, *Proceedings of the Royal Society*, London, A 269, pp. 500-527.
- SAADA, A. S., and F. C. TOWNSEND, 1981, State of the Art: Laboratory strength testing of soils, *Laboratory Shear Strength of Soils*, ASTM Special Technical Publication 740, R. N. Yong and F. C. Townsend, eds., American Society for Testing and Materials, pp. 7-77.
- SCHERTMANN, J. H., 1978, Guidelines for cone penetration test performance and design, *Report FHWA-TS-78-209*, U.S. Department of Transportation, Washington, 145 p.

- SCHOFIELD, A. and C. P. WROTH, 1968, *Critical state soil mechanics*, McGraw-Hill, New York.
- SEED, H. B. and K. L. LEE, 1967, Undrained strength characteristics of cohesionless soils, *J. Soil Mech. Found. Eng. Div.*, ASCE, Vol. 93, No. SM6, pp. 333–360.
- SINGH, R., HENKEL, D. J., and D. A. SANGREY, 1973, Shear and K_0 swelling of overconsolidated clays, *Proceedings of the 8th International Conference on Soil Mechanics and Foundation Engineering*, Vol. 1.2, pp. 367–376.
- SKEMPTON, A. W., 1985, Residual strength of clays in landslides, folded strata, and the laboratory, *Géotechnique*, Vol. 35, No. 1, pp. 3–18.
- SOWERS, G. B., and B. F. SOWERS, 1951, *Introductory Soil Mechanics*, MacMillan, New York.
- TATSUOKA, F., and S. SHIBUYA, 1992, *Deformation characteristics of soils and rocks from field and laboratory tests*, Report of The Institute of Industrial Science, The University of Tokyo, Vol. 37, No. 1, pp. 106–112.
- TAYLOR, 1939, A comparison of results of direct shear and cylindrical compression tests, *Proc. ASTM*.
- YOSHINARI, M., 1967, Compressive strength versus water content, *Proceedings of the Third Asian Regional Conference on Soil Mechanics and Foundation Engineering*, Haifa, Vol. 1, pp. 327–330.

REVIEW QUESTIONS

1. What is the most commonly used theory to describe the failure of soils?
2. Describe the Mohr-Coulomb theory.
3. Draw the evolution of the Mohr circle during an unconfined compression test.
4. Define peak and residual failures.
5. How does the Mohr-Coulomb theory define the orientation of the failure surfaces?
6. Among all the factors influencing the friction angle of coarse-grained soils, which factor has the largest effect?
7. Does the friction angle increase or decrease when the void ratio increases?
8. What is the range of variation for the friction angle in coarse-grained soils?
9. What is the effect of grain angularity on the friction angle of coarse-grained soils?
10. Is the failure envelope of soil strictly obeying the Mohr-Coulomb theory?
11. Define the s and t coordinates, and express the Mohr-Coulomb failure line in terms of s and t .
12. What is the relation between the parameters of the Mohr-Coulomb failure line in σ - τ and s - t spaces.
13. Which is the most reliable conventional laboratory test to determine the failure envelope of soils?
14. Sketch the principles of the triaxial test.
15. What are the different types of triaxial tests?
16. What is the purpose of the consolidation phase in the CD and CU triaxial tests?
17. Define CD, CU and UU triaxial tests.
18. What is the relation between the total and effective stress paths?
19. What are the minimum and maximum values for the friction angle in coarse-grained soils?
20. Is the friction angle different in drained and undrained triaxial tests on coarse-grained soils?

21. Rank the following factors by decreasing order of their influence on the friction angle-confining pressure, void ratio, angularity, and grain size distribution curve.
22. What is the virgin consolidation line?
23. Define the critical state theory.
24. What is the difference between the critical state theory and the Mohr-Coulomb theory?
25. Which are the material parameters of the critical state theory?
26. Give a range of value for the undrained shear strength of fine-grained soils.
27. Does the friction angle increase or decrease with the plasticity index?
28. What is the effect of the liquidity index on the shear strength of fine-grained soils?
29. What is the meaning of apparent and true failure criteria?
30. Draw the typical apparent failure line obtained from UU tests.

7-2 Principles of the Unconfined Compression Test

DEFINITION

As introduced in Chapter 5-4, the unconfined compression test is a rapid means to obtain an approximate value of undrained shear strength S_u for fine-grained soils. As shown in Fig. 1a, the cylindrical soil specimen is loaded axially without a lateral support. The top and bottom areas are assumed to be frictionless (i.e., free of shear stress) and transmit only the axial stress σ_1 , while the lateral surface is free of stress. As schematized in Fig. 1b, a small cubical element inside the specimen undergoes a compressive axial stress σ_1 and no lateral stresses (i.e., $\sigma_2 = \sigma_3 = 0$). In practice, the stresses are not uniform within the sample, mainly due to the effects of shear stresses on the loading caps which are not frictionless. Using Fig. 2, the axial strain ϵ_1 and axial total stress σ_1 are defined as positive in compression:

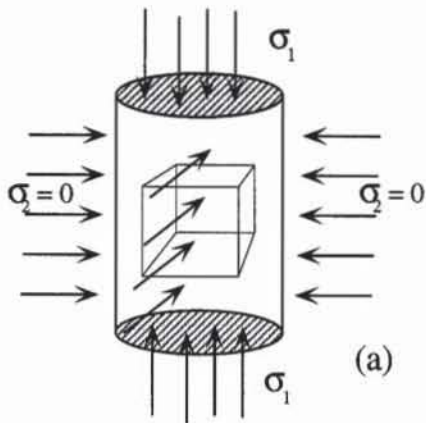
$$\epsilon_1 = \frac{\Delta H}{H_0} \quad \text{and} \quad \sigma_1 = \frac{F}{A} \quad (1)$$

where H_0 is the initial sample height, H the present sample height, $\Delta H = H_0 - H$ the change in sample height, F the applied axial load, and A the average cross-section area of sample.

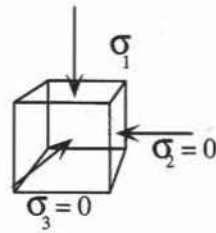
The soil samples which are tested in unconfined compression are usually made of fine-grained soils, fully or partially saturated, with low permeability. When these soils are loaded rapidly, they deform practically at constant volume under undrained conditions, and undergo pore pressure changes that do not have enough time to dissipate. The unconfined compression test is a particular unconsolidated undrained (UU) triaxial test without confining pressure.

FAILURE DURING UNCONFINED COMPRESSION TEST

Figure 3a shows a typical stress-strain response of soils subjected to unconfined compression tests. At the beginning of loading, the axial stress and strain are both



(a)



(b)

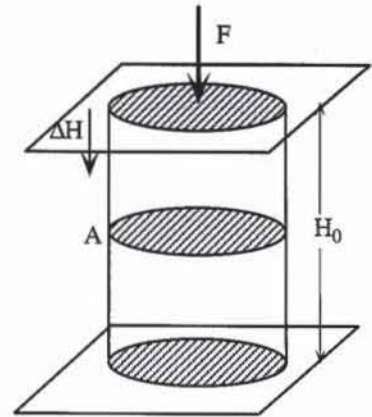


Figure 2 Initial height and change in height of sample.

Figure 1 Stresses within a soil sample subjected to the unconfined compression test.

equal to zero, and the Mohr circle is reduced to point O in Fig. 3b. When the axial stress σ_1 is increased, the sample deforms. At points A , B , and C , the Mohr circle passes through point O and gradually increases size until σ_1 reaches the maximum value $2S_u$ at point C . During loading, pole O of Mohr circle does not move. The unconfined compression test provides only one Mohr circle at failure, which is insufficient to determine the failure envelope in σ - τ space. It is also irrelevant to determine the effective failure envelope because no pore pressure is measured.

When the failure envelope is assumed to be purely cohesive (i.e., $\phi = 0$) as shown in Fig. 3b, the Mohr circle at failure is tangent to the horizontal line $\tau = S_u$. Using pole O as shown in Fig. 3c, the failure surfaces are inclined at 45° with respect to the horizontal direction, and $\sigma = \tau = S_u$ on the failure surface. As shown in Fig. 3d, the Mohr circle of effective stress at failure is obtained by shifting the Mohr circle of total stress by the pore pressure u , the value of which can only be assumed since it is not measured. As established in Chapter 7-1, the effective failure envelope of soils is not purely cohesive. The effective stress Mohr circle at failure is tangent to a failure line of slope $\tan \phi'$ at points (σ'_f, τ_f) where σ'_f and τ_f are the effective normal and shear stresses acting on the failure surface. The inclination of the failure surfaces which is found from pole O and point (σ'_f, τ_f) is $45^\circ + \phi'/2$ instead of 45° . Therefore, the failure planes which are observed in unconfined compression tests are not inclined at 45° as is commonly assumed in practice. Unfortunately, the failure planes are influenced by many factors and do not provide a reliable assessment of ϕ' .

TYPICAL VALUES OF UNDRAINED SHEAR STRENGTH FROM UNCONFINED COMPRESSION TEST

Table 1 classifies the consistency of soils in terms of their undrained shear strength S_u . S_u varies from 3 kPa for soils close to their liquid state, to more than 400 kPa for very hard soils. Table 2 shows compiled results on the undrained shear strength of various clays measured in the unconfined compression (UC) tests, unconsolidated undrained (UU) triaxial tests, and consolidated undrained (CU) triaxial tests. In Table 2, $S_u(\text{CU}) = S_u$, $S_u(\text{UU})$, and $S_u(\text{UC})$ are the undrained shear strength in CU, UU, and UC tests, respectively. $S_u(\text{UC})$ is also referred to as the unconfined shear strength.

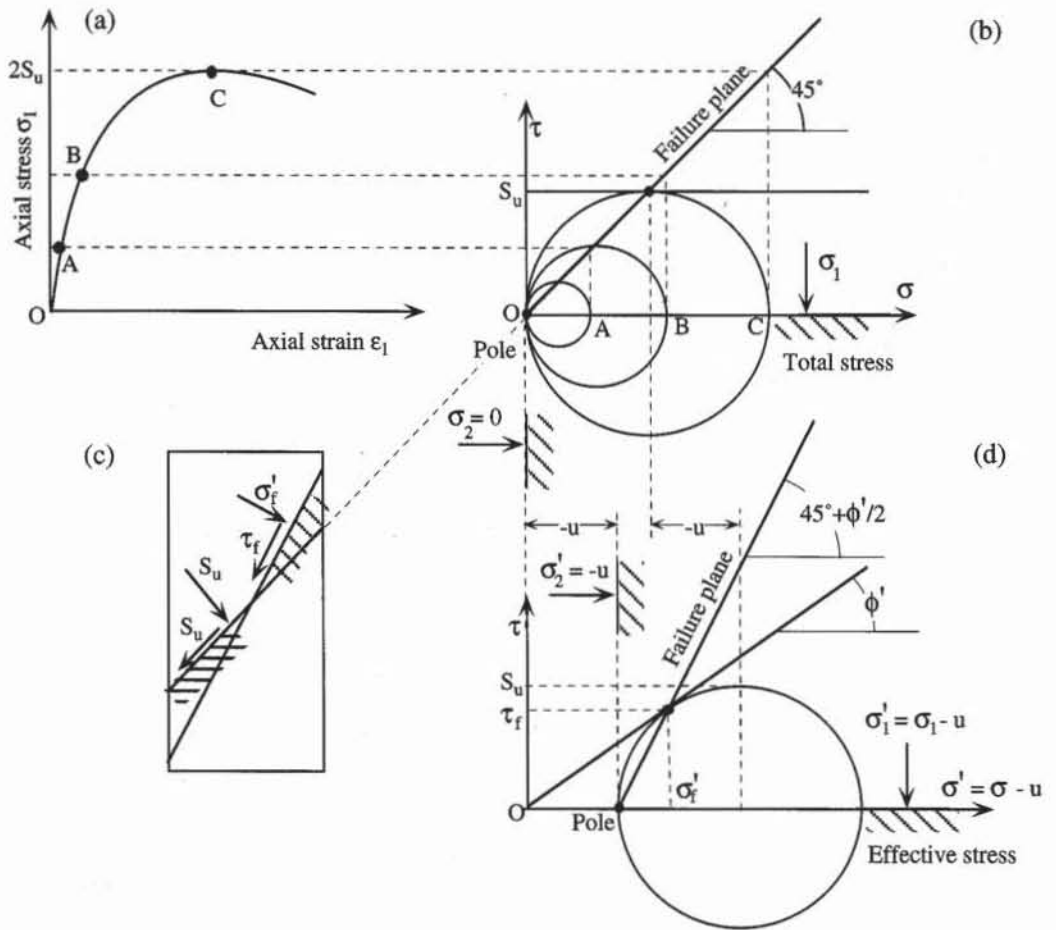


Figure 3 (a) A typical stress-strain response during the unconfined compression test, (b) the corresponding evolution of the Mohr circle in the total stress space, (c) the Mohr circle of effective stress at failure, and (d) the total and effective stresses on the failure planes.

As shown in Fig. 4, $S_u(UC)$ and $S_u(UU)$ are similar, because the data points fall close to the line $S_u(UU) = S_u(UC)$. This result is expected because the unconfined compression test is a UU test without confining pressure. As shown in Fig. 5, $S_u(UC)$ is generally smaller than the undrained shear strength S_u measured from CU triaxial tests. Most points with coordinates $S_u(UC)$ and S_u fall beneath the line $S_u = S_u(UC)$. $S_u(UC)$ is only larger than S_u for some exceptional cases in which soil samples may not have been fully saturated, and had gained strength by drying out.

There can be considerable error in evaluating the undrained shear strength of soils from unconfined compression tests because of sample disturbance and omission of reconsolidation during testing (e.g., Ladd and Lambe, 1963; Noorany and Seed, 1965; Ladd et al., 1977; Ladd, 1991; and Tavenas and Leroueil, 1987). However, in many circumstances such as in the evaluation of older case histories with limited data, the results of more accurate tests (e.g., CU tests) are not available, and the only data available is the unconfined shear strength.

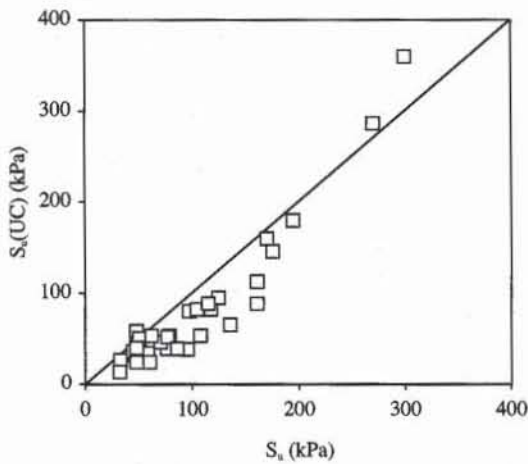


Figure 4 Comparison of the undrained shear strengths S_u measured from unconfined compression (UC) tests and CU triaxial tests (data after Chen and Kulhawy, 1993).

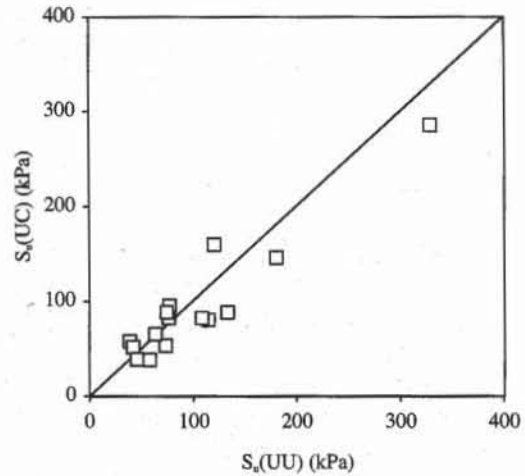


Figure 5 Comparison of the undrained shear strengths S_u measured from unconfined compression (UC) tests and UU triaxial tests (data after Chen and Kulhawy, 1993).

TABLE 1

Typical values of undrained shear strength from unconfined compression tests (Karol, 1969)

Relative consistency	S_u (kPa)
Liquid limit	3
Very soft	5
Medium soft	5-10
Ball moisture	48
Firm or stiff	48-96
Medium hard	96-192
Hard	192-383
Very hard	> 383

EFFECT OF DISTURBANCE ON UNDRAINED SHEAR STRENGTH

Figure 6 shows an example of stress-strain responses for undisturbed and remolded clay samples (Lambe, 1951) in the unconfined compression test. The undisturbed sample is stronger and much stiffer than the remolded sample. The variation in undrained shear strength is characterized by sensitivity S_t , which is the ratio of the undrained shear strengths in the undisturbed and remolded states at the same water content. In Fig. 6, S_t is equal to 7.6, corresponding to the undrained shear strength of 76 and 10 kPa for the undisturbed and remolded specimens, respectively. Additional information on the effect of sensitivity on undrained shear strength can be found in Chapter 7-1.

TABLE 2

Database for the undrained shear strength of various clays measured from unconfined compression tests, and UU and UC triaxial tests (Chen and Kulhawy, 1993).

Site	Soil description	LL (%)	PL (%)	w (%)	Sensitivity	Depth (m)	OCR	S_u (UC) (kPa)	S_u (kPa)	S_u (UU) (kPa)
Gulf of Mexico	Soft plastic clay	111	31	71	2-3	0-6	3.5	26.4	33	
	Firm to stiff plastic clay with silt and sand	73	23	43	2-3	18-32	1.1	39.1	76.6	
		85	20	43	2-3	32-50	1.2	52.8	107.7	
Skabo	Plastic clay with high salt content				5	10.6-16	1.2	32.2	46	
Gotta valley	Lilla Edet clay:			68	50	4-6.8	12	40.8	48	
	marine late glacial	58	25	78	50	10-12.3	1.8	34.2	58	
	plastic clay with	58	29	70	50	16.2-18	1.5	46.2	70	
	high sensitivity	52	15	74	50	10.8-13	1.5	13.1	32	
Drammen	Soft silty clay with thin seams of silt and fine sand	31	16	34	9	5-12	1.3	36.0	45	
		33	19	32	9	18	1.1	24.0	60	
Sault Ste Marie	Varved glacial lake clay with flocculent structure	51	23	45	8	9	1.2	24.0	48	
Hamilton	Firm to stiff grey silty clay (surface desiccated and fissured)	36	24	33		5	3.2	57.8	47.8	39.2
		28	16	26		7	2.5	50.2	50.2	
		45	25	32		11	1.5	52.9	78.9	73.4
		46	27	36		15	1.1	51.6	77	42.4
South Padre Island	Medium to stiff clay	57	26	29		8	1.2	38.2	95.5	58.3
		55	27	25		15	1.2	65.3	136	63.9
		57	29	24		19	6.4	112.7	161	
Kars	Cemented Leda clay	51	23	45		2.5-6	7	52.7	62	
	dark gray plastic clay	56	38	65		6-12	2.5	39.8	48	
Ottawa	Leda clay:	46	14	72	26	6-9	3.1	80.0	97.5	115.1
	moderately	33	8	68	80	9-12	2.2	82.3	117.5	109.3
	preconsolidated clay	34	9	51	114	12-15	2	95.0	125	77.5
	with high plasticity and sensitivity	27	5	36	128	15-18	2	81.9	105	76.7
		38	28	52	84	18-21	1.6	88.6	115	74.8
Southeastern Texas	Very stiff clay with high plasticity	67	30	30		15.2	6.5	145.8	175.7	181.0
		64	23	23		18.3	5.8	159.8	170	120.7
		61	12	26		21.3	2.9	88.6	161	133.6
Empire	Fine gray clay	83	26	46		36.6	1.2	38.7	86.1	45.6
Chicago	Hard silty clay	31	14	43		3.7	17	179.4	195	
		29	16	13		9	20	286.2	270	329.4
		23	14	10		11.6	39	360.0	300	

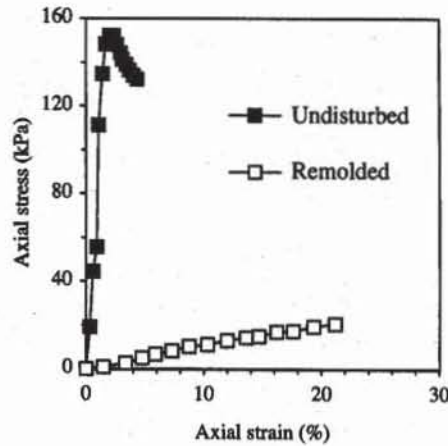


Figure 6 Results of unconfined compression tests on undisturbed and remolded samples of gray silty clay (data after Lambe, 1951).

REFERENCES

- CHEN, Y.-T., and F. H. KULHAWY, 1993, Undrained strength interrelationships among CIUC, UU, and IUC tests, *J. Geotech. Eng., ASCE*, Vol. 119, No. 11, pp. 1732–1750.
- KAROL, R. H., 1969, *Soils and Soil Engineering*, Prentice-Hall, New Jersey, 195 p.
- LADD, C. C., 1991, Stability evaluation during staged constructions, *J. Geotech. Eng., ASCE*, Vol. 117, No. 4, pp. 540–615.
- LADD, C. C., R. FOOTE, K. ISHIHARA, F. SCHLOSSER, and H. G. POULOS, 1977, Stress-deformation and strength characteristics, *Proceedings of the 9th International Conference on Soil Mechanics and Foundation Engineering*, Vol. 2, Tokyo, pp. 421–494.
- LADD, C. C., and T. W. LAMBE, 1963, The strength of “undisturbed” clay determined from undrained tests, *Laboratory shear testing of soils*, Special Technical Publication No. 361, ASTM, Philadelphia, PA, pp. 342–371.
- LAMBE, T. W., 1951, *Soil testing for engineers*, John Wiley & Sons, New York, 165 p.
- LAMBE, T. W., and R. V. WHITMAN, 1979, *Soil Mechanics, SI Version*, John Wiley & Sons, New York, 553 p.
- NOORANY, I., and H. B. SEED, 1965, In-Situ strength characteristics of soft clay, *J. Soil Mech. Found. Eng. Div., ASCE*, Vol. 91, No. 2, pp. 49–80.
- TAVENAS, F., and S. LEROUÉIL, 1987, State-of-the-art on laboratory and in-situ stress-strain-time behavior of soft clays, *Proceedings of the International Symposium on Geotechnical Engineering of Soft Soils*, Mexico City, pp. 1–46.

REVIEW QUESTIONS

1. What soil properties are determined from the unconfined compression test?
2. Draw the evolution of the Mohr circle in parallel to a typical stress-strain curve during an unconfined compression test.
3. Does the pole of the Mohr circle move during the unconfined compression test?
4. What is the theoretical inclination of failure planes predicted for purely cohesive material during an unconfined compression test?

5. Define the axial strain from the displacement and sample height.
6. What is the range of unconfined shear strength for soils?
7. What is the relation between the unconfined shear strength and the undrained shear strength measured from UU and CU triaxial compression tests?
8. What is the effect of the water content on the unconfined shear strength?
9. Define the sensitivity S_t of a clay. What is the range of S_t ? Which clays give the largest values of S_t ?
10. How can Young's modulus be calculated from the results of unconfined compression tests?

EXERCISES

1. Calculate the unconfined shear strengths from the following unconfined compression test results on undisturbed and remolded samples of gray silty clay (data after Lambe, 1951).

Undisturbed		Rmolded	
Axial strain (%)	Axial stress (kPa)	Axial strain (%)	Axial stress (kPa)
0.00	0	0.00	0
0.30	19	1.45	1
0.60	44	3.36	2
0.90	56	4.74	5
1.10	111	5.90	7
1.43	135	7.27	8
1.70	148	8.78	10
2.00	152	10.34	11
2.30	152	12.03	13
2.60	148	13.63	14
2.90	144	14.69	15
3.10	141	16.20	17
3.40	139	17.62	17
3.70	136	19.36	19
4.00	134	21.18	20
4.30	132		

2. Calculate Young's modulus for the undisturbed and remolded samples of gray silty clay from the unconfined compression results of Exercise 1. Compare your results with those reported in Chapter 5-5.

7-3

Unconfined Compression Test

OBJECTIVE

The unconfined compression test is used to measure the unconfined shear strength of fine-grained soils, which is an approximate value of their undrained shear strength. This test is applicable only to cohesive materials such as saturated clays or cemented soils that retain an intrinsic strength without a confining pressure. It is not applicable to dry or cohesionless soils, such as gravels and sands.

EQUIPMENT

The equipment for the unconfined compression test includes:

- Loading device (see Fig. 12), either hand operated or machine driven, capable of providing rates of loading in the range 0.5 to 5 mm/min and with a maximum load capacity of 5 kN.
- Loading ring with 2 kN capacity, accurate to 1 N. The loading ring is equipped with a dial indicator or a LVDT transducer for computer data acquisition.
- Dial indicator or LVDT transducer for measuring axial displacement, having a full range of 25 mm and accurate to 0.01 mm.
- Vernier calipers, suitable for measuring the dimensions of the specimens to the nearest 0.1 mm.
- Trimming frame. A typical trimming frame for 3.5-cm-diameter specimens is shown in Fig. 1. A motorized soil lathe may also be used.
- Sampling tube with extractor with cutting edges to prepare cylindrical specimens.
- Wire saws and knives.
- Miter box or cradle (see Fig. 3) for cutting specimens.
- Watch or clock.



Figure 1 The sample is installed on a trimming frame. The vertical guides are adjusted to obtain the desired sample diameter.

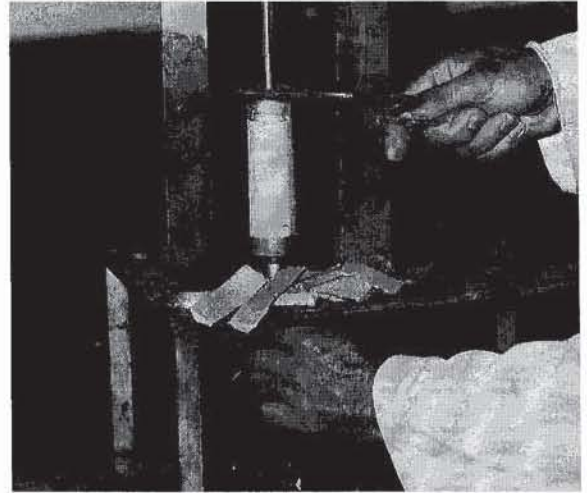


Figure 2 Fragments and scraps from cutting are used to determine the sample water content.

- Balances, sensitive to 0.1 g.
- Equipment necessary to determine water content.

PREPARATION OF SPECIMENS

The test specimens are cut into cylinders which are usually 3.5 cm in diameter. Specimens of larger diameter (e.g., 7 cm) are recommended for undisturbed soils with stratification and cracks. The largest particle in the test specimens should be smaller than 6 mm. The height-to-diameter ratio of the sample should be larger than 2. The specimens may be undisturbed or remolded.

Undisturbed Specimens

Undisturbed specimens are prepared from undisturbed samples of larger size taken in the field. Undisturbed samples are carefully transported and handled in sealed containers that retain the field water content. The test specimens are cut into cylinders by trimming or extruding them:

Trimming specimens

1. Cut a chunk from the undisturbed soil mass which is large enough to cut a specimen. Make a note about the orientation of the vertical direction in the field.
2. Trim the specimen to the required diameter using a trimming device (Fig. 1). The specimen is trimmed by pressing the wire saw against the adjustable

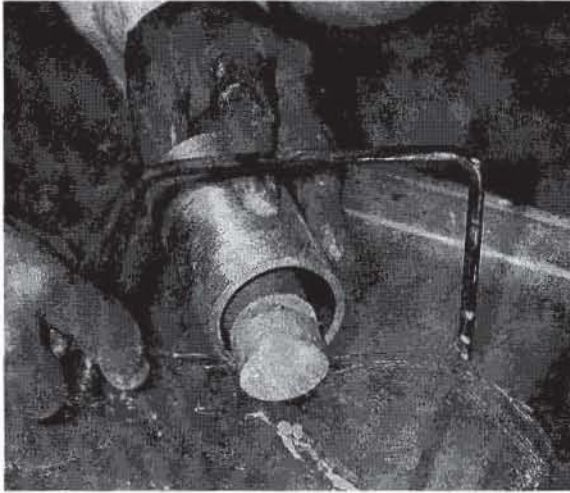


Figure 3 The top and bottom surfaces are cut perpendicular to the specimen axis using a wire saw.

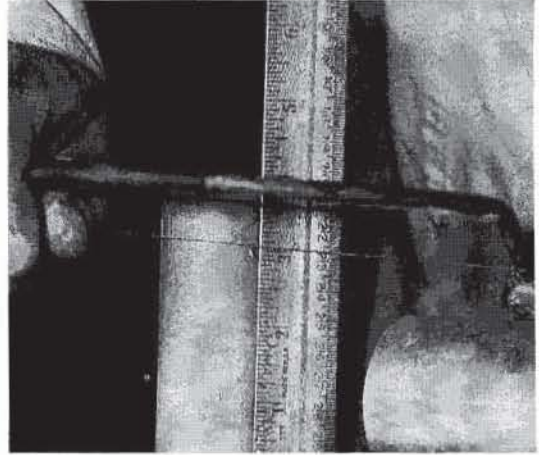


Figure 4 The sample is marked to the desired height.

edges of the trimming frame and by sliding it down. For stiff clays, move the wire saw from the top and bottom toward the middle of the specimen to prevent breaking off pieces at the ends. Remove any small pebbles and fill voids in the specimen with soil from the trimmings. The trimmed specimen is shown in Fig. 2.

3. Cut the specimen to the required length (usually 7 to 9 cm for 3.5-cm-diameter specimens) by using a miter box (Figs. 3 and 4).

4. Measure the weight, height, and diameter of the sample.

5. Test the specimen immediately to prevent loss of moisture.

Extruding specimens

1. Push into the soil the sampling tube, which has a lower cutting edge (Fig. 5), and then remove it with a twisting motion. The soil specimen should now be in the sampling tube (Fig. 6).



Figure 5 The sampling tube with a cutting edge is pushed into the soil.



Figure 6 The soil specimen is now in the sampling tube.



Figure 7 The extractor is assembled to extrude the soil from the sampling tube.



Figure 8 After extruding about 1 cm of soil from the sampling tube, the bottom surface of the sample is cut with a wire saw.

2. Reassemble the extractor and extrude the sample from the sampling tube (Fig. 7).
3. After extruding about 1 cm of soil from the sampling tube, cut the bottom surface of the sample by using a wire saw (Fig. 8).
4. Cut the sample to the desired length by extruding the right amount from the sampling tube (Fig. 9).
5. Same as steps 4 and 5 for trimming specimens.

Remolded Specimens

Remolded specimens are prepared from remolded field samples or specimens that have already been tested. For a meaningful comparison of undisturbed and remolded responses, their water content should be similar to that of the undisturbed specimens.

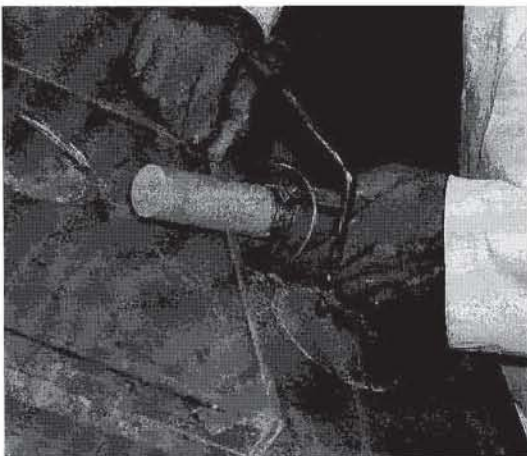


Figure 9 The sample, which is extruded from the sampling tube, is cut to the desired length.



Figure 10 The remolded specimen, which has been compacted in the compaction cylinder, is cut to the desired length.

1. Knead the specimen with the fingers to remold it completely. Avoid trapping air in the specimen.
2. Compact the soil in a cylindrical mold having the internal diameter of the test specimen.
3. Carefully extrude the specimen from the mold, preferably by means of a piston, and plane off the top and bottom of the specimen (Fig. 10).
4. Same as steps 4 and 5 for trimming specimens.

The remolded sample may also be prepared in compaction molds which are larger than the test specimen, and then trimmed and cut as for undisturbed samples.

TEST PROCEDURE

1. Measure the water content of the specimen by using the soil trimmings (see Fig. 2), and measure the specimen weight.
2. Measure the height and diameter of the specimen. When the sample is well trimmed, its diameter D_0 is measured only at its center. When the sample is more irregular, as shown in Fig. 11, the average diameter D_0 is

$$D_0 = \frac{1}{4} (D_1 + 2D_2 + D_3) \quad (1)$$

where D_1 , D_2 , and D_3 are the diameters measured at the top, center, and bottom, respectively, of the specimen.

3. Without delay, to avoid loss of water content, place the specimen on the loading device (Fig. 12). Lower the upper platen or raise the bottom platen so that the upper platen barely touches the specimen and triggers a slight response of the load sensor. Attach the dial indicator or LVDT transducer to the loading device to measure the axial deformation of the specimen.

4. Adjust the rate of axial displacement to obtain a strain rate of about 1% per minute. The complete loading lasts about 20 min to apply 20% of axial strain, which is generally sufficient to reach the unconfined shear strength. Very stiff or brittle materials that fail for small deformations may be tested at a slower rate of strain.

5. As shown in Fig. 13, record simultaneously the axial displacement and load at close time intervals at the beginning, and then at larger intervals. Stop the test when the axial load remains constant or after 20% axial strain.

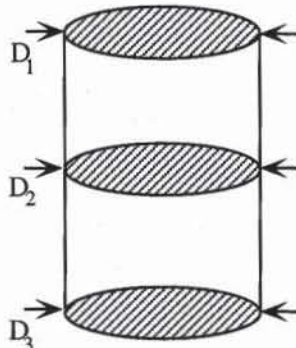


Figure 11 Determination of average diameter of test specimen.

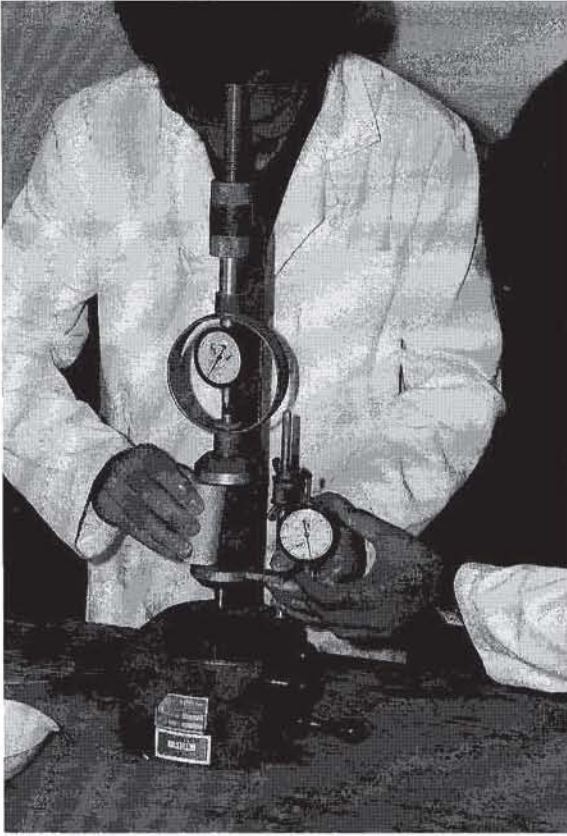


Figure 12 Typical unconfined compression test apparatus. The specimen is placed on the loading frame, and the displacement and force dial gages are adjusted and initialized.

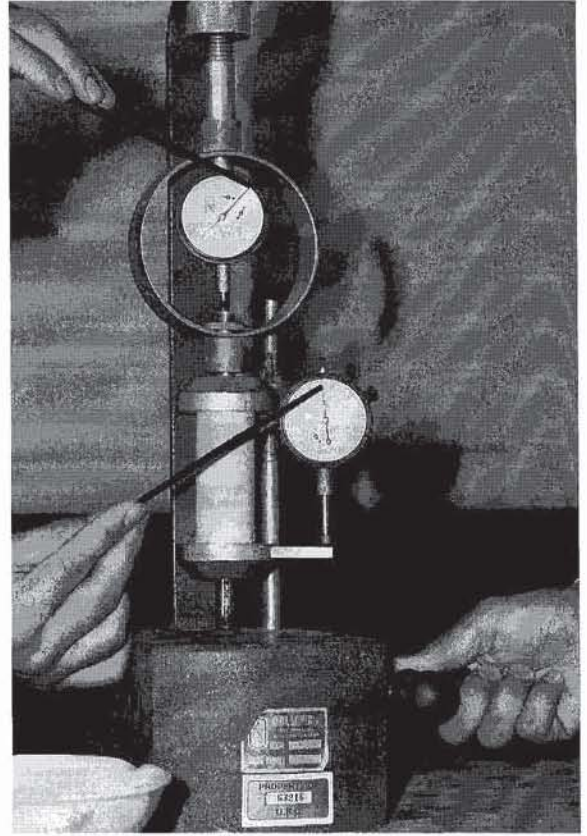


Figure 13 The loading platen is raised by turning the crank at constant speed. Both displacement and force dial readings are recorded at representative time intervals.

6. Record the time to reach the peak strength and the type of failure pattern (e.g., shear or bulge failure), and sketch the failed specimen. Determine the inclination and spacing of the shear bands, if any, in the specimen (Figs. 14 and 15).

7. After the test, determine the water content using the entire specimen or a representative portion of it.

COMPUTATION

The initial state of the tested soil is identified by its water content, total and dry unit weights, void ratio, and degree of saturation. The water content w is

$$w = \frac{W_i - W_d}{W_d} \times 100 \quad (\%) \quad (2)$$

where W_i is the initial weight and W_d is the dry weight of the complete sample or some sample trimmings. The total unit weight γ is

$$\gamma = \frac{W_i}{V_i} \quad (3)$$



Figure 14 When a shear plane occurs, its angle should be recorded. Other modes of failure may also occur and should be reported.

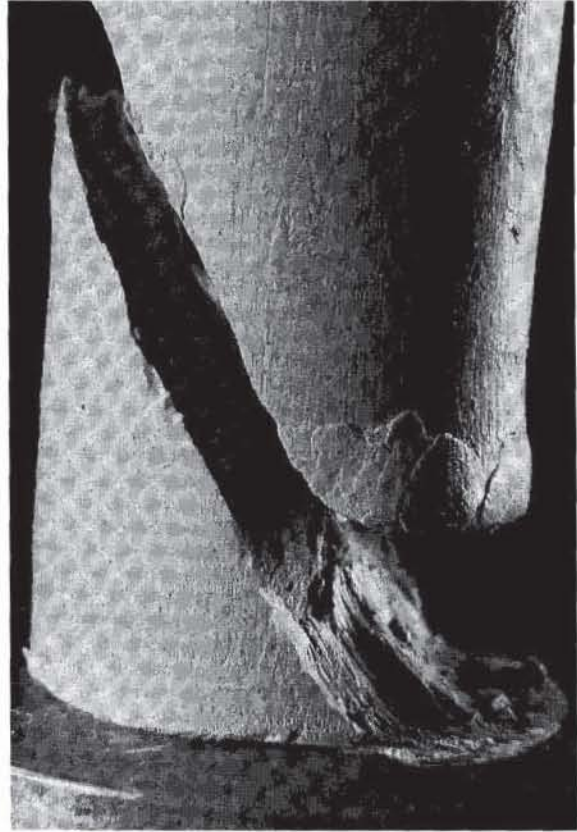


Figure 15 A closer look at the failure plane of the sample of Fig. 14 after lifting up the top part of the sample.

where W_i is the initial sample weight, and V_i is the initial sample volume. The dry unit weight γ_d , void ratio e , and degree of saturation S_r are

$$\gamma_d = \frac{\gamma}{1 + w}, \quad e = \frac{G_s \gamma_w}{\gamma_d} - 1, \quad \text{and} \quad S_r = \frac{G_s w}{e} \quad (4)$$

where G_s is the soil specific gravity. The axial strain ϵ is

$$\epsilon = \frac{\Delta H}{H_0} \times 100 \quad (\%) \quad (5)$$

where H_0 is the initial sample height and ΔH is the change of sample height. The compressive axial stress σ is

$$\sigma = \frac{F}{A_c} \quad \text{and} \quad A_c = \frac{A_i}{1 - \epsilon} \quad (6)$$

where F is the axial load applied to the sample, A_c the corrected area, A_i the initial cross-sectional area of the soil sample, and ϵ the axial strain in real value (not in %). The cross-sectional area of the sample changes during the compression test and is corrected assuming that the sample volume is constant. The unconfined compressive strength of the specimen is the maximum or peak of compressive

stress. When the unconfined shear strength is measured for undisturbed and remolded samples, the sensitivity ratio S_t is also calculated.

EXAMPLE

Figure 16 shows the stress–strain response curves obtained for the unconfined compression test of a clay sample, Fig. 17 shows the input/output data of Fig. 16, and Fig. 18 shows the formulas used in Fig. 17. In reports, the failure mode of the sample should also be sketched. If a failure plane is observed, its orientation must be measured and reported.

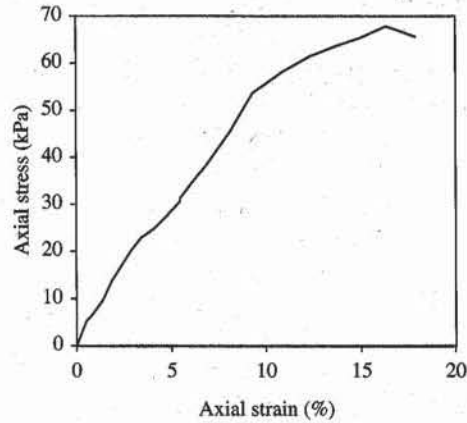


Figure 16 Stress–strain response curve obtained in an unconfined compression test.

REVIEW QUESTIONS

1. What is the purpose of the unconfined compression test?
2. To which types of soil is the unconfined compression test applicable?
3. What are undisturbed and remolded samples?
4. What method can you use to prepare undisturbed samples?
5. What is the typical loading rate for the unconfined compression test?

EXERCISE

1. Derive the relation between the corrected area, initial area, and axial strain (Eq. 6)

	A	B	C	D
1	Unconfined compression test			
2	Analyst name: <i>Sean Smith</i>			
3	Test date: <i>4/13/1993</i>			
4	Sample description: <i>Aardvack modelling clay</i>			
5				
6	Initial height $h_0 = 7.28$			cm
7	Initial diameter $d_0 = 3.39$			cm
8	Mass of wet sample and tare $M_i = 593.80$			g
9	Mass of dry sample and tare $M_d = 572.80$			g
10	Mass of tare $M_t = 466.30$			g
11	Specific gravity $G_s = 2.65$			
12	Initial water content $w = 19.72\%$			
13	Initial unit weight $\gamma = 19.09$			kN/m ³
14	Initial dry unit weight $\gamma_d = 15.95$			kN/m ³
15	Initial void ratio $e_0 = 0.63$			
16	Initial degree of saturation $S_r = 83.12\%$			
17	Young's modulus $E = 616.54$			kPa
18	Unconfined shear strength $S_u = 35.03$			kPa
19				
20	Displacement (mm)	Force (N)	Strain (%)	Stress (kPa)
21	Δh	F	e	s
22	0.00	0.00	0.0	0.0
23	0.37	4.68	0.5	5.2
24	0.62	6.08	0.9	6.7
25	1.02	8.88	1.4	9.7
26	1.37	12.62	1.9	13.8
27	1.75	15.90	2.4	17.2
28	2.09	18.70	2.9	20.2
29	2.49	21.31	3.4	22.9
30	2.98	23.37	4.1	24.9
31	3.37	25.45	4.6	27.0
32	3.96	29.11	5.4	30.6
33	4.00	29.92	5.5	31.4
34	4.49	33.53	6.2	34.9
35	4.99	36.93	6.9	38.2
36	5.90	44.41	8.1	45.3
37	6.78	53.29	9.3	53.7
38	7.97	58.90	11.0	58.3
39	8.98	63.11	12.3	61.4
40	9.99	66.38	13.7	63.6
41	10.93	69.19	15.0	65.3
42	11.91	72.93	16.4	67.7
43	13.06	71.99	17.9	65.6
44	14.08	77.14	19.4	69.1
45	15.09	79.01	20.7	69.5
46	16.05	79.01	22.1	68.4
47	16.67	81.81	22.9	70.1

Figure 17 Example of data set for an unconfined compression test.

	B	C	D
12	Initial water content $w = (M_i - M_d) / (M_d - M_t)$		
13	Initial unit weight $\gamma = (M_i - M_t) / (h_0 \cdot \pi \cdot d_0^2 / 4) \cdot 9.81$		kN/m ³
14	Initial dry unit weight $\gamma_d = \gamma / (1 + w)$		kN/m ³
15	Initial void ratio $e_0 = G_s \cdot 9.8 / \gamma_d - 1$		
16	Initial degree of saturation $S_r = G_s \cdot w / e_0$		
17	Young's modulus $E = \text{SLOPE}(D_{22}:D_{30}, C_{22}:C_{30}) \cdot 100$		kPa
18	Unconfined shear strength $S_u = \text{MAX}(s) / 2$		kPa

	C	D
20	Strain (%)	Stress (kPa)
21	e	s
22	$= Dh / h_0 \cdot 10$	$= F / (\pi \cdot d_0^2 / 4) \cdot (1 - e / 100) \cdot 10$
23	$= Dh / h_0 \cdot 10$	$= F / (\pi \cdot d_0^2 / 4) \cdot (1 - e / 100) \cdot 10$

Figure 18 Formulas used in Fig. 17.

7-4 Principles of the Direct Shear Test

DIRECT SHEAR TEST

As introduced in Chapter 5-4, the direct shear test is used to determine the shear strength of soils on predetermined failure surfaces. The principles of the direct shear test is illustrated in Fig. 1. The soil sample confined inside the upper and lower rigid boxes is subjected to the normal load N and is sheared by the shear force T . If A is the area of surface CD , the shear stress τ acting on surface CD is equal to T/A , and the normal stress σ is equal to N/A . The soil shear strength is the shear stress τ that causes the soil to slip on surface CD . It can be defined by Mohr-Coulomb theory:

$$\tau = c + \sigma \tan \phi \quad (1)$$

where c is the cohesion and ϕ is the friction angle.

STRESS IN THE DIRECT SHEAR TEST

During the direct shear test, the stress state is not completely defined: σ and τ are only measured on the horizontal surface, but are undetermined on other surfaces. Therefore, the stress path during direct shear test cannot be represented in s - t space. However, the Mohr circle can be drawn at failure, assuming that the failure plane is horizontal and the stress state is uniform. As shown in Fig. 2, point M represents the stress on the horizontal surface, and point N the stress on the vertical surface. Pole P is on the same horizontal line as point M when the failure plane is horizontal. The Mohr circle at failure is tangent to AM , and its center B is given by line MB perpendicular to AM . Therefore, the normal stresses σ_y and σ_x acting on horizontal and vertical surfaces, respectively, are related through

$$\sigma_x = 2c \tan \phi + K_s \sigma_y \quad \text{and} \quad K_s = 1 + 2 \tan^2 \phi \quad (2)$$

As shown in Fig. 3, K_s is larger than 1, increases with ϕ , but remains smaller than

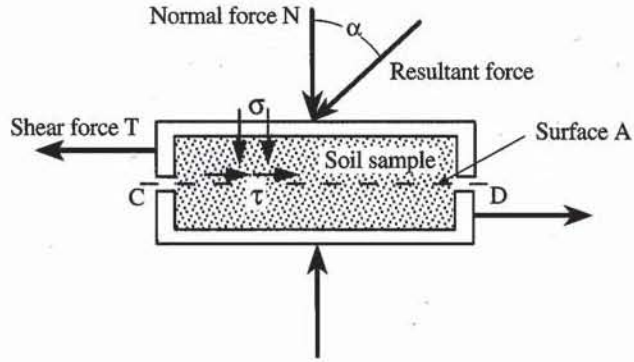


Figure 1 Soil sample in the direct shear box.

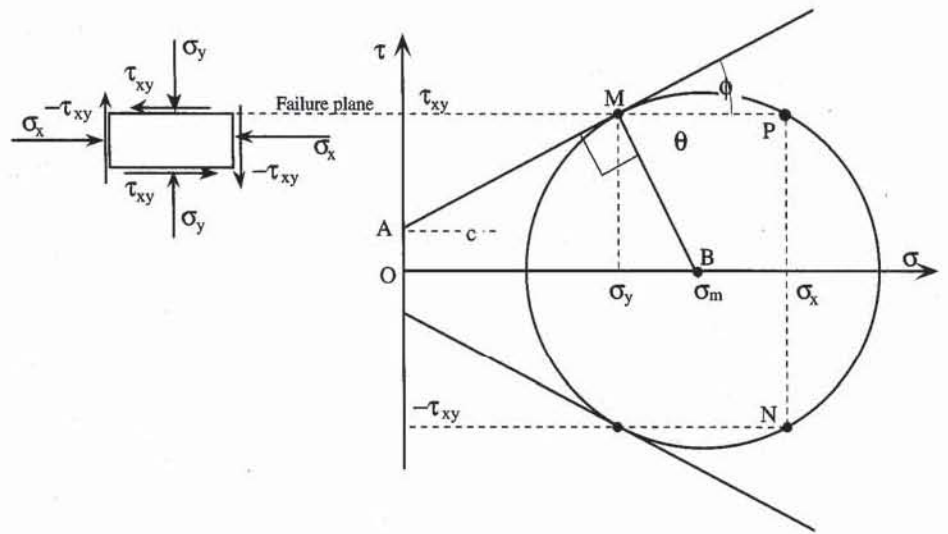


Figure 2 Stress state at failure in direct shear test and its Mohr representation.

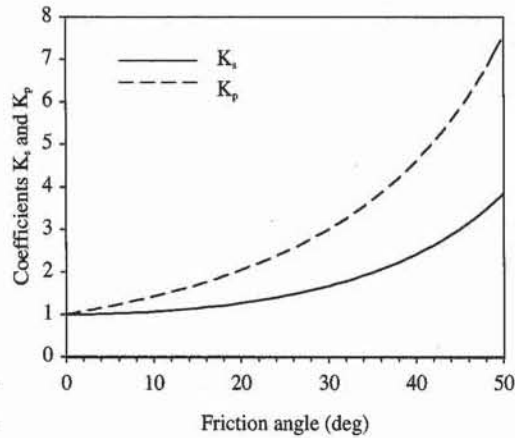


Figure 3 Variation of coefficients K_s and K_p with friction angle.

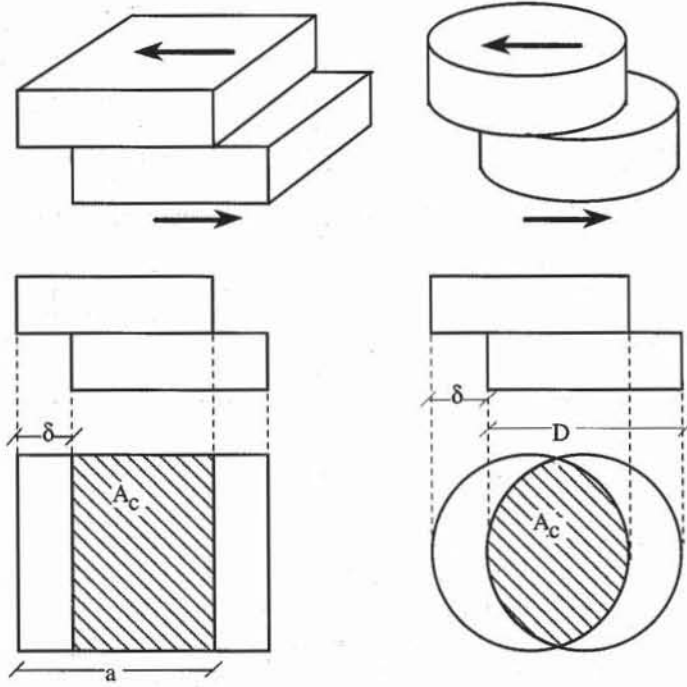


Figure 4 Corrected area for the calculation of shear and normal stresses.

the coefficient K_p of the Rankine theory for passive earth pressure ($K_p = (1 + \sin\phi)/(1 - \sin\phi)$).

As shown in Fig. 4, the contact area between the two specimen halves varies with the relative displacement δ between the lower and upper boxes. The corrected area A_c of the sheared specimen is for the square box of length a ,

$$A_c = a(a - \delta) \tag{3}$$

and for the cylindrical box of internal diameter D ,

$$A_c = \frac{D^2}{2} \left(\theta - \frac{\delta}{D} \sin \theta \right) \tag{4}$$

where $\theta = \cos^{-1} \left(\frac{\delta}{D} \right)$ in radians.

The shear stress τ and normal stress σ on the horizontal surface are calculated from the corrected area A_c , measured lateral force T , and normal force N :

$$\tau = \frac{T}{A_c} \quad \text{and} \quad \sigma = \frac{N}{A_c} \tag{5}$$

The error on the stresses resulting from the error on the contact area is for a square box ($A = a^2$),

$$\frac{\Delta A}{A} = \frac{A - A_c}{A} = \frac{\delta}{a} \tag{6}$$

and for a cylindrical box $\left(A = \frac{\pi D^2}{4}\right)$,

$$\frac{\Delta A}{A} = \frac{A - A_c}{A} = 1 - \frac{2\theta}{\pi} + \frac{2\delta}{\pi D} \sin \theta \quad (7)$$

For a typical sample diameter $D = 6.3$ cm, the error on shear and normal stresses may reach 20% when $\delta = 1$ cm.

STRAIN IN THE DIRECT SHEAR TEST

In the direct shear test, the material response is reported versus shear displacement instead of shear strain, because it is not possible to evaluate shear strain. The direct shear test is therefore not suited for studying the stress-strain relationships of soils.

Figure 5a shows the specimen in its initial state before it is sheared in the direct shear test. The vertical lines in Fig. 5 represent the initial and distorted positions of soil grains which are marked to stand out from the rest of the sample. If the shear strain was uniform, the sheared specimen would become uniformly slanted, as in Fig. 5b. However, the shear strains are never uniform in the direct shear test. As shown in Fig. 5c and d, the deformation is concentrated within the thick or thin shear zones at the interface between the upper and lower boxes. The soil fails at the edges of the box before it fails at the specimen center.

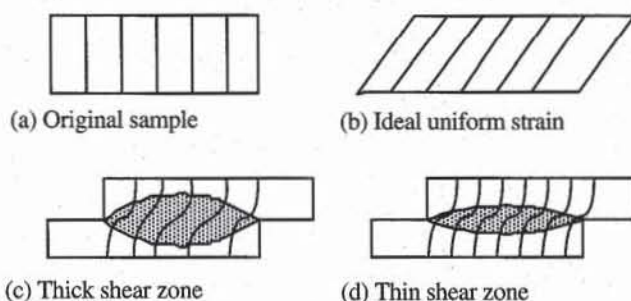


Figure 5 Idealized and observed displacements in the direct shear test (after Lambe, 1951).

DIRECT SHEAR OF COARSE-GRAINED SOILS

Figure 6 shows the typical response of a loose sand subjected to direct shear test. It represents the variation of τ/σ with shear displacement and the corresponding variation of normal displacement. The sand first compacts then dilates under shear.

Figure 7 illustrates the effect of density on the soil response during direct shear tests. For small shear displacement, dense sands have a larger shear strength than loose sands. However, after undergoing a peak failure, dense sands soften with shear strain until they gradually get the same residual strength as loose sands. The peak failure is characterized by the peak friction angle ϕ_p , and the residual failure by the residual friction angle ϕ_r . The peak friction angle ϕ_p is

$$\phi_p = \tan^{-1} \left(\frac{\tau_{\max}}{\sigma} \right) = \tan^{-1} \left(\frac{T_{\max}}{N} \right) \quad (8)$$

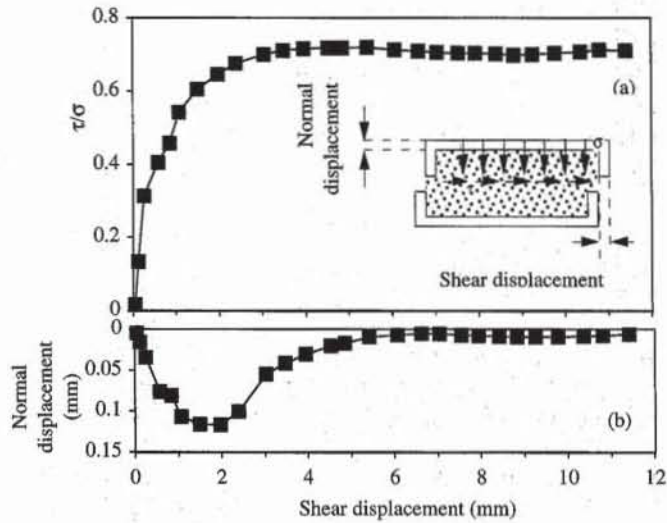


Figure 6 Typical results from a direct shear test on a loose sand (Lambe, 1951).

where τ_{max} is the maximum shear stress, σ the normal stress, T_{max} the maximum shear force, and N the normal load. The residual friction angle ϕ_r is

$$\phi_r = \tan^{-1} \left(\frac{\tau_r}{\sigma} \right) = \tan^{-1} \left(\frac{T_r}{N} \right) \tag{9}$$

where τ_r is the residual shear stress and T_r is the corresponding residual shear force at large lateral displacement. τ/σ is also equal to T/N , which eliminates calculation of the corrected area A_c .

The influence of soil density on ϕ_p is described by the concept of critical void ratio. By definition, the void ratio is critical when the soil fails without a volume change, as shown in Fig. 7. When the void ratio is smaller than critical (e.g., a dense soil), the soil dilates at peak failure. With increasing shear displacement, the void ratio increases until it becomes critical, and the shear stress decreases and gradually merges with the residual shear strength. When the void ratio is larger than critical (e.g., a loose soil), the soil compacts until the void ratio becomes critical, and the shear stress reaches the residual shear strength.

The peak friction angle ϕ_p of coarse-grained soils is also influenced by the normal load amplitude, grain size and shape, grain mineral, and grain size distri-

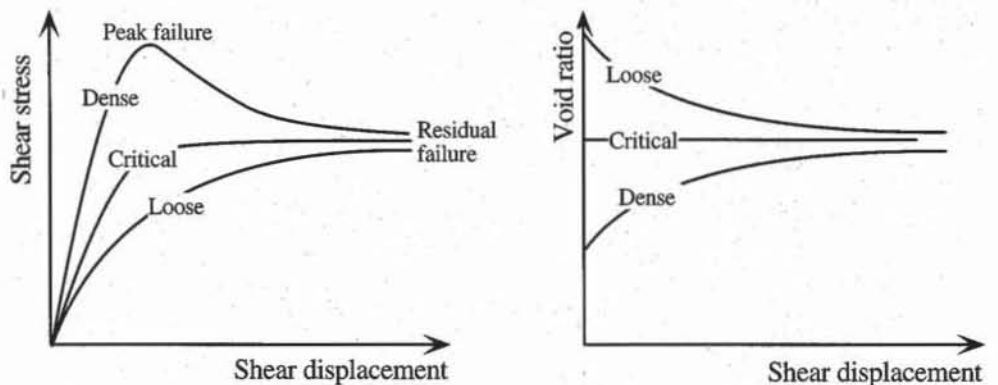


Figure 7 Influence of density on the response of soils subjected to direct shear tests.

bution. Smoothness, rounded corners, and uniform size of the soil grains tend to give lower friction angles. The contributions of these various factors, and typical values of friction angles are presented in Chapter 7-1.

DIRECT SHEAR OF FINE-GRAINED SOILS

Figure 8 shows the typical responses of undisturbed and remolded samples of inorganic clay from Maine which were subjected to the unconsolidated undrained (UU) direct shear test. The samples were sheared in 7 min., which left little time for the excess pore pressure to dissipate. The tests were performed under undrained conditions, without measuring the pore pressure. The undrained shear strength S_u of the remolded and undisturbed specimen is 5 and 40 kPa ($S_u = \tau_{max}$). The value of the sensitivity S_t is 8.

In the case of consolidated drained (CD) direct shear tests, the shearing rate can be selected by following ASTM guidelines (ASTM 3080). The minimum time t_f required to reach failure is

$$t_f = 50 t_{50} = 11.7 t_{90} \quad (10)$$

where t_{50} and t_{90} are the times to complete 50 and 90% of the primary compression, respectively. t_{50} and t_{90} are determined before the application of shear loading, by measuring the settlement of soil samples with time under the constant normal load (see Chapter 6-1). Once t_f is calculated, the lateral displacement δ that is required to reach the soil peak strength is estimated to be 1 to 2 mm for hard clay, 2 to 5 mm for stiff clay, and 8 to 10 mm for plastic clay. The maximum rate v of shearing displacement is then chosen so that it takes at least the time t_f to reach the lateral displacement δ . Typical values of the undrained shear strength, friction angle, and cohesion intercept for various soils can be obtained from Chapter 7-1.

FRICITION ANGLE IN DIRECT SHEAR TEST

Many comparisons have been made between the values of ϕ' measured from direct shear and triaxial tests. Earlier studies (e.g., Taylor, 1939) indicate that the friction angle ϕ'_{DS} during direct shear is generally greater by about 2° than the peak friction angle ϕ'_p during triaxial compression, especially for dense sands. Re-

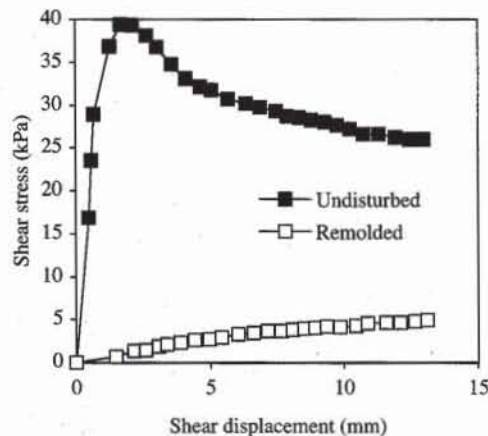


Figure 8 Typical results from a direct shear test on undisturbed and remolded samples of clay (Lambe, 1951).

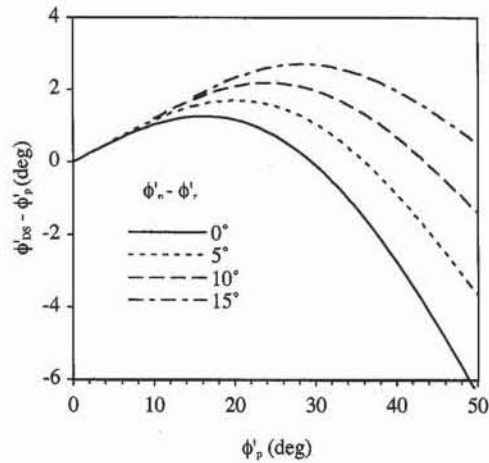


Figure 9 Variation of difference $\phi'_{DS} - \phi'_p$ with ϕ'_p for various values of $\phi'_r - \phi'_p$.

cent studies (e.g., Rowe, 1969; and Kulhawy and Mayne, 1990) show that ϕ'_{DS} is related to ϕ'_p through

$$\phi'_{DS} = \tan^{-1} [\tan (1.12 \phi'_p) \cos \phi'_r] \quad (10)$$

where ϕ'_r is the residual friction angle. In the case of sands, ϕ'_p can be related to ϕ'_r , relative density D_r and stress level as explained in Chapter 7-1. Figure 9 shows the variation of $\phi'_{DS} - \phi'_p$ with ϕ'_p , where ϕ'_{DS} is calculated from Eq. 10, for various constant values of $\phi'_r - \phi'_p$. For small values of ϕ'_p , ϕ'_{DS} can be 2° larger than ϕ'_p , but for larger values of ϕ'_p , ϕ'_{DS} can become 6° smaller than ϕ'_p . Therefore, the friction angle during triaxial compression may be larger or smaller than the friction angle during direct shear, depending on the values of ϕ'_r , relative density and stress level.

There are pros and cons for measuring the shear strength of soils with the direct shear test. The direct shear is inexpensive and reliable for simulating the long term drained failure of fine-grained soils on predetermined failure surfaces. However, it is less reliable for fine-grained soils under undrained conditions, because it does not allow a complete control of the drainage conditions.

REFERENCES

- See Introduction for references to ASTM procedures (pages 4 to 6).
- KULHAWY, F. H., and P. W. MAYNE, 1990, *Manual on Estimating Soil Properties for Foundations Design*, Report EL-9800 to Electric Power Research Institute, Cornell University, Ithaca, New York.
- LAMBE, T. W., 1951, *Soil Testing for Engineers*, John Wiley & Sons, New York, pp. 88-97.
- ROWE, P. W., 1969, The relation between the shear strength of sands in triaxial compression, plane strain and direct shear, *Géotechnique*, Vol. 19, No. 1, pp. 75-86.
- TAYLOR, D. W., 1939, A comparison of results of direct shear and cylindrical compression tests, *Proc. ASTM*.

REVIEW QUESTIONS

1. For which types of engineering analyses do you need the results of direct shear tests?
2. Why is the shear strength of dense sands higher than that of loose sands?
3. Is it possible to plot the evolution of the Mohr stress circle during a direct shear test?
4. Is it possible to determine the state of strain of the tested sample during the direct shear test?
5. Under which assumptions can we determine the normal failure stress on the vertical surface of a sheared sample?
6. What is the effect of the change in the contact area during a direct shear test?
7. In which parts of the soil sample are the strains concentrated during a direct shear test?
8. What is the effect of density on the friction angle of sands?
9. Define *peak* and *residual friction angles*.
10. What is the critical state theory in the case of the direct shear test on sand?

EXERCISES

1. Plot the shear stress and normal displacement versus shear displacement from the direct shear test results on a loose sand shown in Table E1. Calculate the friction angle.

TABLE E1

Shear displacement (mm)	τ/σ	Normal displacement (mm)
0.04	0.02	0.005
0.12	0.13	0.016
0.25	0.31	0.035
0.57	0.40	0.076
0.85	0.46	0.081
1.07	0.54	0.107
1.50	0.60	0.117
1.97	0.64	0.117
2.39	0.68	0.100
3.04	0.70	0.055
3.49	0.71	0.041
3.96	0.72	0.030
4.53	0.72	0.021
4.85	0.72	0.018
5.43	0.72	0.010
6.07	0.71	0.007
6.62	0.71	0.005
7.04	0.71	0.006
7.54	0.70	0.007
7.94	0.70	0.008
8.41	0.70	0.009
8.83	0.70	0.009
9.25	0.70	0.009
9.77	0.70	0.009
10.37	0.71	0.009
10.82	0.71	0.008
11.41	0.71	0.007

2. Given the direct shear test results of Table E1, calculate the normal and shear stresses that are acting at failure on the horizontal and vertical surfaces, provided that the failure plane is horizontal and that the stresses are uniform. The normal stress on the horizontal surface is 50 kPa.
3. Derive the relation between the normal stresses on vertical and horizontal surfaces at failure assuming that the stress state is uniform, and that the failure plane is horizontal.
4. Plot the relative error on the contact area versus the shear displacement for a circular shear box of 6.35 mm diameter. Define the range of displacement for which the relative error on the contact area is less than 5%.
5. Calculate the undrained shear strength of the undisturbed and remolded samples whose direct shear test results are shown in Table E2.

TABLE E2

Undisturbed		Remolded	
Shear displacement (mm)	Shear stress (kPa)	Shear displacement (mm)	Shear stress (kPa)
0.00	0.00	0.00	0.00
0.49	16.82	1.48	0.67
0.57	23.54	2.16	1.32
0.68	28.91	2.59	1.45
1.26	36.89	3.06	1.89
1.68	39.39	3.38	2.11
2.10	39.31	3.88	2.35
2.63	38.10	4.41	2.58
3.01	36.78	4.96	2.72
3.57	34.75	5.41	2.95
4.11	33.13	6.05	3.30
4.64	32.12	6.60	3.43
5.07	31.74	7.13	3.67
5.68	30.74	7.63	3.69
6.34	30.16	8.08	3.82
6.87	29.77	8.51	3.95
7.49	29.29	8.90	4.08
7.88	28.69	9.35	4.20
8.34	28.51	9.86	4.13
8.79	28.23	10.44	4.27
9.29	28.05	10.89	4.60
9.74	27.66	11.58	4.64
10.22	27.17	12.11	4.67
10.73	26.58	12.66	4.80
11.31	26.62	13.11	4.93
11.94	26.24		
12.45	25.96		
12.98	25.99		

Normal stress = 31.92 kPa

7-5

Direct Shear Test

OBJECTIVE

The direct shear test is used to measure the friction angle, cohesion, and undrained shear strength of soils for stability analysis of foundations, slopes, and retaining walls.

EQUIPMENT

The equipment for the direct shear test includes:

- Direct shear loading machine with a counterbalance system for the application of normal load (see Figs. 1 and 6).
- Direct shear box (see Figs. 3 to 5).
- Assortment of slotted weights for applying the normal load. The total weight should be at least 100 kg. For the typical 6.35-cm-diameter shear box, it takes a mass of 32.3 kg to create a normal stress equal to 100 kPa.
- Two dial gages for measuring vertical and horizontal displacements sensitive to 0.01 mm with a full range of 2.5 cm. The dial gages may be replaced by calibrated LVDT transducers of similar range and sensitivity.
- One calibrated load ring for measuring the shear force. A capacity of 2 kN is suitable for most purposes. A larger capacity (e.g., 5 or 10 kN) may be required for larger normal loads. The load ring may be replaced by a load transducer of similar range.
- A 2.5-cm ball bearing for applying the normal load to the sample cap.
- Specimen cutter for trimming samples of cohesive soil.
- Tamper for compacting cohesionless soil.
- Balance, sensitive to 0.1g.
- Timer and calipers.
- Spoons and straightedge.

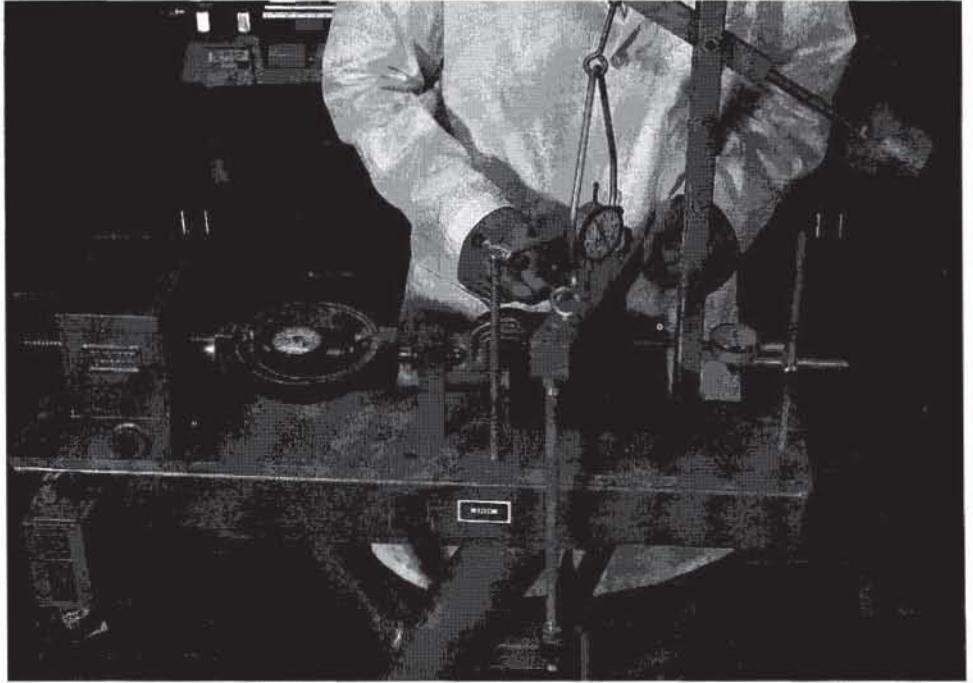


Figure 1 General view of the direct shear equipment.

Direct Shear Box

As shown in Figs. 2 and 3, the direct shear box is made of a lower part (base) and an upper part with a swan neck yoke. The sample is between two porous stones, which are toothed or serrated as shown in Fig. 4 to minimize the slippage at the interface between soil and shear box and to improve the transfer of the shear load to the soil. The porous stones are also used to drain water from saturated samples. The setscrews are used to adjust the spacing between the upper and lower parts of the shear box. Two mounting pins maintain the position of these two parts during the sample fabrication and are removed before the beginning of the shear phase. The base is fixed to the loading frame and occasionally contains water when the soil sample is to remain saturated. The normal load is applied to the soil sample through a ball bearing and a rigid cap. The lateral load is applied to the upper part through the swan neck yoke.

As shown in Fig. 5, some particular shear boxes are designed to simplify preparation of cohesive soil samples. They take samples right out of the field sam-

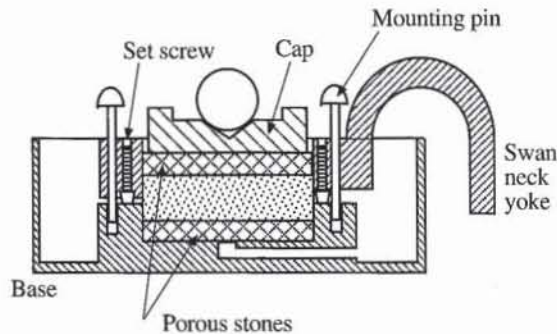


Figure 2 Schematic view of the direct shear box.

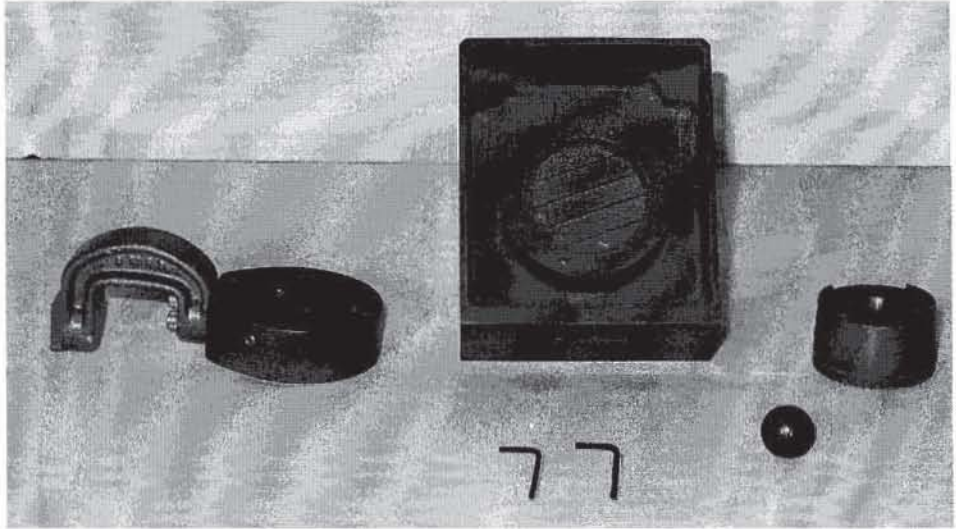


Figure 3 Shear box components.

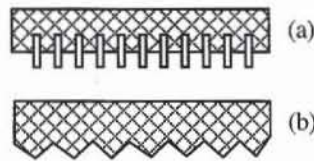


Figure 4 Detail of (a) serrated and (b) toothed porous stones for the direct shear box.

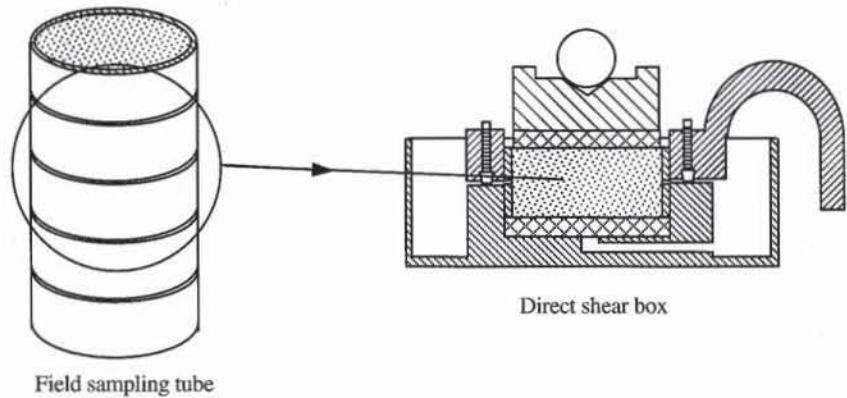


Figure 5 Shear box assorted to field sampling tube.

pling tubes. During field exploration, a stack of rings is first placed in the field sampling tube, which becomes filled with the soil to be tested when it is pushed into the ground. In the laboratory, two full rings are sliced from the field sample using a wire saw and are directly mounted in the shear box.

Loading Unit

The direct shear test can be controlled by either displacement or force. When it is force controlled, the shear force is gradually increased at a prescribed rate and the resulting displacement is measured. When displacement controlled, the upper part of the shear box is laterally pushed at a specified rate and the resulting shear

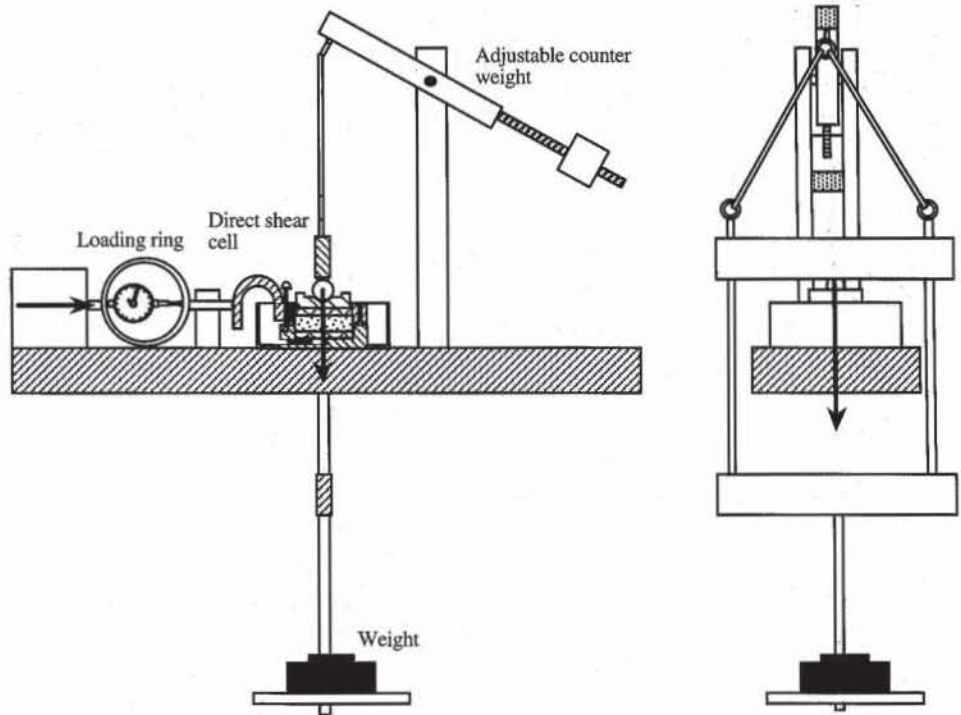


Figure 6 The loading unit and its counterweight mechanism.

force is measured. Displacement-controlled units are preferred because they give the residual shear strength of soils.

Good displacement-controlled equipment has a controllable rate of lateral displacement ranging from 5 to 0.0005 mm/min and a full displacement of about 10 mm. With this range of speed, it takes from 2 min to about 14 days to move 10 mm. A rate of 0.5 to 1 mm/min is appropriate to perform a quick test in 10 to 20 min. The rate of displacement is generally controlled by an electrical motor and a gearbox. As shown in Fig. 6, the shear force is measured by the proving ring attached to the yoke of the direct shear box. The lateral and vertical displacements are measured with dial gages or LVDT transducers.

As shown in Fig. 6, the loading unit also applies normal force to the soil specimen. The counterweight system is balanced so that the empty weight hanger applies no normal force to the sample. The normal load is then obtained directly by adding weights suspended on a weight hanger.

TEST PROCEDURE

There are two different test procedures, depending on whether the soil to be tested is coarse grained (e.g., sands), or fine grained (e.g., clays and silts).

Coarse-Grained Soil

1. Measure the internal diameter of the cylindrical cell (or the internal side length for square cell).
2. Balance the counterweight system so that it applies a small but negligible normal force.

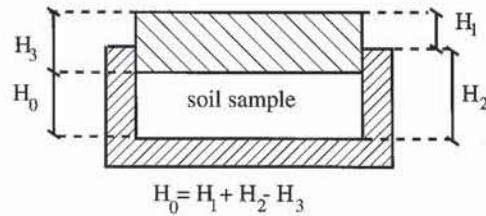


Figure 7 Determination of the initial height H_0 of sample.

3. Weigh the cap and the ball bearing, as their weight is not counterbalanced by the counterweight mechanism and must be added to the weights on the weight hanger.

4. Assemble the direct shear box, and mount it on the direct shear machine. Insert the mounting pins to align the upper and lower parts of the direct shear box.

5. Adjust the gap between the two parts of the shear box by turning the set-screws. In theory, the spacing should be larger than the diameter of the largest particle to prevent the top part from riding up on the grains that get caught in the gap. In practice, a spacing of approximately 0.5 mm is satisfactory. Too close a spacing is indicated by a snapping and crushing of grains, accompanied by jerky readings.

6. Measure the depth H_2 of the shear box and the height H_3 of the top cap as shown in Fig. 7.

7. Weigh the dish filled with the sand to be tested.

8. While the pins hold the two parts of the shear box together, pour in the sand slowly to obtain a loose specimen (Fig. 8). Compact the sand with a tamper or vibrate the container to obtain denser specimens. The cell should be filled with enough material so that the top cap is quite above the shear plane (Fig. 9).



Figure 8 Filling the shear box with sand.

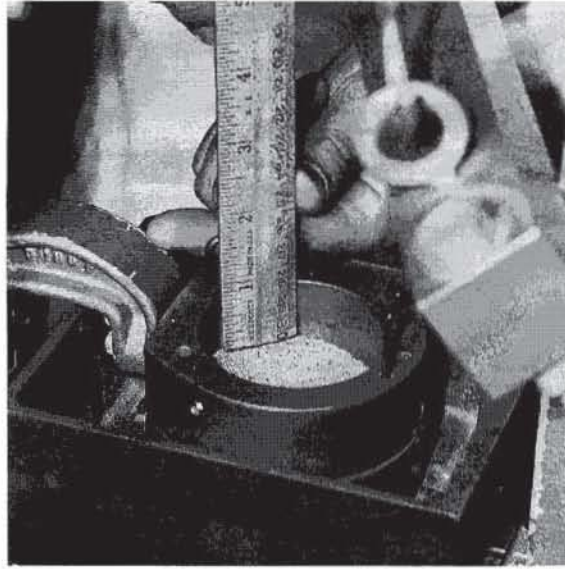


Figure 9 The specimen should be thick enough for the bottom of the loading cap to be quite above the plane separating the upper and lower parts of the shear box.

9. Weigh the dish and the leftover sand to determine the weight of the soil used in the test.

10. Level the soil surface inside the shear cell, put on the cap and ball bearing, and position the counterweight system (Figs. 10 and 11).

11. Put the amount of dead weight on the balanced mechanism which is required to apply the desired normal load.

12. Measure the initial height H_0 of the soil specimen by measuring the distance H_1 as shown in Fig. 7.

13. Attach the dial gages or displacement transducers that measure shear and normal displacements as shown in Fig. 10.

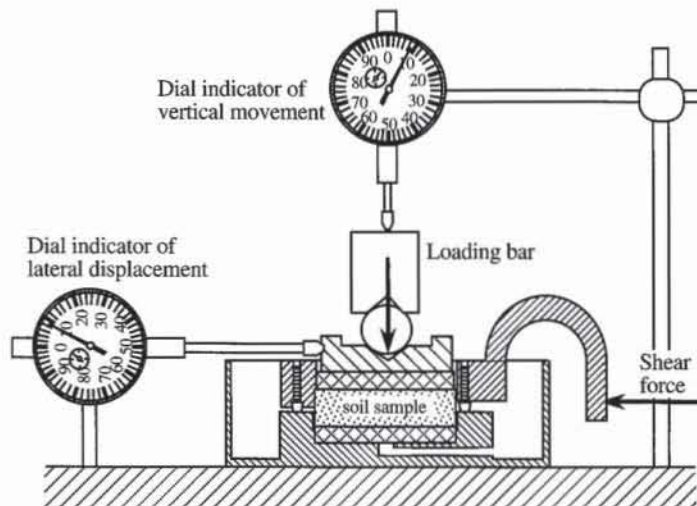


Figure 10 The shear box and the dial gages.

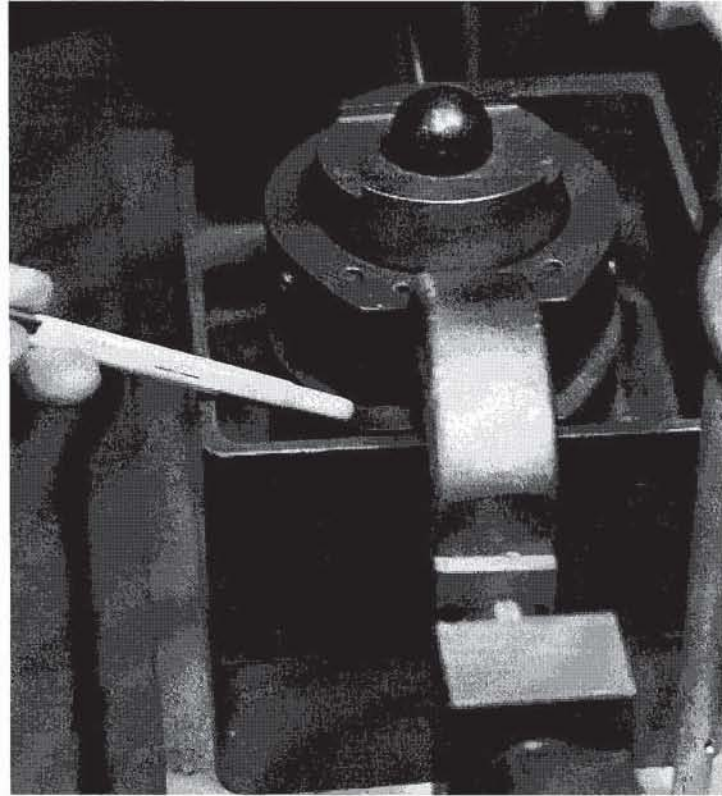


Figure 11 The shear box is assembled and the two mounting pins are removed.

14. Before beginning the shear loading, carefully check that no pin or screw is left to hold the two parts of the shear box together.

15. Adjust the rate of shear displacement to approximately 1 mm/min. If dial gages are used to measure displacement and forces, select a rate of shearing that is convenient for reading the dial gages simultaneously. For a maximum lateral displacement of 1 cm and a rate of 1 mm/min, the test duration is 10 min. For sands, the effect of the displacement rate on the friction angle is generally negligible within the range 3 to 0.1 mm/min.

16. Start the loading. Measure the shear force, time, and shear and normal displacements at convenient time intervals. Continue the test until the horizontal displacement becomes approximately 1 cm or until the shear force becomes constant, whichever comes first.

Fine-Grained Soil

In the case of fine-grained soils, the direct shear test can be performed under CU or CD conditions (see Chapter 5-4). In the CU test, the sample is first consolidated under the action of the normal load, and then quickly sheared. In the CD test, the sample is consolidated as for the CU test, but is sheared very slowly so that no excess pore pressure builds up.

CU test

- 1.** Same as steps 1 to 4 for coarse-grained soils.

2. Turn the set screws so that there is no gap at all between the two parts of the shear box.
3. Measure the depth H_2 of the shear box and the height H_3 of the top cap as shown in Fig. 7.
4. Put the amount of dead weight on the balanced mechanism to apply the desired normal load.
5. Measure the initial height H_0 of the soil specimen by measuring the distance H_1 as shown in Fig. 7.
6. Add water in the direct shear box to cover the soil specimen completely.
7. Attach the dial gages or displacement transducers that measure shear and normal displacements (Fig. 10), and record their initial readings.
8. Measure the vertical settlement of the sample with time until the end of the primary consolidation is detected (see Chapter 6-1).
9. Adjust the gap between the two parts of the shear box to the smallest possible setting that minimizes the friction resistance between these two parts.
10. Check that no pin or screw holds together the two parts of the shear box.
11. Adjust the rate of shearing displacement to approximately 1 mm/min. The loading rate should be fast enough to approach the undrained condition.
12. Start the shear loading. Measure the shear force, time, and shear and normal displacements at convenient time intervals. Continue the test until the horizontal displacement becomes approximately 1 cm.

CD test. The CD test is similar to the CU test, except for the determination of the shearing rate that prevents the excess pore pressure from building up in the sample.

1. Same as steps 1 to 7 of the CU test.
2. Measure the vertical settlement of the sample with time, and determine the time t_{90} to reach 90% of the primary consolidation (see Chapter 6-1).
3. Same as steps 9 to 10 of the CU test.
4. Estimate the lateral displacement δ required to reach the soil peak strength. Typically, $\delta = 1$ to 2 mm for hard clay, $\delta = 2$ to 5 mm for stiff clay, and $\delta = 8$ to 10 mm for plastic clay. Calculate the minimum time t_f required for failure by using the empirical relation $t_f = 11.7 t_{90}$ (ASTM D3080). Calculate the maximum rate v of shearing displacement so that it takes the time t_f to reach the lateral displacement δ (i.e., $v = \delta/t_f$). Select the shearing rate of the equipment that is closest to v .
5. Start the shear loading. Measure the shear force, time, and shear and normal displacements at convenient time intervals. Continue the test until the lateral displacement becomes approximately 1 cm or until the shear force becomes constant, whichever comes first.

COMPUTATIONS

The results of the direct shear test should identify the characteristics of the tested soil. For dry soil specimens of coarse grain, the dry unit weight γ_d and void ratio e are

$$\gamma_d = \frac{W_i}{V_i} \quad \text{and} \quad e = \frac{G_s \gamma_w}{\gamma_d} - 1 \quad (1)$$

where γ_w is the water unit weight, W_i the initial sample weight, V_i the initial sample volume, and G_s the soil specific gravity. For wet specimens of fine-grained soils, the water content w is

$$w = \frac{W_i - W_d}{W_d} \times 100 \quad (\%) \quad (2)$$

where W_i is the initial weight and W_d is the dry weight of the complete sample or some sample trimmings. The total unit weight γ , dry unit weight γ_d , void ratio e , and degree of saturation S_r of wet soil samples are

$$\gamma = \frac{W_i}{V_i}, \quad \gamma_d = \frac{\gamma}{1+w}, \quad e = \frac{G_s \gamma_w}{\gamma_d} - 1, \quad \text{and} \quad S_r = \frac{G_s w}{e} \quad (3)$$

For coarse-grained soils and fine-grained soils tested under CD conditions, the results of a direct shear test should include the peak and residual friction angles, the shear displacements at which they are observed, and the graphs τ/σ and normal displacement versus shear displacement. The shear stress τ , normal stress σ , and ratio τ/σ are

$$\sigma = \frac{N}{A_c}, \quad \tau = \frac{T}{A_c}, \quad \text{and} \quad \frac{\tau}{\sigma} = \frac{T}{N} \quad (4)$$

where T is the measured lateral force, N the normal force, and A_c the corrected area of the sheared specimen, which is a function of the shear displacement δ . In contrast to τ and σ , τ/σ is determined without A_c . The peak friction angle ϕ_p and residual friction angle ϕ_r are

$$\phi_p = \tan^{-1} \frac{T_{\max}}{N} \quad \text{and} \quad \phi_r = \tan^{-1} \frac{T_r}{N} \quad (5)$$

where T_{\max} is the maximum shear force and T_r is the residual shear force.

For fine-grained soils tested under CU conditions, the results of the direct shear test should include the undrained shear strength, the shear displacements at which it is observed, and graphs of τ/σ versus shear displacement.

EXAMPLE

Figures 12 to 15 show results obtained for a dense fine uniform sand. Figures 12 and 13 show graphs of τ/σ and normal displacement versus shear displacement, Fig. 14 shows the corresponding input/output data, and Fig. 15 lists the formulas used in Fig. 14. During shear, the dense material first compacts, then dilates.

REFERENCES

See Introduction for references to ASTM procedures (pages 4 to 6).

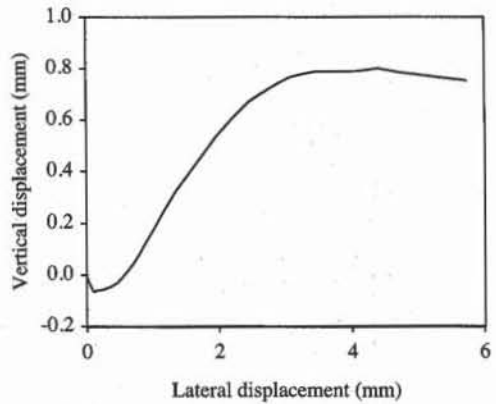
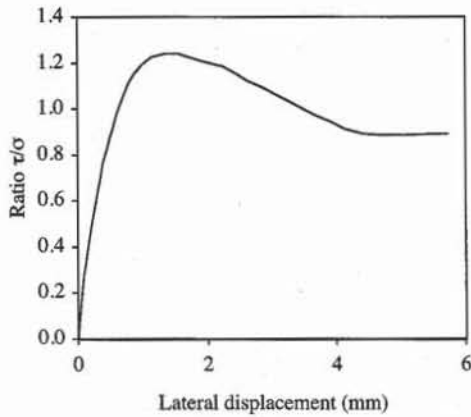


Figure 12 Variation of τ/σ with lateral displacement during a direct shear test of dense fine sand.

Figure 13 Variation of vertical displacement with lateral displacement corresponding to Fig. 12.

	B	C	D
6	Mass of specimen $M = 84$		g
7	Vertical load $N = 19.392 \cdot 9.8$		N
8	Specific gravity $G_s = 2.65$		
9	Initial height $h_0 = 1.545$		cm
10	Diameter $d_0 = 6.33$		cm
11	Dry unit weight $\gamma_d = M \cdot 9.81 / (\pi \cdot h_0 \cdot d_0^2 / 4)$		kN/m ³
12	Void ratio $e = G_s \cdot 9.8 / \gamma_d - 1$		
13	Maximum friction angle $\phi_p = \text{ATAN}(\text{MAX}(\text{ratio})) \cdot 180 / \pi$		deg
14	Displacement at peak $\delta_p = \text{INDEX}(d, \text{MATCH}(\text{MAX}(\text{ratio}), \text{ratio}, 0))$		mm
15	Residual friction angle $\phi_r = \text{ATAN}(D61) \cdot 180 / \pi$		deg
16	Displacement at residual $\delta_r = A61$		mm
17	Normal stress $\sigma = N \cdot 9.81 / (\pi \cdot d_0^2 / 4)$		kPa

D	
19	Ratio
20	τ/σ
21	$=T/N$
22	$=T/N$

Figure 15 Formulas used in Fig. 14.

REVIEW QUESTIONS

1. What is the purpose of a direct shear test? Which soil properties does it measure?
2. Why do we use mounting pins in a direct shear test? Can you predict what will happen if you do not remove them during the test?
3. Why are the porous stones of a direct shear box serrated or provided with teeth?
4. What is the rationale for determining the spacing between the two parts of a direct shear box? What are the effects of a poorly selected spacing?
5. What is the purpose of the counterweight mechanism in direct shear apparatus?
6. What is the range of the rate of shear displacement that is typically achievable with a direct shear loading device?
7. Under which circumstances and for which soils should a very slow shearing speed be used?
8. Give an approximate duration for a very slow direct shear test.

	A	B	C	D
1	Direct Shear Test			
2	Analyst name: <i>Robertus B. Kurniawan</i>			
3	Test date: <i>April 20, 1993</i>			
4	Sample Description: <i>Dense uniform sand</i>			
5				
6	Mass of specimen M = 84.00		g	
7	Vertical load N = 190.04		N	
8	Specific gravity $G_s = 2.65$			
9	Initial height $h_0 = 1.55$		cm	
10	Diameter $d_0 = 6.33$		cm	
11	Dry unit weight $\gamma_d = 16.95$		kN/m ³	
12	Void ratio $e = 0.53$			
13	Maximum friction angle $\phi_p = 51.11$		deg	
14	Displacement at peak $\delta_p = 1.35$		mm	
15	Residual friction angle $\phi_r = 41.73$		deg	
16	Displacement at residual $\delta_r = 5.74$		mm	
17	Normal stress $\sigma = 59.24$		kPa	
18				
19	Lateral displacement (mm)	Vertical displacement (mm)	Lateral force (N)	Ratio
20	d		T	τ/σ
21	0.00	0.00	0.0	0.00
22	0.02	-0.02	13.7	0.07
23	0.05	-0.04	30.8	0.16
24	0.08	-0.05	46.5	0.24
25	0.09	-0.06	52.4	0.28
26	0.12	-0.06	61.5	0.32
27	0.15	-0.06	72.6	0.38
28	0.19	-0.06	86.4	0.45
29	0.23	-0.06	99.5	0.52
30	0.27	-0.06	110.6	0.58
31	0.31	-0.05	122.4	0.64
32	0.35	-0.05	132.9	0.70
33	0.39	-0.04	145.3	0.76
34	0.46	-0.03	157.7	0.83
35	0.50	-0.02	166.2	0.87
36	0.55	-0.01	174.1	0.92
37	0.59	0.01	182.6	0.96
38	0.64	0.02	190.5	1.00
39	0.70	0.05	200.9	1.06
40	0.79	0.08	211.4	1.11
41	0.88	0.12	219.3	1.15
42	1.00	0.17	227.1	1.20
43	1.14	0.24	233.0	1.23
44	1.35	0.32	235.6	1.24
45	1.55	0.39	235.6	1.24
46	1.97	0.54	229.1	1.21
47	2.25	0.62	225.1	1.18
48	2.45	0.67	219.3	1.15
49	2.62	0.70	213.4	1.12
50	2.87	0.74	207.5	1.09
51	3.07	0.76	201.6	1.06
52	3.27	0.78	196.3	1.03
53	3.47	0.79	190.5	1.00
54	3.68	0.79	184.6	0.97
55	3.91	0.79	179.3	0.94
56	4.12	0.79	173.4	0.91
57	4.42	0.80	169.5	0.89
58	4.72	0.79	168.2	0.89
59	5.02	0.77	168.2	0.89
60	5.33	0.77	168.9	0.89
61	5.74	0.75	169.5	0.89

Figure 14 Example of data set for a direct shear test.

9. Is the shear strength of coarse-grained soils influenced by the rate of shearing in a direct shear test? On what basis is the rate of shearing selected for coarse-grained soils?
10. How many and which types of direct shear tests are possible to perform on fine-grained soils?
11. What are the basic steps of a CU direct shear test on a fine-grained soil?
12. What are the basic steps of a CD direct shear test on a fine-grained soil?
13. How is the shearing rate determined for the CD direct shear tests of fine-grained soils?

EXERCISES

1. Plot the exact and approximate variation of area correction and define the range of displacement for which the error on the contact area is less than 5%.
2. Process the following results of a direct shear test on a loose and a dense sample of fine sand.

Sample description	Dense uniform sand	Loose uniform sand
Weight of specimen	84.00 g	68.00 g
Vertical load	190.04 N	190.04 N
Specific gravity	2.65	2.65
Initial height	1.53 cm	1.51 cm
Initial diameter	6.35 cm	6.35 cm
Normal stress	58.92 kPa	58.92 kPa

Dense uniform sand				Loose uniform sand			
Lateral displacement (mm)	Vertical displacement (mm)	Lateral force (N)	τ/σ	Lateral displacement (mm)	Vertical displacement (mm)	Lateral force (N)	τ/σ
0.00	0.00	0.00	0.00	0.00	0.00	0.00	0.00
0.02	0.00	15.05	0.08	0.05	0.01	17.02	0.09
0.04	0.00	29.45	0.15	0.09	0.01	29.45	0.15
0.06	0.00	45.16	0.24	0.14	0.01	41.89	0.22
0.08	0.00	54.98	0.29	0.18	0.01	50.40	0.27
0.10	0.00	66.76	0.35	0.23	0.01	61.52	0.32
0.14	0.00	85.08	0.45	0.30	0.01	75.92	0.40
0.20	0.00	103.41	0.54	0.40	0.01	93.59	0.49
0.26	-0.01	117.81	0.62	0.49	0.00	107.99	0.57
0.30	-0.02	130.24	0.69	0.53	0.00	121.74	0.64
0.34	-0.03	138.10	0.73	0.55	0.00	129.59	0.68
0.40	-0.04	147.92	0.78	0.60	0.00	140.06	0.74
0.44	-0.04	153.81	0.81	0.63	0.00	145.95	0.77
0.54	-0.06	163.62	0.86	0.70	-0.01	155.77	0.82
0.60	-0.07	167.55	0.88	0.72	-0.02	159.70	0.84
0.68	-0.10	173.44	0.91	0.76	-0.03	165.59	0.87
0.74	-0.11	177.37	0.93	0.80	-0.04	169.51	0.89
0.80	-0.12	179.33	0.94	0.82	-0.04	171.48	0.90
0.89	-0.14	183.26	0.96	0.86	-0.04	175.40	0.92
0.99	-0.17	183.91	0.97	0.88	-0.05	177.37	0.93
1.09	-0.20	185.22	0.97	0.90	-0.05	179.33	0.94
1.29	-0.25	185.22	0.97	0.96	-0.07	183.26	0.96
1.48	-0.30	185.88	0.98	1.12	-0.10	186.53	0.98
1.58	-0.32	185.88	0.98	1.16	-0.11	188.49	0.99

(cont.)

Dense uniform sand				Loose uniform sand			
Lateral displacement (mm)	Vertical displacement (mm)	Lateral force (N)	τ/σ	Lateral displacement (mm)	Vertical displacement (mm)	Lateral force (N)	τ/σ
1.79	-0.36	187.18	0.98	1.31	-0.15	187.84	0.99
1.89	-0.38	186.53	0.98	1.42	-0.17	187.18	0.98
2.01	-0.40	182.60	0.96	1.56	-0.20	184.57	0.97
2.13	-0.41	179.33	0.94	1.69	-0.22	180.64	0.95
2.33	-0.43	176.71	0.93	1.86	-0.25	176.71	0.93
2.51	-0.45	172.13	0.91	2.06	-0.25	171.48	0.90
2.74	-0.47	168.20	0.89	2.23	-0.27	166.90	0.88
2.89	-0.48	166.24	0.87	2.51	-0.27	159.04	0.84
2.99	-0.49	166.24	0.87	2.62	-0.28	157.73	0.83

7-6

Principles of Triaxial Tests

INTRODUCTION

As introduced in Chapter 5-4, the triaxial test is used to determine the stress-strain-strength characteristics of soils under drained or undrained conditions. This test reproduces in the laboratory the initial effective stresses and stress changes of soils in the field, in a more realistic way than unconfined compression and direct shear tests. Here we review the principles of triaxial tests, check the saturation of triaxial specimens, and select the loading rate of triaxial tests. Typical triaxial test results can be found in Chapter 7-1.

TYPES OF TRIAXIAL TEST

As shown in Fig. 1, in a triaxial test the cylindrical soil specimen is encased within a rubber sleeve inside a pressure chamber. The lower and upper loading platens have porous disks connected to the drainage system for saturating and/or draining the soil specimen. The confining pressure σ_3 is applied by adjusting the chamber pressure, and the axial stress σ_1 is applied by pushing the piston. There are three main types of triaxial test, which are labeled CD, UU, and CU. The first letter, C or U, refers to the consolidation stage and stands for *consolidated* or *unconsolidated*. The second letter, D or U, refers to the drainage condition during shear and stands for *drained* or *undrained*. Hereafter we present only the CD, CU and UU triaxial compression tests with isotropic consolidation. Information on other types of triaxial test in Chapter 5-4 can be found in Head (1986).

During CD and CU tests, the soil sample is first consolidated to an initial effective stress state. Consolidation is an important step in testing frictional materials, whose elastic properties and shear strength depend largely on effective stresses. As shown in Fig. 1, during an isotropic consolidation, the soil specimen is subjected to hydrostatic pressure. The drainage is opened, and the interstitial water filling the soil voids can drain freely. The time required to complete consolidation is almost negligible for coarse-grained soils with high permeability, but can

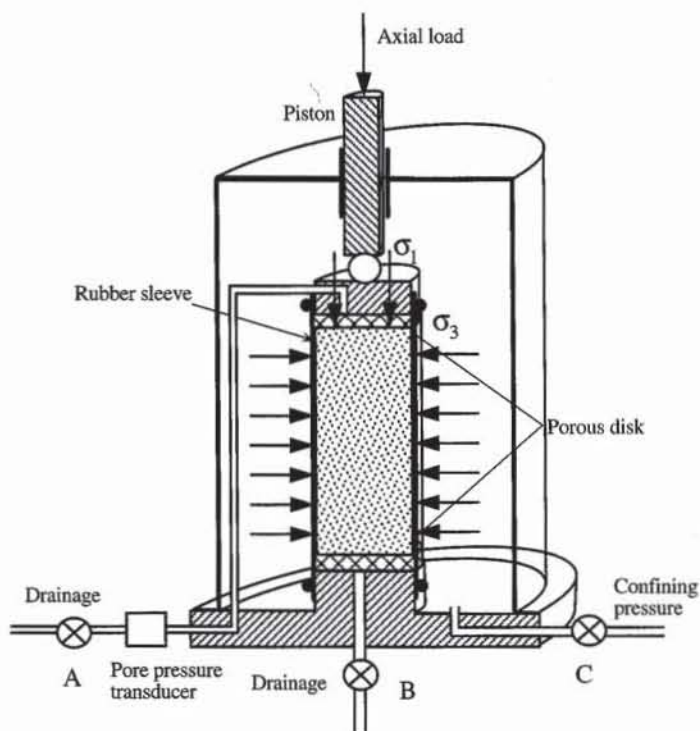


Figure 1 Experimental setup of triaxial test.

be long for fine-grained soils with low permeability.

Figure 2 schematizes the stress loading in σ - τ and s - t spaces during the axial compression after consolidation. As shown in Fig. 2, the axial stress σ_1 is increased while σ_3 is kept constant. The Mohr circle of total stress expands from point A (Fig. 2b) and the corresponding total stress path is AB in s - t space (Fig. 2c).

During CD tests, the drainage is opened and the excess pore pressure remains equal to zero. The total stress path AB is also an effective stress path. For fine-grained soils, the axial loading must be applied very slowly so that the excess pore pressure has time to dissipate through the drainage system.

CU triaxial tests are similar to CD tests except for the drainage which is closed during axial compression. This lack of drainage constrains the volume change of fully saturated specimens and creates an excess pore pressure. As shown in Fig. 2c, the prescribed total stress path AB does not coincide with the nonlinear effective stress path AB'. The effective stress path AB' and effective Mohr circles are related to their total stress counterparts through the measured excess pore pressure as shown in Fig. 2b and c.

During UU triaxial tests, the consolidation phase is omitted and the sample is sheared without knowing its effective stress, but the compression phase is the same as that of CU tests.

SATURATION OF SPECIMENS

The triaxial specimen must be fully saturated to measure its volume change in drained tests and to generate pore pressure in undrained tests. Its degree of saturation S_r is checked directly in the triaxial cell by determining the coefficient B

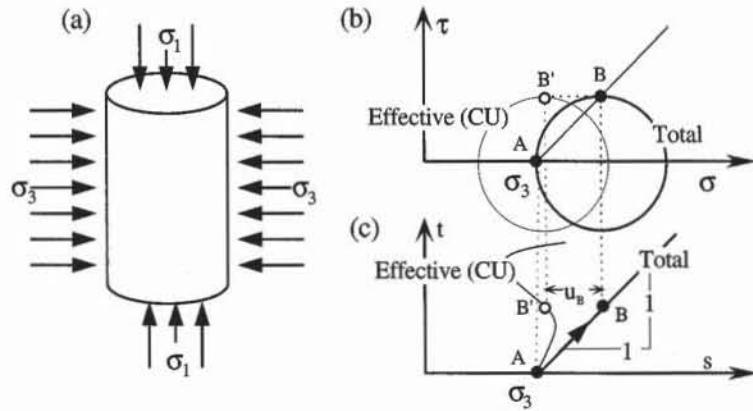


Figure 2 CU and CD triaxial compressions: (a) applied stresses, (b) effective and total stress Mohr circles in σ - τ space, and (c) effective and total stress paths in s - t space.

$$B = \frac{\Delta u}{\Delta \sigma_3} \tag{3}$$

where $\Delta \sigma_3$ is a small increase in confining pressure applied to the sample, and Δu is the resulting change in pore pressure measured under undrained conditions. $\Delta \sigma_3$ should be small enough (e.g., 5 to 10 kPa) to prevent the consolidation of partially saturated specimens. During the total stress increase $\Delta \sigma_3$, the volume change ΔV_{sk} of the sample is equal to the volume change ΔV_f of interstitial water

$$\Delta V_{sk} = V_{sk} \frac{\Delta \sigma'_3}{B_s} = V_{sk} \frac{\Delta \sigma_3 - \Delta u}{B_s} = \Delta V_f = V_f \frac{\Delta u}{B_f} = n V_{sk} \frac{\Delta u}{B_f} \tag{4}$$

where $\Delta \sigma'_3$ is the change in effective stress, V_{sk} the initial volume of soil, B_s the bulk modulus of soil, $V_f = n V_{sk}$ the initial volume of water, B_f the bulk modulus of interstitial water, and n the porosity. Using Eq. 4, B is

$$B = \frac{1}{1 + n \frac{B_s}{B_f}} \tag{5}$$

The interstitial water of nearly saturated soils is a mixture of water and gas which has the following bulk modulus B_f (Bardet and Sayed, 1993):

$$\frac{1}{B_f} = \frac{1}{B_w} + \frac{1 - S_r}{p_B} \tag{6}$$

where S_r is the degree of saturation, B_w the bulk modulus of pure water (2,200 MPa), and p_B the absolute fluid pressure, also referred to as backpressure. $p_B = 101$ kPa for water at atmospheric pressure. As shown in Fig. 3, Eq. 6 predicts that B_f is strongly influenced by S_r . Using Eqs. 5 and 6, and neglecting B_s compared to B_w , B and S_r are related through

$$B \approx \frac{1}{1 + n \frac{B_s}{p_B} (1 - S_r)} \quad \text{and} \quad S_r = 1 - \frac{p_B}{n B_s} \left(\frac{1}{B} - 1 \right) \tag{7}$$

Figure 4 shows the effect of S_r on B at various ratios B_s/p_B . These effects are especially important for soils with large bulk modulus. Under undrained conditions, this effect is reduced, but not eliminated with large back pressure p_B .

Eq. 7 implies that the sample is fully saturated when $B = 1$. In practice, $B \geq 99.5\%$ is satisfactory for undrained tests, and $B \geq 98\%$ is acceptable for drained tests. When B is too small, S_r can be increased under drained conditions by increasing the back pressure p_B and introducing additional deaired water into the voids, which will forces some air to be absorbed into solution. p_B and σ_3 should be simultaneously increased so that the differential pressure across the triaxial membrane does not change. The increase in backpressure Δp_B required to increase S_r from an initial value S_0 to a final value S_f is given by Lowe and Johnson (1960):

$$\frac{\Delta p_B}{p_B} = \frac{0.98 (S_f - S_0)}{100 - 0.98 S_f} \quad (8)$$

where p_B is the initial back pressure, and S_f and S_0 are in percent. For instance, Eq. 9 indicates that the backpressure p_B should be increased by 495 kPa to get a final saturation $S_f = 100\%$, when $S_0 = 90\%$ and p_B was initially atmospheric ($p_B = 101$ kPa).

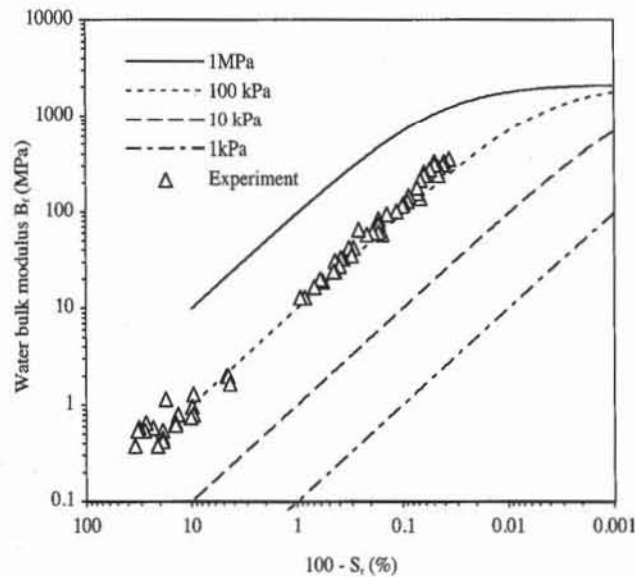


Figure 3 Variation of bulk modulus of water with water pressure and degree of saturation S_r (after Bardet and Sayed, 1993).

RATE OF LOADING FOR CU AND CD TESTS

In CU and CD triaxial tests, the loading rate is selected so that the pore pressure remains uniform within the tested specimen.

In the CD test, the excess pore pressure should remain negligible. The loading rate must be slow enough to allow for the excess pore pressure to dissipate through the pervious boundaries. The loading rate of the CD triaxial test is selected by first determining the time t_f required to reach failure by from Table 1

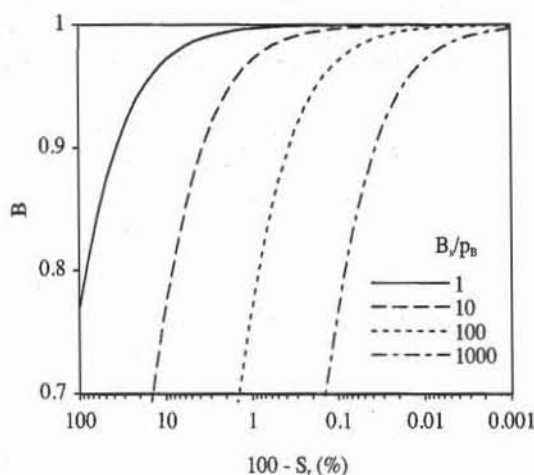


Figure 4 Variation of coefficient B versus degree of saturation S_r ($n = 0.3$) for various normalized values of soil bulk moduli B_s/p_B .

(after Head, 1986). In Table 1, t_{100} is the time to complete the primary compression, which can be determined by measuring the volume change during the consolidation phase of the triaxial test (see Chapter 6-1 for the determination of t_{100}). The side drain of Table 1 refers to a thin filter paper which is wrapped around the sample to shorten the duration of the consolidation phase.

The axial strain ϵ_p required to reach the soil peak strength is then estimated. The maximum rate v of axial displacement is chosen so that axial strain ϵ_p is reached after time t_f :

$$v = \frac{\epsilon_p H_0}{12.7 t_{100}} \quad (9)$$

where H_0 is the initial sample height.

TABLE 1
Time t_f to reach failure (after Head, 1986)

Type of test	No side drain	With side drain
CU	$0.51 \times t_{100}$	$1.8 \times t_{100}$
CD	$8.5 \times t_{100}$	$14 \times t_{100}$

In the CU test, the pore pressure should be distributed uniformly, although its overall value varies when the sample is sheared. The loading rate is determined by using Table 1 as for CD tests. The loading rate of CU tests is about 10 times faster than those of CD tests. During CU tests, the pore water is practically immobile, and the excess pore pressure is more rapidly and uniformly distributed than during CD tests.

REFERENCES

- BARDET, J. P., and H. SAYED, 1993, Velocity and attenuation of compressional waves in nearly saturated soils, *Soil Dyn. Earthquake Eng.*, Vol. 12, No. 7, pp. 391-402.

- BISHOP, A. W., and D. J. HENKEL, 1962, *The Measurement of Soil Properties in the Triaxial Test*, 2nd ed., Edward Arnold, London, pp. 228.
- HEAD, K. H., 1986, *Manual of Soil Laboratory Testing, Volume 3: Effective Stress Tests*, John Wiley & Sons, New York, pp. 951-956, 1001-1053.
- HOLTZ, R. D., and W. D. KOVACS, 1981, *An Introduction to Geotechnical Engineering*, Prentice-Hall, Englewood Cliffs, NJ, pp. 449-519.
- LAMBE, T. W., and R. V. WHITMAN, 1979, *Soil Mechanics, SI Version*, John Wiley & Sons, pp. 116-121, 135-150.
- LOWE, J., and T. C. JOHNSON, 1960, Use of backpressure to increase degree of saturation of triaxial test specimens, *Proceedings of the ASCE Research Conference on Shear Strength of Cohesive Soils*, Boulder, CO, pp. 819-836.

REVIEW QUESTIONS

1. How many types of triaxial tests are there?
2. Define UU, CU, and CD triaxial tests.
3. Sketch a typical triaxial cell with its basic components.
4. Define the B coefficient. What is it used for?
5. How is the rate of loading defined for CD triaxial tests?

7-7

Triaxial Tests on Coarse-Grained Soils

OBJECTIVE

There are two main types of triaxial tests for coarse-grained soils: CU and CD tests. CD tests are used to determine the cohesion and friction angle for various densities and confining pressures, while CU tests are used to calculate the undrained shear strength. UU triaxial tests are not performed on coarse-grained soils.

EQUIPMENT

The equipment for triaxial tests on coarse-grained soils includes:

- Loading frame with a 50 kN capacity (Fig. 1). Strain- or stress-controlled loading devices may be used to load the soil specimen. Strain-controlled devices compress the specimen at a predetermined rate of displacement, whereas stress-controlled devices vary the axial load at a fixed rate. Strain-controlled devices are preferable because they are capable of detecting the strain-softening properties of soils. Strain-controlled devices should have a loading speed of about 1 mm/min.
- Triaxial cell. As shown in Fig. 2, the triaxial cell consists primarily of a head plate, a baseplate, and a transparent plastic cylinder. The baseplate has an inlet to pressurize the chamber and two inlets to saturate and drain the specimen through its base and cap. The head plate has a vent valve to let air out when the chamber is filled with fluid. The cylinder, head plate, and baseplate are tightly held together by tie rods, and their joints are sealed with rubber gaskets. The piston friction is reduced using linear ball bushings. Leakage around the piston is reduced by means of O-rings. For cohesionless soils, the sample diameter is about 7.5 cm.
- Calibrated load ring for measuring the axial force. A capacity of 20 kN is suitable for most purposes. A larger capacity (e.g., 50 kN) may be required for high confining pressure. The load ring may be replaced by a load transducer of similar capacity.

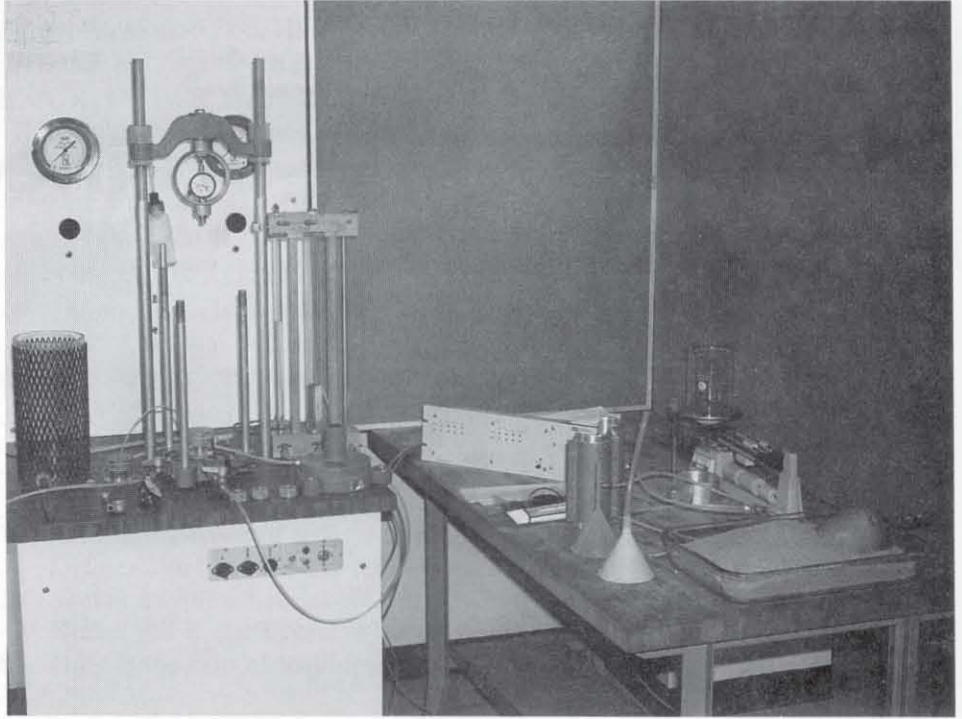


Figure 1 Loading frame device and triaxial test equipment. On the left table, the dismantled triaxial cell includes the upper and lower caps, the head plate, the base plate, and the transparent plastic cylinder reinforced with a steel mesh. On the right table, the equipment for the sample fabrication includes the split mold, membranes and O-rings, vacuum grease, funnels of various sizes, and a scale.

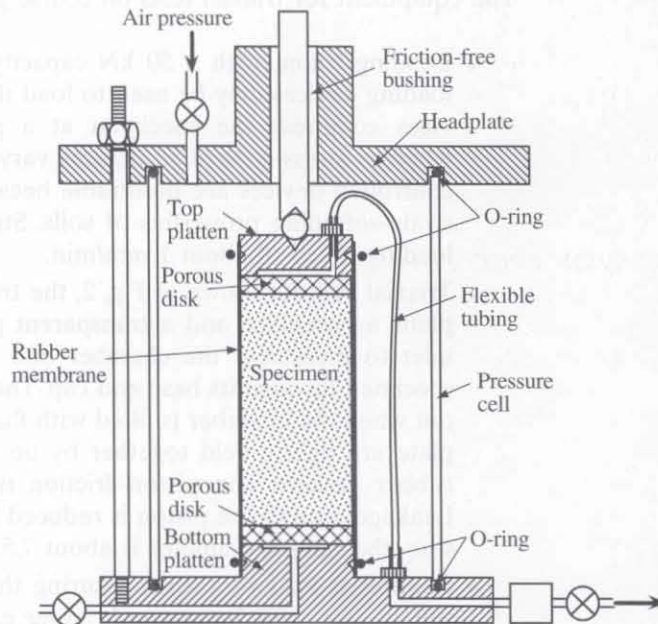


Figure 2 Components of the triaxial cell.

- Pressure transducer for measuring the pore pressure during CU tests. The transducer range should be 0 to 1000 kPa. It should have a bleed valve for saturation.
- Two pressure gages for measuring the confining pressure and backpressure, with a capacity of 1000 kPa.
- Dial gage for measuring the axial displacements sensitive to 0.01 mm and having a full range of 2.5 cm. The dial gage may be replaced by a calibrated LVDT transducer having similar range and sensitivity.
- Base and head caps. These are constructed of a lightweight noncorrosive material and have porous stones and drainage connections.
- Rubber sleeves. These encase the specimen and provide a reliable protection against leakage, with the minimum lateral restraint to the specimen. Membrane thickness ranges from 0.05 to 0.25 mm. They should be carefully inspected prior to use and should be discarded if they have flaws or pinholes.
- Four O-rings of diameter slightly smaller than the base and head caps are required to fasten the membrane.
- Equipment for preparing specimens. A split mold is required to hold the rubber sleeve and construct cohesionless soils (see Fig. 4). The internal diameter of the mold (e.g., 7.5 cm) will give the approximate diameter of the specimen. A funnel or spoon for placing the material inside the mold, and a tamping hammer or vibratory equipment are also necessary.
- Saturation equipment. An air regulator and a pressure gage for controlling the backpressure, similar to those used to control the chamber pressure. A calibrated burette or standpipe capable of measuring volume changes. This burette, which is connected to the backpressure line, measures the volume change of the specimen during the isotropic and shear phases of the triaxial test.

Other items of equipment are as follows:

- Deaired water produced as in Chapter 4-2.
- Vacuum grease.
- Vacuum and air pressure supply.
- Balance sensitive to 0.01 g.
- Equipment necessary to determine specific gravity.

PREPARATION OF SPECIMENS

1. Weigh an amount of material slightly larger than the one to be used for the test specimen.

2. Place the membrane with two O-rings on the bottom platen, then assemble and mount the split mold. Fold back the membrane on the top rim of the mold as shown in Fig. 3.

3. Evacuate the air between the membrane and the membrane stretcher using a vacuum pump (see Fig. 3).

4. Pour the sand inside the forming jacket by means of a funnel or a spoon (see Fig. 4 and the sample construction in Chapter 4-2). The desired density may be achieved by vibrating the specimen. A specimen that is properly formed generally deforms in a symmetric way when it is tested.

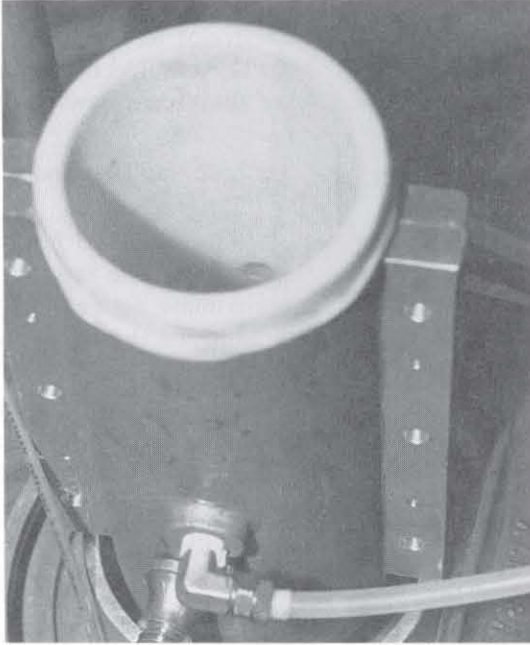


Figure 3 The split mold is mounted on the bottom cap. The membrane is stretched in place by applying vacuum.

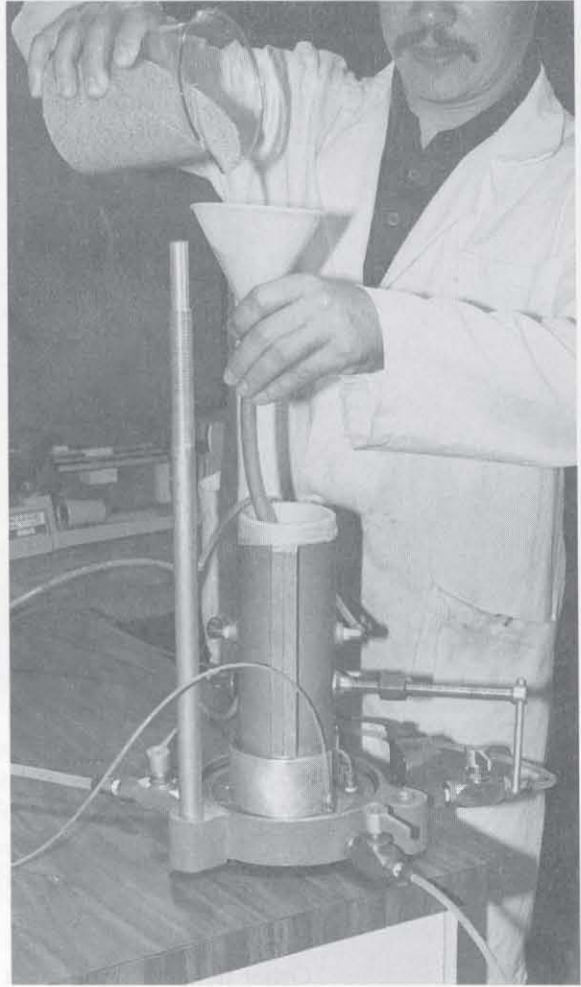


Figure 4 Loose samples are constructed by pouring sand into the mold with a funnel. Denser samples are obtained by tamping or vibrating.

5. Weigh the unused material to calculate the dry sample weight.
6. After having filled the forming jacket with sand to the desired height, place the specimen cap on top of specimen, roll the membrane over the specimen cap and base, and fasten it with O-rings (see Fig. 5).
7. As shown in Fig. 6, open valve *D*, close valve *E*, and connect connector *I* to the vacuum line. This applies vacuum to the inside of the sample through valve *D*. If there is a leak or hole in the membrane, bubbles will keep forming in the bubble trap. If the leak is too important, the sample must be discarded and a new sample must be prepared. In the absence of bubbles, open and remove the split mold (see Fig. 7). The sample is now held together by an internal vacuum. Its initial height and diameter are now measured. The vacuum intensity should be kept to a small value (e.g., -20 kPa) to avoid the consolidation of the specimen.
8. Assemble the triaxial chamber (see Fig. 8) and place it on the loading device.
9. Disconnect connector *G* and open valve *F* to fill the triaxial cell with water (Fig. 9).

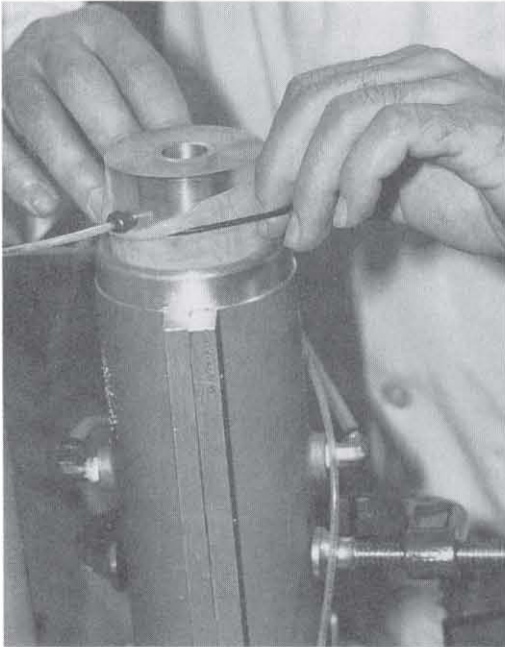


Figure 5 After placing the cap on top of the specimen, the membrane is rolled over the top cap and is fastened by using O-rings.

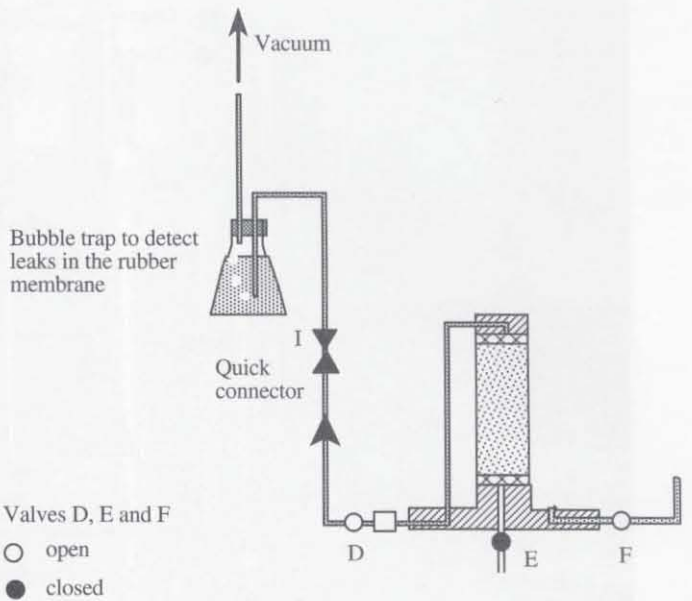


Figure 6 Application of vacuum inside the sample.



Figure 7 Once the vacuum is applied internally to the sample, the split mold is removed.

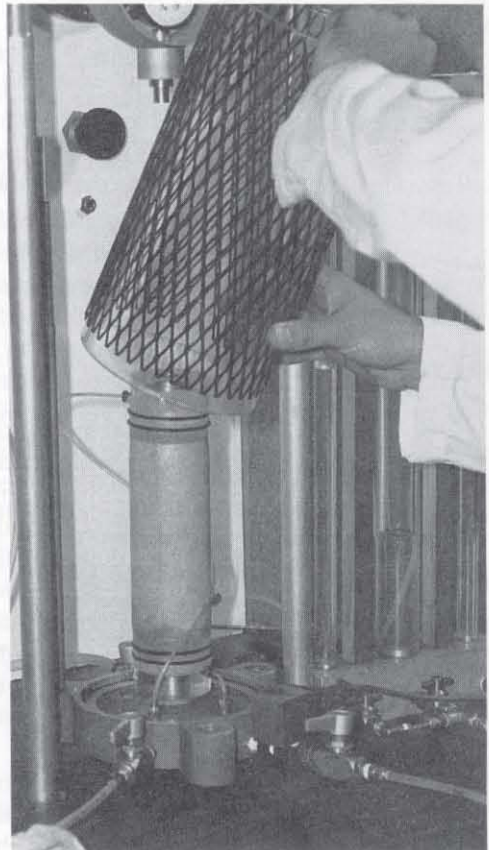


Figure 8 The triaxial cell is assembled by adding the transparent chamber and the top plate, and by securing the mounting bolts firmly.

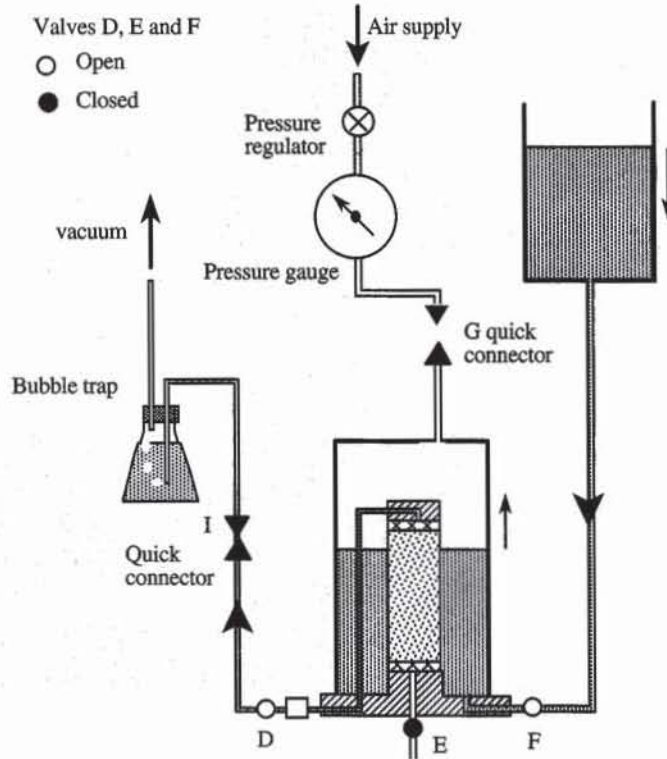


Figure 9 Filling of triaxial cell with water, and application of a small confining pressure to hold the sample together.

10. When the triaxial chamber is almost completely filled with water, close valve *F* and connect the *G* connector.

11. Apply a small amount of confining pressure with the pressure regulator (e.g., 20 kPa), then close valve *D*. At this stage the sample is held together by the external confining pressure, no longer by the internal vacuum.

SATURATION OF SPECIMENS

The triaxial samples for CU and CD triaxial tests must be fully saturated before being isotropically consolidated and sheared. The saturation is tested by closing the drainage system, by applying a small increase $\Delta\sigma_3$ in confining pressure, and by measuring the resulting change in pore pressure Δu . The sample is fully saturated when the coefficient $B = \Delta u / \Delta\sigma_3 = 1$, and partially saturated when $B < 1$.

For CU tests, complete saturation ($B \geq 99.5\%$) is required to generate a meaningful pore pressure. Otherwise, a partial saturation results in erroneous pore pressure and undrained shear strength. The degree of saturation can be increased by increasing the backpressure and confining pressure simultaneously so that the soil effective stress and differential pressure across the sample membrane do not change.

For CD tests, saturation is not as critical as for CU tests because it is used only to measure volume change. Partial saturation leads only to slightly underestimating the volume change. $B \geq 98\%$ is satisfactory for drained tests.

The drainage lines and porous disks should be fully saturated with deaired water. The drainage lines are as short as possible and made of thick-walled, small-

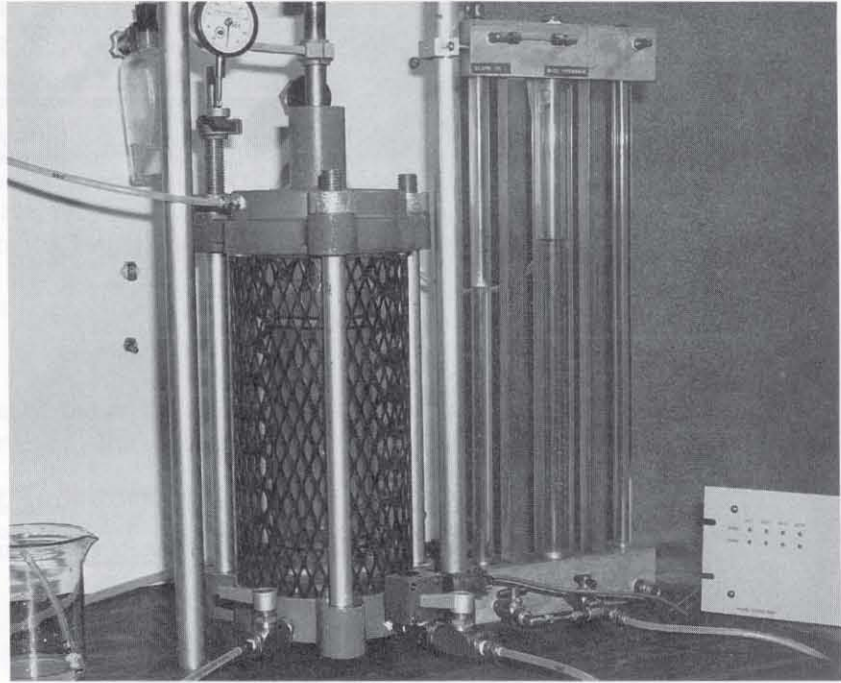


Figure 10 Triaxial cell and volume-change and saturation burette.

bore tubing to ensure minimum changes in volume when the applied pressure varies. During the saturation phase, the chamber pressure should be only slightly higher than the backpressure (e.g., 20 kPa) in order to hold the specimen without consolidating it. The specimen is saturated as follows:

1. Fill the saturation burette (Fig. 10) with deaired water. As shown in Fig. 11, disconnect connector *H*, close valve *B*, and open valve *A*. Close valve *A* when the saturation burette is almost full.
2. Open valves *E* and *D* and close valve *C*. Reconnect connector *H* to the backpressure line and apply 20 kPa of backpressure. Open valve *B*. As shown in Fig. 11, the water of the saturation burette is pushed through the soil specimen until there are no more air bubbles in the saturation line. If necessary, the saturation burette may be refilled with deaired water.
3. To check the saturation, close valves *B*, *D*, and *E*, increase the confining pressure by 10 kPa, measure the resulting increase in pore pressure Δu , and calculate the *B* coefficient. If its value is not satisfactory, repeat steps 1 and 2.
4. If the repetition of steps 1 and 2 does not increase the *B* coefficient, open valves *E* and *B* and apply equal increments of confining pressure and backpressure simultaneously. Check the *B* coefficient again and if necessary, increase confining and backpressures within reasonable limits. The backpressure must always remain slightly smaller than the confining pressure: otherwise, the sample either consolidates or collapses. If the value of *B* is not satisfactory, repeat steps 2 to 4. One may also saturate the samples after the consolidation phase.
5. Open valve *A* to adjust the water level at the middle of the volume-change burette. Close valve *A*, open valves *C* and *E*, and record the level in the measuring burette. The saturation phase is now completed.

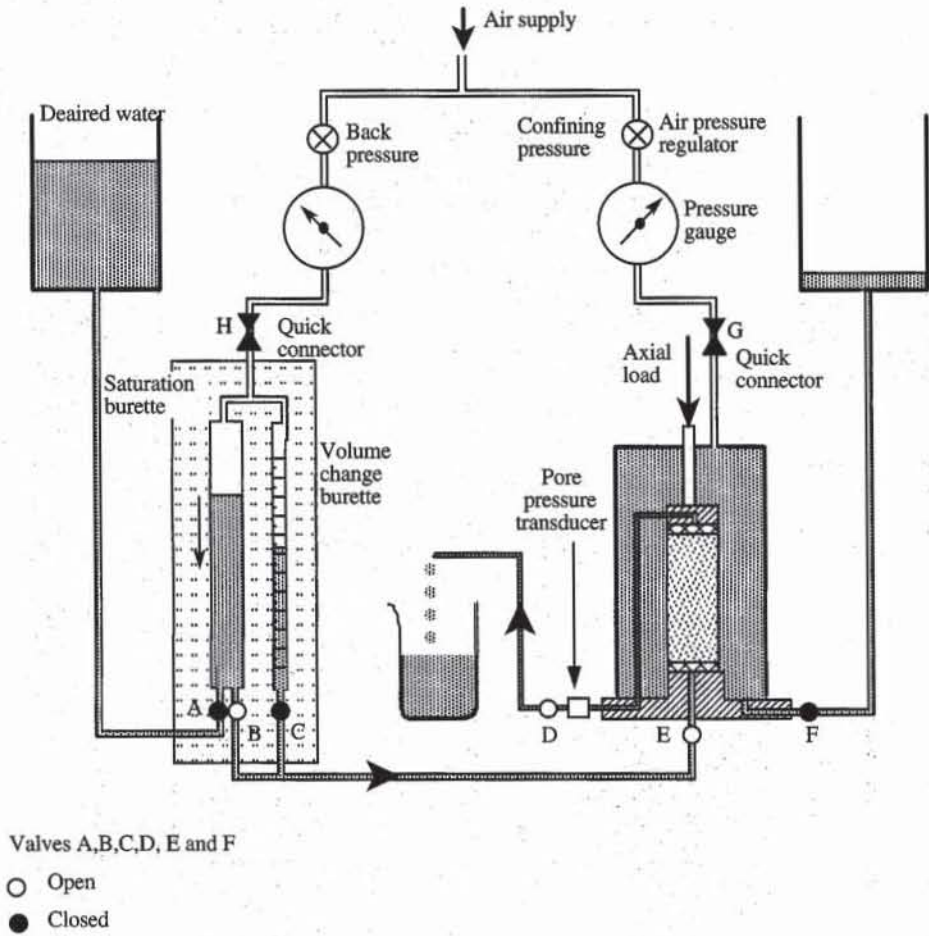


Figure 11 Schematic diagram showing the saturation of soil sample.

CONSOLIDATION PHASE

After saturation, the sample can be isotropically or K_0 consolidated.

For isotropic consolidation, keep the backpressure constant, and increase the cell pressure until the difference between the cell pressure and backpressure becomes equal to the desired confining pressure. Open valves C and E, and let the specimen consolidate under the applied confining pressure. Measure the volume change in the volume-change burette.

For K_0 consolidation, the vertical effective stress σ'_1 is increased with the radial effective stress σ'_3 to reach the initial effective stress state at which $\sigma'_1 = K_0 \sigma'_3$ where K_0 is the coefficient of earth pressure at rest. K_0 consolidation is not covered in this book. Additional information can be found in Head (1986).

SHEAR PHASE

For drained triaxial tests, valves B and D are closed and valves C and E are open. The volume change of the sample is measured in the volume-change burette. For undrained tests, valves D and E are closed and the pore pressure is measured using the pore pressure transducer.

1. Select a loading rate, about 0.5% of axial strain per minute.
2. Start loading and record simultaneously the applied axial load, piston displacement, and volume change for drained tests (porewater pressure for undrained tests).
3. After having completed the axial loading (20 to 25% axial strain), release the back pressure and decrease the confining pressure to 30 kPa. Open valve *F* to flush the pressure fluid gently from the pressure cell. Close valve *F* when the chamber is empty, remove the confining pressure, and then dismantle the triaxial cell.

COMPUTATIONS

Figure 12 shows the height, average area, and total volume of the sample after construction, after saturation, after consolidation, and during shear.

After Construction

The initial dry density γ_{d0} and void ratio e_0 of the sample are

$$\gamma_{d0} = \frac{W}{V_0} \quad \text{and} \quad e_0 = \frac{G_s \gamma_w}{\gamma_{d0}} - 1 \tag{1}$$

where W is the dry weight of the sample, $V_0 = H_0 A_0$ the initial sample volume, $A_0 = \pi D_0^2 / 4$ the average cross-sectional area of the initial sample, D_0 the initial diameter, G_s the soil specific gravity, and γ_w the water unit weight.

After Saturation

During the saturation phase, the sample size is assumed to be constant. There is no accurate way to measure its volume change while it is saturated. As shown in Fig. 12, the heights, average areas, and volumes of the samples are the same after construction and after saturation. As mentioned previously, the upward flow of interstitial water must be slow to prevent the sample from expanding or compacting while it is saturated.

After Consolidation

The volume V_c of the sample after the isotropic consolidation is

$$V_c = V_0 - \Delta V_c \tag{2}$$

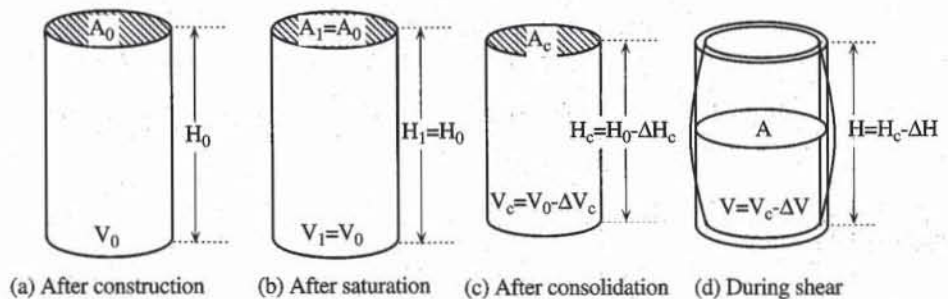


Figure 12 Height, average area, and volume of sample after the construction phase, saturation phase, and consolidation phase, and during the shear phase.

where ΔV_c is the volume change caused by consolidation and measured on the volume-change burette. The specimen height H_c and average area A_c after consolidation are calculated by assuming that axial and radial strains are equal:

$$H_c = H_0 \left(1 - \frac{1}{3} \frac{\Delta V_c}{V_0} \right) \quad \text{and} \quad A_c = \frac{V_c}{H_c} = A_0 \frac{1 - \Delta V_c/V_0}{1 - \Delta V_c/3V_0} \quad (3)$$

After consolidation, the dry unit weight γ_{dc} and void ratio e_c are

$$\gamma_{dc} = \frac{W}{V_c} \quad \text{and} \quad e_c = \frac{G_s \gamma_w}{\gamma_{dc}} - 1 \quad (4)$$

During Shear

During the shear phase, the volume V and height H of the specimen are

$$V = V_c - \Delta V \quad \text{and} \quad H = H_c - \Delta H \quad (5)$$

where ΔV is the volume change and ΔH is the height change. Both ΔV and ΔH are measured from the beginning of the shear phase. ΔV is positive when the sample compacts, and ΔH is positive when the sample shortens. The axial strain ϵ_1 and volumetric strain ϵ_v are

$$\epsilon_1 = \frac{\Delta H}{H_c} \quad \text{and} \quad \epsilon_v = \frac{\Delta V}{V_c} \quad (6)$$

The average cross-sectional area A of the sample is

$$A = \frac{V}{H} = \frac{V_c - \Delta V}{H_c - \Delta H} = \frac{V_c}{H_c} \frac{1 - \frac{\Delta V}{V_c}}{1 - \frac{\Delta H}{H_c}} = A_c \frac{1 - \epsilon_v}{1 - \epsilon_1} \quad (7)$$

The shear stress t and normal stress s are

$$t = \frac{1}{2} (\sigma_1 - \sigma_3) = \frac{P}{A} \quad \text{and} \quad s = \frac{1}{2} (\sigma_1 + \sigma_3) = t + \sigma_3 \quad (8)$$

where P is the net applied axial load, σ_1 the axial stress, and σ_3 the constant confining pressure. $P = 0$ at the beginning of the shear phase. During the drained test, total and effective stresses are equal because there is no pore pressure (i.e., $u = 0$):

$$s' = s \quad \text{and} \quad t' = t \quad (9)$$

Young's modulus is calculated from the initial slope of the $t - \epsilon_1$ curve:

$$E = 2 \frac{\Delta t}{\Delta \epsilon_1} \quad (10)$$

where Δt is the increase in t corresponding to the increase $\Delta \epsilon_1$ in ϵ_1 . The Poisson ratio is calculated from the initial slope of the $\epsilon_v - \epsilon_1$ curve:

$$\nu = \frac{1}{2} \left(1 - \frac{\Delta \epsilon_v}{\Delta \epsilon_1} \right) \quad (11)$$

where $\Delta\varepsilon_v$ is the increase in ε_v corresponding to $\Delta\varepsilon_1$. The residual and peak friction angles are calculated using the following relation (assuming $c' = 0$):

$$\phi' = \sin^{-1} \left(\frac{\sigma'_1 - \sigma'_3}{\sigma'_1 + \sigma'_3} \right) = \sin^{-1} \left(\frac{t}{s'} \right) = \sin^{-1} \left(\frac{t}{t + \sigma_3 - u} \right) \quad (12)$$

During the undrained triaxial test ($\varepsilon_v = 0$), Eq. 7 becomes

$$A = \frac{A_c}{1 - \varepsilon_1} \quad (13)$$

The effective shear stress t' and normal stress s' are

$$s' = s - u, \quad \text{and} \quad t' = t \quad (14)$$

The shear modulus G is calculated from the initial slope of the $t - \varepsilon_1$ curve:

$$G = \frac{1}{6} \frac{\Delta t}{\Delta \varepsilon_1} \quad (15)$$

where Δt is the increase in t corresponding to $\Delta\varepsilon_1$. The peak friction angle is calculated from the maximum ratio t'/s' by using the following relation:

$$\phi'_p = \sin^{-1} \left(\frac{t'}{s'} \right)_{\max} \quad (16)$$

Example of a Drained Triaxial Test

The results of the drained triaxial test are summarized by reporting the initial dry unit weight and void ratio of the specimen and by plotting the variation of shear stress t and volumetric strain ε_v versus axial strain ε_1 . The results should include the initial Young's modulus and Poisson ratio, the peak and residual friction angles, the failure modes of the specimen, and the inclination of shear bands, if any.

Figures 13 to 15 show an example of drained triaxial test results on a fine uniform sand in a loose state. Figure 13 shows the stress-strain and volumetric responses versus axial strain, Fig. 14 shows the input/output data, and Fig. 15 lists the formulas used in Fig. 14.

Example of a Undrained Triaxial Test

The results of the undrained triaxial test are summarized by reporting the initial dry unit weight and void ratio of the specimen and by plotting the variation of shear stress t and pore pressure u versus axial strain ε_1 , and the $s'-t$ stress path. The results should include the initial shear modulus, the peak and residual undrained shear strengths, the peak and residual friction angles ϕ'_p and ϕ'_r , the failure modes of the specimen, and the inclination of shear bands, if any.

Figures 16 to 18 show an example of undrained triaxial test results on a fine uniform sand in a loose state. Figure 16 shows the stress-strain and pore pressure responses versus axial strain, and the effective $s'-t$ stress path, Fig. 17 shows the input/output data, and Fig. 18 lists the formulas used in Fig. 17. As shown in Fig. 16, the loose sand undergoes a peak failure, softens, and then hardens as the pore pressure decreases. The residual undrained shear strength is larger than the peak undrained shear strength.

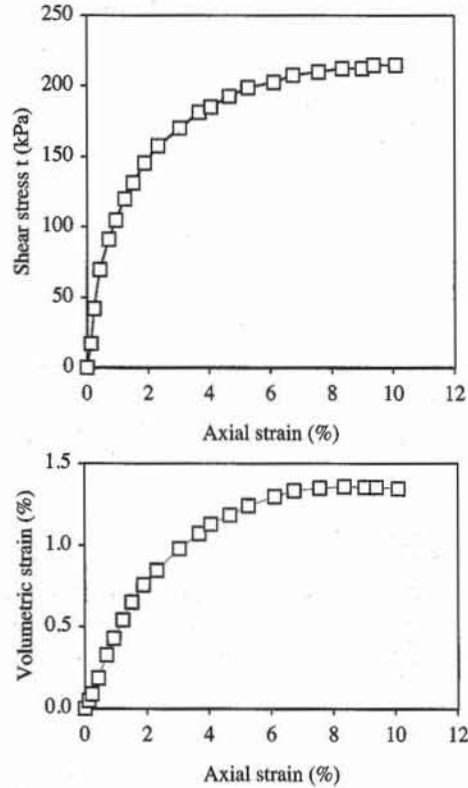


Figure 13 Stress-strain and volumetric responses of loose Hostun sand during drained triaxial test.

REVIEW QUESTIONS

1. Which soil properties are determined from CD and CU triaxial tests on coarse-grained sand?
2. Describe briefly the preparation of a sand specimen.
3. What is the purpose of the split mold?
4. Why do we use a rubber membrane in triaxial tests?
5. How is it possible to detect a small leak in a rubber membrane?
6. Why should the vacuum be kept to a low level during sample construction?
7. How is saturation checked in triaxial tests?
8. Why should the sample be saturated in CU and CD tests?
9. How is the corrected area defined in a CD triaxial test?

	A	B	C	D	E	F
1	Drained triaxial test					
2	Analyst name: <i>A. Comtet</i>					
3	Date: <i>Apr-78</i>					
4	Sample identification: <i>Loose Hostun sand</i>					
5						
6	Weight of dry sample $W = 1164$ g					
7	Initial height of sample $h_0 = 19.5$ cm					
8	Initial sample diameter $D_0 = 6.95$ cm					
9	Soil specific gravity $G_s = 2.65$					
10	Confining pressure $\sigma_3 = 200$ kPa					
11	Back pressure $\sigma_b = 0$ kPa					
12	Saturation coefficient $B = 99$ %					
13	Rate of loading $v = 2$ mm/min					
14	Initial void ratio $e_0 = 0.684$					
15	Initial dry unit weight $\gamma_{d0} = 15.42$ kN/m ³					
16	Volume change during consolidation $\Delta V_c = 1.00$ cm ³					
17	Void ratio after consolidation $e_c = 0.682$					
18	Dry unit weight after consolidation $\gamma_d = 15.44$ kN/m ³					
19	Height after consolidation $h_c = 19.49$ cm					
20	Volume after consolidation $V_c = 738.77$ cm ³					
21	Area after consolidation $A_c = 37.90$ cm ²					
22	Initial Young's modulus $E = 37.14$ MPa					
23	Initial Poisson ratio $\nu = 0.30$					
24	Peak friction angle $\phi_p = 31.19$ deg					
25	Residual friction angle $\phi_r = 31.19$ deg					
26						
27	Axial displacement (mm)	Axial force (kN)	Volume change (cm ³)	Axial strain (%)	Shear stress (kPa)	Volumetric strain (%)
28	Δh	F	ΔV	ϵ_p	t	e_v
29	0.00	0.000	0.00	0.00	0.0	0.00
30	0.02	0.127	-0.36	0.12	16.8	0.05
31	0.04	0.319	-0.67	0.22	42.0	0.09
32	0.08	0.529	-1.36	0.43	69.6	0.18
33	0.14	0.692	-2.43	0.71	91.0	0.33
34	0.18	0.799	-3.17	0.94	104.8	0.43
35	0.24	0.915	-4.01	1.23	119.9	0.54
36	0.29	1.003	-4.82	1.51	131.2	0.65
37	0.37	1.112	-5.58	1.89	145.0	0.76
38	0.45	1.212	-6.24	2.33	157.6	0.84
39	0.59	1.317	-7.22	3.05	170.1	0.98
40	0.72	1.412	-7.91	3.67	181.4	1.07
41	0.79	1.446	-8.33	4.06	185.1	1.13
42	0.91	1.513	-8.76	4.67	192.6	1.19
43	1.03	1.571	-9.16	5.27	198.8	1.24
44	1.19	1.614	-9.59	6.12	202.6	1.30
45	1.32	1.665	-9.84	6.76	207.5	1.33
46	1.48	1.699	-9.97	7.58	210.0	1.35
47	1.63	1.733	-10.03	8.36	212.4	1.36
48	1.76	1.746	-10.01	9.02	212.4	1.36
49	1.83	1.774	-9.99	9.40	214.9	1.35
50	1.97	1.787	-9.95	10.10	214.8	1.35

Figure 14 Example of data set for drained triaxial test on sand.

	D	E	F
14	Initial void ratio $e_0 = =Gs*9.8/gd0-1$		
15	Initial dry unit weight $\gamma_{d0} = =W/(PI()*d0^2/4*h0)*9.8$		kN/m ³
16	Volume change during consolidation $\Delta V_c = 1$		cm ³
17	Void ratio after consolidation $e_c = =Gs*9.8/gd-1$		
18	Dry unit weight after consolidation $\gamma_d = =W/(PI()*d0^2/4*h0-DVc)*9.8$		kN/m ³
19	Height after consolidation $h_c = =h0*(1-DVc/(h0*PI()*d0^2/4)/3)$		
20	Volume after consolidation $V_c = =h0*PI()*d0^2/4-DVc$		
21	Area after consolidation $A_c = =Vc/hc$		
22	Initial Young's modulus $E = =SLOPE(E29:E31,D29:D31)*2/10$		
23	Initial Poisson ratio $\nu = =(1-SLOPE(F29:F31,D29:D31))/2$		
24	Peak friction angle $\phi_p = =ASIN(MAX(q)/(MAX(q)+sc))*180/PI()$		
25	Residual friction angle $\phi_r = =ASIN(E50/(E50+sc))*180/PI()$		

	D	E	F
	Axial strain (%)	Shear stress (kPa)	Volumetric strain (%)
27			
28	eps	t	ev
29	=Dh/hc*100	=F/Ac*(1-eps/100)/(1-ev/100)/2*10000	=-DV/Vc*100
30	=Dh/hc*100	=F/Ac*(1-eps/100)/(1-ev/100)/2*10000	=-DV/Vc*100

Figure 15 Formulas used in Fig. 14.

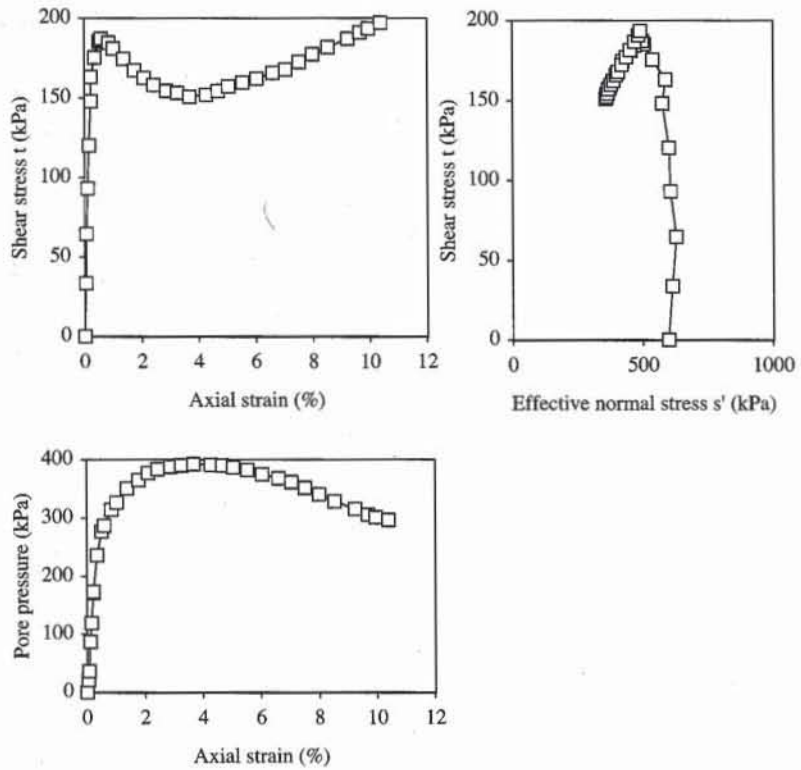


Figure 16 Stress-strain and pore pressure responses, and effective $s'-t$ stress path of loose Hostun sand during undrained triaxial test.

	A	B	C	D	E	F	G
1	Undrained triaxial test						
2	Analyst name: <i>A. Comtet</i>						
3	Date: <i>Apr-78</i>						
4	Sample identification: <i>Loose Hostun sand</i>						
5							
6	Weight of dry sample $W = 1185$ g						
7	Initial height of sample $h_0 = 20.1$ cm						
8	Initial sample diameter $D_0 = 6.92$ cm						
9	Soil specific gravity $G_s = 2.65$						
10	Confining pressure $\sigma_3 = 600$ kPa						
11	Back pressure $\sigma_b = 0$ kPa						
12	Saturation coefficient $B = 99$ %						
13	Rate of loading $v = 2$ mm/min						
14	Initial void ratio $e_0 = 0.691$						
15	Initial dry unit weight $\gamma_{d0} = 15.36$ kN/m ³						
16	Volume change during consolidation $\Delta V_c = 2.00$ cm ³						
17	Void ratio after consolidation $e_c = 0.686$						
18	Dry unit weight after consolidation $\gamma_d = 15.40$ kN/m ³						
19	Height after consolidation $h_c = 20.08$ cm						
20	Volume after consolidation $V_c = 753.96$ cm ³						
21	Area after consolidation $A_c = 37.54$ cm ²						
22	Shear modulus $G = 14.45$ MPa						
23	Peak friction angle $\phi_p = 25.14$ deg						
24	Residual friction angle $\phi_r = 23.20$ deg						
25	Peak undrained shear strength $S_u = 197.09$ kPa						
26	Residual undrained shear strength $S_{ur} = 197.09$ kPa						
27							
28	Axial displacement (mm)	Axial force (kN)	Pore pressure (kPa)	Axial strain (%)	Shear stress (kPa)	Effective normal stress (kPa)	t/s'
29	Δh	F	u	eps	t	s'	ratio
30	0.00	0.000	0.00	0.00	0.0	600.0	0.00
31	0.01	0.252	20.80	0.04	33.6	612.8	0.05
32	0.01	0.486	36.29	0.07	64.6	628.3	0.10
33	0.02	0.700	87.26	0.12	93.1	605.8	0.15
34	0.03	0.905	118.72	0.15	120.3	601.6	0.20
35	0.04	1.114	171.12	0.22	148.0	576.9	0.26
36	0.04	1.228	173.14	0.22	163.2	590.1	0.28
37	0.07	1.323	236.03	0.35	175.6	539.6	0.33
38	0.10	1.399	276.99	0.52	185.3	508.3	0.36
39	0.12	1.413	286.83	0.59	187.0	500.2	0.37
40	0.17	1.397	314.12	0.85	184.5	470.4	0.39
41	0.20	1.373	326.23	1.01	181.0	454.8	0.40
42	0.28	1.329	350.02	1.38	174.5	424.5	0.41
43	0.36	1.280	364.59	1.77	167.4	402.8	0.42
44	0.42	1.245	376.39	2.10	162.3	385.9	0.42
45	0.49	1.215	383.18	2.44	157.9	374.7	0.42
46	0.58	1.194	387.56	2.88	154.5	366.9	0.42
47	0.66	1.188	390.58	3.26	153.1	362.5	0.42
48	0.74	1.177	391.76	3.69	151.0	359.2	0.42
49	0.86	1.194	391.00	4.29	152.2	361.2	0.42
50	0.94	1.216	389.66	4.68	154.4	364.7	0.42
51	1.01	1.243	387.17	5.05	157.2	370.0	0.42
52	1.11	1.270	381.83	5.55	159.8	377.9	0.42
53	1.22	1.297	374.22	6.05	162.2	388.0	0.42
54	1.33	1.333	367.74	6.61	165.7	398.0	0.42
55	1.42	1.355	360.89	7.06	167.7	406.8	0.41
56	1.51	1.401	351.01	7.53	172.5	421.5	0.41
57	1.61	1.446	340.13	8.00	177.2	437.1	0.41
58	1.72	1.492	328.77	8.54	181.7	453.0	0.40
59	1.86	1.546	315.49	9.24	186.9	471.4	0.40
60	1.95	1.588	305.09	9.69	191.0	485.9	0.39
61	2.00	1.615	301.25	9.97	193.7	492.4	0.39
62	2.09	1.652	296.85	10.40	197.1	500.2	0.39

Figure 17 Example of data set for undrained triaxial test on sand.

	D	E	F
14	Initial void ratio $e_0 = =Gs*9.8/gd0-1$		
15	Initial dry unit weight $\gamma_{d0} = =W/(PI()*D0^2/4*h0)*9.8$		kN/m ³
16	Volume change during consolidation $\Delta V_c = 2$		cm ³
17	Void ratio after consolidation $e_c = =Gs*9.8/gd-1$		
18	Dry unit weight after consolidation $\gamma_d = =W/(PI()*D0^2/4*h0-DVc)*9.8$		kN/m ³
19	Height after consolidation $h_c = =h0*(1-DVc/(h0*PI()*D0^2/4)/3)$		cm
20	Volume after consolidation $V_c = =h0*PI()*D0^2/4-DVc$		cm ³
21	Area after consolidation $A_c = =Vc/Hc$		cm ²
22	Shear modulus $G = =SLOPE(E30:E32,D30:D32)/6/10$		MPa
23	Peak friction angle $\phi_p = =ASIN(MAX(ratio))*180/PI()$		deg
24	Residual friction angle $\phi_r = =ASIN(G62)*180/PI()$		deg
25	Peak undrained shear strength $S_u = =MAX(q)$		kPa
26	Residual undrained shear strength $S_{ur} = =E62$		kPa

	D	E	F	G
	Axial strain (%)	Shear stress (kPa)	Effective normal stress (kPa)	t/s'
28				
29	eps	t	s'	ratio
30	=Dh/Hc*100	=F/Ac*(1-eps/100)*10000/2	=sc+q-u	=q/p
31	=Dh/Hc*100	=F/Ac*(1-eps/100)*10000/2	=sc+q-u	=q/p

Figure 18 Formulas used in Fig. 17.

EXERCISES

1. From elasticity theory, derive the relation between Young's modulus E and the Poisson ratio ν and the initial slopes of the $t-\epsilon_1$ and $\epsilon_v-\epsilon_1$ curves for CD triaxial tests.
2. From elasticity theory, derive the relation between shear modulus G and the initial slope of the $t-\epsilon_1$ curve for CU triaxial tests.

7-8 Triaxial Tests on Fine-Grained Soils

OBJECTIVE

There are three different types of triaxial tests for fine-grained soils: UU, CU, and CD tests. The CD tests are used to determine the friction angle for various densities and confining pressures, while UU and CU tests are used to define the undrained shear strength.

EQUIPMENT

The equipment for fine-grained soils is similar to that of coarse-grained soils described in Chapter 7-7. The differences are

- Loading devices. For CU and UU tests, the loading rate is about 0.05 to 2 mm/min. For CD tests, the loading speed should cover a wider range (i.e., 1 to 0.0005 mm/min).
- Triaxial cell. Smaller than for cohesionless soils. The sample diameter is about 2.5 to 3 cm.
- Membrane stretcher (Fig. 1).
- Trimming equipment similar to that used for the unconfined compression test.

PREPARATION OF SPECIMENS

The test specimen is trimmed into a cylinder as described in Chapter 7-3. As shown in Fig. 1a, two O-rings are mounted on the suction membrane stretcher, and the rubber membrane is placed as shown in Fig. 1b. The rubber membrane is drawn tightly to the membrane by applying suction (Fig. 1c) and is lowered around the soil sample (Fig. 1d). When the membrane stretcher is at the position shown in Fig. 1d, the suction is released so that the membrane sticks to the spec-

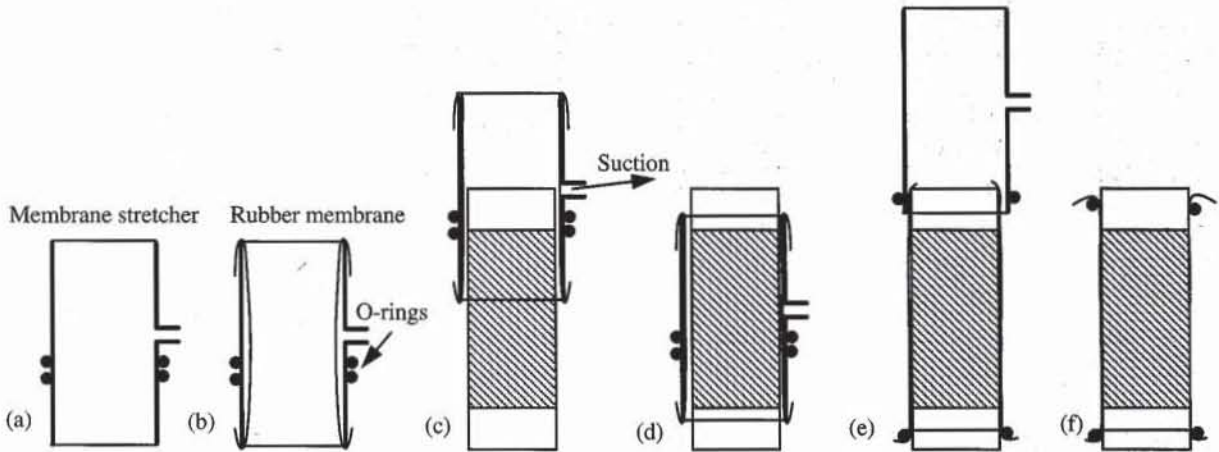


Figure 1 Successive stages to fit the rubber membrane to the cylindrical soil specimen.

imen. The membrane is rolled on the head and base caps and fastened on the base cap with an O-ring (Fig. 1e). The membrane stretcher is removed and the upper O-ring positioned on the head plate.

SATURATION OF SPECIMENS

The triaxial samples for UU, CU, and CD triaxial tests must be fully saturated before being isotropically consolidated and sheared. The saturation phase of fine-grained soils is simpler than that of coarse-grained soils, provided that the specimens were initially saturated and remain saturated during trimming. The saturation of partially saturated specimens may be extremely tedious otherwise. The saturation is checked as for cohesionless soils, by calculating the B coefficient from an isotropic increment. For CU tests, $B \geq 99.5\%$ is required to generate meaningful pore pressure. For CD and UU tests, the saturation is not as critical as for CU tests. $B > 98\%$ is considered satisfactory for drained tests.

UU, CU AND CD TRIAXIAL TESTS

The consolidation and shear phases of the CU and CD tests for fine-grained soils are similar to those of coarse-grained soils. In UU tests, the consolidation phase is performed rapidly, with closed rather than opened drainage. The pore pressure is generally not recorded during UU tests.

EXAMPLE

The results of CU tests are summarized by reporting the initial dry unit weight, water content, and void ratio of the specimen, and by plotting the variation of shear stress t and pore pressure u versus axial strain ϵ_1 , and the $s'-t$ stress path. The results should include the initial shear modulus, the peak and residual undrained shear strengths, the failure modes of the specimen, and the inclination of shear bands, if any. The results of UU tests are reported as those of CU tests but without the pore pressure variation and effective stress paths. The results of CD tests are reported as those for coarse-grained soils.

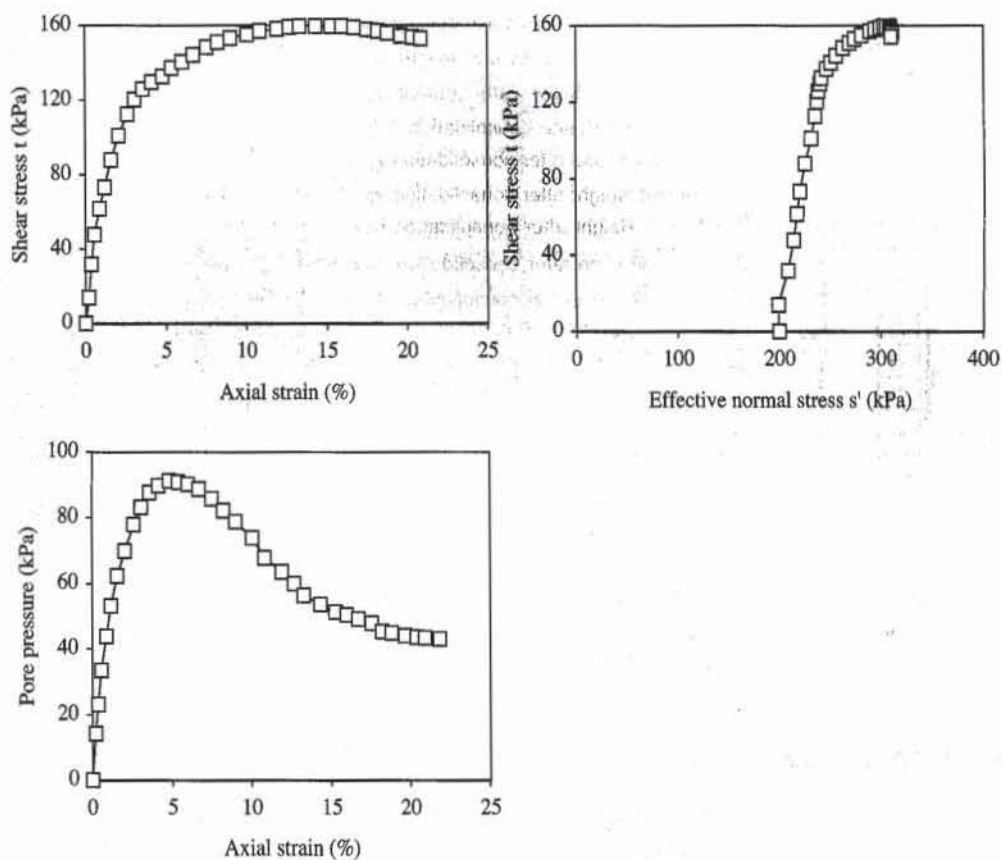


Figure 2 Stress-strain response, pore pressure response, and effective stress path of kaolinite during CU triaxial test.

Figures 2 to 4 show an example of CU triaxial test results on a normally consolidated clay. Figure 2 shows the stress-strain response, pore pressure response, and effective $s'-t$ stress path, Fig. 3 shows the input/output data, and Fig. 4 lists the formulas used in Fig. 3.

	A	B	C	D	E	F	G
12		Saturation coefficient $B =$		99 %			
13		Rate of loading $v =$		0.5 mm/min			
14		Initial void ratio $e_0 =$		0.696			
15		Initial wet density $\gamma_0 =$		19.30 kN/m ³			
16		Initial dry unit weight $\gamma_{d0} =$		15.37 kN/m ³			
17		Initial water content $w_0 =$		25.55%			
18		Volume change during consolidation $\Delta V_c =$		0.40 cm ³			
19		Void ratio after consolidation $e_c =$		0.686			
20		Dry unit weight after consolidation $\gamma_d =$		15.46 kN/m ³			
21		Height after consolidation $h_c =$		7.09 cm			
22		Volume after consolidation $V_c =$		65.97 cm ³			
23		Area after consolidation $A_c =$		9.31 cm ²			
24		Shear modulus $G =$		1.49 MPa			
25		Peak friction angle $\phi_p =$		34.41 deg			
26		Residual friction angle $\phi_r =$		29.43 deg			
27		Peak undrained shear strength $S_u =$		159.80 kPa			
28		Residual undrained shear strength $S_{ur} =$		151.55 kPa			
29							
		Axial displacement (mm)	Axial force (kN)	Pore pressure (kPa)	Axial strain (%)	Shear stress (kPa)	Effective normal stress (kPa)
30							t/s'
31		Δh	F	u	eps	t	s'
32		0.00	0.000	0.0	0.00	0.0	200.0
33		0.01	0.026	14.1	0.18	13.8	199.7
34		0.03	0.059	23.0	0.35	31.7	208.7
35		0.04	0.089	33.4	0.57	47.7	214.3
36		0.06	0.116	43.9	0.87	61.7	217.8
37		0.08	0.138	53.2	1.18	73.4	220.3
38		0.11	0.166	62.3	1.58	87.8	225.5
39		0.15	0.192	69.9	2.08	100.8	230.9
40		0.19	0.215	78.1	2.64	112.7	234.6
41		0.22	0.231	83.3	3.07	120.2	236.9
42		0.25	0.243	87.8	3.59	125.8	238.0
43		0.30	0.252	89.9	4.17	129.7	239.9
44		0.34	0.259	91.3	4.84	132.6	241.3
45		0.38	0.270	90.9	5.40	137.3	246.4
46		0.43	0.279	90.2	6.04	140.7	250.5
47		0.48	0.288	88.8	6.72	144.3	255.5
48		0.54	0.299	85.7	7.54	148.5	262.8
49		0.59	0.306	82.1	8.24	151.0	268.9
50		0.64	0.313	78.8	9.02	153.1	274.3
51		0.71	0.321	73.9	10.06	155.0	281.1
52		0.77	0.328	67.8	10.85	156.9	289.1
53		0.85	0.334	63.6	11.95	158.1	294.4
54		0.90	0.339	59.9	12.71	159.1	299.2
55		0.95	0.343	56.4	13.33	159.5	303.0
56		1.02	0.347	53.7	14.35	159.4	305.8
57		1.09	0.351	51.2	15.29	159.8	308.6
58		1.13	0.353	50.4	15.97	159.5	309.1
59		1.19	0.355	49.2	16.72	158.7	309.5
60		1.25	0.356	47.8	17.54	157.6	309.8
61		1.29	0.357	45.4	18.20	157.0	311.7
62		1.33	0.358	44.9	18.79	156.0	311.1
63		1.40	0.358	44.0	19.67	154.3	310.2
64		1.45	0.359	43.7	20.37	153.6	309.9
65		1.48	0.360	43.5	20.91	152.9	309.4
66		1.55	0.361	43.1	21.86	151.6	308.5

Figure 3 Example of data set for CU triaxial test on clay.

	C	D	E
14	Initial void ratio $e_0 = =Gs*9.8/gd0-1$		
15	Initial wet density $\gamma_0 = =Ww/(PI()*D0^2/4*h0)*9.8$		kN/m ³
16	Initial dry unit weight $\gamma_{d0} = =Wd/(PI()*D0^2/4*h0)*9.8$		kN/m ³
17	Initial water content $w_0 = =(Ww-Wd)/Wd$		
18	Volume change during consolidation $\Delta V_c = 0.4$		cm ³
19	Void ratio after consolidation $e_c = =Gs*9.8/gd-1$		
20	Dry unit weight after consolidation $\gamma_d = =Wd/(PI()*D0^2/4*h0-DVc)*9.8$		kN/m ³
21	Height after consolidation $h_c = =h0*(1-DVc/(h0*PI()*D0^2/4)/3)$		cm
22	Volume after consolidation $V_c = =h0*PI()*D0^2/4-DVc$		cm ³
23	Area after consolidation $A_c = =Vc/hc$		cm ²
24	Shear modulus $G = =SLOPE(E32:E34,D32:D34)/6/10$		MPa
25	Peak friction angle $\phi_p = =ASIN(MAX(G32:G66))*180/PI()$		deg
26	Residual friction angle $\phi_r = =ASIN(G66)*180/PI()$		deg
27	Peak undrained shear strength $S_u = =MAX(E32:E66)$		kPa
28	Residual undrained shear strength $S_{ur} = =E66$		kPa

	D	E	F	G
30	Axial strain (%)	Shear stress (kPa)	Effective normal stress (kPa)	t/s'
31	eps	t	s'	ratio
32	=Dh/h0*100	=F/Ac*(1-eps/100)*10000/2	=sc+q-u	=q/p
33	=Dh/h0*100	=F/Ac*(1-eps/100)*10000/2	=sc+q-u	=q/p

Figure 4 Formulas used in Fig. 3.



8

Elements of Experimental Techniques

- 8-1** Review of data modeling
- 8-2** Review of statistics
- 8-3** Error analysis
- 8-4** Dimensions and units
- 8-5** Report writing

8-1

Review of Data Modeling

INTRODUCTION

The modeling of data is a common exercise in engineering and science. It consists of determining the parameters of theoretical relations that give the best agreement between theoretical and experimental results. Four methods are presented here: linear regression, polynomial regression, interpolation, and nonlinear optimization.

LINEAR REGRESSION

Linear regression finds the straight line that best fits a set of data points, thus providing a linear relationship between two variables. Linear regression consists of fitting a set of n data points (x_i, y_i) to the straight-line model

$$y = Ax + B \quad (1)$$

where A is the slope and B is the intercept of the straight line with the y axis. The accuracy of fit between the straight line and data points can be evaluated by defining the total deviation E , which is the sum of the squared distances between data points and fitted points:

$$E = \sum_{i=1}^n (Ax_i + B - y_i)^2 \quad (2)$$

The best fit is obtained when E is minimum, that is, when

$$\frac{\partial E}{\partial A} = 0 \quad \text{and} \quad \frac{\partial E}{\partial B} = 0 \quad (3)$$

Equations 2 and 3 imply that

$$\frac{\partial E}{\partial A} = 2 \sum_{i=1}^n x_i (Ax_i + B - y_i) = 0 \quad \text{and} \quad \frac{\partial E}{\partial B} = 2 \sum_{i=1}^n (Ax_i + B - y_i) = 0 \quad (4)$$

Equation 4 is a system of two linear equations with two unknowns, A and B :

$$A \sum_{i=1}^n x_i^2 + B \sum_{i=1}^n x_i = \sum_{i=1}^n x_i y_i \quad (5)$$

$$A \sum_{i=1}^n x_i + Bn = \sum_{i=1}^n y_i$$

The values of A and B are

$$A = \frac{n \sum_{i=1}^n x_i y_i - \sum_{i=1}^n x_i \sum_{i=1}^n y_i}{n \sum_{i=1}^n x_i^2 - \left(\sum_{i=1}^n x_i \right)^2} \quad \text{and} \quad B = \frac{\sum_{i=1}^n y_i \sum_{i=1}^n x_i^2 - \sum_{i=1}^n x_i \sum_{i=1}^n x_i y_i}{n \sum_{i=1}^n x_i^2 - \left(\sum_{i=1}^n x_i \right)^2} \quad (6)$$

In Excel, linear regression is carried out by using the built-in functions SLOPE, INTERCEPT, and LINEST.

POLYNOMIAL REGRESSION

Linear regression analysis is generalized to nonlinear regression by using polynomials of order m :

$$P(x) = a_m x^m + a_{m-1} x^{m-1} + \dots + a_1 x + a_0 \quad (7)$$

where the $m + 1$ coefficients a_m, a_{m-1}, \dots, a_1 , and a_0 define a polynomial of order m . Equation 7 may also be written

$$P(x) = \sum_{j=0}^m a_j x^j \quad (8)$$

Polynomial regression consists of fitting a set of n data points (x_i, y_i) to a polynomial model. Linear regression is a particular polynomial regression corresponding to $m = 1$, $A = a_1$, and $B = a_0$. The accuracy of the fit between the polynomial line and data points is evaluated by the sum E of the squared distances between data points and fitted points:

$$E = \sum_{i=1}^n [P(x_i) - y_i]^2 \quad (9)$$

The best fit is obtained when E is minimum, that is, when the following $m + 1$ equations are satisfied:

$$\frac{\partial E}{\partial a_j} = 0 \quad \text{for } j = 0, 1, \dots, m \quad (10)$$

Equation 10 implies that

$$\sum_{i=1}^n [P(x_i) - y_i] \frac{\partial P(x_i)}{\partial a_j} = 0 \quad \text{for } j = 0, 1, \dots, m \quad (11)$$

Equation 11 becomes, after some algebraic manipulations:

$$\sum_{k=0}^m \sum_{i=1}^n x_i^{k+j} a_k = \sum_{i=1}^n y_i x_i^j \quad \text{for } j = 0, 1, \dots, m \quad (12)$$

Equation 12 can also be written

$$\sum_{k=0}^m G_{jk} a_k = H_j \quad \text{for } j = 0, 1, \dots, m \quad (13)$$

where $G_{jk} = \sum_{i=1}^n x_i^{k+j}$ and $H_j = \sum_{i=1}^n y_i x_i^j$. By using a matrix notation, Eq. 13 becomes

$$\mathbf{GA} = \mathbf{H} \quad (14)$$

The polynomial coefficients are therefore

$$\mathbf{A} = \mathbf{G}^{-1}\mathbf{H} \quad (15)$$

where \mathbf{G}^{-1} is the inverse matrix of \mathbf{G} , and $A_j = a_j$. For a quadratic polynomial,

$$\mathbf{A} = \begin{pmatrix} a_0 \\ a_1 \\ a_2 \end{pmatrix}, \quad \mathbf{G} = \begin{pmatrix} n & \sum_{i=1}^n x_i & \sum_{i=1}^n x_i^2 \\ \sum_{i=1}^n x_i & \sum_{i=1}^n x_i^2 & \sum_{i=1}^n x_i^3 \\ \sum_{i=1}^n x_i^2 & \sum_{i=1}^n x_i^3 & \sum_{i=1}^n x_i^4 \end{pmatrix}, \quad \text{and} \quad \mathbf{H} = \begin{pmatrix} \sum_{i=1}^n y_i \\ \sum_{i=1}^n x_i y_i \\ \sum_{i=1}^n x_i^2 y_i \end{pmatrix} \quad (16)$$

and for a cubic polynomial,

$$\mathbf{A} = \begin{pmatrix} a_0 \\ a_1 \\ a_2 \\ a_3 \end{pmatrix}, \quad \mathbf{G} = \begin{pmatrix} n & \sum_{i=1}^n x_i & \sum_{i=1}^n x_i^2 & \sum_{i=1}^n x_i^3 \\ \sum_{i=1}^n x_i & \sum_{i=1}^n x_i^2 & \sum_{i=1}^n x_i^3 & \sum_{i=1}^n x_i^4 \\ \sum_{i=1}^n x_i^2 & \sum_{i=1}^n x_i^3 & \sum_{i=1}^n x_i^4 & \sum_{i=1}^n x_i^5 \\ \sum_{i=1}^n x_i^3 & \sum_{i=1}^n x_i^4 & \sum_{i=1}^n x_i^5 & \sum_{i=1}^n x_i^6 \end{pmatrix}, \quad \text{and} \quad \mathbf{H} = \begin{pmatrix} \sum_{i=1}^n y_i \\ \sum_{i=1}^n x_i y_i \\ \sum_{i=1}^n x_i^2 y_i \\ \sum_{i=1}^n x_i^3 y_i \end{pmatrix} \quad (17)$$

Besides E , the R^2 values are used to measure the quality of fitting:

$$R^2 = 1 - \frac{\sum_{i=1}^n [y_i - P(x_i)]^2}{\sum_{i=1}^n y_i^2 - \frac{1}{n} \left(\sum_{i=1}^n y_i \right)^2} \quad (18)$$

R^2 varies from 0 to 1, the best fitting corresponding to $R^2 = 1$.

EXAMPLE OF REGRESSION USING BUILT-IN AND USER-DEFINED FUNCTIONS

Figure 1 shows a series of data points. The x coordinate is the temperature, and the y coordinate is the water unit mass. In Excel, regression analysis may be performed by using built-in functions or user-defined functions.

Figure 2 shows the linear, quadratic, and cubic fits of the data points of Fig. 1, which were obtained by using the built-in function Trendline. Trendline is based on Eqs. 1 to 18. The optimum regression coefficients and the R^2 values are also shown in Fig. 2. The quadratic and cubic regressions fit data better than the linear regression. In Fig. 2, their fitted results are so similar that they can only be distinguished by their R^2 values, which indicate a small advantage for the cubic regression.

	A	B
	Temperature (°C)	Unit mass (g/cm ³)
1		
2	x	y
3	4	1.00000
4	16	0.99897
5	17	0.99880
6	18	0.99862
7	19	0.99844
8	20	0.99823
9	21	0.99802
10	22	0.99780
11	23	0.99757
12	24	0.99733
13	25	0.99708
14	26	0.99682
15	27	0.99655
16	28	0.99627
17	29	0.99598
18	30	0.99568

Figure 1 Example of series of data point for regression analysis.

The calculations of linear, quadratic, and cubic regression analysis are detailed in the user-defined functions FIT1, FIT2, and FIT3 of Fig. 3. The arrays X and Y represent the cell ranges containing the x and y data, respectively. The coefficients of G and H are calculated using the built-in functions COUNT, SUM, and SUMPRODUCT; then

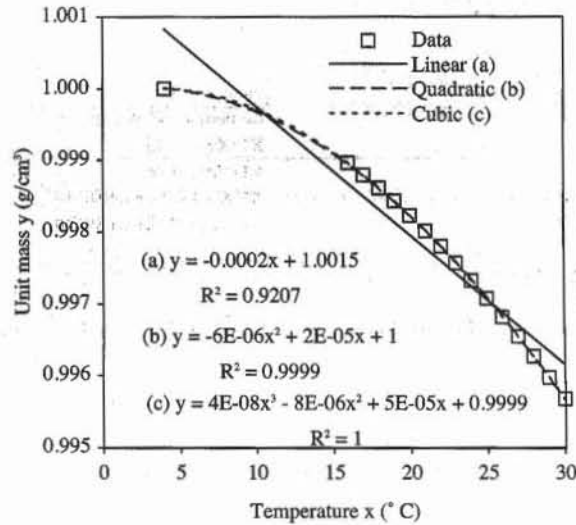


Figure 2 Regression analysis with Trendline.

$$n = \text{COUNT}(X), \quad \sum_{i=1}^n x_i = \text{SUM}(X), \quad \sum_{i=1}^n x_i^2 = \text{SUMPRODUCT}(X, X), \quad (19)$$

$$\sum_{i=1}^n x_i y_i = \text{SUMPRODUCT}(X, Y), \quad \text{and} \quad \sum_{i=1}^n x_i^2 y_i = \text{SUMPRODUCT}(X, X, Y), \text{ etc.}$$

The matrix \mathbf{G} is inverted using the built-in function MINVERSE, and \mathbf{G}^{-1} and \mathbf{H} are multiplied using MMULT. Figure 4 shows the coefficients calculated using FIT1, FIT2, and FIT3, and Fig. 5 shows the formulas of Fig. 4. FIT1, FIT2, and FIT3 determine exactly the same coefficients as Trendline.

INTERPOLATION

In some engineering calculations, it is only necessary to interpolate a set of tabulated data, without the need for a regression analysis. The problem is to find y corresponding to a known value x , based on n tabulated data points (x_i, y_i) , where x_i either continuously increases (i.e., $x_1 \leq x_2 \leq \dots \leq x_{n-1} \leq x_n$) or decreases (i.e., $x_1 \geq x_2 \geq \dots \geq x_{n-1} \geq x_n$). The linearly interpolated value of y corresponding to x is

$$y = y_i + \frac{y_{i+1} - y_i}{x_{i+1} - x_i} (x - x_i) \quad \text{if } (x - x_i)(x - x_{i+1}) \leq 0 \quad \text{and } x_i \neq x_{i+1} \quad (20)$$

In some instances, such as the determination of grain size corresponding to 10% by weight finer on a grain size distribution curve, the linear interpolation is carried out on a semilogarithmic graph having a logarithmic y axis. In this case, referred to as semilog interpolation, Eq. 20 becomes

	A	B	C	D
1	FIT1	Name of function		
2	=RESULT(64)	Result of function is an array		
3	=ARGUMENT("X",64)	Input X-array		
4	=ARGUMENT("Y",64)	Input Y-array		
5	=COUNT(X)	n= number of element in X and Y		
6	=SUM(X)	$X_1+X_2+\dots+X_n$		
7	=SUM(Y)	$Y_1+Y_2+\dots+Y_n$		
8	=SUMPRODUCT(X,X)	$X_1^2+X_2^2+\dots+X_n^2$		
9	=SUMPRODUCT(X,Y)	$X_1Y_1+X_2Y_2+\dots+X_nY_n$		
10	=A5*A8-A6*A6			
11	=IF(A10=0,RETURN("ERR"))			
12	=(A7*A8-A6*A9)/A10			
13	=(A5*A9-A6*A7)/A10			
14	=RETURN(A12:A13)			
15				
16	FIT2	Fit quadratic polynomial by linear regression		
17	=RESULT(64)			
18	=ARGUMENT("X",64)	Input X-array		
19	=ARGUMENT("Y",64)	Input Y-array		Space for vector
20	=COUNT(X)	349	8231	15.96216
21	=SUM(X)	8231	201889	348.06384
22	=SUMPRODUCT(X,X)	201889	5095943	8207.227
23	=SET.VALUE(B20,A21)	Form matrix		
24	=SET.VALUE(C20,A22)			
25	=SET.VALUE(B21,A22)			
26	=SET.VALUE(C21,SUMPRODUCT(X,X,X))			
27	=SET.VALUE(B22,C21)			
28	=SET.VALUE(C22,SUMPRODUCT(X,X,X,X))			
29	=SET.VALUE(D20,SUM(Y))	Form vector		
30	=SET.VALUE(D21,SUMPRODUCT(X,Y))			
31	=SET.VALUE(D22,SUMPRODUCT(X,X,Y))			
32	=RETURN(MMULT(MINVERSE(A20:C22),D20:D22))			

	A	B	C	D	E
34	FIT3	Fit cubic polynomial by linear regression			
35	=RESULT(64)				
36	=ARGUMENT("X",64)	Input X-array			
37	=ARGUMENT("Y",64)	Input Y-array			Space for vector
38	=COUNT(X)	349	8231	201889	15.96216
39	=SUM(X)	8231	201889	5095943	348.06384
40	=SUMPRODUCT(X,X)	201889	5095943	131689249	8207.227
41	=SUMPRODUCT(X,X,X)	5095943	131689249	3470452391	201271.75128
42	=SET.VALUE(B38,A39)	Form matrix			
43	=SET.VALUE(C38,A40)				
44	=SET.VALUE(D38,A41)				
45	=SET.VALUE(B39,A40)				
46	=SET.VALUE(C39,A41)				
47	=SET.VALUE(D39,SUMPRODUCT(X,X,X,X))				
48	=SET.VALUE(B40,A41)				
49	=SET.VALUE(C40,D39)				
50	=SET.VALUE(D40,SUMPRODUCT(X,X,X,X,X))				
51	=SET.VALUE(B41,D39)				
52	=SET.VALUE(C41,D40)				
53	=SET.VALUE(D41,SUMPRODUCT(X,X,X,X,X,X))				
54	=SET.VALUE(E38,SUM(Y))	Form vector			
55	=SET.VALUE(E39,SUMPRODUCT(X,Y))				
56	=SET.VALUE(E40,SUMPRODUCT(X,X,Y))				
57	=SET.VALUE(E41,SUMPRODUCT(X,X,X,Y))				
58	=RETURN(MMULT(MINVERSE(A38:D41),E38:E41))				

Figure 3 User-defined functions for linear (FIT1), quadratic (FIT2), and cubic (FIT3) regressions.

	A	B	C	D
20		FIT1	FIT2	FIT3
21	a ₀	1.001542072	1.000000202	0.999910033
22	a ₁	-0.000179121	2.43481E-05	5.20192E-05
23	a ₂		-5.63002E-06	-7.51229E-06
24	a ₃			3.60518E-08

Figure 4 Results of regression analysis with FIT1, FIT2, and FIT3.

	A	B	C	D
20		FIT1	FIT2	FIT3
21	a ₀	=FIT1(x,y)	=FIT2(x,y)	=FIT3(x,y)
22	a ₁	=FIT1(x,y)	=FIT2(x,y)	=FIT3(x,y)
23	a ₂		=FIT2(x,y)	=FIT3(x,y)
24	a ₃			=FIT3(x,y)

Figure 5 Formulas used in Fig. 4.

$$\ln(y) = \ln(y_i) + \frac{\ln(y_{i+1}) - \ln(y_i)}{x_{i+1} - x_i} (x - x_i)$$

if $(x - x_i)(x - x_{i+1}) \leq 0$ and $x_i \neq x_{i+1}$ (21)

Equation 21 can also be written

$$\ln \frac{y}{y_i} = \frac{x - x_i}{x_{i+1} - x_i} \ln \frac{y_{i+1}}{y_i}$$

(22)

or equivalently,

$$y = y_i \left(\frac{y_{i+1}}{y_i} \right)^{\frac{(x-x_i)}{(x_{i+1}-x_i)}}$$

(23)

EXAMPLE OF INTERPOLATION

In Table 1 there are seven data points. The x component is the grain size, and the y component is the percent finer. In Fig. 6, the data are plotted using semilog axes. The problem is to find the grain size D₃₀ corresponding to 30 percent finer. The solution is given in Table 1, and the EXCEL formulas are given in Fig. 7. The user-defined functions INTERL and INTER that perform the linear and semilog interpolation are listed in Fig. 8. Both INTERL and INTER check first that the input arrays are defined in columns, search the two components that bracket the input Value, and finally, perform a linear interpolation for the entry Value. As shown in Table 1 and Fig. 6, the linear and semilog interpolations give slightly different results. In contrast to the linear interpolation, the semilog interpolation gives an interpolated point that is exactly on one of the segments of Fig. 6.

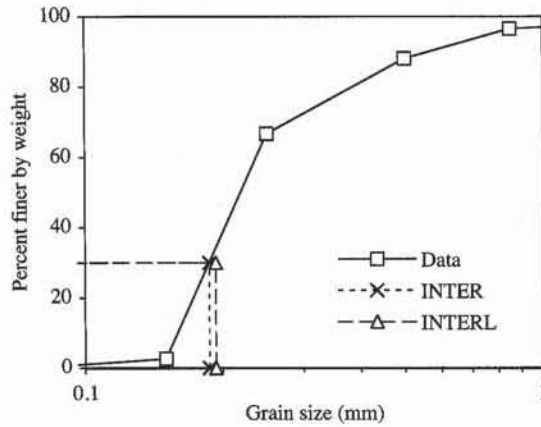


Figure 6 Graph corresponding to data of Table 1, and linear and semilinear interpolation.

	A	B
10	Semilog interpolation	
11	D ₃₀ = =INTER(30,B2:B8,A2:A8)	
12		
13	Linear interpolation	
14	D ₃₀ = =INTERL(30,B2:B8,A2:A8)	
15		

Figure 7 Formulas used in Fig. 6.

TABLE 1

Data set for interpolation

	A	B
1	Grain size (mm)	Percent finer
2	4.750	100.00
3	2.000	98.90
4	0.850	96.48
5	0.500	88.17
6	0.250	66.67
7	0.150	2.52
8	0.075	0.05
9		0.00
10	Semilog interpolation	
11	D ₃₀ = 0.187 mm	
12		
13	Linear interpolation	
14	D ₃₀ = 0.193 mm	
15		

NONLINEAR OPTIMIZATION WITH CONSTRAINTS

Some spreadsheet programs have the capabilities of performing nonlinear optimization with constraints. In principle, constrained optimization consists of finding the values of m variables p_1, p_2, \dots, p_m that minimize the function $f(p_1, p_2, \dots, p_m)$, with inequality or equality constraints on p_1, p_2, \dots, p_m . In general, the con-

	A	B
1	INTER	Linear Interpolation returns interpolated result corresponding to Value given two arrays X and Y in columns (x-logy axis)
2	=RESULT(1)	
3	=ARGUMENT("Value",1)	
4	=ARGUMENT("X",64)	
5	=ARGUMENT("Y",64)	
6	=IF(OR(ROWS(X)<>ROWS(Y),COLUMNS(X)>1,COLUMNS(Y)>1),RETURN(#VALUE!))	
7	=FOR("I",1,ROWS(X)-1)	
8	= IF(AND((INDEX(X,I+1)-Value)*(INDEX(X,I)-Value)<=0,INDEX(X,I+1)<>INDEX(X,I)))	
9	= RETURN(INDEX(Y,I)*(INDEX(Y,I+1)-INDEX(Y,I))*((Value-INDEX(X,I))/(INDEX(X,I+1)-INDEX(X,I))))	
10	= END.IF()	
11	=NEXT()	
12	=RETURN(#VALUE!)	
13		
14	INTERL	Linear Interpolation returns interpolated result corresponding to Value given two arrays X and Y in columns
15	=RESULT(1)	
16	=ARGUMENT("Value",1)	
17	=ARGUMENT("X",64)	
18	=ARGUMENT("Y",64)	
19	=IF(OR(ROWS(X)<>ROWS(Y),COLUMNS(X)>1,COLUMNS(Y)>1),RETURN(#VALUE!))	
20	=FOR("I",1,ROWS(X)-1)	
21	= IF(AND((INDEX(X,I+1)-Value)*(INDEX(X,I)-Value)<=0,INDEX(X,I+1)<>INDEX(X,I)))	
22	= RETURN(INDEX(Y,I)+(INDEX(Y,I+1)-INDEX(Y,I))*((Value-INDEX(X,I))/(INDEX(X,I+1)-INDEX(X,I))))	
23	= END.IF()	
24	=NEXT()	
25	=RETURN(#VALUE!)	

Figure 8 User-defined functions INTER and INTERL for linear and semilinear interpolations.

straints assign an admissible range of values for the variables, which eliminates unrealistic solutions. A detailed description of these numerical techniques is beyond the scope of this book. We only present an example relevant to soil mechanics.

In the case of the consolidation test, the problem is to find the values of parameters $p_1 = d_0$, $p_2 = d_{100}$, and $p_3 = C_v$ (i.e., $m = 3$) that minimize the error function $E(p_1, p_2, p_3)$:

$$E = \sum_{i=1}^n (d_i - d_i^p)^2 \tag{24}$$

between n experimental dial readings d_i at time t_i , $i = 1, \dots, n$, and the corresponding fitted dial readings d_i^p :

$$d_i^p = d_0 + (d_{100} - d_0)U(C_v t_i) \quad \text{and} \quad U(x) = \begin{cases} \sqrt{\frac{4}{\pi}}x & \text{if } x < 0.2827 \\ 1 - \frac{8}{\pi^2} \exp\left(-\frac{\pi^2}{4}x\right) & \text{if } x \geq 0.2827 \end{cases} \tag{25}$$

We impose the following constraint on d_0 , d_{100} , and C_v :

$$d_0 \geq d_1, \quad d_{100} \leq d_n, \quad d_{100} \geq d_0, \quad \text{and} \quad C_v \geq 0 \tag{26}$$

where d_1 represents the first dial readings, and d_n represents the last dial readings. Figure 9 shows the data points to be fitted, and Fig. 10 lists the formulas used in Fig. 9. Figure 11 compares the experimental and fitted data points.

	A	B	C	D	E	F
1	Time (min)	Displacement (cm)	Fitted displacement (cm)			
2	0.0	0.0000	0.0350	$d_0 = 0.0350$ cm $d_{100} = 0.1234$ cm $C_v = 0.0400$ 1/min Error E = 0.0000		
3	0.3	0.0445	0.0449			
4	0.5	0.0483	0.0491			
5	1.0	0.0551	0.0549			
6	2.0	0.0635	0.0632			
7	4.0	0.0762	0.0748			
8	8.0	0.0912	0.0908			
9	15.0	0.1067	0.1070			
10	30.0	0.1173	0.1196			
11	60.0	0.1217	0.1232			
12	120.0	0.1232	0.1234			
13	240.0	0.1245	0.1234			
14	480.0	0.1245	0.1234			
15	1440.0	0.1245	0.1234			

Figure 9 Data set and results of nonlinear optimization with constraints.

	C
1	Fitted displacement (cm)
2	=E2+(E3-E2)*U(E4*A2)
3	=E2+(E3-E2)*U(E4*A3)
4	=E2+(E3-E2)*U(E4*A4)
5	=E2+(E3-E2)*U(E4*A5)
6	=E2+(E3-E2)*U(E4*A6)
7	=E2+(E3-E2)*U(E4*A7)
8	=E2+(E3-E2)*U(E4*A8)
9	=E2+(E3-E2)*U(E4*A9)
10	=E2+(E3-E2)*U(E4*A10)
11	=E2+(E3-E2)*U(E4*A11)
12	=E2+(E3-E2)*U(E4*A12)
13	=E2+(E3-E2)*U(E4*A13)
14	=E2+(E3-E2)*U(E4*A14)
15	=E2+(E3-E2)*U(E4*A15)

	D	E
5	Error E =	=SUMPRODUCT(B3:B15-C3:C15,B3:B15-C3:C15)

Figure 10 Formulas used in Fig. 9.

In Excel, the nonlinear optimization with constraints is performed using SOLVER. The parameters C_v , d_0 , and d_{100} to be optimized are in cells E2, E3, and E4, and the function to minimize is in cell E5. At the beginning of the calculations, C_v , d_0 , and d_{100} were set equal to 0.01, d_1 , and d_n . When SOLVER is called, it displays the window of Fig. 12. Set the cell to be optimized (e.g., E5), and select the minimum option. Define the cells to be changed by separating them with a comma, then add the constraints of Eq. 26. When all the input is performed, start the optimization. The calculation may take a few minutes, depending on the computer speed and the number of data points. In most cases, with the SOLVER default options, the optimization converges without a problem when the variables are properly constrained and initialized. SOLVER provides additional options for difficult optimizations (refer to the Microsoft Excel User's Manual for the options available).

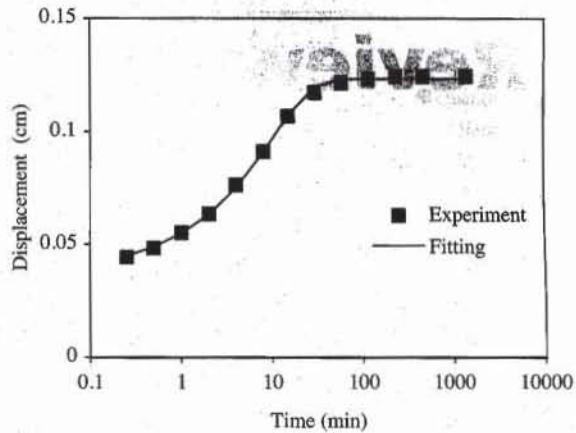


Figure 11 Comparison of experimental and fitted data points.

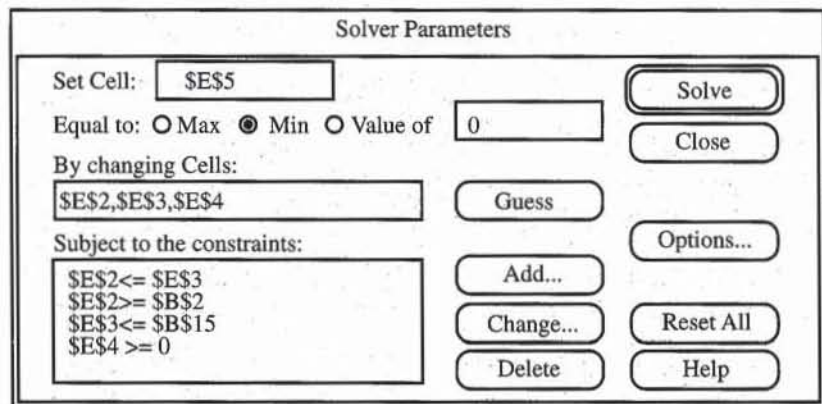


Figure 12 SOLVER's window.

REVIEW QUESTIONS

1. What is the difference between interpolation, linear regression, and nonlinear optimization?
2. What is the principle of linear regression?
3. Which quantity measures the accuracy of a linear regression fitting?
4. By using a linear interpolation, find the value of y corresponding to x between data points (x_1, y_1) and (x_2, y_2) .
5. Name the EXCEL functions that are used to perform linear regression.

8-2 Review of Statistics

In this chapter, we review some basic definitions in statistics and introduce statistical concepts relevant to grain size distributions of soils.

HISTOGRAM, FREQUENCY PLOT, AND CUMULATIVE FREQUENCY

Table 1 displays the distribution of glass beads. The glass beads are sorted in size categories; each is characterized by a minimum and a maximum size. For instance, there are 148 particles having a diameter between 12 and 14 mm, and the corresponding mass is 340.5 g. The total number of particles is 1565, and the total mass

TABLE 1
Distribution of a set of glass beads

Size (mm)	Number of glass beads	Weight (g)	Weight distribution (%)	Quantity distribution (%)	Cumulative weight distribution (%)	Cumulative quantity distribution (%)
0	0	0.00	0.0	0.00	0.00	0.00
2	141	3.99	0.2	9.01	0.20	9.01
4	183	23.95	1.2	11.69	1.40	20.70
6	362	130.03	6.5	23.13	7.90	43.83
8	325	248.11	12.4	20.77	20.30	64.60
10	230	320.58	16.0	14.70	36.32	79.30
12	148	340.50	17.0	9.46	53.34	88.75
14	85	300.41	15.0	5.43	68.36	94.19
16	47	241.81	12.1	3.00	80.44	97.19
18	24	172.39	8.6	1.53	89.06	98.72
20	13	126.08	6.3	0.83	95.36	99.55
22	6	76.45	3.8	0.38	99.18	99.94
24	1	16.36	0.8	0.06	100.00	100.00
26	0	0.00	0.0	0.00	100.00	100.00
	1565	2000.65				

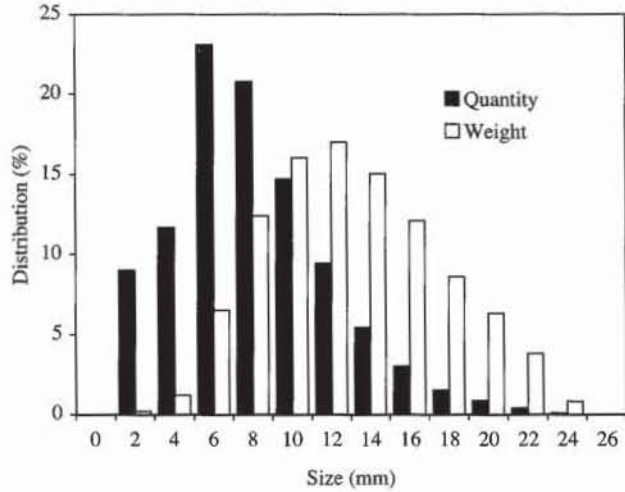


Figure 1 The histograms for the distributions of quantity and weight of the set of glass beads.

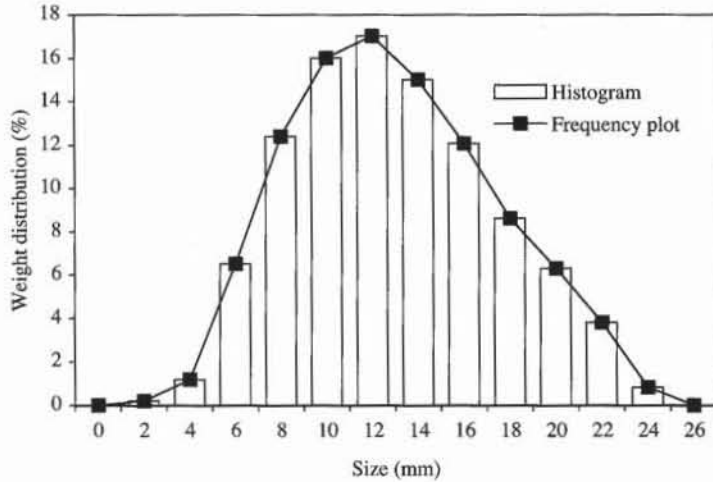


Figure 2 The histogram and frequency plot representations for the weight distribution of Table 1.

is 2000.65 g. The distributions of weight and quantity are expressed in percent. They are obtained by dividing the quantity, or mass, in each size category by the total quantity, or mass.

A distribution may be represented by using several graphical means. Figure 1 shows the histogram plot for the weight and quantity distributions. The fourth size range contains the largest number of beads, whereas the seventh size range has the largest mass. Distribution may also be represented as a frequency plot (continuous line) instead of a histogram (Fig. 2). The continuous line of the frequency plot connects the average size of each size category.

Figure 3 shows the cumulative distribution of weight and quantity. The cumulative distribution for a given size x is obtained by adding all the distributions for the category size smaller than x . While the distributions of weight and quantity vary up and down, the cumulative distributions always increase from 0 to 100.

In contrast to sets of glass beads, real soils have particles whose size varies from 0.001 to 100 mm. The smallest clay particles may reach a total number 10^{10} times larger than the number of coarser gravel particles. This large disparity in

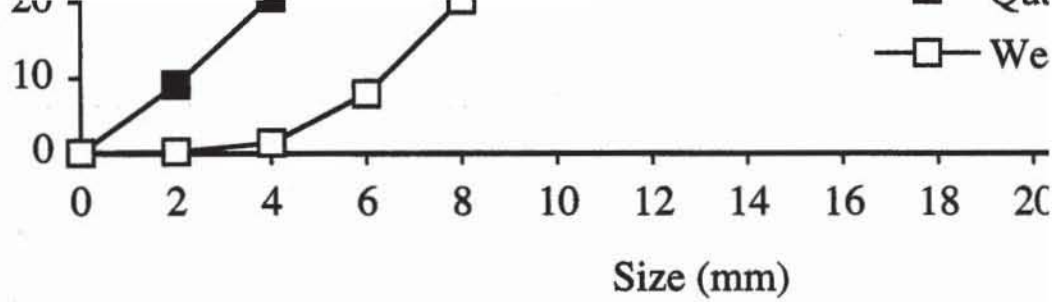


Figure 3 Cumulative frequency plots of the distribution and weight of the set of glass beads.

the quantity of particle sizes and the impossibility of counting are the main reasons for selecting a weight distribution instead of a size distribution of soils.

MEAN AND STANDARD DEVIATION

A distribution is generally characterized by three statistics: mean, standard deviation, and range. The range is the difference between the smallest and largest values in the data set. It is a measure of the spread of the data. For instance, the range is 24 mm for the distribution of glass beads. For a data set sorted in M groups, each group having f_i frequency and average value m_i , the mean or average value μ is

$$\mu = \frac{\sum_{i=1}^M m_i f_i}{\sum_{i=1}^M f_i}$$

In the case of glass beads, m_i and f_i are the average size and frequency of a particle size range, respectively. For instance, in the case of Table 1, $m_6 = 11$ mm and $f_6 = 16\%$ for the sixth particle size range. Equation 1 may be simplified because the sum of coefficients

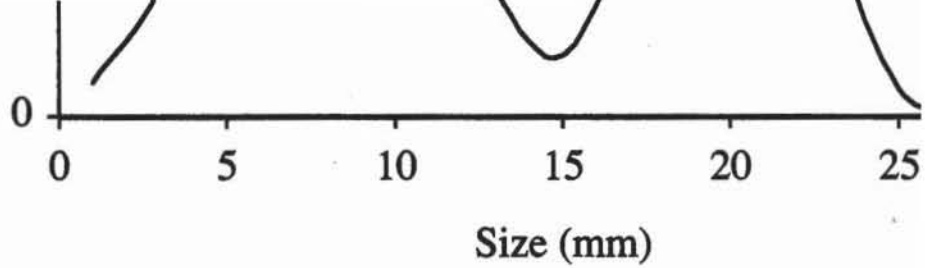


Figure 4 An example of bimodal distribution

When $\sum_{i=1}^M f_i = 1$, Eq. 3 becomes

$$\sigma = \sqrt{\sum_{i=1}^M (m_i - \mu)^2 f_i} = \sqrt{\sum_{i=1}^M m_i^2 f_i - \mu^2}$$

By applying Eq. 4 to the data of Table 1, $\sigma = 4.43$ mm.

The mean, range, and standard deviation are general characteristics that describe distributions that have a unique peak. The distribution is called *unimodal*. However, the mean, range, and standard deviation are not as meaningful for describing complicated distributions with several peaks. For example, an example of a *bimodal* distribution (i.e., two peaks), which is formed by mixing a uniform gravel and a uniform fine sand, for instance, is defined more accurately with two values for mean and standard deviation than with a single value for mean and standard deviation.

DISTRIBUTION

Several functions have been proposed to describe various distributions. Only a few examples available in spreadsheet programs are listed below.

EXPONENTIAL DISTRIBUTION

The exponential distribution is

$$f(x, \lambda) = \lambda e^{-\lambda x}$$

WEIBULL DISTRIBUTIONS

The Weibull distribution is

$$f(x) = \frac{\alpha}{\beta^\alpha} x^{\alpha-1} e^{-(x/\beta)^\alpha} \tag{8}$$

Its cumulative distribution is

$$F(x, \alpha, \beta) = \int_0^x f(t) dt = 1 - e^{-(x/\beta)^\alpha} \tag{9}$$

When $\alpha = 1$, the Weibull distribution becomes the exponential distribution with $\lambda = 1/\beta$.

NORMAL AND LOGNORMAL DISTRIBUTIONS

The normal distribution is

$$f(x, \mu, \sigma) = \frac{1}{\sqrt{2\pi}\sigma} e^{-(x-\mu)^2/2\sigma^2} \tag{10}$$

The lognormal distribution is obtained by replacing x by $\ln(x)$ in Eq. 10.

As shown in Figs. 5 and 6, the normal distribution fits the weight distribution of Table 1. Fig. 7 gives the data set, and Fig. 8 lists the formulas used in Fig. 7. The average and standard deviation are calculated using Eqs. 2 and 4.

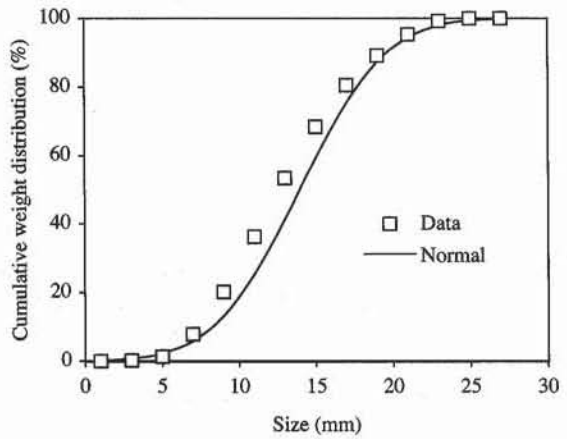
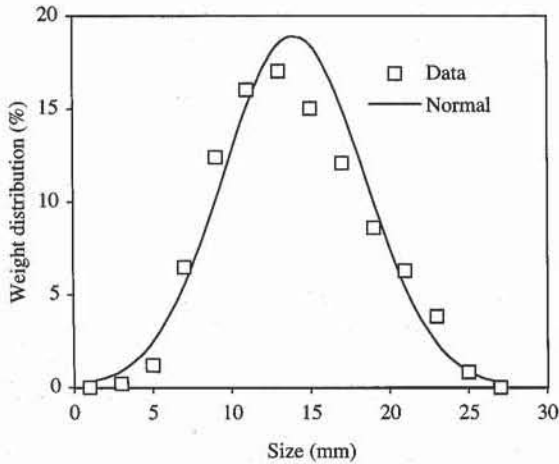


Figure 5 Weight distribution of Table 1 fitted by normal distribution.

Figure 6 Weight distribution of Table 1 fitted by cumulative normal distribution.

OTHER DISTRIBUTIONS

Besides exponential, Weibull, and normal distributions, there are other types of distributions, such as gamma, Poisson, and Student- t .

	A	B	C	D	E
1		Data		Fitting	
2	Size (mm)	Weight distribution (%)	Cumulative weight distribution	Normal	Normal cumulative
3	d	f			
4	1	0.00	0.00	0.26	0.17
5	3	0.20	0.20	0.89	0.67
6	5	1.20	1.40	2.46	2.16
7	7	6.50	7.90	5.52	5.82
8	9	12.40	20.30	10.13	13.16
9	11	16.02	36.32	15.15	25.21
10	13	17.02	53.34	18.50	41.41
11	15	15.02	68.36	18.43	59.24
12	17	12.09	80.44	14.98	75.32
13	19	8.62	89.06	9.94	87.20
14	21	6.30	95.36	5.38	94.37
15	23	3.82	99.18	2.38	97.92
16	25	0.82	100.00	0.86	99.36
17	27	0.00	100.00	0.25	99.84
18	Average size $\mu =$		13.96	mm	
19	Standard dev $\sigma =$		4.44	mm	

Figure 7 Examples of weight distribution fitted by a normal distribution.

	D	E
2	Normal	Normal cumulative
3		
4	=100/EXP((d-m)^2/2/s^2)/SQRT(2*PI()*s)	=NORMDIST(d,m,s,TRUE)*100
5	=100/EXP((d-m)^2/2/s^2)/SQRT(2*PI()*s)	=NORMDIST(d,m,s,TRUE)*100

	B	C	D
18	Average size $\mu =$	=SUMPRODUCT(f,d)/100	mm
19	Standard dev $\sigma =$	=SQRT(SUMPRODUCT(d,d,f)/100-m^2)	mm

Figure 8 Formulas used in Fig. 7.

REVIEW QUESTIONS

1. Define *histogram* and *frequency plots* of a distribution.
2. What is the relation between a distribution and a cumulative distribution? Assuming that $f(x)$ is a continuous distribution, define the cumulative distribution $F(x)$. Conversely, assuming that $F(x)$ is a cumulative distribution, define the distribution $f(x)$.
3. Why is a weight distribution preferable to a quantity distribution when characterizing the grain size distribution of real soils?
4. Assume that a data set is sorted in M groups of data, each having an average value x_i and each containing m_i elements. Define the average and standard deviation of the data set.
5. Same as question above but assume that m_i represents the percentage of elements instead of the number of components. Simplify the definitions of the average and standard deviation of the complete data set.
6. What are unimodal and bimodal distributions?
7. Name three probability distributions.

EXERCISES

1. Define a weight distribution and a quantity distribution for the following set of glass beads:

5 beads of 3 mm diameter

10 beads of 5 mm diameter

20 beads of 7 mm diameter

10 beads of 9 mm diameter

5 beads of 9 mm diameter

Assume the same unit mass for all glass beads.

2. Define a cumulative weight distribution and a cumulative quantity distribution for the set of glass beads in Exercise 1.
3. Plot the distribution and cumulative distribution of a bimodal distribution that has the following averages and standard deviations: $\mu_1 = 10$ mm, $\sigma_1 = 5$ mm, and $\mu_2 = 100$ mm, $\sigma_2 = 10$ mm. Identify the shape of a gap-graded grain size distribution curve.

8-3

Error Analysis

CAUSES AND TYPES OF EXPERIMENTAL ERRORS

Errors creep into all experiments regardless of the care that is exerted. Some errors are of a random nature, and some are due to gross blunders on the part of the experimenter. The latter type may be detected and fixed after scrutinizing the experimental results, especially when they show a gross deviation from expected results. The former type of error may be systematic, which causes the readings to be incorrect by the same amount for some unknown reason, or random errors, which result from fluctuations in the measuring instruments. The random errors in reading a well-calibrated and operational instrument are generally comparable to the instrument accuracy.

UNCERTAINTY ANALYSIS

Kline and McClintock (1953) presented a method of estimating the uncertainties of experimental results based on the uncertainties of various primary experimental measurements. Consider that the result y is a function of n independent variables x_1, x_2, \dots, x_n :

$$y = y(x_1, x_2, \dots, x_n) \quad (1)$$

The variables x_1, x_2, \dots, x_n are considered independent when they are separately measured (i.e., they are not calculated one from the other). The uncertainties in the measurement of x_i are denoted Δx_i . For instance, if x_i is a weight, the uncertainty Δx_i is the scale accuracy at which the weight x_i can be measured. The accuracy of an instrument is generally specified by its manufacturer. When the uncertainties of all the independent variables are given, the uncertainty of the result is

$$\Delta y = \sqrt{\left(\frac{\partial y}{\partial x_1} \Delta x_1\right)^2 + \left(\frac{\partial y}{\partial x_2} \Delta x_2\right)^2 + \dots + \left(\frac{\partial y}{\partial x_n} \Delta x_n\right)^2} \quad (2)$$

One may also evaluate Δy by using the following alternative formula:

$$\Delta y = \left| \frac{\partial y}{\partial x_1} \Delta x_1 \right| + \left| \frac{\partial y}{\partial x_2} \Delta x_2 \right| + \dots + \left| \frac{\partial y}{\partial x_n} \Delta x_n \right| \quad (3)$$

In both formulas, the errors generated by each independent variable add up. The more variables there are, the larger is the error. By definition, Δy is called the *absolute error* on y , whereas $\Delta y/y$ is called the *relative error* on y . The relative error is dimensionless and is expressed in percent, while the absolute value has the same dimension as y (i.e., $[\Delta y] = [y]$).

EXAMPLES

Equations 2 and 3 apply to the determination of water content w in the plastic limit test. The result $y = w$ is calculated as follows:

$$w = \frac{W_w - W_d}{W_d - W_c} \times 100 \quad (\%) \quad (4)$$

where W_c is the weight of the container, W_w the weight of the container and wet soil, and W_d the weight of the container and dry soil. The independent variables are $x_1 = W_c$, $x_2 = W_w$, and $x_3 = W_d$ because W_c , W_w , and W_d are measured independently. The partial derivatives of w with respect to W_c , W_w , and W_d are

$$\frac{\partial w}{\partial W_c} = \frac{W_w - W_d}{(W_d - W_c)^2} = \frac{w}{W_d - W_c}, \quad \frac{\partial w}{\partial W_w} = \frac{1}{W_d - W_c}, \quad \text{and} \quad \frac{\partial w}{\partial W_d} = \frac{W_c - W_w}{(W_d - W_c)^2} \quad (5)$$

Since W_c , W_w , and W_d are measured using the same scale,

$$\Delta W_c = \Delta W_w = \Delta W_d = \Delta W \quad (6)$$

Applying Eq. 2 to w , one obtains the relative error of w :

$$\begin{aligned} \frac{\Delta w}{w} &= \Delta W \frac{\sqrt{(W_w - W_d)^2 + (W_w - W_c)^2 + (W_d - W_c)^2}}{(W_d - W_c)^2} \\ &= \frac{\Delta W}{W_d - W_c} \sqrt{1 + w^2 + \left(\frac{W_w - W_c}{W_d - W_c}\right)^2} \end{aligned} \quad (7)$$

As shown in Eq. 7, the error on w is proportional to the error of the weight measurement. Figure 1 shows an example of experimental results for the liquid limit test. In this case, the error in weight measurement is set equal to the scale accuracy (i.e., $\Delta W = 0.01$ g). The relative and absolute errors for each determination of w are given in Fig. 1. Figure 2 lists the formulas used in Fig. 1.

The error can also be calculated using Eq. 3 instead of Eq. 2. First, it is convenient to take the logarithm of w :

$$\ln(w) = \ln(W_w - W_d) - \ln(W_d - W_c) \quad (8)$$

then to differentiate it:

$$\begin{aligned} \frac{dw}{w} &= \frac{d(W_w - W_d)}{W_w - W_d} - \frac{d(W_d - dW_c)}{W_d - W_c} \\ &= \frac{dW_c}{W_d - W_c} + \frac{dW_w}{W_w - W_d} - \frac{(W_w - W_c)dW_d}{(W_w - W_d)(W_d - W_c)} \end{aligned} \tag{9}$$

The infinitesimal variations dW_c , dW_w , and dW_d are then replaced by the errors ΔW_c , ΔW_w , and ΔW_d that are all set equal to ΔW , and the relative error on w becomes

$$\frac{\Delta w}{w} = \Delta W \left(\frac{1}{|W_d - W_c|} + \frac{1}{|W_w - W_d|} + \frac{|W_w - W_c|}{|W_w - W_d||W_d - W_c|} \right) \tag{10}$$

Because $W_d > W_c$, $W_w > W_d$, and $W_w > W_c$, Eq. 10 becomes

$$\frac{\Delta w}{w} = \frac{2\Delta W(W_w - W_c)}{(W_w - W_d)(W_d - W_c)} \tag{11}$$

As shown in Fig. 1, Eq. 3 generates larger errors than Eq. 2 and therefore is a more conservative error estimate.

In Fig. 3, the absolute errors are represented by using vertical bars centered on the data points. The height of each error bar is equal to the absolute error on w . In Excel, these error bars are plotted by selecting the graph, by using **Insert Error Bars**, and by entering the range of absolute error on w as **Y Error Bars**.

Another example may be taken from the one-point liquid limit test. In this simplified procedure, the liquid limit LL is calculated from the water content w associated with N blows:

$$LL = w \left(\frac{N}{25} \right)^{A'} \tag{12}$$

where A' is the slope of flow line. The error of N can be taken to be zero, because it is improbable that the number of blows be miscounted. The independent variables are $x_1 = w$ and $x_2 = A'$. The partial derivatives of LL with respect to w and A' are

$$\frac{\partial LL}{\partial w} = \frac{LL}{w} \quad \text{and} \quad \frac{\partial LL}{\partial A'} = LL \ln \frac{N}{25} \tag{13}$$

Therefore, the error of LL is

$$\frac{\Delta LL}{LL} = \sqrt{\left(\frac{\Delta w}{w} \right)^2 + \left(\ln \frac{N}{25} \Delta A' \right)^2} \tag{14}$$

When $N = 25$, $\Delta LL/LL = \Delta w/w$. Figure 4 shows $\Delta LL/LL$ calculated by using $\Delta w/w = 1\%$ and four values of $\Delta A'$ (i.e., $\Delta A' = 0.01, 0.02, 0.05,$ and 0.08). As illustrated in Fig. 4, error analysis can be used to assess the effects of each measurement on the final results and to select the optimal measurement conditions, which produce the smallest errors. In the one-point liquid limit test, it is recommended to select a blow count N as close as possible to 25, in order to decrease the error on LL . It is clear that the liquid limit cannot be determined more accurately than the water content itself.

	A	B	C	D	E	F	G	H	I	J	K	
1	Liquid limit											
2	Analyst name: <i>Henry T. Guapo</i>											
3	Sample description: <i>Aardvark modeling clay</i>											
4	Scale accuracy $\Delta W = 0.01$ g						Eq. 2		Eq. 3			
5	set number	Container mass (g)	Mass of wet soil and container (g)	Mass of dry soil and container (g)	Number of blows	Water content (%)	Relative error on water content	Absolute error on water content (%)	Relative error on water content	Absolute error on water content (%)	Water content fitted (%)	
6		W_c	W_w	W_d	N	w	$\Delta w/w$		$\Delta w/w$			
7	1	47.72	59.89	57.05	24	30.44	0.18%	0.05	0.92%	0.28	30.70	
8	2	43.21	59.76	55.95	31	29.91	0.13%	0.04	0.68%	0.20	29.76	
9	3	45.17	61.25	57.45	22	30.94	0.14%	0.04	0.69%	0.21	31.02	
10	4	45.81	58.26	55.26	19	31.75	0.18%	0.06	0.88%	0.28	31.56	

Figure 1. Example of error calculation for liquid limit test.

	F	G	H	I	J
5	Water content (%)	Relative error on water content	Absolute error on water content (%)	Relative error on water content	Absolute error on water content (%)
6	w	$\Delta w/w$		$\Delta w/w$	
7	$=100 \cdot (W_w - W_d) / (W_d - W_c)$	$=DW \cdot \text{SQRT}((W_w - W_d)^2 + (W_d - W_c)^2 + (W_w - W_c)^2) / (W_d - W_c)^2$	$=G7 \cdot w$	$=2 \cdot DW \cdot (W_w - W_c) / (W_w - W_d) / (W_d - W_c)$	$=I7 \cdot w$
8	$=100 \cdot (W_w - W_d) / (W_d - W_c)$	$=DW \cdot \text{SQRT}((W_w - W_d)^2 + (W_d - W_c)^2 + (W_w - W_c)^2) / (W_d - W_c)^2$	$=G8 \cdot w$	$=2 \cdot DW \cdot (W_w - W_c) / (W_w - W_d) / (W_d - W_c)$	$=I8 \cdot w$

Figure 2. Formulas used in Fig. 1.

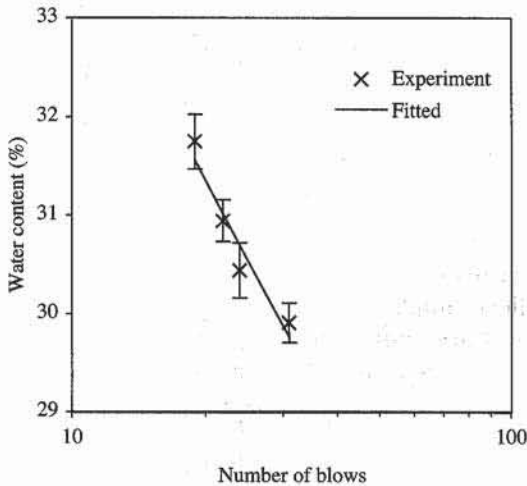


Figure 3 Error in water content resulting from error in the measurement of weight (Eq. 3).

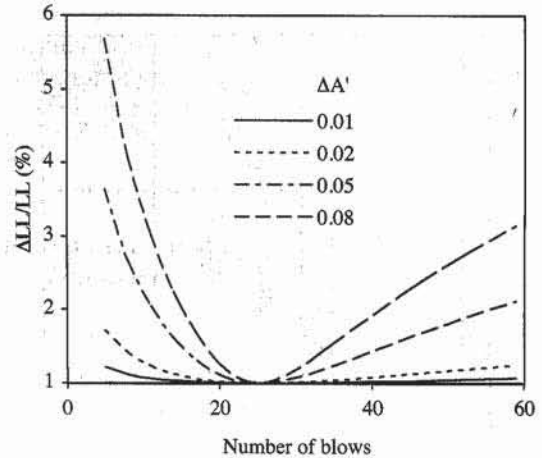


Figure 4 Variation of relative error of liquid limit versus number of blows N for various errors of coefficient A' ($\Delta A' = 0.01, 0.02, 0.05,$ and 0.08).

REFERENCE

KLINE, S. J., and F. A. MCCLINTOCK, 1953, Describing uncertainties in single-sample experiments, *Mech. Eng.*, January, p. 3.

EXERCISES

1. Define two different types of errors in experiments. Illustrate your general definitions with an example of your choice.
2. Define *relative error* and *absolute error*.
3. What is the purpose of error analysis?
4. How can error analysis be used to improve an experimental procedure?
5. In pipette analysis, the grain size D (mm) is calculated as follows:

$$D = \sqrt{\frac{30\eta H}{(G_s - 1)981\rho_w t}}$$

where t is the time (min) after the beginning of sedimentation, G_s the specific gravity of soil particles, ρ_w the unit mass of water (g/cm^3) at temperature T , η the viscosity of water ($\text{g}/\text{cm} \cdot \text{s}$) at temperature T , and H the sampling depth (cm). Calculate the relative error of D as a function of the error of each variable.

6. In pipette analysis (dry method), the percentage p by weight of particles with diameter smaller than D is

$$p = 100 \frac{V_t}{V} \frac{M_s - M_b - M_d}{M_o} \quad (\%)$$

where M_o is the total mass of oven-dried soil in suspension, M_b the mass of empty bottle used to collect the pipette sample, M_s the mass of bottle and sample of oven-dried soil, V_t the total volume of suspension, V the volume

of the pipette, and M_d the mass of the dispersing agent in volume V . Calculate the relative error of p as a function of the error of each variable.

7. In pipette analysis (wet method), the percentage p by weight of particles with diameter smaller than D is

$$p = 100 \frac{\rho_s V_t}{\rho_s V - M_{dw}} \frac{M_{sw} - M_b - M_{dw}}{M_o} \quad (\%)$$

where M_o is the total mass of oven-dried soil in suspension, M_b the mass of the empty bottle used to collect sample, M_{sw} the mass of the bottle and sample of soil suspension, V_t the total volume of suspension, V the volume of the pipette, ρ_s the unit mass of solids, and M_{dw} the mass of water and dispersing agent in volume V . Calculate the relative error of p as a function of the error of each variable.

8. In the determination of unit weight by the buoyancy method, the total unit mass of soil is

$$\rho = \rho_w \frac{M}{M_P - M_I - (\rho_w / \rho_P) (M_P - M)}$$

where M is the mass of the soil, M_P the mass of the soil and paraffin wax, M_I the immersed mass of the soil and wax, ρ_w the unit mass of water ($\rho_w \approx 1.0 \text{ g/cm}^3$), and ρ_P the unit mass of wax. Calculate the relative error of ρ as a function of the error of each variable.

8-4

Dimensions and Units

The comparison of experimental results obtained from different sources requires certain standard units of length, weight, time, temperature, and electrical quantities. The National Institute of Standards and Technologies has the primary responsibility of maintaining these standards in the United States. In this section we present the dimensions, units, and unit conversions that are useful in soil mechanics.

DIMENSIONS

A dimension is a physical variable used to describe the behavior or nature of a physical system. For instance, the length of a rod is a dimension. Dimensions are not to be confused with units. When the rod is said to be 2 meters long, the length dimension was measured with the unit *meter*. Most of the physical quantities used in soil mechanics can be expressed in terms of the following dimensions: length, mass, time, force, and temperature. Their notations are listed in Table 1.

TABLE 1
Notation of physical dimensions used in soil mechanics

Notation	Dimension
L	length
M	mass
T	time
Θ	temperature
F	force

DIMENSIONAL ANALYSIS

Physical variables can be related by physical laws. Their relations can be derived by using dimensional analysis, a simplified form of calculus that we illustrate with

a few examples. In dimensional analysis, the dimension of variable x is noted $[x]$. When x has no dimension, $[x] = 1$.

In Table 1, L , M , T , and θ are independent dimensions, but F is related to other dimensions. Using Newton's second law of motion, the mass m moving with acceleration a is subjected to the force f :

$$f = ma \quad (1)$$

The dimension of f is force (i.e., $[f] = F$). Similarly, $[m] = M$. By using dimensional analysis,

$$[f] = [m][a] \quad (2)$$

Because the acceleration a is the second-order derivative of displacement x with respect to time t , the acceleration dimension is

$$[a] = \left[\frac{d^2x}{dt^2} \right] = [x][t]^{-2} = LT^{-2} \quad (3)$$

where $[x] = L$ and $[t] = T$. Therefore, F is related to M , L , and T through

$$F = MLT^{-2} \quad (4)$$

As another example, consider Stokes' law, which gives the drag force f applied by a fluid moving with velocity v onto a sphere of radius d :

$$f = 3\pi\eta vd \quad (5)$$

where η is the fluid viscosity. Using dimensional analysis,

$$[f] = [\eta][v][d] \quad (6)$$

$[3\pi] = 1$ because 3π is dimensionless. The dimension of velocity v is

$$[v] = LT^{-1} \quad (7)$$

Therefore, the dimension of η is mass divided by length and time:

$$[\eta] = [f][v]^{-1}[d]^{-1} = FL^{-1}TL^{-1} = MLT^{-2}L^{-1}TL^{-1} = ML^{-1}T^{-1} \quad (8)$$

UNITS

Units are not be confused with dimensions. Units are used to report the measurement of dimensions. In general, there are several units for the same dimension. For instance, the length of a rod may be 2 meters, or 200 centimeters. One of the most common systems of units is the International System of units, referred to as the SI units system. Table 2 lists the names and notations of basic SI units. Table 3 gives a list of derived SI units for the physical quantities in soil mechanics.

Table 4 lists the standard multiplier prefixes used in the SI system. For instance, $1 \times 10^6 \text{ N} = 1000 \text{ kN} = 1 \text{ MN}$, or $1 \times 10^{-6} \text{ m} = 1 \text{ }\mu\text{m}$.

TABLE 2
Basic SI units

Dimension	Unit	Symbol
Length	meter	m
Mass	kilogram	kg
Time	second	s
Electric current	ampere	A
Temperature	kelvin	K
Luminous intensity	candela	Cd
Plane angle	radian	rad
Solid angle	steradian	sr

TABLE 3
Derived SI units

Dimension	Unit	Symbol
Area	square meter	m ²
Volume	cubic meter	m ³
Unit mass	kilogram per cubic meter	kg/m ³
Frequency	hertz	Hz (or s ⁻¹)
Velocity	meter per second	m/s
Angular velocity	radian per second	rad/s
Acceleration	meter per squared second	m/s ²
Angular acceleration	radian per squared second	rad/s ²
Volumetric flow rate	cubic meter per second	m ³ /s
Force	newton	N (or kg · m/s ²)
Pressure	newton per squared meter, Pascal	N/m ² , Pa
Surface tension	newton per meter	N/m
Work	joule, newton meter	J, N · m
Diffusivity	meter squared per second	m ² /s

TABLE 4
Standard prefixes and multiples
in SI units (after Holman and Gadja, 1984)

Symbol	Multiple/ submultiple	Prefix
10 ¹²	tera	T
10 ⁹	giga	G
10 ⁶	mega	M
10 ³	kilo	k
10 ²	hecto	h
10	deka	da
10 ⁻¹	deci	d
10 ⁻²	centi	c
10 ⁻³	milli	m
10 ⁻⁶	micro	μ
10 ⁻⁹	nano	n
10 ⁻¹²	pico	p
10 ⁻¹⁵	femto	f
10 ⁻¹⁸	atto	a

CONVERSION OF UNITS

A physical quantity can be reported in terms of several units. It is common to convert a physical quantity from one unit system to another. For instance, a pressure can be converted from Pa to atm (atmospheric pressure). Erroneous unit

conversions can generate dramatic engineering mistakes, such as errors of several orders of magnitude. In soil mechanics in the United States, British units (e.g., pound, quart, foot, or inch) are still commonly used, although the SI units are recommended in engineering practice and required in technical publications.

Unit conversions can easily be performed with spreadsheets. The user-defined function UNITS in Chapter 9-3 performs such a conversion task. It was used in the appendix to generate the conversion factors for the units of length, area, volume, time, velocity, force stress, unit weight, and diffusivity.

REFERENCE

HOLMAN, J. P., and W. J. GADJA, Jr., 1984, *Experimental Methods for Engineers*, McGraw-Hill Book Company, New York.

REVIEW QUESTIONS

1. Define *dimension* and *unit*. Give an example of a dimension and a unit.
2. Name five basic dimensions.
3. Which is the most commonly used systems of units?
4. List 10 different units for length.
5. Find the basic dimensions of energy by using dimensional analysis.



8-5

Report Writing

INTRODUCTION

Many books have been written on the subject of report writing (e.g., Tarabian 1973). Here, we only review some basic requirements for a good report for engineering and academic purposes. The importance of good report writing and data representation cannot be overemphasized. The best experiment or the most brilliant discovery is worthless unless the information is communicated effectively to other people. In report writing, as in any communication exercise, the author must first identify his or her relative position to the reader with whom he or she intends to share the information. The author could be a student writing to the laboratory instructor, a laboratory technician to an engineering company, or an engineer to a client. The following presentation pertains primarily to the first situation, where a student has to write a report to a laboratory instructor.

ORGANIZATION OF REPORTS

The organization of a report depends largely on its volume; a 10-page report generally requires less structure than a 1000-page doctoral dissertation. Our recommendations apply to the laboratory reports that students will write to their laboratory instructor and supervisor, those reports involving generally less than a total of 10 pages. Our comments are also adapted to the generation of reports accompanied with spreadsheet results.

A carefully constructed outline is always the best starting point to write a report. It will help the writer to make sure that all pertinent information is included. The writer may decide to omit some elements of the recommended outline in particular circumstances.

Front Matter

Front matter includes the title page, with the author's name and affiliation, date of the work, sponsor of the report if any, a table of contents, and an optional list of nomenclature, tables, and figures.

- The title page should contain the minimum, but necessary, amount of information. Its main function is to identify the report. It is generally typed in larger characters that are clearly laid out.
- The table of contents should list the main headings and subheadings of the report. It is a good practice to number each page of the report and to indicate the heading page numbers in the table of contents.
- A list of nomenclature should be included when the author uses abbreviations and mathematical notations that are not common knowledge.
- A list of tables and a list of figures are required when there are numerous figures and tables throughout the text, a profusion of which may confuse everybody, including the author.

Abstracts

The abstract summarizes the main points of a report and should reflect in a few words the outcome of the work. Keep in mind that an abstract is often what people read first. Although the abstract comes first, it is generally written after the body of the report has been completed.

Introduction

The purpose of an introduction is to lay down the background of the problem that is to be solved in the report. A reference to past work on similar subjects is strongly encouraged. A good introduction should explain why a particular report has been written. It should always spell out the objectives of the present work. In practice, the objectives are generally specified by the instructor or by the client.

Experimental Apparatus and Procedure

The description of the experimental equipment and procedure may be extremely brief (e.g., ASTM D-854). It tells the reader how the test was performed. There is no need to copy a well-known procedure except when there have been deviations from it.

Results of Experiments

The results should be in clear tabular and graphical presentations. The spreadsheet programs provide added presentation benefits, of which the author should take full advantage. As a golden rule, all numbers should be reported with their units. A number without a unit implicitly assumes that the corresponding variable is dimensionless. Would you like to be paid 100 cents rather than 100 dollars? The same rule applies to the labels along the vertical and horizontal axes of a graph. Always remember that a good graph or table should stand on its own without the need for additional information.

Interpretation of Results

The interpretation of experimental results always engages the responsibility of the author, who has to answer the following question: Are my results in agreement with existing theories, or are they contradicting them? Again, remember that the experiment has been performed for a specific objective. This section should tell if the experimental results fail, meet, or exceed expectations. The reasons for failure or success should be made as clear as possible. In cases where the

author would develop an challenging or apologetic mood, it is recommended that there be a separate section entitled "Discussion." You may include in a discussion section what you did not like, or what you believe should be done.

Conclusions

An honest conclusion collects only the main points that have been made in the body of the report. It should make sure that all the objectives of the report that were spelled out in the introduction have been addressed properly. It should not bring a new topic or problem, which is bound to confuse the reader. Many readers will read only the abstract and the conclusion. In general, the conclusion and the abstract are always the last sections to be written in a report. But avoid copying the same sentences in the abstract and conclusion, at the risk of testing the patience of your readers.

Acknowledgments

Should you feel the need to recognize the contribution of some of your colleagues to your work, an acknowledgment is the appropriate place to express your gratitude. Please be precise, and acknowledge your sponsor if any. What about your laboratory partners who collected data for you during the experiment?

References

Rare, and generally poor, are the technical reports that contain no references to past work. References may be cited in the text in various ways. We recommend referring to the work by the author's last name followed by the publication year (e.g., Terzaghi 1943). Numbering the references in the text is another recognized practice. The references should be listed alphabetically in a separate section after the conclusion. They should be typed in a consistent format. You may refer to the format of the references typed in this book.

Appendix

To keep a report clear and concise, it is very often necessary to open a separate section after the main body of the report: the appendix or appendices. An appendix may contain data or graphs that are useful but not fundamental to comprehending the report. In the appendix you may include the calibration of measuring instruments, or details of the formulas you have used to perform the calculations in the spreadsheets.

EXAMPLE

Most computer programs have a wealth of features for preparing reports, which should be used sparingly with the sole goal of clarifying the report. The author should try to refrain from abusing the bells and whistles of these computer programs, an excess of which may obscure the main message. A report should have a consistent style throughout the headings, text, numbers, and figures.

Hereafter, we provide an example of a clear and well-organized report, which should meet the requirements of most instructors. It was obtained by combining the use of a word processor and a spreadsheet program: namely Microsoft Word and Excel. The word processor is used to

generate and paginate the report, and the spreadsheet program is used to perform all calculations and graphics. Once all the data have been processed into the spreadsheet, it is copied and inserted into the report for the final presentation. The report is listed in Fig. 1. The cover page is a title page, the function of which is to identify the report by stating the experiment title, name of student, date, and so on. Following the cover page, the first page contains the table of contents, the abstract, the introduction, and the experimental equipment and procedure. It accounts for the selection of a particular sieving technique (e.g., dry versus wet technique). The second page combines the experimental results and their interpretation. The measured and calculated data are reported in tables and figures that are numbered (e.g., Table 1 and Fig. 1) and that are referred to in the text by using these numbers (e.g., Table 1 and Fig. 1). All the tables and figures should have a caption that identifies them and describes their contents concisely. All the numbers in the tables have a unit (e.g., grain size in mm) unless if they are dimensionless (e.g., coefficient of uniformity). The third page presents the experimental results as a graph, with labeled axes, and gives the discussion, conclusion, and references. The fourth and fifth pages are the appendices. They contain the details of the calculations that are useful to detect the possible errors of measurement and/or data processing.

REFERENCES

TURABIAN, K. L., 1973, *A Manual for Writers*, 4th ed., University of Chicago Press, Chicago.

EXERCISES

1. Name the 10 different sections in a well-organized report.
2. What is the purpose of a table of contents?
3. What is the function of an introduction?
4. What is the main difference between an abstract and a conclusion?

Grain size analysis with sieve

CE468L laboratory report No. 1

by M. Kapuskar

7 September 1996

Civil Engineering Department
University of Southern California
Los Angeles CA 90089-2531

Figure 1 Example of a laboratory report.

Custom functions used in formulas

et

the grain size distribution curve of soil sample
Marina District of San Francisco, California
analysis. Based on the coefficients of un
sample is classified as a fine-grained uni

ction and objective

The objective of the report is to define
by using a sieve analysis for soil sample
San Francisco, California. The grain size
the relative proportion of different gra

experimental equipment and procedure

The experimental equipment and procedure
titled "Grain size analysis with sieve" of
consists of sorting soil grains by size

60	0.250	40.90
100	0.150	122.00
200	0.075	4.70
pan		0.10

Total mass $M_{tot} = 190.20$ g

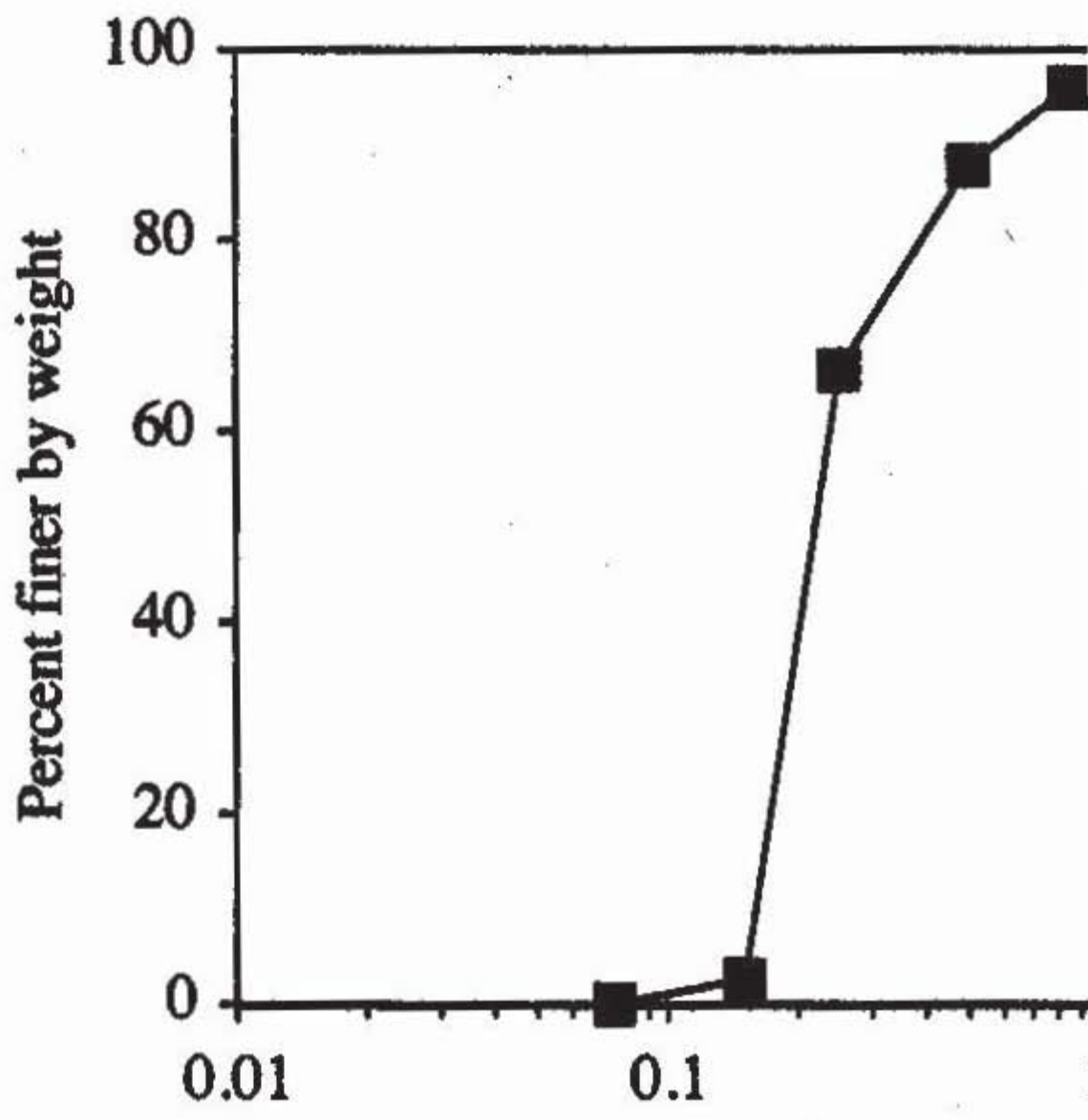
$D_{10} = 0.159$ mm

C_u

$D_{30} = 0.187$ mm

C_c

$D_{60} = 0.238$ mm



Sample mass $M_0 = 191.10$

US sieve number	Sieve opening (mm) d	Mass retained (g) M
4	4.750	0.00
10	2.000	2.10
20	0.850	4.60
35	0.500	15.80
60	0.250	40.90
100	0.150	122.00
200	0.075	4.70
pan		0.10

Total mass $M_{tot} = 190.20$ g

$D_{10} = 0.159$ mm

C_u

$D_{30} = 0.187$ mm

C_c

$D_{60} = 0.238$ mm

las used in Table 1

A	B	C	
US sieve number	Sieve opening (mm) d	Mass retained (g) M	Mass M_0

List of variables used in Table 1

Variable name	Cell(s) location
d	=B10:B16
D.10	=B19
D.30	=B20
D.60	=B21
M	=C10:C17
M0	=B6
Mp	=D10:D17
Mtot	=C18
p	=E10:E16

Custom functions used in formulas of Table 1

	A
1	INTER
2	=RESULT(1)
3	=ARGUMENT("Value",1)
4	=ARGUMENT("X",64)
5	=ARGUMENT("Y",64)
6	=IF(OR(ROWS(X)<>ROWS(Y),ROWS(X)<1,ROWS(Y)<1),RETURN(#VALUE!))
7	=FOR("I",1,ROWS(X)-1)
8	= IF(AND((INDEX(X,I+1)-Value)*(INDEX(X,I)-Value)<=0,INDEX(X,I+1)<>INDEX(X,I)))
9	= RETURN((INDEX(Y,I)*(INDEX(Y,I+1)/INDEX(Y,I))^(Value-INDEX(X,I)))/(INDEX(X,I+1)-INDEX(X,I))))
10	= END.IF()
11	=NEXT()
12	=RETURN(#VALUE!)

- 4 -

Figure 1 (cont.)



9

Data Processing with Spreadsheets


- 9-1** Basics of spreadsheets
- 9-2** User-defined functions
- 9-3** Worked examples

9-1

Basics of Spreadsheets

INTRODUCTION

Spreadsheet programs such as Lotus 123 and Microsoft Excel are common software for personal computers. Originally intended for business applications, spreadsheets are now capable of performing sophisticated calculations in engineering and science. Spreadsheets are convenient for entering and processing data and displaying it as two- and three-dimensional graphs. Intuitively mastered after a few hours of training, spreadsheets are becoming the most used technique for processing data in the geotechnical laboratory. In this book, we selected Excel (Microsoft Corp. 1994a,b) because it works on Apple and Windows computers. However, our spreadsheet approach to data processing is general enough to be adapted to other spreadsheet programs.

In the following section, we introduce some basic spreadsheet definitions and review their features relevant to the processing of laboratory data. This section, which may be too elementary for experienced users, ends with a list of exercises and questions to probe basic knowledge of spreadsheets. These questions may help users test their understanding and identify the features they should know. The text here applies to both the Macintosh and Windows versions of Excel. The only difference is that the COMMAND key, denoted  for Macintosh, should be replaced by the Control key (CTRL) in Windows.

WORKSHEETS AND WORKBOOKS

As shown in Fig. 1, a spreadsheet (or worksheet) is a matrix of cells to enter data, text or formulas. The columns are numbered from A to Z, then AA, AB to IV, and the rows are numbered from 1 to 16384. Cells are referenced by column then by row. For example, cell B2 is located in column B and row 2. The active cell where the action takes place is highlighted and its name is displayed in the reference area. A cell range is a group of connected cells, columns, and rows. Ranges are referred to by the cells at their extremities (e.g., B:D, 5:7, B2:E5, or C2:F2).

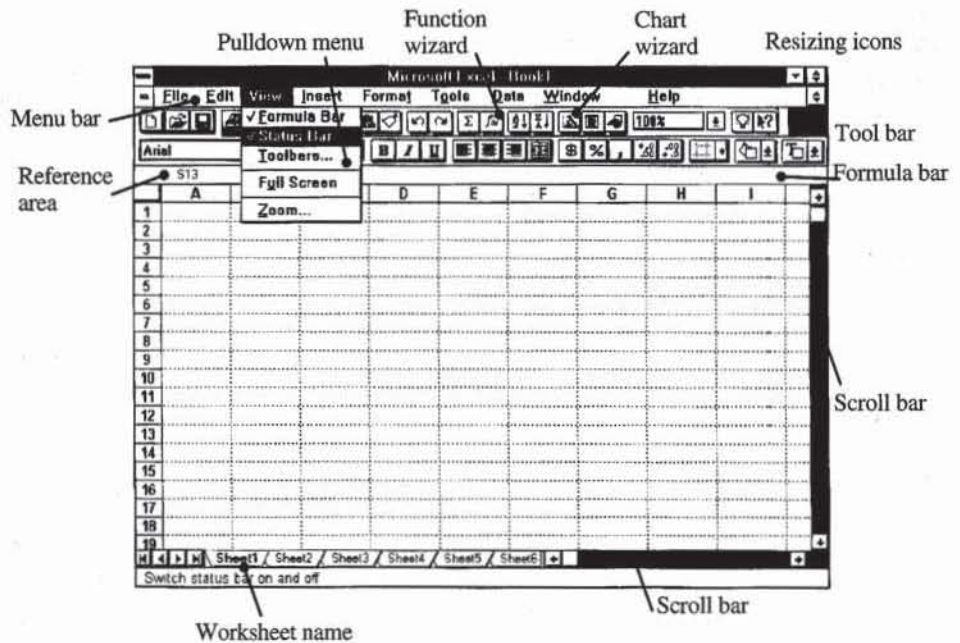


Figure 1 Typical Excel window and some of its parts.

Excel collects several worksheets into workbooks. As shown in Fig. 1, the worksheets are displayed by clicking on their names once and are renamed by clicking twice. Workbooks are useful to organize related materials (e.g., specific types of experiments and projects).

Figure 1 identifies several elements of a workbook. The menu bar displays several pull-down menus (e.g., View) with their specific commands. Some of these commands are listed in Table 1. The title bar displays the name of the workbook. The formula bar displays the data or formula in the active cell. The scroll bars are used to display the rest of the worksheet. The status bar displays various messages or information about the current command. The tool bar contains several icons of commonly used commands. The window may be resized by dragging its lower right corner or double clicking on the icon at the upper right corner.

FORMULAS

By definition, a formula is a mathematical expression that calculates a result from two or more values. Formulas consist of numbers, mathematical operators (+, -, *, /, ^), functions (e.g., COS, SIN), and references to other cells (e.g., B2) or range references (e.g., B2:D10). Cells and cell ranges may be called by using names (e.g., A). All formulas must begin with an equal sign. They are entered and edited as text or numbers. The following are examples of formulas:

- | | |
|-----------|--|
| = B4 | The cell containing the formula takes the values in cell B4. |
| = B4/B2 | Divides the contents of cell B4 by that of cell B2. |
| = B4 + B2 | Adds the contents of cell B4 with that of cell B2. |

The mathematical operators obey the common rule of operator precedence. The order of the calculation is %, ^, *, and /, +, and - . You may use parentheses to overrule this operator precedence. The result of a formula is calculated and

TABLE 1

Main functions of pull-down menus of the Macintosh version of Excel. In Windows, the COMMAND (⌘) key should be replaced by the Control (CTRL) key

Name	Shortcut	Definitions
File Save	⌘S	To save an existing workbook or to save and name a new one.
File Save As ...		To save the workbook under a different name or in a different folder or floppy disk.
File New	⌘N	To open a new workbook.
File Open	⌘O	To open an existing workbook.
File Close	⌘W	To close the workbook, which can also be done by clicking on the close icon.
File Quit	⌘Q	To finish using Excel. Remember to save your work from time to time when working and before closing it.
File Print	⌘P	To print a worksheet.
Edit Redo	⌘Y	To repeat the last action.
Edit Undo	⌘Z	To undo the last action.
Edit Copy	⌘C	To copy a cell or cell range to another location. You may also copy by dragging the selection with the mouse while pressing the Option key.
Edit Paste..	⌘V	To paste a cell or cell range that was copied to another location. You may also paste by dragging the selection with the mouse while pressing the Option key
Edit Cut	⌘X	To cut and copy a cell or cell range that is to be pasted somewhere else. You may also move the selection by dragging it with the mouse.
Edit Insert	⌘I	To insert a single cell or whole rows and columns.
Edit Clear	⌘B	To clear data quickly. You can completely remove the cell contents, format, formula, or attached notes by using the options of Edit Clear .
Edit Delete	⌘K	To delete cells or cell ranges. Erroneous deletions can be rectified by using Undo .
Insert Name Paste	⌘`	To display the names of all defined variables or arrays.
Insert Name	⌘L	To switch between the displays of formulas and results.
	Enter	To name a variable or array.
		To enter an array formula.

displayed in the active cell. You switch between the display of formulas and results by using ⌘`.

When a formula is copied or moved from one cell to another, the cells that it references are adjusted to compensate for the movement. For instance, as shown in Fig. 2, the formula = A4 + B5 in cell B4 becomes = C8 + D9 when copied to cell D8. The column letter and row number are both shifted, in most cases avoiding the redefinition of the formula.

When the cell reference is to remain unchanged after copying, absolute cell references are used instead of relative references. Absolute references are defined by adding \$ before the column letter and/or row number. As shown in Fig. 2, \$A\$4 is not changed by copying from cell B6 to cell D11, whereas B5 is changed. A mixed reference is partially absolute and partially relative (e.g., \$A4 in cell B8). As shown in Fig. 2, the row number changes, but not the column letter, when cell B8 is copied to cell D14.

Formulas having cells or cell ranges (e.g., B43 + C2 or SUM(A3:B40)) are more difficult to read than mathematical relations with simpler variable names (e.g., = x + t or SUM(T)). Cells or cell ranges can be assigned a name by using ⌘ L. If the variable applies only to the present worksheet, its name should be preceded by the worksheet name and ! (e.g., *Example!x* for variable *x* in worksheet *Example*). The names used in the workbook are defined in the pulldown menu of the reference cell. They can also be listed with their locations by using the list option of **Insert Name Paste ...** The use of variables is highly recommended because it greatly simplifies formulas.

	A	B	C	D	E
1					
2					
3					
4		=A4+B5			
5					
6		=\$A\$4+B5			
7					
8		=\$A4+B7		=C8+D9	
9					
10					
11				=\$A\$4+D10	
12					
13					
14				=\$A10+D13	
15					
16					

Figure 2 Effect of copying formulas in spreadsheets.

BUILT-IN FUNCTIONS

Excel provides built-in functions to construct complex formulas, some of which are listed in Table 2 by categories. The mathematical, trigonometric, and statistical functions are the most commonly used in processing laboratory measurements. The built-in functions may be entered directly or by using the Formula Wizard. The Formula Wizard displays the available functions and their arguments to be completed. Additional help on built-in functions can be obtained from the interactive help.

TABLE 2

List of functions available in Excel

(a) Mathematical and trigonometric functions	
<u>ABS(number)</u>	absolute value of a number
<u>ACOS(number)</u>	arccosine of a number (in radian)
<u>ACOSH(number)</u>	inverse hyperbolic cosine of a number
<u>ASIN(number)</u>	arcsine of a number (in radian)
<u>ASINH(number)</u>	inverse hyperbolic sine of a number
<u>ATAN(number)</u>	arctangent of a number
<u>ATAN2(x_num,y_num)</u>	arctangent from x- and y- coordinates
<u>ATANH(number)</u>	inverse hyperbolic tangent of a number
<u>COS(number)</u>	cosine of a number
<u>COSH(number)</u>	hyperbolic cosine of a number
<u>EVEN(number)</u>	rounds a number to the nearest integer
<u>EXP(number)</u>	exponential of a number
<u>FACT(number)</u>	factorial of a number
<u>INT(number)</u>	rounds a number down to the nearest integer
<u>LOG(number, base)</u>	logarithm of a number to a specified base
<u>LOG10(number)</u>	base-10 logarithm of a number
<u>MDETERM(array)</u>	matrix determinant of an array
<u>MINVERSE(array)</u>	matrix inverse of an array
<u>MMULT(array1,array2)</u>	matrix product of two arrays
<u>PI()</u>	value pi
<u>RAND()</u>	random number between 0 and 1
<u>SIGN(number)</u>	sign of a number
<u>SIN(number)</u>	sine of a number
<u>SINH(number)</u>	hyperbolic sine of a number

TABLE 2 (cont.)

List of functions available in Excel

(a) Mathematical and trigonometric functions	
<u>SQRT</u> (number)	square root of a number
<u>SUM</u> (number1,number2,.....)	add the arguments
<u>SUMPRODUCT</u> (array1,array2,.....)	sum of the products of corresponding components
<u>TAN</u> (number)	tangent of a number
<u>TANH</u> (number)	hyperbolic tangent of a number
(b) Information functions	
<u>ISBLANK</u> (value)	TRUE if the value is blank
<u>ISLOGICAL</u> (value)	TRUE if the value is a logical value
<u>ISNUMBER</u> (value)	TRUE if the value is a number
<u>ISTEXT</u> (value)	TRUE if the value is text
(c) Statistical functions	
<u>AVERAGE</u> (number1,number2,.....)	average of the arguments
<u>COUNT</u> (value1,value2,.....)	counts how many numbers are in the lists of arguments
<u>COUNTA</u> (value1,value2,.....)	counts how many values are in the lists of arguments
<u>GROWTH</u> (known_y's,known_x's,new_x's,const)	returns values of an exponential trend
<u>LINEST</u> (known_y's,known_x's,const,stat)	returns the parameters of a linear trend
<u>LOGEST</u> (known_y's,known_x's,const,stat)	returns the parameters of an exponential trend
<u>MAX</u> (number1,number2,.....)	maximum value in a list of arguments
<u>MIN</u> (number1,number2,.....)	minimum value in a list of arguments
<u>SLOPE</u> (known_y's,known_x's)	slope of the linear regression line
<u>INTERCEPT</u> (known_y's,known_x's)	intercept of the linear regression line
<u>TREND</u> (known_y's,known_x's,new_x's,const)	returns values along a linear trend
(d) Lookup and reference functions	
<u>COLUMNS</u> (array)	returns the number of columns of an array
<u>INDEX</u> (array, row_num,column_num)	chooses a component of an array
<u>ROWS</u> (array)	returns the number of rows of an array
<u>TRANSPOSE</u> (array)	returns the transpose of an array
(e) Logical functions	
<u>AND</u> (logical1, logical2,.....)	returns TRUE if all its arguments are TRUE
<u>FALSE</u> ()	returns the logical value FALSE
<u>IF</u> (logical1, value_if_true,value_if_false)	TRUE if the value is not text
<u>NOT</u> (logical)	reverses the logic of its arguments
<u>OR</u> (logical1, logical2,.....)	returns TRUE if any argument is TRUE
<u>TRUE</u> ()	returns the logical value TRUE
(f) Text functions	
<u>CHAR</u> (number)	returns the character specified by the code number
<u>EXACT</u> (text1,text2)	check to see if two text values are identical
<u>FIND</u> (find_text, within_text,start)	finds one text value within another (case sensitive)
<u>LEFT</u> (text, num_chars)	returns the leftmost characters from a text string
<u>LEN</u> (text)	returns the number of characters in a text string
<u>LOWER</u> (text)	convert text to lower case
<u>RIGHT</u> (text, num_chars)	returns the rightmost characters from a text string
<u>TRIM</u> (text)	removes spaces from text
<u>UPPER</u> (text)	convert text to upper case

ARRAY FORMULAS

An array formula produces an output array (i.e., a cell range). For instance, the built-in linear regression function LINEST fills in several cells for output instead of a single cell. Array formulas are displayed in the formula bar between braces

	A	B		A	B
1	x	y	1	x	y
2	1	-1.00	2	1	=RAND()
3	2	-0.64	3	2	=RAND()
4	3	-0.18	4	3	=RAND()
5	4	-0.79	5	4	=RAND()
6	5	-0.07	6	5	=RAND()
7	6	-0.02	7	6	=RAND()
8	7	-0.31	8	7	=RAND()
9	8	-0.25	9	8	=RAND()
10	9	-0.22	10	9	=RAND()
11	10	-0.01	11	10	=RAND()
12	Slope	y-intercept	12	Slope	y-intercept
13	0.080	-0.783	13	=LINEST(B2:B10, A2:A10)	=LINEST(B2:B10, A2:A10)

Figure 3 Example of results and array formula for linear regression.

{ } [e.g., {=LINEST(B2:B11,A2:A11)}]. Array formulas are edited by selecting a cell range, entering the formula, and using **Shift + Enter** instead of Enter. As shown in Fig. 3, the array formula {=LINEST(B2:B11,A2:A11)} in cells A13:B13 calculates the slope and intercept of a linear regression for a series of x and y data. The left figure shows the results, and the right one displays the formulas.

FORMATS

The column width and row height may be adjusted by dragging the pointer at the top right edge of the column heading (or bottom edge of the row heading). The column width (or row height) may be optimized by double clicking. Columns or rows may also be hidden by using **Format Row Hide** or **Format Column Hide**.

As shown in Table 3, numbers can be displayed by using various formats of **Format Cells Numbers**. When ##### is displayed, the column width is too narrow for the selected format. The text alignment may be defined by using the left, right, or center options of the **Format Cells Alignment**. The overwriting of cells may be prevented by selecting the **Wrap** option of **Alignment**.

TABLE 3
Examples of formats for numbers

Format	Display
0.00E+00	1.23E+03
0.00	1234.00
#,##0.00	1,234.00
#,##0.00%	123,400.00%
0.0 "m"	1234.0 m

The style (e.g., bold, italic), font (e.g., Geneva, Time, Symbol), size of font (e.g., 12 pt, 14 pt), and color of cells can be modified by using the options of **Format Cells Font**. Borders and shading can also be added by using **Format Cells Borders**. By default, grid lines are displayed on the spreadsheet screen. They may be hidden by options in **Tools Options View**. Shading and various gray levels can also be added by using **Format Cells Pattern**.

PRINTING YOUR WORKSHEET

In the dialog box of **File Page Setup...** you may select the landscape or portrait orientations, paper size, margin positions, scaling, and range of pages to be printed. You may center horizontally and/or vertically your print on each page. You may add or delete the row and column headings, grid lines, headers (e.g., titles), and footers (e.g., page numbers). You may print a smaller area of the worksheet by using **File PageSetup Set Print Area...** and define your own page breaks by using **Insert Page Break**. You may preview the print on the screen by using **File Print Preview...** While previewing, you may interactively setup the pages and margins. You may select the page range and number of copies to be printed in the Print dialog box.

CREATING CHARTS

Excel offers several types of two- or three-dimensional charts, including pie, bar, column, area, and line graphs. Charts are created by using the Chart Wizard as follows. Click on the Chart Wizard Icon, open a plotting window in the worksheet with the mouse, and enter the input as required by the Chart Wizard.

Charts can be copied, moved, and resized. They are edited by double clicking on them. A title is added to the chart or the axes by using **Insert Titles**. The font, size, orientation, and alignment of axis labels, scales, tick marks, line thicknesses, number formats, fonts, and patterns may be changed by double clicking on the axis. The same technique also applies to change the minimum and maximum intervals along the axis, to reposition the x and y axes, and to select a logarithmic axis.

Two-dimensional x - y line graphs and scattered point charts are the most commonly used for representing laboratory results. The line styles and data point symbols are changed by double clicking on them. New data sets may be added to the same chart by using **Insert New Data...** The series can also be reordered. Multiple data sets may be labeled with legends by using **Insert Legend**. The legends may be repositioned by dragging them to a new position.

REFERENCES

- Microsoft Corporation, 1994a, Microsoft Excel, *User's Guide, Version 5*.
Microsoft Corporation, 1994b, Microsoft Excel, *Visual Basic User's Guide, Version 5*.

EXERCISES

1. Name 10 different parts in a spreadsheet.
2. Do you know how to:

Resize and move a worksheet window?

Save a worksheet with the same name or with a new name?

Open a new or existing workbook?

Move between worksheets?

Close a workbook?

Enter and edit text, numbers, dates and times?

Fill in a series of data?

- Use undo and redo?
 - Select a cell range?
 - Copy, move, and erase data?
 - Copy or move a worksheet to another workbook?
 - Insert and delete individual cells, rows, and columns?
 - Write and enter formulas?
 - Display formulas instead of their results?
 - Copy formulas?
 - Use the formula wizard?
 - Enter an array formula?
 - Format and align numbers?
 - Define names for variables and arrays that are local to a worksheet?
 - Enter formulas with named variables?
 - List all the variables defined in the workbook?
 - Rename a variable?
 - Change the display format?
 - Change alignment?
 - Center text over multiple columns?
 - Change the font?
 - Add a border around a cell or cell range?
 - Shade a cell range?
 - Change column width and row height?
 - Apply existing styles to a cell range?
 - Change the default display format and alignment?
 - Create styles?
 - Change the print setup?
 - Choose the print area?
 - Adjust page breaks?
 - Preview a print job?
 - Print a worksheet?
 - Create and save charts?
 - Choose the chart type?
 - Print a chart?
 - Resize a chart?
 - Add a title and legend to a chart?
 - Format text on a chart?
 - Change scale and tick marks?
 - Select a logarithmic axis and change the axis intersection?
3. What are relative and absolute cell references (addresses)?
 4. What are styles for Excel spreadsheets? What are their advantages?
 5. What is an array formula?
 6. What are worksheets and workbooks?
 7. Which is the easiest way to define a formulas with built-in functions?

9-2 User-defined Functions

INTRODUCTION

A user-defined function is created by combining formulas and built-in functions, and is used as other built-in functions. A user-defined function may be created by using a macrosheet or Visual Basic. A macrosheet looks like a spreadsheet but contains functions and commands instead of input data. It is the original programming language of spreadsheets. Visual Basic is a more recent and advanced programming language that is similar to Basic and other computer languages. For instance, Fig. 1 shows the user-defined function SIND, which calculates the sine of angles in degrees, in the macrosheet language and Visual Basic.

MACROSHEET USER-DEFINED FUNCTIONS

In a macrosheet, a user-defined function is a succession of formulas, ordered in a column with a specific structure. The first line contains its name (e.g., SIND in Fig. 1). The second line defines its output type, which may be a number, a text, a logical, a reference, an error message, an array, or a combination of the above. The output type is defined by RESULT followed by a data type. The various data types are listed in Table 1. If the result is a number or a text, the data type is 3. RESULT must come before any other formulas. If you omit the data type, the data type is assumed to be 7 by default (i.e., a number, a text, or a logical). In the example of Fig. 1, the result of SIND is a number.

	A
1	SIND
2	=RESULT(1)
3	=ARGUMENT("X",1)
4	=RETURN(SIN(PI()*X/180))

```
Const Pi = 3.141592654
Function Sind(x)
Sind = Sin(Pi * x / 180)
End Function
```

Figure 1 Example of user-defined function in a macrosheet (left) and Visual Basic (right).

TABLE 1
Data type for functions
ARGUMENT and RESULT

Value	Data type
1	Number
2	Text
4	Logical
8	Reference
16	Error
64	Array

Like built-in functions, user-defined functions have input variables. Each input variable must individually be defined by using ARGUMENT in the column under RESULT. ARGUMENT specifies the name and type of each input variable name. The name is entered as text between double quote marks. For instance, in Fig. 1, the angle in degree is named X. ARGUMENT specifies the data type in a similar way to RESULT. This type may be a number, a text, a logical, a reference, an error message, an array, or a combination of the above.

Following ARGUMENT, the users define the formulas that perform the main operation of their function. These formulas may invoke cell references within the worksheet and names of variables defined by ARGUMENT or **Ⓜ**. For instance, the calculation is performed in cell A4 of Fig. 1 by using the variable named X by ARGUMENT. A user-defined function is terminated by using RETURN, which branches the calculation back to the worksheet.

Writing a User-Defined Function

There are two steps in defining a user-defined function: (1) creating it and (2) naming it. A new macrosheet is created within a workbook by choosing **Insert Macro MS Excel 4.0 Macro**. The same macrosheet may contain several user-defined functions. A user-defined function is named by selecting its first cell, by choosing **Insert Name Define (or Ⓜ)**, by entering the function name in the **Name** box, and by selecting the **Function** option.

Using a User-Defined Function in a Worksheet


You may use a user-defined function by using the Function Wizard, which lists the active user-defined functions after the built-in functions. In the window of the Function Wizard, replace the arguments of the user-defined function with cell(s) or cell range(s). When the desired user-defined functions do not appear in this list, check that their names have been defined with **Ⓜ** and that their macrosheet is open.

VISUAL BASIC USER-DEFINED FUNCTIONS

In Visual Basic, a user-defined function is created within a workbook by **Insert Module**. It starts with **Function** followed by the function name and ends with **End Function**. The function type can be **Single** or **Variant**, depending on whether it returns a number or an array (other types besides **Single** and **Variant** are also available as specified in the Visual Basic User's Guide). On the line after **Function**, the types of the function arguments should be defined. When the arguments are undefined, they are considered as **Variant**. Visual Basic has its own built-in func-


```
Function MyLinest(X,Y) As Variant
    Slope = Application.SLOPE(Y,X)
    Intercept = Application.INTERCEPT(Y,X)
    MyLinest = Array(Slope,Intercept)
End Function
```

Figure 2 Example of Visual Basic function using built-in macrosheet functions.

tions, which in most cases have spellings similar to those of macrosheet built-in functions. Some built-in macrosheet functions are called from within Visual Basic by using the prefix Application (Fig. 2). Visual Basic is a powerful language that extends the capabilities of macrosheets. Its functions are linked automatically to the workbook and do not need to be defined with .

REFERENCE

Microsoft Corporation, 1994, Microsoft Excel, *Visual Basic User's Guide, Version 5*.

EXERCISES

1. What is a user-defined function?
2. What is a macrosheet? What is the main difference between a worksheet and a macrosheet?
3. What is the basic structure of a user-defined function in a macrosheet?
4. How do you use an existing user-defined function?
5. How do you define the input and output of a user-defined function?
6. Write a user-defined function that calculates the cosine of an angle in degrees.
7. What is Visual Basic?

9-3 Worked Examples

EXAMPLE 1: SUPERIMPOSED GRAPHS

EXERCISE

Plot functions $\sin(2\theta)$ and $\cos(2\theta)$ on the same graph when angle θ varies from 0 to 180° . Format the graph as shown in Fig. 1 and tabulate the data as shown in Fig. 2.

STEPS

The table of Fig. 1 is obtained as follows:

- Create a new workbook with File New.
- Enter the table headings in cells A3, B3, and C3.
- Enter 0 in cell A4.
- Select range A4:A40 with the mouse.
- In the dialog box of **Edit Fill Series**, enter 5 for step value. Cells A4 to A40 now display the θ values.
- Press ⌘L and enter Example1!q to name the range A4:A40 (or abcd!q if abcd is the name of your worksheet). q stands for the Greek symbol θ , which cannot be used.
- Enter $= \sin(2*Pi()/180*q)$ in cell B4 and $= \cos(2*Pi()/180*q)$ in cell C4 (Fig. 3).
- Select cells B4:C4 and press ⌘C .
- Select range B4:C40 and press ⌘V . All the number of Fig. 1 should now be displayed.
- Move to cell A43 and list the names and locations of the variables in the workbook by using **Insert Name Paste ... Paste Link**.
- Adjust the column widths by double clicking on the edges of the column headings or by dragging them.

$$\frac{2\theta \times \pi}{180}$$

$$\frac{\theta}{180} = \frac{\pi}{P.D}$$

- Select the range B4:C40 use **Format Cells Numbers ...**, or $\text{Ctrl}+1$, and enter the format 0.00.
- Select the range A3:C40 and choose the horizontal centering option of **Format Cells Alignment...**
- Edit cells A3, B3, and C3 to obtain the symbol θ with **Format Cells Font**.
- Define the table border with **Format Cells Border** so that your table looks like that of Fig. 1.

The chart of Fig. 2 is obtained as follows:

- Click on the Chart Wizard Icon and open a plotting window by dragging the mouse on the spreadsheet.
- Select the range A3:C40 by using the mouse, then press **Next >**.
- Select the XY scatter chart type, then press **Next >**.
- Select the option with connected points and linear axes, then press **Next >**.

	A	B	C
3	θ (deg)	$\sin(2\theta)$	$\cos(2\theta)$
4	0	0.00	1.00
5	5	0.17	0.98
6	10	0.34	0.94
7	15	0.50	0.87
8	20	0.64	0.77
9	25	0.77	0.64
10	30	0.87	0.50
11	35	0.94	0.34
12	40	0.98	0.17
13	45	1.00	0.00
14	50	0.98	-0.17
15	55	0.94	-0.34
16	60	0.87	-0.50
17	65	0.77	-0.64
18	70	0.64	-0.77
19	75	0.50	-0.87
20	80	0.34	-0.94
21	85	0.17	-0.98
22	90	0.00	-1.00
23	95	-0.17	-0.98
24	100	-0.34	-0.94
25	105	-0.50	-0.87
26	110	-0.64	-0.77
27	115	-0.77	-0.64
28	120	-0.87	-0.50
29	125	-0.94	-0.34
30	130	-0.98	-0.17
31	135	-1.00	0.00
32	140	-0.98	0.17
33	145	-0.94	0.34
34	150	-0.87	0.50
35	155	-0.77	0.64
36	160	-0.64	0.77
37	165	-0.50	0.87
38	170	-0.34	0.94
39	175	-0.17	0.98
40	180	0.00	1.00

Figure 1 Variation of $\sin(2\theta)$ and $\cos(2\theta)$ with θ .

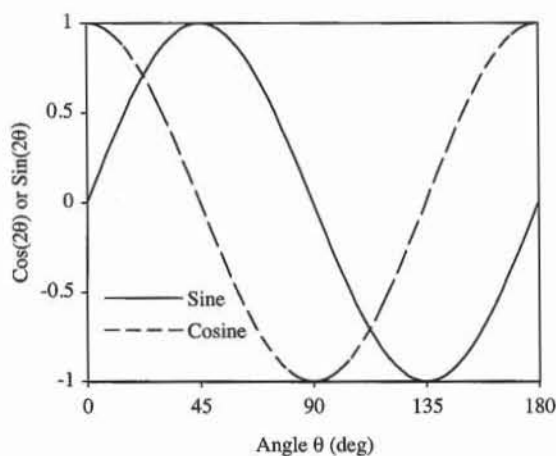


Figure 2 Plots of $\sin(2\theta)$ and $\cos(2\theta)$.

- Assign the data series in columns, using the first column for X data. Assign the legend in the first row, enter “Angle (deg)” for the X-category axis title and “Cosine or Sine” for the Y-values axis title, then press **Finish**.

A chart should now be displayed in Excel’s built-in format. In the following steps, you will modify this graph so that it looks like Fig. 2.

- Select the chart by double clicking on it.
- Double click on the shaded area to display the **Format Plot Area** dialog box. Select a border and no area, then press OK.
- Double click on the vertical axis to display the **Format Axis** dialog box. In **Patterns**, select outside major tick marks and no minor tick marks. Move to **Scale** and enter 0.5 for major unit and -1 for the value at which the X axis crosses the vertical axis. Move to **Font** and select 10-pt Times.
- Double click on the horizontal axis to display the **Format Axis** dialog box. In **Patterns**, select outside major tick marks and no minor tick marks. Move to **Scale** and enter 180 for maximum and 45 for major unit. Move to **Font** and select 10-pt Times.
- Double click on the series of Cosine data points to display the **Format Data Series** dialog box. In **Patterns**, select a solid line and no marker. In **Names and Values**, enter Cosine for name, then press OK.
- Double click on the series of Sine data points to display the **Format Data Series** dialog box. In **Patterns**, select a dashed line and no marker. In **Names and Values**, enter Sine for name, then press OK.
- Drag the box containing the series labels to the location shown in Fig. 2.
- Double click on the box to display the **Format Labels** dialog box. Select no border and no area, then press OK.
- Double click on the horizontal axis title to edit it and introduce the symbol θ . Type the letter q , select it, and change its font from Times to Symbol. Note that you cannot edit graph labels that are set equal to the contents of spreadsheet cells.

	A	B	C
3	θ (deg)	sin(2θ)	cos(2θ)
4	0	=SIN(2*PI()/180*q)	=COS(2*PI()/180*q)

Figure 3 Formulas used in Fig. 1.

- Double click on the vertical axis title to edit it and introduce q as shown in Fig. 2.
- You may drag the chart and scale it by using its edge points.

EXAMPLE 2: FITTING OF DATA POINTS WITH A POWER RELATION

EXERCISE

Find the power relation between U.S. sieve number N and mesh opening d in Fig. 4, and compare the fitted and original results on a log-log graph. Use the built-in functions TREND, SLOPE, INTERCEPT, and LINEST, and fit data by using Trendline.

STEPS

- In a new workbook, enter column headings in cells A8:C9 and numbers in cell range A10: B38, and format them as shown in Fig. 4.
- Assign the name N to the range A10:A38, using **Alt**. In the same way, assign the name d to the range B10:B38. You may use the reference area or **Insert Name Paste ... Paste Link** to verify the names.
- Select the range C10:C38, type the formula as shown in cell C10 of Fig. 5, and press **Enter**. The cell range C10:C38 should be filled as shown in Fig. 4.
- Use the Chart Wizard, to plot the ranges C10:C38 versus A10:A38 as a solid line and the ranges B10:B38 versus A10:A38 as discrete points. Select logarithmic axes and define titles for axes as shown in Fig. 6.
- Select the range C41:D41, type the formula with **LINEST** in cell C41 as shown in Fig. 7, and press **Enter**. The results of Fig. 8 should be displayed. The final result is $d = 10^b N^a$, where d is the mesh opening (mm), N the U.S. sieve number, a the slope of linear regression ($a = -1.085$), and b the intercept of linear regression ($b = 1.360$).
- In cells C42 and C43, enter the formulas of Fig. 7 to obtain a and b by using SLOPE and INTERCEPT.
- Use the Chart Wizard to plot the ranges B10:B38 versus A10:A38 as discrete points. Format the graph as shown in Fig. 9.
- Select the data points and use **Insert Trendline...** In **Options**, select to display the equation and R^2 value on the chart. In **Type**, select the power relation. You should obtain the graph of Fig. 9, and the equation displayed by Trendline should yield the same results as those found by LINEST, SLOPE, and INTERCEPT.

Arrays

Using

12

21

	A	B	C
8	US sieve number	Sieve opening (mm)	Fitted sieve opening (mm)
9	N	d	
10	4	4.750	5.098
11	5	4.000	4.002
12	6	3.350	3.284
13	7	2.800	2.778
14	8	2.360	2.404
15	10	2.000	1.887
16	12	1.700	1.548
17	14	1.400	1.310
18	16	1.180	1.133
19	18	1.000	0.997
20	20	0.850	0.890
21	25	0.710	0.699
22	30	0.600	0.573
23	35	0.500	0.485
24	40	0.425	0.420
25	45	0.355	0.369
26	50	0.300	0.329
27	60	0.250	0.270
28	70	0.212	0.229
29	80	0.180	0.198
30	100	0.150	0.155
31	120	0.125	0.127
32	140	0.106	0.108
33	170	0.090	0.087
34	200	0.075	0.073
35	230	0.063	0.063
36	270	0.053	0.053
37	325	0.045	0.043
38	400	0.038	0.035

Figure 4 U.S. sieve number, sieve opening, and fitted values.

	C
	Fitted sieve opening (mm)
8	
9	
10	=10^TREND(LOG10(d),LOG10(N),LOG10(A10))
11	=10^TREND(LOG10(d),LOG10(N),LOG10(A11))
12	=10^TREND(LOG10(d),LOG10(N),LOG10(A12))

Figure 5 Formula for defining fitted points for chart.

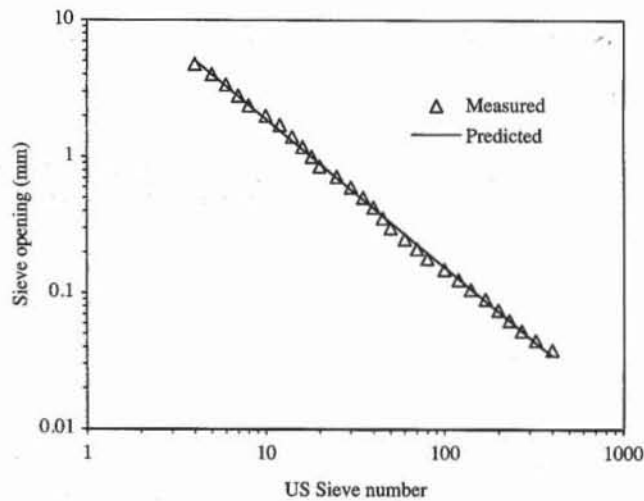


Figure 6 Comparison of data points and results fitted by using TREND.

	B	C	D
41	Slope, intercept = =LINEST(LOG10(d),LOG10(N))		=LINEST(LOG10(d),LOG10(N))
42	Slope = =SLOPE(LOG(d),LOG(N))		
43	Interecept = =INTERCEPT(LOG(d),LOG(N))		

Figure 7 Formulas used in Fig. 8.

	A	B	C	D
40	Result of linear regression analysis using LINEST			
41	Slope, intercept =		-1.08461	1.36039
42	Slope =		-1.08461	
43	Interecept =		1.36039	

Figure 8 Results of linear regression analysis with built-in functions LINEST, SLOPE, and INTERCEPT.

10 ^ Inter * x ^ Slope

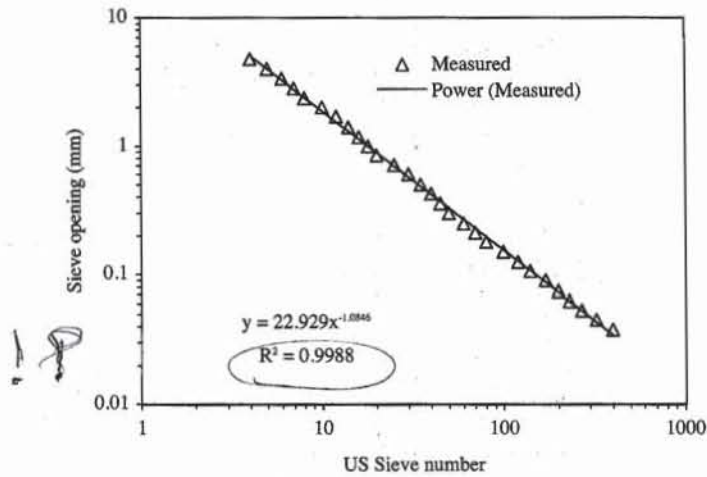


Figure 9 Comparison of data points and results fitted by using Trendline.

EXAMPLE 3: CUBIC POLYNOMIAL FITTING OF DATA POINTS

EXERCISE

Find the two cubic polynomials that describe the variations of water viscosity and water unit mass with temperature. The data measured are listed in Fig. 10. Plot the fitted and measured viscosity and unit mass versus temperature (Fig. 11). Use the method in Chapter 8-1 to determine the polynomial coefficients, and compare your results with those obtained by Trendline.

STEPS

- In a new workbook, enter and format the heading and data of the table in Fig. 10.
- Assign the names T , hw , and rw to cell ranges A8:A23, B8:B23, and C8:C23. Unfortunately, neither the Greek symbols η and ρ nor superscripts or subscripts can be used for variable names.

	A	B	C
6	Temperature (°C)	Viscosity (g/s/cm)	Unit mass (g/cm ³)
7	T	η_w	ρ_w
8	4.0	0.01567	1.00000
9	16.0	0.01111	0.99897
10	17.0	0.01083	0.99880
11	18.0	0.01056	0.99862
12	19.0	0.01030	0.99844
13	20.0	0.01005	0.99823
14	21.0	0.00981	0.99802
15	22.0	0.00958	0.99780
16	23.0	0.00936	0.99757
17	24.0	0.00914	0.99733
18	25.0	0.00894	0.99708
19	26.0	0.00874	0.99682
20	27.0	0.00855	0.99655
21	28.0	0.00836	0.99627
22	29.0	0.00818	0.99598
23	30.0	0.00801	0.99568

Figure 10 Measured variations of water viscosity and water unit mass with temperature.

	A	B	C
48	Temperature (°C)	Viscosity (g/s/cm)	Unit mass (g/cm ³)
49	T_a		
50	1.0	0.01721	0.99995
51	2.0	0.01668	0.99998
52	3.0	0.01616	1.00000
53	4.0	0.01567	1.00000
54	5.0	0.01520	0.99999
55	6.0	0.01474	0.99996
56	7.0	0.01430	0.99992
57	8.0	0.01389	0.99986
58	9.0	0.01348	0.99980
59	10.0	0.01310	0.99972
60	11.0	0.01273	0.99962
61	12.0	0.01238	0.99951
62	13.0	0.01204	0.99940
63	14.0	0.01172	0.99926
64	15.0	0.01141	0.99912
65	16.0	0.01111	0.99897
66	17.0	0.01083	0.99880
67	18.0	0.01056	0.99862
68	19.0	0.01030	0.99843
69	20.0	0.01005	0.99823
70	21.0	0.00981	0.99802
71	22.0	0.00958	0.99780
72	23.0	0.00936	0.99757
73	24.0	0.00914	0.99733
74	25.0	0.00894	0.99708
75	26.0	0.00874	0.99682
76	27.0	0.00855	0.99655
77	28.0	0.00836	0.99627
78	29.0	0.00818	0.99598
79	30.0	0.00801	0.99568

Figure 11 Fitted variations of water viscosity and water unit mass.

- Define the 16 entries of matrix *A* in cell range A25:D28, as shown in Fig. 12, and assign the name *A* to this range by using **⌘L**.
- Select the range A30:D33, type the formula of cell A30 shown in Fig. 12, and press **⌘Enter**. Assign the name *AI* to the range A30:D33 by using **⌘L**.
- Enter the formulas for the vectors *Bh* and *Br* in cell ranges A36:A39 and A42:A45, as shown in Fig. 12, and assign the names *Bh* and *Br* to these ranges by using **⌘L**.
- Select the range C36:C39, type the contents of cell C36 shown in Fig. 12, and press **⌘Enter**. The coefficients of the cubic polynomial should be as shown in Fig. 13. Assign the names *A_0*, *A_1*, *A_2*, and *A_3* to cells C36 to C39 by using **⌘L**. The names *a1*, *a2*, and *a3* cannot be used because they conflict with cell names.
- Select the range C42:C45, type the contents of cell C42 shown in Fig. 12, and press **⌘Enter**. Assign the names *B_0*, *B_1*, *B_2*, and *B_3* to cells C42 to C45.
- Define the table of Fig. 11 showing cells A48:C79. Use the edit Fill series to generate the temperature data. Enter the formulas in cells B50 and C50, as shown in Fig. 14, and copy them to range B50:C79.

	A	B	C	D
24	Matrix A			
25	=COUNT(T)	=SUM(T)	=SUMPRODUCT(T,T)	=SUMPRODUCT(T,T,T)
26	=B25	=C25	=D25	=SUMPRODUCT(T,T,T,T)
27	=B26	=C26	=D26	=SUMPRODUCT(T,T,T,T,T)
28	=B27	=C27	=D27	=SUMPRODUCT(T,T,T,T,T,T)
29	Inverse matrix A ⁻¹			
30	=MINVERSE(A)	=MINVERSE(A)	=MINVERSE(A)	=MINVERSE(A)
31	=MINVERSE(A)	=MINVERSE(A)	=MINVERSE(A)	=MINVERSE(A)
32	=MINVERSE(A)	=MINVERSE(A)	=MINVERSE(A)	=MINVERSE(A)
33	=MINVERSE(A)	=MINVERSE(A)	=MINVERSE(A)	=MINVERSE(A)
34	Nonlinear regression for viscosity (cubic)			
35	Vector Bh	Polynomial coefficients		
36	=SUM(hw)	a ₀ = =MMULT(AI,Bh)		
37	=SUMPRODUCT(T,hw)	a ₁ = =MMULT(AI,Bh)		
38	=SUMPRODUCT(T,T,hw)	a ₂ = =MMULT(AI,Bh)		
39	=SUMPRODUCT(T,T,T,hw)	a ₃ = =MMULT(AI,Bh)		
40	Nonlinear regression for unit mass (cubic)			
41	Vector Br	Polynomial coefficients		
42	=SUM(rw)	b ₀ = =MMULT(AI,Br)		
43	=SUMPRODUCT(T,rw)	b ₁ = =MMULT(AI,Br)		
44	=SUMPRODUCT(T,T,rw)	b ₂ = =MMULT(AI,Br)		
45	=SUMPRODUCT(T,T,T,rw)	b ₃ = =MMULT(AI,Br)		

Figure 12 Formulas used in Fig. 13.

	A	B	C	D
24	Matrix A			
25	16	349	8231	201889
26	349	8231	201889	5095943
27	8231	201889	5095943	131689249
28	201889	5095943	131689249	3470452391
29	Inverse matrix A ⁻¹			
30	6.975278585	-1.6770185	0.1042623	-0.0018996
31	-1.677018533	0.4732953	-0.031107	0.000582945
32	0.104262304	-0.0311065	0.0020889	-3.9654E-05
33	-0.001899598	0.0005829	-3.97E-05	7.595E-07
34	Nonlinear regression for viscosity (cubic)			
35	Vector Bh	Polynomial coefficients		
36	0.15719	a ₀ = 0.0177717		
37	3.25593	a ₁ = -0.000568		
38	74.93481	a ₂ = 1.115E-05		
39	1806.32571	a ₃ = -1.02E-07		
40	Nonlinear regression for unit mass (cubic)			
41	Vector Br	Polynomial coefficients		
42	15.96216	b ₀ = 0.99991		
43	348.06384	b ₁ = 5.202E-05		
44	8207.227	b ₂ = -7.51E-06		
45	201271.7513	b ₃ = 3.605E-08		

Figure 13 Results of cubic polynomial regression.

- Use the Chart Wizard to plot the measured and fitted data, as shown in Figs. 15 and 16.

Cubic polynomial fitting with Trendline.

- Use the Chart Wizard to plot the measured data, as shown in Figs. 17 and 18.

	A	B	C
48	Temperature (°C)	Viscosity (g/s/cm)	Unit mass (g/cm ³)
49	T _a		
50	1	=A_0+A_1*Te+A_2*Te^2+A_3*Te^3	=B_0+B_1*Te+B_2*Te^2+B_3*Te^3
51	2	=A_0+A_1*Te+A_2*Te^2+A_3*Te^3	=B_0+B_1*Te+B_2*Te^2+B_3*Te^3

Figure 14 Formulas used in Fig. 2.

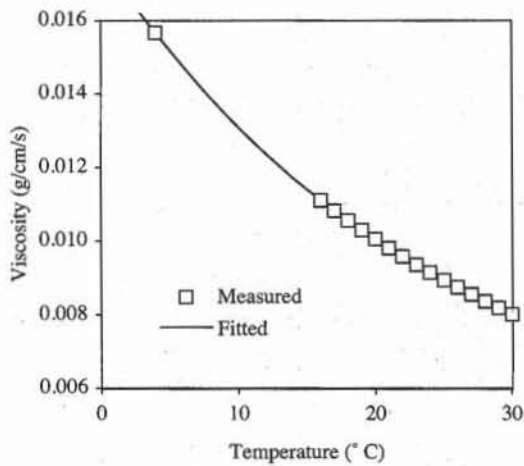


Figure 15 Variation of measured and fitted viscosity with temperature.

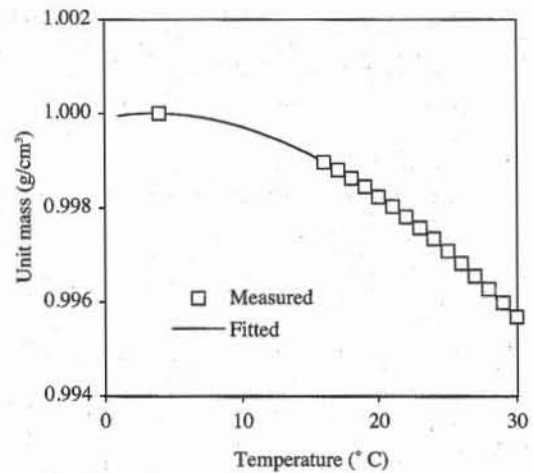


Figure 16 Variation of measured and fitted unit mass with temperature.

- Select the data points, and use **Insert Trendline**. In **Options**, select the display of equation and R^2 value, and in **Type**, select the polynomial fitting with a degree equal to 3. The results obtained by Trendline should be identical to those obtained in the preceding section.

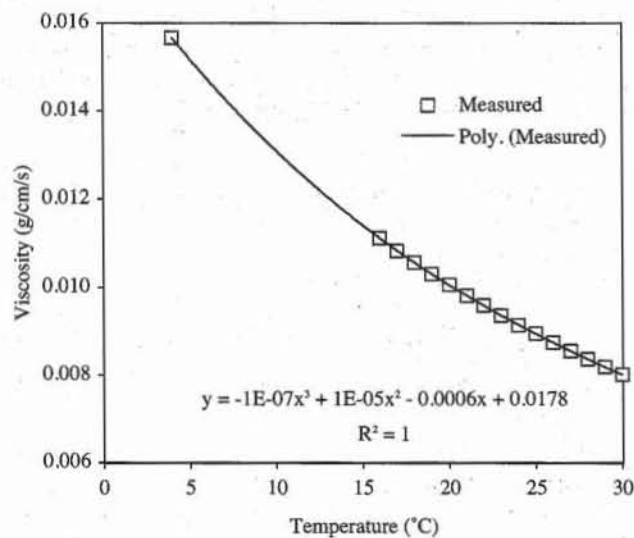


Figure 17 Variation of water viscosity with temperature fitted by using Trendline.

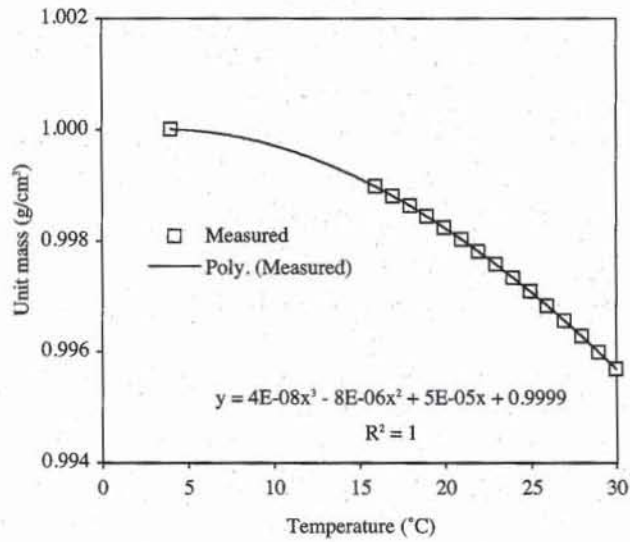


Figure 18 Variation of water unit mass with temperature fitted by using Trendline.

EXAMPLE 4: USER-DEFINED FUNCTIONS FOR UNIT MASS AND VISCOSITY OF WATER

EXERCISE

Write two user-defined functions to calculate the water viscosity η in $\text{g/cm}\cdot\text{s}$ and the water unit mass ρ_w (g/cm^3) as a function of the temperature T ($^\circ\text{C}$).

$$\eta = 0.0178 - 5.684 \times 10^{-4}T + 1.115 \times 10^{-5}T^2 - 1.017 \times 10^{-7}T^3$$

$$\rho_w = 0.99991 + 5.202 \times 10^{-5}T - 7.512 \times 10^{-6}T^2 + 3.605 \times 10^{-8}T^3$$

Write a user-defined function in the macrosheet and Visual Basic languages. Plot the variations of water viscosity and water unit mass on the same graph with primary and secondary vertical axes.

STEPS

- In a new workbook, use **Insert Macro MS Excel 4.0 Macro** to create a new macrosheet.
- Type the formulas as shown in Fig. 19.
- Assign the name *VISCO* and *DENSI* to cells A1 and A6 by using **ⓂL**. In both cases, check the **Function** option when naming macros.
- Use **Insert Module** to create the Visual Basic functions VBvisco and VBdensi shown in Fig. 20. The functions are given different names in order not to conflict with the corresponding macrosheet functions. You do not need to define the function names because this is automatically done by Visual Basic.
- In a worksheet created by using **Insert Worksheet**, define the heading

	A	B
1	VISCO	Viscosity of water in g/cm/s
2	=RESULT(1)	
3	=ARGUMENT("T",1)	Temperature in degrees Celsius
4	=RETURN(0.0178-5.684/10^4*T+1.115/10^5*T^2-1.017/10^7*T^3)	
5		
6	DENSI	Density of water in g/cm ³
7	=RESULT(1)	
8	=ARGUMENT("T",1)	Temperature in degrees Celsius
9	=RETURN(0.99991+5.202/10^5*T-7.512/10^6*T^2+3.605/10^8*T^3)	

Figure 19 Macrosheet user-defined function for water viscosity and water unit mass.

```

Viscosity of water in g/cm/s at temperature T in degree Celsius
Function VBvisco(T)
    VBvisco = 0.0178 - 5.684/10^4*T + 1.115/10^5*T^2 - 1.017/10^7*T^3
End Function

'Unit mass of water in g/cm3 at temperature T in degree Celsius
Function VBdensi(T)
    VBdensi = 0.99991 + 5.202/10^5*T - 7.512/10^6*T^2 + 3.605/10^8*T^3
End Function

```

Figure 20 Visual Basic user-defined function for water viscosity and water unit mass.

and column A of Fig. 21 (the formulas used in Fig. 21 are listed in Fig. 22). Use **Edit Fill Series** to generate the temperature data. Assign the name *T* to cells A8:A37 by using **⌘L**.

- Enter the formulas shown in cells B8 and C8, and copy them onto cells B9:C37.
- Use the Chart Wizard to create the graph of Fig. 23. Introduce the secondary axis for the water viscosity, add legends, and format the graph so that it looks like Fig. 23.
- After having tested the macrosheet functions VISCO and DENSI, you may test the Visual Basic functions. Replace VISCO and DENSI with VBvisco and VBdensi by using **⌘H**.

EXAMPLE 5: USER-DEFINED FUNCTION FOR LINEAR REGRESSION

EXERCISE

Write a user-defined function that performs a linear regression in the same way as the built-in function LINEST. Write the user-defined function in the macrosheet and Visual Basic languages. Compare the results of LINEST and your own function in the case of a random series.

STEPS

- In a new workbook, use **Insert Macro MS Excel 4.0 Macro** to create a new macrosheet.
- Type the formulas as shown in Fig. 24.

	A	B	C
6	Temperature (° C)	Viscosity (g/s/cm)	Unit mass (g/cm ³)
7	T		
8	1.0	0.01724	0.99995
9	2.0	0.01671	0.99998
10	3.0	0.01619	1.00000
11	4.0	0.01570	1.00000
12	5.0	0.01522	0.99999
13	6.0	0.01477	0.99996
14	7.0	0.01433	0.99992
15	8.0	0.01391	0.99986
16	9.0	0.01351	0.99980
17	10.0	0.01313	0.99972
18	11.0	0.01276	0.99962
19	12.0	0.01241	0.99951
20	13.0	0.01207	0.99940
21	14.0	0.01175	0.99926
22	15.0	0.01144	0.99912
23	16.0	0.01114	0.99897
24	17.0	0.01086	0.99880
25	18.0	0.01059	0.99862
26	19.0	0.01033	0.99843
27	20.0	0.01008	0.99823
28	21.0	0.00984	0.99802
29	22.0	0.00961	0.99780
30	23.0	0.00939	0.99757
31	24.0	0.00917	0.99733
32	25.0	0.00897	0.99708
33	26.0	0.00877	0.99682
34	27.0	0.00858	0.99655
35	28.0	0.00839	0.99627
36	29.0	0.00821	0.99598
37	30.0	0.00804	0.99568

Figure 21 Variation of water unit mass and viscosity with temperature.

	A	B	C
6	Temperature (° C)	Viscosity (g/s/cm)	Unit mass (g/cm ³)
7	T		
8	1	=VISCO(T)	=DENSI(T)
9	2	=VISCO(T)	=DENSI(T)

Figure 22 Formulas used in Fig. 21.

- Assign the name *MYLINEST* to cell B1 by using **Alt**. Check the **Function** option when defining the name. Assign the names *n*, *Ax*, *AY*, *Axx*, *Axy*, and *D* to cells A5 to A10. These names should be preceded by the macrosheet name and ! for these local variables to be declared only in the macrosheet.
- Use **Insert Module** and create the Visual Basic function *VBLINEST* of Fig. 25. You do not need to name it.
- In a new worksheet created with **Insert Worksheet**, type cells A5:A15 and B5 as shown in Fig. 26.
- Enter the formula of Fig. 27 in cell B6 and copy it in range B6:B15, as shown in Fig. 26. Assign the names *x* and *y* to the ranges A6:A15 and B6:B15 by using **Alt**.
- Select range C17:D17, use the Function Wizard to call *LINEST*, complete the arguments as shown in Fig. 27, and press **Enter**.
- Select range C19:D19, use the Function Wizard to call *MYLINEST*, complete the arguments as shown in Fig. 27, and press **Enter**. The results of *MYLINEST* and *LINEST* should be identical.

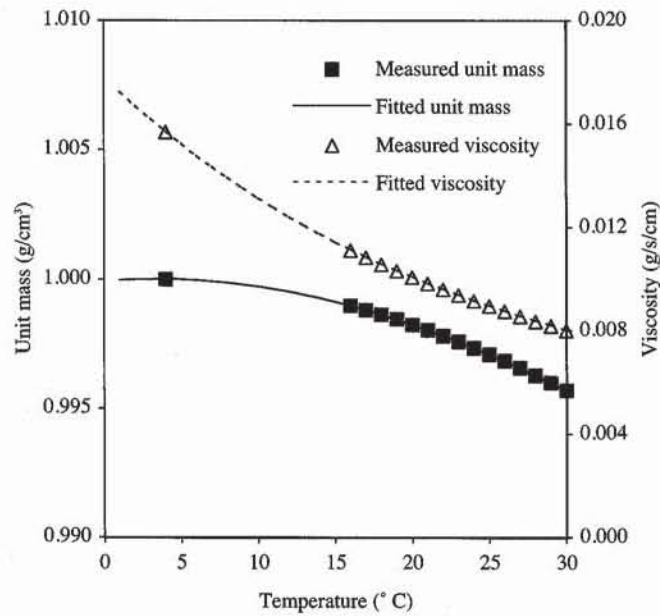


Figure 23 Variation of water unit mass and water viscosity with temperature.

	A	B	C
1		MYLINEST	name of function
2		=RESULT(64)	result of function is an array
3		=ARGUMENT("Y",64)	input array y
4		=ARGUMENT("X",64)	input array x
5	n	=COUNT(X)	n= number of element in arrays X and Y
6	Ax	=SUM(X)	$X_1+X_2+\dots+X_n$
7	Ay	=SUM(Y)	$Y_1+Y_2+\dots+Y_n$
8	Axx	=SUMPRODUCT(X,X)	$X_1^2+X_2^2+\dots+X_n^2$
9	Axy	=SUMPRODUCT(X,Y)	$X_1*Y_1+X_2*Y_2+\dots+X_n*Y_n$
10	D	=n*Axx-Ax^2	
11		=IF(D=0,RETURN("ERR"))	
12		=(n*Axy-Ax*Ay)/D	
13		=(Ay*Axx-Ax*Axy)/D	
14		=RETURN(TRANSPOSE(B12:B13))	return slope and intercept on the same row

Figure 24 Macrosheet user-defined function MYLINEST for linear regression.

- After having tested the macrosheet function MYLINEST, you may test the Visual Basic function VBlinest. Replace MYLYNEST with VBlinest by using H.

```

Function VBlinest(Yarray, Xarray) As Variant
    Dim N As Integer, x As Single, y As Single,
        xx As Single, xy As Single, Slope As Single,
        Intercept As Single
    N = 0
    x = 0
    y = 0
    xx = 0
    xy = 0
    For Each c In Xarray
        N = N + 1
        x = x + Xarray(N)
        y = y + Yarray(N)
        xx = xx + Xarray(N)^2
        xy = xy + Xarray(N)*Yarray(N)
    Next
    Slope = (N*xy - x*y)/(N*xx - x^2)
    Intercept = (y*xx - x*xy) / (N*xx - x^2)
    VBlinest = Array(Slope, Intercept)
End Function
    
```

Figure 25 Visual basic user-defined function VBlinest for linear regression.

	A	B	C	D
5	x	y		
6	1	0.397		
7	2	0.503		
8	3	0.914		
9	4	0.680		
10	5	0.062		
11	6	0.268		
12	7	0.867		
13	8	0.528		
14	9	0.809		
15	10	0.271		
16	Result of built-in function LINEST			
17	Slope, intercept = -0.00090043 0.535050422			
18	Result of user-defined function MYLINEST			
19	Slope, intercept = -0.00090043 0.535050422			

Figure 26 Results of linear regression with LINEST and user-defined function MYLINEST.

	A	B	B	C	D
5	x	y			
6	1	=RAND()			
7	2	=RAND()			
17	Slope, intercept =		=LINEST(y,x)	=LINEST(y,x)	
18	Slope, intercept =		=MYLINEST(y,x)	=MYLINEST(y,x)	

Figure 27 Formulas used in Fig. 26.

EXAMPLE 6: USER-DEFINED FUNCTION FOR UNIT CONVERSION

EXERCISE

Write the user-defined function UNITS that converts the number X from a system of unit U into another unit V . Dimensions and UNITS are covered in Chapter 8-4.

PRINCIPLES OF UNIT CONVERSION

The user-defined function UNITS converts the value X initially in unit U into another compatible unit, V . The unit dimensions include length, area, volume, force, stress, unit weight, time, velocity, and diffusivity. Most metric and English units are considered. The converted value Y in new unit V of the value X in original unit U is obtained as follows:

$$Y = X * \text{UNITS}(U, V) \quad (9)$$

where U is the case-insensitive spelling of the old unit and V is the case-insensitive spelling of the new unit. The spelling of all the units is defined in Fig. 28. For instance, to convert 10 atm into kPa, enter the following formula:

$$= 10 * \text{UNITS}(\text{"atm"}, \text{"kPa"}) \quad (10)$$

Figure 28 also gives the basic conversion factors used by UNITS. When AU and AV are the conversion factors of units U and V , respectively, then

$$Y = X * AV / AU \quad (11)$$

Figure 29 and 30 show the macrosheet and Visual Basic versions of the user-defined function for unit conversion. New units may be added provided that the new units names are spelt in lowercase, and that the extreme left column and bottom row of the table of unit names and conversion factors is left blank.

STEPS

- In a new workbook, use **Insert Macro MS Excel 4.0 Macro** to create a new macrosheet.
- Type the formulas and data as shown in Figs. 28 and 29. Assign the name UNITS to cell A1 by using **Alt**. Check the function option when naming UNITS. Assign the name A to range E2:R20 of Fig. 28. Also assign the names i , j , and Av to cells C5, C6, and B10. The variable names A , i , j , and Av should be preceded by the macrosheet name and ! for having local variables (e.g., Macros!A).
- Use **Insert Module** to create the Visual Basic function VBUNITS shown in Fig. 30. You do not need to define the function name. The third argument of function VBUNITS is the table defined in UNITS.

	D	E	F	G	H	I	J
1	DIMENSION Table 1						
2	length	inch	ft	ang	micron	mm	cm
3		1	0.0833333333333	254000000	25400	25.4	2.54
4	area	inch2	ft2	cm2	m2	ha	acre
5		1	0.0069444	6.4516	0.00064516	0.000000064516	0.000000159423
6	volume	inch3	ft3	cm3	m3	gal	quart
7		1	0.0005787037	16.387064	0.000016387064	0.004329	0.017316
8	force	kg	dyne	gr	pound	tonl	ton
9		1	980665	1000	2.2046223	0.00098420653	0.0011023113
10	stress	atm	bar	cmhg	mmhg	ftwater	kg/cm2
11		1	1.0133	76	760	33.899	1.03323
12	unit weight	gr/cm3	t/m3	kg/m3	pci	pcf	kn/m3
13		1	1	1000	0.036127292	62.427961	9.8039
14	time	ms	s	mn	hr	day	month
15		1	0.001	0.00001666666	0.0000002777777	0.000000011574074	0.00000000038057
16	velocity	cm/s	micron/s	m/mn	ft/mn	mile/hr	ft/yr
17		1	10000	0.6	1.9685	0.022369	1034643.6
18	consolidation	cm2/s	cm2/month	cm2/yr	m2/month	m2/yr	inch2/s
19		1	2628000	31536000	262.8	3153.6	0.155

	D	K	L	M	N	O	P	Q
1	DIMENSION							
2	length	m	yard	mile	km			
3		0.0254	0.02777777	0.0000157	0.0000254			
4	area	mile2						
5		0.000000000249098						
6	volume	pint	l	ml				
7		0.034632	0.0163852	16.3852				
8	force	kip	t	n	kn	ounce		
9		0.0022046223	0.001	9.80665	0.00980665	32.1512		
10	stress	gr/cm2	kg/m2	t/m2	psf	psi	ton/ft2	kpa
11		1033.23	10332.3	10.3323	2116.22	14.696	1.0581	101.325
12	unit weight							
13								
14	time	yr						
15		0.00000000003171416						
16	velocity							
17								
18	consolidation	inch2/month	inch2/yr	ft2/month	ft2/yr			
19		4151600	4888200	2882.998	33944.7			

Figure 28 Table of data used in user-defined function UNITS.

	A	B	C
1		UNITS	Convert from
2		=RESULT(3)	one unit to another
3		=ARGUMENT("OLD",2)	New unit name in " "
4		=ARGUMENT("NEW",2)	Old unit name in " "
5		=SET.VALUE(i,1)	9
6		=WHILE(NOT(ISBLANK(INDEX(A,i,1))))	10
7		= SET.VALUE(j,1)	Above space is reserved
8		= WHILE(NOT(ISBLANK(INDEX(A,i,j))))	for counters i and j.
9		= IF(EXACT(INDEX(A,i,j),LOWER(NEW)))	For input, check spelling
10	AV	= INDEX(A,i+1,j)	of unit names in Table 1
11		= SET.VALUE(j,1)	Units may be added
12		= WHILE(NOT(ISBLANK(INDEX(A,i,j))))	into Table 1. However
13		= IF(EXACT(INDEX(A,i,j),LOWER(OLD)))	the named array A
14		= RETURN(AV/INDEX(A,i+1,j))	should have one more
15		= ELSE()	row and column than
16		= SET.VALUE(j,j+1)	Table 1. The unit
17		= END.IF()	names should be in lower
18		= NEXT()	case in Table 1.
19		= RETURN("ERROR")	
20		= ELSE()	
21		= SET.VALUE(j,j+1)	
22		= END.IF()	
23		= NEXT()	
24		= SET.VALUE(i,i+2)	
25		=NEXT()	
26		=RETURN("ERROR")	

Figure 29 User-defined function UNITS for unit conversion.

```

Function VBunits(OldUnit, NewUnit, AllUnits)
  Dim x, i, j
  i = 1
  Do Until IsEmpty(AllUnits(i, 1))
    j = 1
    Do Until IsEmpty(AllUnits(i, j))
      If AllUnits(i, j) = LCase(NewUnit) Then
        x = AllUnits(i + 1, j)
        j = 1
        Do Until IsEmpty(AllUnits(i, j))
          If AllUnits(i, j) = LCase(OldUnit) Then
            VBunits = x / AllUnits(i + 1, j)
            Exit Function
          Else
            j = j + 1
          End If
        Loop
        MsgBox "Check the units"
        Exit Function
      Else
        j = j + 1
      End If
    Loop
    i = i + 2
  Loop
  MsgBox "Check the units"
End Function

```

Figure 30 Visual Basic user-defined function for unit conversion.

	A	B	C	D	E	F	G	H
4	Examples of unit conversion with UNITS							
5	From feet to cm		X =	12.4 ft	=	377.95	cm	
6	From psf to kPa		X =	50 psf	=	2.39	kPa	
7	From pcf to kN/m ³		X =	120 pcf	=	18.85	kN/m ³	
8	From m/s ² to ft ² /yr		X =	0 cm ² /s	=	33.94	ft ² /yr	

	G
5	=D5*UNITS(E5,H5)
6	=D6*UNITS(E6,H6)
7	=D7*UNITS(E7,H7)
8	=D8*UNITS(E8,H8)

Figure 31 Example for user-defined function UNITS.

- In a new worksheet, define the table and formulas of Fig. 31. You should find the results of Fig. 31.
- After having tested the macrosheet function UNITS, you may test the Visual Basic function VBunits. Replace UNITS with VBunits by using **ⓂH**. You will also need to add the third argument of VBunits, which contains the table of Fig. 28 [e.g., D5*VBunits(E5,H5,Macros!A) in cell G5 of Fig. 31].

EXAMPLE 7: USER-DEFINED FUNCTION FOR GRADE ASSIGNMENT

EXERCISE

Write a user-defined function that gives the course grade for numeric grades between 0 and 100. The custom function should specify the lower limit to get an A, B, C, and D and should automatically assign + and - in each grade category.

STEPS


- In a new workbook, use **Insert Macro MS Excel 4.0 Macro** to create a new macrosheet.
- Type the formulas as shown in Fig. 32. *A1*, *B1*, *C1*, and *D1* are the lower

	A	B
1	Grade	Grading program
2	=RESULT(2)	returns a letter grade
3	=ARGUMENT("G",1)	Number between 0 and 100
4	=ARGUMENT("A1",1)	Lower limit to get A
5	=ARGUMENT("B1",1)	Lower limit to get B
6	=ARGUMENT("C1",1)	Lower limit to get C
7	=ARGUMENT("D1",1)	Lower limit to get D
8	=IF(G>=(2*100/3+A1/3),RETURN("A+"))	
9	=IF(G>=(100/3+2*A1/3),RETURN("A"))	
10	=IF(G>=A1,RETURN("A-"))	
11	=IF(G>=(2*A1/3+B1/3),RETURN("B+"))	
12	=IF(G>=(A1/3+2*B1/3),RETURN("B"))	
13	=IF(G>=B1,RETURN("B-"))	
14	=IF(G>=(2*B1/3+C1/3),RETURN("C+"))	
15	=IF(G>=(B1/3+2*C1/3),RETURN("C"))	
16	=IF(G>=C1,RETURN("C-"))	
17	=IF(G>=(2*C1/3+D1/3),RETURN("D+"))	
18	=IF(G>=(C1/3+2*D1/3),RETURN("D"))	
19	=IF(G>=D1,RETURN("D-"))	
20	=RETURN("F")	

Figure 32 User-defined function for grade assignment.

	A	B	C		C
4	Student Name	Exam grade (/100)	Course grade	4	Course grade
5	Mary Absent	10	F	5	=Grade(B5,90,75,60,50)
6	Joe Doe	85	B+	6	=Grade(B6,90,75,60,50)
7	Kathy Greats	90	A-	7	=Grade(B7,90,75,60,50)
8	Paul Reagan	70	C+	8	=Grade(B8,90,75,60,50)
9	Ian Smith	65	C	9	=Grade(B9,90,75,60,50)

Figure 33 Example for user-defined function Grade and formulas used to call it.

limits to get an A, B, C, and D. Assign the name Grade to cell A1 by using L.

- In a new worksheet, define the example of Fig. 33 and enter the formulas of Fig. 33 to get the course grade.

EXAMPLE 8: USER-DEFINED FUNCTION FOR CUBIC POLYNOMIAL REGRESSION

EXERCISE

Write a user-defined function that calculates the coefficients of cubic polynomial regression. Compare the results obtained with your function with those of Example 3 in the case of the variation of the viscosity and unit mass of water with temperature.

STEPS

- In a new workbook, use **Insert Macro MS Excel 4.0 Macro** to create a new macrosheet.
- Type the formulas and data as shown in Fig. 34. Assign the name FIT3

	A	B
19	FIT3	Fit cubic polynomial by linear regression
20	=RESULT(64)	Input X-array
21	=ARGUMENT("X",64)	Input Y-array
22	=ARGUMENT("Y",64)	
23	=COUNT(X)	349
24	=SUM(X)	8231
25	=SUMPRODUCT(X,X)	201889
26	=SUMPRODUCT(X,X,X)	5095943
27	=SET.VALUE(B23,A24)	Form matrix
28	=SET.VALUE(C23,A25)	
29	=SET.VALUE(D23,A26)	
30	=SET.VALUE(B24,A25)	
31	=SET.VALUE(C24,A26)	
32	=SET.VALUE(D24,SUMPRODUCT(X,X,X,X))	
33	=SET.VALUE(B25,A26)	
34	=SET.VALUE(C25,D24)	
35	=SET.VALUE(D25,SUMPRODUCT(X,X,X,X,X))	
36	=SET.VALUE(B26,D24)	
37	=SET.VALUE(C26,D25)	
38	=SET.VALUE(D26,SUMPRODUCT(X,X,X,X,X,X))	
39	=SET.VALUE(E23,SUM(Y))	Form vector
40	=SET.VALUE(E24,SUMPRODUCT(X,Y))	
41	=SET.VALUE(E25,SUMPRODUCT(X,X,Y))	
42	=SET.VALUE(E26,SUMPRODUCT(X,X,X,Y))	
43	=RETURN(MMULT(MINVERSE(A23:D26),E23:E26))	

Figure 34 User-defined function for cubic fitting.

to cell A19 by using **⌘L**. Do not forget to check the function option when naming user-defined functions.

- In a new worksheet, enter and format the heading and data of the table in Fig. 35.
- Assign the names *T*, *hw*, and *rw* to cell ranges A7:A22, B7:B22, and C7:C22 by using **⌘L**.
- Select the range B24:B27, type the formula of cell B24 shown in Fig. 36, and press **⌘Enter**. Same thing for the range B29:B32. You should find the same coefficients as in Example 3.

	A	B	C
5	Temperature (° C)	Viscosity (g/s/cm)	Unit mass (g/cm ³)
6	T	η_w	ρ_w
7	4.0	0.01567	1.00000
8	16.0	0.01111	0.99897
9	17.0	0.01083	0.99880
10	18.0	0.01056	0.99862
11	19.0	0.01030	0.99844
12	20.0	0.01005	0.99823
13	21.0	0.00981	0.99802
14	22.0	0.00958	0.99780
15	23.0	0.00936	0.99757
16	24.0	0.00914	0.99733
17	25.0	0.00894	0.99708
18	26.0	0.00874	0.99682
19	27.0	0.00855	0.99655
20	28.0	0.00836	0.99627
21	29.0	0.00818	0.99598
22	30.0	0.00801	0.99568
23	Nonlinear regression for viscosity (cubic)		
24	a ₀ = 0.017771671		
25	a ₁ = -0.000568441		
26	a ₂ = 1.11479E-05		
27	a ₃ = -1.01686E-07		
28	Nonlinear regression for unit mass (cubic)		
29	b ₀ = 0.999910033		
30	b ₁ = 5.20192E-05		
31	b ₂ = -7.51229E-06		
32	b ₃ = 3.60518E-08		

Figure 35 Results of cubic polynomial regression for unit mass and viscosity of

	A	B
23	Nonlinear	
24	a ₀ = =FIT3(T,hw)	
25	a ₁ = =FIT3(T,hw)	
26	a ₂ = =FIT3(T,hw)	
27	a ₃ = =FIT3(T,hw)	
28	Nonlinear	
29	b ₀ = =FIT3(T,rw)	
30	b ₁ = =FIT3(T,rw)	
31	b ₂ = =FIT3(T,rw)	
32	b ₃ = =FIT3(T,rw)	

Figure 36 Formulas used in Fig. 35.

Appendix: Conversion Factors

LENGTH

To the unit below, multiply by

	inch	ft	ang	micron	mm	cm	m	yard	mile	km
inch	1	0.08333333	254.000E+6	25400	25.4	2.54	0.0254	0.02777777	15.700E-6	25.400E-6
ft	12	1	3.048E+9	304800	304.8	30.48	0.3048	0.33333324	0.000188	0.0003048
ang	3.937E-9	328.084E-12	1	0.0001	100.000E-9	1E-08	1E-10	109.361E-12	6.18E-14	100.000E-15
micron	39.370E-6	3.281E-6	10.000E+3	1	0.001	0.0001	0.000001	1.094E-6	6.18E-10	1.000E-9
mm	0.03937	0.00328084	10.000E+6	1000	1	0.1	0.001	0.00109361	6.18E-07	0.000001
cm	0.393701	0.0328084	100.000E+6	10000	10	1	0.01	0.01093613	6.18E-06	0.00001
m	39.37008	3.2808399	10.000E+9	1000000	1000	100	1	1.09361299	0.000618	0.001
yard	36.00001	3.000E+0	9.144E+9	914400.3	914.400256	91.44003	0.9144	1	0.000565	0.0009144
mile	63694.27	5307.85563	16.178E+12	1.618E+9	1617834.39	161783.4	1617.834	1769.28471	1	1.617834395
km	39370.08	3280.8399	1E+13	1.000E+9	1000000	100000	1000	1093.61299	0.61811	1

AREA

To the unit below, multiply by

	inch ²	ft ²	cm ²	m ²	ha	acre	mile ²
inch ²	1	0.0069444	6.4516	0.000645	64.516E-9	159.423E-9	249.098E-12
ft ²	144.00092	1	929.036346	0.092904	9.290E-6	22.957E-6	35.870E-9
cm ²	0.155000	0.0010764	1	0.0001	10.000E-9	24.711E-9	38.610E-12
m ²	1550.0031	10.763842	10000	1	0.0001	0.0002471	386.103E-9
ha	15500031	107638.42	100.000E+6	10000	1	2.4710614	0.003861027
acre	6272620.6	43559.587	40.468E+6	4046.844	0.4046844	1	0.001562497
mile ²	4.014E+9	27.878E+6	25.900E+9	2.590E+6	258.99847	640.00112	1

VOLUME

To the unit below, multiply by

	inch ³	ft ³	cm ³	m ³	gal	quart	pint	l	ml	
To convert from this unit	inch ³	1	0.0005787	16.3871	16.387E-6	0.004329	0.01732	0.03463	0.01639	16.3852
	ft ³	1728	1	28316.8	0.02831685	7.480512	29.922	59.8441	28.3136	28313.626
	cm ³	0.06102	35.315E-6	1	0.000001	0.0002642	0.00106	0.00211	0.001	1
	m ³	61023.7	35.314666	1000000	1	264.17179	1056.69	2113.375	1000	1.00E+6
	gal	231	0.1336807	3785.42	0.00378542	1	4	8	3.78498	3784.985
	quart	57.7501	0.0334202	946.354	0.00094635	0.25	1	2	0.9462425	946.24625
	pint	28.875	0.0167101	473.177	0.00047318	0.125	0.5	1	0.47312	473.12312
	l	61.0307	0.0353187	1000	0.00100011	0.2642018	1.05681	2.11361	1	1000
	ml	0.06103	35.319E-6	1	1.000E-6	264.202E-6	1.057E-3	0.00211	0.001	1

TIME

To the unit below, multiply by

	ms	s	mn	hr	day	month	yr	
To convert from	ms	1	0.001	16.667E-6	277.778E-9	11.574E-9	380.570E-12	31.714E-12
	s	1000	1	0.0166667	0.00027778	11.574E-6	380.570E-9	31.714E-9
	mn	60000.024	60.00002	1	0.0166667	0.00069444	22.834E-6	1.903E-6
	hr	3600000.1	3600	59.999978	1	0.04166667	0.001370052	0.0001142
	day	86400001	86400	1439.9994	23.9999995	1	0.032881248	0.0027401
	month	2.628E+9	2627637	43793.941	729.899283	30.4124708	1	0.0833333
	yr	31.532E+9	31531657	525527.4	8758.79323	364.949726	12.00000252	1

VELOCITY

To the unit below, multiply by

	cm/s	micron/s	m/mn	ft/mn	mile/hr	ft/yr	
To convert from	cm/s	1	10000	0.6	1.9685	0.022369	1034644
	micron/s	0.0001	1	0.00006	0.000197	2.24E-06	103.4644
	m/mn	1.666667	16666.67	1	3.280833	0.037282	1724406
	ft/mn	0.508001	5080.01	0.304801	1	0.011363	525600
	mile/hr	44.70473	447047.3	26.82284	88.00125	1	46253458
	ft/yr	9.67E-07	0.009665	5.8E-07	1.9E-06	2.16E-08	1

FORCE

To the unit below, multiply by

	kg	dyne	gr	pound	tonl	ton	kip	t	N	kN	ounce
kg	1	980665	1000	2.204622	0.0009842	0.0011023	0.002205	1.000E-3	9.80665	0.0098067	32.151E+0
dyne	1.020E-6	1	0.00102	2.248E-6	1.004E-9	1.124E-09	2.248E-9	1.020E-9	0.00001	10.000E-9	32.785E-6
gr	0.001	980.665	1	0.002205	984.207E-9	1.102E-6	2.205E-6	0.000001	0.009807	9.807E-6	0.0321512
pound	0.453592	444822.2	453.5924	1	0.0004464	0.0005	0.001	0.0004536	4.448222	0.0044482	14.583541
tonl	1016.047	996.4E+6	1016047	2240	1	1.12	2.24	1.0160469	9964.016	9.9640164	32667.127
ton	907.1847	889.6E+6	907184.7	2000	0.8928572	1	2	0.9071847	8896.443	8.8964433	29167.078
kip	453.5924	444.8E+6	453592.4	1000	0.4464286	0.5000001	1	0.4535924	4448.222	4.4482223	14583.541
t	1000	980.7E+6	1000000	2204.622	0.9842065	1.1023113	2.204622	1	9806.65	9.80665	32151.2
N	0.101972	100000	101.9716	0.224809	0.0001004	0.0001124	0.000225	0.000102	1	0.001	3.27851
kN	101.9716	100.0E+6	101971.6	224.8089	0.1003611	0.1124045	0.224809	0.1019716	1000	1	3278.51
ounce	0.031103	30501.66	31.10304	0.06857	30.612E-6	34.285E-6	68.570E-6	31.103E-6	0.305017	0.000305	1

STRESS AND PRESSURE

To the unit below, multiply by

	atm	bar	cmHg	mmHg	ftwater	kg/cm ²	gr/cm ²	kg/m ²	t/m ²	psf	psi	ton/ft ²	kPa
atm	1	1.0133	76	760	33.899	1.0332	1033.2	10332	10.3323	2116.2	14.696	1.0581	101.32
bar	0.986875	1	75.002	750.02	33.454	1.0197	1019.7	10197	10.1967	2088.4	14.503	1.04421	99.995
cmHg	0.013158	0.0133329	1	10	0.446	0.0136	13.595	135.95	136.0E-3	27.845	0.1934	0.01392	1.3332
mmHg	0.001316	0.00133333	0.1	1	0.0446	0.0014	1.3595	13.595	0.0136	2.7845	0.0193	1.392E-3	0.1333
ftwater	0.029499	0.0298917	2.242	22.42	1	0.0305	30.48	304.8	0.3048	62.427	0.4335	0.03121	2.989
kg/cm ²	0.967839	0.980711	73.556	735.556	32.809	1	1000	10000	10	2048.2	14.223	1.02407	98.066
gr/cm ²	967.8E-6	980.7E-6	0.0736	0.7356	0.0328	0.001	1	10	0.01	2.0482	0.0142	0.00102	0.0981
kg/m ²	96.784E-6	98.071E-6	0.0074	0.0736	0.0033	0.0001	0.1	1	0.001	0.2048	0.0014	0.0001	0.0098
t/m ²	0.096784	98.071E-3	7.3556	73.556	3.2809	0.1	100	1000	1	204.82	1.4223	0.10241	9.8066
psf	472.5E-6	478.825E-6	0.0359	0.3591	0.016	0.0005	0.4882	4.8824	0.00488	1	0.0069	0.0005	0.0479
psi	68.046E-3	0.0689507	5.1715	51.715	2.3067	0.0703	70.307	703.07	0.70307	144	1	0.072	6.8947
ton/ft ²	0.94509	0.95766	71.827	718.27	32.038	0.9765	976.5	9765	9.76496	2000	13.889	1	95.761
kPa	0.00986	10.000E-3	0.75006	7.5006	0.3346	0.0102	10.197	101.97	0.10197	20.885	0.145	0.01044	1

UNIT WEIGHT

To the unit below, multiply by

	gr/cm ³	t/m ³	kg/m ³	pci	pcf	kN/m ³
gr/cm ³	1	1	1000	0.036127	62.42796	9.8039
t/m ³	1	1	1000	0.036127	62.42796	9.8039
kg/m ³	0.001	0.001	1	3.61273E-05	0.062428	0.009804
pci	27.6799	27.6799	27679.9	1	1728	271.3714
pcf	0.016018	0.016018	16.01846	0.000579	1	0.157043
kN/m ³	0.102	0.102	102.0002	0.003685	6.367666	1

DIFFUSIVITY

To the unit below, multiply by

To convert from this unit

	cm ² /s	cm ² /month	cm ² /yr	m ² /month	m ² /yr	inch ² /s	inch ² /month	inch ² /yr	ft ² /month	ft ² /yr
cm ² /s	1	2628000	31536000	262,8	3153,6	0,155	4151600	4888200	2882,998	33944,7
cm ² /month	380,518E-9	1	12	0,0001	0,0012	58,980E-9	1,579756	1,860046	0,001097	0,012917
cm ² /yr	31,710E-9	0,083333	1	8,333E-6	0,0001	4,915E-9	0,131646	0,155004	91,419E-6	0,001076
m ² /month	0,0038052	10000	120000	1	12	589,802E-6	15797,56	18600,46	10,97031	129,1655
m ² /yr	0,0003171	833,3333	10000	0,083333	1	49,150E-6	1316,464	1550,038	0,914193	10,76379
inch ² /s	6,4516129	16954839	203,458E+6	1695,484	20345,81	1	26784516	31536774	18599,99	218998,1
inch ² /month	240,871E-9	0,633009	7,59610752	63,301E-6	0,00076	37,335E-9	1	1,177426	0,000694	0,008176
inch ² /yr	204,574E-9	0,537621	6,45145452	53,762E-6	0,000645	31,709E-9	0,849311	1	0,000589	0,006944
ft ² /month	0,0003469	911,5511	10938,6132	0,091155	1,093861	53,763E-6	1440,029	1695,527	1	11,7741
ft ² /yr	2,94597E-05	77,42004	929,040469	0,007742	0,092904	4,566E-6	122,3048	144,0048	0,084932	1



Data Sheets

- Sieve analysis
- Hydrometer analysis
- Pipette analysis
- Buoyancy analysis
- Liquid limit test
- Plastic limit test
- Shrinkage test
- Determination of unit weight of soils
- Specific gravity test
- Compaction test
- Sand cone method
- Constant head permeability test
- Falling head permeability test
- Consolidation test
- Unconfined compression test
- Direct shear test
- Drained triaxial test
- Undrained triaxial test

Note: Additional datasheets can be printed from the Excel datafiles on the floppy disk provided with Experimental Soil Mechanics.

Sieve analysis

Analyst name: _____
 Test date: _____
 Sample description: _____
 Total sample mass = _____ g

US sieve number	Sieve opening (mm)	Mass retained (g)

Sieve analysis

Analyst name: _____

Test date: _____

Sample description: _____

Total sample mass = _____ g

ASTM Sieve number	Sieve opening (mm)	Mass retained (g)
4	4.750	
5	4.000	
6	3.350	
7	2.800	
8	2.360	
10	2.000	
12	1.700	
14	1.400	
16	1.180	
18	1.000	
20	0.850	
25	0.710	
30	0.600	
35	0.500	
40	0.425	
45	0.355	
50	0.300	
60	0.250	
70	0.212	
80	0.180	
100	0.150	
120	0.125	
140	0.106	
170	0.090	
200	0.075	
230	0.063	
270	0.053	
325	0.045	
400	0.038	

Hydrometer analysis

Analyst name: _____
 Test date: _____
 Sample description: _____

Mass in suspension $W_0 =$ _____ g
 Specific unit weight $G_s =$ _____
 Dispersing agent correction $C_d =$ _____ g/L
 Meniscus correction $C_m =$ _____ g/L
 Cylinder diameter $d_c =$ _____ cm
 Hydrometer bulb volume $V_b =$ _____ cm³

Graduation mark on hydrometer stem (g/L) R_s	Distance to bulb center (cm) H_s
0	
10	
20	
30	
40	
50	
60	

Time (min) t	Hydrometer reading(g/L) R_t	Temperature (°C) T_e

Pipette analysis

Analyst: _____
 Test date: _____
 Sample: _____

Wet method

Total soil mass in suspension = _____ g
 Soil specific gravity = _____
 Pipette volume = _____ mL
 Total volume of suspension = _____ mL
 Mass of sampled water, agent and bottle = _____ g
 Mass of bottle = _____ g

Time (min)	Sampling depth (cm)	Temperature (°C)	Mass of bottle (g)	Mass of sample and bottle (g)

Shrinkage Test

Analyst name: _____
 Test date: _____
 Sample description: _____

WAX METHOD	Sample No.1	Sample No.2
Mass of coated dish (g)		
Mass of coated dish + wet soil (g)		
Mass of coated dish + dry soil (g)		
Volume of wet soil (cm ³)		
Mass of soil and wax (g)		
Buoyant Mass of soil and wax (g)		
Unit mass of wax (g/cm ³)		

Shrinkage Test

Analyst name: _____
 Test date: _____
 Sample description: _____

WAX METHOD	Sample No.1	Sample No.2
Mass of coated dish (g)		
Mass of coated dish + wet soil (g)		
Mass of coated dish + dry soil (g)		
Volume of wet soil (cm ³)		
Mass of soil and wax (g)		
Buoyant Mass of soil and wax (g)		
Unit mass of wax (g/cm ³)		

Shrinkage Test

Analyst name: _____
 Test date: _____
 Sample description: _____

MERCURY METHOD	Sample No.1	Sample No.2
Mass of coated dish (g)		
Mass of coated dish + wet soil (g)		
Mass of coated dish + dry soil (g)		
Volume of wet soil (cm ³)		
Mass of dish (g)		
Mass of dish + displaced mercury (g)		
Unit mass of Mercury (g/cm ³)		

Shrinkage Test

Analyst name: _____
 Test date: _____
 Sample description: _____

MERCURY METHOD	Sample No.1	Sample No.2
Mass of coated dish (g)		
Mass of coated dish + wet soil (g)		
Mass of coated dish + dry soil (g)		
Volume of wet soil (cm ³)		
Mass of dish (g)		
Mass of dish + displaced mercury (g)		
Unit mass of Mercury (g/cm ³)		

Unit Weight of soils

Analyst name: _____

Test date: _____

Sample description: _____

SOIL UNIT WEIGHT	Sample 1	Sample 2	Sample 3
Mass of soil sample (g)			
Mass of waxed soil (g)			
Mass of immersed soil (g)			
Mass of trimmed sample (g)			
Mass of dry sample (g)			

WAX UNIT WEIGHT	Sample 1	Sample 2
Mass of immersed iron block (g)		
Mass of wax block (g)		
Mass of immersed iron and wax blocks (g)		

Unit Weight of soils

Analyst name: _____

Test date: _____

Sample description: _____

SOIL UNIT WEIGHT	Sample 1	Sample 2	Sample 3
Mass of soil sample (g)			
Mass of waxed soil (g)			
Mass of immersed soil (g)			
Mass of trimmed sample (g)			
Mass of dry sample (g)			

WAX UNIT WEIGHT	Sample 1	Sample 2
Mass of immersed iron block (g)		
Mass of wax block (g)		
Mass of immersed iron and wax blocks (g)		

Unit Weight of soils

Analyst name: _____
 Test date: _____
 Sample description: _____

SOIL UNIT WEIGHT	Sample 1	Sample 2	Sample 3
Mass of soil sample (g)			
Mass of waxed soil (g)			
Mass of immersed soil (g)			
Mass of trimmed sample (g)			
Mass of dry sample (g)			

WAX UNIT WEIGHT	Sample 1	Sample 2
Mass of immersed iron block (g)		
Mass of wax block (g)		
Mass of immersed iron and wax blocks (g)		

Unit Weight of soils

Analyst name: _____
 Test date: _____
 Sample description: _____

SOIL UNIT WEIGHT	Sample 1	Sample 2	Sample 3
Mass of soil sample (g)			
Mass of waxed soil (g)			
Mass of immersed soil (g)			
Mass of trimmed sample (g)			
Mass of dry sample (g)			

WAX UNIT WEIGHT	Sample 1	Sample 2
Mass of immersed iron block (g)		
Mass of wax block (g)		
Mass of immersed iron and wax blocks (g)		

Specific Gravity

Analyst name: _____
Test date: _____
Sample description: _____

	Sample 1	Sample 2
Mass of flask and water (g)		
Mass of flask, soil and water (g)		
Mass of evaporating dish (g)		
Mass of evaporating dish and dry soil (g)		

Specific Gravity

Analyst name: _____
Test date: _____
Sample description: _____

	Sample 1	Sample 2
Mass of flask and water (g)		
Mass of flask, soil and water (g)		
Mass of evaporating dish (g)		
Mass of evaporating dish and dry soil (g)		

Specific Gravity

Analyst name: _____
Test date: _____
Sample description: _____

	Sample 1	Sample 2
Mass of flask and water (g)		
Mass of flask, soil and water (g)		
Mass of evaporating dish (g)		
Mass of evaporating dish and dry soil (g)		

Specific Gravity

Analyst name: _____
 Test date: _____
 Sample description: _____

	Sample 1	Sample 2
Mass of flask and water (g)		
Mass of flask, soil and water (g)		
Mass of evaporating dish (g)		
Mass of evaporating dish and dry soil (g)		

Specific Gravity

Analyst name: _____
 Test date: _____
 Sample description: _____

	Sample 1	Sample 2
Mass of flask and water (g)		
Mass of flask, soil and water (g)		
Mass of evaporating dish (g)		
Mass of evaporating dish and dry soil (g)		

Specific Gravity

Analyst name: _____
 Test date: _____
 Sample description: _____

	Sample 1	Sample 2
Mass of flask and water (g)		
Mass of flask, soil and water (g)		
Mass of evaporating dish (g)		
Mass of evaporating dish and dry soil (g)		

Compaction test

Analyst name: _____
Test date: _____
Sample description: _____

Diameter of mold (cm) _____
Height of mold (cm) = _____
Mass of mold (g) = _____
Specific gravity G_s = _____

Mass of soil and mold (g)	Mass of can and wet soil (g)	Mass of can and dry soil (g)	Mass of can (g)

Compaction test

Analyst name: _____

Test date: _____

Sample description: _____

Diameter of mold (cm) _____

Height of mold (cm) = _____

Mass of mold (g) = _____

Specific gravity G_s = _____

Mass of soil and mold (g)	Mass of can and wet soil (g)	Mass of can and dry soil (g)	Mass of can (g)

Sand cone method

Analyst name: _____
 Test date: _____
 Sample description: _____

Measurement in the field

Mass of jar and sand before use $M_i =$ _____ g
 Mass of jar and sand after use $M_e =$ _____ g
 Mass of collected soil $M =$ _____ g

Water content in the laboratory

Mass of can and wet soil (g) M_w
 Mass of can and dry soil (g) M_d
 Mass of can (g) M_t

Sample 1	Sample 2

Calibration in the laboratory

Diameter of mold $D =$ _____ cm
 Height of mold $H =$ _____ cm

	Sample 1	Sample 2
Mass of mold and sand (g) M_{ms}		
Mass of empty mold (g) M_m		
Mass of jar and sand before filling cone (g) M_{j_b}		
Mass of jar and sand after filling cone (g) M_{j_a}		

Sand cone method

Analyst name: _____
 Test date: _____
 Sample description: _____

Measurement in the field

Mass of jar and sand before use M_i = _____ g
 Mass of jar and sand after use M_e = _____ g
 Mass of collected soil M = _____ g

Water content in the laboratory

Mass of can and wet soil (g) M_w
 Mass of can and dry soil (g) M_d
 Mass of can (g) M_c

Sample 1	Sample 2

Calibration in the laboratory

Diameter of mold D = _____ cm
 Height of mold H = _____ cm

Mass of mold and sand (g) M_{ms}
 Mass of empty mold (g) M_m
 Mass of jar and sand before filling cone (g) M_{jb}
 Mass of jar and sand after filling cone (g) M_{ja}

Sample 1	Sample 2

Constant Head Permeability

Analyst name: _____
 Test date: _____
 Soil sample: _____

Specific gravity $G_s =$ _____
 Specimen dry mass $M_d =$ _____ g
 Specimen height $H =$ _____ cm
 Specimen diameter $D =$ _____ cm
 Piezometer tap distance $L =$ _____ cm

Trial	1	2	3	4
Piezometer level distance (cm) Δh				
Duration of sampling (s) t				
Mass of water collected & container (g) M_{wc}				
Mass of container (g) M_c				
Water temperature ($^{\circ}\text{C}$) T_e				

Constant Head Permeability

Analyst name: _____
 Test date: _____
 Soil sample: _____

Specific gravity $G_s =$ _____
 Specimen dry mass $M_d =$ _____ g
 Specimen height $H =$ _____ cm
 Specimen diameter $D =$ _____ cm
 Piezometer tap distance $L =$ _____ cm

Trial	1	2	3	4
Piezometer level distance (cm) Δh				
Duration of sampling (s) t				
Mass of water collected & container (g) M_{wc}				
Mass of container (g) M_c				
Water temperature ($^{\circ}\text{C}$) T_e				

Constant Head Permeability

Analyst name: _____
 Test date: _____
 Soil sample: _____

Specific gravity $G_s =$ _____
 Specimen dry mass $M_d =$ _____ g
 Specimen height $H =$ _____ cm
 Specimen diameter $D =$ _____ cm
 Piezometer tap distance $L =$ _____ cm

Trial	1	2	3	4
Piezometer level distance (cm) Δh				
Duration of sampling (s) t				
Mass of water collected & container (g) M_{wc}				
Mass of container (g) M_c				
Water temperature ($^{\circ}C$) T_e				

Constant Head Permeability

Analyst name: _____
 Test date: _____
 Soil sample: _____

Specific gravity $G_s =$ _____
 Specimen dry mass $M_d =$ _____ g
 Specimen height $H =$ _____ cm
 Specimen diameter $D =$ _____ cm
 Piezometer tap distance $L =$ _____ cm

Trial	1	2	3	4
Piezometer level distance (cm) Δh				
Duration of sampling (s) t				
Mass of water collected & container (g) M_{wc}				
Mass of container (g) M_c				
Water temperature ($^{\circ}C$) T_e				

Falling Head Permeability

Analyst Name: _____
Test Date: _____
Soil Sample: _____

Specific gravity $G_s =$ _____
Specimen dry mass $M =$ _____ g
Specimen height $H =$ _____ cm
Specimen diameter $D =$ _____ cm
Diameter of standpipe $d_s =$ _____ cm
Initial height in standpipe $h_0 =$ _____ cm

Time (min) t	Height of water in standpipe (cm) h_t	Temperature (°C) T_e

Falling Head Permeability

Analyst Name: _____

Test Date: _____

Soil Sample: _____

Specific gravity $G_s =$ _____

Specimen dry mass $M =$ _____ g

Specimen height $H =$ _____ cm

Specimen diameter $D =$ _____ cm

Diameter of standpipe $d_s =$ _____ cm

Initial height in standpipe $h_0 =$ _____ cm

Time (min)	Height of water in standpipe (cm)	Temperature (°C)
t	h_t	T_e

Consolidation test

Analyst : _____
Test date: _____
Sample description: _____
Initial sample height = _____ cm
Sample diameter = _____ cm
Initial sample mass = _____ g
Final sample mass = _____ g
Final mass of dry sample = _____ g
Initial dial reading = _____ cm
Final dial reading = _____ cm

Applied stress (kPa)	Elapsed time (min)	Displacement (cm)

Consolidation test

Analyst : _____

Test date: _____

Sample description: _____

Initial sample height = _____ cm

Sample diameter = _____ cm

Initial sample mass = _____ g

Final sample mass = _____ g

Final mass of dry sample = _____ g

Initial dial reading = _____ cm

Final dial reading = _____ cm

Applied stress (kPa)	Elapsed time (min)	Displacement (cm)

Unconfined compression test

Analyst name: _____
 Test date: _____
 Sample description: _____

Initial height $h_0 =$ _____ cm
 Initial diameter $d_0 =$ _____ cm
 Mass of wet sample and tare $M_l =$ _____ g
 Mass of dry sample and tare $M_d =$ _____ g
 Mass of tare $M_t =$ _____ g
 Specific gravity $G_s =$ _____

Displacement (mm) Δh	Force (N) F

Drained triaxial test

Analyst name: _____

Date: _____

Sample identification: _____

Weight of dry sample $W =$ _____ g

Initial height of sample $h_0 =$ _____ cm

Initial sample diameter $D_0 =$ _____ cm

Soil specific gravity $G_s =$ _____

Confining pressure $\sigma_3 =$ _____ kPa

Back pressure $\sigma_b =$ _____ kPa

Saturation coefficient $B =$ _____ %

Rate of loading $v =$ _____ mm/min

Volume change during consolidation $\Delta V_c =$ _____ cm³

Axial displacement (mm) Δh	Axial force (kN) F	Volume change (cm ³) ΔV

DATA SHEET

Undrained triaxial test

Analyst name: _____

Date: _____

Sample identification: _____

Weight of dry sample $W =$ _____ g

Initial height of sample $h_0 =$ _____ cm

Initial sample diameter $D_0 =$ _____ cm

Soil specific gravity $G_s =$ _____

Confining pressure $\sigma_3 =$ _____ kPa

Back pressure $\sigma_b =$ _____ kPa

Saturation coefficient $B =$ _____ %

Rate of loading $v =$ _____ mm/min

Volume change during consolidation $\Delta V_c =$ _____ cm^3

Axial displacement (mm) Δh	Axial force (kN) F	Pore pressure (kPa) u

Undrained triaxial test

Analyst name: _____

Date: _____

Sample identification: _____

Weight of wet sample $W_w =$ _____ g

Weight of dry sample $W_d =$ _____ g

Initial height of sample $h_0 =$ _____ cm

Initial sample diameter $D_0 =$ _____ cm

Soil specific gravity $G_s =$ _____

Confining pressure $\sigma_3 =$ _____ kPa

Back pressure $\sigma_b =$ _____ kPa

Saturation coefficient $B =$ _____ %

Rate of loading $v =$ _____ mm/min

Volume change during consolidation $\Delta V_c =$ _____ cm^3

Axial displacement (mm) Δh	Axial force (kN) F	Pore pressure (kPa) u

INDEX

- A-line, 77**
AASHTO classification system, 116-119
Absolute error, 490
Abstracts (see Report writing)
Accuracy of measurement, 489
Acknowledgments (see Report writing)
Active cell, 509
Activity of clays, 80
 values, 81
Adsorbed water, 75
Alcohol method, 84
Alternate consolidation tests, 314
American Society for Testing and Materials, 4-6
Analog/Digital (A/D) converter, 363
Analogy (see Electrical analogy)
Andreasen pipette, 55-57
Angular distortion, 253
Apparent failure envelope, 399
Appendix (see Report writing)
Array formulas, 513
ASTM, 4-6
Atterberg limits, 75-100
ASTM, 4, 6
 values, 80
Average, 484
Axial strain, 252
- Back pressure, 377, 446, 454**
Balloon density apparatus, 166, 167
Banding sand, 377
Beam-and-weight mechanism, 343
Bernoulli equation, 179
Bimodal distribution, 485
Blow counts, 88
Body forces, 235
Boiling, 181
Boulders, 10
Boundary conditions, 219
British Standard Institutions (BS), 4
Brownian motion, 34
Built-in functions, 512
Bulk modulus
 soils, 278-280
 water (see Water)
Bulk unit weight (see Unit weight)
Buoyancy analysis, 65-73
Buoyant unit weight (see Unit weight)
- Calcium carbide method, 4**
Cambridge notation, 248, 367
Capillary rise, 204
Casagrande apparatus, 77, 86
 method, 213
Cauchy representation of stress, 238-239, 245
Cavitation, 377
CD triaxial test (see Triaxial test)
Cells, 509
Chemically combined water, 76
Chlorite, 76
Clay fraction, 14, 81, 184, 392
Clay, 10, 14, 75-76, 80
Clay-silt-sand mixtures, 14
Coarse-grained soils, 10, 116, 189
Cobbles, 10
Coefficient
 B, 444, 454
 compressibility, 299, 309
 consolidation, 310-312, 317, 320-333
 values, 181-182, 314
 correlation, 315
 curvature, 12, 14
 lateral earth pressure at rest, 265, 282
 permeability, 179, 181-184, 195, 203-204
 values, 184-186
Cofferdam, 230
Cohesion, 363, 367, 373, 390-392
 values, 393
Cohesionless soils, 369
Cohesive soils, 369
Colloids, 34
Columns, 509
Combined grain size analysis, 71
Compacted soils, 125
Compaction, 147-165
 ASTM, 5, 6
 curve, 148
 energy, 149
Complementary seepage problem, 211
Compression index, 301, 304
 values 304-306
Computer data acquisition, 363
Concentration, 35
Conclusion (see Report writing)
Conduction theory, 207
Conductivity, 208
Cone penetrometer apparatus, 77
Confined compression test, 268, 282-283
 consistency of clays, 79
CONSO, 327, 371
Consolidated tests (see Triaxial tests)
Consolidation phase (see Triaxial tests)
Consolidation test, 296-375
 ASTM, 5, 6
 cell, 298, 343-4
 loading device, 343
 theory, 308-310
Consolidometer, 203
Constant head permeability test, 182, 189-201
Constant rate of strain consolidation, 315, 318
Constant-pressure tank, 192
Constitutive equations, 264
Constrained modulus, 278, 282-283, 299
Contour plot, 225
Conversion
 factors, 540
 units, 497
Correlations, 123-125
 compressibility, 304-306
 consolidation, 314
 friction angle, 379-381, 426-427
 permeability, 181-182
 secondary compression, 319-320
 shear modulus, 285, 287, 291
 shrinkage, 103-104
 undrained shear strength, 393-398
Coulomb friction theory, 361
COUNT, 474
Counterweight system, 433
Creating charts, 515
Creep, 263
Critical hydraulic gradient, 180
Critical state
 line, 371, 373, 387
 parameters, 388
 theory, 386-389
Critical void ratio, 425
CRS consolidation, 315, 318
CU triaxial tests (see Triaxial test)
Cumulative distribution, 11, 483
Current (electrical), 209
Cutting edges, 411
- D10, 12, 27, 28, 181**
D30, D60, 12, 27, 28
Darcy's Law, 179
Data modeling, 471
Datum, 179
Deaired water, 191, 454
Deformation, 252
Degree of consolidation, 311
Degree of saturation, 131, 445
DENSI, 50, 62, 69
Density, 1, 4, 6
Dial indicator, 343
Diffusivity, 543
Dimensional analysis, 495
Dimensions, 495
Direct shear test, 5, 269, 421-442
 box, 430
 device, 269, 430
Direction shear cell, 274
Discharge velocity, 178, 195
Discretization, 218
Dispersing agent, 44, 46, 56, 67
Dispersion apparatus, 42
Displacement transducer, 343
Displacement-controlled loading, 361, 432
Distributed granular stress, 245
Distribution, 483
Disturbed samples, 2, 291, 393
Double direct shear apparatus, 269
Double drainage, 311
Double layer, 76
Drag coefficient, 32-3
Drag force, 31-2
Drainage distance, 310
Drainage filters, 17
Drained shear strength (see Shear strength)
Drained triaxial test (see triaxial test)
Dry sieving, 22, 24

- Dry unit mass, 130
 Dry unit weight (see Unit weight)
 Dry-pluviation method, 193
 Dynamic elastic properties, 290
 values, 285–288
- Earth gravity, 235**
 Effective cohesion and friction (see Cohesion and Friction angle)
 Effective stress, 244
 Elastic properties, 261, 277–278
 relations, 278
 values, 283
 Elastic-perfectly plastic, 262
 Elastic-strain hardening, 263
 Elasticity, 277
 Elastoplasticity, 261
 Electric potential, 208
 Electrical analogy, 207–216
 Elevation head, 179
 Elongation, 253
 Engineering classification of soils (see Soil classification)
 Equilibrium
 forces and moments, 237
 stresses, 237
 Equipotential lines, 209
 Error analysis, 489–494
 Excess pore water pressure, 307
 Experimental apparatus and procedure (see Report writing)
 Experimental errors, 489
 Exponential distribution, 485
 Extractor, 155, 160–161
 Extruding specimens, 413
- Failure**
 envelope, 366–390
 plane, 405, 418
 surfaces, 366, 383
 theory, 361–370
 Falling head permeability test, 183, 202–206
 Field compaction, 166–167
 Field sampling, 2, 416
 Field testing, 2
 Fillunger-Terzaghi Postulate, 244
 Filter papers, 362, 447
 Filter requirements, 17
 Fines, 10
 Fine-grained soils, 42, 116
 Finite difference, 217–233
 direct method, 223
 relaxation, 223–224
 Finite element, 264
 FIT1, 474
 FIT2, FIT3, 161, 474
 Fixed wall permeameter, 190
 Flexible wall permeameter, 190
 Floating-ring, 360
 Flocculated, 44
 Flow line, 90, 178, 222
 Flow net, 222, 228, 232
 Fluid unit weight, 179
 Fluid velocity, 177
 Format, 514
 Formula, 510, 512
 Frequency
 distributions, 15
 plot, 483
 Friction
 angle, 363, 366, 390, 426
 coefficient, 363
 values, 373, 378, 393
 Front matter (see Report writing)
 Fuller, 12
 Fully saturated, 130, 444–446
- Gap-graded, 12**
 GDFIT2, GDFIT3, 164
 Generalized square-root-time method, 326
 Grain size analysis, 9–73
 Granular stress, 244
 Gravel, 10
 Grid, 218
 Grooving tool, 86
 Groundwater drainage, 17
 Grouting and chemical injection, 17
- Hazen's Formula, 181, 197**
 Histogram, 483
 Hollow torsional shear test, 275
 Homogeneity, 278
 Hooke's law, 277
 Hydraulic
 conductivity, 177
 gradient, 179, 194, 195, 236
 Hydrostatic pressure, 239
 Hydrometer analysis, 42–54
 ASTM, 4, 6
 152H, 4, 38
- Illite, 76, 78**
 Impervious boundary, 209
 In-situ
 density, 5
 stresses, 265
 testing, 2
 Infinitesimal
 rotations, 254
 strains, 252–254
 Initial compression, 313
 Initial stresses, 265
 INTER, 28, 50, 477
 INTERCEPT, 472, 523
 Interfaces, 220
 INTERL, 50, 477
 Intermediate principal stress, 381
 International System of units, 496
 Interpolation, 475
 Interpretation of results (see Report writing)
 Interstitial water, 76
 Introduction (see Report writing)
 Inviscid, 263
 Irreversible, 261
 Isotropic compression, 371
 Isotropic consolidation, 384, 456
 Isotropic test, 266, 279–280
 Isotropy, 278
 Iteration, 223
- Kaolinite, 76, 78**
 Kozeny-Carman's formula, 182, 197
- Laboratory testing of soils, 266**
 Lade and Duncan, 382
 Laplace's equation, 207
 Linear regression, 471, 530
 Linear shrinkage, 102
 Linear behavior, 261
 LINEST, 472, 513, 523, 530
 Liquefaction, 377
- Liquid limit, 77, 66–95
 values, 80
 Liquid state, 76
 Liquidity index, 79, 388
 Load ring, 411, 430, 449
 Load-controlled loading, 361
 Loading device, 411, 432, 449
 compliance, 365
 Local strain measurement, 289, 290
 Log-time method, 321
 Lognormal distribution, 486
 London clay, 367
 Long-term settlement, 297
 LVDT transducer, 411, 430
- M, 50**
 Macrosheet user-defined function, 501
 Major principal stress, 239, 242
 Marine clays, 306
 Matsuoka and Nakai, 382
 Maximum dry unit weight, 155
 Maximum void ratio, 131
 Mean, 468
 Mechanical shaker, 23
 Medium, 10
 Membrane stretcher, 449
 Meniscus correction, 45
 Mercury, 106
 Mexico City clay, 300
 Microwave oven, 4, 84
 Minimum void ratio, 131
 Minor principal stress, 239, 242
 MINVERSE, 475
 MIT notation, 246, 367
 Mixture of water and soil particles, 36
 Modified compaction test, 155, 160
 Modified flow function, 228
 Modified secondary compression index, 319
 Mohr circle, 241
 Mohr representation, 239, 245
 Mohr strain space, 258
 Mohr stress space, 241
 Mohr-Coulomb failure surface, 365, 382
 Mohr-Coulomb theory, 361
 Montmorillonite, 76, 78
 Mortar, 22
 Mounting pins, 436
- Nevada sand, 287, 289**
 NGI simple shear apparatus, 274
 Nickel-based paint, 212
 NMULT, 475
 Nonlinear optimization, 329, 478
 Nonlinear behavior, 261
 Normal distribution, 486
 Normal stresses, 236
 Normally consolidated, 302–303, 385
 Nuclear methods, 166–167
- Oedometer, 268, 343**
 Ohm's law, 207, 208, 209
 One-dimensional tests, 297
 One-point liquid limit test, 92–95
 Optimum water content, 148, 151, 155
 OPTIMUM2, OPTIMUM3, 161, 164

- Organic soils, 44, 116
 Organization of report (see Report writing)
 Oven drying, 75
 Overburden stress, 265
 Overconsolidated, 302–303, 385
 Overconsolidation ratio, 285, 302, 368
 Oxidation process, 44
- p'-q stress paths, 348, 370**
 p-q representation, 248
 Paraffin wax, 112
 Partially saturated specimens, 445
 Passive earth pressure, 423
 Peak failure, 361, 424
 Peak friction angle, 366, 424, 438
 Peat, 116
 Percent coarser by weight, 11
 Percent finer by weight, 11
 Perfectly plastic, 262
 Permeability, 177–206
 ASTM, 5
 anisotropy, 186
 correlation, 181–182
 influence of compaction, 150
 values, 184–186
 Permeameter, 190, 194, 202
 Pestle, 22
 Pycnometer, 5
 Piezometric head, 179
 Piezometric tap, 190
 Pipette analysis, 6, 55–64
 BS, 6
 Piping, 181
 Plane strain compression test, 275
 Plastic limit, 77, 96–100
 values, 80
 Plastic state, 76
 Plasticity chart, 77
 Plasticity index, 78, 184, 374
 Pneumatic device, 359, 361
 Poisson ratio, 277, 283, 285
 values, 286
 Pole of Mohr circle, 243
 Polynomial regression, 472, 525, 538
 Poorly graded soils, 12
 Pore water pressure, 179, 244
 Porosity, 131, 135
 Porous boundaries, 308
 Porous stones, 190, 415, 416
 Power relation, 368
 Preconsolidation pressure, 302, 303, 384
 Pressure head, 179
 Pressure transducer, 451
 Pretreatment of sample, 43, 44
 Primary compression (consolidation), 313
 Principal directions, 242
 Principal strain, 257
 Principal stress, 238, 242, 247
 Prong plate, 106
 Pull-down menus, 510
- Quick, 181, 382**
- Rammer, 155, 158**
 Range, 484
 Rate independent, 263
 Rate of deformation, 297
 Rate of loading, 426, 436, 446–447, 457
 Rate of settlement, 366
 Rate-dependent, 263
 References (see Report writing)
 Regression analysis, 474
 Relative density, 131
 Relative error, 490
 Relaxation, 263
 Relaxation method, 223
 Remolded, 291, 414
 Report writing, 499–507
 Residual failure, 461
 Residual friction angle, 366, 424
 values, 378–380
 Residual shear strength, 361, 425
 Resistance, 208
 Resistive paper, 212
RESULT, 517
 Results of experiment (see Report writing)
 Reynolds number, 32
 Riffle, 22
 Rigid-body rotation, 254
 Rigid-perfectly plastic, 262
 Road subbase materials, 17
 Rows, 509
 Rubber balloon method, 166
 Rubber membrane, 451, 465
- s-t representation, 246, 364**
 Sacramento River sand, 279, 282–283, 371–373, 375–377
 Sample splitter, 22
 Sampling tube, 411
 San Francisco bay mud, 298
 Sand bath method, 84
 Sand cone method, 166–175
 Sand, 10
 Saturated unit weight (see Unit weight)
 Saturation, 444, 454, 457, 466
 burette, 455
 line, 148
 Secant moduli, 281, 283
 shear modulus, 283, 285
 Young's modulus, 280, 290
 Secondary compression, 313, 319–320, 333
 index, 319
 ratio, 313
 values, 320
 Sedimentation analysis, 31–70
 cylinder, 43
 Seepage, 1
 flow, 221, 228
 quantity, 177
 theory, 207, 217
 Selection
 aggregate materials, 17
 fill materials, 16
 Semisolid state, 76
 Sensitivity, 306, 396, 398, 426
SHANSEP, 390
 Shear modulus, 277, 283,
 correlations, 285, 287, 291
 initial and secant, 283
 Shear strain, 253
 Shear strength envelope, 366
 Shear strength, 2, 360–403
 coarse-grained soils, 370–386
 envelope, 366
 fine-grained soils, 383, 390–391
 Shear stress, 236, 240
 Shear zone, 424
 Sheet-pile wall, 225
 Shear strain, 253
 Shrinkage limit, 77, 101, 104, 106–115
 ASTM, 4
 correlations, 103–104
 mercury method, 106–111
 shrinkage ratio, 101
 wax method, 112–115
 values, 104
 SI unit system, 496
 Sieve analysis, 9–30
 ASTM, 4
 BS, 6
 sieves, 22
 Sign convention
 stress, 240
 strain, 258
 Silt, 10
 Simple shear test, 273, 283
 Single drainage, 311
 SLOPE, 472, 523
 Soaking, 25
 Sodium hexametaphosphate, 43
 Soil classification, 1, 116–126
 AASHTO, 117–119
 ASTM, 4
 USCS, 116–118
 Soil hydrometer, 42
 Solid state, 76
 Solid unit mass, 130
 SOLVER, 331, 480
 Specific gravity, 36, 132, 142
 values, 133–134
 Specific surface, 10
 Specific surface area, 182
 Split mold, 155, 157, 451
 Spreadsheet, 509
 Spring analogy, 307
 Square-Root-Time method, 323
 Stagnation pressure, 32
 Standard (Proctor) compaction test, 150, 155, 158
 Standard deviation, 484
 Statistics, 482–488
 Steady state line, 371
 Stokes, Law, 31
 Strain hardening, 261
 Strain softening, 261
 Strain, 215–260
 tensor, 256
 Stream function, 222
 Stress, 235–250
 invariant, 247
 vector, 236
 Stress-path, 267–274, 385
SUM, 474
SUMPRODUCT, 474
 Suspension, 34
 Swelling
 index, 301, 304
 line, 302, 384
 slope, 384, 388
 values, 305
- Taylor expansion, 218**
 Teflon sphere, 65
 Temperature correction, 46
 Terminal velocities, 36

- Three-dimensional Mohr-Coulomb failure surface, 225, 365
 - strain, 259
 - stress, 246
- Torsional shear test, 269, 275
- Total head, 179, 227
- Total stress failure criterion, 398
- Total stress, 244
- Total unit mass, 130
- TREND**, 523
- Trendline, 523, 525
- Tresca surface, 365
- Triangular classification, 14
- Triaxial test, 270, 273, 280–282, 404, 443–469
 - ASTM 5–6
 - cell, 449, 452, 465
 - compression, 270, 385
 - consolidated drained (CD), 272, 444, 447, 449–469
 - consolidated undrained (CU), 272, 449–469
 - consolidation, 456
 - equipment, 450
 - extension, 270
 - unconsolidated undrained (UU), 272, 449–469
- Trimming, 136, 411, 412, 465
- True triaxial apparatus, 275
- U-line**, 78
- U.S. standard sieves, 24
- Uncertainty, 489
- Unconfined compression test, 5, 6, 269, 280, 404–420
- Unconfined compressive strength, 405, 417
- Unconfined seepage, 213
- Unconsolidated (see Triaxial test)
- Undisturbed samples, 2, 291, 412
- Undrained shear strength, 387–389, 391, 394–405, 404–405, 408
- Undrained triaxial test (see Triaxial test)
- Unified soil classification system, 116–118
- Uniform soils, 12
- Unimodal distribution, 16, 485
- Unit conversion, 534
- Unit mass (see Unit weight)
- Unit weight, 135–136, 542
 - bulk, 130, 166, 173
 - buoyant, 130
 - dry, 130, 134, 166, 173
 - saturated, 130
 - values, 135
- Units, 5, 495
- UNITS**, 498
- User-defined functions, 517
- UU triaxial tests (see triaxial tests)
- Vacuum line**, 452
- Vertical settlement, 299
- Virgin compression line, 301, 387
- Virgin consolidation line, 384
- VISCO**, 50, 62, 69
- Viscosity (see Water)
- Viscous behavior, 263
- Visual Basic user-defined function, 518
- Void ratio, 130, 135, 184
 - values, 134–135
- Voltage, 209
- Volume-change burette, 455
- Volumetric strain, 253, 259, 298
- Von Mises surface, 365
- Water**,
 - bulk modulus, 445–446
 - unit mass, 39
 - viscosity, 31, 39, 181
- Water content, 75, 84–85, 131
 - ASTM, 4, 6
- Water pressure, 227
- Wax unit weight, 138
- Weald clay, 383, 387
- Weibull distribution, 486
- Weight-volume relationships, 129
- Well-graded soils, 12
- Wet sieving, 22, 25
- Wet-pluviation method, 193
- Wire saw, 362
- Workbooks, 509
- Worksheet, 509
- Yield stress**, 261
- Young's modulus, 277, 283, 458
 - initial and secant, 281–282
 - relation to undrained shear strength, 398–399
 - values, 285

SOFTWARE INSTRUCTIONS

What's on the Disk?

The floppy disk included with this book contains all the Excel examples of this book as well as the necessary user-defined functions, i.e., 23 Excel workbook files totaling 1.4 Mb. It is recommended to copy these workbook files, as you need them, onto your hard disk or another floppy disk so that you preserve the original files. The workbook files are readable by Excel (versions 5.0 and later) on a Windows 3.X, Windows 95, Windows NT, or Macintosh-based computer. The 1.44MB floppy disk is DOS formatted. It can also be read by Macintosh computers that have PC Exchange, DOS mounter, or similar software. If your Macintosh displays the alert box *This is not a Macintosh disk, Do you want to initialize it?*, eject the disk, and use Apple File Exchange to transfer the files from the DOS-format disk onto the Macintosh hard drive.

What are these workbooks on the Disk?

The table below gives the correspondence between the workbook files on the floppy disk and the examples in the chapters of the book.

Chapter number	Chapter name	Workbook file
1-2	Sieve analysis	Sieve.xls
1-4	Hydrometer analysis	Hydro.xls
1-5	Pipette analysis	Pipette.xls
1-6	Buoyancy analysis	Buoyan.xls
1-7	Combined grain size analysis	Combine.xls
2-3	Liquid limit test	Liquid.xls
2-5	Plastic limit test	Plastic.xls
2-7 & 2-8	Shrinkage limit analyses with mercury and wax	Shrink.xls
2-9	Engineering classification of soils	Classi.xls
3-2	Unit weight of cohesive soils	Uweight.xls
3-3	Determination of specific gravity	Specific.xls
3-5	Compaction tests	Compac.xls
3-6	Sand cone method	Cone.xls
4-2	Constant head permeability test	Permcons.xls
4-3	Falling head permeability test	Permfall.xls
4-4	Electrical analogy of seepage problems	Elect.xls
4-5	Finite difference solutions of seepage problems	Finite.xls
6-2	Consolidation test	Consol.xls
7-3	Unconfined compression test	Unconf.xls
7-5	Direct shear test	Direct.xls
7-7 & 7-8	Triaxial drained and undrained tests	Triaxial.xls
9-3	Worked examples	Examples.xls

The additional workbook AREADME.XLS describes the contents of these workbooks, and provides users with a few suggestions on how to use them.

The workbooks include the datasheets at the end of the book. The datasheets can be used during the laboratory experiments to take notes and record measurements by hand. The workbooks also include all the tables and graphs of the examples in the book so that the users can process their own data. From within Excel, it is recommended to open the workbook of the selected experiment, and to create a new worksheet in the same workbook by using **Move or Copy Sheet ...** of the **Edit** menu, and checking the **Copy File** option. In this new worksheet, you may enter your own data in place of the old input data which is italicized. You may also use **Ctrl** to display the formulas and not erase them by mistake. You may add and remove lines in the tables of data, provided that you check the formulas and the names of defined variables. The graphs should automatically be modified as you enter new data.

Some worksheets need user-defined functions to perform calculations. These functions should be in Macros or Modules, in the same workbook as the worksheet. Macros are written in the spreadsheet programming language, and Modules are written in Visual Basic, a more advanced computer language. The Visual Basic functions of Modules have been assigned a name starting with **VB** (e.g., **VBfin**) and have the same arguments as Macros in most cases. The examples in the workbooks are using Macros. To use VB functions instead of Macros, the users will have to add **VB** in front of the Macro names in the formulas, and modify their arguments when required.

An error message may be displayed when using the workbook **FINITE.XLS**. This is not a problem because this workbook uses circular references for iterative calculations.

YOU SHOULD CAREFULLY READ THE FOLLOWING TERMS AND CONDITIONS BEFORE OPENING THIS DISKETTE PACKAGE. OPENING THIS DISKETTE PACKAGE INDICATES YOUR ACCEPTANCE OF THESE TERMS AND CONDITIONS. IF YOU DO NOT AGREE WITH THEM, YOU SHOULD PROMPTLY RETURN THE PACKAGE UNOPENED, AND YOUR MONEY WILL BE REFUNDED.

IT IS A VIOLATION OF COPYRIGHT LAWS TO MAKE A COPY OF THE ACCOMPANYING SOFTWARE EXCEPT FOR BACKUP PURPOSES TO GUARD AGAINST ACCIDENTAL LOSS OR DAMAGE.

Prentice-Hall, Inc. provides this program and licenses its use. You assume responsibility for the selection of the program to achieve your intended results, and for the installation, use, and results obtained from the program. This license extends only to use of the program in the United States or countries in which the program is marketed by duly authorized distributors.

LICENSE

You may:

- a. use the program;
- b. copy the program into any machine-readable form without limit;
- c. modify the program and/or merge it into another program in support of your use of the program.

LIMITED WARRANTY

THE PROGRAM IS PROVIDED "AS IS" WITHOUT WARRANTY OF ANY KIND, EITHER EXPRESSED OR IMPLIED, INCLUDING, BUT NOT LIMITED TO, THE IMPLIED WARRANTIES OF MERCHANTABILITY AND FITNESS FOR A PARTICULAR PURPOSE. THE ENTIRE RISK AS TO THE QUALITY AND PERFORMANCE OF THE PROGRAM IS WITH YOU. SHOULD THE PROGRAM PROVE DEFECTIVE, YOU (AND NOT PRENTICE-HALL, INC. OR ANY AUTHORIZED DISTRIBUTOR) ASSUME THE ENTIRE COST OF ALL NECESSARY SERVICING, REPAIR, OR CORRECTION.

SOME STATES DO NOT ALLOW THE EXCLUSION OF IMPLIED WARRANTIES, SO THE ABOVE EXCLUSION MAY NOT APPLY TO YOU. THIS WARRANTY GIVES YOU SPECIFIC LEGAL RIGHTS AND YOU MAY ALSO HAVE OTHER RIGHTS THAT VARY FROM STATE TO STATE.

Prentice-Hall, Inc. does not warrant that the functions contained in the program will meet your requirements or that the operation of the program will be uninterrupted or error free.

However, Prentice-Hall, Inc., warrants the diskette(s) on which the program is furnished to be free from defects in materials and workmanship under normal use for a period of ninety (90) days from the date of delivery to you as evidenced by a copy of your receipt.

LIMITATIONS OF REMEDIES

Prentice-Hall's entire liability and your exclusive remedy shall be:

1. the replacement of any diskette not meeting Prentice-Hall's "Limited Warranty" and that is returned to Prentice-Hall with a copy of your purchase order, or

2. if Prentice-Hall is unable to deliver a replacement diskette or cassette that is free of defects in materials or workmanship, you may terminate this Agreement by returning the program, and your money will be refunded.

IN NO EVENT WILL PRENTICE-HALL BE LIABLE TO YOU FOR ANY DAMAGES, INCLUDING ANY LOST PROFITS, LOST SAVINGS, OR OTHER INCIDENTAL OR CONSEQUENTIAL DAMAGES ARISING OUT OF THE USE OR INABILITY TO USE SUCH PROGRAM EVEN IF PRENTICE-HALL, OR AN AUTHORIZED DISTRIBUTOR HAS BEEN ADVISED OF THE POSSIBILITY OF SUCH DAMAGES, OR FOR ANY CLAIM BY ANY OTHER PARTY.

SOME STATES DO NOT ALLOW THE LIMITATION OR EXCLUSION OF LIABILITY FOR INCIDENTAL OR CONSEQUENTIAL DAMAGES, SO THE ABOVE LIMITATION OR EXCLUSION MAY NOT APPLY TO YOU.

GENERAL

You may not sublicense, assign, or transfer the license or the program except as expressly provided in this Agreement. Any attempt otherwise to sublicense, assign, or transfer any of the rights, duties, or obligations hereunder is void.

This Agreement will be governed by the laws of the State of New York.

Should you have any questions concerning this Agreement, you may contact Prentice-Hall, Inc., by writing to:

Prentice Hall
College Division
Upper Saddle River, NJ 07458

YOU ACKNOWLEDGE THAT YOU HAVE READ THIS AGREEMENT, UNDERSTAND IT, AND AGREE TO BE BOUND BY ITS TERMS AND CONDITIONS. YOU FURTHER AGREE THAT IT IS THE COMPLETE AND EXCLUSIVE STATEMENT OF THE AGREEMENT BETWEEN US THAT SUPERSEDES ANY PROPOSAL OR PRIOR AGREEMENT, ORAL OR WRITTEN, AND ANY OTHER COMMUNICATIONS BETWEEN US RELATING TO THE SUBJECT MATTER OF THIS AGREEMENT.

ISBN: 0-13-374935-5

NOTICE TO CONSUMERS

**THIS BOOK CANNOT BE RETURNED
FOR CREDIT OR REFUND IF THE
PERFORATION ON THE VINYL
DISK HOLDER IS BROKEN OR
TAMPERED WITH.**

Diskette version 1.0 (1/1/97)

Microsoft Excel Data files for Windows and Macs.
DOS formatted 1.4 Mb disk for Windows and Macs.

© 1997 by Prentice-Hall, Inc.
Upper Saddle River, New Jersey, 07458

ISBN 0-13-374935-5



DISK INCLUDED
DO NOT DEMAGNETIZE

PRENTICE HALL
Upper Saddle River, NJ 07458
<http://www.prenhall.com>

BARDET NEW

EXPERIMENTAL SOIL MECHANICS-W/3"DISK
97 PH
0-13-374935-5 5-5554KE-B1-D-13-374935-5



9 780133 749359 98000

01000265197ND

17 B